3-D Modeling of the Erosional Potential of Turbulent Lava

Applied to Lunar Sinuous Rilles

by

Vincenzo Cataldo

A Dissertation Presented in Partial Fullfillment
of the Requirements for the Degree
Doctor of Philosophy

Approved January 2022 by the
Graduate Supervisory Committee:

David A. Williams, Co-Chair
Amanda B. Clarke, Co-Chair
Mark W. Schmeeckle
Mark S. Robinson
Donald M. Burt

ARIZONA STATE UNIVERSITY

May 2022

ABSTRACT

This study has the objective to better constrain the role played by thermal erosion by turbulent lava in the formation of large channels on Mars and the Moon. On Mars, a rigorous one-dimensional model was used to test whether lava might have excavated the Athabasca Valles outflow channel. Calculated erosion depths are much lower than the measured depths of the channel, and suggest a limited role played by thermal erosion in excavating it. On the Moon, the investigation focused on the outer and inner sinuous rilles of Vallis Schröteri. At this site, erosional features cannot be explained by one- and two-dimensional models. The first 3-D model of thermal erosion by turbulent lava on the Moon was created to relate the spatial distribution of erosion rates over the bed and banks of a channel with changes in fluid- and thermodynamic parameters. The turbulence model chosen for each steady-state simulation is the Shear Stress Transport (SST) k-ω model and OpenFOAM is the Computational Fluid Dynamics software used. At the 150-km-long, 4-km-wide, and up-to 700-m-deep outer rille, I aimed to determine maximum erosion rates at/near the lava source and rille segments 1-km-long and 4-km-wide were chosen for the simulations. By adopting the obtained maximum erosion rates of 1 m/day, lava might have taken ~2 years to excavate the 700-m-deep depression. These fast erosion rates were unlikely maintained downstream of the lava source unless lava flowed in a tube. Besides, observational evidence suggests that tectonics and constructional processes likely contributed to rille development. On these grounds, thermal or thermo-mechanical erosion might have contributed to rille formation at a later stage. At the Vallis Schröteri inner rille, 1-km-long and 160-m-wide meandering channels were chosen. In one scenario, lava loses

heat by radiation, in the other flows in a tube. Using the calculated (and conservative) erosion rate of 50 cm/day, it would have taken ~6 months for the 90-m deep inner rille to be excavated. A mechanism of secondary flow circulation analogous to that found in meandering rivers potentially explains meander generation. At each bend, downstream and cross-stream velocity variations lead to local temperature/ erosion enhancements.

TABLE OF CONTENTS

Page

CHAPTER Page

CHAPTER Page

CHAPTER Page

LIST OF TABLES

Table Page

Table Page

Table Page

LIST OF FIGURES

Figure Page

Figure Page

Figure Page

Figure Page

Figure Page

Figure Page

Figure Page

1 INTRODUCTION

Thermal Erosion Models

The partial or complete melting and assimilation of a solid or particulate substrate by flowing lava are defined as thermal erosion, whereas mechanical erosion involves the entrainment of substrate materials that have not chemically interacted with the lava (*Williams et al*., 1998). Thermomechanical erosion implies a combination of the two processes. These processes are important because they cause the removal of substrate during lava flow emplacement, and erosion by flowing lava is a mechanism thought to be responsible for the formation of some lava channels and tubes on Earth and other silicate planets and moons (*Carr*, 1974; *Baker et al*., 1992; *Greeley et al*., 1998; *Schenk and Williams*, 2004; *Head et al*., 2011). Regardless of the mechanism, erosion by lava is most plausible for high-temperature, low-viscosity lavas, especially if they flow turbulently. Thermal erosion has been inferred to have a minor role (i.e., cm's of melting) in the emplacement of carbonatite lavas at Oldoinyo Lengai, Tanzania (*Dawson et al.*, 1990) and in possible planetary lava analogs like industrial sulfur flows (*Greeley et al.*, 1990). It has also been inferred to have a somewhat greater role in the formation of several terrestrial lava tubes (*Greeley*, 1971b, 1972; *Cruikshank and Wood*, 1972; *Swanson*, 1973; *Peterson and Swanson*, 1974; *Wood*, 1981; *Coombs et al.*, 1990; *Peterson et al.*, 1994; *Kauahikaua*, 1996), and in the formation of some lunar sinuous rilles (*Hulme*, 1973, 1982; *Head and Wilson*, 1981), some Martian lava channels (*Carr*, 1974; *Cutts et al.*, 1978; *Baird*, 1984; *Wilson and Mouginis-Mark*, 1984), and some Venusian canali (*Head et al*., 1991; *Baker et al*., 1992; *Komatsu et al*., 1993; *Komatsu and Baker*, 1994; *Bussey et al.*, 1995).

Mathematical Modeling of Lava Emplacement

Over the last 90 years, mathematical models have been used to study volcanic processes such as 1) the cooling and heat loss from lava flows and intrusions (*Lovering*, 1935; *Larsen*, 1945; *Price and Slack*, 1954; *Carslaw and Jaeger*, 1959; *Jaeger*, 1968; *Dragoni*, 1988; *Crisp and Baloga*, 1990, 1994); 2) style and mode of lava emplacement (*Shaw and Swanson*, 1970; *Danês*, 1972; *Hulme*, 1974; *Wadge*, 1978; *Huppert and Sparks*, 1985; *Dragoni et al*., 1986; *Crisp and Baloga*, 1994; *Pinkerton and Wilson*, 1994; *Dragoni et al*., 1995); and 3) contact metamorphism by heat from lava flows and intrusions (*Lovering*, 1936; *Jaeger*, 1957, 1959, 1964). Mathematical models can be analytical when using equations of physical processes to arrive at an exact solution, or numerical when they use repeated iterations of an algorithm to approximate the solution. When it comes to solving simple problems, there is often little difference between exact and approximate solutions; on the contrary, for a complex problem, a numerical solution can be quite different from an exact solution, and the choice of an appropriate methodology is crucial to the success of the operation.

Hulme (1973) first simulated the role played by high-temperature, low-viscosity, and high-density lavas in creating the sinuous rilles on the Moon. *Hulme* (1973) and *Huppert and Sparks* (1985) showed that turbulently flowing, low-viscosity lavas are expected to lose heat mainly by convection rather than conduction. *Huppert et al*. (1984) and *Huppert and Sparks* (1985) used a combination of laboratory experiments and mathematical modeling to simulate the turbulent emplacement of Archean komatiites on

Earth. In subsequent years, all workers used variations of the *Hulme* model and the *Huppert and Sparks* model (*Jarvis*, 1995; *Wilson and Mouginis-Mark*, 2001). Since mathematical modeling was first used for solving problems in physical volcanology, there has been a debate as to what factors might be most important in controlling lava flow emplacement. Several authors argue that topographic control, lava viscosity, variable flow rate, yield strength, flow volume, and hydrostatic pressure gradients exert a primary control on flow dimensions, with heat loss being important only to the formation of the lava crust (*Nichols*, 1939; *Walker*, 1973; *Hulme*, 1974; *Malin*, 1980; *Baloga and Pieri*, 1986; *Dragoni et al*., 1986; *Guest et al*., 1987). Other authors consider heat loss and crust development to be the most important factors determining flow length and width, due to the sensitivity of lava rheology to temperature changes (*Shaw and Swanson*, 1970; *Danês*, 1972; *Huppert et al*., 1984; *Huppert and Sparks*, 1985; *Gregg and Greeley*, 1993; *Crisp and Baloga*, 1990, 1994; *Keszthelyi*, 1995; *Keszthelyi and Denlinger*, 1996; *Sakimoto et al*., 1997). Heat loss and crust development are also thought to exert a strong control on the formation of lava breakouts upstream from an advancing flow front (*Crisp and Baloga*, 1990).

Williams et al. (1998) model of thermal erosion by turbulently flowing lava

The rigorous analytical-numerical model developed by *Williams et al*. (1998) advances the *Huppert and Sparks* (1985) model by including both a geophysical approach and a geochemical approach, thus better constraining the evolving composition and thermal-rheological properties of lava and substrate, and the convective heat transfer to the top of the flow and to the substrate. For a complete description of the model and the

equations adopted, the reader may refer to *Williams et al*. (1998). A couple of years later, *Williams et al*. (2000) adapted their original model to the lunar environment and assessed the effect of bubbles on the emplacement of the lava. Importantly, the *Williams et al*. model was designed for terrestrial localities where model results could be compared to field data. The flow is one-dimensional with thermal erosion in the vertical direction. Lava erupts as a turbulent flow with a thermally mixed interior, convective heat transfer occurs to the top and the base of the flow, and thermal erosion occurs at the base of the flow, providing that the lava temperature is greater than the melting temperature of the substrate and latent heat is released as the flow crystallizes. The model includes (1) the effects of lava rheology changes due to assimilation of eroded substrate and crystallization of mafic minerals in the flowing lava, (2) the lava temperature decrease as the flow moves downstream, and (3) the flow thickness increase as velocity decreases (thickness is used as a proxy for flux, which is conserved as the flow moves downstream). Several algorithms are used to calculate initial values of important temperature- and composition-dependent thermal-physical lava properties, including solidus and liquidus temperatures, liquid density and viscosity, lava-specific heat, and thermal conductivity. However, these algorithms require an initial lava major oxide composition, and a set of topographical parameters associated with the flow is also required to run the model.

What is required to advance the study of thermal-mechanical erosion by flowing lava is a more sophisticated, 3-D modeling approach, over the 1-D modeling of *Williams et al.* (1998). Application of computational fluid dynamics (CFD) software that can model turbulent flow in a lava channel or tube in three dimensions would provide new insights

into the locations and depths of erosion by lava in an evolving system. Specifically, it will reveal changes in fluid-dynamic parameters on a local scale, i.e., in channel cross-section at meander bends, and how those changes relate to variations in flow temperature, hence, thermal erosion rates. Understanding erosion by lava in a sinuous channel system using CFD software would be a major advance on past modeling efforts because no current state-of-the-art 1- and 2-D models are capable of addressing this level of complexity. That is precisely the goal of this work.

2 BACKGROUND ON THERMAL EROSION MODEL AND SENSITIVITY ANALYSIS

Introduction

The purpose of this chapter is to present erosion rate results obtained through application of the new three-dimensional model of thermal erosion by turbulently flowing lava to 1.2-1.5-km-long channel segments of the inner sinuous rille of Vallis Schröteri on the Moon. Erosion rates are obtained from a baseline model that was chosen based on rille knowledge gathered from high-resolution imagery (*Robinson et al*., 2012) and lava and substrate information inferred from remotely-sensed data (*Walker et* al., 1976; *McEwen et* al., 1994; *Mustard et al*., 2011; *Zhang et al*., 2014). Then, a sensitivity analysis is presented, in which variations of baseline model results relate to uncertainty in lava and substrate parameters (lava temperature, thickness, velocity and substrate composition/compaction) and variability of measurable properties (rille width, meander amplitude, and meander wavelength). The sensitivity analysis is performed by choosing a baseline set of model parameters (Tables 2.1, 2.2), running the model with this set of parameters, and then running the model after changing one parameter at a time (Tables 2.3 – 2.9). By comparing the model results between the baseline run and the later runs in which a single parameter has been varied, the sensitivity of the model results to changes in that parameter can be determined.

OpenFOAM^{TM} is the software that was used to obtain model results, which consists of a C++ library of applications called solvers and utilities. Solvers are groups of equations sorted by physical problem (turbulent versus laminar flow, compressible versus

incompressible scenarios) and enable simulation of specific problems of Computational Fluid Dynamics (CFD). Utilities are designed to perform simple pre-and post-processing tasks like those involved in mesh generation. The solver that was chosen is simpleFoam, which is well-suited for the purpose of modeling turbulent, incompressible flow. However, no temperature is specified in the solver, a severe limitation when modeling turbulently flowing lava. As a result, a 3-D temperature model was coupled to simpleFoam. Turbulence modeling is a time-averaging mathematical procedure that introduces two unknowns (Reynolds stresses). Because of this, models that contain two additional transport equations are needed to solve any problem involving turbulence. Two among the most widely used turbulence models are the k-ε and the Shear Stress Transport (SST) k-ω models. The standard "k-ε" model (*Jones and Launder*, 1972; *Launder and Sharma*, 1974) is a high Reynolds number model that does not perform well at channel boundaries (low-Reynolds number regions) if wall functions are not used. The k expression quantifies the turbulent kinetic energy that is produced, convected, and diffused within the flow, and the ε equation approximates turbulent dissipation. The "SST k-ω" model (*Menter*, 1993) switches to a "k-ε" behavior in the free stream and can be used as a low Reynolds number model all the way down to the wall, thanks to the Shear Stress Transport (SST) formulation. Because of this, it is very well-suited to determine erosion rates into the lava substrate.

The baseline model (BM) – input parameters

Table 2.1 shows the input parameters (physical and thermophysical properties of the flow together with the geometric properties of the channel) that identify the baseline

model. There is uncertainty as to the thickness of the lava flows that formed the Vallis Schröteri inner rille. Estimates of the thicknesses of lava flows have varied widely, ranging between 10 and 60 m (*Schaber*, 1973) and 1 and 96 m (*Gifford and El-Baz*, 1981), and representing ranges in eruption conditions as well as available data resolution and measurement techniques. Specifically, *Gifford and El-Baz* (1981) used shadow measurements of lava flow front scarps observed in Lunar Orbiter images and Apollo orbital photographs. Very recently, terrestrial image interpretations were found to overestimate lava flow thicknesses by factors of 1.2 to 3.5 (*Rumpf et al*., 2020), and current measurements of lunar mare flow thicknesses likely overestimate individual flow thicknesses by factors up to 3 (*Rumpf et al*., 2020). Over the last decade, the Lunar Reconnaissance Orbiter (LRO) Narrow Angle Camera (NAC) has provided panchromatic images at ~0.5 m/pixel (*Robinson et al*., 2012), thus greatly improving our ability to interpret meter-scale features. Individual layers of lava have been observed in lunar pit craters and in the walls of impact craters greater than several km in diameter, and a mean layer thickness of 9.7 ± 2.9 m was measured at Bessel crater (*Robinson et al*., 2012). Because of all the above, a value of 10 m is chosen to be representative of the thickness of the lava in the baseline model.

Table 2.1. Baseline model - Input parameters of the flow. The lava substrate is assumed to be consolidated and identical in composition to the flowing lava. The suffix "inlet" stands for lava source; "interface" refers to channel bed and banks, "mg" stands for "melting of ground", "emg" is "effective melting of ground", "freestream" is the channel region that is farthest from channel boundaries, "top" stands for flow top. T is lava temperature, U_x is the horizontal component of flow velocity, ρ is density, υ is kinematic viscosity, υ_t is kinematic turbulent viscosity, Pr is laminar (molecular) Prandtl number, Prt is turbulent Prandtl number, C_p is specific heat capacity of the lava, C_g is specific heat capacity of the lava substrate, L_g is latent heat of fusion of the lava substrate, αt is turbulent thermal diffusivity. As regards the geometric parameters of the channel, "Hydr. R" stands for hydraulic radius (see text), With

reference to the turbulence parameters, k is turbulent kinetic energy and ω is specific turbulence dissipation.

Input physical parameters							
T_{inlet}	$T_{interface}$	U_{x_inlet}	$U_{x\_interface}$	ρ_{lava}	$\rho_{substrate}$	υ_{inlet}	$\upsilon_{interface}$
°C	°C	m s^{-1}	m s^{-1}	kg m^{-3}	kg m^{-3}	m^2 s^{-1}	m^2 s^{-1}
1440 (liq.)	1412	7.0	0.0	2900	3100	1.38 x10^{-4}	4.24 x10^{-4}
υ_{t_inlet}	$\upsilon_{t\_int\_field}$	$\upsilon_{t\_interface}$					
m^2 s^{-1}	m^2 s^{-1}	m^2 s^{-1}					
10^{-3}	10^{-3}	0.0					
Input thermophysical parameters							
T_{mg}	T_{emg}	$Pr_{freestream}$	$Pr_{interface}$	$Prt_{freestream}$	$Prt_{interface}$	$C_{p\_freestream}$	C_g
°C	°C	#	#	#	#	m^2 s^{-2} $°C^{-1}$	m^2 s^{-2} $°C^{-1}$
1080	1160	1409.7	4123.2	0.7	0.85	1570	1500
L_g	αt_{inlet}	αt_{int_field}	$\alpha t_{interface}$				
m^2 s^{-2}	m^2 s^{-1}	m^2 s^{-1}	m^2 s^{-1}				
4.25 x 10^5	10^{-3}	10^{-3}	0.0				
Geometry of the meandering channel							
Depth (h)	Length (l)	Width (w)	Hydr. R.	Meander wavelength λ		Meander amplitude 2A	
m	m	m	m	m		m	
10	1200	160	8.889	800		300	
Calculated input turbulence parameters - SST k-ω model (from Menter, 1993)							
k_{int_field}	k_{inlet}	$k_{interface}$	k_{top}	ω_{int_field}	ω_{inlet}	$\omega_{interface}$	ω_{top}
m^2 s^{-2}	m^2 s^{-2}	m^2 s^{-2}	m^2 s^{-2}	s^{-1}	s^{-1}	s^{-1}	s^{-1}
5.43 x 10^{-6}	7.26 x 10^{-2}	0.0	calculated	3.54	7.91 x 10^{-1}	1.36	calculated

The lava that, at least, contributed to excavating the inner rille flowed over a substrate that likely had a composition analogous to that of the lava that flowed in the primary outer rille. The lava is taken to have a composition analogous to that of the Apollo

12, low-Ti basalt (*Walker et al*., 1976) with a liquidus eruption temperature of 1440°C and a kinematic viscosity of 1.38 x 10^{-4} m^2 s^{-1} (equivalent to a dynamic viscosity of 0.4 Pa s). Turbulent viscosity is assumed to be the same (10^{-3} m^2 s^{-1}) at the lava source and flow core. Given the lava flow thickness, the steady-state velocity of a turbulently flowing gravity current can be obtained by re-arranging equation (8) of *Jarvis* (1995). For a lunar gravity value of 1.62 m s^{-2} and a measured average slope of the ground of 0.2° (*Honda et al.*, 2009; *Cataldo et al*., 2015), the calculated lava velocity is equal to ~4.0 m s^{-1}. That said, by applying *Hulme's* (1973) model of lava flow to 7 lunar rilles, *Wilson and Head* (2017) found Reynolds numbers of order 10^5 and inferred lava flow depths of ~10 m in channels measured to be 100-300 m deep. Flow speeds were within a factor of two of 6 m s^{-1}, i.e., in the range between 3 and 12 m s^{-1}, with very high total erupted volumes in the range 100-2000 km^3, which explains the adopted inlet velocity value of 7 m s^{-1}. At the interface between the flowing lava and the substrate, the temperature is held constant at 1412°C, the 28°C temperature difference between the flow core and the channel boundaries being intermediate between those characterizing 5-m- and 20-m-thick flows (see Table 5.2). The lower temperature assumed at the channel boundaries is tied to a kinematic viscosity that is greater by a factor of ~3 than that found at the lava source and flow core. Flow speed and turbulent viscosity are assumed to be equal to zero at the channel interface, consistent with our understanding of boundary layer theory.

Among the key input thermophysical parameters of the flow, the melting temperature of the ground (1080°C) is taken from *Williams et al*. (1998) and refers to a basaltic composition. From the same authors is also the value of the effective melting

temperature of the ground, which accounts for the viscosity of the lava substrate and, in so doing, reduces the amount of heat being transferred into the substrate itself. The molecular or laminar Prandtl number is calculated at the lava source and flow core ($Pr_{\_freestream}$) as well as at the channel boundaries ($Pr_{\_interface}$). The turbulent Prandtl number is assumed to be equal to 0.7 everywhere in the flow except at flow boundaries (Pr = 0.85). The specific heat capacity at the flow source and core ($C_{p\_freestream}$) and the one at the channel boundaries (C_g) are taken from *Williams et al*. (1998, 2000) and refer to a lava and substrate that are basaltic in composition. The substrate latent heat of fusion is taken from *Williams et al*. (2000) and refers to a consolidated basaltic substrate. Finally, the turbulent thermal diffusivity, α_t, is assumed to be equal to 10^{-3} m^2 s^{-1} whereas at the channel interface it is equal to zero (no turbulent motion).

As regards the geometric parameters of the baseline channel (beside lava depth), the investigated channel length is only 1200 m long because the key objective is that of running steady-state simulations that may reveal how the fluid- and thermodynamic parameters of the flow vary from one channel section to the next. Channel width is equal to 160 m, an average value that was obtained by taking several measurements at rille sections that stretch from the lava source to a downstream distance of ~100-130 km. Measurements were possible thanks to the availability of very high-resolution Lunar Reconnaissance Orbiter (LRO) Narrow Angle Camera (NAC) images of the rille. For an open channel, the hydraulic radius often replaces channel depth, though the two values tend to be very similar (though not quite the same) for channels that are much wider than deeper. For a rectangular channel cross-section, the hydraulic radius is defined as $R_H = A/P$, in

which A is the cross-sectional area of the flow and P its wetted perimeter. The value of A is determined as the product of channel width, b, and channel depth, y, whereas P = 2y + b. As a result, the hydraulic radius can be written as R_H = by / (2y + b). Meander wavelength appears to vary between ~800 and ~1200 m down to a downstream distance of ~130 km from the lava source. Shorter values (in the range 600-700 m) characterize rille sections that are farther from the source than ~130 km. Because of this, a value of 800 m is adopted in the baseline model. Meander amplitude appears to vary more significantly than meander wavelength. This is also due to the abundant occurrence of goose-neck meanders down to distances of ~ 150 km from the lava source. The value chosen in baseline model simulations is equal to 300 m and is representative of a rille section that is located at a downstream distance of ~100 km from the lava source. A similar value of meander amplitude is found at several other rille sections (other than those characterized by goose-neck meanders), which justifies the choice of such a value in baseline simulations.

At the bottom of Table 2.1, the input turbulence parameters are shown for the adopted SST k-ω model. The values of k and ω vary as a function of lava velocity and temperature (through their dependence on flow viscosity) and depending on whether they are calculated at the lava source or at the channel boundaries. When using the SST k- ω model, the choice of appropriate values for the k and ω turbulence parameters is key in ensuring that simulations may converge and provide physically sound results. Because of this, turbulence parameters (except those located at the lava source/channel inlet) were calculated by adopting the expressions shown in *Menter* (1993). The value of the specific

turbulent dissipation rate, ω, away from lava source (inlet) and channel boundaries is given by:

$$\frac{U\infty}{L} < \omega\_{farfield} < 10\,\frac{U\infty}{L} \quad (1)$$

in which U_∞ is freestream lava velocity and L is defined as the appropriate length of the computational domain (taken here to be equal to the hydraulic radius). The following expression is then used to determine ω_{wall}, i.e., the value of ω at channel boundaries:

$$\omega\_{wall} = 10\,\frac{6\upsilon}{\beta 1(\Delta d1)\hat{}2} \quad (2)$$

in which υ is kinematic viscosity at the channel bed and banks, β_1 is a constant equal to 0.075 and Δd_1 is the distance of each finite volume cell from the wall (0.5 m in all runs). The turbulent kinetic energy away from inlet and walls, $k\_{farfield}$, is calculated as follows:

$$10^{-5}\,\frac{U\infty\hat{}2}{Re} < k\_{farfield} < 0.1\,\frac{U\infty\hat{}2}{Re} \quad (3)$$

in which Re is the Reynolds number of the flow. The value of k at the lava source (inlet) is calculated as follows:

$$k\_{inlet} = \frac{3}{2}\,(UI)^2 \quad (4)$$

in which U is inlet lava velocity and I is turbulence intensity. Turbulence intensity is obtained by adopting an expression for fully developed pipe flow (*Ansys*, 2018), as follows:

$$I = 0.16\,Re_{dh}^{(-1/8)} \quad (5)$$

in which Re_{dh} is the Reynolds number based on the pipe hydraulic diameter. The value of the specific turbulent dissipation rate, ω, at the inlet is calculated as follows:

$$\omega\_{inlet} = C_\mu^{3/4}\,\frac{k\hat{}0.5}{l} \quad (6)$$

in which C_μ is the turbulence model constant that usually takes the value 0.09 and l is the turbulent length scale. The l parameter describes the size of large energy-containing eddies in a turbulent flow and is given by:

$$l = 0.07*dh \quad (7)$$

in which dh is the hydraulic diameter of the pipe. As shown in Table 2.1, the value of k at the inlet is always higher than that at the flow core. Also, k is equal to zero at the channel boundaries, a consequence of the fact that lava velocity is equal to zero there. Consistently, the value of ω is lower at the inlet and is higher at the flow core and channel boundaries.

The baseline model (BM) – results

This section is concerned with providing values of maximum and minimum erosion rates across the 1200 m long and 160 m wide channel bed and over the two banks. Fig 2.2a shows a plan view of the channel bed in which the left and right banks are clearly labeled. The lava source is located on the left and the lava flows toward the right end of the channel. The other results concern two channel cross-sections that are cut along two adjacent bend axes (bend 1 and 2) and are located at downstream distances from the source of 400 m and 800 m, respectively. River meanders are a result of erosion occurring at specific locations on channel banks and the observed pattern of erosion tends to repeat itself consistently. The current study investigates how thermal erosion by lava varies between a bend apex and a trough and how erosion at the bed relates to bank erosion. Finally, as in rivers, the intention is to search for erosional patterns, if any.

Across the 1200 m long channel bed shown in Fig. 2.1, thermal erosion is maximum at/near bend troughs and in a channel bed area located in the proximity of the downstream flank of bend 2. Explaining why these maxima and minima occur where they do is beyond the scope of this section but, in Chapter 5, observed variations in erosion rate will be related to observed changes in the key fluid- and thermodynamic parameters within two channel cross-sections cut along two bend axes.

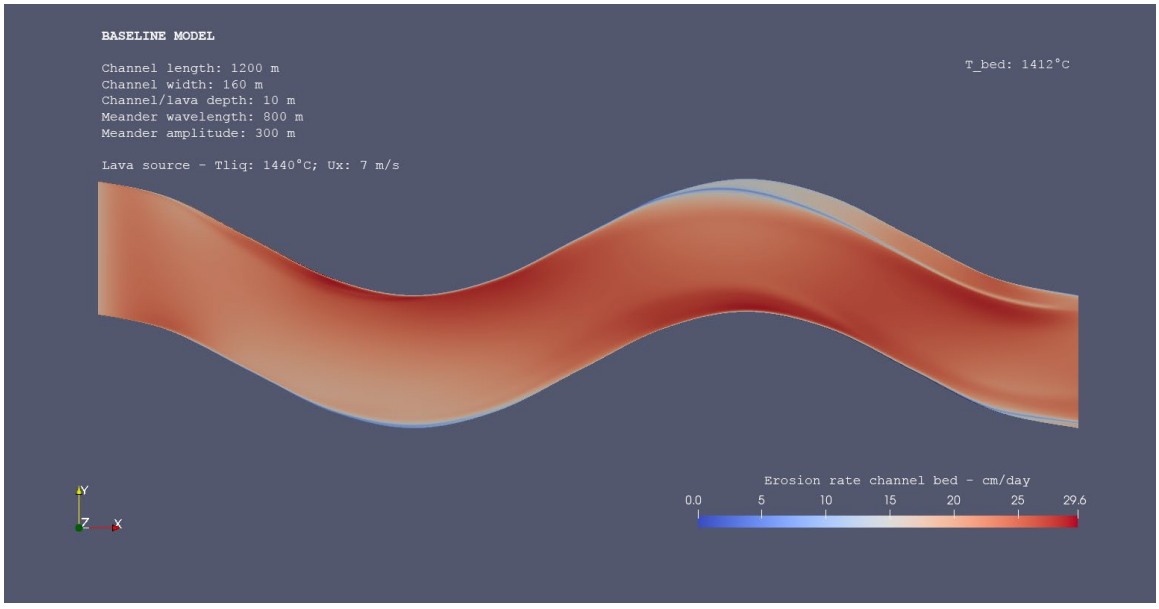

Figure 2.1. Baseline model. Channel length is 1200 m, lava depth is equal to 10 m, meander wavelength is 800 m and meander amplitude is 300 m. Lava flows to the right and is erupted at T=1440° C (liquidus), and initial flow velocity is U_x=7 m s^{-1}. Temperature at channel boundaries (bed and banks) is held constant at T=1412° C. The figure shows maximum and minimum erosion rates at the channel bed. Erosion maxima occur at/near the two bend troughs and in a bed area located in the proximity of the downstream flank of bend 2.

Erosion rates of ~23 cm/day are obtained at/near the channel inlet (lava source). For a straight channel, erosion rates are always highest at the source and the same value or a slightly lower one would be expected at a downstream distance of 1200 m from the source

and anywhere else in the channel. In contrast, erosion rates appear to vary drastically across a 1200 m long and 160 m wide meandering bed, as shown in Table 2.2a.

Table 2.2a. Baseline model – Results in sensitivity analysis. Channel length is 1200 m. Channel/lava depth is equal to 10 m, lava is erupted at T=1440° C (liquidus temperature), and initial flow velocity is U_x=7 m s^{-1}. Temperature at channel boundaries (bed and banks) is held constant at T=1412° C. The table illustrates maximum and minimum erosion rates at the channel bed and banks. The suffixes "Max/Min E.R." stand for maximum and minimum erosion rates.

BASELINE MODEL RESULTS – Channel length = 1200 m. Erosion rates at channel bed and banks			
Obtained Erosion Rates (ER)	Erosion Rate Values	Distance from lava source	Location in the channel
Description	cm/day	m	description
Max ER bed	29.1	299.6	bend 1, 100.4 m upstream of trough, 5 m from right bank.
Min ER bed	1.2	630.6*	bend 2, 169.4 m upstream of bend axis, bed/right bank.
Max ER left bank	28.8	697.7	bend 2, 102.3 m upstream of bend axis, bank top.
Min ER left bank	1.3	1047.9	bend 2, 247.9 m downstream of bend axis, left bank/bed.
Max ER right bank	29.6	293.8	bend 1, 293.8 m downstream of bend axis (inlet), bank top.
Min ER right bank	1.2	630.6*	bend 2, 169.4 m upstream of bend axis, right bank/bed.

Maximum erosion rates of 29.1 cm/day are found in proximity to bend 1 trough (~100 m upstream of it) and next to the right bank (5 m away from it). Still at the bed, minimum erosion rates of 1.2 cm/day are found ~169 m upstream of bend 2 axis and close to the right bank. Table 2.2a also shows maximum and minimum erosion rate at the two channel banks. Because the two channel banks extend from flow top to channel bed, results reveal how close to the top/bed a maximum and minimum of erosion occurs. Maximum erosion rates

are slightly higher over the right bank than over the left bank (29.6 cm/day and 28.8 cm/day, respectively). In line with the results found at the channel bed (Fig. 2.1), the right bank maximum occurs where bend 1 is, at a downstream distance from the lava source that is comparable with the one at which the maximum of bed erosion occurs. The right bank minimum occurs at the same distance from the source at which the bed minimum is found. The left bank maximum is found where bend 2 is – about 102 m upstream of bend axis - whereas the minimum is farther downstream, at a distance from the source of ~249 m. Minimum erosion rates are similar in value to those found at the bed, though the minimum at the right bank (1.2 cm/day) is slightly lower than that at the left bank (1.3 cm/day). Due to the thermal vertical structure of the flow – with a higher temperature and lower viscosity at the top (*Kerr*, 2001) – the maximum of erosion is located at the top of both banks whereas both minima are found at the bank/bed intersection. Interestingly, the right bank minimum of erosion is found at the exact same location the minimum bed erosion occurs.

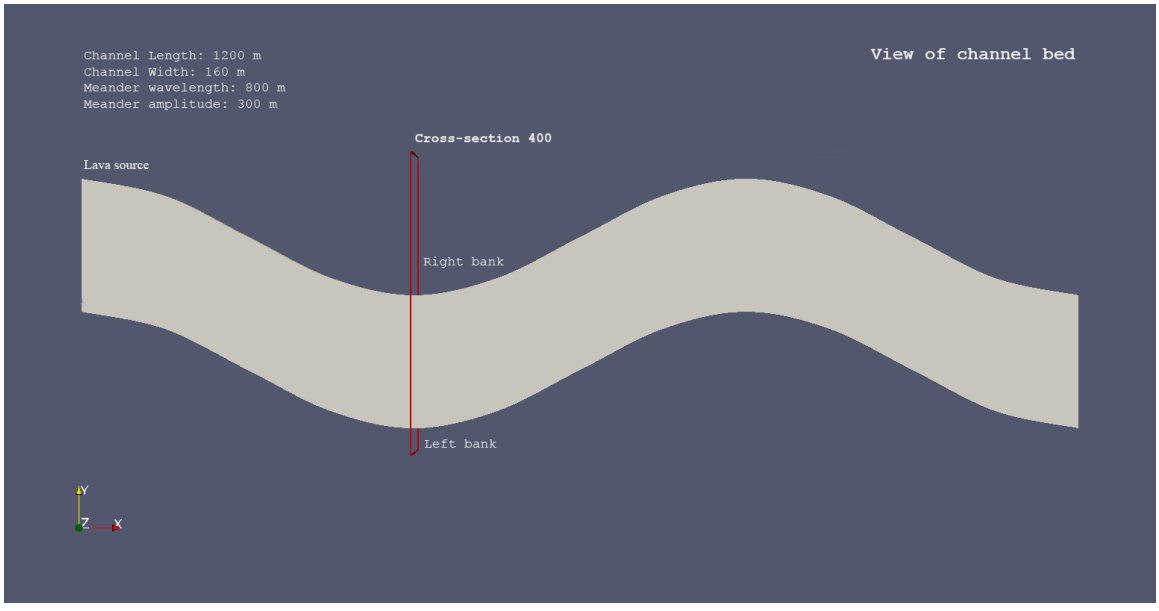

Figure 2.2a. Baseline model. Plan view of channel bed. Bend 1 axis is located at the lava source and Cross-Section CS 400 passes through bend 1 trough at a downstream distance

of 400 m from the lava source (left). The erupted lava flows toward the right end of the channel.

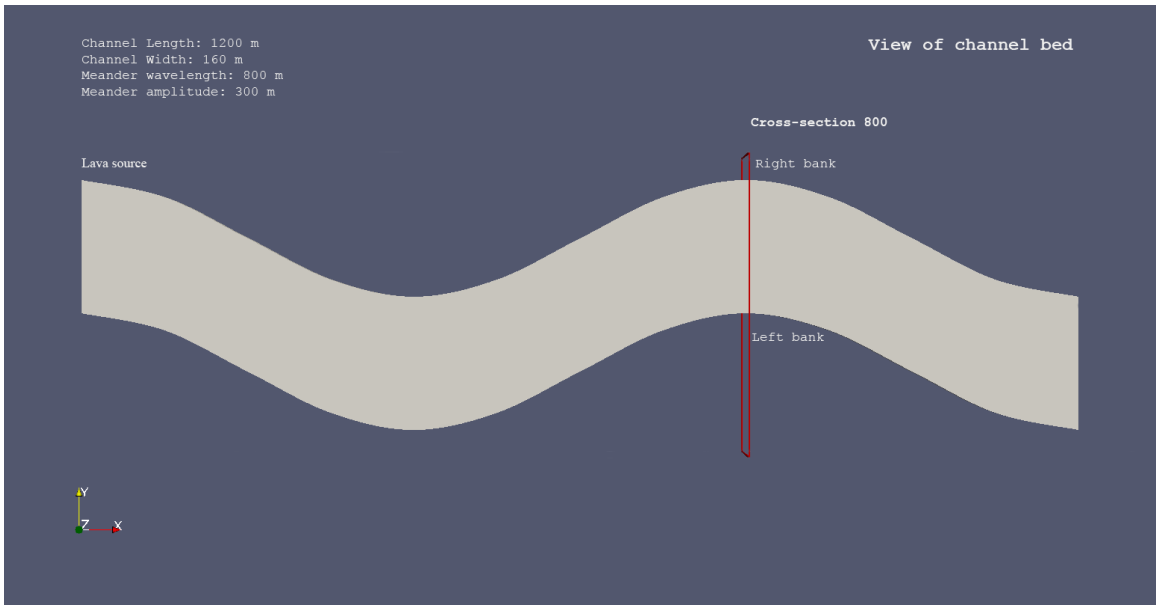

Figure 2.2b. Baseline model. Planar view of channel bed. Bend 2 axis is located at a downstream distance of 800 m from the lava source (left) and Cross-Section CS 800 passes through bend 2 axis. The erupted lava flows toward the right end of the channel.

The final batch of results shows maximum and minimum erosion rates at two channel cross-sections that are cut through bend 1 and bend 2 axes. Figs. 2.2 (a, b) show the two Cross-Sections (CS) of interest, CS 400 that is cut at a downstream distance of 400 m from the lava source and CS 800 that is located 800 m away from it. Maximum and minimum erosion rates and their location in channel cross-section are summarized in Tables 2.2 (b, c) and Figs. 2.4 (a, b). Table 2.2 (b) and Fig. 2.4 refer to CS 400 and shows how erosion rates at the channel bed vary with distance from either of the two banks.

Table 2.2b. Baseline model – Results in sensitivity analysis. The table illustrates maximum and minimum erosion rates at a channel cross-section located 400 m downstream of the lava source and cut along bend 1 trough (see Fig. 2.2a). The suffix "400" stands for cross-section 400 m.

BASELINE MODEL RESULTS – Erosion rates at channel Cross-Section (CS) 400 m			

Obtained Erosion Rates (ER)	Erosion Rate Values	Distance from lava source	Location in channel CS
description	cm/day	m	description
Max E.R. bed$_{400}$	28.8	400.0	~6 m from right bank
Min E.R. bed$_{400}$	5.0	400.0	~1 m from left bank
Max E.R. left bank$_{400}$	10.3	400.0	2-4 m above bed
Min E.R. left bank$_{400}$	4.9	400.0	left bank/bed
Max E.R. right bank$_{400}$	24.4	400.0	bank top
Min E.R. right bank$_{400}$	8.9	400.0	right bank/bed

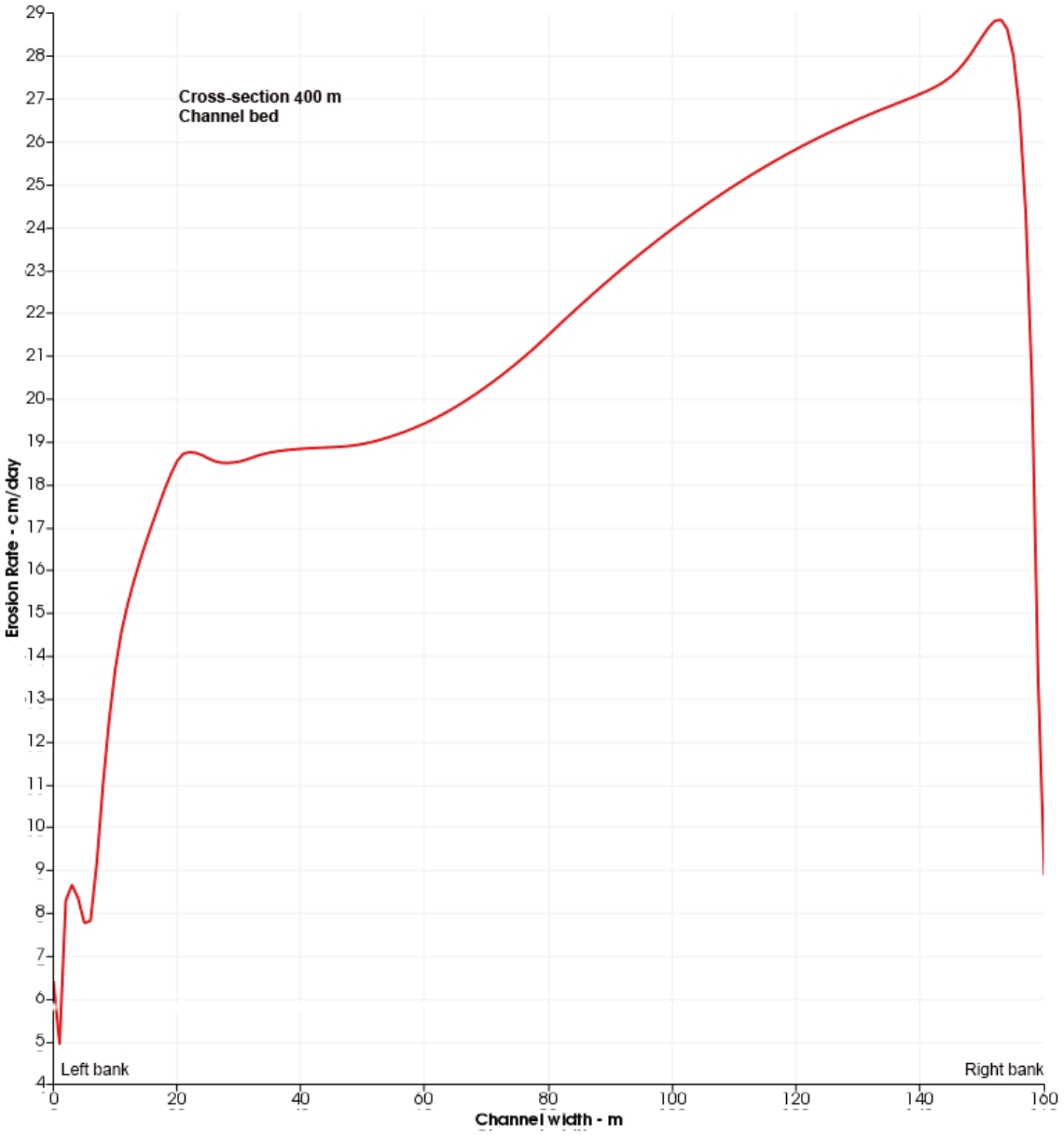

Figure 2.3. Baseline model. Erosion rates at the channel bed for cross-section 400. Erosion rates are highest within ~5 m of the right bank (where the maximum bank erosion occurs as well) and decrease while moving toward the left bank. Within 20 m of the left bank, the decrease in erosion rates is steeper than anywhere else. At the point where the bed intersects the right bank, erosion rates drop to < 9 cm/ day, a consequence of the higher lava viscosity and zero velocity environment that is found at the channel boundaries.

Maximum erosion rates are found in proximity to the right bank, consistent with results shown in Table 2.2b. Erosion rates are highest within ~5 m of the right bank (where a

maximum in bank erosion occurs as well) and decrease while moving toward the left bank. Within 20 m of the left bank, the decrease in erosion rate is steeper than anywhere else. At the right bank/bed interface, erosion rates drop to < 9 cm/day. Noticeably, erosion rates decrease dramatically for points that are located close to the two banks, and more so for points that approach the left bank. Chapter 5 addresses these variations in erosion rate distribution by looking at how downstream and cross-stream lava circulation relate to temperature distribution within the channel and, consequently, erosion rates. Fig. 2.4a and Fig. 2.4b refer to cross-section 400 and illustrate how erosion rates at the two channel banks vary as a function of distance from the flow top (or proximity to the bed). As regards the right bank (Fig. 2.4a), erosion rates are highest at the flow top (24.4 cm/day) and progressively decrease to a minimum value of 8.8 cm/day at the right bank/bed intersection. The decrease becomes faster within ~2 m of the bed. At the left bank, erosion rates progressively increase from a value of 8.3 cm/day at the flow top and reach a value of ~10.3 cm/day at a distance from the bed of 3.8-2.2 m. Within 2 m of the bed, they decrease abruptly until they reach a value of 4.9 cm/day at the left bank/bed interface. The observed sharp decrease in erosion rate is likely a consequence of the decrease in lava temperature, increase in viscosity and reduction in flow velocity that characterizes those portions of the bank that are found in proximity to the bed.

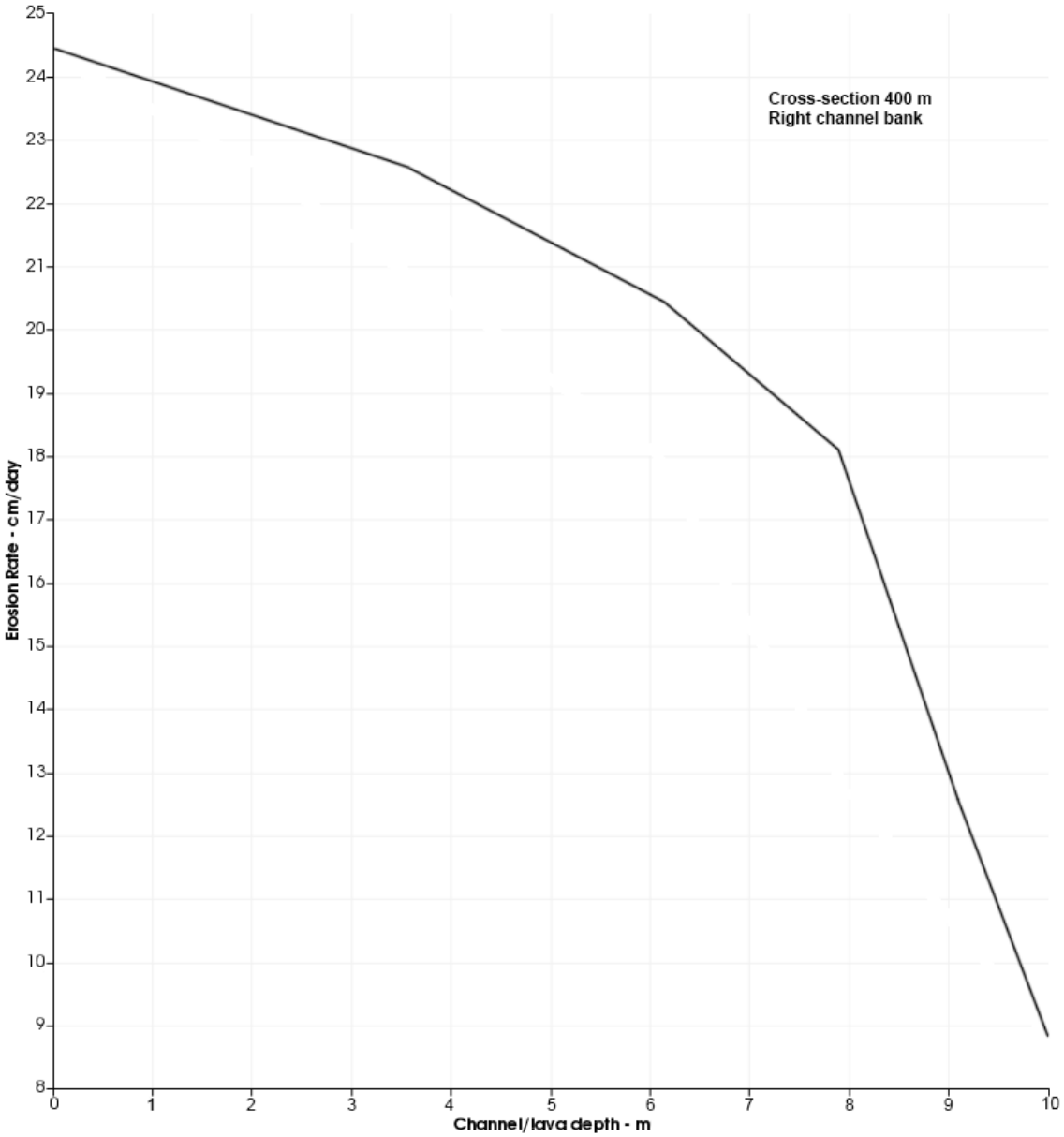

Figure 2.4a. Baseline model. Erosion rates at the right bank for Cross-Section 400. Values on the x-axis display flow depth values that range from 0 to 10 m. Erosion rates are highest at the bank top (24.4 cm/day) and progressively decrease to a minimum value of 8.8 cm/day at the right bank/bed contact. The decrease becomes faster within ~2 m of the same contact.

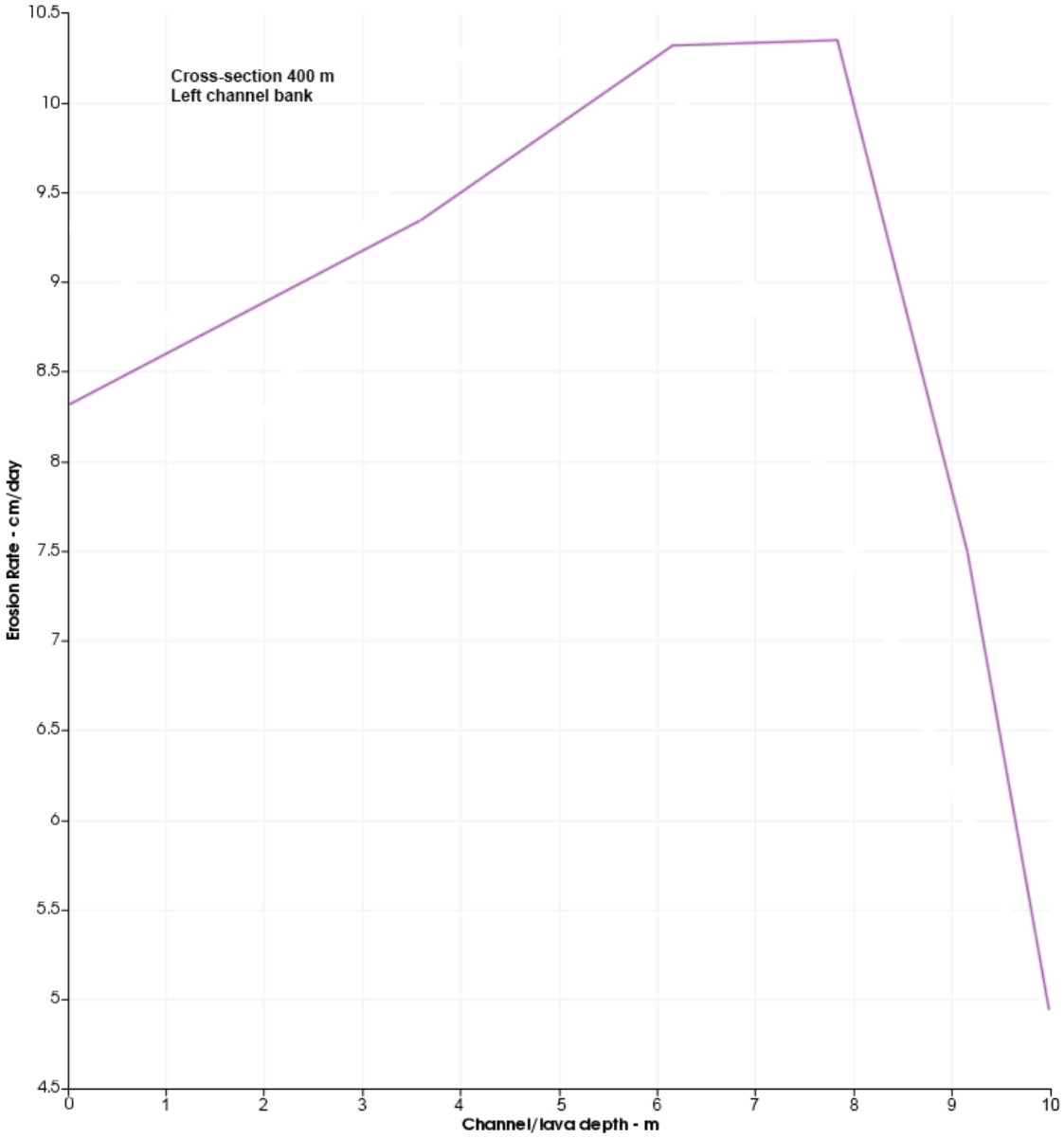

Figure 2.4b. Baseline model. Erosion rates at the left bank for Cross-Section 400. Values on the x-axis display flow depth values that range from 0 to 10 m. Erosion rates progressively increase from a value of 8.3 cm/day at the bank top and reach a value of ~10.3 cm/day at a distance from the bank/bed contact of 3.8-2.2 m. Within 2 m of that contact, they decrease abruptly and reach a value of 4.9 cm/day at the contact itself. Such a sharp decrease is likely a consequence of the decrease in lava temperature, increase in viscosity and reduction in flow velocity that characterizes those portions of the bank that are found in proximity to the bank/bed contact.

Channel cross-section 800 displays an erosional trend that is reversed compared to that observed at cross-section 400, as shown in Table 2.2 (c) and Fig. 2.5.

Table 2.2c. Baseline model results - Results in sensitivity analysis. The table illustrates maximum and minimum erosion rates at a channel cross-section located 800 m downstream of the lava source and cut along bend 2 axis (see Fig. 2.2b). The suffix "800" stands for cross-section 800 m.

BASELINE MODEL RESULTS – Erosion rates at channel Cross-Section (CS) 800 m			
Obtained Erosion Rates (ER)	Erosion Rate Values	Distance from lava source	Location in channel CS
description	cm/day	m	description
Max E.R. bed_{800}	29.0	800.0	~10 m from left bank
Min E.R. bed_{800}	6.1	800.0	~25 m from right bank
Max E.R. $left\ bank_{800}$	26.0	800.0	bank top
Min E.R. $left\ bank_{800}$	9.4	800.0	left bank/bed
Max E.R. $right\ bank_{800}$	15.7	800.0	2-4 m above bed
Min E.R. $right\ bank_{800}$	7.7	800.0	right bank/bed

The maximum erosion rate of 29 cm/day is found at ~10 m from the left bank and thermal erosion decreases as we move toward the right bank, reaching a minimum of 6.1 cm/day at ~25 m from the bank. From that point on, erosion rates increase sharply to 14.6 cm/day out to ~8 m from the bank and finally decrease to a second minimum of 7.8 cm/day at the bed/right bank interface. The observed trend is potentially suggestive of a flow regime that might be at least slightly more chaotic than that found at cross-section 400, for reasons that will become clear in Chapter 5. Fig. 2.6a shows erosion rates at the left bank, which is where the highest rates are found (other than what found at cross-section 400). In line with what observed at the bed, erosion rates are highest at the bank top (26 cm/day) and gently decrease to a value of 24.7 cm/day at a vertical distance of ~4 m from the bank/bed interface. From that point on, they decrease faster and reach a value of 9.3 cm/day at the bank/bed

interface. At the right bank (Fig. 2.6b), erosion rates increase from the bank top (10.4 cm/day) up to a value of 15.7 cm/day at a vertical distance from the bank/bed interface of ~ 4 m. Then, they slightly decrease to a value of 15.4 cm/day at a vertical distance from the interface of ~2 m and finally drop to a value of 7.7 cm/day at the actual interface.

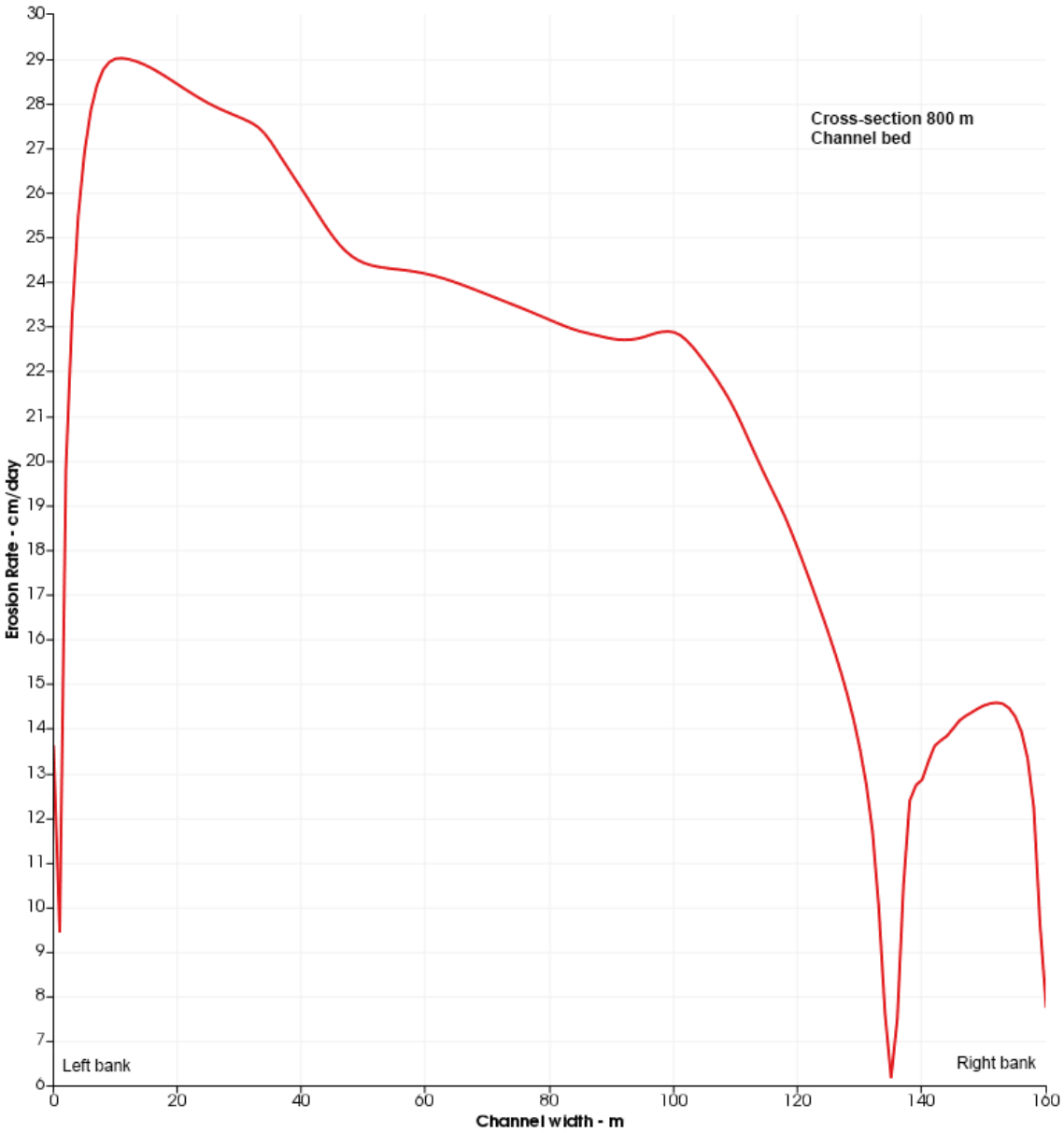

Figure 2.5. Baseline model. Erosion rates at the channel bed for cross-section 800. Erosion rates are highest within ~5 m of the right bank (where the maximum bank erosion occurs as well) and decrease while moving toward the left bank. Within 20

m of the left bank, the decrease in erosion rates is steeper than anywhere else. At the point where the bed intersects the right bank, erosion rates drop to < 9 cm/day, a consequence of the higher lava viscosity and zero velocity environment that is found at the channel boundaries.

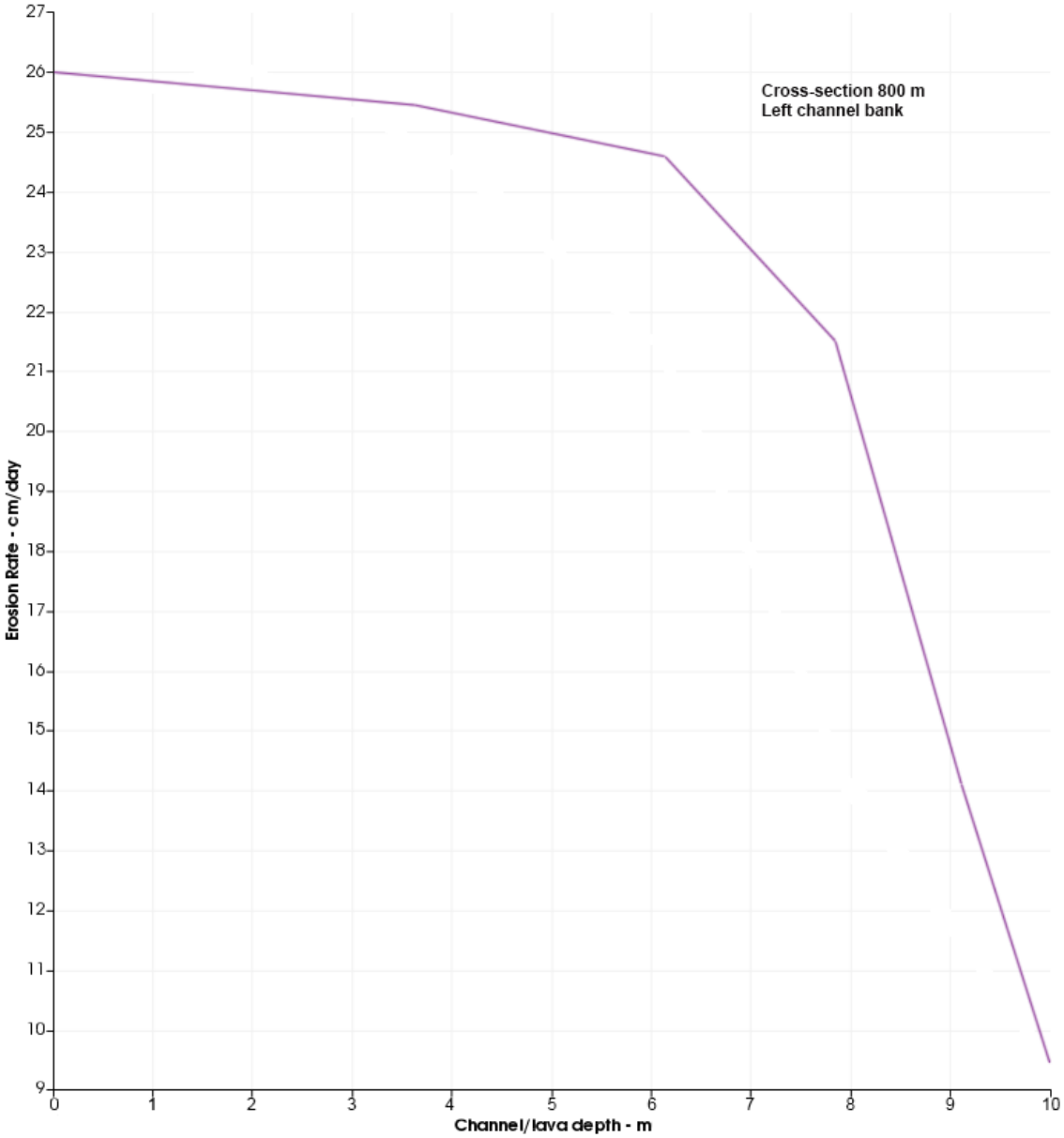

Figure 2.6a. Baseline model. Erosion rates at the left bank for Cross-Section 800. Erosion rates are highest at the bank top (26 cm/day) and gently decrease to 24.7 cm/day at a vertical distance of ~4 m from the bank/bed interface. From that point on, they decrease faster and reach a value of 9.3 cm/day at the bank/bed contact.

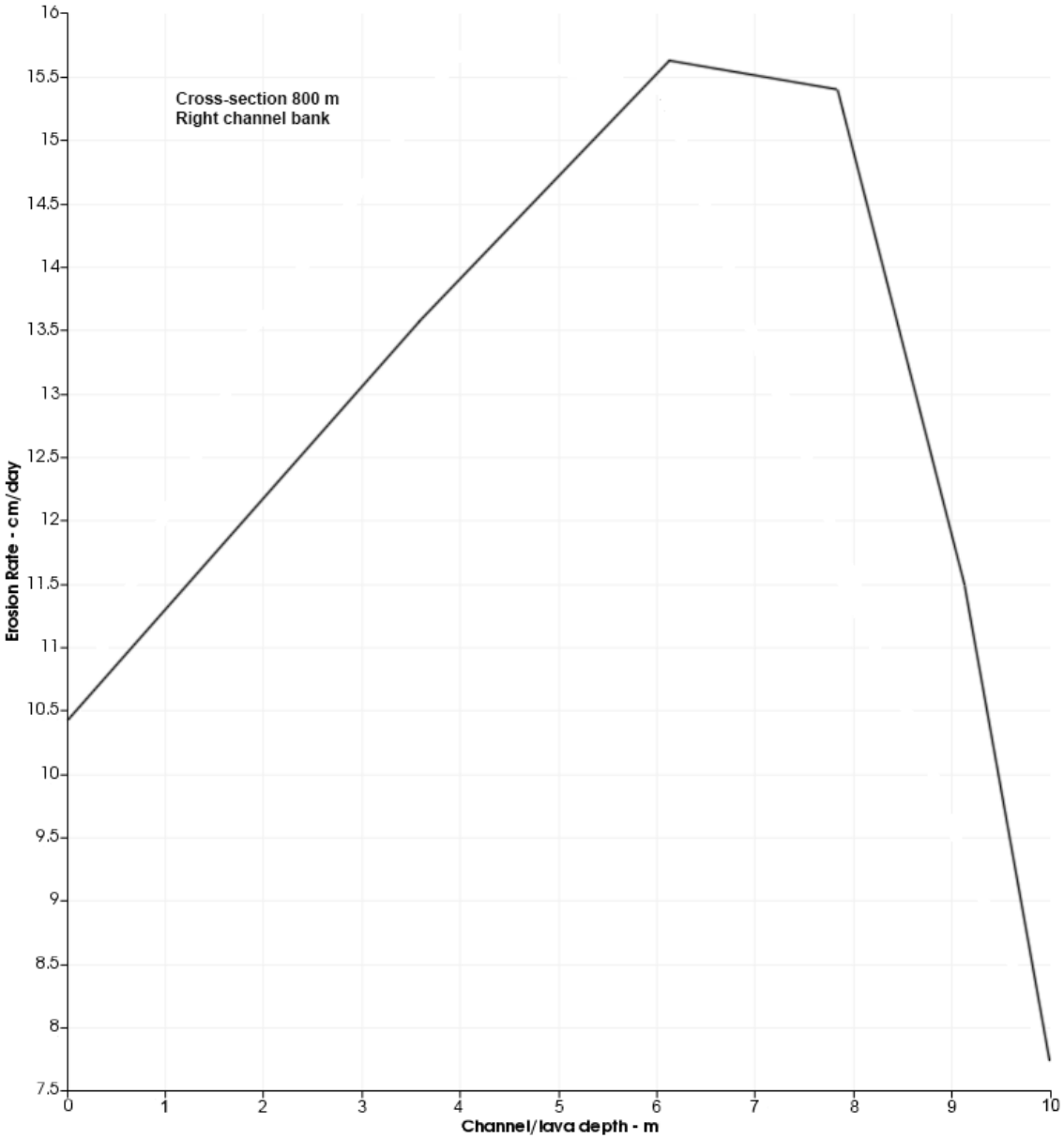

Figure 2.6b. Baseline model. Erosion rates at the right bank for Cross-Section 800. Erosion rates increase from the bank top (10.4 cm/day) up to a value of 15.7 cm/day at a vertical distance from the bank/bed interface of ~ 4 m. They only slightly decrease to a value of 15.4 cm/day at a vertical distance from the bank/bed contact of ~2 m and then sharply decrease to a value of 7.7 cm/day at the contact itself.

Results at bends 1 and 2 reveal the existence of a trend. At both channel cross-sections, maximum erosion rates are found at the bank top and then erosion values progressively

decrease to a minimum at the bank/bed interface. Also, at both bends maximum erosion rates are found at/near the trough. The bank at which erosion rates are comparatively lower than those measured at the bank located on the opposite side of the channel reveals a different distribution of erosion rates. Both the left bank in cross-section 400 and the right bank in cross-section 800 show a peak of erosion that occurs 4-2 m above the bank/bed interface. For reasons that will become clear in Chapter 5, at these two banks the maximum of erosion rates is not found at the bank top.

Sensitivity analysis - Uncertainty in lava/substrate properties

The first part of the sensitivity analysis aims to assess the variation of baseline model (BM) results derived from the adoption of values of lava and substrate physical parameters that are different from those chosen for the BM. There is uncertainty about the physical properties of the lava and the mechanical (compaction) and thermophysical properties of the lava substrate at the inner rille of Vallis Schröteri. Because of this, the sensitivity of BM results to changes in lava and substrate properties is presented first and separate from that resulting from variations in observable/measurable parameters.

Sensitivity of BM results to changes in lava temperature

This section illustrates how a change in lava eruption temperature may affect the magnitude and spatial distribution of thermal erosion rates across a 1200-m-long and 160-m wide channel. Two eruption temperature scenarios alternative to that chosen in the baseline model are here presented. The lava that formed the Vallis Schröteri inner rille

could have been erupted at a temperature of 1630° C (190° C higher than liquidus). The choice of this extremely high temperature value is supported by arguments put forward by *Wiekzorek et* al. (2000). Based on geophysical studies and thermal modeling, these authors suggested that mare basalts could have been superheated to ~1630° C at 3.5 Ga in their source region, which enabled the denser lunar basalts to ascend to the lunar surface using buoyancy alone. In the other temperature scenario, lava is erupted at a sub-liquidus temperature of 1400° C, a temperature at which the resulting lava dynamic viscosity is equal to 1.98 Pa s and the kinematic viscosity is 6.8×10^{-4} m^2 s^{-1}. At that temperature, the expected fraction of small olivine crystals thought to have been suspended in the lava (see Eq. 1, Chapter 3) is equal to 14 vol.%. Such conditions might still be supportive of a Newtonian flow regime, a condition that is necessary for the presented 3-D model of thermal erosion to provide reliable results. In both temperature scenarios, a temperature gap of 28° C is assumed between the flow top/core and the channel bed and banks, which is based on the theoretical argument presented in Chapter 4 (p. 169).

Fig. 2.7 shows the channel bed in plan view and displays the spatial variation of erosion rates for a scenario in which lava is erupted at the temperature of 1630° C (superheated lava). Erosion rates increase up to a value of 54.2 cm/day. Though the spatial distribution of erosion rates might look identical to that shown in Fig. 2.1 (baseline model) a more careful observation reveals important differences between the two scenarios (see Tables 2.3a, b and Fig. 2.8).

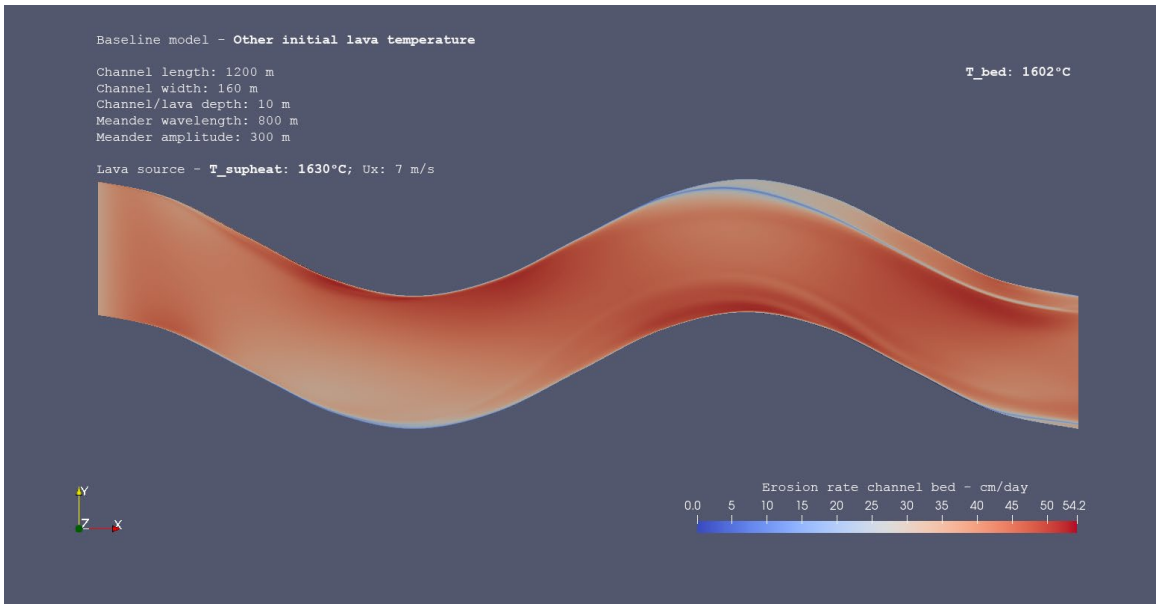

Figure 2.7. Sensitivity of baseline model results to changes in lava eruption temperature. The case for a lava flow erupted at a superheated temperature of 1630° C. Channel length is 1200 m, lava depth is equal to 10 m, meander wavelength is 800 m and meander amplitude is 300 m. Lava flows to the right and initial flow velocity is U_x=7 m s^{-1}. Temperature at channel boundaries (bed and banks) is held constant at T=1602° C. The figure shows maximum and minimum erosion rates at the channel bed. Though the spatial distribution of erosion rates might look identical to that shown in Fig. 2.1 (baseline model) a more careful observation reveals important differences between the two scenarios.

Table 2.3a illustrates how erosion rates vary at the channel bed and banks for a scenario of superheated lava. Maxima and minima of erosion migrated 20-90 m farther downstream of the lava source compared to their BM locations, except for the location of the right bank maximum, which is unchanged. As already seen in the BM run, the points of minimum erosion at the bed and right bank coincide. The observed trend of migration and the fact that the maximum of bank erosion (54.2 cm/day) is located on the left bank instead of the right one (as seen in the BM) suggest that the different eruption temperature might be responsible for affecting lava circulation and lead to a different distribution of erosion rates at both the channel bed and the two banks.

Table 2.3a. Sensitivity of baseline model (BM) results to changes in lava eruption temperature. The table illustrates maximum and minimum erosion rates at the channel bed and banks. Results refer to lavas erupted at a temperature of 1630° C (superheated). Temperature at channel boundaries (bed and banks) is held constant at T=1602° C.

SENSITIVITY OF BM RESULTS TO CHANGES IN ERUPTION TEMPERATURE - Superheated lava. Erosion rates at channel bed and banks			
Obtained Erosion Rates (ER)	Erosion Rate Values	Distance from lava source	Location in the channel
description	cm/day	m	description
Max ER bed	52.0	305.8	bend 1, 305.8 m downstream of bend axis (inlet), within 5 m of right bank.
Min ER bed	1.8	655.5*	bend 2, 144.5 m upstream of bend axis, bed/right bank.
Max ER left bank	54.2	781.2	bend 2, 18.8 m upstream of bend axis, bank top.
Min ER left bank	1.9	1065.1	bend 2, 265.1 m downstream of bend axis, left bank/bed.
Max ER right bank	53.2	293.8	bend 1, 293.8 m downstream of bend axis, 3.5 m down from bank top.
Min ER right bank	1.7	655.5*	bend 2, 144.5 m upstream of bend axis, right bank/bed.

Table 2.3b and Fig. 2.8 show how values of erosion rate at the bed vary across channel cross-section 400, i.e., the section cut through bend 1 trough.

Table 2.3b. Sensitivity of baseline model (BM) results to changes in lava eruption temperature. The table illustrates maximum and minimum erosion rates for superheated lava, at a channel cross-section located 400 m downstream of the lava source and cut along bend 1 trough (see Fig. 2.2a).

SENSITIVITY OF BM RESULTS TO CHANGES IN ERUPTION TEMPERATURE - Superheated lava. Erosion rates at channel Cross-Section (CS) 400 m			
Obtained Erosion Rates (ER)	Erosion Rate Values	Distance from lava source	Location in channel CS
description	cm/day	m	description

Max E.R. bed$_{400}$	51.0	400.0	~6 m from right bank
Min E.R. bed$_{400}$	8.4	400.0	~1 m from left bank
Max E.R. left bank$_{400}$	23.4	400.0	bank top
Min E.R. left bank$_{400}$	8.8	400.0	left bank/bed
Max E.R. right bank$_{400}$	45.9	400.0	bank top
Min E.R. right bank$_{400}$	15.7	400.0	right bank/bed

Maximum erosion rates of 51 cm/day are found at the bed within ~6 m of the right bank contact (where the maximum bank erosion occurs as well) and decrease toward the left bank. Within 20 m of the left bank, the decrease in erosion rates is faster than elsewhere until erosion rates reach a minimum value of 8.4 cm/day at the bed/bank contact. Figs. 2.9 (a, b) show how erosion rates vary at the two channel banks. At the right bank, minimum values of erosion rate are higher (15.7 cm/day) than those at the left bank/bed contact. Importantly, the occurrence of a maximum of bank erosion at the right bank is in stark contrast with the maximum of bank erosion found at the left bank over the entire 1200-m-long channel (Table 2.3a). This apparent discrepancy will be resolved in the section of Chapter 5 dedicated to secondary flow circulation. Another important difference between the temperature-modified simulation and the baseline model is that the maximum of bank erosion at the left bank is located at the bank top and not at a vertical distance of 2-4 m from the bank/bed contact. Also, differences in erosion magnitude between left and right bank are more pronounced in this temperature-modified run than in the baseline model. Values of 45.9 cm/day are obtained at the right bank whereas the maximum erosion rate at the opposite bank does not get any higher than 23.4 cm/day. All these results suggest that a higher lava temperature not only has the potential to affect the magnitude of thermal erosion but also its horizontal and vertical distribution across the channel. Minimum

erosion rates always occur at the bank/bed contact because those channel portions are characterized by lower lava temperatures (and associated higher viscosities) and lava velocities reaching a value of 0 m s^{-1} at channel boundaries.

If we allow the eruption temperature to decrease to the sub-liquidus value of 1400°C, magnitude and distribution of erosion rates change as shown in Table 2.3c. Maximum values at the bed and right bank are no higher than 11.1 cm/day and minimum values are as low as 0.4 cm/day (see also Fig. 2.10). Importantly, the maximum of erosion is found at the bank top at the right bank and ~4 m above the bank/bed contact at the left bank (see Figs. 2.11 a, b). Adopting a lower eruption temperature and its associated higher flow viscosity causes all points (but one) of maximum and minimum erosion to migrate upstream by 4-19 m compared to those listed in Table 2.2a (baseline model). The much lower shift in position compared to the 20-90 m shift found for a scenario of superheated lava might, at least, partially result from the fact that the 40° C temperature difference between the liquidus and sub-liquidus scenarios is much smaller than the 190° C temperature difference between the BM and the superheated scenario. Contrary to this trend, the maximum erosion rate at the bed is found downstream of its baseline model counterpart, ~794 m from the lava source and within 2-4 m of the left bank. Once again, a discrepancy exists between the above location and the location of the maximum bed erosion at channel cross-section 400, the latter being within ~6 m of the right bank (see also Fig. 2.10).

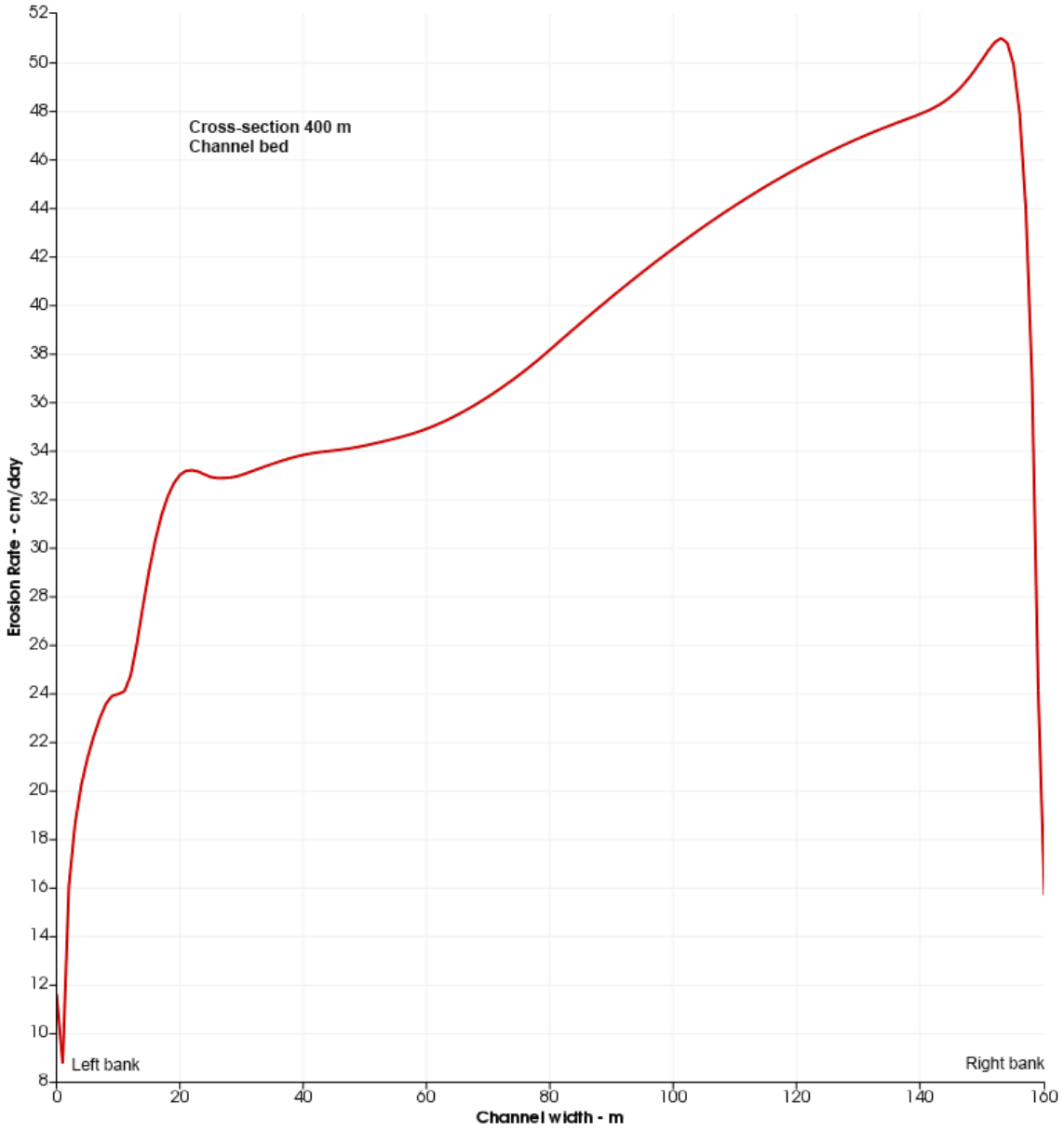

Figure 2.8. Erosion rates at the channel bed for cross-section 400. The case for lava erupted at a superheated temperature of 1630° C. Erosion rates are highest within ~6 m of the right bank (where the maximum bank erosion occurs as well) and decrease toward the left bank. Within 20 m of the left bank, the decrease in erosion rates is faster than elsewhere. At the bed/right bank contact, erosion rates reach a minimum value of 8.4 cm/day, a likely consequence of the higher lava viscosity and zero velocity environment found at channel boundaries.

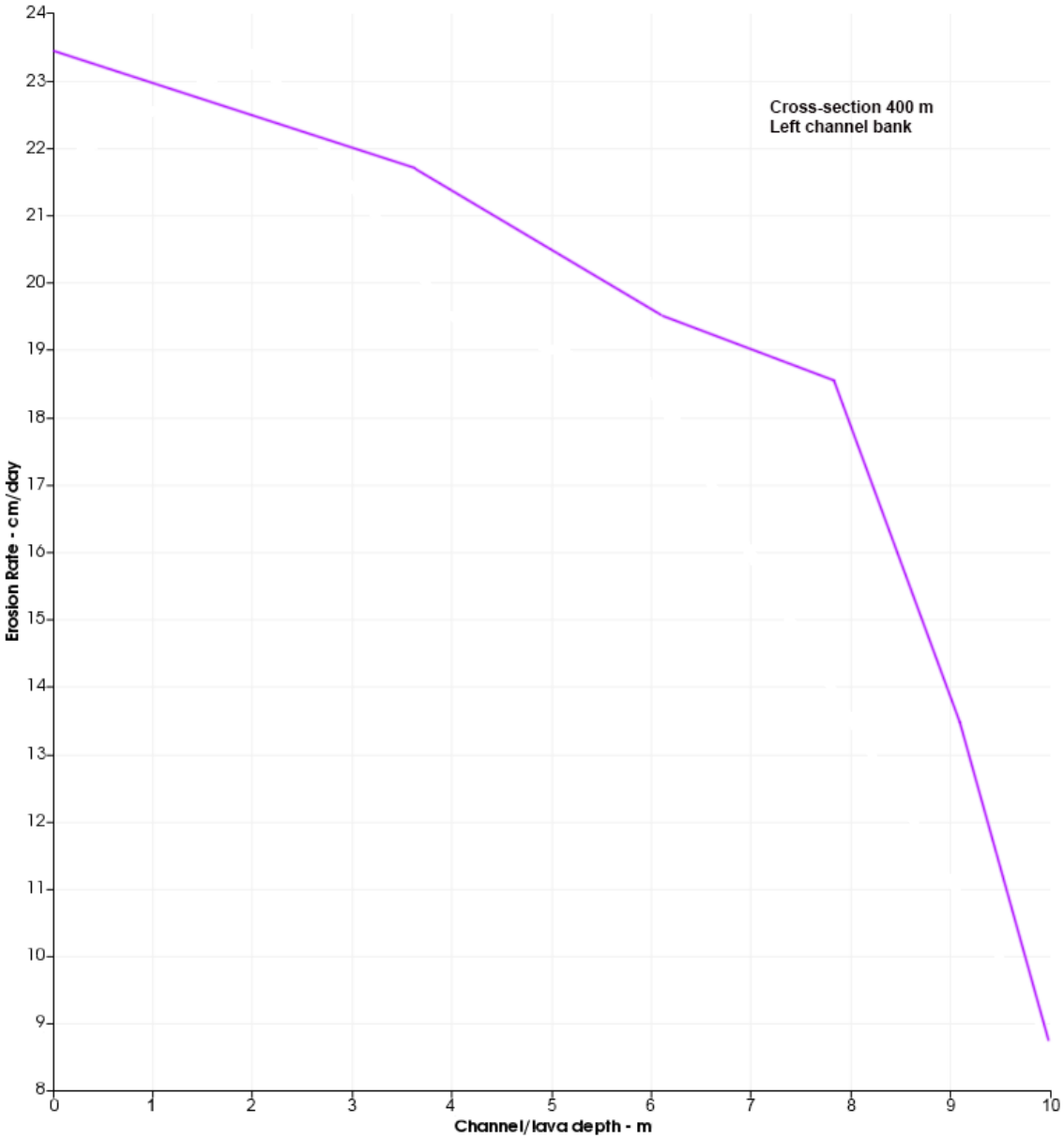

Figure 2.9a. Erosion rates at the left bank for cross-section 400. The case for lava erupted at a superheated temperature of 1630° C. Maximum erosion rates of 23.4 cm/day are found at the bank top. Erosion rates progressively decrease till they reach a minimum value of 8.8 cm/day at the bank/bed contact. The decrease is faster once the vertical distance to the contact is ≤ 2 m.

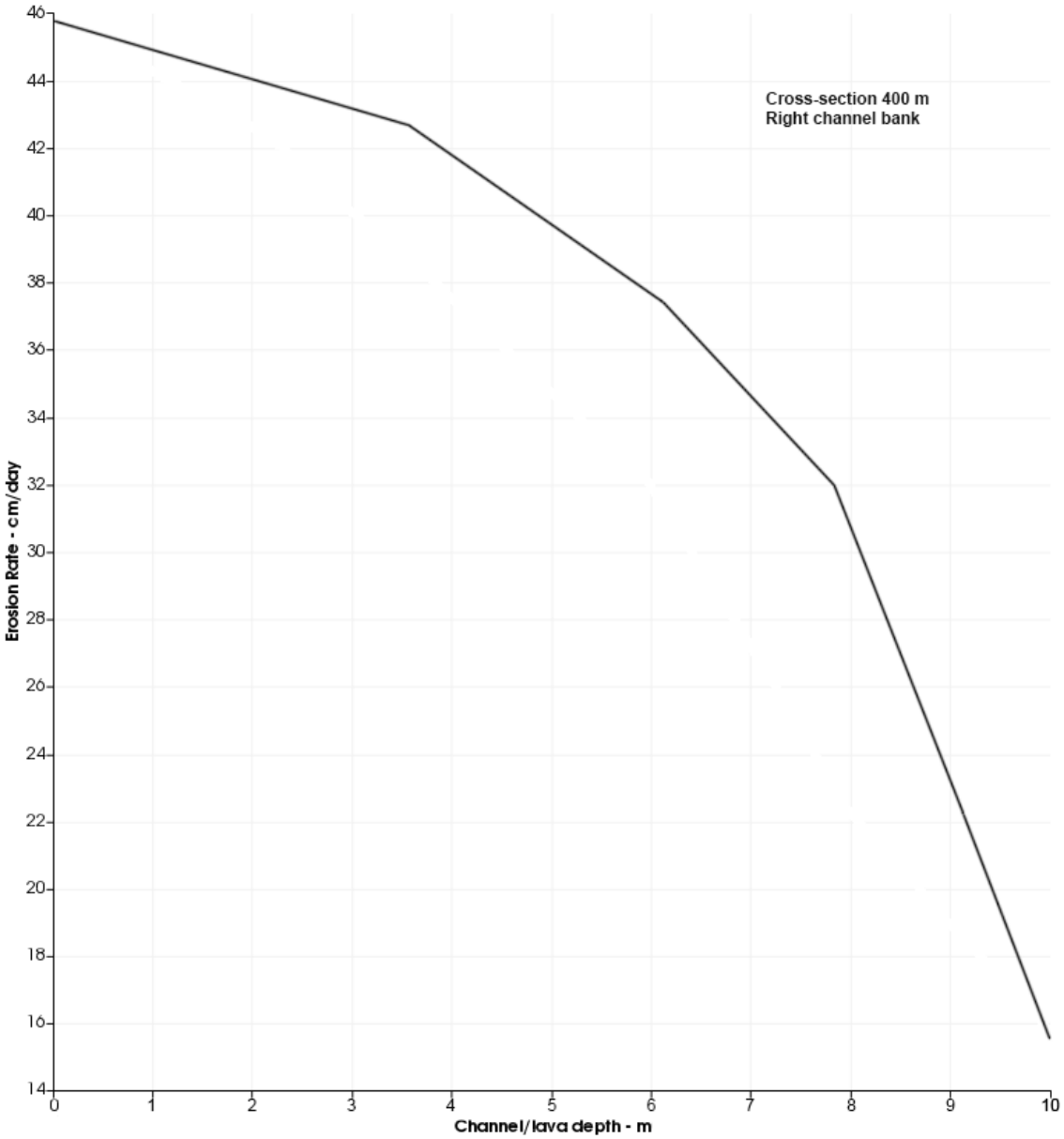

Figure 2.9b. Erosion rates at the right bank for cross-section 400. The case for lava erupted at a superheated temperature of 1630° C. Maximum erosion rates of 45.9 cm/day are found at the bank top. Erosion rates decrease faster and faster as the vertical distance to the underlying bank/bed contact is reduced till a minimum value of 15.7 cm/day is reached at the contact itself.

Table 2.3c. Sensitivity of baseline model (BM) results to changes in lava eruption temperature. The table illustrates maximum and minimum erosion rates at the channel bed and banks. Results refer to lavas erupted at a sub-liquidus temperature of 1400° C. Temperature at channel boundaries (bed and banks) is held constant at T=1372° C.

SENSITIVITY OF BM RESULTS TO CHANGES IN ERUPTION TEMPERATURE – Sub-liquidus lava. Erosion rates at channel bed and banks			
Obtained Erosion Rates (ER)	Erosion Rate Values	Distance from lava source	Location in the channel
description	cm/day	m	description
Max ER bed	11.1	793.7	bend 2, 6.3 m upstream of bend axis, 2-4 meters from left bank.
Min ER bed	0.4	619.1*	bend 2, 180.9 m upstream of bend axis, bed/right bank.
Max ER left bank	10.1	693.8	bend 2, 106.2 m upstream of bend axis, bank top.
Min ER left bank	0.4	1028.7	bend 2, 228.7 m downstream of bend axis, left bank/bed.
Max ER right bank	11.1	291.9	bend 1, 291.9 m downstream of bend axis (inlet), bank top.
Min ER right bank	0.4	619.1*	bend 2, 180.9 m upstream of bend axis, right bank/bed.

When looking at channel cross-section 400 (Table 2.3d), the distribution of erosion rates at the bed and banks is analogous to that shown in BM. Though erosion rates are reduced in magnitude compared to those in the baseline model (maximum values at the bed are no higher than 10.7 cm/day), the maximum of erosion at the left bank occurs once again at a vertical distance from the bank/bed contact of 2-4 m (see also Fig. 2.11a).

Table 2.3d. Sensitivity of baseline model (BM) results to changes in lava eruption temperature. The table illustrates maximum and minimum erosion rates for lava erupted at T=1400° C (sub-liquidus), at a channel cross-section located 400 m downstream of the lava source and cut along bend 1 trough (see Figs. 2.11 a, b).

SENSITIVITY OF BM RESULTS TO CHANGES IN ERUPTION TEMPERATURE – Sub-liquidus lava. Erosion rates at channel Cross-Section (CS) 400 m			

Obtained Erosion Rates (ER)	Erosion Rate Values	Distance from lava source	Location in channel CS
description	cm/day	m	description
Max E.R. bed$_{400}$	10.7	400.0	~8 m from right bank
Min E.R. bed$_{400}$	1.5	400.0	~1 m from left bank
Max E.R. left bank$_{400}$	3.8	400.0	2-4 m above bed
Min E.R. left bank$_{400}$	1.5	400.0	left bank/bed
Max E.R. right bank$_{400}$	8.4	400.0	bank top
Min E.R. right bank$_{400}$	3.3	400.0	right bank/bed

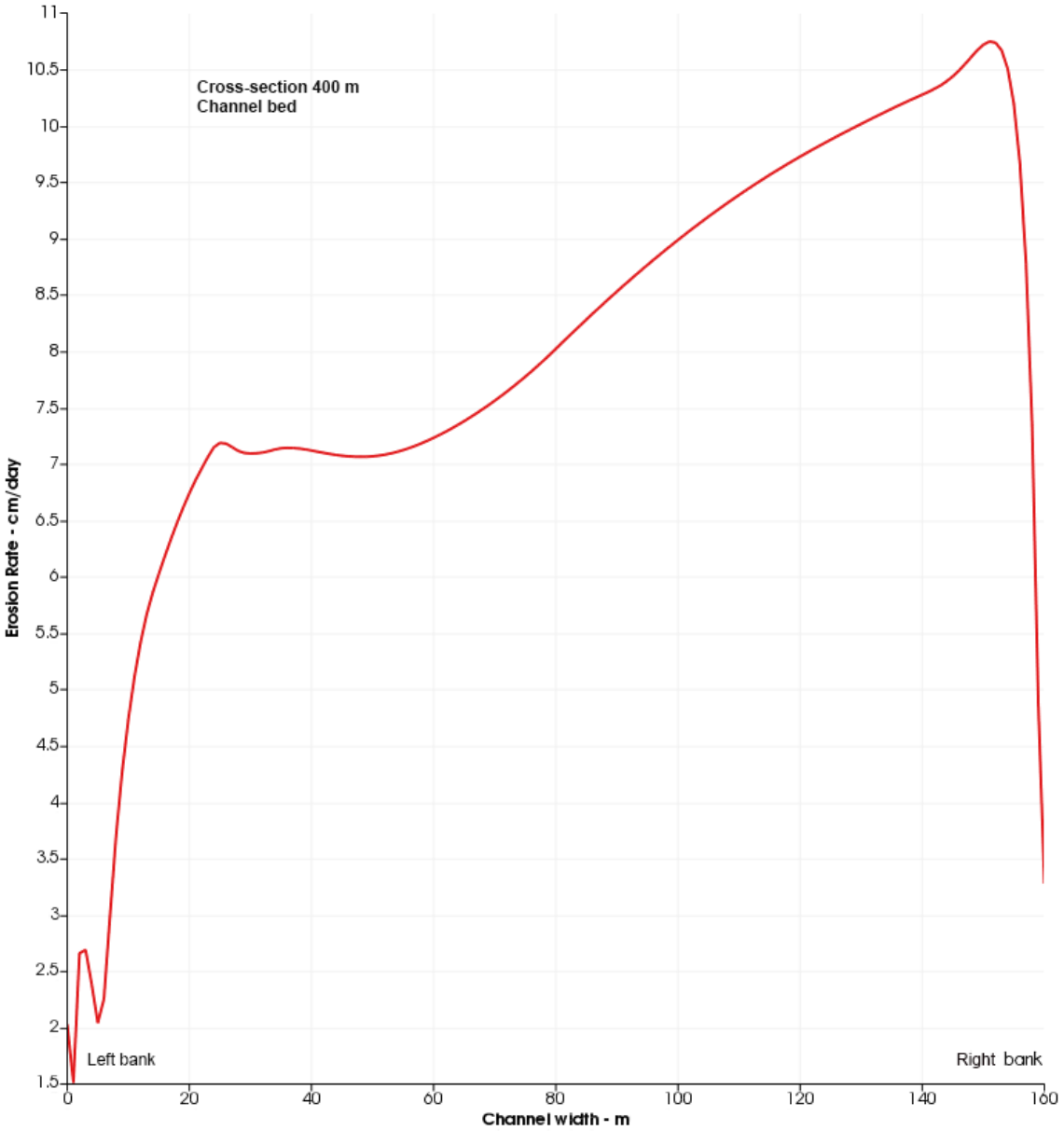

Figure 2.10. Erosion rates at the channel bed for cross-section 400. The case for lava erupted at a sub-liquidus temperature of 1400° C. Erosion rates are highest (10.7 cm/day) within ~8 m of the right bank and lowest (1.5 cm/day) within ~1 m of the left bank. The decrease in erosion rate as the left bank is approached is very similar to that shown in previously described scenarios.

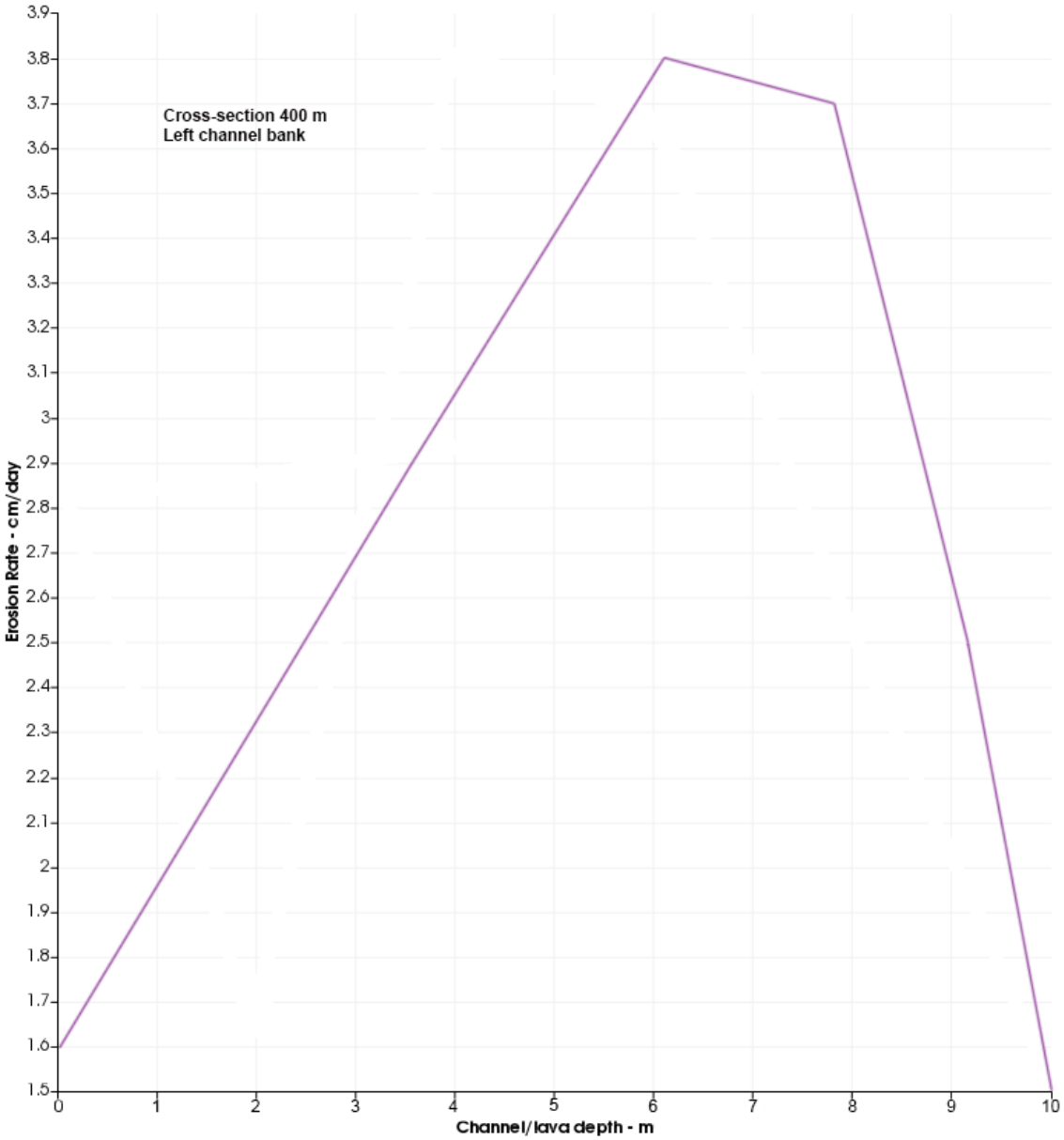

Figure 2.11a. Erosion rates at the left bank for cross-section 400. The case for lava erupted at a sub-liquidus temperature of 1400° C. Maximum erosion rates of 3.8 cm/day are found at a vertical distance from the bank top of ~6 m, i.e., ~4 m above the bank/bed contact. At the bank top, erosion rates reach a maximum value of 1.6 cm/day, whereas the minimum value (1.5 cm/day) is found at the bank/bed contact in line with expectations.

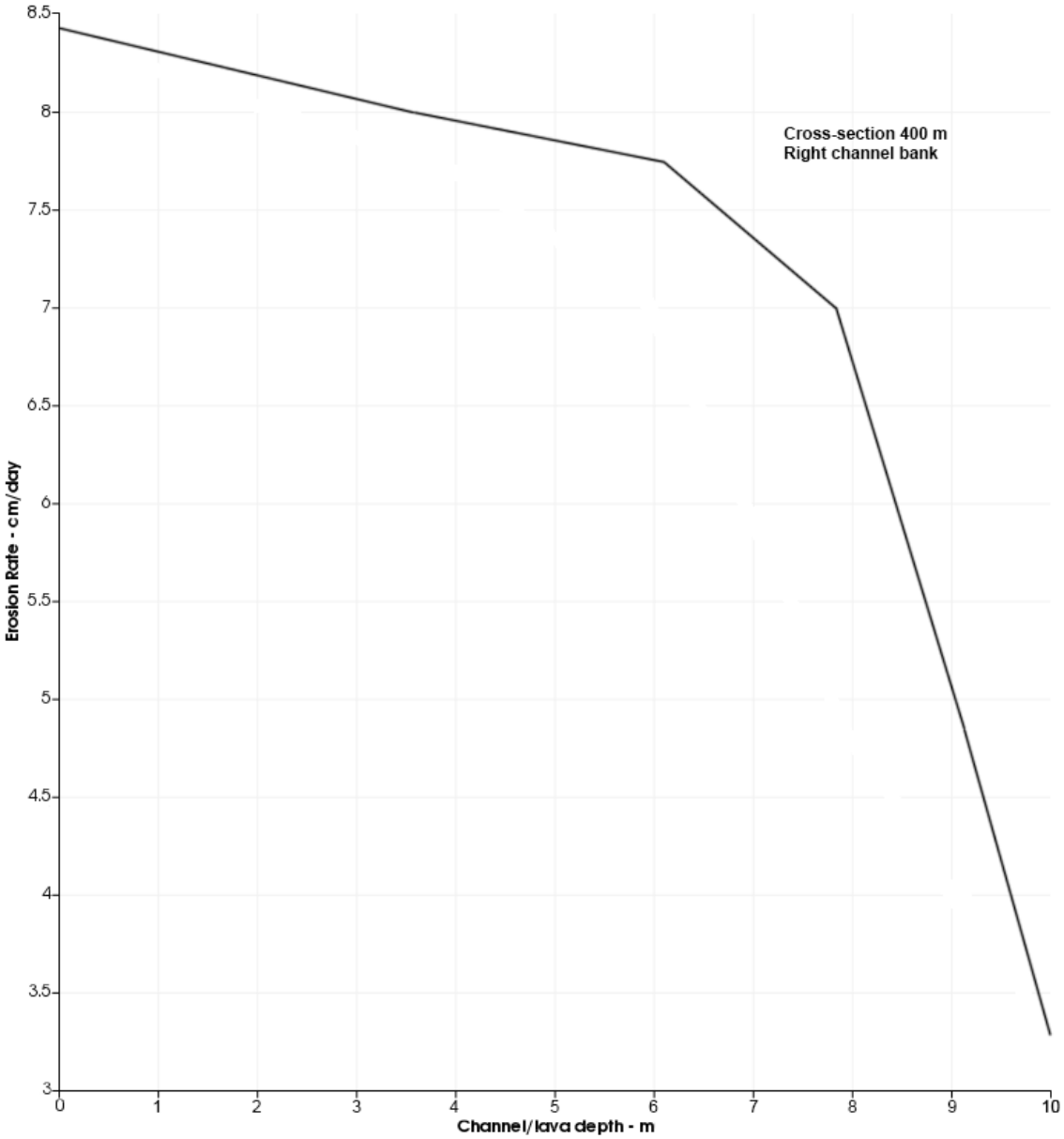

Figure 2.11b. Erosion rates at the right bank for cross-section 400. The case for lava erupted at a sub-liquidus temperature of 1400° C. Maximum erosion rates of 8.4 cm/day are found at the bank top and a minimum of 3.3 cm/ day is obtained at the bank/bed contact. Erosion rates decrease from bank top to bottom and the decrease becomes faster starting at a vertical distance of ~4 m from the underlying bank/bed contact. In line with what seen before, within ~2 m of the contact, erosion rates drop drastically from 7 to 3.3 cm/day.

How temperature-modified results compare with BM results

Table 2.3e shows how temperature-modified model results compare with baseline model results. Ratios higher than 1 indicate that erosion rate values are higher than those obtained from the baseline results. The opposite applies if ratio values are lower than 1.

Table 2.3e. Sensitivity of baseline model results to changes in lava eruption temperature, T_e - temperature ratios.

Obtained Erosion Rates	$Ratio_{all\_channel}$ (Super_heated/BM)	$Ratio_{400}$ (Super_heated/BM)	$Ratio_{all\_channel}$ (Sub_liquidus/BM)	$Ratio_{400}$ (Sub_liquidus/BM)
	#	#	#	#
Max E.R. bed	1.79	1.77	0.38	0.37
Min E.R. bed	1.50	1.70	0.33	0.30
Max E.R. left bank	1.88	2.27	0.35	0.37
Min E.R. left bank	1.46	1.80	0.31	0.31
Max E.R. right bank	1.80	1.88	0.37	0.34
Min E.R. right bank	1.42	1.76	0.33	0.37

Ratios calculated at channel cross-section 400 are higher than those obtained from measurements conducted across the entire 1200-m-long channel. Contrary to this, maximum erosion rates at the bed (across the entire 1200-m-long channel) are lower at channel cross-section 400. For a lava that is erupted at a superheated temperature of 1630°C, the highest ratios (1.88-2.27) are associated with values of maximum erosion at the left bank, especially those obtained at channel cross-section 400. Because the highest maximum erosion rate values (both in the BM and temperature-modified runs) occur at the right bank, there might be some process that enhances erosion rates at the left bank. Other ratios that range from 1.80 to 1.88 are those associated with maximum erosion rates at the right bank. All ratios obtained from minimum erosion rate values fall below the calculated ratio average (~1.64), except those that occur at channel cross-section 400. Once again, an

in-depth analysis of lava circulation might be needed to uncover the cause of the observed increase in erosion rates at meander bends.

For a lava that is erupted at a sub-liquidus temperature of 1400°C, all the ratios are lower than 1 because erosion rate values are lower than those obtained in the BM. Similar trends to those observed in the higher temperature scenario are found here though less pronounced. Ratios referred to channel cross-section 400 are higher than those referring to the 1200-long channel by only a factor of 1.12 (at best) and the trend is sometimes reversed (the minimum erosion rates ratio at the bed and the maximum erosion rates ratio at the right bank are lower at channel cross-section 400 than over the 1200-m-long channel). It might be worth exploring if a lower lava temperature (and associated higher viscosity) could lead to the observed trend inversion.

Sensitivity of BM results to changes in lava velocity

This section deals with the sensitivity of BM results to changes in lava velocity at the source. The goal is to test how adding and subtracting 3 m s^{-1} to/from the baseline value, thus obtaining velocities of 4 and 10 m s^{-1}, affects magnitude and spatial distribution of erosion rates across the channel and at channel cross-section 400. A velocity of 10 m s^{-1} is probably a bit too high when considering a steady-state eruption of lava that flows within a 10-m-deep channel in the low-gravity lunar environment and over a substrate with a gentle slope of ~0.2° (see Eq. 8 in *Jarvis*, 1995), which is why the 10 m s^{-1} velocity value is only used here for sensitivity analysis purposes. The angle at which the lava flows outward from the inlet was held the same for both velocity scenarios, for the purpose of

minimizing any changes in erosion rates tied to variations in initial flow geometry. Table 2.4a shows the magnitude and spatial distribution of erosion rates across the 1200-m-long channel section of study for lava that travels at a velocity of 4 m s^{-1}. Expectedly, they are lower than those obtained by running the baseline model and their spatial distribution is changed. The maximum erosion rate at the bed occurs ~500 m downstream of the point at which it was found in the baseline model. The remaining two maxima appear to have shifted a short distance from their BM location or have not moved at all, the left bank maximum being 2 m upstream of its BM location and the right bank sitting still at a downstream distance of 294 m from the lava source. In sharp contrast to this, the minimum erosion rate at the bed is located ~410 m downstream of the point it is found in the BM whereas the left and right bank minima are shifted upstream of their BM location by 2 and 6 m, respectively. Interestingly, the bed and left bank minima occupy the same place in the channel, whereas in the baseline model the minimum of bed erosion is where the minimum of right bank erosion is, i.e., on the opposite side of the channel.

Table 2.4a. Sensitivity of baseline model (BM) results to changes in lava velocity at the source. The table illustrates maximum and minimum erosion rates at the channel bed and banks. Results refer to lavas erupted at a velocity U_x=4 m s^{-1}. All other flow BM parameters are unchanged.

SENSITIVITY OF BM RESULTS TO CHANGES IN LAVA VELOCITY AT THE SOURCE – U_x = 4 m s^{-1}. Erosion rates at channel bed and banks			
Obtained Erosion Rates (ER)	Erosion Rate Values	Distance from lava source	Location in the channel
description	cm/day	m	description
Max ER bed	17.0	797.9	bend 2, 2.1 m upstream of bend axis, within 5 m of left bank.
Min ER bed	0.7	1042.1*	bend 2, 242.1 m downstream of bend axis, bed/left bank.

Max ER left bank	16.4	695.7	bend 2, 104.3 m upstream of bend axis, bank top.
Min ER left bank	0.7	1042.1*	bend 2, 242.1 m downstream of bend axis, left bank/bed.
Max ER right bank	17.8	293.8	bend 1, 293.8 m downstream of bend axis (inlet), bank top.
Min ER right bank	0.7	624.9	bend 2, 175.1 m upstream of bend axis, right bank/bed.

The spatial distribution of erosion rates in channel cross-section 400 is almost identical to that in the BM, except for a minor shift (~1 m) of the maximum of bed erosion away from the right bank (see Table 2.4b).

Table 2.4b. Sensitivity of baseline model (BM) results to changes in lava velocity at the source. The table illustrates maximum and minimum erosion rates at a channel cross-section located 400 m downstream of the lava source and cut along bend 1 trough (see Fig. 2.2a). Results refer to lavas erupted at a velocity U_x=4 m s^{-1}. All other flow BM parameters are unchanged.

SENSITIVITY OF BM RESULTS TO CHANGES IN LAVA VELOCITY AT THE SOURCE – U_x = 4 m s^{-1}. Erosion rates at channel Cross-Section (CS) 400 m			
Obtained Erosion Rates (ER)	Erosion Rate Values	Distance from lava source	Location in channel CS
description	cm/day	m	description
Max E.R. $bed_{\_400}$	17.3	400.0	~7 m from right bank
Min E.R. $bed_{\_400}$	2.9	400.0	~1 m from left bank
Max E.R. $left\ bank_{\_400}$	6.2	400.0	2-4 m above bed
Min E.R. $left\ bank_{\_400}$	2.9	400.0	left bank/bed
Max E.R. $right\ bank_{\_400}$	14.2	400.0	bank top
Min E.R. $right\ bank_{\_400}$	5.3	400.0	right bank/bed

The maximum bank erosion of 14.2 cm/day is at the right bank and the left bank maximum of 6.2 cm/day is found at a vertical distance of 2-4 m from the bank/bed contact (see Figs. 2.12 a, b). At the top of the left bank, erosion rates reach a maximum value <

4.1 cm/day, whereas the minimum erosion rate value of 2.9 cm/day is found at the bank/bed contact in line with expectations. At the right bank, the maximum is located at the bank top and the minimum of 5.3 cm/day is found at the bank/bed contact. Erosion rates decrease from bank top to bottom and the decrease becomes faster starting at a vertical distance from the bank/bed contact of ~4 m. Within ~2 m of the contact, erosion rates drop drastically from ~11 to 5.3 cm/day.

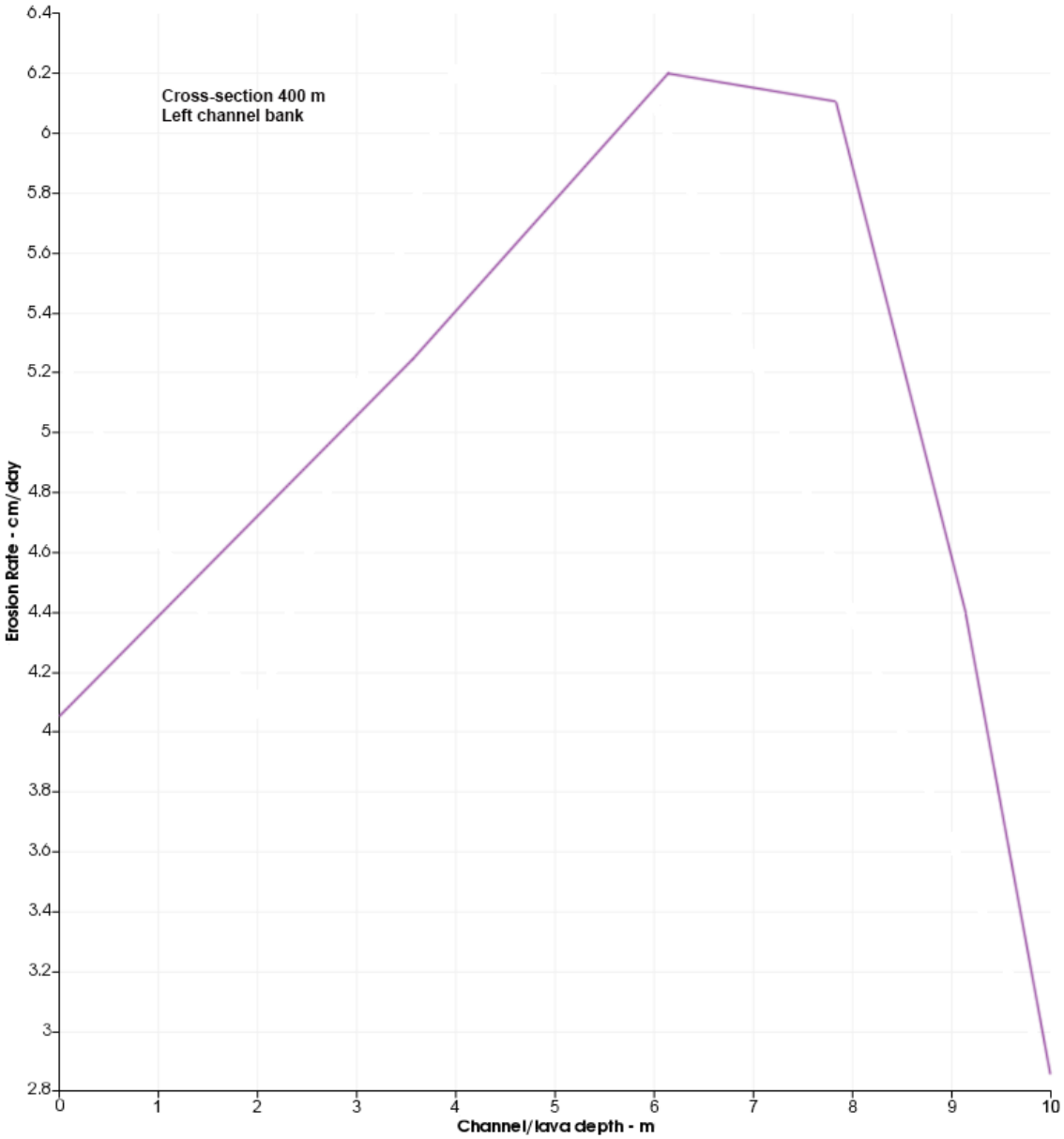

Figure 2.12a. Erosion rates at the left bank for cross-section 400. The case for a lava velocity of 4 m s^{-1} at the source. Maximum erosion rates of 6.2 cm/day are found at a vertical distance from the bank top of ~6 m, i.e., ~4 m above the bank/bed contact. At the bank top, erosion rates reach a maximum value < 4.1 cm/day, whereas the minimum erosion rate value (2.9 cm/day) is found at the bank/bed contact in line with expectations.

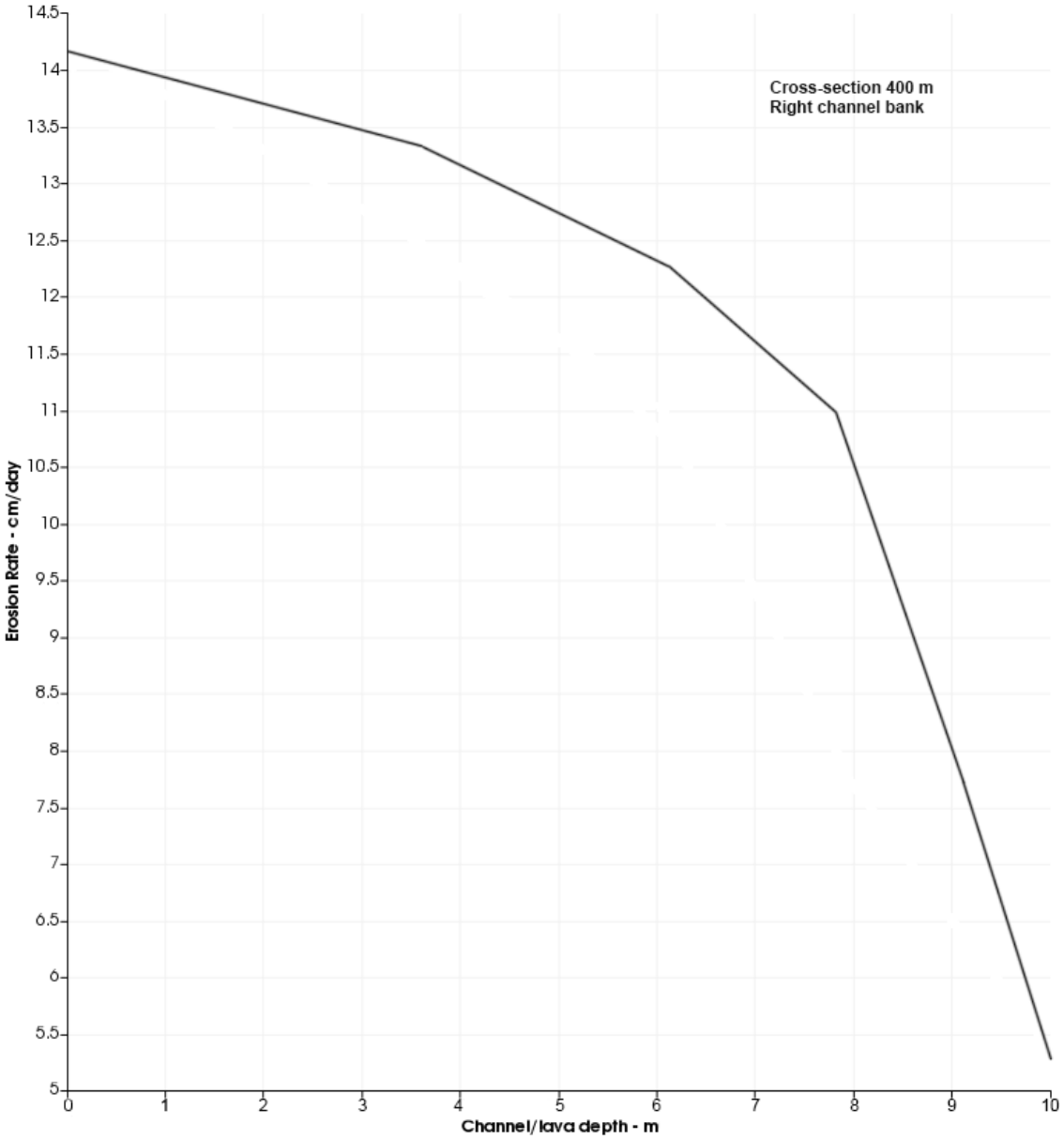

Figure 2.12b. Erosion rates at the right bank for cross-section 400. The case for a lava velocity of 4 m s^{-1} at the source. The maximum erosion rate of 14.2 cm/ day is located at the bank top and the minimum of 5.3 cm/day is found at the bank/bed contact. Erosion rates decrease from bank top to bottom and the decrease becomes faster starting at a vertical distance from the bank/bed contact of ~4 m. Within ~2 m of the contact, erosion rates drop from ~11 to 5.3 cm/day.

Table 2.4c illustrates values of erosion rates for lava that flows at a velocity of 10 m s^{-1} at the source. Once again, the location of the erosion maxima and minima has changed.

Three maxima of erosion (at the bed, right and left banks) are found at the same location as in the BM, whereas all minima are shifted downstream of the place they are in the baseline model (minima of bank erosion by only a few meters, the minimum of bed erosion by ~420 m). Consistent with previous observations, the maximum of bed erosion is still occurring a few meters (~5 m) from the bed/right bank contact and bank maxima are found at the bank top. All minima are found at the bed/bank contact. In line with what seen in the slower velocity scenario, the bed and left bank minima still occupy the same place in the channel, though they are found ~10 m downstream of their previous location. The new batches of results that refer to velocity- and temperature-modified versions of the baseline model prove that variations of both temperature and velocity affect the spatial distribution of erosion rates in the lava channel. Table 2.4d shows the spatial distribution of erosion rates at channel cross-section 400. Though erosion values are higher than in previous simulations (due to the faster lava velocity), their distribution appears almost identical to that seen in the BM, except for a minor shift (~2 m) of the maximum bed erosion away from the bed/right bank contact.

Table 2.4c. Sensitivity of baseline model (BM) results to changes in lava eruption velocity. The table illustrates maximum and minimum erosion rates at the channel bed and banks. Results refer to lavas erupted at a velocity U_x=10 m s^{-1}. All other flow BM parameters are unchanged.

SENSITIVITY OF BM RESULTS TO CHANGES IN LAVA VELOCITY AT THE SOURCE – U_x = 10 m s^{-1}. Erosion rates at channel bed and banks			
Obtained Erosion Rates (ER)	Erosion Rate Values	Distance from lava source	Location in the channel
description	cm/day	m	description
Max ER bed	40.2	299.6	bend 1, 299.6 m downstream of bend axis (inlet), within 5 m of right bank.

Min ER bed	1.5	1051.7*	bend 2, 251.7 m downstream of bend axis, bed/left bank.
Max ER left bank	41.2	697.6	bend 2, 102.4 m upstream of bend axis, bank top.
Min ER left bank	1.6	1051.7*	bend 2, 251.7 m downstream of bend axis, left bank/bed.
Max ER right bank	41.1	293.8	bend 1, 293.8 m downstream of bend axis (inlet), bank top.
Min ER right bank	1.6	634.4	bend 2, 165.5 m upstream of bend axis, right bank/bed.

Table 2.4d. Sensitivity of baseline model (BM) results to changes in lava eruption velocity. The table illustrates maximum and minimum erosion rates at a channel cross-section located 400 m downstream of the lava source and cut along bend 1 trough (see Fig. 2.2a). Results refer to lavas erupted at a velocity U_x=10 m s^{-1}. All other flow BM parameters are unchanged.

SENSITIVITY OF BM RESULTS TO CHANGES IN LAVA VELOCITY AT THE SOURCE – U_x = 10 m s^{-1}. Erosion rates at channel Cross-Section (CS) 400 m			
Obtained Erosion Rates (ER)	Erosion Rate Values	Distance from lava source	Location in channel CS
description	cm/day	m	description
Max E.R. $bed_{\_400}$	39.9	400.0	~7 m from right bank
Min E.R. $bed_{\_400}$	6.8	400.0	~1 m from left bank
Max E.R. left $bank_{\_400}$	14.2	400.0	2-4 m above bed
Min E.R. left $bank_{\_400}$	6.8	400.0	left bank/bed
Max E.R. right $bank_{\_400}$	34.3	400.0	bank top
Min E.R. right $bank_{\_400}$	12.2	400.0	right bank/bed

At the left bank, maximum erosion rates of 14.2 cm/day are found at a vertical distance from the bank top of ~8 m, i.e., ~2 m above the bank/bed contact. At the bank top, erosion rates are equal to 13.8 cm/day. Erosion values then increase downward till the maximum of 14.2 cm/day is reached (~2 m above the bank/bed contact). From there, erosion rates drop drastically to a value of 6.8 cm/day at the contact. At the right bank, the maximum erosion rate of 34.3 cm/day is located at the bank top and the minimum of 12.2 cm/day is

found at the bank/bed contact. Erosion rates progressively decrease from bank top to bottom, but their decrease is much faster at a distance from the contact of ~2 m.

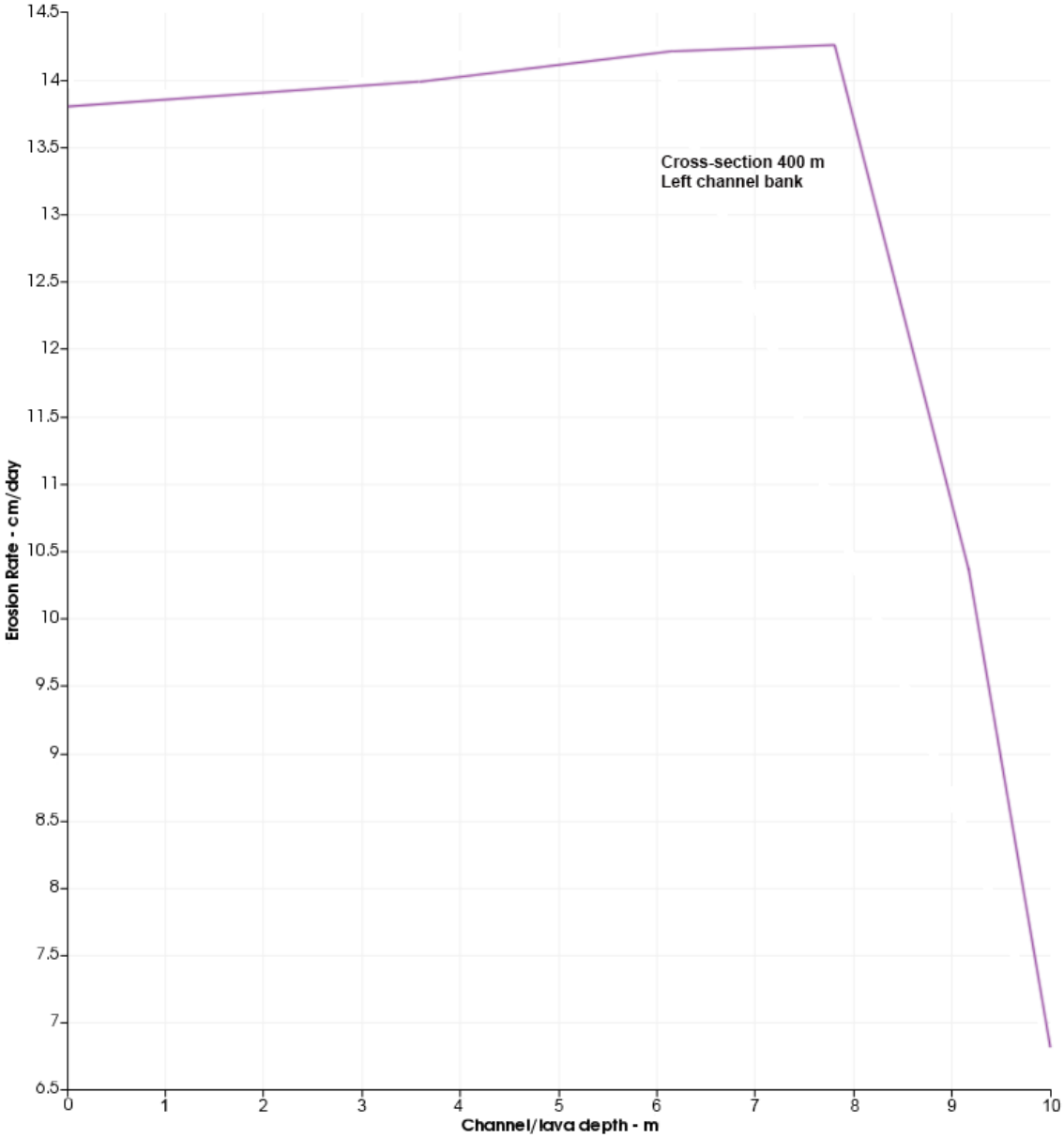

Figure 2.13a. Erosion rates at the left bank for cross-section 400. The case for a lava velocity of 10 m s^{-1} at the source. Maximum erosion rates of 14.2 cm/day are found at a vertical distance from the bank top of ~8 m, i.e., ~2 m above the bank/bed contact. At the bank top, erosion rates are equal to 13.8 cm/day. Then, they increase to 14.2 cm/day, ~ 2 m above the contact. From that point on,

erosion rates drop drastically to a value of 6.8 cm/day at the bank/bed contact.

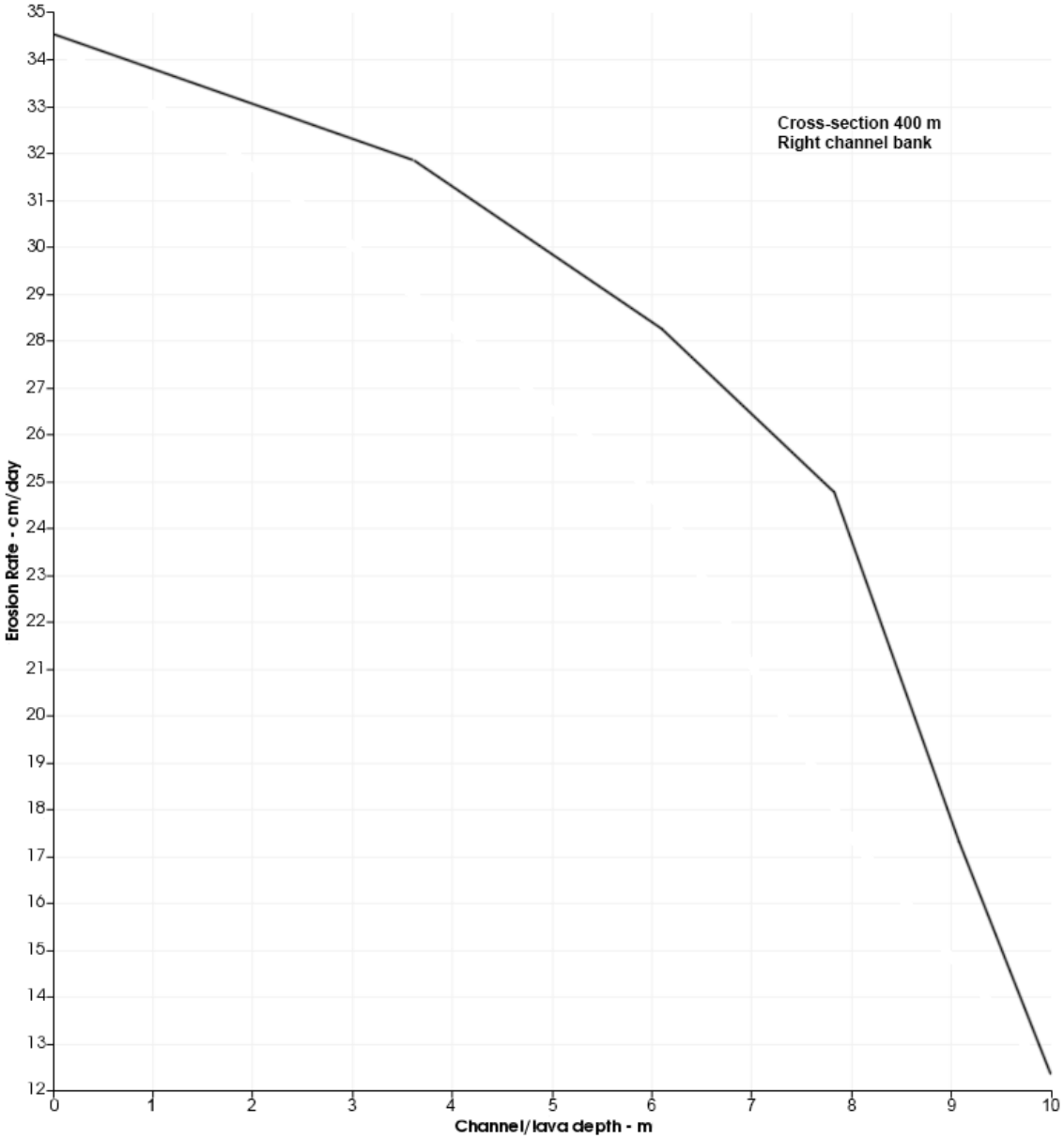

Figure 2.13b. Erosion rates at the right bank for cross-section 400. The case for a lava velocity of 10 m s^{-1} at the source. The maximum erosion rate of 34.3 cm/day is located at the bank top and the minimum of 12.2 cm/day is found at the bank/ bed contact, in line with expectations. Erosion rates decrease from bank top to bottom faster and faster as the contact with the bed is approached, but their decrease is much faster starting at a vertical distance from the contact of ~2 m.

How velocity-modified results compare with BM results

Table 2.4e illustrates how lava velocities at the source that are slower and faster than 7 m s^{-1} (BM value) affect the magnitude of erosion rates across the 1200-m-long channel and channel cross-section 400. As regards the 4 m s^{-1} velocity scenario, all ratios are < 1 because a slower lava velocity is conducive to lower erosion rates (holding other flow parameters equal) and in the range 0.54-0.60. The opposite applies to the faster velocity scenario of 10 m s^{-1}, for which ratios are in the range between 1.23 and 1.43.

As seen before, a difference in value exists between ratios obtained at the 1200-m-long channel and those at channel cross-section 400. For a lava velocity of 4 m s^{-1}, ratios obtained at the left bank of channel cross-section 400 are higher than those calculated across the whole channel by a factor of 1.05-1.09. At the right bank, while the ratio of erosion minima is higher by a factor of 1.03 than its counterpart calculated at the whole channel, the erosion maximum shows an inverse trend (0.58 versus 0.60 for the whole channel). Interestingly, the maximum and minimum ratios at the bed are identical in values. Perhaps, a slower lava velocity affects erosion rate values at the bends more than anywhere else in the channel. For a lava velocity of 10 m s^{-1}, both the maximum and minimum ratios at the right bank are higher at cross-section 400 than elsewhere in the channel, whereas only the minimum ratio is higher at the left bank. The left bank maximum ratio shows an inverse trend analogous to that shown by the right bank maximum ratio for a velocity of 4 m s^{-1}. As for the slower velocity scenario, maximum bed erosion ratios are identical across the 1200-m-long channel and at cross-section 400, whereas minimum ratios are higher at cross-section 400. The observed variations may sound confusing for a start, yet they prove

how efficient velocity and temperature variations can be in altering the distribution of erosion rates at meander bends and, to varying extents, over the entire meandering channel.

Table 2.4e. Sensitivity of baseline model results to changes in initial lava velocity, U_x – velocity ratios.

Obtained Erosion Rates	$Ratio_{\_all\_channel}$ (Ux=4 m/s/BM)	$Ratio_{\_400}$ (Ux = 4 m/s/BM)	$Ratio_{\_all\_channel}$ (Ux = 10 m/s /BM)	$Ratio_{\_400}$ (Ux = 10 m/s /BM)
	#	#	#	#
Max E.R. bed	0.60	0.60	1.38	1.38
Min E.R. bed	0.58	0.58	1.25	1.36
Max E.R. left bank	0.57	0.60	1.43	1.38
Min E.R. left bank	0.54	0.59	1.23	1.39
Max E.R. right bank	0.60	0.58	1.39	1.41
Min E.R. right bank	0.58	0.60	1.33	1.37

Sensitivity of BM results to changes in lava thickness

This section deals with changes in lava thickness and how these changes affect erosion rate distribution across the channel and at channel cross-section 400. Based on what stated on lava flow thicknesses in the lunar maria and at sinuous rille sites, a lower-end value of 5 m and an upper-end value of 20 m are chosen here. Table 2.5a shows how adopting a lava thickness of 5 m instead of 10 m affects erosion rates magnitude and their spatial distribution at the 1200-m-long channel and cross-section 400. The maximum and minimum of bed erosion are shifted downstream of the position they are found in the baseline model, the maximum by 113 m and the minimum by 436 m. The maximum is now located at only 12.5 m from the bend trough, the minimum 267 m downstream of bend 2 axis. The left and right bank erosion maxima are shifted upstream of their BM location (by 8 m and 23 m, respectively) and they are both far from bend axes. Erosion minima are shifted downstream of their BM locations, and they too are located far from bend axes. The

minima of bed and left bank erosion are located at the same place in the channel, whereas in the baseline model this feature was shared by the minima of bed and right bank erosion.

Table 2.5a. Sensitivity of baseline model (BM) results to changes in channel depth h (equal to lava thickness here). The table illustrates maximum and minimum erosion rates at the channel bed and banks. Results refer to a lava thickness of h = 5 m. All other flow BM parameters are unchanged, except for the temperature at channel boundaries, which is equal to T = 1420° C (see text).

SENSITIVITY OF BM RESULTS TO CHANGES IN LAVA THICKNESS – h = 5 m. Erosion rates at channel bed and banks			
Obtained Erosion Rates (ER)	Erosion Rate Values	Distance from lava source	Location in the channel
description	cm/day	m	description
Max ER bed	20.9	412.5	bend 2, 12.5 m downstream of bend 1 trough, within 5 m of right bank.
Min ER bed	1.0	1067.0*	bend 2, 267.0 m downstream of bend axis, bed/left bank.
Max ER left bank	19.7	690.0	bend 2, 110.0 m upstream of bend axis, bank top.
Min ER left bank	1.0	1067.0*	bend 2, 267.0 m downstream of bend axis, left bank/bed.
Max ER right bank	21.6	270.8	bend 1, 270.8 m downstream of bend axis (inlet), 2.7 m down from bank top.
Min ER right bank	1.2	642.1	bend 2, 157.9 m upstream of bend axis, right bank/bed.

Table 2.5b. Sensitivity of baseline model (BM) results to changes in channel depth h (equal to lava thickness here). The table illustrates maximum and minimum erosion rates at a channel cross-section located 400 m downstream of the lava source and cut along bend 1 trough (see Fig. 2.2a). Results refer to a lava thickness of h = 5 m. All other flow BM parameters are unchanged, except for the temperature at channel boundaries, which is equal to T = 1420° C (see text).

SENSITIVITY OF BM RESULTS TO CHANGES IN LAVA THICKNESS – h = 5 m. Erosion rates at channel Cross-Section (CS) 400 m			
Obtained Erosion Rates (ER)	Erosion Rate Values	Distance from lava source	Location in channel CS

description	cm/day	m	description
Max E.R. bed$_{400}$	20.5	400.0	~10 m from right bank
Min E.R. bed$_{400}$	3.0	400.0	~1 m from left bank
Max E.R. left bank$_{400}$	5.2	400.0	3 m from bank top
Min E.R. left bank$_{400}$	2.9	400.0	left bank/bed
Max E.R. right bank$_{400}$	12.9	400.0	3 m down from bank top
Min E.R. right bank$_{400}$	6.8	400.0	right bank/bed

Table 2.5b shows the erosion rates distribution at channel cross-section 400. In contrast to what seen in the baseline model, the maximum erosion rate at the bed (20.5 cm/day) is located farther away (~10 m) from the bed/right bank contact (see also Fig. 2.14). The minimum value of 3.0 cm/day is found within ~1 m of the left bank. The decrease in erosion rate as the left bank is approached is very similar to that shown in previously described scenarios. At the bed/right bank contact, the minimum erosion rate is equal to 6.8 cm/day. At the left bank, the maximum erosion rate of 5.2 cm/day is located at a vertical distance of 2 m from the underlying contact (see also Fig. 2.15a), the same distance found for a 10-m-thick lava channel. At the bank top, erosion rates are equal to ~4.1 cm/day. Erosion rates then increase downward till the maximum of 5.2 cm/day is reached. From that point down to the bank/bed contact, erosion rates drop drastically to a value of 2.9 cm/day at the contact itself. At the right bank, the maximum erosion rate of 12.9 cm/day is located at a vertical distance of ~2 m from the underlying contact. At the bank top, erosion rates are equal to 12.6 cm/day and keep increasing downwards until the vertical distance of ~2 m from the contact is reached. From there downwards, erosion rates drop drastically and reach a value of 6.8 cm/day at the bank/bed contact.

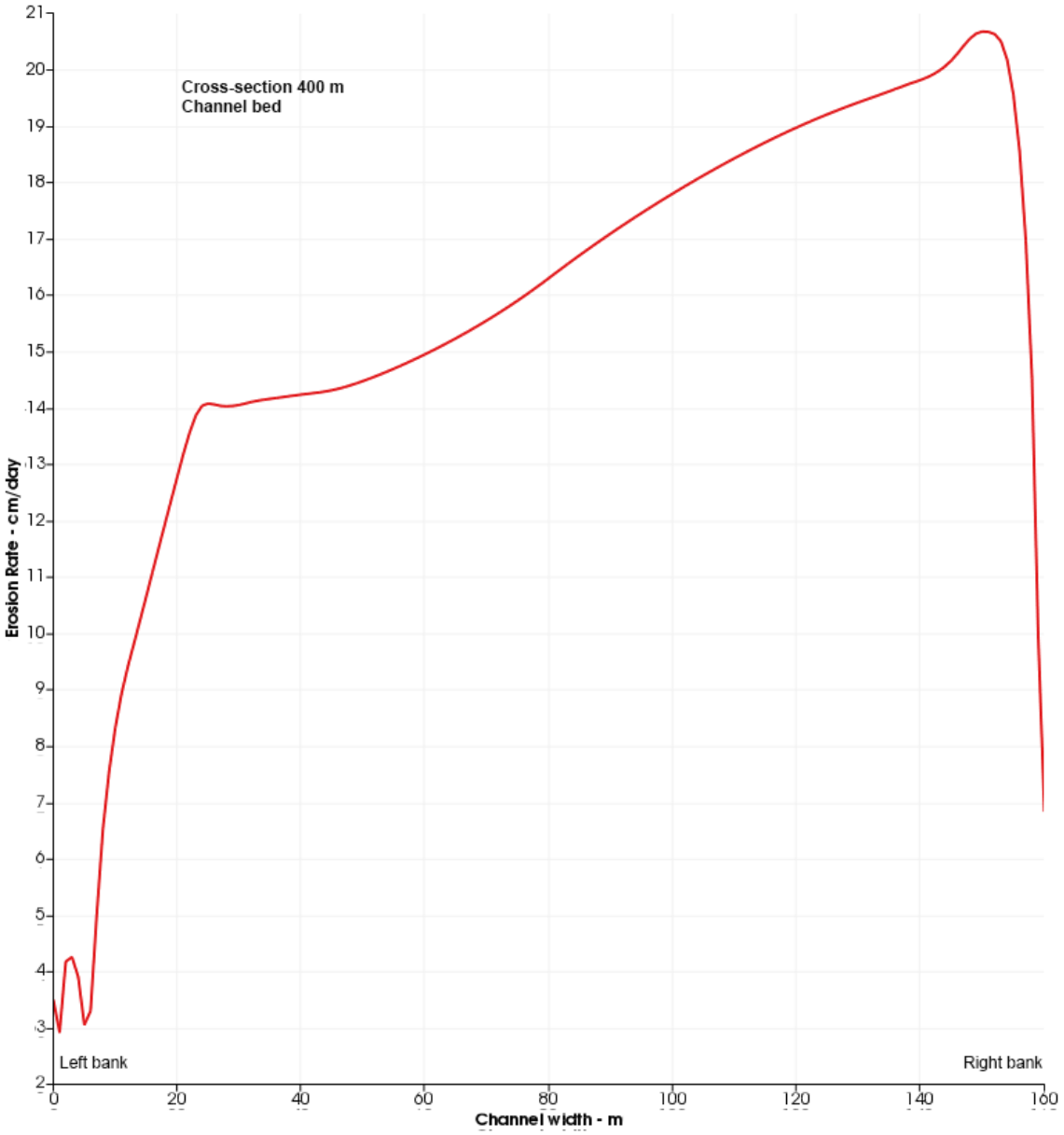

Figure 2.14. Erosion rates at the channel bed for cross-section 400. The case for a lava thickness of 5 m. The maximum value of 20.5 cm/day is obtained at a horizontal distance of ~10 m from the right bank whereas the minimum value of 3.0 cm/day is found within ~1 m of the left bank. The decrease in erosion rate as the left bank is approached is very similar to that shown in previously described scenarios. At the bed/right bank contact, the minimum erosion rate is equal to 6.8 cm/day.

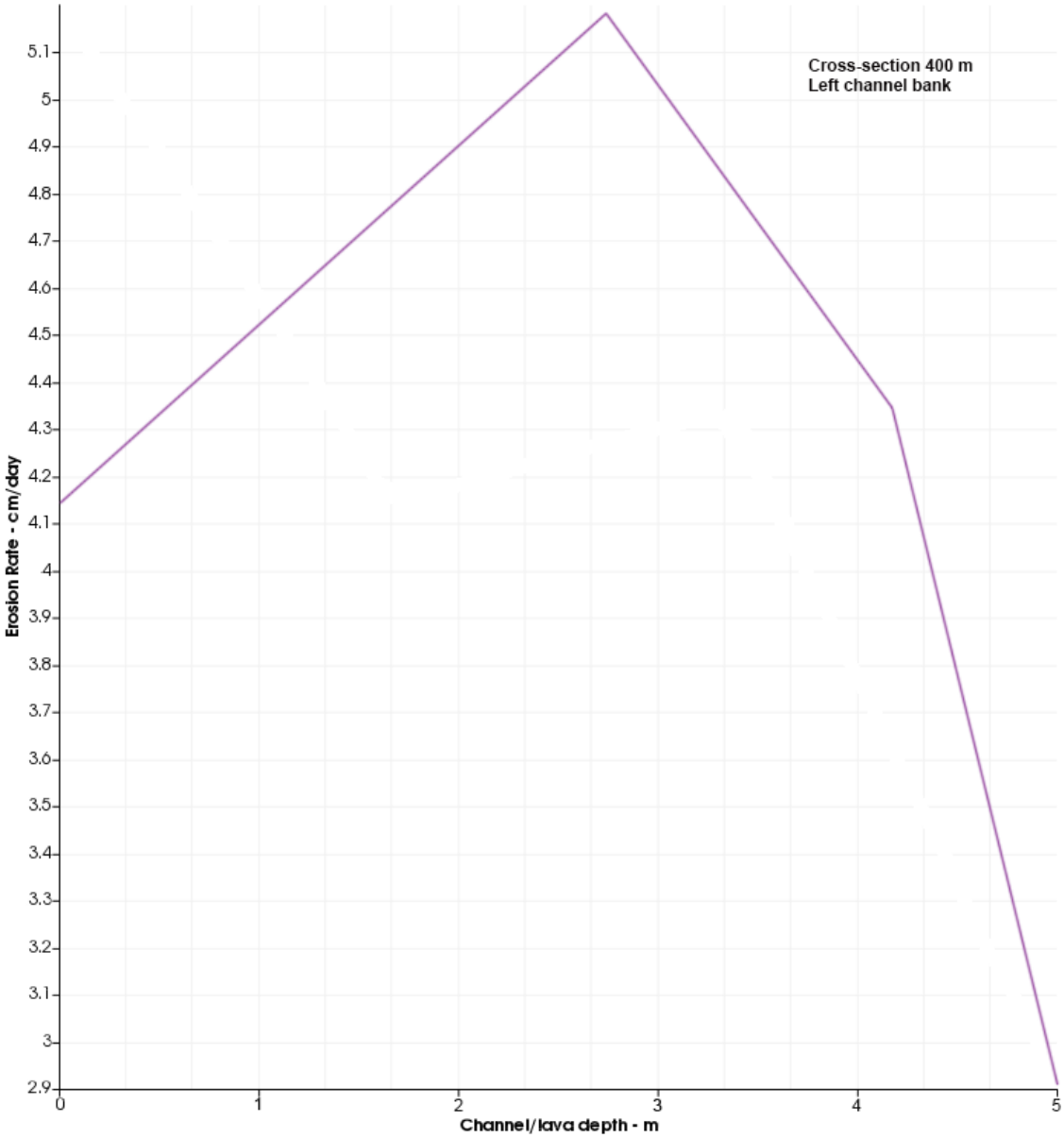

Figure 2.15a. Erosion rates at the left bank for cross-section 400. The case for a lava thickness of 5 m. Maximum erosion rates of 5.2 cm/day are found at a vertical distance from the bank top of ~3 m, i.e., ~2 m above the bank/ bed contact. At the bank top, erosion rates are equal to ~4.1 cm/day. Erosion rates then increase downwards till the maximum of 5.2 cm/day is reached (~2 m above the bank/bed contact). From that point down, erosion rates drop drastically to a value of 2.9 cm/day at the contact.

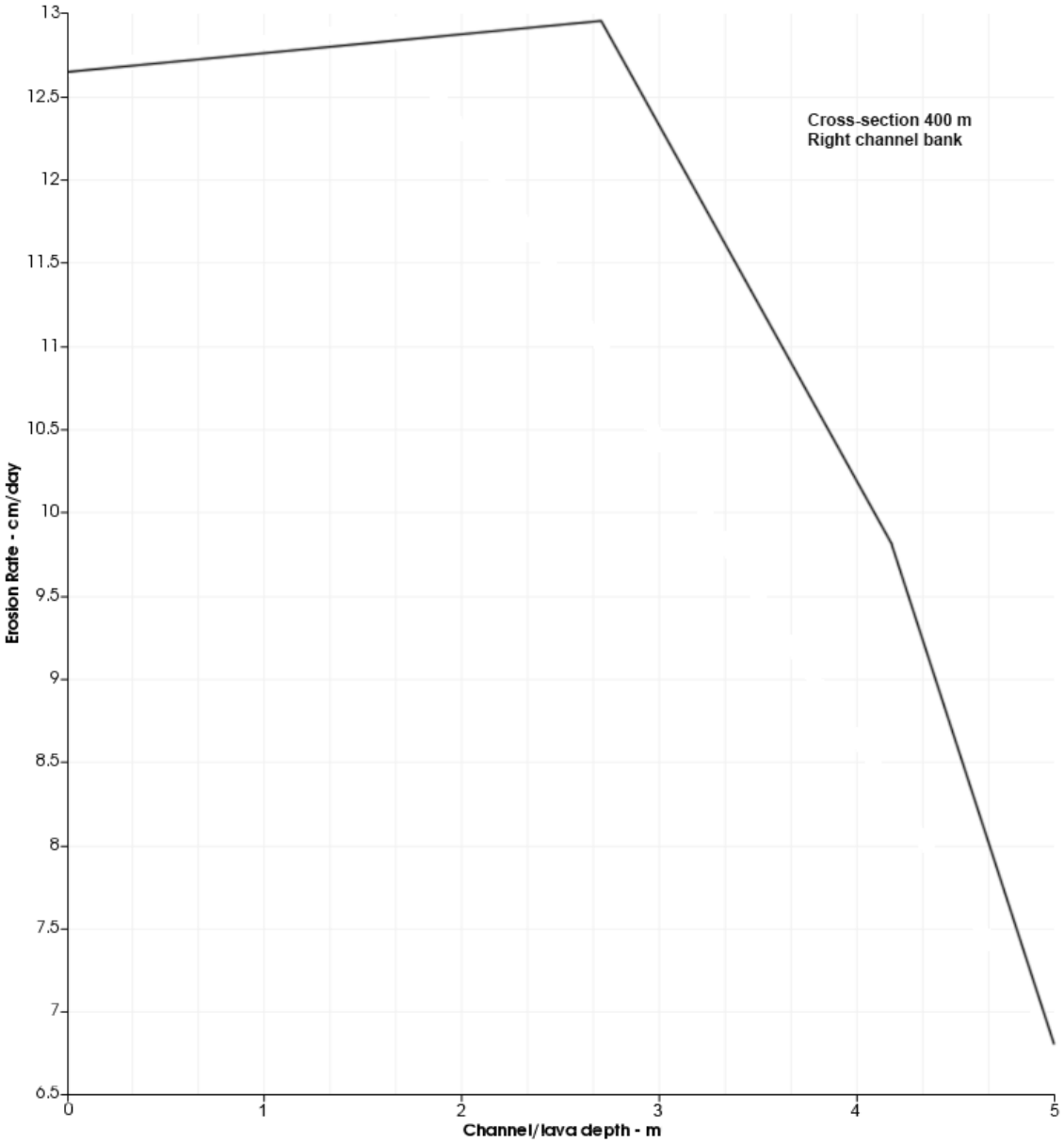

Figure 2.15b. Erosion rates at the right bank for cross-section 400. The case for a lava thickness of 5 m. The maximum erosion rate of 12.9 cm/day is located at a vertical distance of ~2 m from the underlying bank/bed contact. At the bank top, erosion rates are equal to 12.6 cm/day and they keep increasing downwards until the vertical distance of ~2 m from the contact is reached. From that point downward, erosion rates drop to 6.8 cm/day at the bank/bed contact.

Table 2.5c show how baseline model results change by considering a lava thickness of 20 m. Compared to the lower thickness scenario, the distribution of maxima and minima of

erosion is once again changed. All but one erosion rate maxima are shifted downstream of their BM locations, the exception being the maximum erosion rate at the right bank that is found at the same location as in the BM. All erosion rate minima are shifted upstream of their BM locations. Interestingly, all minima were shifted downstream of their BM locations in the scenario involving a 5-m-thick lava. Most maxima and minima are found at channel locations that are far from bend axes, with the only exception of the maximum erosion rate at the left bank that is located 8.4 meters upstream of bend 2 axis. Finally, the bed and right bank minima are found at the same place in the channel (as in the baseline model).

Table 2.5c. Sensitivity of baseline model (BM) results to changes in channel depth h (equal to lava thickness here). The table illustrates maximum and minimum erosion rates at the channel bed and banks. Results refer to a lava thickness of h = 20 m. All other flow BM parameters are unchanged, except for the temperature at channel boundaries, which is equal to T = 1400° C (see text).

SENSITIVITY OF BM RESULTS TO CHANGES IN LAVA THICKNESS – h = 20 m. Erosion rates at channel bed and banks			
Obtained Erosion Rates (ER)	Erosion Rate Values	Distance from lava source	Location in the channel
description	cm/day	m	description
Max ER bed	42.8	1082.3	bend 2, 282.3 m downstream of bend axis, 28 m from right bank.
Min ER bed	1.3	615.3*	bend 2, 184.7 m upstream of bend axis, bed/right bank.
Max ER left bank	42.3	791.6	bend 2, 8.4 m upstream of bend axis, bank top.
Min ER left bank	1.8	1030.6	bend 2, 230.6 m downstream of bend axis, left bank/bed.
Max ER right bank	43.2	293.8	bend 1, 293.8 m downstream of bend axis (inlet), 11.7 m from bank top.

Min ER right bank	1.3	615.3*	bend 2, 184.7 m upstream of bend axis, right bank/bed.

When looking at channel cross-section 400 (Table 2.5d), the distribution of erosion rates at the bed is very similar to that shown in the baseline model (except for the higher values referring to the thicker lava scenario). Erosion rates reach 39.8 cm/day at the bed and 42.3 cm/day at the right bank.

Table 2.5d. Sensitivity of baseline model (BM) results to changes in channel depth h (equal to lava thickness here). The table illustrates maximum and minimum erosion rates at a channel cross-section located 400 m downstream of the lava source and cut along bend 1 trough (see Fig. 2.2a). Results refer to a lava thickness of h = 20 m. All other flow BM parameters are unchanged, except for the temperature at channel boundaries, which is equal to T = 1400° C (see text).

SENSITIVITY OF BM RESULTS TO CHANGES IN LAVA THICKNESS – h = 20 m. Erosion rates at channel Cross-Section (CS) 400 m			
Obtained Erosion Rates (ER)	Erosion Rate Values	Distance from lava source	Location in channel CS
description	cm/day	m	description
Max E.R. bed_{400}	39.8	400.0	~7 m from right bank
Min E.R. bed_{400}	5.3	400.0	~1 m from left bank
Max E.R. $left\ bank_{400}$	23.5	400.0	from flow top to ~7 m down
Min E.R. $left\ bank_{400}$	5.2	400.0	left bank/bed
Max E.R. $right\ bank_{400}$	42.3	400.0	bank top
Min E.R. $right\ bank_{400}$	12.1	400.0	right bank/bed

Perhaps, the most intriguing difference is represented by the shape of the erosion rate curve at the left bank (see Fig. 2.16a), which looks somewhat different from its BM counterpart (Fig. 2.4b). In the 10-m-thick (BM) scenario, the maximum is reached at a vertical distance of 4-2 m from the bank/bed contact whereas in the 20 m thick channel the maximum is much closer to the bank top, at a vertical distance of ~6 m from the bank/bed contact.

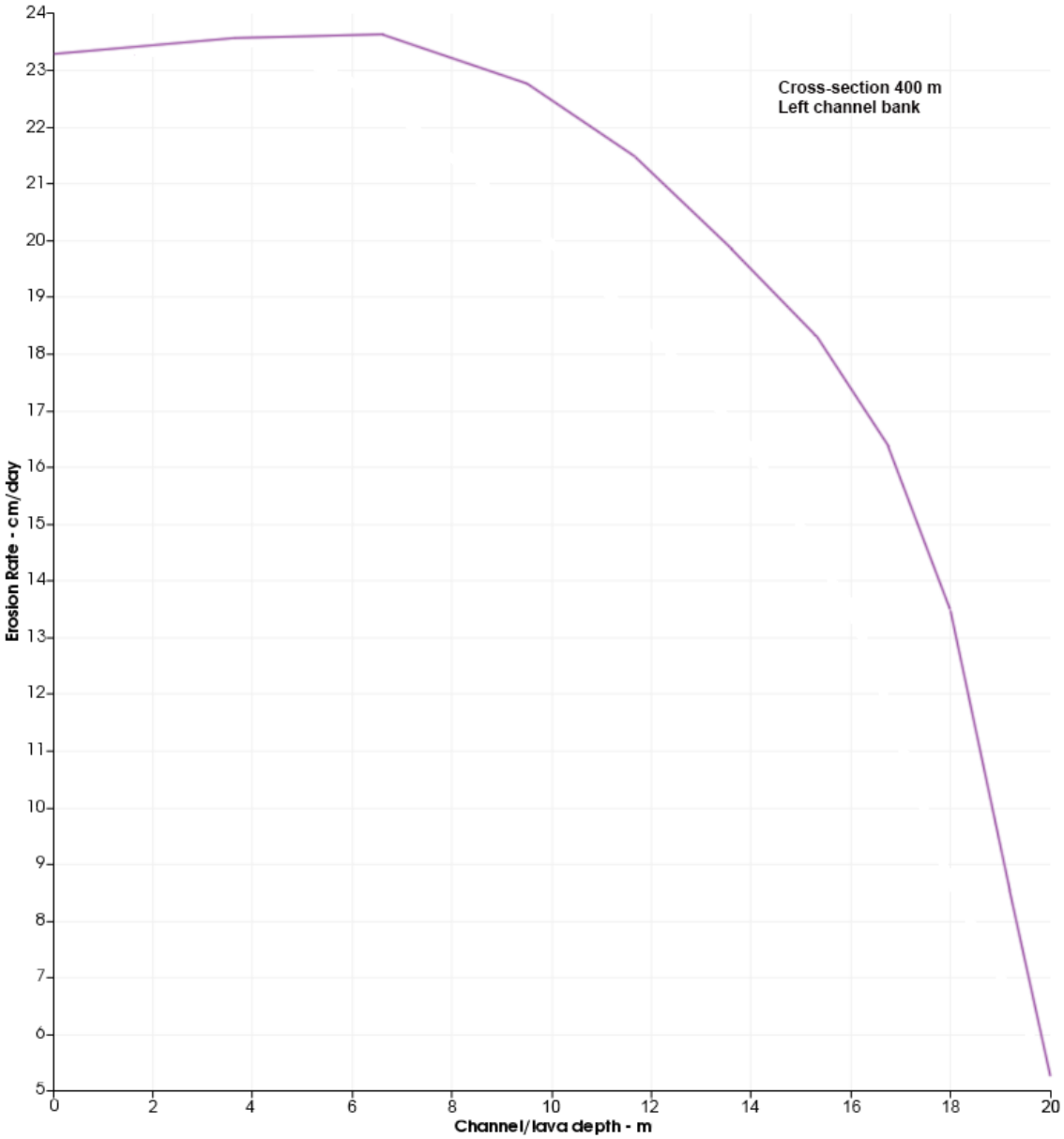

Figure 2.16a. Erosion rates at the left bank for cross-section 400. The case for a lava thickness of 20 m. The maximum erosion rate of 23.5 cm/day is found at a vertical distance from the bank top of ~6 m, i.e., ~14 m above the bank/bed contact. At the bank top, erosion rates are equal to ~23.3 cm/day and they increase downward till they reach the maximum value of 23.5 cm/day. From that point downward, they decrease faster and faster as the vertical distance from the bank/bed contact is reduced until they reach 5.2 cm/day at the contact.

At the right bank (Fig. 2.16b), the maximum erosion rate of 42.3 cm/day is located at the bank top. From that point downward, erosion rates decrease faster and faster till a vertical

distance of ~6 m from the bank/bed contact is reached. Then they continue decreasing - though at a slower pace - till the vertical distance from the underlying contact is equal to ~3 m. From there, they drop drastically to the minimum of 12.1 cm/day at the contact itself.

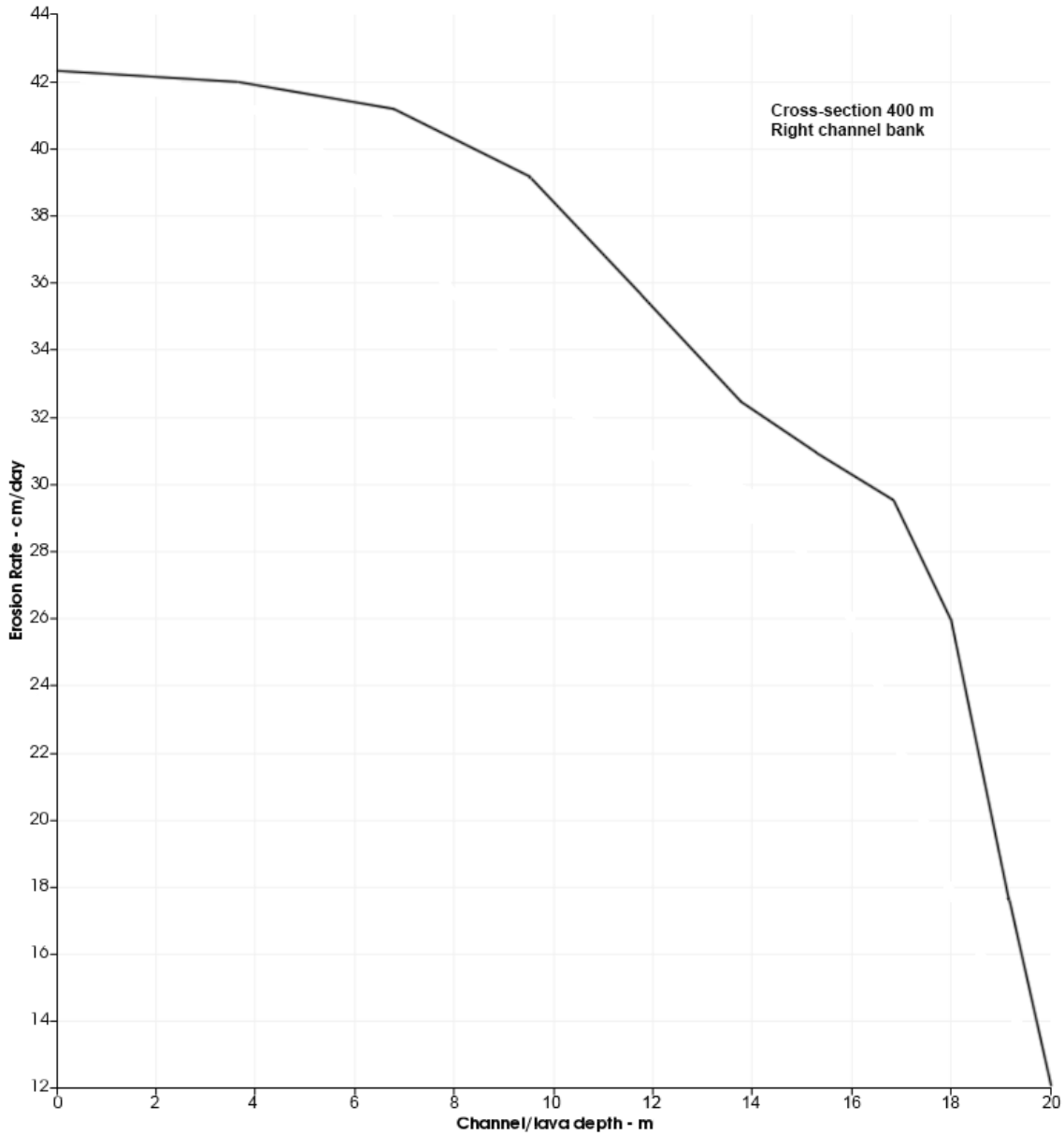

Figure 2.16b. Erosion rates at the right bank for cross-section 400. The case for a lava thickness of 20 m. The maximum erosion rate of 42.3 cm/day is located at the bank top. From that point downward, erosion rates decrease faster and faster till a vertical distance of ~6 m from the bank/bed contact is reached. Then they continue decreasing at a slower pace till the vertical distance from the contact is equal to ~3

m. From there, they drop drastically to the minimum of 12.1 cm/day at the bank/bed contact.

How thickness-modified results compare with BM results

Table 2.5e shows ratios obtained from maxima and minima of erosion for a 1200-m-long channel and a channel cross-section cut through a meander axis (cross-section 400). In line with expectations, for a 5-m-thick flow, all ratios are < 1 whereas they are > 1 for a flow that is 20 m thick (because a thicker flow has a higher erosive power than a comparatively thinner flow, holding other factors equal). For a 5-m-thick flow, all ratios obtained at the 1200-m-long channel are higher by a factor of 1.01-1.38 than those at cross-section 400. We have seen so far that ratios obtained at cross-section 400 tend to be higher than those calculated over the entire channel when the flowing lava has a high erosive power (superheated lava, lava flowing at high velocity). At channel cross-section 400, for those scenarios in which the flowing lava is not highly erosive (lava erupted at a sub-liquidus temperature or flowing at a very low velocity) we have seen ratios that are lower than their counterpart values that refer to the 1200-m-long channel. It is known that a thin flow has a lower erosive power than a thicker flow, holding other factors equal. The result that ratios at cross-section 400 can be lower than those at the 1200-m-long channel by a factor of 1.38 suggests that a low lava thickness might be especially effective in hampering erosion at meander bends (the reason will be explained in Chapter 5). For the thicker lava scenario in Table 2.5e, all maxima ratios are higher at cross-section 400 than at the 1200-m-long channel, except the one obtained at the bed. This result is likely explained by the observed enhanced erosion at channel bends, associated with the 20-m-thick flow.

Remarkably, the value of the ratio at the left bank (at cross-section 400, equal to 2.28) is greater than that at the 1200-m-long channel by a factor of 1.55. A similar value of ratio (2.27) was obtained from maxima of left bank erosion for a scenario of superheated lava (Table 2.3e). In conclusion, variations in flow thickness are very effective in engendering large variations in erosion rate magnitude and distribution, especially at meander bends.

Table 2.5e. Sensitivity of baseline model results to changes in initial lava thickness, h.

Obtained Erosion Rates	$Ratio_{all\_channel}$ (h = 5 m/BM)	$Ratio_{400}$ (h = 5 m/BM)	$Ratio_{all\_channel}$ (h = 20 m/BM)	$Ratio_{400}$ (h = 20 m/BM)
	#	#	#	#
Max E.R. bed	0.72	0.71	1.47	1.38
Min E.R. bed	0.83	0.60	1.08	1.06
Max E.R. left bank	0.68	0.50	1.47	2.28
Min E.R. left bank	0.77	0.59	1.38	1.06
Max E.R. right bank	0.73	0.53	1.46	1.73
Min E.R. right bank	1.01	0.76	1.08	1.36

Sensitivity of BM results to changes in lava substrate

In this section, we explore how changes in the thermal and mechanical properties of the lava substrate may affect the magnitude and spatial distribution of erosion rates in a 1200-m-long channel and at a channel cross-section cut parallel to the axis of bend 1 at a downstream distance of 400 m from the lava source. At the Vallis Schröteri inner rille, the lava substrate likely consists of consolidated lava of similar composition to the lava that flowed within the Vallis Schröteri primary rille. The latter is a sinuous rather than meandering channel that is up to 4.5-km-wide (*Garry et al*., 2008; *Honda et al*., 2009) and encases the narrower and highly meandering inner rille. A thorough spectral analysis of the materials that cover the Aristarchus plateau that includes the Vallis Schröteri rille site has

revealed an extreme heterogeneity in composition (*Mustard et al*., 2011). As a result, the possibility that the substrate might consist of – at least over discrete segments of the rille – unconsolidated highland material cannot be ruled out. Though information on the thermo-physical properties of a few mineral species expected to occur in lunar highland materials is available, it is difficult to derive the thermo-physical properties of an entire lava substrate. The Apollo landing missions revealed a lunar surface of highly fragmented, impact weathered material (regolith) on both the mare and highland crusts (*Wilhelms*, 1987). On older surfaces (highlands), the regolith or mega-regolith may extend to several kilometers. The highland material comprising the Aristarchus plateau likely contains a substantially thick surface regolith that may have served as a mechanically weakened substrate for the Vallis Schröteri lavas. Based on this, we assume that at least a fraction of the material that constitutes the inner rille lava substrate might have characteristics analogous to those of an unconsolidated granular regolith. The physical and thermo-physical properties of a lunar granular regolith are described by *Colozza* (1991) and *Richter* (1993). The University of Arizona determined the melting point of a simulated lunar regolith and found a lower-end temperature of 1017°C and an upper-end value of 1300°C (*Richter*, 1993). An expression for the specific heat of regolith material was obtained from a curve fit and interpolation of experimental data given in *Robie et al*. (1970) and was later adopted by *Colozza* (1991) and *Richter* (1993). Using this expression, a value of specific heat of 1438 J kg^{-1} $°C^{-1}$ is calculated for a substrate melting temperature of 1100°C. The latent heat of fusion was calculated to be 161.2 kJ kg^{-1} on average and regolith density varies between 1600 and 2000 kg m^{-3} (*Richter*, 1993).

Fig. 2.17 shows erosion rate values at the channel bed for a scenario in which the lava substrate consists of granular regolith material with a melting temperature T_{mg} = 1100°C, density ρ_g = 2000 kg m^{-3}, latent heat of fusion L_g = 161.2 kJ kg^{-1} and specific heat capacity C_g = 1438 J kg^{-1} $°C^{-1}$. From now on, this substrate will be referred to as "unconsolidated 1".

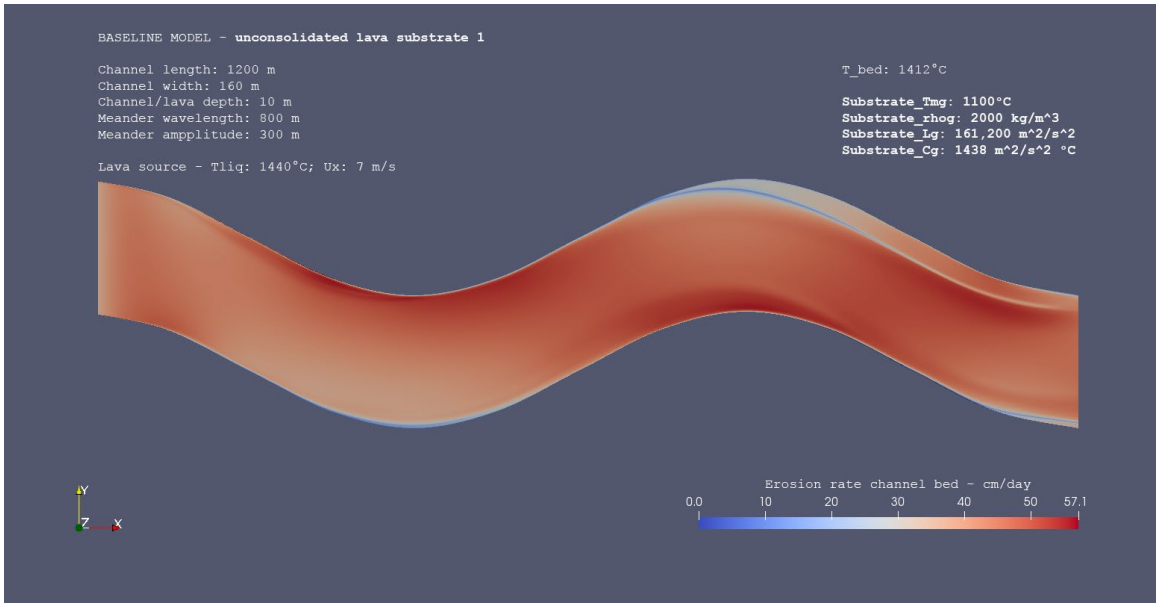

Figure 2.17. Erosion rates at the channel bed for a lava channel that has the same identical characteristics adopted in the baseline model (BM), except for the lava substrate that is modeled as unconsolidated ("unconsolidated 1"). The physical and thermal properties of the substrate are taken from *Richter* (1993) and Robie (1970) and adapted for the Vallis Schröteri environment. All other geometric and flow parameters are held the same as in BM.

Table 2.6a shows how maximum and minimum erosion rates vary for a 1200-m-long and 160-m-wide lava channel identical to the baseline model channel, exception made for the mechanical and thermal properties of the lava substrate (here "unconsolidated 1").

Table 2.6a. Sensitivity of baseline model (BM) results to changes in lava substrate (an unconsolidated substrate with thermal and mechanical properties analogous to those of granular regolith, *Colozza,* 1990*; Richter et al.*, 1993). The table illustrates maximum and

minimum erosion rates at the channel bed and banks. All other flow BM parameters are unchanged.

SENSITIVITY OF BM RESULTS TO CHANGES IN LAVA SUBSTRATE – unconsolidated 1. Channel length = 1200 m. Erosion rates at channel bed and banks			
Obtained Erosion Rates (ER)	Erosion Rate Values	Distance from lava source	Location in the channel
description	cm/day	m	Description
Max ER bed	56.0	299.6	bend 1, 100.4 m upstream of bend trough, within 5 m of right bank.
Min ER bed	2.3	630.6*	bend 2, 169.4 m upstream of bend axis, bed/right bank.
Max ER left bank	55.5	697.6	bend 2, 102.4 m upstream of bend axis, bank top.
Min ER left bank	2.4	1047.9	bend 2, 247.9 m downstream of bend axis, left bank/bed.
Max ER right bank	57.1	293.8	bend 1, 106.2 m upstream of bend trough, bank top.
Min ER right bank	2.3	630.6*	bend 2, 169.4 m upstream of bend axis, right bank/bed.

** The x, y, and z coordinates of every ER value are identical to those in the baseline model (BM).

Throughout the channel, erosion maxima and minima are found at the same locations they are in the baseline model, a consequence of the identical channel geometry and distribution of initial physical and thermal flow parameters in the two model versions. The only point that has moved downstream of its BM location by 50 m is the maximum erosion at the bed. As in the baseline model, the bed and right bank minima are located at the same downstream distance from the lava source, i.e., 631 m. No maxima or minima are found in the proximity of bend axes. Because of the lower melting temperature and density of substrate, erosion maxima and minima are almost twice as high as those obtained in the BM. Also, the latent heat of fusion that is lower by a factor of ~3 than the value used in the

baseline model together with the lower specific heat capacity of the substrate likely contributed to the observed increase in erosion rates. The bank maximum is still found at the right bank and the ratio of maximum erosion rate at right bank to maximum erosion rate at left bank is almost identical to that found in the baseline model. Table 2.6b shows how adopting the substrate properties defined as "unconsolidated 1" affects erosion rates distribution at channel cross-section 400. Once again, all maxima and minima are almost twice as high as those obtained at cross-section 400 of the baseline model. Another similarity is that the maximum bed erosion of 55.1 cm/day is slightly lower than that obtained at the 1200-m-long channel (56.0 cm/day) and the maximum erosion rate at the right bank is much higher than the one measured at the left bank (by a factor of ~2.4). In comparison, the right bank erosion maximum is only ~1.03 times higher than the left bank erosion maximum at the 1200-m-long channel. A local process might be at work at/in the proximity of bend 1 axis and could potentially explain the enhanced erosion at the right bank. Erosion minima are much higher than those observed at the long channel segment, and this is especially true for the right bank minimum of 17.1 cm/day.

Table 2.6b. Sensitivity of baseline model (BM) results to changes in lava substrate (an unconsolidated substrate with thermal and mechanical properties analogous to those of granular regolith, *Colozza,* 1990*; Richter et al.*, 1993). The table illustrates maximum and minimum erosion rates at a channel cross-section located 400 m downstream of the lava source and cut along bend 1 trough (see Fig. 2.2a). All other flow BM parameters are unchanged.

SENSITIVITY OF BM RESULTS TO CHANGES IN LAVA SUBSTRATE – unconsolidated 1. Channel length = 1200 m. Erosion rates at Cross-Section 400 m			
Obtained Erosion Rates (ER)	Erosion Rate Values	Distance from lava source	Location in channel CS
description	cm/day	m	description
Max E.R. bed_{400}	55.1	400.0	~7 m from right bank

Min E.R. bed$_{400}$	9.5	400.0	~1 m from left bank
Max E.R. left bank$_{400}$	19.8	400.0	~6.1 m down from bank top
Min E.R. left bank$_{400}$	9.4	400.0	left bank/bed
Max E.R. right bank$_{400}$	46.9	400.0	bank top
Min E.R. right bank$_{400}$	17.1	400.0	right bank/bed

The spatial distribution of erosion rates at the bed of channel cross-section 400 is almost identical to that observed at the BM channel cross-section, hence it is not shown here. The same applies to the erosional trends observed at the left and right bank of the same channel cross-section. Expectedly, changing the physical and thermal properties of the lava substrate is not conducive to a change in the spatial distribution of erosion rates and it only affects their magnitude.

The other unconsolidated scenario chosen here, "unconsolidated 2", adopts the lower-end melting temperature T_{mg} = 1017°C and the lower-end density of 1600 kg m^{-3}. A value of specific heat of 1409.6 J kg^{-1} $°C^{-1}$ is calculated for the substrate melting temperature of 1017°C and the values of other thermo-physical parameters are held the same (Fig. 2.18). "Unconsolidated 2" is presented for the purpose of testing the sensitivity of the model to extreme changes in substrate thermophysical properties though it might not be representative of a real-life scenario. This is because a lunar substrate made of granular regolith will likely melt over a range of temperatures rather than at the lowest melting temperature value. A similar argument can be made for the value of 1600 kg m^{-3} that is assigned to regolith density.

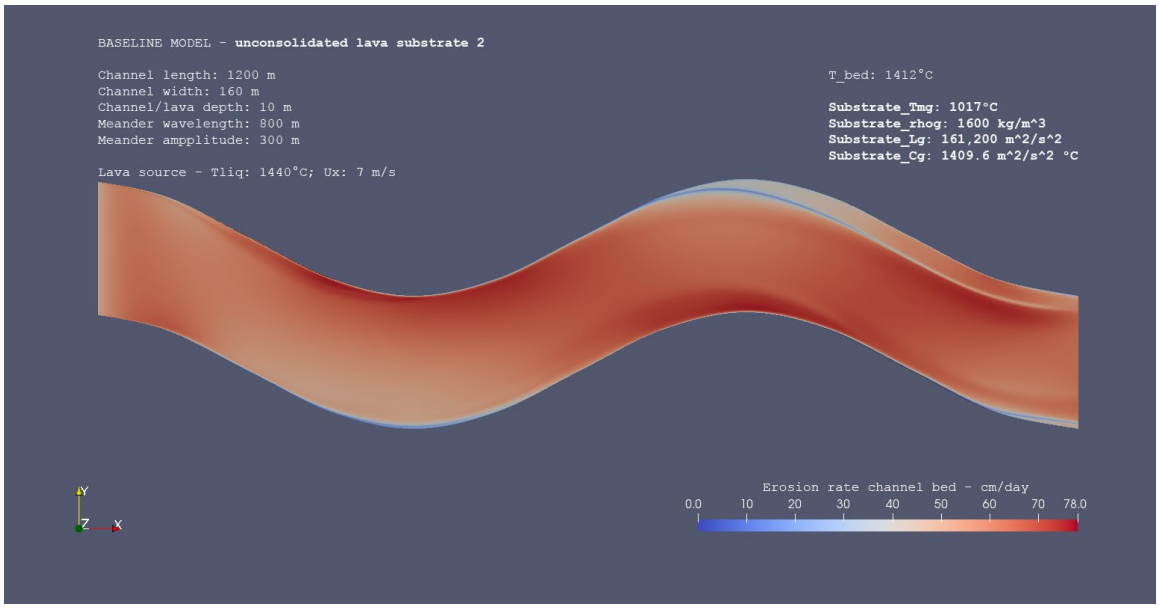

Figure 2.18. Erosion rates at the channel bed for a lava channel that has the same identical characteristics adopted in the baseline model (BM), except for the lava substrate that is modeled as unconsolidated ("unconsolidated 2"). The physical and thermal properties of the substrate are taken from *Richter* (1993) and Robie (1970) and are adapted for the Vallis Schröteri environment. All other geometric and flow parameters are held the same as in BM.

Table 2.6c shows how an unconsolidated substrate (of granular regolith) defined by the physical and thermal properties listed in Fig. 2.18 affects magnitude and spatial distribution of erosion rates across a 1200-m-long rille segment. Maxima and minima values are higher than those obtained from the "unconsolidated 1" scenario by a factor of ~1.4, an increase that arises from the lower melting temperature and density of the "unconsolidated 2" substrate. The specific heat capacity of the latter substrate is also lower than the value chosen for the former scenario though its small variation (from 1438 to 1409.6 J kg^{-1} $°C^{-1}$) is unlikely to play a major role in the observed increase in erosion rates. As compared to the baseline model, erosion rate values are higher by a factor of ~2.6. The spatial distribution of maxima and minima across the channel is almost identical to that shown in

the baseline model (as well as that in the previous scenario), except for the location of the right bank erosion maximum that is shifted 2 m upstream of its BM location. Also, the bed maximum is shifted 50 m downstream of its baseline location (as in "unconsolidated 1").

Table 2.6c. Sensitivity of baseline model (BM) results to changes in lava substrate (unconsolidated 2 - with lower density, melting point, and specific heat capacity than unconsolidated 1, see text). The table illustrates maximum and minimum erosion rates at the channel bed and banks. All other flow BM parameters are unchanged.

SENSITIVITY OF BM RESULTS TO CHANGES IN LAVA SUBSTRATE – unconsolidated 2. Channel length = 1200 m. Erosion rates at channel bed and banks			
Obtained Erosion Rates (ER)	Erosion Rate Values	Distance from lava source	Location in the channel
description	cm/day	m	description
Max ER bed	76.5	299.6	bend 1, 100.4 m upstream of bend trough, within 5 m of right bank.
Min ER bed	3.1	630.6*	bend 2, 169.4 m upstream of bend axis, bed/right bank.
Max ER left bank	75.8	697.6	bend 2, 102.4 m upstream of bend axis, bank top.
Min ER left bank	3.3	1047.9	bend 2, 247.9 m downstream of bend axis, left bank/bed.
Max ER right bank	78.0	291.9	bend 1, 108.1 m upstream of bend trough, bank top.
Min ER right bank	3.1	630.6*	bend 2, 169.4 m upstream of bend axis, right bank/bed.

When looking at the magnitude and spatial distribution of erosion rates at channel cross-section 400 (Table 2.6d), the trend shown in Table 2.6b is repeated though values are higher by a factor of ~1.4. Erosion rates are higher than their BM counterpart values by a factor of ~2.6. The maximum erosion at the bed (75.5 cm/day) is slightly lower than that found at the long channel section (76.5 cm/day) and the gap separating the right bank maximum from the left bank maximum (64.1-27.1 cm/day) is much larger than the one observed at

the 1200-long channel segment (78.0-75.8 cm/day). Once again, a process responsible for modifying erosion rates distribution likely occurs at/in the proximity of a bend axis.

Table 2.6d. Sensitivity of baseline model (BM) results to changes in lava substrate (unconsolidated 2 - with lower density, melting point, and specific heat capacity than unconsolidated 1, see text). The table illustrates maximum and minimum erosion rates at a channel cross-section located 400 m downstream of the lava source and cut along bend 1 trough (see Fig. 2.2a). All other flow BM parameters are unchanged.

SENSITIVITY OF BM RESULTS TO CHANGES IN LAVA SUBSTRATE – unconsolidated 2. Channel length = 1200 m. Erosion rates at Cross-Section (CS) 400 m			
Obtained Erosion Rates (ER)	Erosion Rate Values	Distance from lava source	Location in channel CS
description	cm/day	m	description
Max E.R. bed_{400}	75.5	400.0	~7 m from right bank
Min E.R. bed_{400}	12.9	400.0	~1 m from left bank
Max E.R. left $bank_{400}$	27.1	400.0	6-8 m down from bank top
Min E.R. left $bank_{400}$	12.9	400.0	left bank/bed
Max E.R. right $bank_{400}$	64.1	400.0	bank top
Min E.R. right $bank_{400}$	23.3	400.0	right bank/bed

The spatial distribution of erosion rates at the channel bed of cross-section 400 (Fig. 2.19) is almost identical to those observed in the "unconsolidated 1" and BM scenarios, the only difference being the erosion rate magnitude. Also, Figs. 2.20 (a, b) show the similarities between the distribution of erosion rates at the banks of channel cross-section 400 and their distribution at cross-section 400 of the baseline model (Figs. 2.4 a, b).

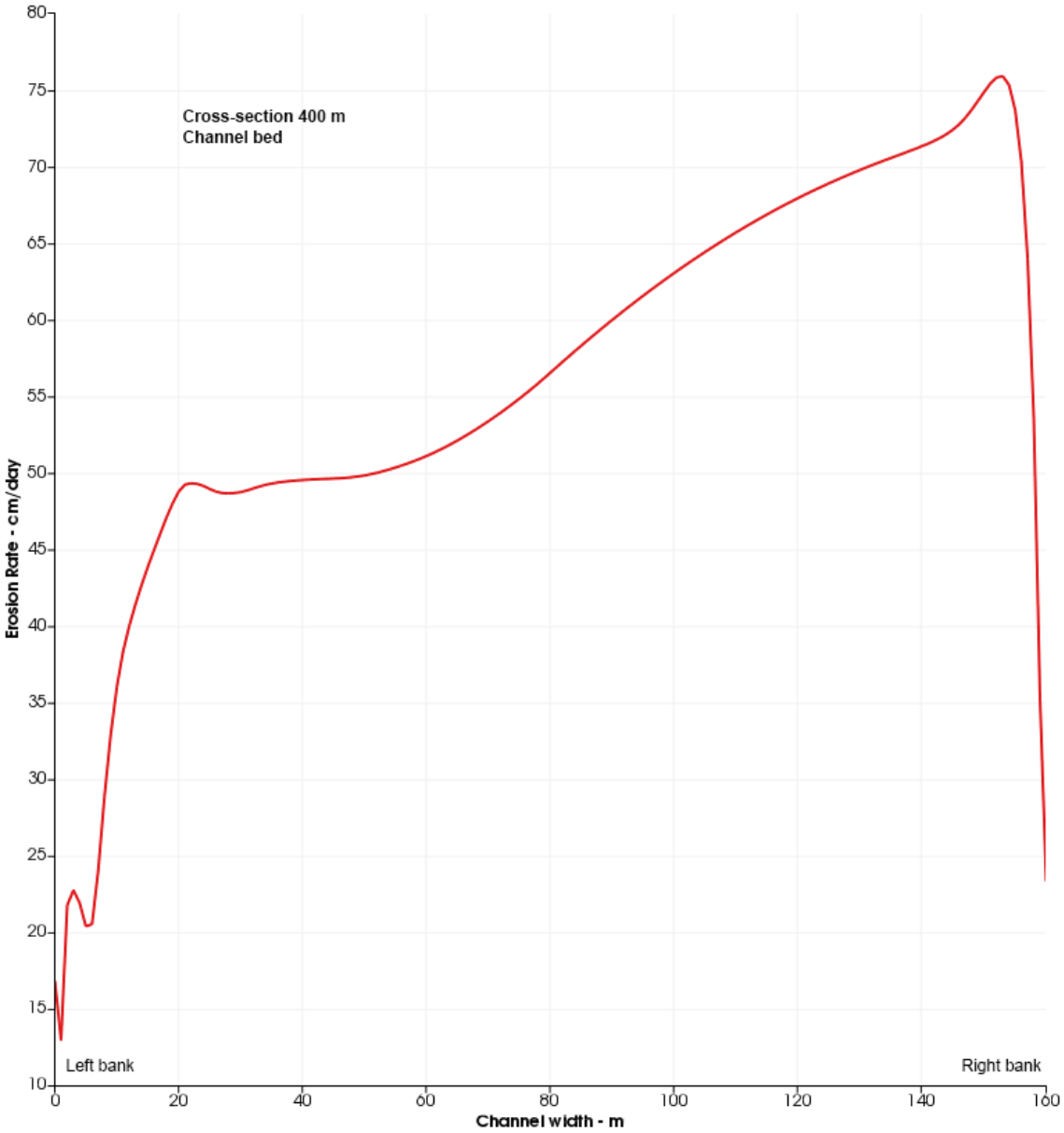

Figure 2.19. Erosion rates at the channel bed for cross-section 400. Channel geometry and initial flow conditions are identical to those assumed for the baseline model, exception made for the lava substrate that is taken to be unconsolidated with the lowest allowed melting temperature and density ("unconsolidated 2", see text). Erosion rate distribution is almost identical to that shown in the baseline model (see Fig. 2.3), though values are higher by a factor of ~2.6.

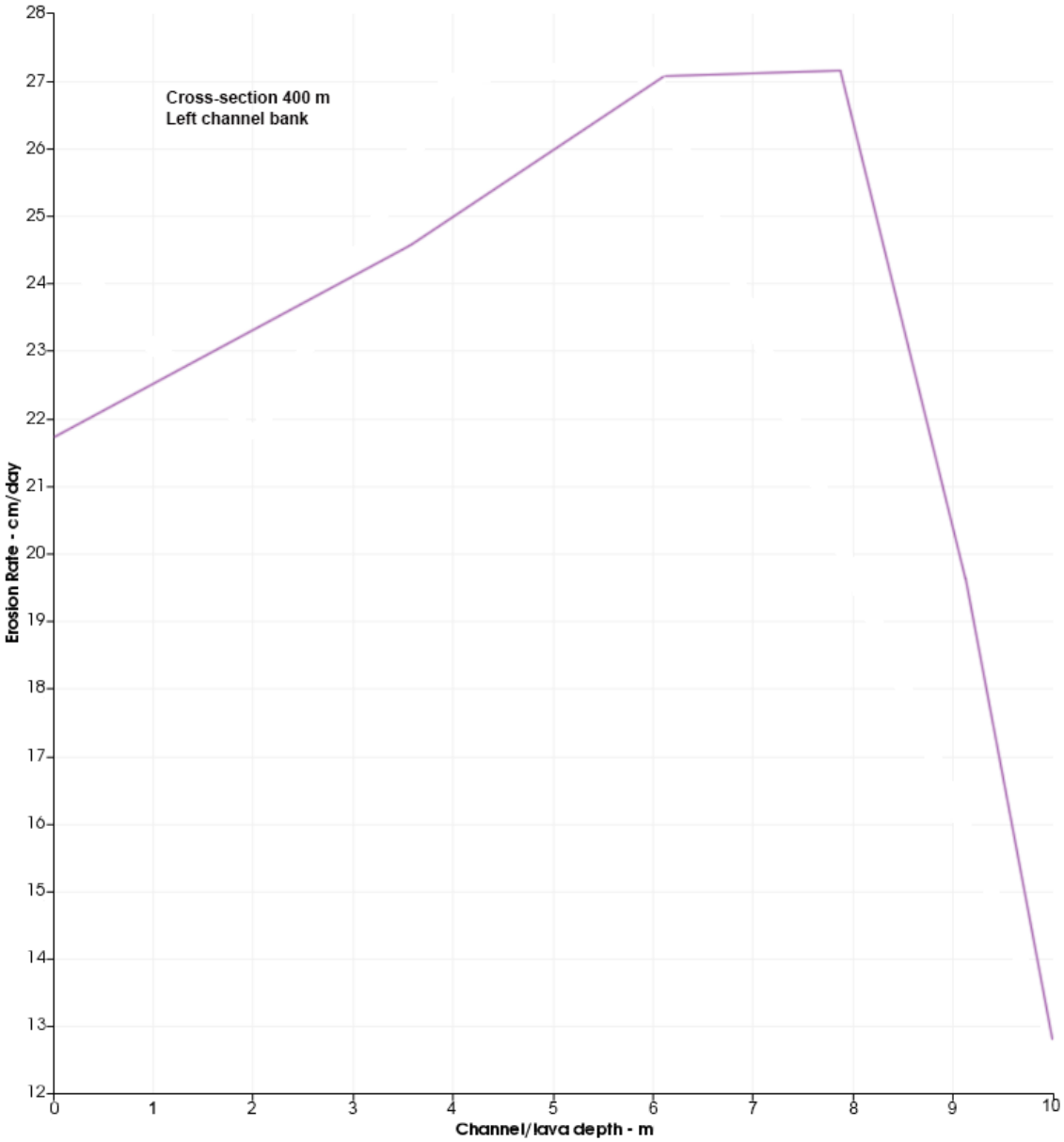

Figure 2.20a. Erosion rates at the left bank for cross-section 400. Channel geometry and initial flow conditions are identical to those assumed in the baseline model, the only difference being represented by the occurrence of an unconsolidated lava substrate of granular regolith with the lowest allowed melting temperature and density ("unconsolidated 2", see text). The plot looks almost identical to that shown in Fig. 2.4b (BM), and the only difference is that erosion rate values are higher by a factor of ~2.6.

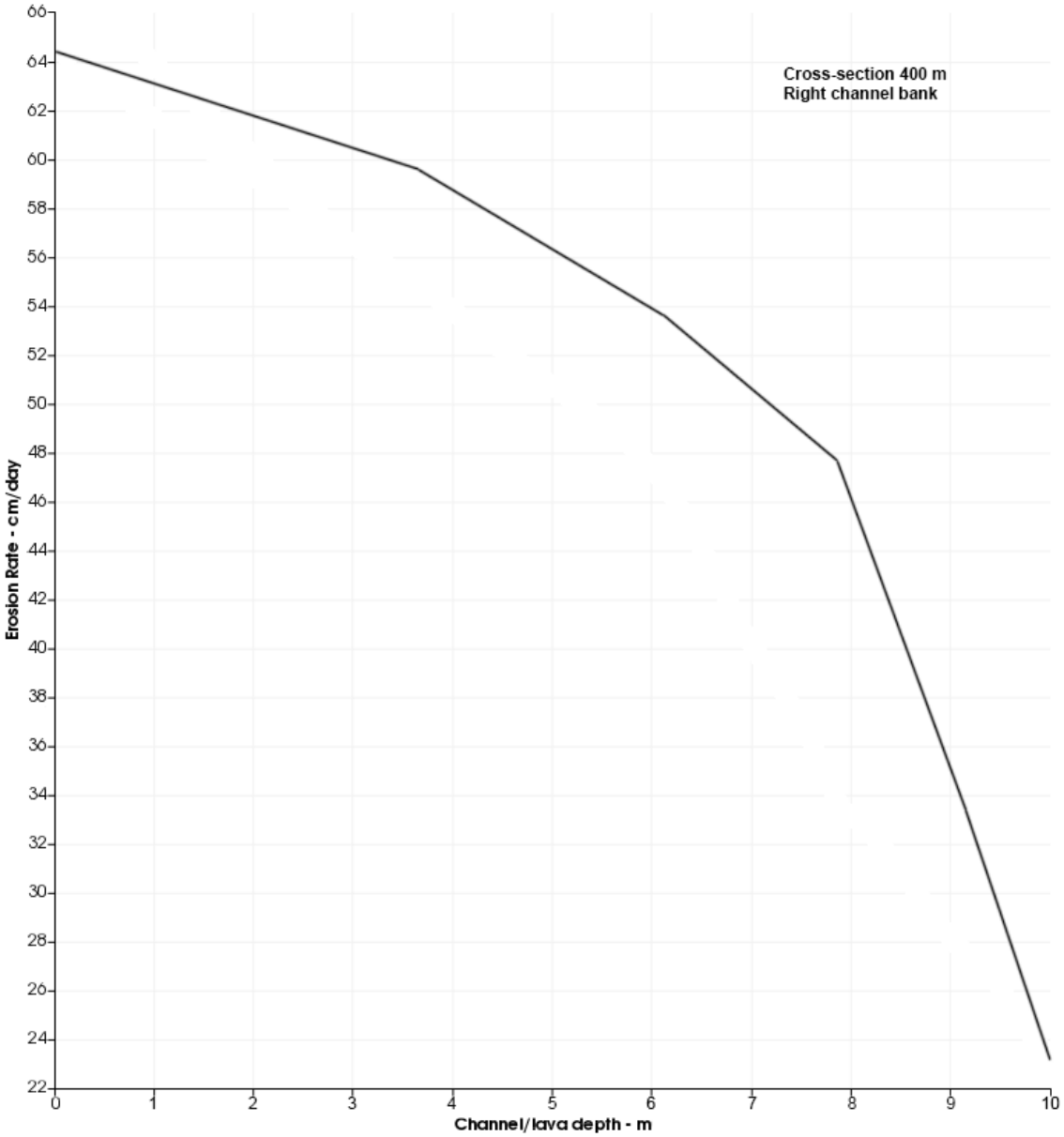

Figure 2.20b. Erosion rates at the right bank for cross-section 400. Channel geometry and initial flow conditions are identical to those assumed in the baseline model, the only difference being represented by the occurrence of an unconsolidated lava substrate of granular regolith with the lowest allowed melting temperature and density ("unconsolidated 2", see text). The plot looks almost identical to that shown in Fig. 2.4a (BM), and the only difference is that erosion rate values are higher by a factor of ~2.6.

How substrate-modified results compare with BM results

Table 2.6e shows ratios of erosion maxima and minima at a 1200 m-long rille segment and a channel cross-section that is cut parallel to bend axis 1 at a downstream distance of 400 m from the lava source. The higher ratios – in the range between 1.85 and 2.63 - compared to those obtained in previous scenarios imply a higher sensitivity of the model to changes in substrate physical and thermal properties. No value is equal to or lower than 1 because erosion rate values associated with the two unconsolidated lava substrates are always higher than those obtained from the consolidated basaltic substrate assumed for the baseline scenario. The values obtained at the 1200-m-long channel segment are very similar to those obtained at channel cross-section 400. This result stands out from those obtained before and is a likely consequence of the fact that, for the two modeled scenarios, channel geometry and initial flow parameters are identical to those adopted in the baseline model. The presence of two unconsolidated lava substrates appears to boost erosion rates values without significantly modifying their spatial distribution. A noticeable exception to this trend is found at/in the proximity of bend 1 axis and concerns erosion minima, especially those at the two channel banks. For the “unconsolidated 1” and “unconsolidated 2” scenarios, the ratios obtained from erosion minima at the left bank of the 1200-m-long channel (1.85 and 2.54, respectively) are lower than those calculated from erosion minima at the left bank of cross-section 400 (1.92 and 2.63, respectively). Also, the ratios obtained from right bank minima are identical for the “unconsolidated 1” scenario whereas they differ for the scenario involving a substrate with lower melting temperature and density. In contrast, bank maxima values are similar if not identical for both scenarios.

Table 2.6e. Sensitivity of baseline model results to changes in substrate thermal and mechanical properties: results are shown for two unconsolidated substrates with thermal and mechanical properties analogous to those of granular regolith (*Colozza*, 1990; *Richter et al*., 1993).

Obtained Erosion Rates	$Ratio_{all\_channel}$ (unconsol_1/BM)	$Ratio_{400}$ (unconsol_1/BM)	$Ratio_{all\_channel}$ (unconsol_2/BM)	$Ratio_{400}$ (unconsol_2/BM)
	#	#	#	#
Max E.R. bed	1.92	1.91	2.63	2.62
Min E.R. bed	1.92	1.90	2.58	2.58
Max E.R. left bank	1.93	1.92	2.63	2.63
Min E.R. left bank	1.85	1.92	2.54	2.63
Max E.R. right bank	1.93	1.92	2.63	2.63
Min E.R. right bank	1.92	1.92	2.58	2.62

Sensitivity analysis – Variations in rille geometry

The second part of the sensitivity analysis is concerned with quantifying the sensitivity of BM results to changes in the observed geometry of the Vallis Schröteri inner rille. The availability of LROC NAC high-resolution images allows for extraction of measurements at this lunar site. The values of meander amplitude, meander wavelength and rille width that are adopted were averaged over several measurements performed over the entire rille path (from source to terminus).

Sensitivity of BM results to changes in meander amplitude

In this section, we explore the impact of meander geometry on flow conditions and, hence, erosion rates distribution at the 1200-m-long channel and, locally, at cross-section 400. At the Vallis Schröteri inner rille, meander amplitude appears to be mostly bimodal because it does not vary with continuity over the entire lava channel. Goose-neck meanders are abundant and characterized by amplitude values of several hundred meters. That said,

a careful inspection of those meanders reveals that they likely formed in response to the presence of obstacles in the channel. Probably, those obstacles compelled the flow to follow a highly meandering path, which resulted in the generation of the observed goose-neck shape. Because of this, this section does not account for those extreme meander amplitudes and, instead, explores how a variation in amplitude within 50-100 m of the 300 m BM value affects erosion rates magnitude and distribution. Fig. 2.21 shows a 1200-m-long channel with meander amplitude 2A = 250 m, i.e., 50 m lower than that adopted in the baseline model.

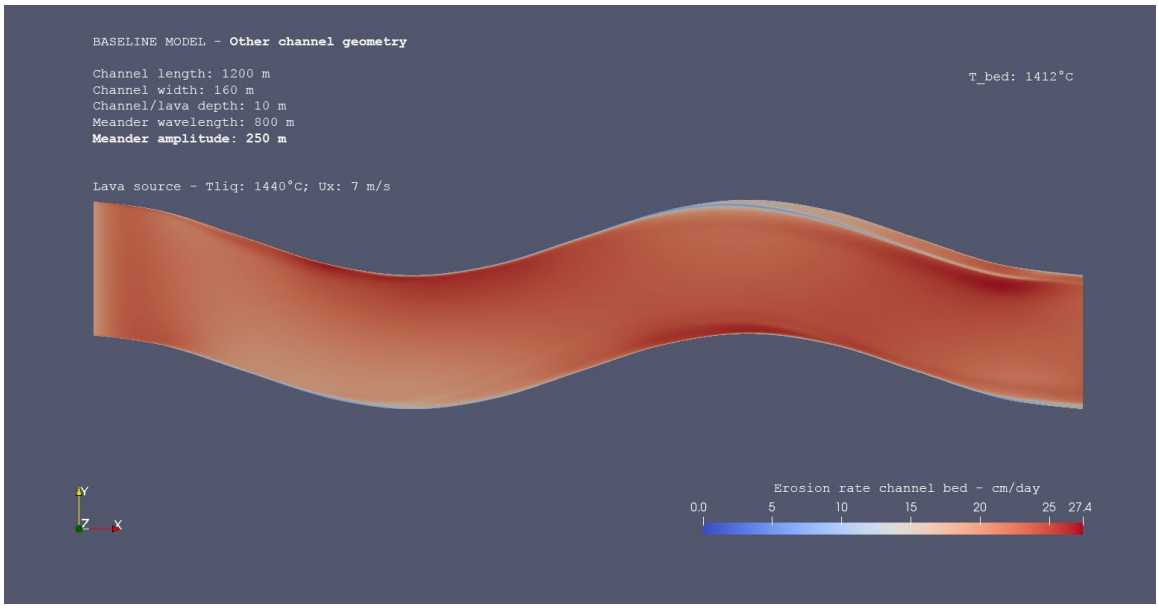

Figure 2.21. Erosion rates at the channel bed for a 1200-m-long channel with meander amplitude 2A = 250 m (50 m lower than that adopted in the baseline model). Meanders are more flattened compared to their BM shape and meander wavelength is held the same as in the baseline model (800 m). All other flow parameters are also held the same as in the baseline model.

Table 2.7a shows that most erosion maxima and minima are shifted downstream of their BM locations, except for the minimum erosion rate at the left bank and the right bank maximum that are shifted upstream by 791 and 2 m, respectively. The left bank maximum

occurs at a location that is very close to bend 2 axis and the bed minimum and right bank maximum are found at the same place in the channel, i.e., ~131 m upstream of bend 2 axis. In the baseline model, the bed minimum and right bank maximum are too in the same place, though upstream (38 m) of the location reported here.

Table 2.7a. Sensitivity of baseline model (BM) results to changes in meander amplitude (2A = 250 m instead of 300 m in BM). The table illustrates maximum and minimum erosion rates at the channel bed and banks. All other flow BM parameters are unchanged.

SENSITIVITY OF BM RESULTS TO CHANGES IN MEANDER AMPLITUDE – 2A = 250 m. Erosion rates at channel bed and banks			
Obtained Erosion Rates (ER)	Erosion Rate Values	Distance from lava source	Location in the channel
description	cm/day	m	description
Max ER bed	27.5	1096.1	bend 2, 296.1 m downstream of bend axis, ~25 m from right bank.
Min ER bed	1.1	668.6*	bend 2, 131.4 m upstream of bend axis, bed/right bank.
Max ER left bank	28.5	773.5	bend 2, 26.5 m upstream of bend axis, bank top.
Min ER left bank	1.4	256.9	bend 1, 256.9 m downstream of bend axis (inlet), left bank/bed.
Max ER right bank	25.4	292.2	bend 1, 292.2 m downstream of bend axis (inlet), 3.5 m down from bank top.
Min ER right bank	1.1	668.6*	bend 2, 131.4 m upstream of bend axis, right bank/bed.

Table 2.7b shows the erosion rate distribution at cross-section 400. The maximum erosion at the bed (24.6 cm/day) is lower than that obtained from the baseline model (28.8 cm/day). Fig. 2.22 also reveals that the maximum is located at a horizontal distance of ~10 m from the right bank (instead of 6 m in BM). The minimum value of 7.3 cm/day is found within ~1 m of the left bank and is higher than its BM counterpart (5 cm/day). At the bed/right

bank contact, a minimum of 7.4 cm/day is found, which is lower than that obtained from BM (9 cm/day). The fluctuations in erosion rate values that are typically seen in the proximity of the left bank are absent here.

Table 2.7b. Sensitivity of baseline model (BM) results to changes in meander amplitude (2A = 250 m instead of 300 m as in BM). The table illustrates maximum and minimum erosion rates at a channel cross-section located 400 m downstream of the lava source and cut along bend 1 trough (see Fig. 2.2a). All other flow BM parameters are unchanged.

SENSITIVITY OF BM RESULTS TO CHANGES IN MEANDER AMPLITUDE – 2A = 250 m. Erosion rates at channel Cross-Section (CS) 400 m			
Obtained Erosion Rates (ER)	Erosion Rate Values	Distance from lava source	Location in channel CS
Description	cm/day	m	description
Max E.R. $bed_{\_400}$	24.6	400.0	~10 m from right bank
Min E.R. $bed_{\_400}$	7.3	400.0	~1 m from left bank
Max E.R. left $bank_{\_400}$	18.3	400.0	bank top
Min E.R. left $bank_{\_400}$	7.3	400.0	left bank/bed
Max E.R. right $bank_{\_400}$	22.9	400.0	bank top
Min E.R. right $bank_{\_400}$	7.4	400.0	right bank/bed

At the bed of cross-section 400, erosion rates are lower than those found over the entire channel segment and lower than their BM counterparts. At the left bank, Fig. 2.23a shows that the maximum erosion rate of 18.3 cm/day is much higher than its BM counterpart (10.3 cm/day) and is found at the bank top (in BM, it was found at a vertical distance of ~4-2 m from the underlying bank/bed contact). Moving from the bank top downward, erosion rates decrease faster and faster as the vertical distance from the contact decreases until they reach a value of 7.3 cm/day at the contact itself. The fastest drop in erosion rate values occurs within ~2 m of the bank/bed contact. At the right bank, Fig. 2.23b shows a maximum erosion rate of 22.9 cm/day that is lower than the 24.4 cm/day BM value though is still

located at the bank top as in BM. Erosion rates decrease at a progressively faster pace as the vertical distance from the underlying bank/bed contact becomes shorter, and reach a minimum value of 7.3 cm/day at the bank/bed contact. As usual, the fastest drop in erosion rate values occurs within ~2 m of the contact itself.

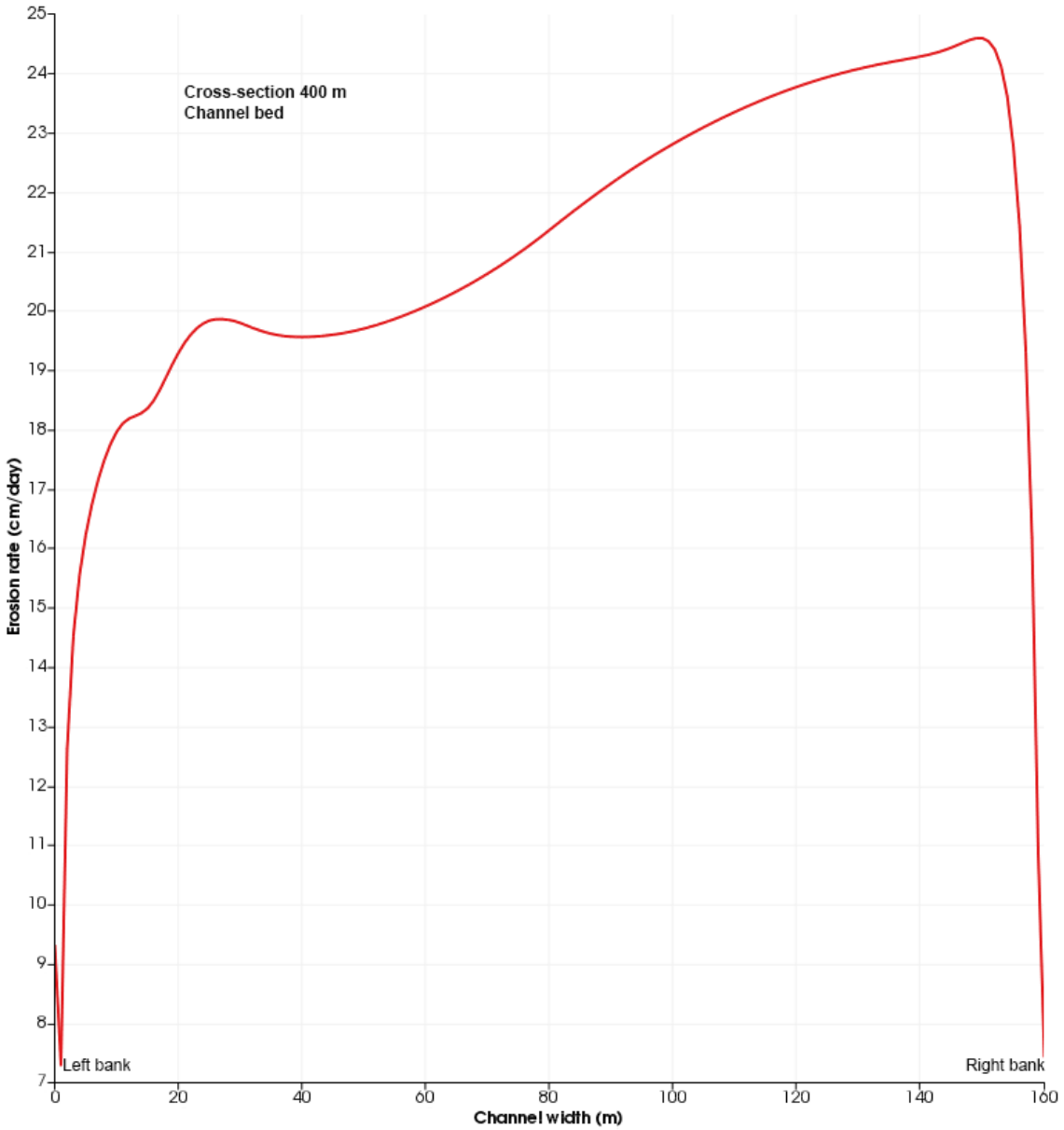

Figure 2.22. Erosion rates at the channel bed for cross-section 400. The case for a lower meander amplitude (2A = 250 m). The maximum value of 24.6 cm/day is lower than that obtained from the baseline model (28.8 cm/day). It is at a horizontal

distance of ~10 m from the right bank (instead of 6 m in BM). The minimum value of 7.3 cm/day is found within ~1 m of the left bank and is higher than its BM counterpart (5 cm/day). At the bed/right bank contact, a minimum of 7.4 cm/day is found, which is lower than that obtained in BM (9 cm/day).

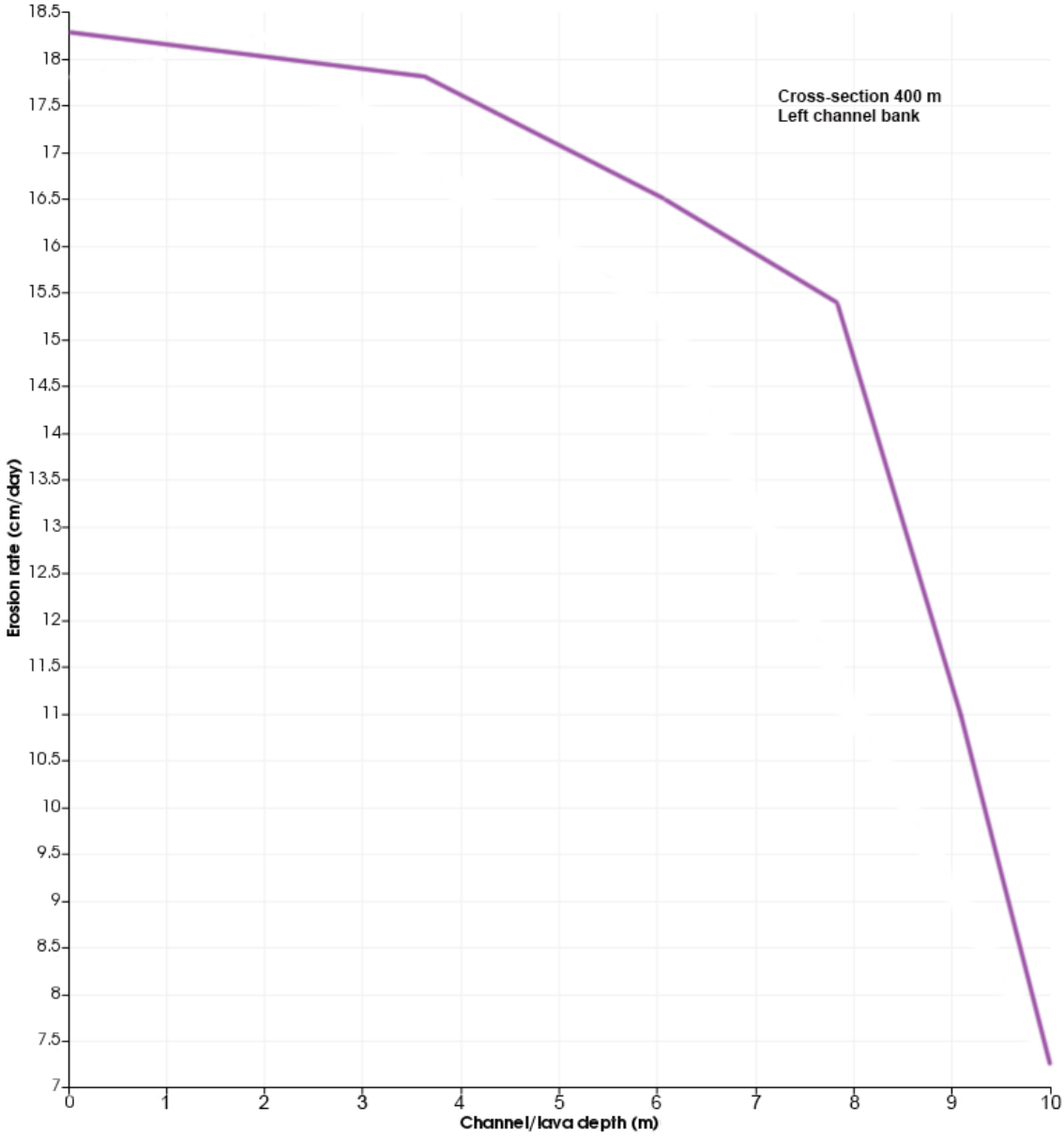

Figure 2.23a. Erosion rates at the left bank for cross-section 400. The case for a lower meander amplitude (2A = 250 m). The maximum erosion rate of 18.3 cm/day is much higher than its BM counterpart (10.3 cm/day) and is found at the bank top (in BM, it was at a vertical distance of ~4-2 m from the underlying bank/bed contact). Moving from the bank top downward, erosion rates fast increase as distance from the contact becomes shorter, and reach a value of 7.3 cm/day at the bank/bed contact. The fastest decrease occurs within 2 m of contact.

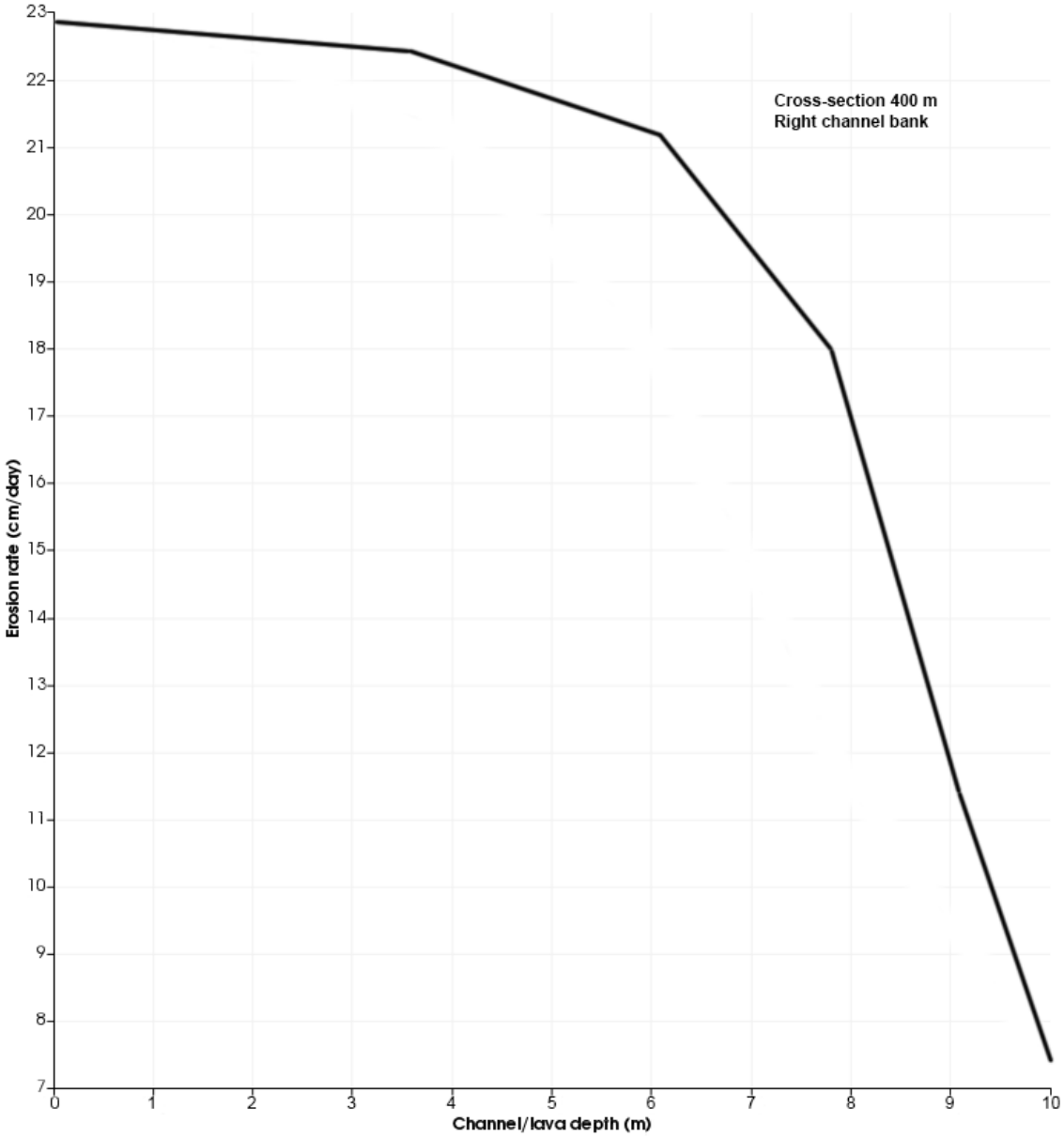

Figure 2.23b. Erosion rates at the right bank for cross-section 400. The case for a lower meander amplitude (2A = 250 m). The maximum erosion rate of 22.9 cm/ day is lower than the 24.4 cm/day BM value and is located at the bank top as in BM. Erosion rates decrease at a progressively faster pace as the vertical distance from the bank/bed contact becomes smaller, and reach a minimum value of 7.3 cm/day (lower than the 8.9 cm/day BM value) at the bank/bed contact. The fastest drop in erosion rate values occurs within ~2 m of the contact itself.

Table 2.7c shows how erosion rates vary for a channel with meander amplitude equal to 400 m (100 m higher than in the baseline model). All erosion maxima and minima are shifted upstream of their BM locations, except for the bed maximum that is shifted ~510 m downstream of its BM location and the right bank maximum that occupies the same place. The bed maximum is very close to bend 2 axis (9 m downstream of that location) and this scenario is the first (among those considered up to this moment) for which there are no two maxima or minima that are located at the same place in the channel. The maximum bank erosion is found at the right bank (38.4 cm/day versus 28.2 cm/day at the right bank). Noticeably, maxima of erosion at the bed (37.5 cm/day) and right bank (38.4 cm/day) are much higher than those found in the baseline and lower meander amplitude scenarios. At the bed and right bank, erosion rates are a factor of ~1.3 higher than their BM values of 29.1 and 29.6 cm/day, respectively. Erosion minima at the bed and left bank are much lower than their BM counterparts (0.1 versus 1.2-1.3 cm/day). In contrast, the minimum at the right bank is identical to the BM value.

Table 2.7c. Sensitivity of baseline model (BM) results to changes in meander amplitude (2A = 400 m instead of 300 m in BM). The table illustrates maximum and minimum erosion rates at the channel bed and banks. All other flow BM parameters are unchanged.

SENSITIVITY OF BM RESULTS TO CHANGES IN MEANDER AMPLITUDE – 2A = 400 m. Erosion rates at channel bed and banks			
Obtained Erosion Rates (ER)	Erosion Rate Values	Distance from lava source	Location in the channel
description	cm/day	m	Description
Max ER bed	37.5	809.0	bend 2, 9.0 m downstream of bend axis, within 5 m of left bank.
Min ER bed	0.1	388.8	bend 1, 388.8 m downstream of bend axis (inlet), bed/left bank.

Max ER left bank	28.2	91.4	bend 1, 91.4 m downstream of bend axis (inlet), 7.8 m from bank top.
Min ER left bank	0.1	393.3	bend 1, 393.3 m downstream of bend axis (inlet), left bank/bed.
Max ER right bank	38.4	294.0	bend 1, 294.0 m downstream of bend axis (inlet), bank top.
Min ER right bank	1.3	616.3	bend 2, 183.7 m upstream of bend axis, right bank/bed.

By looking at the erosion rate distribution at channel cross-section 400 (Table 2.7d), we see that the maximum erosion at the bed (see also Fig. 2.24) is much higher than the BM value (37.1 versus 28.8 cm/day). Moreover, it is located at a horizontal distance of ~12 m from the right bank (instead of 6 m in BM).

Table 2.7d. Sensitivity of baseline model (BM) results to changes in meander amplitude (2A = 400 m instead of 300 m as in BM). The table illustrates maximum and minimum erosion rates at a channel cross-section located 400 m downstream of the lava source and cut along bend 1 trough (see Fig. 2.2a). All other flow BM parameters are unchanged.

SENSITIVITY OF BM RESULTS TO CHANGES IN MEANDER AMPLITUDE – 2A = 400 m. Erosion rates at channel Cross-Section (CS) 400 m			
Obtained Erosion Rates (ER)	Erosion Rate Values	Distance from lava source	Location in channel CS
description	cm/day	m	Description
Max E.R. $bed_{\_400}$	37.1	400.0	~12 m from right bank
Min E.R. $bed_{\_400}$	0.8	400.0	~1 m from left bank
Max E.R. $left\ bank_{\_400}$	1.7	400.0	6.1 m from bank top
Min E.R. $left\ bank_{\_400}$	0.8	400.0	left bank/bed
Max E.R. $right\ bank_{\_400}$	25.6	400.0	6.1 m from bank top
Min E.R. $right\ bank_{\_400}$	12.3	400.0	right bank/bed

The minimum bed erosion of 0.8 cm/day is found within ~1 m of the left bank and is much lower than its BM counterpart (5 cm/day). At the bed/right bank contact, a minimum of

12.3 cm/day is found (see also Fig. 2.25b), which is higher than that obtained in BM (9 cm/day). Fig. 2.24 displays a peak in erosion rates at a horizontal distance of ~55 m from the left bank, which was absent in previous scenarios. Besides, the fluctuations in erosion rate usually seen within 10 m of the bed/left bank contact are absent here. A totally different trend is observed at the left bank (Fig. 2.25a). Here, the maximum erosion rate of 1.7 cm/day is much lower than its BM counterpart (10.3 cm/day) and is located at the bank top. In the baseline model, it was found at a vertical distance of ~4 m from the underlying bank/bed contact. Moving downward from the bank top, erosion rates decrease until they reach a value of 0.09 cm/day at the bank/bed contact.

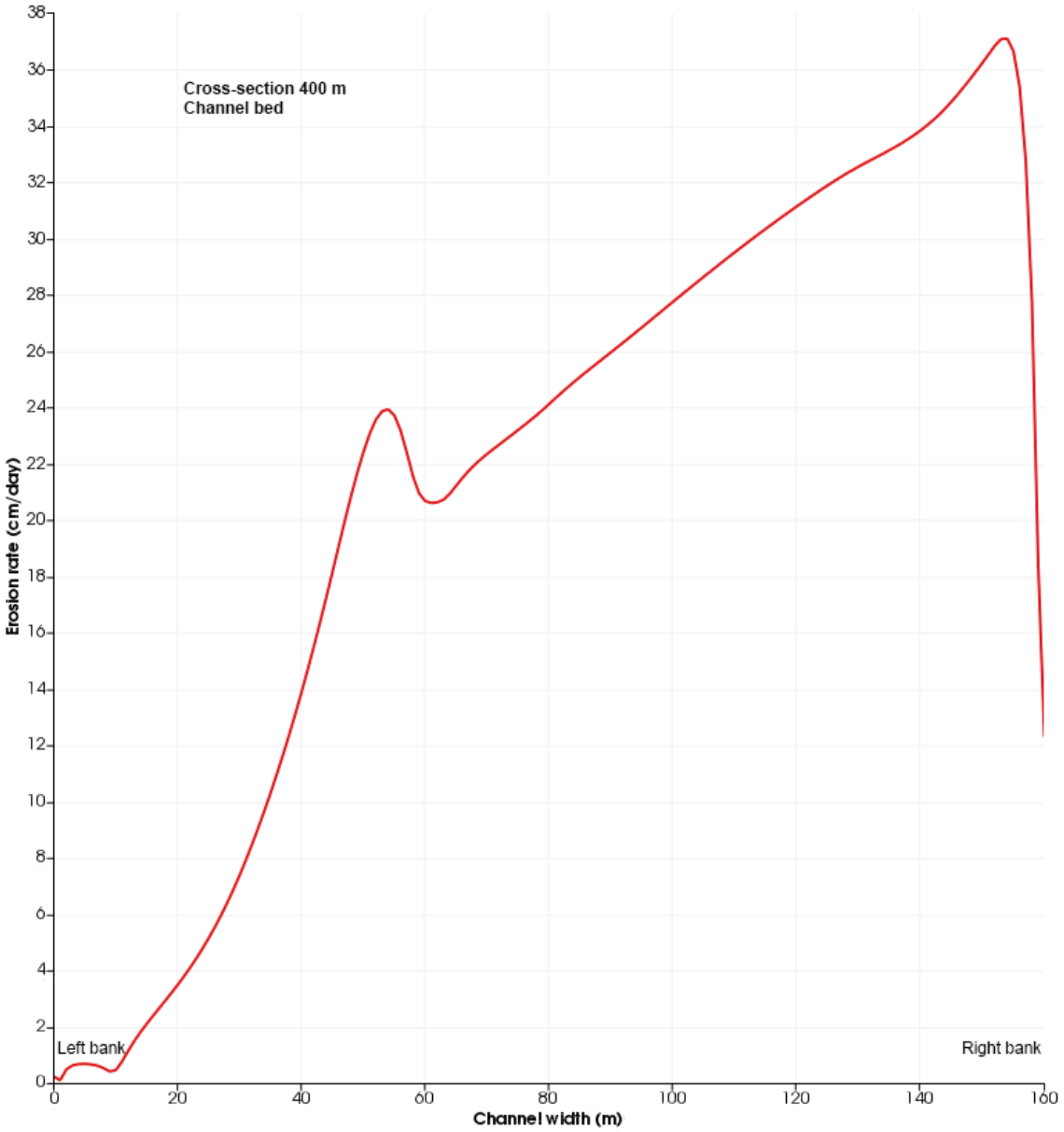

Figure 2.24. Erosion rates at the channel bed for cross-section 400. The case for a higher meander amplitude (2A = 400 m). The maximum value of 37.1 cm/day is much higher than that obtained from the baseline model (28.8 cm/day). Moreover, it is located at a horizontal distance of ~12 m from the right bank (instead of 6 m in BM). The minimum value of 0.8 cm/day is found within ~1 m of the left bank and is much lower than its BM counterpart (5 cm/day). At the bed/ right bank contact, a minimum of 12.3 cm/day is found, which is higher than that obtained in BM (9 cm/day). The peak in erosion rates at a horizontal distance of ~50 m from the left bank is absent in previous scenarios. Besides, the fluctuations in erosion rate usually seen within 10 m of the left bank are absent here.

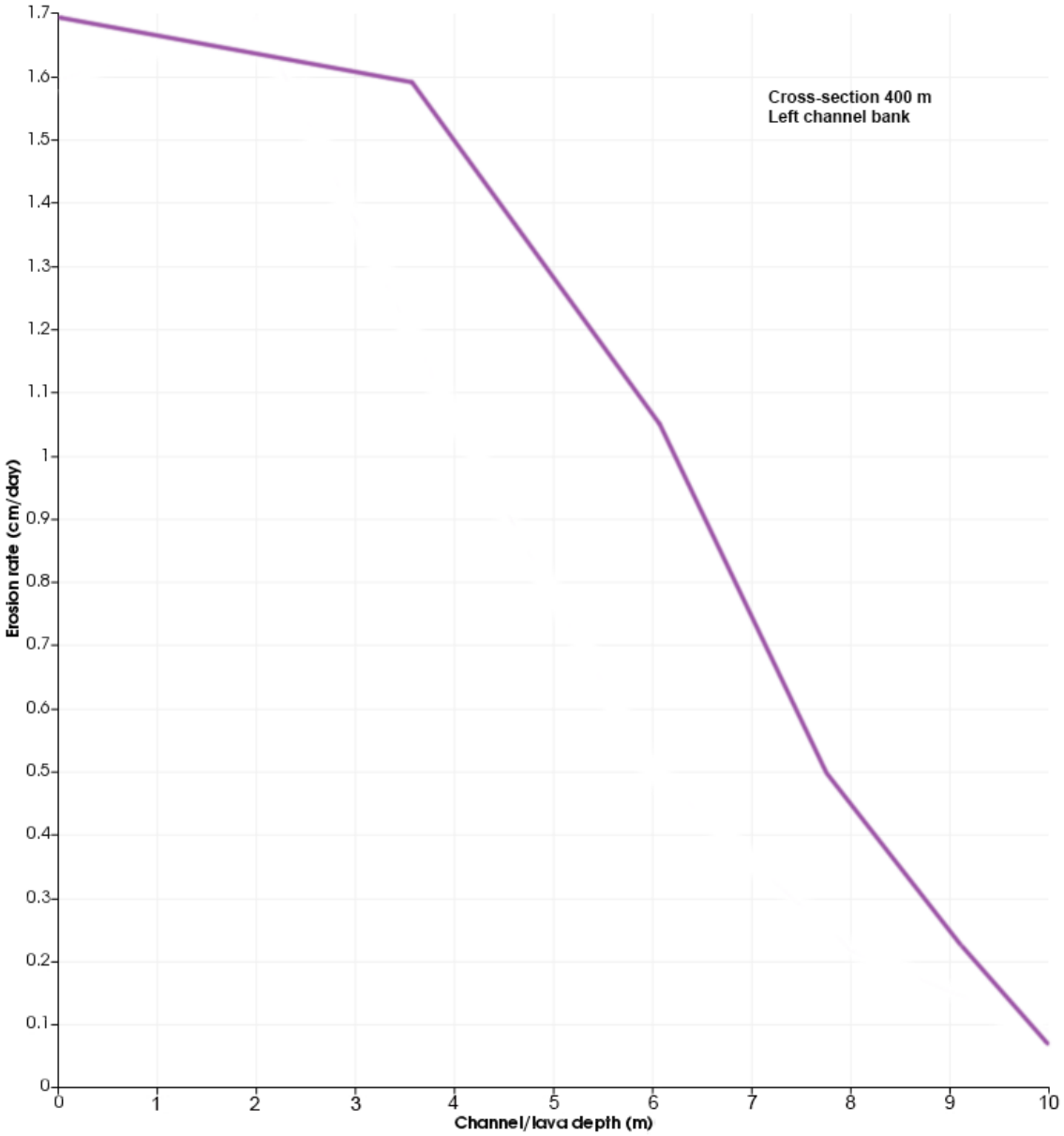

Figure 2.25a. Erosion rates at the left bank for cross-section 400. The case for a higher meander amplitude (2A = 400 m). The maximum erosion rate of 1.7 cm/ day is much lower than its BM counterpart (10.3 cm/day) and – in contrast to BM where is found at a vertical distance of ~4 m from the bank/bed contact – is located at the bank top. From the bank top, erosion rates decrease initially slowly and then rapidly until they reach a value of ~0.09 cm/day at the bank/bed contact. The sharpest drop in erosion rates occurs within 4-2 m of the bank/bed contact.

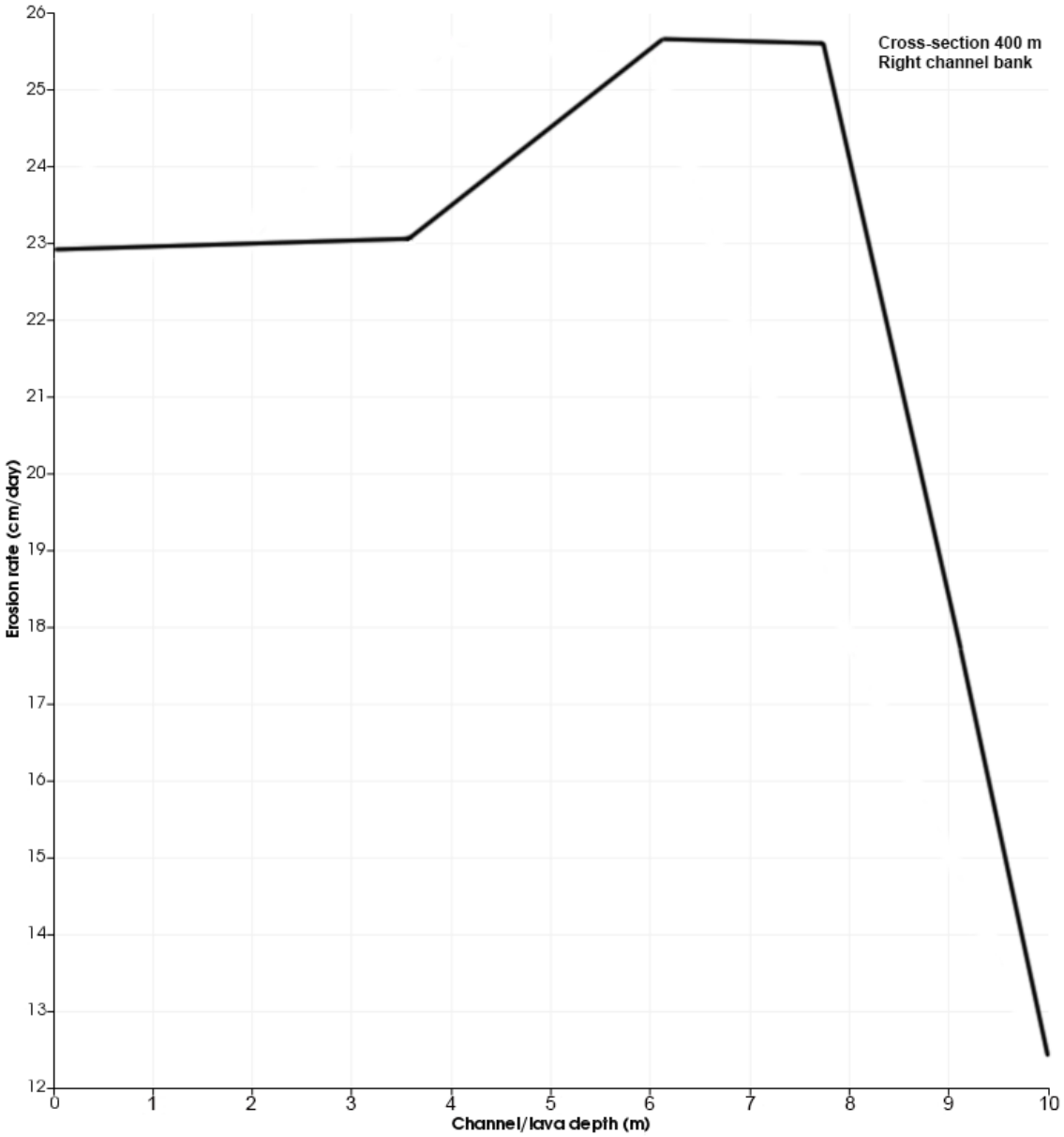

Figure 2.25b. Erosion rates at the right bank for cross-section 400. The case for a higher meander amplitude (2A = 400 m). The maximum erosion rate of 25.6 cm/day is higher than the 24.4 cm/day BM value and higher than that associated with the low meander amplitude scenario. Instead of occurring at the bank top (as in BM), the maximum is located at a vertical distance of 4-2 m from the underlying bank/bed contact. At the bank top, an erosion rate of 22.9 cm/day is measured. While moving down the bank, values increase until they reach the 25.6 cm/day maximum. At that point, erosion rates drop to a minimum of 12.3 cm/day (higher than the 8.9 cm/day BM value) at the contact.

At the right bank (Fig. 2.25b), the maximum erosion rate of 25.6 cm/day is higher than the 24.4 cm/day BM value and instead of being found at the bank top (as in BM) is located at a vertical distance of ~4 m from the underlying bank/bed contact. At the bank top, an erosion rate of 22.9 cm/day is measured. While moving down the bank, values increase until they reach the 25.6 cm/day maximum. At that point, erosion rates level off and then drop and reach a minimum of 12.3 cm/day (higher than the 8.9 cm/day BM value) at the contact itself.

How meander amplitude-modified results compare with BM results

Table 2.7e illustrates ratios of erosion maxima and minima at the 1200-m-long channel and cross-section 400. Ratios that refer to the modified version of the baseline model that adopts a value of meander amplitude equal to 250 m are both < 1 and > 1. What stands out is the pattern observed at the left bank in contrast to the results obtained elsewhere in the channel. At the left bank, ratios are always greater than 1 - even as high as 1.5 and 1.8 - except in one case where the value is still very close to 1 (0.99). In stark contrast, any other ratios obtained elsewhere in the channel are in the range between 0.83 and 0.94. At channel cross-section 400, the described trend is more pronounced than at the 1200-m-long rille section. As a result, erosion rates produced by lava flowing within a low-amplitude rille appear to be almost anywhere lower than those obtained from the baseline model, except at the left bank. This trend underlines a fluid- and thermodynamic complexity that will be revealed and explained in the theorethical study section of Chapter 5. For a scenario in which meander amplitude is higher (here 2A = 400 m) than the 300 m

baseline value, an almost opposite trend is found. Ratios greater than 1 are found at the bed and right bank whereas those calculated at the left bank are always much lower than 1 (0.16) and even approaching 0 (minimum of erosion at the left bank of the 1200-m-long channel). At cross-section 400, the ratio obtained from bed erosion maxima (1.29) is identical to that found at the 1200-m-long channel, and the maximum of erosion at the right bank is lower than its longer channel counterpart value (1.30). Furthermore, erosion minima at the bed and left bank are very low and identical to those found at the long channel segment. These results show that a lava that flows within a rille with meanders of high amplitude produces erosion rates at the bed and right bank, which are much higher than those generated by an analogous lava that flows within a channel with meanders of lower amplitude. This is a very important result that might have impacted rille evolution in time, as discussed in Chapter 6.

Table 2.7e. Sensitivity of baseline model results to changes in initial channel geometry: changes in meander amplitude, amplitude ratios.

Obtained Erosion Rates	$Ratio_{all\_channel}$ (2A = 250 m/BM)	$Ratio_{400}$ (2A = 250 m/BM)	$Ratio_{all\_channel}$ (2A = 400 m/BM)	$Ratio_{400}$ (2A = 400 m/BM)
	#	#	#	#
Max E.R. bed	0.94	0.85	1.29	1.29
Min E.R. bed	0.92	1.5	0.08	0.16
Max E.R. left bank	0.99	1.8	0.98	0.16
Min E.R. left bank	1.10	1.5	0.08	0.16
Max E.R. right bank	0.86	0.94	1.30	1.05
Min E.R. right bank	0.92	0.83	1.08	1.38

Sensitivity of BM results to changes in meander wavelength

In this section, we first explore how a meander wavelength of 1000 m affects erosion rates at a channel that is now 1450 m long (see Fig. 2.26) and at a channel cross-

section that is cut at a downstream distance of 500 m from the lava source. Once again, channel cross-section 500 is designed in such a way to pass through bend 1 trough.

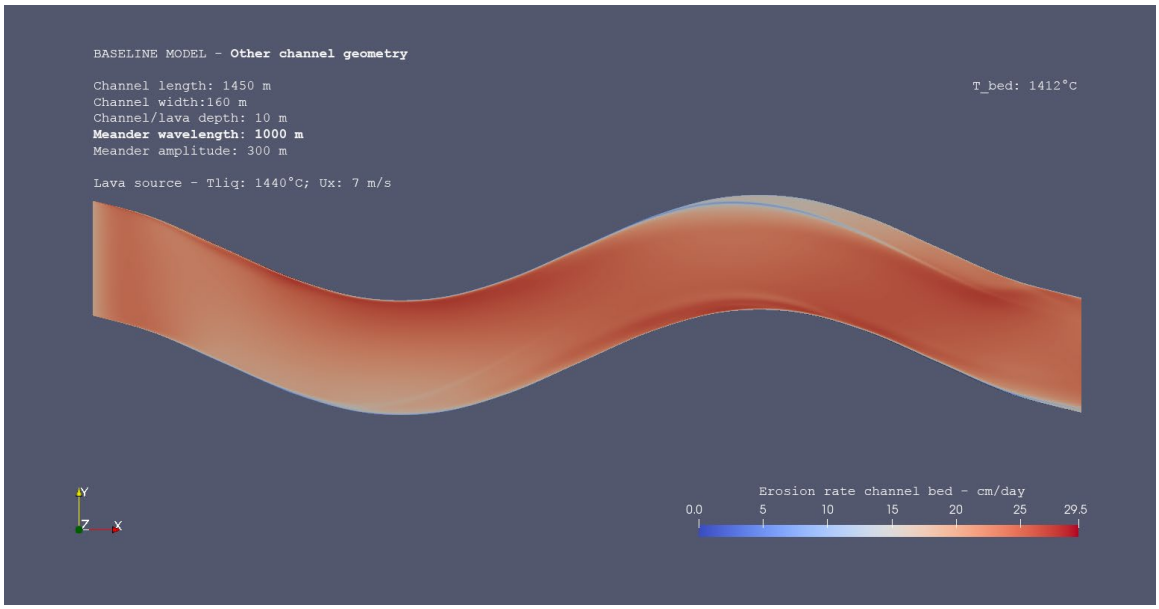

Figure 2.26. Erosion rates at the channel bed for a 1450-m-long channel with meander wavelength λ = 1000 m (200 m longer than that adopted in the baseline model). Meanders appear more flattened compared to their BM shape though meander amplitude is held the same as in the baseline model (300 m). All other flow parameters are held the same as in the baseline model.

Table 2.8a shows that all erosion maxima and minima (except for the left bank minimum) are shifted downstream of their BM locations by 43-744 meters. No erosion maximum or minimum is really close to a bend axis and the nearest of all to a bend is the left bank maximum that is located ~54 m upstream of bend 2 axis. Similar to the baseline model, the erosion minima at the bed and the right bank are found at the same place in the channel, though here they are 175 m downstream of their BM location. For the 1450-m-long channel, the maximum erosion rate at the bed is a bit lower than its baseline model counterpart (27.3 cm/day versus 29.1 cm/day). The maximum bank erosion occurs at the left bank (29.5

cm/day) and not at the right bank (28.2 cm/day) as for the BM. Erosion minima have values that are almost identical to those in the baseline model.

Table 2.8a. Sensitivity of baseline model (BM) results to changes in meander wavelength (λ = 1000 m instead of the 800 m BM value). Channel length is 1450 m. The table illustrates maximum and minimum erosion rates at the channel bed and banks. All other flow BM parameters are unchanged.

SENSITIVITY OF BM RESULTS TO CHANGES IN MEANDER WAVELENGTH – λ = 1000 m. Channel length = 1450 m. Erosion rates at channel bed and banks			
Obtained Erosion Rates (ER)	Erosion Rate Values	Distance from lava source	Location in the channel
description	cm/day	m	description
Max ER bed	27.3	343.1	bend 1, 343.1 m downstream of bend axis (inlet), within ~5 m of right bank.
Min ER bed	1.2	806.1*	bend 2, 193.9 m upstream of bend axis, bed/right bank.
Max ER left bank	29.5	946.2	bend 2, 53.8 m upstream of bend axis, bank top.
Min ER left bank	1.3	304.4	bend 1, 195.6 m upstream of bend trough, left bank/bed.
Max ER right bank	28.2	337.3	bend 1, 162.7 m upstream of bend trough, 6.1 m from bank top.
Min ER right bank	1.3	806.1*	bend 2, 193.9 m upstream of bend axis, right bank/bed.

Table 2.8b shows erosion rates magnitude and distribution at channel cross-section 500. The maximum erosion at the bed is lower than its BM counterpart (26.7 cm/day versus 28.8 cm/day). The maximum is reached at ~10 m from the bed/right bank contact and the minimum is found within 1 m of the left bank. The bank maximum is found at the right bank (as for the BM) but its magnitude is lower than the BM one (19.5 cm/day versus 24.4 cm/day).

Table 2.8b. Sensitivity of baseline model (BM) results to changes in meander wavelength (λ = 1000 m instead of the 800 m BM value). The table illustrates maximum and minimum erosion rates at a channel cross-section located 500 m downstream of the lava source and cut along bend 1 trough (see Fig. 2.2a). All other flow BM parameters are unchanged.

SENSITIVITY OF BM RESULTS TO CHANGES IN MEANDER WAVELENGTH – λ = 1000 m. Erosion rates at channel Cross-Section (CS) 500 m			
Obtained Erosion Rates (ER)	Erosion Rate Values	Distance from lava source	Location in channel CS
description	cm/day	m	description
Max E.R. bed_{500}	26.7	500.0	~10 m from right bank
Min E.R. bed_{500}	5.4	500.0	~1 m from left bank
Max E.R. left $bank_{500}$	17.3	500.0	bank top
Min E.R. left $bank_{500}$	5.4	500.0	left bank/bed
Max E.R. right $bank_{500}$	19.5	500.0	bank top
Min E.R. right $bank_{500}$	7.5	500.0	right bank/bed

The left bank maximum (17.3 cm/day) is much higher than its BM counterpart (10.3 cm/day) and is located at the bank top (Fig. 2.27a). From there, erosion rates decrease very slowly down to a vertical distance of ~3.5 m from the bank top. Then, they decrease faster and faster until they reach a minimum value of 5.4 cm/day at the bank/bed contact. Erosion rates drop drastically once the vertical distance of ~2 m from the bank/bed contact is reached. At the right bank (Fig. 2.27b), the maximum erosion rate of 19.5 cm/day (lower than the 24.4 cm/day BM value) is located at the bank top as in BM. Erosion rates decrease very slowly down to a vertical distance of ~4 m from the bank/bed contact where the high value of 18.7 cm/day is found. From that point downward and starting at a vertical distance of ~2 m from the bank/bed contact, erosion rates drop very rapidly and reach a minimum value of 7.5 cm/day at the contact itself.

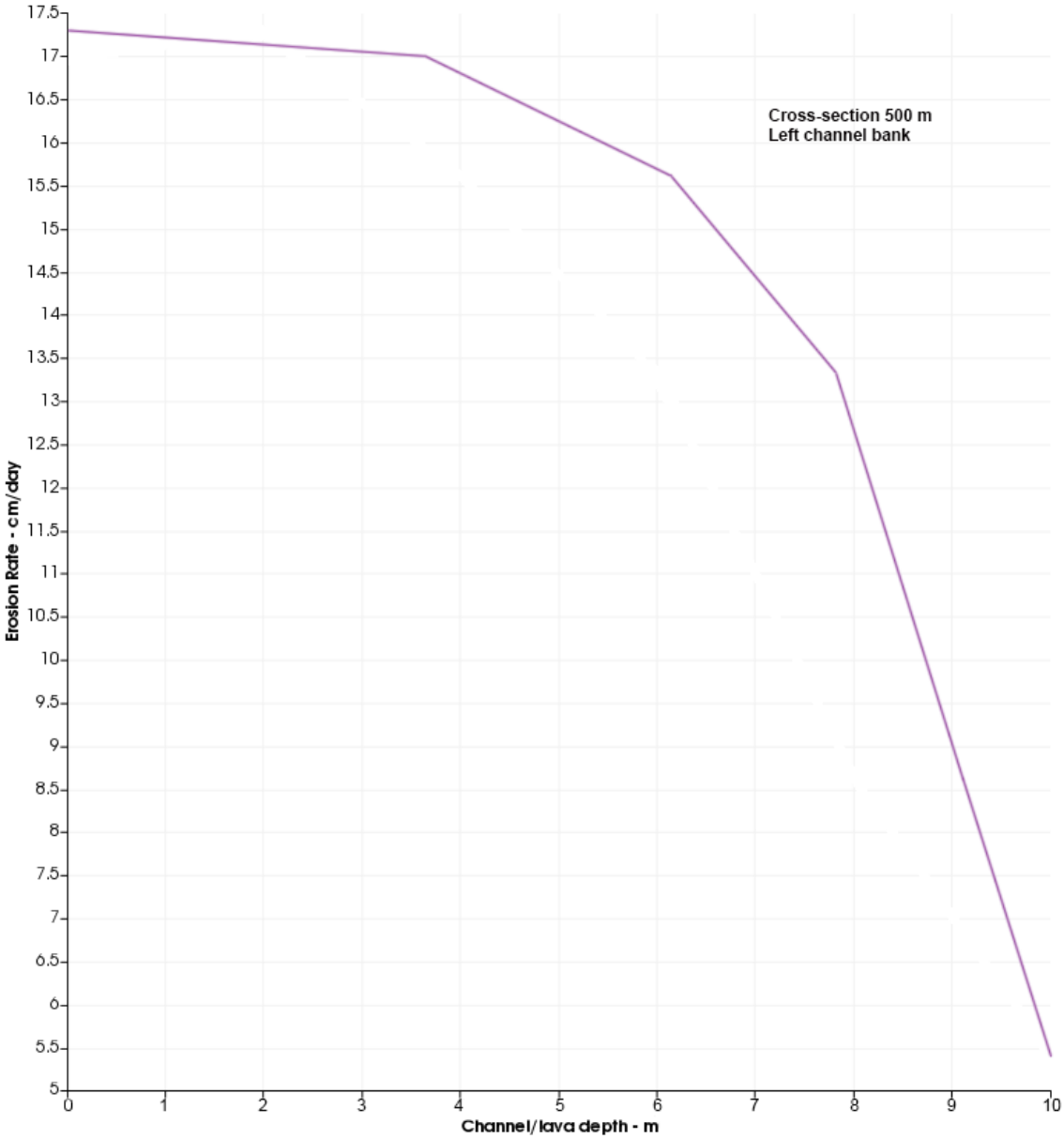

Figure 2.27a. Erosion rates at the left bank for cross-section 400. The case for a longer meander wavelength, λ = 1000 m. The maximum erosion rate of 17.3 cm/ day is much higher than its BM counterpart (10.3 cm/day) and is located at the bank top. From there, erosion rates decrease very slowly down to a vertical distance of ~3.5 m from the bank top. Then, they decrease faster and faster, and reach a minimum value of 5.4 cm/day at the bank/bed contact. Erosion rates drop drastically once the vertical distance of ~2 m from the contact is reached.

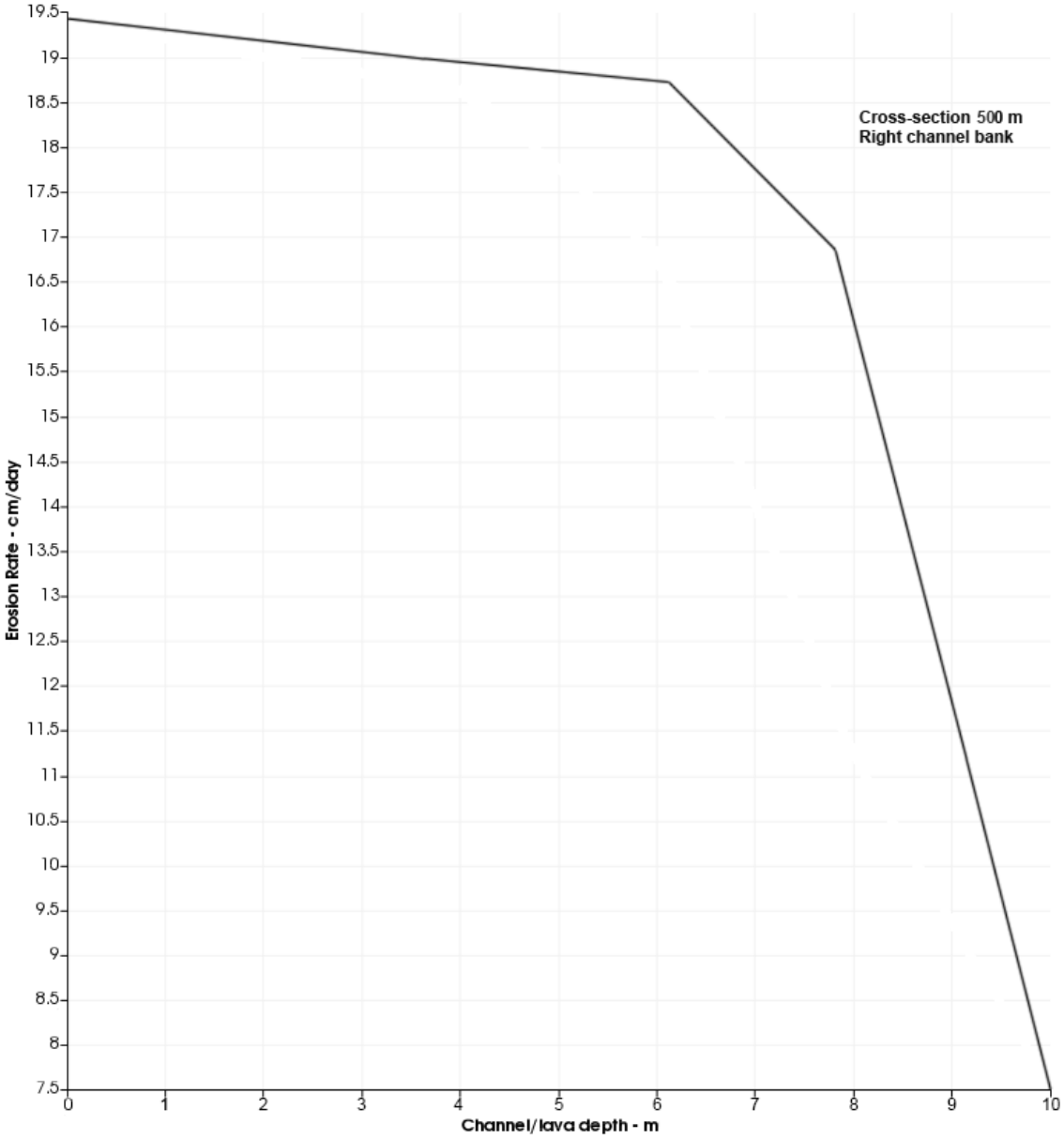

Figure 2.27b. Erosion rates at the right bank for cross-section 400. The case for a longer meander wavelength, λ = 1000 m. The maximum erosion rate of 19.5 cm/ day (lower than the 24.4 cm/day BM value) is located at the bank top as in BM. Erosion rates decrease very slowly down to a vertical distance of ~4 m from the bank/bed contact where the high value of 18.7 cm/day is found. From that point downward and starting at a vertical distance of ~2 m from the bank/bed contact, erosion rates drop very rapidly and reach a minimum value of 7.5 cm/day at the contact itself.

Table 2.8c shows how an even longer meander wavelength, λ = 1200 m, affects erosion rates magnitude and distribution in a channel that is 1500 m long and at a channel cross-section that is cut parallel to bend 1 trough at a downstream distance of 600 m from the lava source.

Table 2.8c. Sensitivity of baseline model (BM) results to changes in meander wavelength (λ = 1200 m instead of the 800 m BM value). Channel length = 1500 m. The table illustrates maximum and minimum erosion rates at the channel bed and banks. All other flow BM parameters are unchanged.

SENSITIVITY OF BM RESULTS TO CHANGES IN MEANDER WAVELENGTH – λ = 1200 m. Channel length = 1500 m. Erosion rates at channel bed and banks			
Obtained Erosion Rates (ER)	Erosion Rate Values	Distance from lava source	Location in the channel
description	cm/day	m	description
Max ER bed	25.8	1175.3	bend 2, 24.7 m upstream of bend axis, 5 m from right bank.
Min ER bed	3.0	974.0*	bend 2, 226.0 m upstream of bend axis, bed/right bank.
Max ER left bank	27.4	1077.3	bend 2, 122.7 m upstream of bend axis, bank top.
Min ER left bank	4.0	381.8	bend 1, 218.2 m upstream of bend trough, left bank/bed.
Max ER right bank	26.7	1500.0	bend 2, 300 m downstream of bend axis, bank top.
Min ER right bank	3.0	974.0*	bend 2, 226.0 m upstream of bend axis, right bank/bed.

All erosion rate maxima and minima (except for the left bank minimum) are shifted downstream of their BM locations by 343-1206 m. The observed trend is very similar to that seen for the channel with λ = 1000 m though each erosion maximum/minimum is shifted farther downstream in the channel with λ = 1200 m. As before, the erosion minima at the bed and right bank are found at the same place in the channel, though the new location

is much farther downstream than the location shown in the λ = 1000 m channel. The erosion maximum at the bed of 25.8 cm/day is lower than that found in the λ = 1000 m channel (27.3 cm/day) and much lower than the one obtained at the baseline channel (29.1 cm/day). It is found at a place in the channel that is close to bend 2 axis (~24.7 m upstream of that). The maximum bank erosion is found at the left bank and is equal to 27.4 cm/day, analogous to what found at the channel with λ=1000 m and different from the baseline model (λ = 800 m), the latter showing maxima of bank erosion at the right bank. Additionally, erosion minima at both banks are higher than their BM counterpart values (3.0-4.0 cm/day versus 1.2-1.3 cm/day). Table 2.8d shows erosion rates magnitude and distribution at channel cross-section 600.

Table 2.8d. Sensitivity of baseline model (BM) results to changes in meander wavelength (λ = 1200 m instead of the 800 m BM value). The table illustrates maximum and minimum erosion rates at a channel cross-section located 600 m downstream of the lava source and cut along bend 1 trough. All other flow BM parameters are unchanged.

SENSITIVITY OF BM RESULTS TO CHANGES IN MEANDER WAVELENGTH – λ = 1200 m. Channel length = 1500 m. Erosion rates at channel Cross-Section 600 m			
Obtained Erosion Rates (ER)	Erosion Rate Values	Distance from lava source	Location in channel CS
description	cm/day	m	description
Max E.R. bed_{600}	24.6	600.0	~12 m from right bank
Min E.R. bed_{600}	6.7	600.0	bed/right bank
Max E.R. left $bank_{600}$	16.5	600.0	2-4 m above bed
Min E.R. left $bank_{600}$	8.2	600.0	left bank/bed
Max E.R. right $bank_{600}$	20.0	600.0	bank top - ~4 m down.
Min E.R. right $bank_{600}$	6.7	600.0	right bank/bed

The maximum erosion rate of 24.6 cm/day at the bed is much lower than the value reported in Table 2.2b (28.8 cm/day, BM, cross-section 400). The left bank maximum is higher than

its BM counterpart (16.5 cm/day versus 10.3 cm/day), whereas the right bank maximum is lower than the BM one (20.0 cm/day versus 24.4 cm/day). The erosion minima at the bed and left bank are also higher than their BM counterpart whereas only the minimum erosion rate at the right bank is lower than that found in BM (6.7 cm/day versus 8.9 cm/day). Fig. 2.28 shows how erosion rates at the bed vary at cross-section 600. The maximum value is located at a horizontal distance of ~12 m from the right bank (instead of 6 m in BM). A low value of 8.2 cm/day is found within ~1 m of the left bank. That said, the minimum erosion rate of 6.7 cm/day is found at the bed/right bank contact, which is also unusual. The minimum value is higher than its BM counterpart (5 cm/day). Finally, while moving toward the left bank, the erosion rate curve does not drop as rapidly as it does in the scenarios seen before, which proves that erosion rates at the left bank are higher than usual. At the left bank (Fig. 2.29a), the maximum of 16.5 cm/day is higher than the value of 10.3 cm/day found at cross-section 400, BM. Besides, it is located at a vertical distance of 4-2 m from the bed. From the bank top (erosion rate of 14.6 m/day) downwards, erosion rates increase steadily till the maximum of 16.5 cm/day is reached. Then, they drop drastically until they reach a minimum value of 8.2 cm/day at the bank/bed contact. At the right bank (Fig. 2.29b), the maximum erosion rate of 20.0 cm/day (lower than the 24.4 cm/day BM value) is located at the bank top as in BM. From that point downwards, erosion rate values level off to a vertical distance of 6.5 m from the bank/bed contact. Then, they start decreasing first slowly and then faster and faster until they drop to a minimum value of 6.7 cm/day at the bank/bed contact. The fastest drop begins at a vertical distance from the contact of ~2 m.

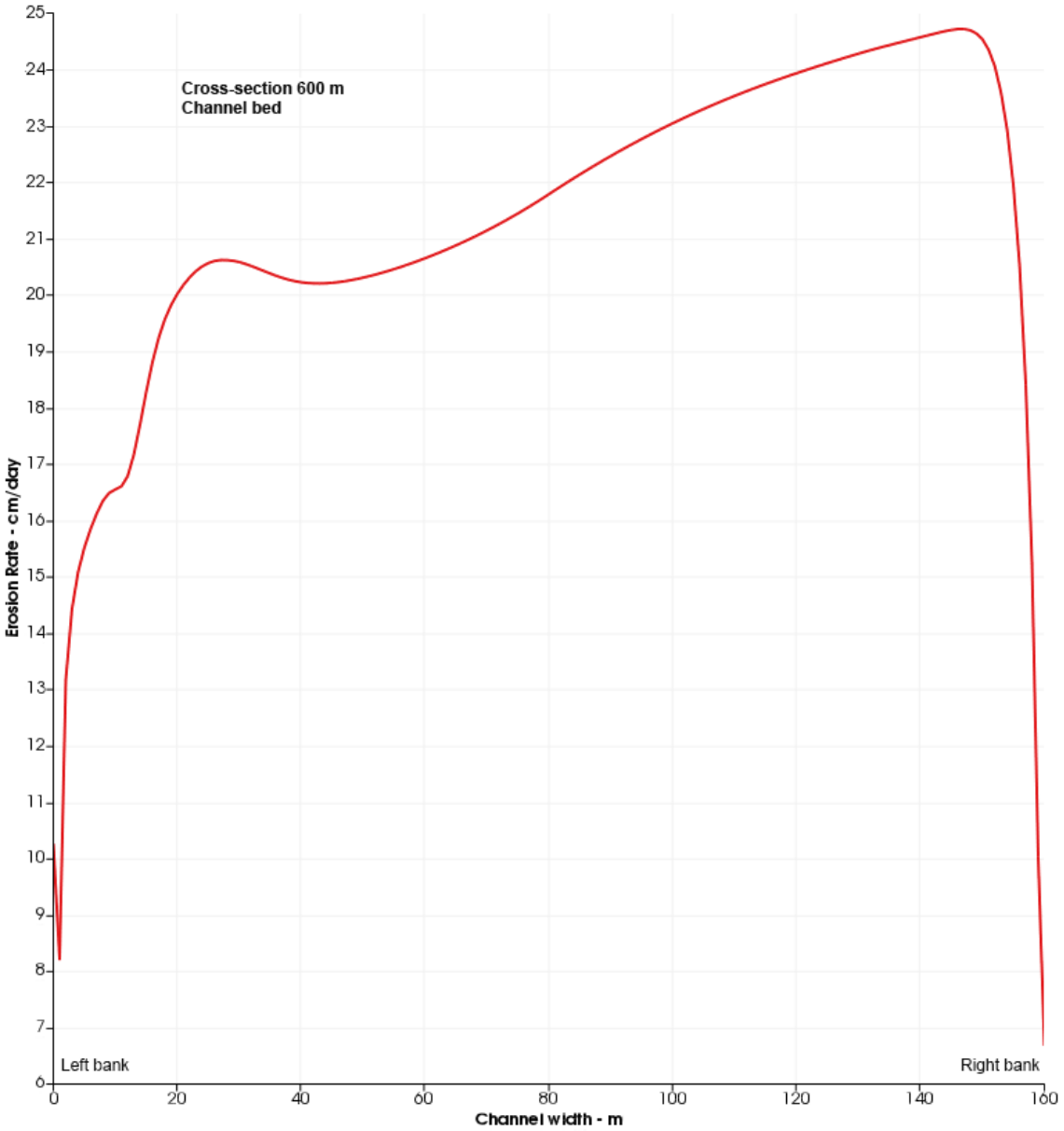

Figure 2.28. Erosion rates at the channel bed for cross-section 400. The case for a longer meander wavelength, λ = 1200 m. The maximum value of 24.6 cm/day is much lower than the value of 28.8 cm/day that refers to BM, cross-section 400. Moreover, it is located at a horizontal distance of ~12 m from the right bank (instead of 6 m in BM). A low value of 8.2 cm/day is found within ~1 m of the left bank. That said, the minimum erosion rate of 6.7 cm/day is found at the bed/right bank contact, which is also unusual. The minimum value is higher than its BM counterpart (5 cm/day). Finally, while moving toward the left bank, the erosion rate curve does not drop as rapidly as it does in the scenarios seen before, which proves that erosion rates at the left bank are higher than usual.

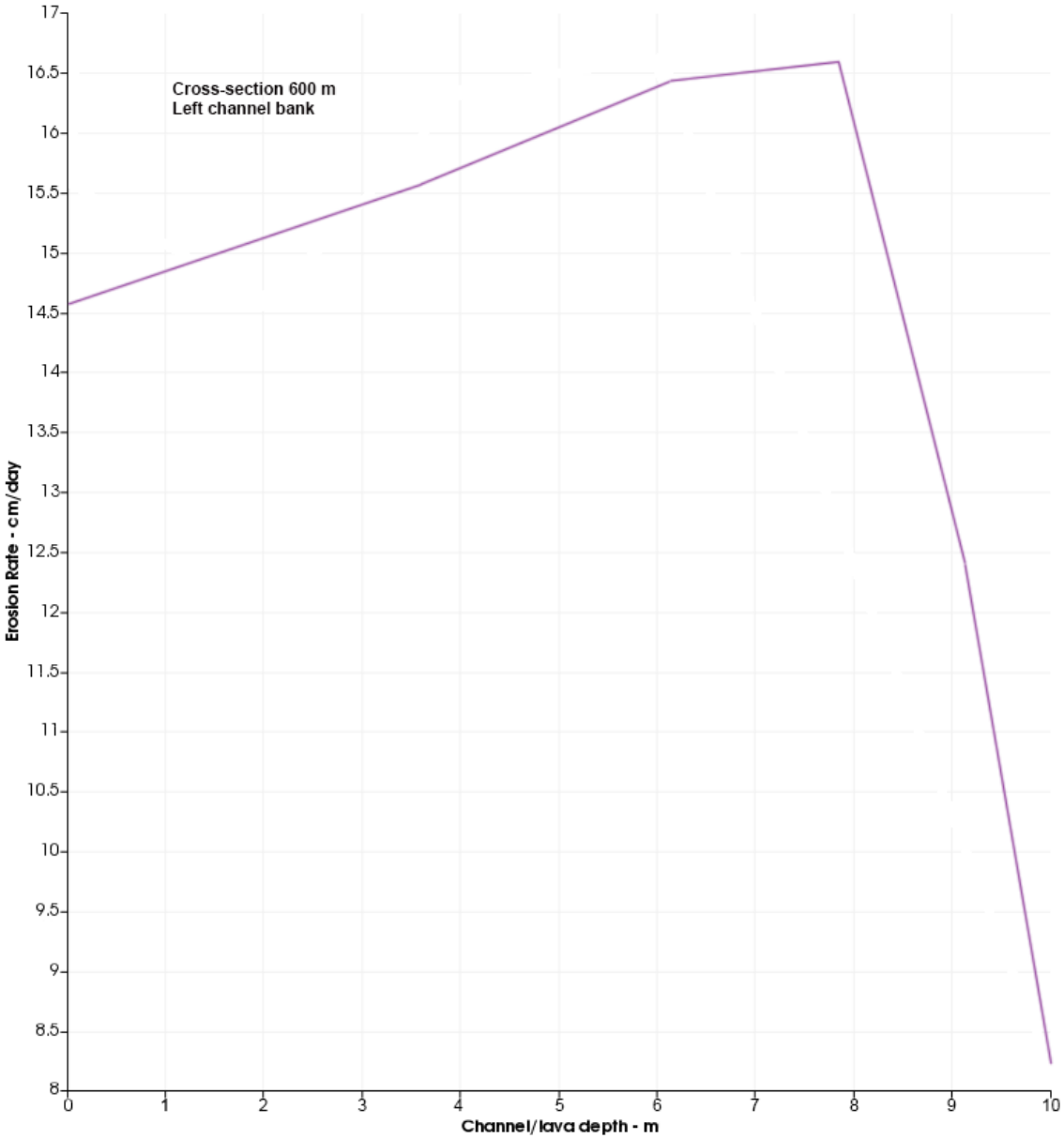

Figure 2.29a. Erosion rates at the left bank for cross-section 400. The case for a longer meander wavelength, λ = 1200 m. The maximum erosion rate of 16.5 cm/day is much higher than its BM counterpart (10.3 cm/day) and is located at a vertical distance of 4-2 m from the bank/bed contact. From the bank top (erosion rate of 14.6 m/day) downwards, erosion rates increase steadily till the maximum of 16.5 cm/day is reached. Then, they drop drastically until they reach a minimum value of 8.2 cm/day at the bank/bed contact.

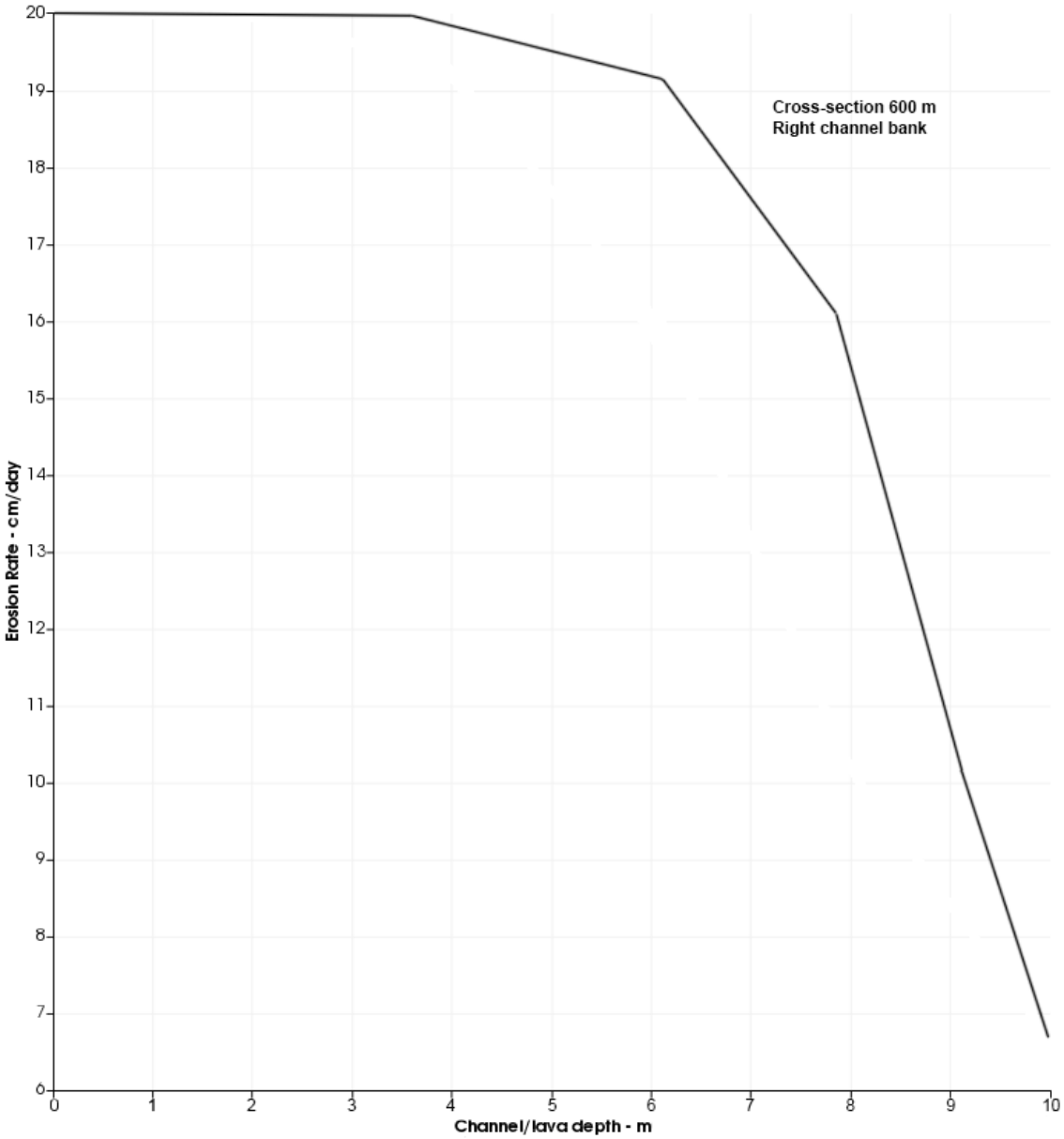

Figure 2.29b. Erosion rates at the right bank for cross-section 400. The case for a longer meander wavelength, λ = 1200 m. The maximum erosion rate of 20.0 cm/ day (lower than the 24.4 cm/day BM value) is located at the bank top as in BM. From that point downwards, erosion rate values level off to a vertical distance of 6.5 m from the bank/bed contact. From that point on, they start decreasing first slowly and then faster and faster until they drop to a minimum value of 6.7 cm/day at the bank/bed contact. The fastest drop begins at a vertical distance from the contact of ~2 m.

How meander wavelength-modified results compare with BM results

Table 2.8e illustrates ratios of erosion maxima and minima obtained at two channels of different length and meander wavelength (λ = 1000 m and 1200 m). Both values of wavelength are longer than the wavelength λ = 800 m adopted in the baseline model. First, we consider a 1450-m-long channel with meander wavelength λ = 1000 m. In this channel, a cross-section is cut parallel to bend 1 trough at a downstream distance of 500 m from the lava source. Ratios obtained from erosion maxima and minima are mostly > 1. Exceptions to this are represented by the ratios obtained from bed erosion maxima (0.94) and right bank erosion maxima (0.95). At channel cross-section 500, ratios are higher than those obtained at the whole channel, except for those calculated from maxima at the bed and minima at the right bank. The observed distribution of erosion rates at the bed and two channel banks explains the ratio distribution in Table 2.8e. The highest ratios are those obtained at channel cross-section 500 and at the left bank, where erosion rates are much higher than their BM counterpart values. Interestingly, at cross-section 400, maximum erosion rates are still found at the right bank in contrast to what found at the 1450-m-long channel where bank erosion maxima are obtained at the left bank. Besides, ratios calculated from minima are always > 1, the only exception being the ratio obtained at cross-section 400 from minima at the right bank. For a 1500-m-long channel of meander wavelength λ = 1200 m, ratios obtained from minima are the highest, with values of 2.50 at the bed and right bank and 3.08 at the left bank. In stark contrast to this, ratios from maxima are all < 1, the lowest value of 0.89 belonging to the bed maximum. At channel cross-section 600, the only ratio (obtained from erosion maxima) that is > 1 is the one at the left bank (1.59).

Other maxima ratios range between 0.82 (right bank) and 0.85 (bed). Ratios obtained from minima are still > 1 (except for the one at the right bank), though lower in magnitude compared to those at the 1500-m-long channel. To summarize, making meander wavelength longer – from 800 m (BM) to 1000 m – leads to an increase of minimum erosion rates and a decrease in maximum erosion rates where they are highest (bed and right bank). At the left bank, maximum erosion rates are always increased, more so at channel cross-section 500. An even longer meander wavelength of 1200 m causes maximum erosion rates to decrease further and minimum erosion rates to increase further. The steepest and most homogeneous increase in minimum erosion rates is seen at the 1500-m-long channel.

Table 2.8e. Sensitivity of baseline model results to changes in initial channel geometry: changes in meander wavelength (λ = 1000 and 1200 m).

Obtained Erosion Rates	$Ratio_{all\_channel}$ (λ = 1000 m/BM)	$Ratio_{500}$ (λ = 1000 m/BM)	$Ratio_{all\_channel}$ (λ = 1200 m/BM)	$Ratio_{600}$ (λ = 1200 m/BM)
	#	#	#	#
Max E.R. bed	0.94	0.93	0.89	0.85
Min E.R. bed	1.01	1.08	2.50	1.64
Max E.R. left bank	1.02	1.68	0.95	1.59
Min E.R. left bank	1.01	1.10	3.08	1.67
Max E.R. right bank	0.95	0.80	0.90	0.82
Min E.R. right bank	1.08	0.84	2.50	0.75

Sensitivity of BM results to changes in channel width

In this section, we explore how changes in channel width affect the magnitude and spatial distribution of erosion rates in a 1200-m-long channel and at a channel cross-section cut parallel to the axis of bend 1 at a downstream distance of 400 m from the lava source

(see Fig. 2.2a). Fig. 2.30 shows the erosion rates distribution at the bed of a channel that is wider (w = 200 m) than the BM one (w = 160 m).

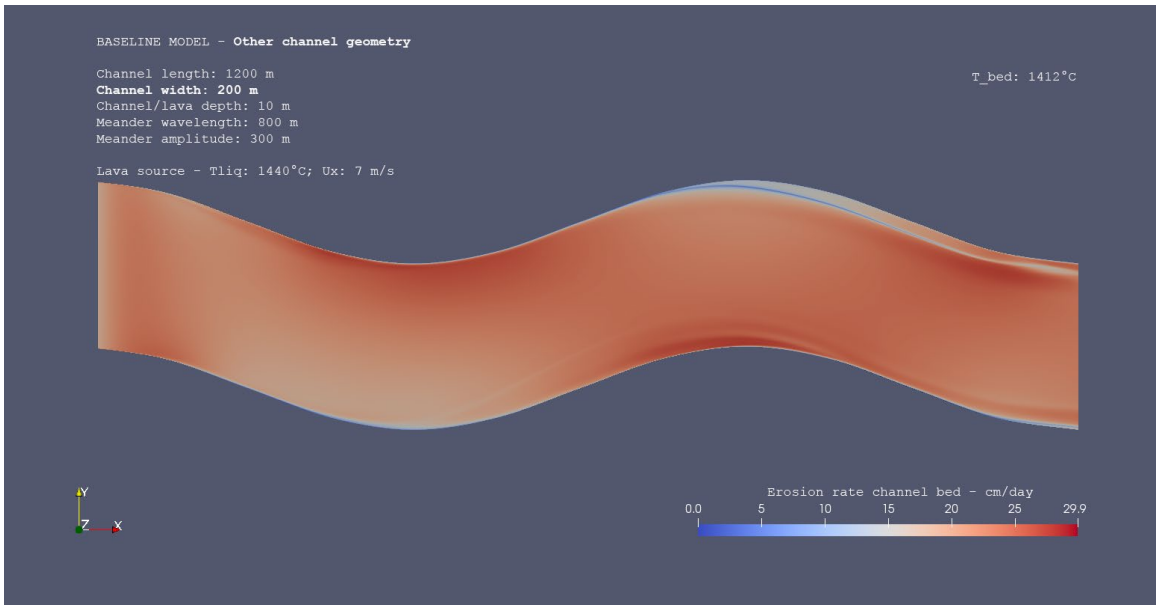

Figure 2.30. Erosion rates at a channel bed that is wider (w = 200 m) than the baseline bed (w = 160 m). All other geometric and flow parameters are held the same as in the baseline model.

Table 2.9a shows how erosion rates magnitude and spatial distribution change across the 1200-m-long channel and at channel cross-section 400. Both the bed and left bank maxima are shifted downstream of their BM location by 497 and 90 m, respectively, and their new locations are within 12.3 m of bend 2 axis. Instead, the right bank maximum is located 2 m upstream of its BM location. The bed and right bank minima occupy the same place in the channel (as they do in the baseline model) and are both shifted downstream of their BM location by 10 m. The left bank minimum is the one to have undergone the greatest shift of all - 809 m upstream of its BM location. Erosion rate values are different from those in the baseline model. The maximum erosion rate at the bed is lower (27.6 cm/day versus 29.1 cm/day at BM) and the left bank maximum is higher (29.9 cm/day versus 28.8 cm/day).

The left bank maximum is also the highest (peak) bank maximum (right bank maximum is equal to 28.4 cm/day). All minima are slightly lower than their BM counterparts (1.0-1.1 versus 1.2-1.3).

Table 2.9a. Sensitivity of baseline model (BM) results to changes in channel width (w = 200 m instead of the 160 m BM value). The table illustrates maximum and minimum erosion rates at the channel bed and banks. All other flow BM parameters are unchanged.

SENSITIVITY OF BM RESULTS TO CHANGES IN CHANNEL WIDTH – w = 200 m. Channel length = 1200 m. Erosion rates at channel bed and banks			
Obtained Erosion Rates (ER)	Erosion Rate Values	Distance from lava source	Location in the channel
description	cm/day	m	description
Max ER bed	27.6	795.9	bend 2, 4.1 m upstream of bend axis, within 5 m of left bank.
Min ER bed	1.0	641.0*	bend 2, 159.0 m upstream of bend axis, bed/right bank.
Max ER left bank	29.9	787.7	bend 2, 12.3 m upstream of bend axis, bank top.
Min ER left bank	1.1	239.0	bend 1, 239.0 m downstream of bend axis (inlet), left bank/bed.
Max ER right bank	28.4	291.8	bend 1, 108.2 m upstream of bend trough, 3.5 m down from bank top.
Min ER right bank	1.0	641.0*	bend 2, 159.0 m upstream of bend axis, right bank/bed.

Table 2.9b refers to channel cross-section 400 and shows how erosion rates and their distribution differ from those shown in Table 2.9a. The bank maximum is found at the right bank and its value (26.1 cm/day) is much higher than the left bank maximum (15.1 cm/day). The bed maximum (27.1 cm/day) is lower than its BM counterpart (28.8 cm/day) and all erosion minima are much higher than those shown in Table 2.9a and similar in values to

(or, with reference to the right bank minimum, lower than) those found in the baseline model.

Table 2.9b. Sensitivity of baseline model (BM) results to changes in channel width (w = 200 m instead of the 160 m BM value). The table illustrates maximum and minimum erosion rates at a channel cross-section located 400 m downstream of the lava source and cut along bend 1 trough (see Fig. 2.2a). All other flow BM parameters are unchanged.

SENSITIVITY OF BM RESULTS TO CHANGES IN CHANNEL WIDTH – w = 200 m. Channel length = 1200 m. Erosion rates at channel Cross-Section (CS) 400 m			
Obtained Erosion Rates (ER)	Erosion Rate Values	Distance from lava source	Location in channel CS
description	cm/day	m	description
Max E.R. bed_{400}	27.1	400.0	~12 m from right bank
Min E.R. bed_{400}	5.3	400.0	~1 m from left bank
Max E.R. left $bank_{400}$	15.1	400.0	bank top
Min E.R. left $bank_{400}$	5.3	400.0	left bank/bed
Max E.R. right $bank_{400}$	26.1	400.0	bank top - ~3.5 m down.
Min E.R. right $bank_{400}$	6.7	400.0	right bank/bed

Fig. 2.31 shows the erosion rate distribution at the bed of channel cross-section 400 for the 200-m-wide channel. The maximum value of 27.1 cm/day is located at a horizontal distance of ~12 m from the right bank (instead of 6 m in BM). The minimum value of 5.3 cm/day is found within ~1 m of the left bank and is slightly higher than its BM counterpart (5 cm/day). At the bed/right bank contact, the lowest erosion rate is equal to 6.8 cm/day. Erosion rate values drop drastically within ~1 m of the left and right banks. Within ~1 m of the right bank, values drop from the observed maximum of 27.1 cm/day to a value of 6.8 cm/day. At the left bank (Fig. 2.32a), the maximum erosion rate of 15.1 cm/day is higher than its BM counterpart (10.3 cm/day) and is located at the bank top and not at a vertical distance of 4-2 m from the bank/bed contact (BM). From the bank top, erosion

rates decrease faster and faster as the distance from the bank/bed contact becomes shorter until a minimum erosion rate of 5.3 cm/day is obtained. The fastest drop occurs within ~2 m of the bank/bed contact. At the right bank (Fig. 2.32b), the maximum erosion rate of 26.1 cm/day (higher than the 24.4 cm/day BM value) is located at the bank top as in BM. From that point downwards, erosion rates start decreasing first slowly and then faster and faster until they drop to a minimum value of 6.7 cm/day at the bank/bed contact. The fastest drop begins at a vertical distance of ~2 m from that contact.

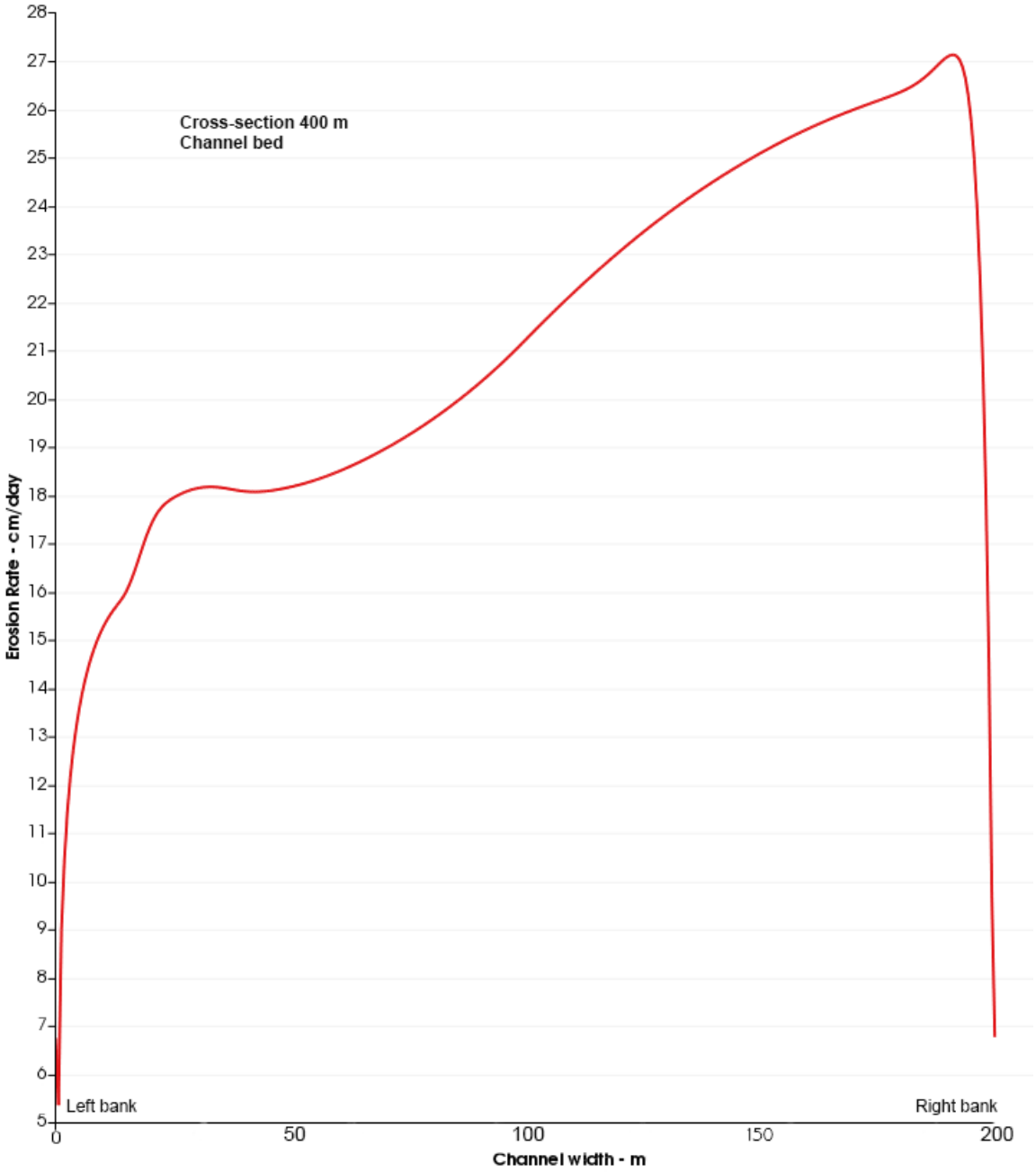

Figure 2.31. Erosion rates at the channel bed for cross-section 400. The case for a channel wider than the BM, w = 200 m. The maximum value of 27.1 cm/day is lower than the value of 28.8 cm/day that refers to BM, cross-section 400. Moreover, it is located at a horizontal distance of ~12 m from the right bank (instead of 6 m in BM). The minimum value of 5.3 cm/day is found within ~1 m of the left bank and is slightly higher than its BM counterpart (5 cm/day). At the bed/right bank contact, the lowest erosion rate is equal to 6.8 cm/day. Erosion rate values drop drastically within ~1 m of the left and right banks. Within ~1 m of

left and right banks. Within ~1 m of the right bank, values drop from the observed maximum of 27.1 cm/day to a value of 6.8 cm/day.

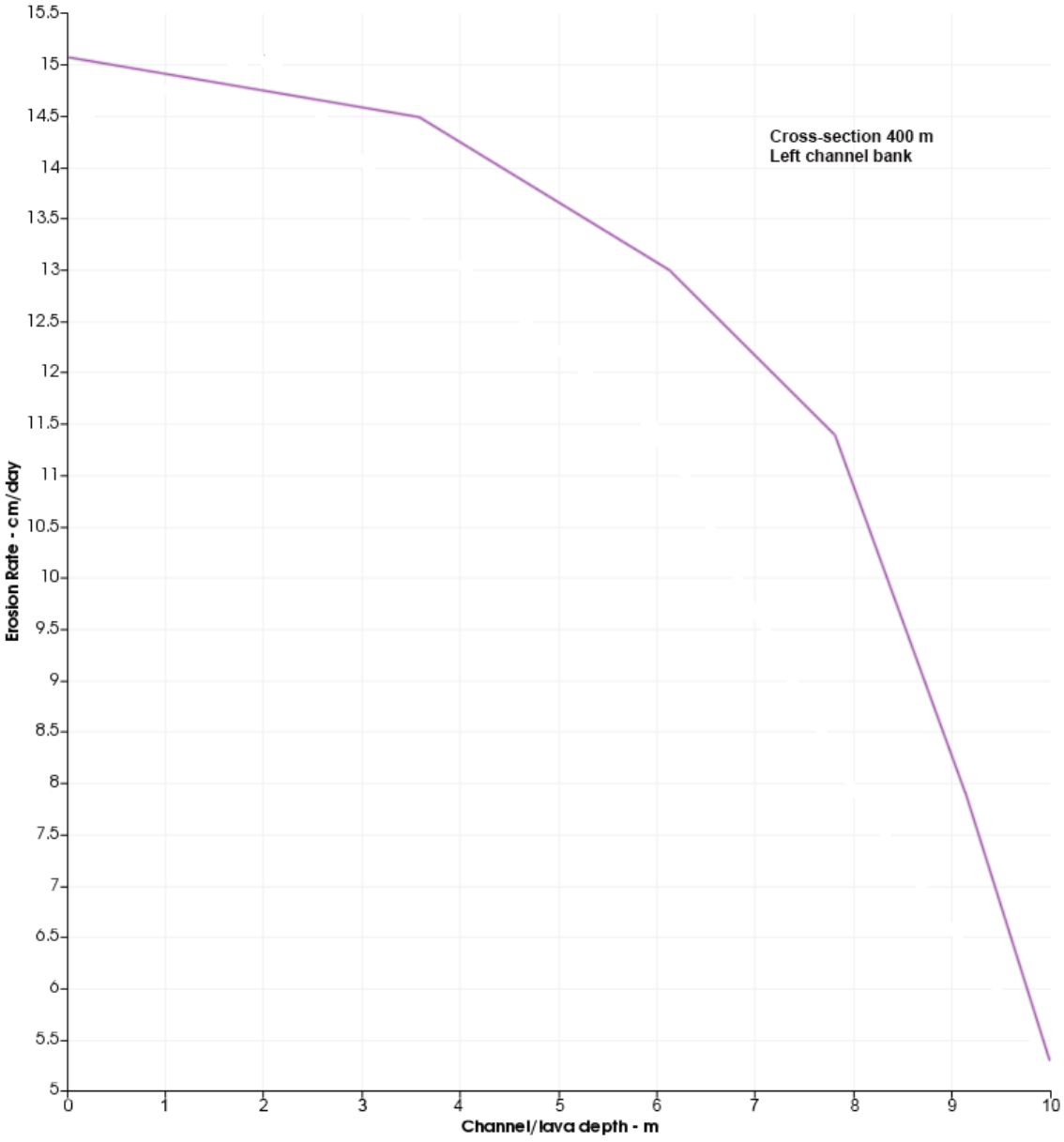

Figure 2.32a. Erosion rates at the left bank for cross-section 400. The case for a channel wider than the BM, w = 200 m. The maximum erosion rate of 15.1 cm/ day is higher than its BM counterpart (10.3 cm/day) and is located at the bank top and not at a vertical distance of 4-2 m from the bank/bed contact as in BM. From the bank top, erosion rates decrease faster and faster as the distance from the bank/bed contact is reduced until a minimum erosion rate of 5.3 cm/day is obtained. The fastest drop occurs within ~2 m of the bank/bed contact.

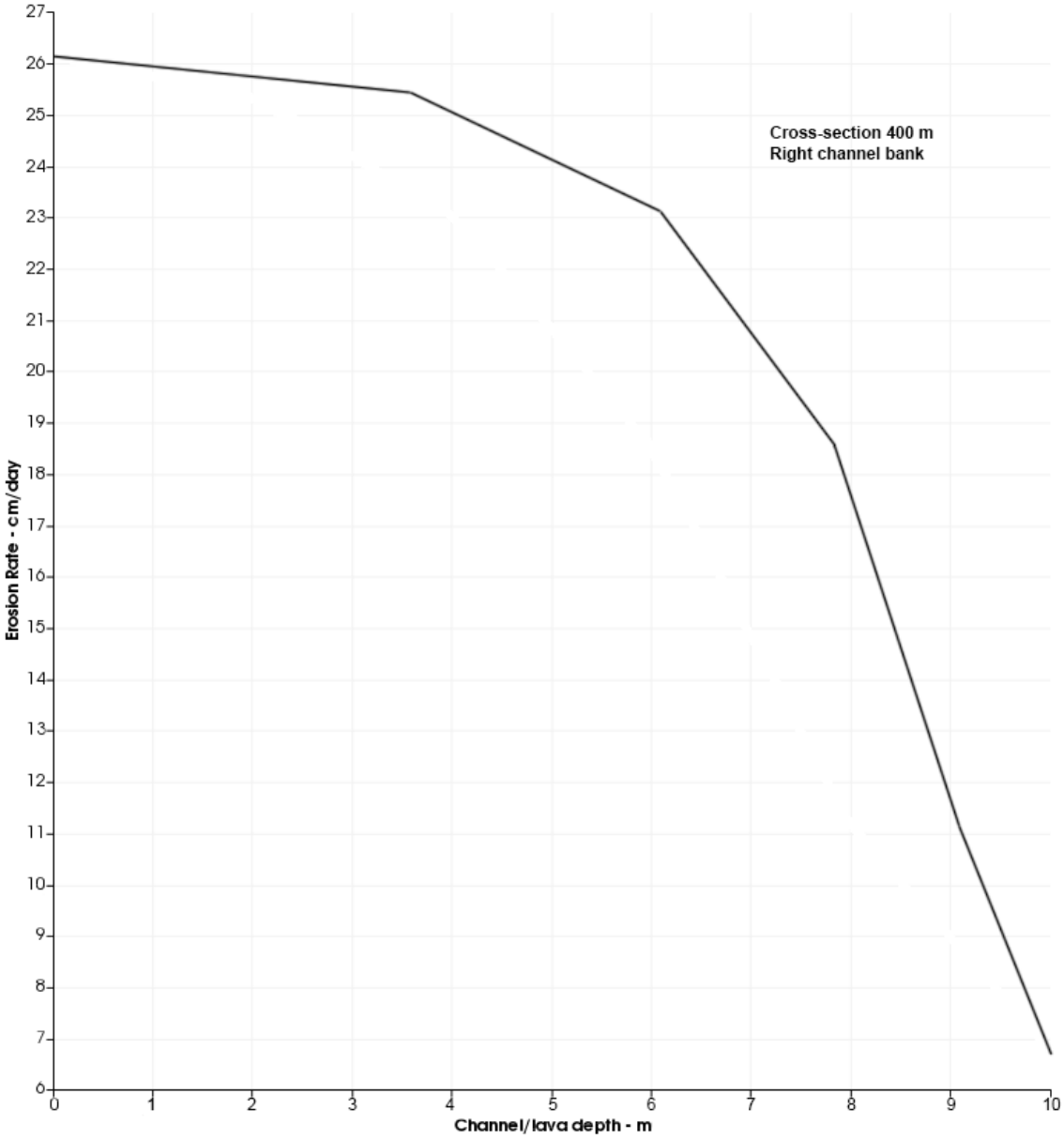

Figure 2.32b. Erosion rates at the right bank for cross-section 400. The case for a channel wider than the BM, w = 200 m. The maximum erosion rate of 26.1 cm/day (higher than the 24.4 cm/day BM value) is located at the bank top as in BM. From that point downwards, erosion rates start decreasing first slowly and then faster and faster until they drop to a minimum value of 6.7 cm/day at the bank/bed contact. The fastest drop begins at a vertical distance of ~2 m from that contact.

After having examined a channel that is 40 m wider than the baseline channel (w = 160 m), we will now consider a channel that is 40 m narrower (w = 120 m) (see Fig. 2.33).

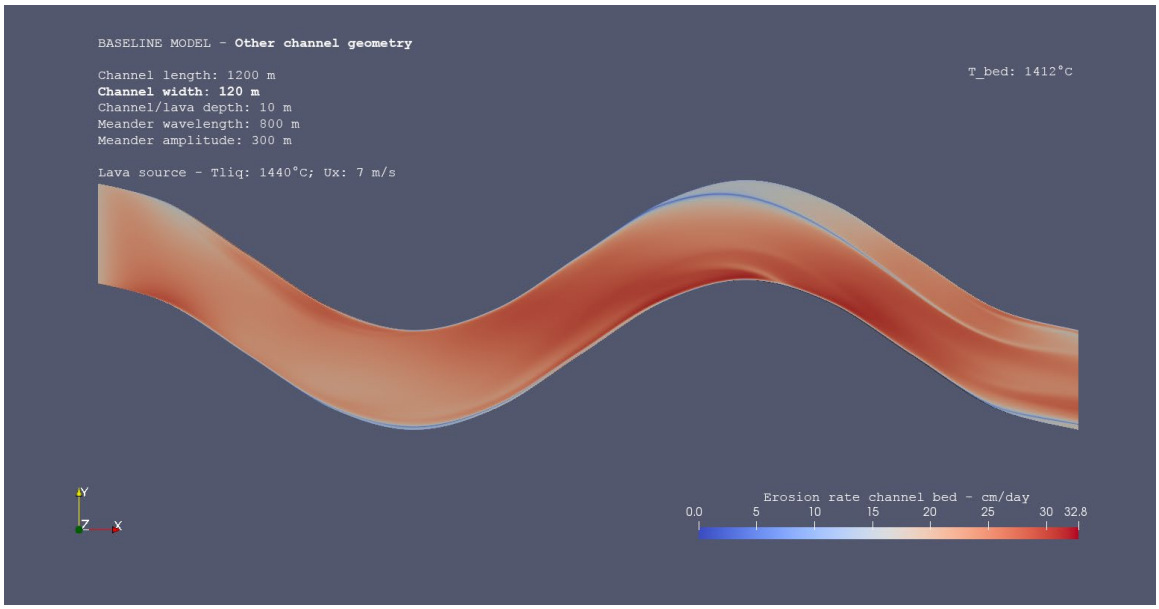

Figure 2.33. Erosion rates at a channel bed that is narrower (w = 120 m) than the baseline channel (w = 160 m). Meander amplitude is held the same as in the baseline model (BM), though the reduced width may give the impression that the amplitude is changed. All other geometric and flow parameters are held the same as in BM.

Table 2.9c shows how the magnitude and spatial distribution of erosion rates has changed compared to that in the baseline model. The bed and right bank maxima are moved 497 m and 805 m downstream of their BM locations, respectively. The bed maximum is located at only 4.3 m from bend 2 axis, whereas the right bank maximum is over the flank of bend 2. The bed and right bank minima occupy almost the same place in the channel, which is 8 m downstream of its BM counterpart location. The left bank minimum is the only minimum to have moved 805 m upstream of its BM location. Erosion rate values vary significantly from those in the previous case study (w = 200 m) and the baseline model. The maximum erosion rate at the bed (31.5 cm/day) is higher than that in the BM (29.1 cm/day). The

maximum bank erosion occurs at the left bank (32.8 cm/day) and is higher than its BM counterpart. The left bank maximum is also the highest value of erosion rate across the entire channel. Erosion minima (0.8-0.9) are lower than those in the baseline model (1.2-1.3).

Table 2.9c. Sensitivity of baseline model (BM) results to changes in channel width (w = 120 m instead of the 160 m BM value). The table illustrates maximum and minimum erosion rates at the channel bed and banks. All other flow BM parameters are unchanged.

SENSITIVITY OF BM RESULTS TO CHANGES IN CHANNEL WIDTH – w = 120 m. Channel length = 1200 m. Erosion rate at channel bed and banks			
Obtained Erosion Rates (ER)	Erosion Rate Values	Distance from lava source	Location in the channel
description	cm/day	m	description
Max ER bed	31.5	795.7	bend 2, 4.3 m upstream of bend axis, within 5 m of left bank.
Min ER bed	0.9	639.3*	bend 2, 160.7 m upstream of bend axis, bed/right bank.
Max ER left bank	32.8	94.3	bend 1, 94.3 m downstream of bend axis (inlet), 7.8 m down from bank top.
Min ER left bank	0.9	243.1	bend 1, 156.9 m upstream of bend trough, left bank/bed.
Max ER right bank	29.9	1099.3	bend 2, 299.3 m downstream of bend axis, bank top.
Min ER right bank	0.8	639.3*	bend 2, 160.7 m upstream of bend axis, right bank/bed.

Table 2.9d shows the magnitude and distribution of erosion rates at channel cross-section 400. The maximum bed erosion (26.2 cm/day) is lower than its BM counterpart value (28.8 cm/day) and the bank erosion maximum is found at the right bank (20.9 cm/day) as in the baseline model, but it is lower in value (BM value = 24.4 cm/day). Erosion minima values are also somewhat different from the BM ones. The left bank minimum (7.3 cm/day) is

higher than the BM one (4.9 cm/day) and the right bank minimum (5.0 cm/day) is lower than its BM counterpart value (8.9 cm/day).

Table 2.9d. Sensitivity of baseline model (BM) results to changes in channel width (w = 120 m instead of the 160 m BM value). The table illustrates maximum and minimum erosion rates at a channel cross-section located 400 m downstream of the lava source and cut along bend 1 trough (see Fig. 2.2a). All other flow BM parameters are unchanged.

SENSITIVITY OF BM RESULTS TO CHANGES IN CHANNEL WIDTH – w = 120 m. Channel length = 1200 m. Erosion rates at channel Cross-Section (CS) 400 m			
Obtained Erosion Rates (ER)	Erosion Rate Values	Distance from lava source	Location in channel CS
description	cm/day	m	description
Max E.R. bed_{400}	26.2	400.0	~8 m from right bank
Min E.R. bed_{400}	5.0	400.0	bed/right bank
Max E.R. left $bank_{400}$	13.4	400.0	6.1 m down from bank top
Min E.R. left $bank_{400}$	7.3	400.0	left bank/bed
Max E.R. right $bank_{400}$	20.9	400.0	bank top - ~3.5 m down.
Min E.R. right $bank_{400}$	5.0	400.0	right bank/bed

Fig. 2.34 shows the magnitude and spatial distribution of erosion rates at the bed of channel cross-section 400. The bed maximum (26.2 cm/day) is located at a horizontal distance of ~8 m from the right bank (instead of 6 m in BM). The minimum value of 5.0 cm/day is found at the bed/right bank contact and is identical to the BM value that is located at the bed/left bank contact instead. At the horizontal distance of ~7 m from the bed/left bank contact, the second-lowest erosion rate is equal to 5.8 cm/day (dip in Fig. 2.34). Going from the right to the left, the erosion rate curve does not decrease as fast as in previous scenarios. Because of this, erosion rates as high as 22.2 cm/day are still found within 20 m of the left bank. On the opposite side of the channel, erosion rates drop drastically within ~1 m of the bed/right bank contact. At the left bank (Fig. 2.35a), the maximum erosion rate

of 13.4 cm/day is higher than its BM counterpart (10.3 cm/day) and is located at a vertical distance of 4-2 m from the bank/bed contact. From the bank top (erosion rate of 7.9 cm/day) downwards, erosion rates increase steadily and rapidly till the maximum of 13.4 cm/day is reached. Then, they drop drastically and reach a minimum value of 7.3 cm/day at the bank/bed contact.

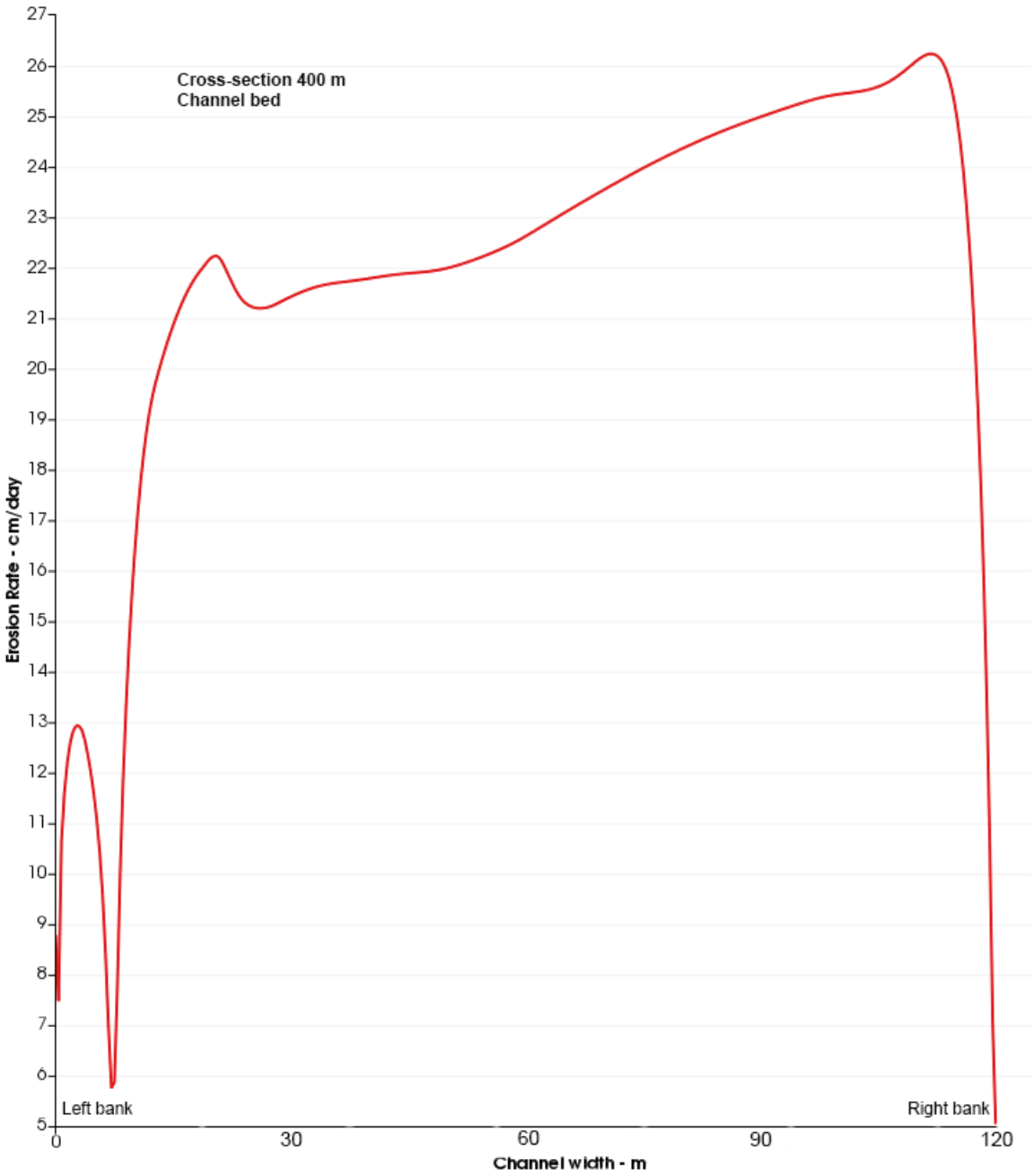

Figure 2.34. Erosion rates at the channel bed for cross-section 400. The case for a channel narrower than the BM one, w = 120 m. The maximum value of 26.2 cm/day is lower than the value of 28.8 cm/day (BM, cross-section 400). Moreover, it is located at a horizontal distance of ~8 m from the right bank (instead of 6 m in BM). The minimum value of 5.0 cm/day is found at the bed/right bank contact and is identical to the BM value located at the bed/left bank contact. The curve does not decrease fast as in other scenarios. As a

result, erosion rates as high as 22.2 cm/day are found within 20 m of the left bank. On the opposite side of the channel, erosion rates drop drastically within ~1 m of the bed/right bank contact.

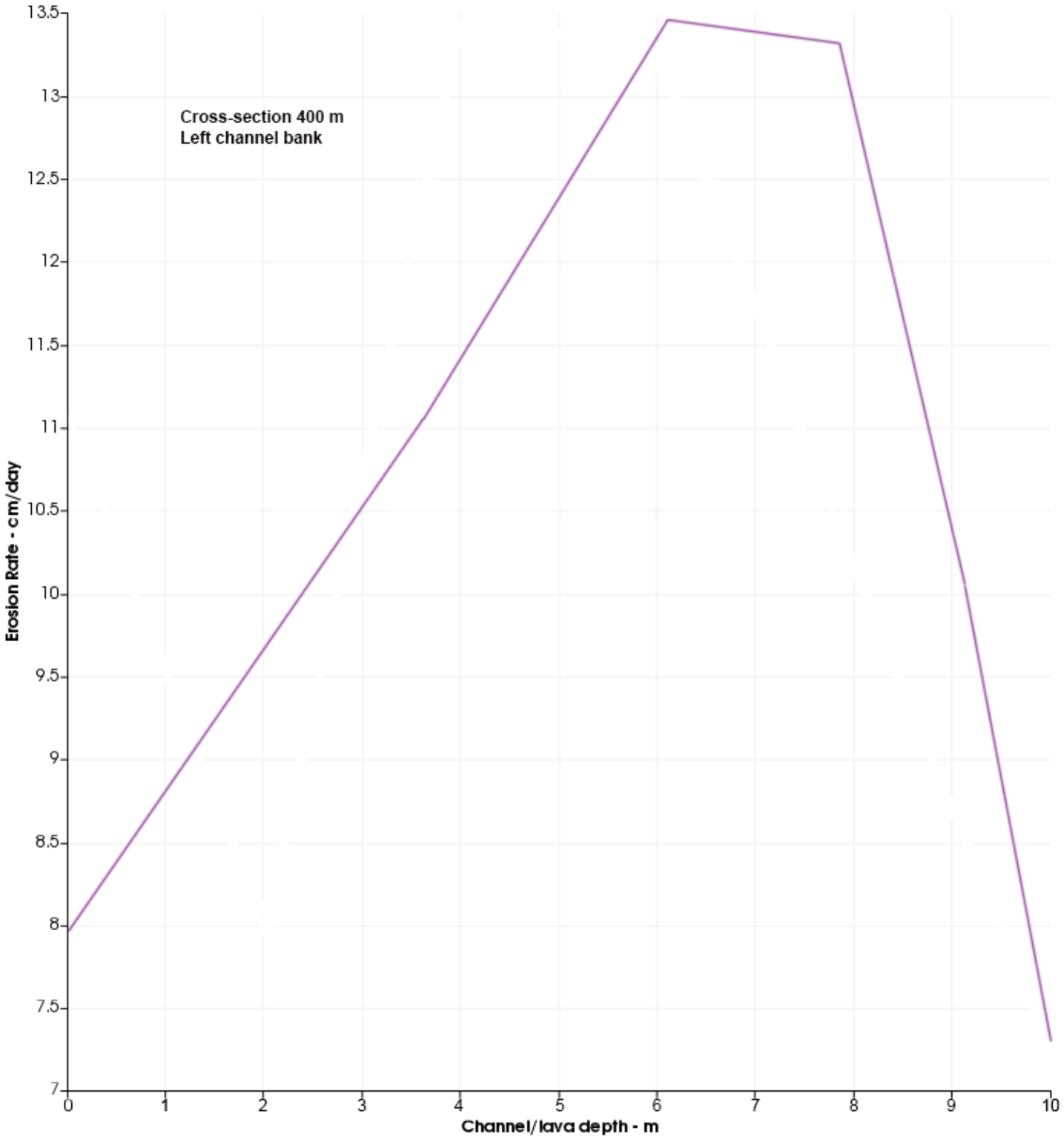

Figure 2.35a. Erosion rates at the left bank for cross-section 400. The case for a channel narrower than the BM channel, w = 120 m. The maximum erosion rate of 13.4 cm/day is higher than its BM counterpart (10.3 cm/day) and is located at a vertical distance of 4-2 m from the bank/bed contact. From the bank top (erosion rate of 7.9 cm/day) downwards, erosion rates increase rapidly till the maximum of 13.4 cm/day is reached. The minimum is 7.3 cm/day.

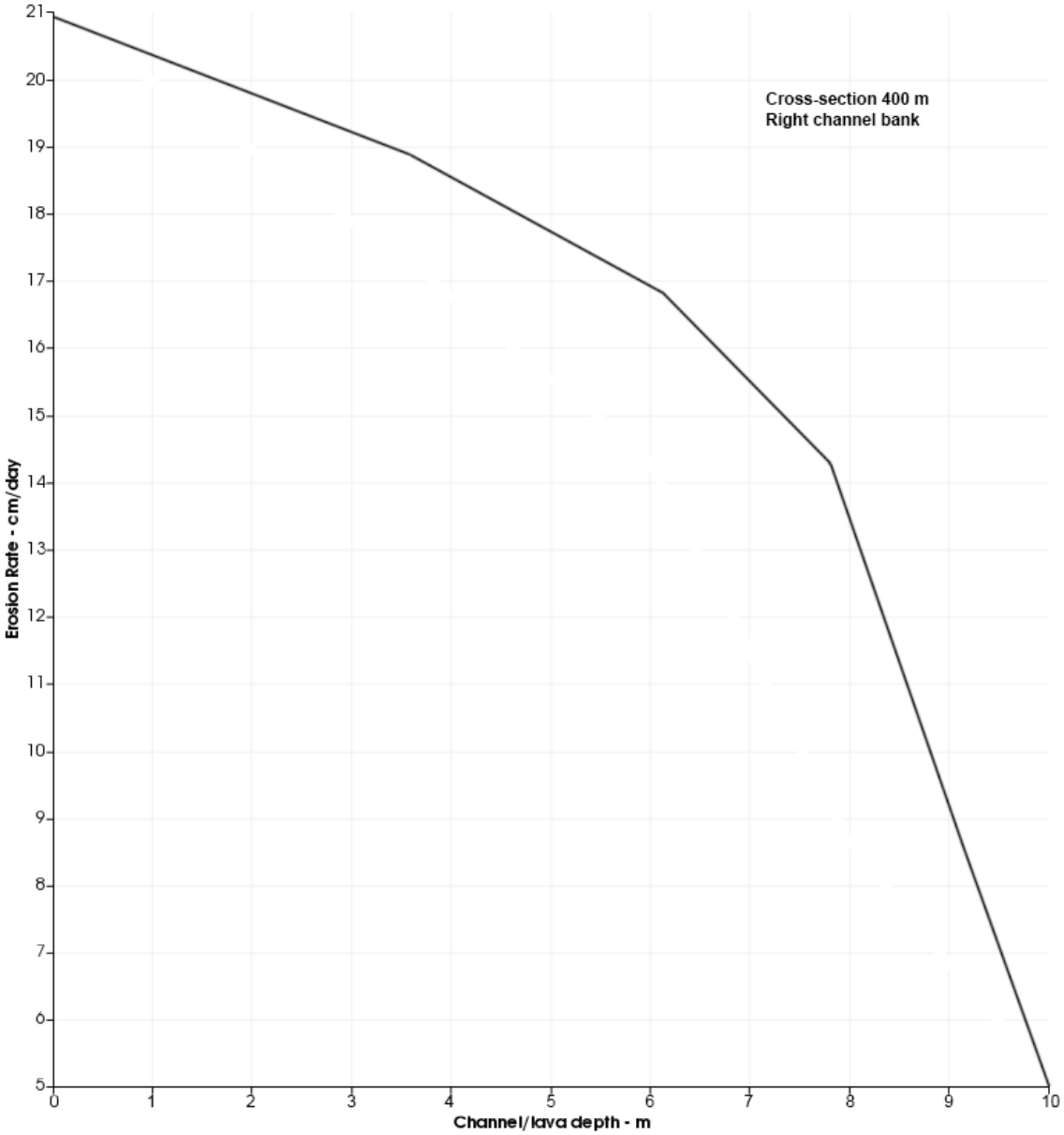

Figure 2.35b. Erosion rates at the right bank for cross-section 400. The case for a channel narrower than the BM channel, w = 120 m. The maximum erosion rate of 20.9 cm/day is much higher than its BM counterpart (10.3 cm/day) and is located at the bank top and not at a vertical distance of 4-2 m from the bank/bed contact as in BM. From the bank top, erosion rates decrease faster and faster as the distance from the bank/bed contact is reduced until a minimum erosion rate of 5.0 cm/day is reached at the contact. The fastest drop occurs within ~2 m of the contact itself.

At the right bank (Fig. 2.35b), the maximum erosion rate of 20.9 cm/day is much higher than its BM counterpart (10.3 cm/day) and is located at the bank top and not at a vertical distance of 4-2 m from the bank/bed contact as in BM. From the bank top, erosion rates decrease faster and faster as the distance from the bank/bed contact is reduced until a minimum erosion rate of 5.0 cm/day is reached at the contact. The fastest drop occurs within ~2 m of the same contact.

How width-modified results compare with BM results

Table 2.9e illustrates ratios of erosion maxima and minima obtained at two channels of identical length and different width (w = 120 m and w = 200 m). Ratios at the channel that is narrower (w = 120 m) than the baseline channel (w = 160 m) are higher and lower than 1. At the 1200-m-long channel, all ratios obtained from erosion maxima are higher than 1, the highest value being at the left bank (where the highest erosion rates are found). Ratios obtained from erosion minima are all lower than 1, the lowest value being located at the right bank (where the lowest erosion minimum is found). At channel cross-section 400, ratios obtained from erosion maxima are lower than 1, except for the ratio calculated at the left bank that has the highest value of all (1.30). This apparent discrepancy can be explained as follows: even though the highest erosion rate values at cross-section 400 are obtained at the right bank, the values found at the left bank are much higher than their BM counterparts.

For a channel that is wider (w = 200 m) than the baseline channel (w = 160 m), a similar trend to the one seen at the narrower channel arises. At the 1200-m-long channel,

ratios obtained from erosion maxima are lower than those obtained at the narrower channel. Moreover, their values are always lower than 1, except for the ratio obtained at the left bank of the channel. The latter statement implies that all (but one) the erosion maxima obtained at the 1200-m-long channel are lower than their BM counterparts. In contrast, ratios obtained from erosion minima are higher than those obtained at the narrower channel though still lower than 1 in value. The latter statement implies that erosion minima at the 200-m-wide channel are all lower than their BM counterpart values. At channel cross-section 400, ratios that are calculated from erosion maxima are (all but one at the bed) higher than 1 and higher than those obtained at cross-section 400 of the narrower channel. This implies that erosion maxima are higher than their BM counterpart values and higher than those obtained at the narrower channel cross-section 400. The differences in behavior found at the long channel segment and cross-section 400 underline a complexity that will be explained in the theoretical study section of Chapter 5. The enhanced thermal erosion at the bed and banks of cross-section 400 is likely counteracted (to some extent, at least) by the increased heat loss by conduction into the lava substrate (a consequence of the increase in flow surface area, *Keszthelyi*, 1995). Ratios calculated from erosion minima are higher than 1 (except for the one obtained at the right bank). This implies that even erosion minima are higher than their BM counterparts at the cross-section of a channel that is wider than the baseline channel. The same erosion minima are also lower than those calculated at a similar cross-section of a narrower channel, which suggests there might exist an inverse correlation between erosion maxima and minima at meander bends.

Table 2.9e. Sensitivity of baseline model results to changes in initial channel geometry: changes in channel width.

Obtained Erosion Rates	$Ratio_{all\_channel}$ (w = 120 m/BM)	$Ratio_{400}$ (w = 120 m/BM)	$Ratio_{all\_channel}$ (w = 200 m/BM)	$Ratio_{400}$ (w = 200 m/BM)
	#	#	#	#
Max E.R. bed	1.08	0.91	0.95	0.94
Min E.R. bed	0.75	1.16	0.83	1.06
Max E.R. left bank	1.14	1.30	1.04	1.47
Min E.R. left bank	0.69	1.49	0.85	1.08
Max E.R. right bank	1.01	0.86	0.96	1.07
Min E.R. right bank	0.67	0.56	0.83	0.75

Significance of results

The results presented here confirm that the new 3-D model outputs flow scenarios of a much higher level of complexity than those obtainable with one- and two-dimensional approaches. The magnitude and spatial distribution of erosion rates vary from rille bed to banks, and a pattern exists at rille cross-sections cut parallel to bend axes. At bend 1, erosion rates are always higher at the inner (right) bank than at the outer (left) bank, with only a few exceptions occasionally represented by flow scenarios for which either channel or meander geometry are modified. The 3-D model shows correct behavior based on predictions from available lower-dimensional models. As regards lava/substrate physical properties, temperature and velocity increases (at the lava source) are always conducive to higher erosion rates, regardless of channel location. A thick flow always leads to erosion rates that are higher than those produced by thinner lava. And a substrate that is unconsolidated and has a low melting temperature is excavated faster than a consolidated substrate of higher melting temperature, holding other flow parameters equal. As regards the measurable properties of the rille, an increase in meander amplitude leads to higher erosion rates (both at the rille bed and the bends) than those generated by lava flowing

through a channel with meanders of a lower amplitude. Increasing meander wavelength causes erosion rates at the bed and right bank to decrease, whereas erosion at the left bank and erosion minima are higher than their BM counterparts. Finally, for a rille segment that is wider than the baseline channel, erosion at the bed is always lower than in the BM whereas erosion at the right bank is either higher or lower than in the BM depending on whether the bank portion of interest is located at cross-section 400 or away from the bend axis, respectively. A caveat is represented by the fact that, for a channel or tube that is wider than another, a larger amount of heat is lost by conduction into the underlying substrate (*Keszthelyi*, 1995), which likely counteracts (at least to some extent) the increase in thermal erosion. The non-homogeneous magnitude and spatial distribution of erosion rates at channel cross-sections is indicative of an underlying fluid and thermodynamic complexity that is revealed and explained in Chapter 5.

3 PAPER 1: MARS, ATHABASCA VALLES (CATALDO ET AL., 2015)

Abstract

The Athabasca Valles flood lava is presumably the most recent (<50 Ma) and best-preserved effusive lava flow on Mars and is inferred to have been emplaced turbulently. The *Williams et al.* (2005) model of thermal erosion by turbulent lava has been applied to the topography of "Proximal Athabasca", the 75-km-long upstream portion of the Athabasca Valles channel. For emplacement volumes of 5,000 and 7,500 km^3 and average flow thicknesses of 20 and 30 m, the duration of the eruption varies between ~11 and ~37 days, in agreement with *Jaeger et al.* (2010). The erosion of the lava substrate is investigated for three lava eruption temperatures (1270°, 1260°, and 1250°C), and volatile contents equivalent to 0-65 vol.% vesicles. The largest erosion depths of 3.8-7.5 m are at the source, for 20-m-thick and vesicle-free flows erupted at their liquidus temperature (1270°C). A substrate containing 25% ice by volume leads to the high end of the modeled erosion. A lava temperature 20 °C below liquidus reduces erosion depths by a factor of ~2.2. By assuming that flow viscosity increases with increasing bubble content in the lava, a 30-50% vesicles presence leads to erosion depths ~1.8-2.4 times lower than those relative to non-vesicular lava. The presence of 25% ice in the substrate increases erosion depths by a factor of 1.3. Nevertheless, in all cases, the modeled erosion depths for a lava flow consistent with the emplacement volume and flow duration constraints, are far less than the depth of the channel (~35-100 m). We conclude that thermal erosion by flowing lava does not appear to have had a major role in excavating Athabasca Valles.

Introduction

Flood lava at Athabasca Valles

Athabasca Valles is a 300-km-long outflow channel located in north-central Elysium Planitia, Mars. It has a crater retention age of 20 Ma or less (e.g., *Berman and Hartmann,* 2002; *Burr et al.,* 2002), but the channel may be older because those ages date the lava coating the channel (*McEwen et al.,* 2012). *Jaeger et al.* (2007, 2010) studied in great detail the thin flow that drapes the Athabasca channel system - the best preserved and presumably youngest flood lava on Mars (*Plescia*, 1990). The flow issued simultaneously from a series of vents located along a nearby fissure that is part of the Cerberus Fossae, and extended southwest for about 300 km through Athabasca Valles. It then emptied into a basin named Cerberus Palus and spread over the surrounding plains, flowing out to as much as ~1,400 km from its source (Fig. 1, from *Jaeger et al*., 2010). Ages in the range 0.5-10 Ma and <50 Ma were derived, based on the observed superposition of secondary impact craters onto the flow (*Jaeger et al.*, 2010 and references therein). Depth estimates that reflect the thickness of the congealed lava where it pooled on the Cerberus Palus plain, are in the range 20-30 m, and refer to the volume of the partially degassed lava that *Jaeger et al.* (2010) calculated to be in the range 5,000-7,500 km^3. As a result, the volume of lava including vesicles that flowed out of the vent may have been somewhat higher. Flow depths of 80-100 m were reached in the center of the channel at peak flow, reflecting the variability in channel floor topography. At its height, the flow locally overtopped the channel banks. Subsequently, its level dropped more than 50 m from its high stand, as fluid lava drained downstream into the distal basin of Cerberus Palus (*Jaeger et al.*, 2007). The total width of the Athabasca channel is~30-50

km (with an average value of 39 km), and the average slope is 0.063 ± 0.007% (0.036˚± 0.004 ˚).

Instrumentation aboard the Mars Reconnaissance Orbiter (MRO) was used to investigate the emplacement of the flow and its composition. Specifically, the 27-117 cm/pixel color and stereo High Resolution Imaging Science Experiment (HiRISE; *McEwen et al.*, 2007) images, together with the ~6 m/pixel Context Camera (CTX; *Malin et al.*, 2007) images enabled flow margins and flow contacts to be resolved, thanks to a favorable mix of high spatial resolution and wide area coverage. Flood lavas are characterized by large volumes and areal coverage. Early quantitative studies suggested that they were emplaced in a turbulent fashion (*Shaw and Swanson*, 1970), but detailed examination of the lava morphologies suggested laminar emplacement under a thick insulating crust (*Self et al*., 1998). On Earth, the study of features diagnostic of inflation in flood lavas indicates emplacement in a laminar flow regime (*Hon et al.,* 1994) and long eruption durations (*Self et al*., 1998). The Athabasca lava flow is thin within a distance of 75 km from its source (proximal Athabasca), and gradually thickens in the downstream direction. Thus, the flow apparently deflated rather than inflated in its proximal reaches before solidifying (*Jaeger et al*., 2010). The same authors found that the flow was likely emplaced during a single event, over a period of a few to several weeks and, at peak discharge, was marginally to fully turbulent (with a Reynolds number Re=860-300,000; the transition to turbulence occurs around Re=500-2,000). The Reynolds number is here defined as: $Re=2\rho_b u r_h/\eta$, where ρ_b is the bulk density of the lava, u is the speed of the flow, r_h is the hydraulic radius of the lava (equal to the 'wetted' perimeter divided by the cross-sectional area), and η is

the dynamic viscosity of the flow. They used reasonable physical properties for the lava and the dimensions of the channel to obtain flow velocity and lava flux (following *Keszthelyi et al*., 2006), and derived information on flow regime. The composition of the lava is difficult to determine because the region is overlain by sufficient dust to obscure substrate mineralogy (*Bandfield et al*., 2000; *Christensen et al*., 2001). However, mineralogical maps produced from data collected utilizing the Compact Reconnaissance Imaging Spectrometer (CRISM), with a spatial resolution of 15-19 m/pixel (*Murchie et al*., 2007), provided some insight into the composition of the Athabasca flood lava. CRISM data confirmed that the Athabasca flood lava is spectrally similar to the mafic-ultramafic materials seen by Spirit in Gusev crater (*Jaeger et al*., 2010) - the so-called "Adirondack" type lavas – which show a composition intermediate to that of a basalt and a picrobasalt (*McSween et al*., 2004, 2008) and comparable with terrestrial high-Mg basalts or komatiitic basalts (*Gellert et al*., 2004). However, a range of mafic to ultramafic compositions were considered plausible.

Thousands of ring-mound landforms (*Jaeger et al*., 2007) occur exclusively on the flow surface, often near channel margins. HiRISE observations cast light on these landforms, whose origin was highly controversial. They are now thought to be hydrovolcanic or rootless cones, formed when ice and/or groundwater heated by the overlying lava flow vented in steam explosions (*Jaeger et al*., 2010; *Dundas and Keszthelyi*, 2013).

Thermal erosion by turbulent lava at Athabasca

The partial or complete melting and assimilation of a solid or particulate substrate by flowing lava is defined as thermal erosion, whereas mechanical erosion involves the entrainment of xenoliths or xenocrysts that have not chemically interacted with the lava (*Williams et al*., 1998). Thermo-mechanical erosion implies a combination of the two processes. These processes are important because they cause the removal of substrate to different extents during lava flow emplacement, and erosion by lava is a mechanism thought to be responsible for the formation of some lava channels and tubes on the Earth and other silicate planets and moons (*Carr,* 1974*; Baker et al.,* 1992*; Greeley et al.,* 1998*; Schenk and Williams,* 2004; *Head et al.,* 2011). Regardless of whether the mechanism is thermal or mechanical, erosion by lava is most plausible for high-temperature, low-viscosity lavas, especially if they flow turbulently. For Mars, erosion by lava has been considered a possible mechanism for the generation of at least some of the channels occurring in volcanic areas as an alternative to flowing water (*Carr*, 1974; *Baird*, 1984; *Cutts et al*., 1978; *Wilson and Mouginis-Mark*, 1984, 2001; *Leverington*, 2011; *Williams et al*., 2005; *Hurwitz et al*., 2010). *Dundas and Keszthelyi* (2014) described evidence for local mechanical erosion by a turbulent flood lava flow in Kasei Valles on Mars but found that the flow was far from adequate to erode that large channel. However, Athabasca Valles and several other relatively shallow outflow channels are found in the Elysium Planitia region. The smaller scale of those channels, and evidence for extensive recent flood volcanism, make it necessary to understand and quantify the potential for erosion by lava there.

The first mathematical model of erosion by turbulent lava was by *Hulme* (1973), who simulated the role played by high-temperature, low-viscosity, and high-density lavas in excavating the sinuous rilles on the Moon. *Hulme* (1973) and *Huppert and Sparks* (1985) showed that low-viscosity lavas that flow turbulently are expected to lose heat mainly by convection rather than conduction. *Huppert et al*. (1984) and *Huppert and Sparks* (1985) used a combination of laboratory experiments and mathematical modeling to reproduce the turbulent flow and emplacement of Archean komatiites on Earth. In the subsequent years, all workers used variations on the *Hulme* and *Huppert and Sparks* models.

The rigorous analytical-numerical model developed by *Williams et al.* (1998) advances the *Huppert and Sparks* (1985) model by involving both a geophysical and geochemical approach, thus better constraining the composition and thermal-rheological properties of lava and substrate, and the convective heat transfer to the top of the flow and to the substrate. Furthermore, it was designed for terrestrial localities where model results could be compared to field data. The *Williams et al.* (1998, 2000, 2005) model has been used to investigate thermal erosion by turbulent lava under various conditions on the Earth, the Moon, Mars, and Io, and calculates erosion rates and depths with time, as a function of distance from the source.

Jaeger et al. (2010) suggested that the brief duration of the Athabasca Valles Flood Lava eruption implied little thermal erosion but did not quantify the plausible amount. Here we adapt and apply the *Williams et al.* (2000, 2005) model to "proximal Athabasca", the upstream portion of Athabasca Valles which stretches out to a distance of ~75 km from the lava source. Our objective is to investigate whether the Athabasca lava may have flowed

turbulently out to the maximum distance traveled and determine erosion rates and depths across the entire length of proximal Athabasca. We want to assess what role, if any, thermal erosion could have had in the formation of Athabasca Valles. We then compare model results with available observations.

Method: The model

The flow is one-dimensional (in the x direction) with thermal erosion in the z direction. Lava erupts as a turbulent flow with a thermally mixed interior, convective heat transfer occurs to the top and the base of the flow, and thermal erosion occurs at the base of the flow, providing that the lava temperature is greater than the melting temperature of the substrate, and latent heat is released as the flow crystallizes. The model includes: (1) the effects of lava rheology changes due to assimilation of eroded substrate and crystallization of mafic minerals in the flowing lava, (2) the lava temperature decrease as the flow moves downstream, and (3) the flow thickness increase as velocity decreases (thickness is used as proxy for flux, which is conserved as the flow moves downstream). From the initial values of the lava thermal-physical properties, several algorithms are used to calculate initial values of important temperature- and composition-dependent thermal-physical lava properties, such as solidus and liquidus temperatures, liquid density and viscosity, lava specific heat and thermal conductivity, etc. However, these algorithms require an initial lava major oxide composition. Additionally, a set of topographical parameters associated with the flow is required to run the model. We have listed the complete set of input values, including the composition, the thermal/rheological properties

of lava and substrate, and the topographic parameters, as follows: liquid temperatures (T_{liq}) were calculated using MELTS (*Ghiorso and Sack*, 1995) and the solid temperatures (T_{sol}) are taken from experimental data of *Arndt* (1976); liquid density (ρ_l) was calculated using the method of *Bottinga and Weill* (1970) and density changes as a function of evolving pressure, temperature, and composition were obtained by adopting the partial molar volume coefficients of *Mo et al*. (1982); liquid viscosity (μ_l) was calculated using the method of *Shaw* (1972); specific heat (c) was calculated from the heat capacity data of *Lange and Navrotsky* (1992); and the temperature-dependent heat of fusion (L_l) is approximated using expressions for the mineral representing the highest volume percentage of the rock (here forsteritic olivine, from *Navrotsky* (1995)). The density (ρ_{gas}) and specific heat of water vapor (c_{gas}) were taken from *Serway and Jewett* (2014). Two values of ground slope were considered, one referring to the proximal portion of the Athabasca channel and the other averaged over the entire flow length (α=0.06° and α=0.036°, respectively, from *Jaeger et al*. (2010)).

The initial physical parameters of the lava are used in a series of auxiliary equations to calculate additional lava properties at the vent and at progressively increasing distances downstream. Lava crystallinity X is given by the ratio of the degree of undercooling divided by the range of crystallization, as follows:

$$X = \frac{(T_{liq} - T)}{(T_{liq} - T_{sol})} \quad (1)$$

in which T_{liq} is liquidus temperature, T_{sol} is solidus temperature, and T is lava temperature at the vent and then at progressively increasing downstream distances. Crystallinity is calculated by assuming constant liquidus and solidus temperatures rather than a range of values, and a linear growth (in the crystal fraction) with cooling, the latter assumption giving an adequate approximation for lavas crystallizing a single silicate phase (olivine) (*Williams et al*., 2000). Crystal growth and the presence of vesicles (which will be discussed later) in the lava interior are the only parameters in calculating bulk viscosity, although the strength of the crust may also influence the bulk motion of the flow. The bulk viscosity, μ_b, is expressed as a function of the initial liquid viscosity, μ_l, by the Roscoe-Einstein equation (2a):

$$\mu_b = \mu_l \left(1 - \frac{X}{0.6}\right)^{-2.5}, \qquad \mu_b = \mu_l \exp\left[2.5 + \left(\frac{X}{0.6 - X}\right)^{0.48}\right] \frac{X}{0.6} \qquad (2a, b)$$

at crystal fractions X < 0.3 and by the *Pinkerton and Stevenson* (1992) relation (2b), at crystal fractions X > 0.3. Equations (2a) and (2b) assume that the crystals remain in suspension during flow emplacement, which is strongly indicated during turbulent flow (*Huppert and Sparks*, 1985). Following this, flow velocity u, friction coefficient λ, and Reynolds number Re (3 a,b,c) are calculated iteratively:

$$u = \sqrt{\frac{4\,g\,h\sin(\alpha)}{\lambda}}, \qquad \lambda = [0.79\ln(Re) - 1.64]^{-2},$$

$$\mathrm{Re} = \frac{2\,\rho_b u\,h}{\mu_b}\,, \qquad \mathrm{Pr} = \frac{c_l\,\mu_b}{k_{eff}} \quad (3a,b,c,4)$$

in which g is acceleration due to gravity, h is flow thickness, α is ground slope, and ρ_b is bulk density of the flow (liquid + crystals). The value of Re = 2000 is chosen as the theoretical limit on turbulent flow in conduits. Another calculated composition-dependent thermal-physical property of the lava is the Prandt number Pr, the ratio of momentum diffusivity to thermal diffusivity (4), in which c_l is lava specific heat and k_{eff} is the effective lava thermal conductivity in the thermal boundary layers at the base and top of the flow, respectively (5a,b) (*Williams et al*., 1998). The effective thermal conductivity is expressed as:

$$k_{eff} = \frac{0.0013\,(T - T_{mg})}{\dfrac{\ln\,(2.16 - 0.0013\,T_{mg})}{(2.16 - 0.0013\,T)}}\,, \qquad k_{eff} = \frac{0.0013\,(T - T_{sol})}{\dfrac{\ln\,(2.16 - 0.0013\,T_{sol})}{(2.16 - 0.0013\,T)}} \qquad (5a,b)$$

In (5a), T_{mg} is the effective melting temperature of the substrate (which for a given value of μ_g maximizes thermal erosion). Unlike *Hulme* (1973) and *Huppert and Sparks* (1985), *Williams et al.* (1998) adopt more than one expression for the convective heat transfer coefficient (h_T), and we use here one that includes the effects for turbulent sheet flows:

$$h_T = \frac{0.0296\,k_{eff}\,\mathrm{Re}^{4/5}\,\mathrm{Pr}^{1/3}}{h}\left(\frac{\mu_b}{\mu_g}\right)^{0.14} \qquad (6)$$

in which μ_g, the viscosity of the melted substrate, is calculated as a function of T_{mg} and is equal to 35.6 Pa s for a substrate that is basaltic in composition (*Williams et al*., 1998). The ratio of the lava bulk viscosity to the viscosity of the melted substrate in (6) has the effect of reducing heat transfer compared to that found in fluids with constant physical properties.

Lava thermal erosion rate, u_m, as modified from *Huppert and Sparks* (1985), is given by:

$$u_m = \frac{h_T(T - T_{mg})}{E_{mg}}, \qquad E_{mg} = \rho_g[c_g(T_{mg} - T_a) + L_g] \tag{7a, b}$$

in which E_{mg} is the energy required to melt the substrate, ρ_g is substrate density, c_g is substrate specific heat, T_a is ambient temperature of the surface, and L_g is heat of fusion required to melt the substrate. Lava thermal erosion rates enable estimates of erosion depth to be made by simply multiplying erosion rate values (varying as a function of distance from lava source) by the elapsed time t since flow began, assuming steady flow conditions. The erosion rate is used to calculate the degree of contamination of the lava by assimilated substrate, given by:

$$S(x) = 1 - \frac{Q_0}{Q(x)}, \qquad Q(x) = Q_0 + \int_0^x u_m \, dx \tag{8a, b}$$

in which Q_0 is the initial flow rate and Q(x) is the flow rate at any given distance from the source. Finally, the following mass expressions:

$$M_{new} = M_{old}\,(1-\Delta S) + M_{asm}\,(\Delta S), \qquad M_{new} = M_{old}\,(1-\Delta X) + M_{olv}\,(\Delta X) \qquad (9a,b)$$

are used to calculate the compositional change in the liquid lava due to the assimilation of thermally eroded substrate S and the crystallization of minerals (olivine) X at each model distance increment. Here, M_{new} is the major oxide composition of the lava at the current distance from the source, M_{old} is the major oxide composition of the lava at the previous distance increment, M_{asm} is the major oxide composition of the substrate, and M_{olv} is the olivine major oxide composition. Equation (9b) is used in conjunction with partition coefficient and stoichiometric algorithms to calculate M_{olv} at each model increment of distance. The newly calculated lava composition from (9b) is then used to recalculate the temperature- and composition-dependent thermal, rheological, and fluid dynamic properties of the lava at each distance increment downstream.

Lava temperature is the key parameter that advances the model, which decreases as the flow moves downstream. This model of lava cooling with distance is given by the following 1st order ordinary differential equation (modified from *Huppert and Sparks*, 1985):

$$\rho_b c_l h u \frac{dT}{dx} =$$

$$-h_T\left(T - T_{mg}\right) - h_T(T - T_{sol}) - \frac{\rho_b c_l\, h_T\left(T - T_{mg}\right)^2}{E_{mg}} + \rho_b c_l hu \frac{dT}{dx}\, \frac{L_l\, X'(T)}{c_l} \qquad (10)$$

in which L_l is the lava heat of fusion and X'(T) represents the increasing volume fraction of olivine crystals in the lava with decreasing temperature, equal to $-1/625°C^{-1}$ (derived from the slope of the liquidus, Fig. 2, *Usselman et al.* (1979)). Because the physical properties of the lava are changing with distance, (10) must be solved at each increment of distance from the eruption source using a fourth order Runge-Kutta numerical method. Once a new temperature (from equation (10)) and a new lava composition (from equations (9)) are obtained, the new thermal, rheological, and fluid dynamic parameters are calculated at that distance. In doing so, the physical and geochemical evolution of the lava flow at progressively increasing downstream distances from the source is simulated.

The effect of bubbles on the emplacement of the lava is also assessed in the *Williams et al*. (2000) model. In order to account for such an effect, the bulk density and effective viscosity and specific heat equations found in *Williams et al.* (2000) have replaced their counterpart expressions within the sequence of algorithms mentioned above. By defining a parameter for the fraction of the lava consisting of vesicles (f_v), the effect on these physical properties can be assessed by the following equations:

$$\rho_{eff} = f_v\left(\rho_{gas}\right) + (1 - f_v)\rho_b\,, \qquad c_{eff} = f_v\left(c_{gas}\right) + (1 - f_v)c_l \qquad (11, 12)$$

$$\mu_{eff} = \mu_b\left[\frac{1}{1 - (1.3\, f_v)^{1/3}}\right] \qquad (13)$$

in which the subscript 'eff' refers to liquid plus crystals and/or bubbles, gas refers to the volatile gas in the vesicles, b refers to bulk (liquid plus crystals), and l refers to liquid. Equation (13), which is recommended by *Pinkerton and Stevenson* (1992) to assess the effect of bubbles on lava viscosity, is from *Sibree* (1934), and is valid for foams with values of f_v up to 75%.

To simulate thermal erosion over an unconsolidated substrate, the *Williams et al*. (1998, 2005) model considers the possible effects of particle disaggregation due to melting of ice and vaporization of intergranular water. Once intergranular water reaches the boiling point, it vaporizes. Because water expands as it changes phase from liquid to vapor, the expansion may fragment the unconsolidated substrate, and lead to mechanical mixing (mechanical erosion) with the lava before subsequent melting and assimilation by it (thermal erosion). A similar process of thermo-mechanical erosion can be described by energy conservation, as follows:

$$\rho_b c_l h \frac{dT}{dt} = -h_T\left(T - T_{vap}\right) - h_T(T - T_{sol}) - \frac{h_T\left(T - T_{vap}\right)E_{hg}}{E_{dg}} + \rho_l h \frac{dT}{dt} L_l X'(T) \quad (14a)$$

in which E_{dg} is the energy required to disaggregate the ground, given by:

$$E_{dg} = (1 - f_w)\, \rho_g\, c_g\, (T_{vap} - T_a) + f_w\, \rho_w\, [c_w\, (T_{vap} - T_a) + L_{vap}] \quad (14b)$$

and E_{hg} is the energy required to heat the disaggregated ground up to the lava temperature:

$$E_{hg} = (1 - f_w)\,\rho_g\,\{c_g\,(T - T_{vap}) + L_g\}\,f_w\,\rho_w\,c_{vap}\,(T - T_{vap}) \quad (14c)$$

in which f_w is the volume fraction of ice/water in the substrate, ρ_w and c_w are the density and specific heat of water/ice in the substrate, respectively, T_{vap} is the temperature at which all substrate water is vaporized, L_{vap} is the latent heat of vaporization of water, and c_{vap} is the specific heat of the water vapor. Finally, the erosion rate is given by:

$$u_m = \frac{h_T\left(T - T_{vap}\right)}{E_{dg}} \quad (15)$$

This erosion rate determines the upflow velocity of steam produced by vaporization of intergranular ice/water. The model predicts that particles up to the size of very fine sand (<0.1 mm) can be physically removed from the substrate, i.e., mechanically eroded, in this manner.

Finally, the calculated lava thermal erosion rate and degree of contamination of the lava by assimilated substrate enable estimates of erosion depth to be made by simply multiplying erosion rate values (varying as a function of distance from the lava source) by the elapsed time t since flow began, assuming steady flow conditions.

Model assumptions

The user-friendly interface of the C-written code makes the *Williams et al*. model especially adaptable to simulate various eruption conditions and planetary environments. Key input parameters of the model comprise: 1) The major oxide composition of the erupted lava and underlying substrate, 2) An initial value of lava thickness, 3) Amounts of ice in the substrate of: 0 vol% (consolidated substrate); 25 vol% (unconsolidated substrate), 4) The slope of the substrate.

Both lava and substrate are assumed to have a composition similar to that measured by Spirit at Gusev crater, with an estimated liquid viscosity of 2.8 Pa s and a liquidus temperature of 1270°C (1543 K) (*Jaeger et al.*, 2010), which well suit a turbulent emplacement regime. However, no real constraint on the eruption temperature exists (*Jaeger et al.*, 2010), which has led us to choose three values of eruption temperature (1270°C, 1260°C, and 1250°C) to investigate the extent to which a similar temperature variation may affect the key physical parameters of the flow along with erosion rates and depths. With bubbles and cooling (and crystallization), *Greeley et al.* (2005) suggested that a value of 50 Pa s might be more realistic for the bulk viscosity of the lava during emplacement. To assess the effect of bubbles on the emplacement of the lava as well as the ability of the modified flow to erode the substrate, we have followed the methodology adopted by *Williams et al.* (2000) and let the Athabasca turbulent lava contain 30-65% by volume of bubbles at the vent. The presence of bubbles in the lava is expected to decrease lava density and increase flow viscosity at low strain rates (*Pinkerton and Stevenson*, 1992), whereas at high strain rates bubbles will deform, reducing flow viscosity (*Spera et al.*, 1988). More recently, the effects of gas volume fractions and frequency of oscillation on

the elastic and viscous components of bubble deformation were investigated by *Llewellin et al*. (2002) and are analyzed in depth in the discussion. In the case of turbulent flow, high strain rates rather than low ones should be expected, but this is a scenario for which the effect of bubbles has not been assessed. In order to account for such an effect, the bulk density, effective viscosity and specific heat equations found in *Williams et al.* (2000) have replaced their counterpart expressions within the sequence of algorithms mentioned in the previous section.

The hydraulic radius of the lava is taken to be in the range 20-68 m, the latter value matching previously estimated upper end volumetric flux rates (*Jaeger et al.,* 2010), although we include results for an 80-m-thick flow. Observations from Digital Terrain Models indicate that the deepest parts of the channel center are as much as 100 m below the high-lava marks. Importantly, for the very wide and shallow proximal Athabasca channel, the value of the hydraulic radius very closely approximates flow depth (*Shaw and Swanson*, 1970).

The lava substrate is assumed to be dry and consolidated as well as ice-rich and unconsolidated. Rootless cones provide evidence that water or ice was present in the shallow subsurface at the time of the eruption. To simulate thermal erosion over an unconsolidated substrate, the *Williams et al*. (2005) model considers the possible effects of particle disaggregation (i.e., mechanical erosion) due to melting of ice and vaporization of intergranular water. Therefore, eq. (14a,b,c) calculate the energy required to vaporize the water and disaggregate the ground. All of the water is assumed to be vaporized in the process, with the maximum volume fraction of water present in the substrate pore space

being equal to 25%. Another important assumption is that the ice is melted first, followed by the rock.

The average slope of the substrate is calculated to be equal to 0.06° at proximal Athabasca, but we also adopt the value of 0.036°, which is averaged across the entire length of the Athabasca channel (*Jaeger et al.,* 2010), to test the impact of a lower slope of the ground on erosion rates and depths. Along with all the important temperature- and composition- dependent thermal physical properties of the lava, the model outputs decreasing flow velocities and increasing flow thicknesses, which are then multiplied by channel width to obtain 3-D flow rates. From these, we derive an estimate of the duration of the flow by using the available range of flow volumes (*Jaeger et al.*, 2010).

Results

Results are grouped in two separate sets: one set assesses the influence of different eruption temperatures and lava thicknesses on erosion rates and erosion depths into the lava substrate; the other set, while keeping the eruption temperature the same, describes the extent to which the likely presence of bubbles in the lava may cause the effective viscosity of the flow to increase, and lead to a reduced amount of thermal erosion.

Erosion rates and depths for 3 eruption temperatures at proximal Athabasca

Fig. 3 shows a linear relationship between crystal growth and decreasing lava temperatures. This is obtained by assuming that liquidus and solid temperatures are constant, and only a single silicate phase (olivine) crystallizes from the lava, the latter

assumption being consistent with the lava temperatures output. Figure 4 to 8 show how the density and viscosity of the flow vary as a function of decreasing lava temperatures and increasing downstream distances. Fig. 4 shows how lava thickness and downstream distances affect the rate of variation of both liquid and bulk flow densities. The eruption temperature is held at 1270°C (liquidus). For a 20-m-thick lava flow, the liquid density decreases from 2820 to ~2813 kg/m^3 over the 75-km-long proximal channel, whereas it reaches the minimum value of ~2819 kg/m^3, for a 68-m-thick flow. Bulk density values are always higher than liquid values for the same flow thickness and at similar distances from the lava source.

Table 2 shows the strong control exerted by temperature on flow viscosity. Flow viscosity and lava thickness increase as velocities and lava temperatures decrease with increasing distance from the lava source. Figs. 5 and 6 refer to an eruption temperature of 1270°C (liquidus) and show how flow viscosities increase faster for a 20-m-thick flow – from ~2.3 to ~4.1 Pa s through the end of proximal - which helps explain why turbulent flow conditions are more easily achieved and maintained by thicker lavas. Figs. 7 and 8 show the impact of a lower eruption temperature of 1250°C on the rate of variation in viscosity with increasing downstream distances and decreasing lava temperatures, respectively. Bulk viscosity values decrease by only a factor of ~1.4 relative to the ~1.7 factor obtained for lavas erupted at the liquidus temperature, this being likely a consequence of the presence of crystals and higher flow viscosities of ~14 Pa s at time of eruption compared to the liquidus temperature scenario.

At proximal Athabasca, the measured average slope of the ground of ~0.06° is responsible for the higher flow velocities - in the range 4.5-11.0 m/s - and flow rates that reach 3.4 x 10^{-2} km^3/s (Table 2). By comparison, Table 3 lists the key flow parameters concerning the other portions of the Athabasca main channel, which are characterized by a lower slope of the ground (0.036°, from *Jaeger et al*., 2010), and which enabled determination of average flow rates lower than those obtained at proximal by a factor of ~1.3 and total flow durations ranging from 2.2 to 37.2 days and obtained from 80-m and 20-m-thick lava flows, respectively. Flow velocities range between ~4.0 and 11.0 m/s, and fall within previously estimated values (*Jaeger et al.*, 2010) if thicknesses are equal to or larger than 30 m. Lava temperatures decrease by less than 8°C from initial eruption values over the 75-km-long proximal Athabasca channel, the largest temperature drop occurring for a 20-m-thick flow erupted at the liquidus temperature. Because of this, a 20-m-thick lava flow is unlikely to have flowed fully turbulently out to a distance of ~1,400 km from the vent (Table 3, Figure 9). Average bulk densities range from 2820 kg/m^3 (for an 80-m-thick flow erupted at the liquidus temperature) to 2798 kg/m^3, for a 20-m-thick flow and a lava temperature in the range 1250°-1246°C. Bulk viscosities never exceed ~20 Pa s, for the same interval of lava temperatures and flow thicknesses. This likely results from our model assumption of a thermally-mixed interior, which well suits a fully turbulent regime, with Reynolds numbers in the range $3.6x10^4$-$2.1x10^6$, the higher values being associated with liquidus lava temperatures and flows thicker than 30 m, as also shown in Figure 10.

Table 3 shows that a flow of thickness equal to or larger than 30 m may have flowed turbulently out to a distance of ~1400 km from the vent, thus covering the total distance

traveled by the Athabasca flood lava (see also Fig. 9). This last result adds further support to the idea that the entire flow was likely emplaced during a single event, and over a short time. Calculated effusion rates vary by a factor of ~8 for thicknesses in the range 20-68 m and up to ~10, if the bank-full flow thickness of 80 m is included (Tables 2, 3). Flow rates increase mainly as a function of increasing flow thickness and, to a lesser extent, increasing lava temperature (a result of the reduced viscosity). The duration of the flow is necessarily approximate since flow rate is expected to vary with time. As a result, the values examined in Table 3 are plausible average values for the main effusive event. A roughly order-of-magnitude difference between peak and mean flux is observed for smaller terrestrial fissure eruptions (e.g., *Wadge*, 1981). This would not only affect the erosion rate but also the spatial distribution of erosion, since the higher fluxes will inundate and erode some areas that would be untouched at lower eruption rate. If we assume an average flow thickness in the range 20-30 m (*Jaeger et al.*, 2010), and refer to the emplacement of the total flow out to a distance of ~1,400 km from the vent, we obtain flow durations in the range ~11-37 days, in agreement with previous results from *Jaeger et al.* (2010). The 11-day time refers to a total lava volume of 5,000 km^3, a flow thickness of 30 m and an eruption temperature of 1270°C (liquidus). If we assume for the total non-vesicular lava volume to range between 5,000 and 7,500 km^3, a flow that on average is 20-m thick and is erupted at a temperature of 1250°C will take 3-5 additional days to be emplaced, respectively, compared to a similar flow of identical thickness, which is erupted at a temperature of 1270°C.

Table 4 shows erosion rates and depths as a function of eruption temperature, flow thickness, and substrate slope. Calculated values range from a minimum of 0.05 m/day, for a 20-m-thick flow erupted at 1250 °C, to a maximum of 0.36 m/day for an 80-m-thick flow that is erupted at the liquidus temperature and is flowing over a substrate with 25% ice (by volume). Higher lava temperatures generate higher erosion depths and, for a given lava thickness, depth values are always higher near the vent. For a 20-m-thick flow, a 20°C difference in eruption temperature yields a 2.1-4.2 m difference in erosion depth values at the lava source (see also Figure 11). Fig. 12 shows maximum erosion depths—obtained by assuming a total flow volume of 7,500 km^3—plotted against distance from lava source. The presence of ice in substrate pore space makes erosion depth values higher by a factor of 1.3, compared to a "dry" scenario. The 20-m-thick flow erupted at a temperature of 1250°C, which is associated with the lowest erosion rate, generated an erosion depth of 3.3 m at the lava source (Table 4) in a period of ~37 days (Table 3). Importantly, flow duration is the most important parameter in determining the total amount of thermal erosion, and higher erosion rates are not necessarily associated with larger erosion depths.

In summary, our range of modeled erosion depths (0.4-7.5 m), consistent with the proposed emplacement volumes and duration of the Athabasca flow, is far less than the depth of the channel (~35-100 m), regardless of the parameters used. Thus, our modeling suggests that thermal erosion does not appear to have had a major role in the formation of Athabasca Valles.

Lava vesicles in the flowing lava

The likely occurrence of vesicles in the flow has the effect of either increasing or decreasing the "effective" viscosity of the flow, depending on bubble shapes and strain rates (*Llewellin*, 2002), the term "effective" implying that liquid, solid (olivine crystals) and gas phases (H_2O vapor) may coexist in the lava during flow emplacement. In our calculations, we assume that lava viscosity increases with increasing proportions of gas bubbles in the flow. The eruption temperature is held constant at 1270°C, and the liquid bulk density and viscosity of the non-vesicular flow remain constant and equal to 2820 kg/m^3 and ~2.3 Pa s, respectively. Table 5 shows values of Reynolds number, flow rates, total volumes, and erosion rates and depths, which refer to lava flows of different thickness, containing 30-65% by volume of vesicles at the Proximal Athabasca source region. Erosion depths were calculated by referring to total vesicular volumes of 6,500, 7,500 and 8,250 km^3, which were obtained by adding the contribution of 30%, 50%, and 65% of vesicles, respectively, to the original 5,000 km^3 estimate.

Total flow durations were obtained from the newly-calculated flow rates and total vesicular volumes, and are similar to those found for non-vesicular flows (Table 3), exception made for the ~49 days taken by a 20-m-thick flow containing 65% vesicles. A 30-m-thick flow that contains 30 vol% vesicles is defined by a bulk density of 1974 kg/m^3, an effective viscosity of 8.6 Pa s, and a velocity of 4.9 m/s. This flow is estimated to erode the underlying substrate at rates of ~0.09-0.12 m/day, which are about half the values that are obtained by a similar non-vesicular flow, and determines maximum erosion depths of the substrate of 1.2-1.6 m. A non-vesicular flow of similar thickness would yield a maximum erosion depth of 2.2-2.9 m. If the same flow contained 50% vesicles, maximum

erosion depths would be lower – of order 0.9-1.3 m. These results show that amounts of vesicles in the range 30-50% have the potential to reduce erosion depths by a factor of ~1.8-2.4, if compared to their non-vesicular counterparts. In the case of a 30-m-thick flow containing 65% vesicles, maximum erosion depths at the lava source are of order 0.6-0.8 m, a factor of ~3.6 lower than those pertaining to a similar scenario where vesicularity is not accounted for.

Could a 30-m-thick flow that originally contains 30% vesicles travel a large distance and still flow turbulently? First, it must be noted that vesicularity is likely to decrease downstream of the source region and over time. Second, the Reynolds number characterizing this vesicular flow at the source region (6.7×10^4) is higher by a factor of ~1.2 compared to the value (5.6×10^4) referred to a flow of similar thickness, which is erupted at a temperature of 1250°C (Table 3) and is found to flow turbulently out to the total distance traveled by the Athabasca flood lava (Fig. 9). For an amount of vesicles as large as 50%, the Reynolds number of a 30-m-thick flow at the source is equal to 2.1×10^4, a factor of ~2.6 lower than 5.6×10^4. This flow would be characterized by a bulk density of 1411 kg/m^3 and an effective flow viscosity of ~17 Pa s. For a lava flow containing 65% vesicles, the flow regime always turns to laminar at a downstream distance that depends on the initial value of the lava flow thickness. The effective viscosity of the flow increases to ~42 Pa s and the bulk density becomes as low as 988 kg/m^3.

In summary, our model results suggest that if the Athabasca lavas were enriched in gas (derived either from juvenile volatiles or from assimilation of water vapor from melting of substrate ice), then they would have been even less capable of thermal erosion to depths

sufficient to produce the Athabasca channel. Lava-draped craters with depressed interiors (implying volume loss from closed depressions) suggest that a significant volume of gas was lost from the flow after eruption (*Jaeger et al.,* 2010), so the lava was probably highly vesicular near the vent.

Discussion

In this section, we will discuss the possible sources of error for the model. Three values of eruption temperature (liquidus and 10 and 20 degrees below) were chosen to investigate the extent to which this physical parameter may have affected the other physical parameters of the flow and, ultimately, erosion rates and depths. The *Williams et al*. (1998) program shows that, if the lava temperature decreases more than 20° C below liquidus, the dynamic viscosity of the flow increases much faster as a function of distance from the lava source. Specifically, once an eruption temperature of 1243° C is chosen, the model stops producing turbulent flow scenarios. As a result, we do not expect the minimum eruption temperature to have been much lower than what we model, if turbulent flow conditions truly characterized the Athabasca flood lava, and a negligible source of error is expected to arise from this approximation.

The lava substrate underlying the Athabasca flow was assumed to be of the same composition and temperature as the lava. Yet, the substrate could have a lower melting temperature, since it is composed of Elysium Rise lavas that could be different from the Cerberus Fossae flood lavas. Notwithstanding this, both the presence of ice in substrate pore space and its level of consolidation appear to have a higher impact than a change in

composition on maximum erosion rates and depths, as shown in *Williams* et al. (1998, 2005). The rootless cones that pepper the floor of Athabasca Valles (*Jaeger et al.,* 2007) may indicate that a non-homogeneous substrate existed, originally, at several locations along the Valles. Also, rootless cones could have been caused by atmospherically emplaced ground ice, since it would be difficult for lava erosion to reach deep ice layers (*Dundas and Keszthelyi*, 2013).

Another potential source of error in our model could result from our assumption of low strain rates in assessing the impact of bubbles on flow viscosity. *Llewellin et al*. (2002) developed a semi-empirical constitutive model for the visco-elastic rheology of bubble suspensions with gas volume fractions < 0.5 and small deformations (capillary number = Ca <<1). Their model was validated against observations of the deformation of suspensions of nitrogen bubbles in a Newtonian liquid (golden syrup) subjected to forced oscillations over a range of frequencies, f. In the case of steady flow conditions, shear conditions have remained constant for a time significantly longer than the relaxation time of the bubbles (*Llewellin et al*., 2002). In a similar scenario, at low f, which occur at low Ca values, bubbles remain approximately spherical in shape and increasing gas volume proportions, f_v, lead to an increase in viscosity. At high f, which correspond to high Ca values, bubbles are significantly elongate and viscosity decreases as the proportion of gas bubbles increases. Hence, viscosity can increase or decrease with increasing f_v depending on the conditions of strain. To date, the behavior of bubble-bearing turbulent lava has not been reproduced in any experimental setting. If we assumed that the viscosity of the bubble-rich flow became lower than that of the bubble-free flow by an order of magnitude, thus reaching a

value of ~0.23 Pa s, maximum erosion depths for 20-m-thick lava flows - will be higher by a factor of ~2.3. Even if such a decrease in viscosity with increasing bubble contents was the case, other factors such as variations in effusion rates with time of eruption would likely act against a monotonic decrease in viscosity, due to the variations in strain rates associated with it. Other factors, such as local variations in ground slope, could also counteract such a trend of decrease in flow viscosity, especially along the comparatively steeper and more irregular portion of the proximal Athabasca channel.

The enhanced cooling caused by the impact of bubbles on thermophysical properties is not fully included in our analysis, though we do include the reduced lava density which represents the predominant effect of bubbles (*Keszthelyi,* 1994). Consideration of these additional assumptions and conditions, while contributing to a more complete knowledge of the processes that may have occurred during the flow and emplacement of the Athabasca flood lava, is unlikely to lead to significantly higher erosion rates and erosion depths of the lava substrate.

Results show that the short flow duration poses a severe constraint on the ability of the lava to thermally erode the substrate. Instead, mechanical erosion does not require long flow durations to determine high levels of erosion of the lava substrate, for reasons that will become clear next. *Ciesla and Keszthelyi* (2000) suggested that many lava flows are close to reaching the critical stresses necessary to fracture underlying rock and entrain the fragments in the flow. They came to this conclusion by using a simple quantitative model of the stresses generated at the base of an active lava flow, a model based on Hallet's study of glacial erosion (*Hallet*, 1996). In the model, the lava is assumed to flow in a laminar

fashion over a horizontal saw-toothed shaped substrate and a cavity filled with a rotating pool of lava forms in the process. The authors derived an expression from *Hallet* (1996), which enables determination of the average normal stress at the flow/substrate contact and, ultimately, calculation of the tensile stress in the rock. The latter was found to approximate or even reach the critical stresses required to fracture coherent crystalline rock. At Athabasca, a similar scenario appears to be further supported by the presence of landforms that are consistent with (but not diagnostic of) mechanical erosion by lava (*Keszthelyi et al.*, 2014). In the case of short flow duration, the effect of mechanical erosion could be much stronger than thermal erosion because 1) larger entrained blocks do not reach thermal equilibrium with the flowing lava and 2) there may be a substantial porosity in the removed material (*Keszthelyi et al.*, 2014). The same authors finally place an upper limit on the amount of mechanical erosion obtainable at Athabasca Valles using thermal considerations. Specifically, rock is of order 1000 K colder than the lava and the lava will freeze if cooled ~100 K, so the entrained rock should be no more than 10% of the erupted volume. Given the large distance traveled by the lava (~1,400 km), an order of magnitude less entrainment is likely more realistic. Using the available volume estimates of 5,000 and 7,500 km^3 (*Jaeger et al*., 2010), this corresponds to an order of ~100-1000 km^3 of erosion. Athabasca Valles is roughly 300 km x 30 km in area (~10,000 km^2), so a maximum of <100 m, and more realistically ~10 m average downcutting is allowed and a non-uniform erosion – with some tens of meters of downcutting - could be reached locally. This is broadly consistent with results from Kasei Valles, where a similar turbulent lava flow is thought to have eroded large volumes at cataracts but had much lesser effects elsewhere (*Dundas and*

Keszthelyi, 2014). Elements from available mechanical and thermo-mechanical models of erosion by lava could be incorporated into a new version of the model to test the validity of the predictions concerning the Athabasca flood lava.

Conclusions

The Athabasca flood lava was probably emplaced turbulently, over a time of a few to several weeks (*Jaeger et al.,* 2010). We adapt the *Williams et al.* (2000, 2005) model to investigate how effective the mechanism of thermal erosion by turbulent lava could have been in eroding the lava substrate along the ~75-km-long upstream portion of the main Athabasca channel, i.e., at proximal Athabasca. Eruption temperatures within 20°C of the liquidus value (1270°C) were considered, and proportions of bubbles of 30%, 50%, and 65% by volume were assumed to coexist with the liquid phase within the flowing lava. For emplacement volumes of 5,000 and 7,500 km^3 and average lava flow thicknesses of 20 and 30 m, we find flow durations of ~11 to ~37 days, consistent with previous results from *Jaeger et al.* (2010). The highest values of erosion depth are found at the lava source for a 20-m-thick flow that is erupted at the liquidus temperature (1270°C) and flows free of bubbles over a substrate that contains 25% by volume of ice. The calculated erosion depths are never higher than 7.5 m, far less than the channel depth.

The results reveal how important flow duration is in determining the effectiveness of thermal erosion in melting the lava substrate. The maximum value of erosion depth obtained is far lower than the depth of the channel, which reaches values of 80-100 m at several locations (*Jaeger et al.*, 2010). Therefore, some additional mechanism besides

thermal erosion must have been at work to erode Athabasca Valles. One possibility is that the channel was pre-existing, produced either by aqueous floods or by a series of previous lava flows with modest erosional effectiveness. In order to better understand the latter possibility, mechanical erosion by lava must be examined in more detail. Specifically, in the case of short flow durations, mechanical erosion is expected to be more effective than thermal erosion, because it physically removes portions of substrate that are not given sufficient time to become assimilated into the flowing lava. These entrained fragments and blocks could then contribute to eroding the substrate further by abrasion. An advanced version of the current model will include a mechanical/thermo-mechanical mechanism of erosion, which will account for the geometrical and compositional characteristics of the Athabasca lava substrate.

Acknowledgements

The investigation by V.C. and D.A.W. was supported by NASA Planetary Geology and Geophysics grant NNX12AR66G. We used data obtained from the NASA Planetary Data System, and the Ronald Greeley Center for Planetary Studies (the NASA Regional Planetary Information Facility at ASU). We are grateful to all those who were involved in analyzing the data collected by the High Resolution Imaging Science Experiment (HiRISE), Context (CTX), and Compact Reconnaissance Imaging Spectrometer for Mars (CRISM) instruments onboard the Mars Reconnaissance Orbiter (MRO) spacecraft. Specifically, the data contained in the Jaeger et al. (2007, 2010) papers enabled production of our results.

Finally, we are grateful for the constructive comments by journal reviewers, and an anonymous U.S.G.S. reviewer.

4 PAPER 4: MOON, VALLIS SCHRÖTERI OUTER RILLE (CATALDO ET AL., IN REVISION)

Abstract

Results of the first 3-D model of thermal erosion by turbulently flowing lava on the Moon were obtained at the Vallis Schröteri primary rille. Maximum erosion rates (at the lava source) in the range 6.9 cm/day – 2.8 m/day are found for eruption temperatures that vary from 1630°C (superheated lavas) to the liquidus temperature of 1440°C and a sub-liquidus value of 1400°C. The lava substrate has been modeled as both consolidated and unconsolidated. Thermal considerations limit our ability to derive erosion depth measurements from any value of maximum erosion rate calculated by the model. Based on the same considerations, any values within 1 m/day are predicted to be consistent with the geochemical and geophysical evolution of the lava over time and, hence, provide reliable estimates of erosion depths of the lava substrate. By assuming a constant maximum erosion rate of 1 m/day over time, it might have taken ~ 2 years for the lava to excavate the Cobra Head region, the ~700 m deep depression located at the head of the primary rille.

The occurrence of structural patterns associated with the Imbrium basin adjustment along the Vallis Schröteri rille segments and its location on the Aristarchus Plateau, a tilted block thought to have formed in response to the Imbrium impact strongly support a tectonic origin for the rille. At a later moment in time, the rille was likely excavated farther into the substrate by a process of thermal and/or a combination of thermal and mechanical erosion by lava. While favoring a combined tectonic and erosional origin for the rille, we cannot

totally rule out a constructional component in the process – especially in light of the recent finds by the "Gravity Recovery And Interior Laboratory" (GRAIL).

Introduction

Sinuous rilles are narrow, winding valleys that occur primarily within the lunar maria. In size they are typically a few hundred meters to a km wide, several hundred meters deep and can be tens of kilometers to over hundred kilometers long (*Spudis*, 2015). Some originate in highlands terrain, but all trend downslope and empty into mare material. There is a consensus that these features are lava channels though their formation mechanism is still highly debated.

Vallis Schröteri (Fig. 4.1) is the largest sinuous rille on the Moon and includes an outer primary rille (investigated in this study) that stretches out to a distance of ~150 km from its source region, and a sinuous and highly meandering inner rille that extends ~50 km farther downstream (*Cataldo et al.*, 2022, manuscript in preparation). Vallis Schröteri sits atop the Aristarchus Plateau, a block of ancient highland crust that was uplifted during formation of the Imbrium basin (*Moore*, 1965; *Guest*, 1973; *Zisk et al.*, 1977) as the crust readjusted following the impact that occurred ~3.85 b.y. ago (*Wilhelms*, 1987). The parallelogram-shaped Plateau lies just outside the main topographic ring of the Imbrium impact basin (*Mustard et al*., 2011), and rises 1-1.5 km above the surrounding Oceanus Procellarum sloping away from it to the west (*Zisk et al*., 1977). Part of the high topography associated with the Aristarchus Plateau likely existed prior to the formation of the Imbrium basin (*Mustard et al*., 2011).

Melosh (1976) suggested that radial faults - thought to have formed with the formation of the Imbrium basin - continued to be active for at least 600 Ma on the Moon. His suggestion was inferred from the observation of radial faults cutting mare basalts, 600 Ma after the formation of Imbrium basin (*Taylor*, 1975). More recently, other investigators noticed that many structures associated with the Imbrium impact are not radial to the basin, thereby implying an endogenic or structural origin (*Hartmann*, 1964; *Strom*, 1964).

The primary rille of Vallis Schröteri might have formed, in part, by exploitation of pre-existing tectonic structures (*Zisk et al*., 1977). Besides, the Aristarchus Plateau hosts many other rilles that extend into the mare basalts to the east of the Aristarchus crater, and are thought to have formed by a combination of thermal and mechanical erosion and construction of cooled levees (*Campbell et al*., 2008).

Cataldo et al. (2015) carried out a preliminary investigation of the Vallis Schröteri primary rille using the rigorous 1.5-dimensional model of thermal erosion by turbulently flowing lava of *Williams et al.* (1998, 2000). Preliminary results of that investigation show that thermal erosion unlikely played a key role in the formation of the rille, and tectonics might have contributed to the shape of the rille we see today. In this paper, we will use the *Cataldo et al.* (2020) 3-D model of thermal erosion by turbulently flowing lava to calculate maximum erosion rates and – whenever possible - depths at the Vallis Schröteri primary rille. The collected information and model results will be used to formulate a better testable hypothesis of formation for the Vallis Schröteri primary rille.

A constructional and erosional origin for lunar sinuous rilles

Some authors interpret rilles to be mainly constructional features that were partly roofed over to form lava tubes (*Spudis et al.*, 1988, 2015; *Komatsu and Baker*, 1992; *Gregg and Greeley*, 1993). Other authors support an origin by thermal erosion of the substrate by turbulently flowing lava (*Hulme*, 1973, 1982; *Head and Wilson*, 1981; *Wilson and Head*, 1981; *Williams et al*., 1998, 2000; *Kerr*, 2009) or thermo-mechanical erosion (*Williams et al.*, 1998, 2000; *Fagents and Greeley*, 2001; *Siewert and Ferlito*, 2008). Constructional fe-

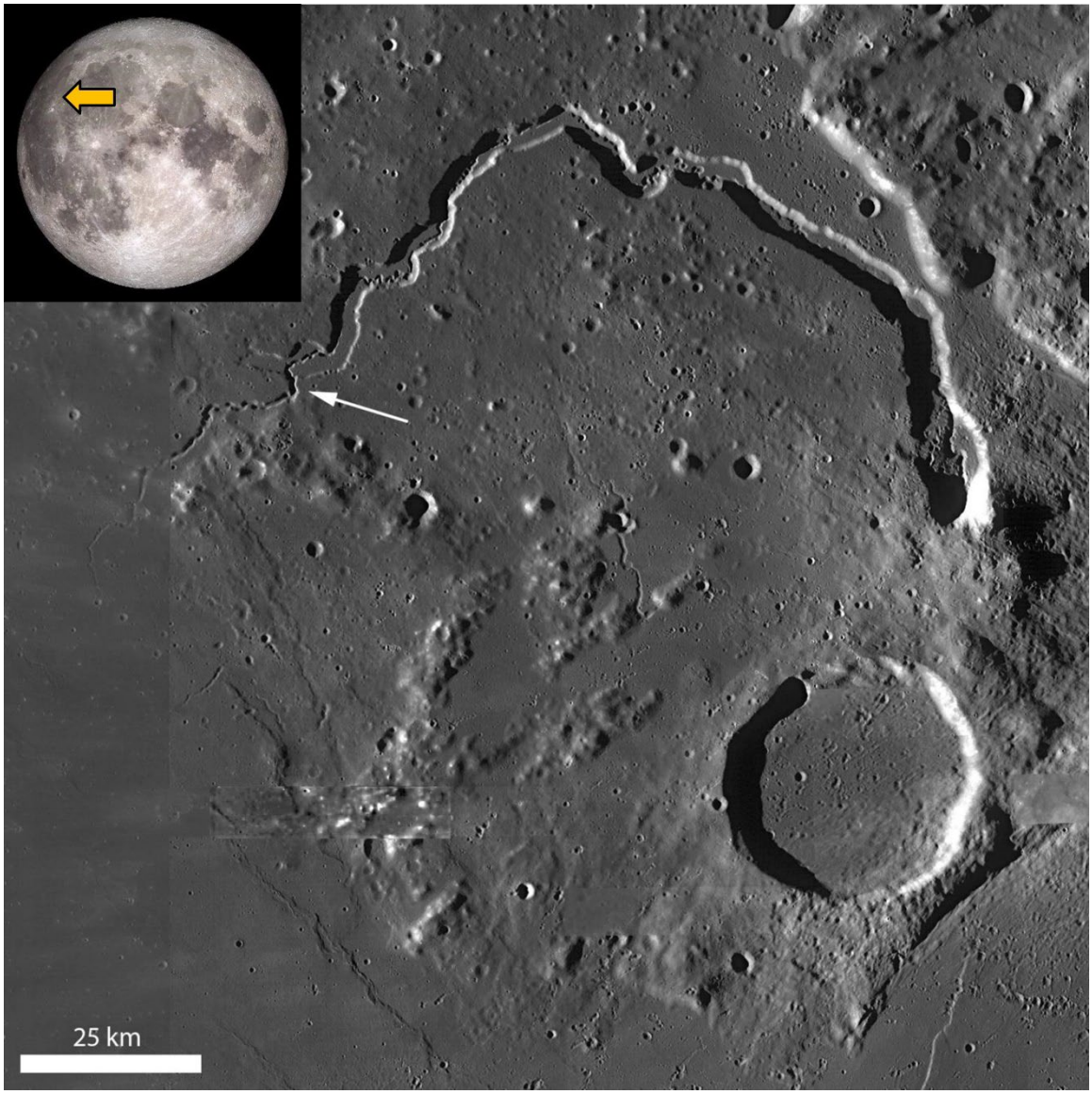

Fig. 4.1. LROC image showing part of the Aristarchus Plateau with the Vallis Schröteri sinuous rille and the Herodotus impact crater. The upper left inset shows the location of the rille on the Moon's near side. The rille source region (Cobra Head) is closer to the crater and the white arrow points at the location where the primary rille ends and the inner rille crosses it. LROC WAC mosaic, 100/pixel, NASA/GSFC/Arizona State University.

atures form as the result of marginal cooling of a lava flow. As the flow cools inward from the margins, levees form and bound the fastest-moving portion of the flow until a channel is formed (*Hulme*, 1974). These channels tend to be shallow and develop within an initial sheet flow. They might also develop a structurally stable crust at the surface or, alternatively, form within the substrate and lead to a lava tube (*Greeley*, 1971). On the Moon, subsurface tube structures were identified in the Marius Hills region (*Haruyama et al*., 2009; *Boyd et al*., 2011; *Huang et al*., 2011), and they look totally different from the laterally continuous, nearly parallel walls that bound the wide channels that characterize the largest sinuous rilles. Importantly, the latter channels appear to lack levees and are a few to several hundred of meters deep. Because of this, several authors interpreted them to have formed by thermal and/or thermo-mechanical erosion into the lava substrate, with lava flowing in a turbulent fashion in an open channel that likely developed a thin surface crust (e.g., *Williams et al*., 1998, 2000). One of the largest sinuous rilles on the Moon, Hadley Rille, is located just inside the rim of the Imbrium basin and was examined by the Apollo 15 crew (*Spudis et al*., 1988). This rille fits in the category of large, deep channels we just described and, hence, it might have formed by thermal or thermo-mechanical erosion of the lava substrate. That said, numerous structural and topographic depressions in the area were probably produced by regional deformation associated with basin adjustment and were later followed by basalt flows that established Hadley Rille (*Spudis*

et al., 1988). Specifically, the mountain material (Apennine Bench) surrounding the rille contains scarps, cracks and grabens that tend to be oriented in directions radial and concentric to Imbrium basin structural trends (*Spudis et al*., 1988). Last but not least, the trends of individual segments of Hadley Rille are coincident with these regional structural patterns. The same authors argue that some erosion by lava probably occurred and caused individual depression segments to connect. Nevertheless, the rille was predominantly constructional in origin, and formed by accretion of lava along the walls of pre-existing Apennine Bench cracks, generally narrowing the width of the depressions that later became the rille. Several authors support the idea that the large majority of lunar sinuous rilles formed by thermal and/or a combination of thermal and mechanical erosion of the lava substrate.

Method

The 3-D Cataldo et al. (2020) model of thermal erosion

We created a 3-D model of thermal erosion by turbulently flowing lava to assess how channel bank erosion relates to erosion at the channel bed, something that is not addressable by one- or two-dimensional models. When applied to sinuous rilles, a 3-D model has the unique advantage of revealing the details of flow circulation and how flow velocity and viscosity at meander bends relate to the same flow parameters at the channel centerline. Besides, it reveals how erosion rates vary with changing flow rate, flow temperature, and meander/channel geometry.

The new model uses the resources made available by OpenFOAM, a C++ library of applications called solvers and utilities. Solvers enable simulation of specific problems of Computational Fluid Dynamics (CFD), whereas utilities are designed to perform simple pre-and post-processing tasks like those involved in mesh generation. The OpenFOAM finite volume software is extremely versatile because users can create their own solvers and utilities or modify existing ones. Finally, it allows for grid design that can be tailored to the scenario of interest.

The Finite-Volume Method

A thorough description of the method is found in *Moukalled et al*. (2016). The term finite volume refers to the small volume surrounding each node point in a mesh. Analogous to other numerical methods developed for the simulation of fluid flow, the finite volume method transforms a chosen set of partial differential equations into a system of linear algebraic equations. The discretization process involves two basic steps: in the first step, the partial differential equations are integrated and transformed into conservation equations over an individual volume or cell. In the second step, interpolation profiles are chosen to approximate the variation of the variables within the cell and relate the surface values of the variables to their cell values. This later step leads to the algebraic equations previously mentioned.

A key advantage of this methodology is the fact that the flux entering a given volume is identical to that leaving the same volume, i.e. the method is conservative. Furthermore, a key ingredient in the implementation of the methodology is setting up the

geometrical support framework for the problem at hand, which also allows for unstructured meshes.

Turbulence modeling

The motion of a turbulent lava flow – an incompressible fluid – can be described by the Navier-Stokes momentum equations in the x, y, and z direction. To reduce the large computational cost associated with a direct solution of the Navier-Stokes equations, statistical analyses can be used to simplify the resolution of turbulent flows. Specifically, the time-dependent nature of turbulence together with its wide range of time scales suggest that statistical averaging techniques can be applied to approximate fluctuations. The process of time-averaging introduces two new unknowns (Reynolds stresses) into the system of equations and is applicable to Netwonian fluids only because Reynolds stresses are assumed to be a linear function of the mean velocity gradients (*Moukalled et al*., 2016). The process of calculating Reynolds stresses is referred to as turbulence modeling and consists of finding two additional transport equations. Two among the most widely used turbulence models are the k-epsilon (k-ε) and SST k-omega (k-ω) models. Each of the two models contains two additional transport equations. The standard "k-ε" model (*Jones and Launder*, 1972; *Launder and Sharma*, 1974) is a high Reynolds number model that does not perform well in cases of adverse pressure gradients and flow separation. The k expression quantifies the turbulent kinetic energy that is produced, convected, and diffused within the flow, and the ε equation approximates turbulent dissipation. The "SST k-ω" model (*Menter*, 1993) switches to a "k-ε" behavior in the free stream and can be used as a

low Reynolds number model all the way down to the wall, thanks to the Shear Stress Transport (SST) formulation. Omega is the rate of dissipation of the turbulent eddies or, in other words, the rate at which turbulent kinetic energy is converted into internal thermal energy per unit volume and time (*Moukalled et al*., 2016). Thanks to the SST formulation, the SST k- ω model is very well-suited to determine erosion rates into the lava substrate and is especially effective in cases of adverse pressure gradients and flow separation. In this paper, we will present results obtained with the SST k- ω model.

Modifying SimpleFoam – The Steady-State Solver for turbulent flow

Although our model adopts an initial value of flow velocity at the lava source (inlet value in the three directions, U_x, U_y, and U_z), the velocity field within the flowing lava is not known and has to be computed by solving the set of Navier-Stokes equations. For incompressible flows, this task is complicated by the strong coupling that exists between pressure and velocity and by the fact that pressure does not appear as a primary variable in either the momentum or continuity equations (*Moukalled et al*., 2016). The Semi Implicit Method for Pressure Linked Equations (SIMPLE) algorithm was specifically designed to reformulate the Navier-Stokes equations in terms of a momentum and a pressure equation, which are then discretized and solved sequentially. The sequence is repeated until the velocity and pressure fields satisfy both mass and momentum conservation (*Patankar and Spalding*, 1972). The simpleFoam solver that is made available in the OpenFOAM library is well-suited for the purpose of modeling turbulent, incompressible flow. The key input parameters of the flow are velocity and pressure, and flow is investigated in steady

conditions. However, no initial temperature is specified in the solver, a severe limitation when modeling turbulently flowing lava.

To solve the temperature limitation inherent in the solver, we coupled a 3-D temperature model to simpleFoam. The first step was to choose an energy expression that could be applicable to a fixed control volume and fit a scenario of turbulently flowing lava. An energy equation can be written in terms of specific internal energy, specific enthalpy, specific total enthalpy, or temperature. An energy expression written in terms of temperature assumes that the flow is Newtonian because the specific enthalpy of the flow is only a function of pressure and temperature variations (*Moukalled et al*., 2016). Such an assumption is consistent with a scenario of turbulently flowing lava for which lava temperatures are assumed to be above at or near the liquidus value. Finally, our steady-state energy expression as a function of temperature can be written as:

$$\nabla \left[\rho\, c_p\, \mathbf{v}\, T\right] = \nabla \left[k\, \nabla T\right] \qquad \text{Eq. (1)}$$

in which ρ is density of the liquid lava, c_p is lava specific heat capacity, **v** is the velocity vector (**v** = v_x, v_y, v_z), T is lava temperature, and k is lava thermal conductivity. Because we are dealing with an incompressible fluid, lava density is taken as a constant. If we normalize Eq. (1) by density, we obtain:

$$\nabla \left[\, c_p\, \mathbf{v}\, T\right] = \nabla \left[\frac{k}{\rho}\, \nabla T\right] \qquad \text{Eq. (2)}$$

Conveniently, the lava *effective thermal diffusivity* α_{eff} can be expressed as a function of lava thermal conductivity, k, as follows:

$$\alpha_{\text{eff}} = \frac{k}{\rho\, c_p} \qquad \text{Eq. (3)}$$

If we solve for k and then substitute (3) into (2), we obtain:

$$\nabla \left[c_p\, \mathbf{v}\, T \right] = \nabla \left[c_p \alpha_{\text{eff}} \nabla T \right] \qquad \text{Eq. (4a)}$$

or

$$\nabla \left[\mathbf{v}\, T \right] = \nabla \left[\alpha_{\text{eff}} \nabla T \right] \qquad \text{Eq. (4b)}$$

The left-hand side term in (4a) is a convection term and the right-hand side one is a diffusion term and they are both normalized by density. Eq. (4b) represents the temperature model that was coupled to the SimpleFoam solver, and the suffix "eff" stands for effective. The *effective thermal diffusivity* accounts for the laminar and turbulent components of diffusivity, and is given by:

$$\alpha_{\text{eff}} = \frac{\upsilon}{\text{Pr} + \alpha_t} \qquad \text{Eq. (5)}$$

in which υ is the kinematic viscosity of the lava, Pr is the molecular (laminar) Prandtl number and α_t is the kinematic turbulent thermal diffusivity that is expressed as:

$$\alpha_t = \frac{\upsilon_t}{Pr_t} \quad \text{Eq. (6)}$$

Deriving the erosion rate expression

The one-dimensional expression that allows determination of the erosion rate into the lava substrate, u_m, is obtained by adopting the approach taken by *Hulme* (1973), *Huppert and Sparks* (1985) and *Williams et al*. (1998, 2000), as follows:

$$u_m = \frac{h_T(T_l - T_m)}{\rho_g[c_g(T_m - T_0) + L_g]} \quad \text{Eq. (7)}$$

in which the numerator represents the convective heat flux to the base of the flow and the denominator defines the energy required to melt the ground. Specifically, h_T is the convective heat transfer coefficient, T_l is the temperature of the liquid lava, T_m is the temperature of melting of the ground, ρ_g is the density of the lava substrate, c_g is the substrate specific heat capacity, T_0 is substrate temperature away from the lava/substrate interface, and L_g is latent heat of fusion of the ground. Equation 7 calculates the steady-state rate of advance of the ground/lava interface, when thermal equilibrium is assumed at the lava/ground interface.

To find an expression that can be used in our model, we must equate the numerator of Eq. (7) to a heat flux expression that contains thermal diffusivity and temperature gradient of the lava in a direction perpendicular to the lava/substrate interface, as follows:

$$h_T(T_l - T_m) = -\rho c_p \alpha_{eff} \frac{\partial T}{\partial n} \quad \text{Eq. (8)}$$

in which the left-hand side term represents the convective heat flux to the base of the flow and $\frac{\partial T}{\partial n}$ is the temperature gradient of the lava in a direction perpendicular to the channel bed and banks. The convective heat transfer coefficient can be expressed as (*Kakac et al*., 1987):

$$h_T = \frac{0.027\, k\, Re^{0.8} Pr^{0.33}}{h} \left(\frac{\mu_b}{\mu_g}\right)^{0.14} \quad \text{Eq. (9)}$$

in which Re is the Reynolds number of the flow, expressed as:

$$Re = \frac{U\,L}{\upsilon} \quad \text{Eq. (10)}$$

in which U is flow velocity, L is the characteristic length of the flow (here the hydraulic diameter of the channel) and υ is the kinematic viscosity of the lava. In Eq. (9), h is lava thickness μ_b is the bulk dynamic viscosity of the flow and μ_g is the dynamic viscosity of the lava substrate. Equation 9 shows how the value of the heat transfer coefficient is influenced by flow thickness, and also accounts for the viscosity of the substrate. By combining (8) and (7), we obtain:

$$u_m = \frac{-\rho\, c_p\, \alpha_{eff}\, \frac{\partial T}{\partial n}}{\rho_g[c_g(T_m - T_0)+L_g]} \quad \text{Eq. (11)}$$

which is used to calculate erosion rates into the channel bed and banks. In the following section, we will describe the key input parameters and assumptions of the model. This will help identify the flow parameters in (9) that are most effective in determining variations in erosion rate.

Model input parameters and assumptions

The current investigation aims to provide an estimate of maximum erosion rates into rille bed and banks at the primary rille of Vallis Schröteri. The input parameters of the model can be divided into physical, thermo-physical and turbulence parameters of the flowing lava. Among the physical parameters, initial flow velocities are assumed to be equal to 5 and 10 m s^{-1}, values that fall within the range of velocities obtained by *Wilson and Head* (2017) for eruptions at lunar rille sites. The temperature of the lava at time of eruption is taken to vary from 1630°C (superheated) to 1440°C (liquidus), and 1400°C (sub-liquidus). Superheated lavas might have been erupted on the lunar surface at temperatures up to ~200°C above their liquidus value, if their rising speed through the crust was sufficiently high to minimise heat loss to the surrounding rocks (*Arndt*, 1994; *Kerr et al.*, 1996). The 1630°C value was chosen by *Williams et al*. (2000) to calculate erosion rates into the lava substrate by superheated lavas on the Moon. The initial kinematic viscosity of the lava is taken to be equal to 1.38 x 10^{-4} m^2 s^{-1}, the equivalent of the dynamic

viscosity value of 0.4 Pa s reported in *Williams et al*. (2000). Our model adopts the *Dragoni et al*. (1986) temperature-dependent viscosity that – though it was originally used for the purpose of investigating flow behavior in the Bingham laminar regime – can be used to model the evolution of lava temperature and viscosity so long as flow rate is fixed (a scenario for which flow height and velocity are both independent of lava yield stress and flow regime is Newtonian (*Dragoni et al*., 1986). The vertical distribution of temperatures within the flow is analogous to that modeled by previous authors (*Kerr*, 1996; *Siewert and Ferlito*, 1998), with higher temperature values at the flow top and core and lower values at the channel bed. Also, we assume for lava temperature and viscosity at the channel banks to be the same as those at the channel bed. The actual temperature values at the channel bed and banks were chosen based on our understanding of how convective heat flux is transported to the base of the flow. Holding the initial lava temperature and viscosity equal, the higher the flow thickness the higher the convective heat flux to flow boundaries, i.e., the value of the left-hand side term of Eq. (8). As a result, the temperature gap occurring between the flow top (and core) and the boundaries will be greater for a thicker flow. As lava temperature decreases, viscosity increases at both the channel bed and banks. Table 1 shows the values of calculated lava temperatures at the flow boundaries for the three chosen values of lava thickness (5, 10 and 20 m). It also shows calculated values of the laminar Prandtl number of the flowing lava, which range from a minimum of 570 for a superheated lava that is erupted at a temperature of 1630°C to a maximum of 26,685 at the channel boundaries and for a lava temperature of 1360°C and a flow kinematic viscosity of 3.4 x 10^{-3} m^2 s^{-1}. The specific heat capacity of the lava is assumed to have a value of 1570 J kg^{-}

^{1} °C^{-1} at the liquidus temperature and above, and the specific heat of the lava substrate (consolidated) is chosen at the effective temperature of melting of the lava substrate (*Williams et al*., 2000). Both values of specific heat decrease with decreasing lava temperature though they also vary depending on whether the substrate is consolidated or not. Values of the latent heat of crystallization and fusion are taken to be equal to 433,700 and 500,000 J kg^{-1} for the lava and substrate, respectively (*Williams et al*., 2000); a value for the kinematic turbulent thermal diffusivity, α_t, must also be specified at the inlet, and we take that value to be equal to 10^{-6} m^2 s^{-1}.

The model assumes steady-state flow conditions, an assumption justified by the likely long-lasting duration of eruptive events associated with the formation of lunar sinuous rilles (*Wilson and Head*, 2017). The liquidus temperature of the lava was previously calculated to be equal to 1440°C. Clementine data shows that low-titanium basalts characterize the portion of the Aristarchus plateau where the rille is found (*Zhang et al*., 2014), and the chosen liquidus temperature is that of the lunar low-Ti picritic basalt sample 12002 (*Walker et al*., 1976). The substrate is assumed to have a composition of a "pure" ferroan anorthosite (PFA) (*Warren*, 1990), and is modeled as consolidated and unconsolidated. The thickness of individual lava layers is taken to vary from 5 to 20 m, values that are consistent with those observed by the Apollo 15 crew at Hadley Rille (*Spudis et al*., 1988).

A thorough spectral analysis of the materials that cover the Aristarchus plateau out to the Vallis Schröteri rille site has revealed an extreme heterogeneity in composition (*Mustard et al*., 2011). As a result, it is difficult to model the thermo-physical properties of

an unconsolidated substrate in that lunar region. The Apollo landing missions revealed a lunar surface of highly fragmented, impact weathered material (regolith) on both the mare and highland crusts (*Wilhelms*, 1987). On younger surfaces (mare) the regolith may occur at depths of only a few meters, while on older surfaces (highlands) the regolith or mega-regolith may extend to several kilometers. The highland material comprising the Aristarchus plateau likely contains a substantially thick surface regolith that may have served as a mechanically weakened substrate for the Vallis Schröteri lavas. Based on this, we assume that at least a fraction of the material that is outcropping on the walls of the primary rille might have characteristics analogous to those of an unconsolidated granular regolith. *Colozza* (1991) provided a thermo-physical analysis of the lunar regolith and reported that the material remains in granular form up to a temperature of 1100°C, and then it begins to melt. Since the regolith is a mixture of compounds, it melts over a range of temperatures comprised between 1100°C and 1400°C (*Langseth et al*., 1973). An expression for the specific heat of regolith material was obtained from a curve fit and interpolation of experimental data given in *Robie et al*. (1970). Using this expression, we calculated a value of specific heat of 1438 J kg^{-1} $°C^{-1}$ for a substrate melting temperature of 1100°C, though it is important to remember that the value increases up to 1515 J kg^{-1} $°C^{-1}$ at the temperature at which the regolith is completely melted (1400°C). The latent heat of fusion was previously calculated to be 161.2 kJ kg^{-1} on average (*Richter*, 1993), and regolith density varies between 1600 and 2000 kg m^{-3} (*Colozza*, 1991; *Richter*, 1993). In order to maximize erosion rate values, we have adopted the lower end density value in our simulations.

Table 4.1 illustrates the physical and thermophysical parameters of the flow that are used as input values of the model. For each of the three values of lava thickness h (5, 10 and 20 m), we assign eruption temperatures of 1630°C, 1440°C and 1400°C, two values of flow velocity at the channel inlet (5 and 10 m s^{-1}) and initial flow kinematic viscosities of 1.4 x 10^{-4} and 6.8 x 10^{-4} m^2 s^{-1}. Prior to running our 3-D model of thermal erosion by turbulently flowing lava, a few calculations were necessary to determine temperature values at the channel boundaries. The illustrated temperature values were determined by first calculating the heat transfer coefficient and convective heat flux to the base of the flow for each value of lava thickness and for the two values of flow rate adopted. At channel boundaries (bed and banks), flow temperatures decrease with increasing lava thickness. Flow rates also play an important role because lava temperatures at channel boundaries tend to be higher at higher flow rates, holding other flow parameters equal. Finally, the laminar Prandtl number is calculated from the kinematic viscosity of the flow, eruption temperature and thermal conductivity of the lava.

Input turbulence parameters of the SST k-omega model

Initial values of turbulent kinetic energy k and rate of dissipation ω were calculated for a mesh designed to be 1,000 m long, 4,000 m wide and 5 to 20 m thick. This mesh geometry is representative of a limited portion of the Vallis Schröteri primary rille channel though it is ideal for the purpose of determining maximum erosion rates at/near the lava source. A mesh that is much shorter than the length of the rille allows for a high mesh

resolution (closest finite volume cell to channel bed/banks 0.5 m away from channel walls) while keeping computational cost low.

Each model run requires input values of k and omega at inlet and channel boundaries. These input values were calculated for each individual run – as described in *Menter* (1993) and are shown in Table 4.1. Turbulence intensity varies as a function of the Reynolds number of the flow and depends on physical flow parameters such as lava velocity and viscosity and the geometry of the channel. Initially calculated turbulence intensities were in the range 2.4×10^{-2} - 3.0×10^{-2} but they were increased by a factor of ~2.3 (see Table 4.1), following a necessary increase of k value at the channel inlet. Tweaking k values at the inlet is common practice in turbulence modeling because it serves the purpose of obtaining inlet values that are consistent with those obtained downstream of that point. Table 4.1 refers to eruption temperatures in the 1440°C (liquidus) and a constant flow kinematic viscosity of 1.4×10^{-4} $m^2 s^{-1}$. For eruption temperatures lower than the liquidus value, k and ω have similar values to those shown in Table 4.1 except for the "ω_{bound}" value that changes with increasing flow viscosity.

Results

Maximum erosion rates at the lava source

In this section, we present results of the first 3-D model of thermal erosion by turbulently flowing lava on the Moon – as applied to the primary rille of Vallis Schröteri. As mentioned before, we ran steady-state simulations concerning a 1 km long and 4 km wide section of the rille because we are mostly interested in obtaining information on

maximum erosion rates at/near the lava source (here named Cobra Head). Fig.4.2 shows maximum erosion rates into the channel bed and banks for lava that is 5 to 20 m in thickness and travels at speeds of 5 and 10 m s^{-1}. The lava is assumed to flow over a consolidated basaltic substrate that has a composition identical to that of the lava. In our simulations, maximum erosion rates at the channel bed appear to be the same as those obtained at the channel banks. Importantly, this study does not focus on the geometry of erosion at channel bed/banks, something that has instead been thoroughly explored at the Vallis Schröteri inner rille (*Cataldo et al*., 2022, manuscript in preparation). Eruption temperatures vary from a maximum value of 1630°C - consistent with superheated magma that was likely fast-ascending through the lunar crust - to the liquidus value of 1440°C and a sub-liquidus temperature of 1400°C. In our model, flow viscosity is temperature-dependent, and the highest kinematic viscosity is equal to 7.53 x 10^{-3} m^2 s^{-1}, equivalent to a dynamic viscosity of 21.8 Pa s. This viscosity value is found at the channel bed and banks of a 20-m thick flow erupted at the sub-liquidus temperature of 1400°C and traveling at a speed of 5 m s^{-1}. Maximum erosion rates appear to drop drastically soon after the lava cools below the liquidus temperature, a likely effect of the increase in flow viscosity that is accompanied by a decrease in the Reynolds number of the flow. For eruption temperatures in the range 1630°C - 1440°C, the kinematic viscosity of the flow remains constant at a value of ~1.4 x 10^{-4} m^2 s^{-1}, equivalent to a dynamic viscosity of 0.4 Pa s. This probably explains the gradual decrease in erosion rates with decreasing lava temperature over that temperature range that is shown in Fig. 4.2. Even for an eruption temperature that is slightly lower than the liquidus value (40 degrees lower), a 20-m thick flow that travels at a speed of 10 m s^{-1}

can erode into the lava substrate at a rate no faster than 29.5 cm/day, whereas for a lava that is erupted at the liquidus temperature, maximum erosion rates already increase to a value of 76 cm/day.

The parameter that appears to have the strongest influence on erosion rates is flow rate. Regardless of the initial lava temperature and flow thickness, a flow that travels at a speed of 10 m s^{-1} is conducive to maximum erosion rates that are higher by a factor of 1.8-1.9 than those associated with a flow of similar thickness that travels at half the speed. With regard to the role played by lava thickness, a flow that is 10 m thick is responsible for erosion rates that are higher by a factor of ~1.5-1.6 than those produced by a 5-m thick flow traveling at the same speed. And a 20-m thick flow is associated with values of erosion rates that are higher by a factor of ~1.3-1.4 than those produced by a 10-m thick flow that travels at the identical speed.

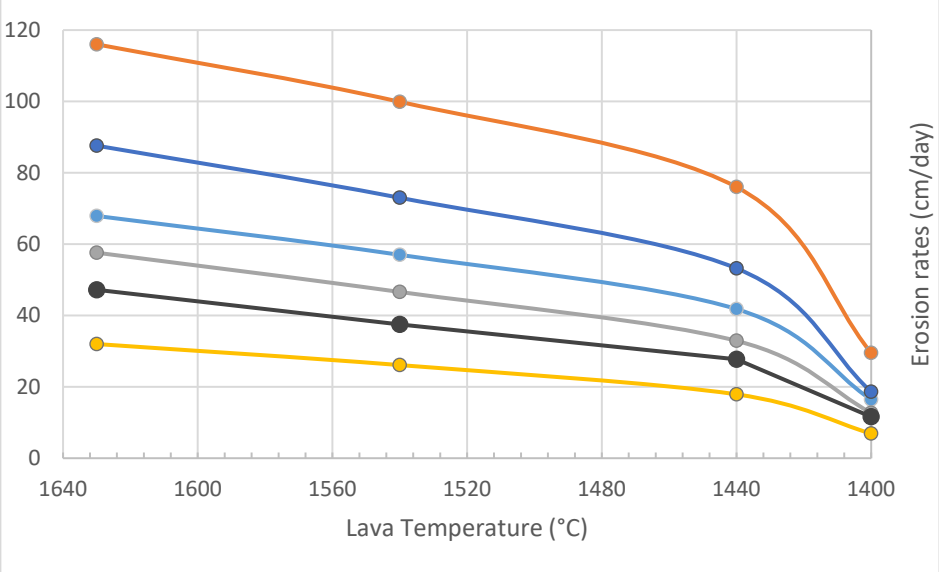

Fig 4.2. Graph shows how flow rate and lava thickness affect maximum erosion rates at channel bed and banks. Flow speed varies from 5 to 10 m s^{-1}, and values of flow thickness of 5, 10 and 20 m are considered. The lava is assumed to flow over a consolidated basaltic substrate with composition equal to that of the lava. The temperature of the lava at time of eruption goes from 1630°C (superheated)

to 1440°C (liquidus) and 1400°C (sub-liquidus). Red: 20 m thick, 10 m s^{-1}; blue: 10 m thick, 10 m s^{-1}; pale blue: 20 m thick, 5 m s^{-1}; grey: 5 m thick, 10 m s^{-1};gre -en: 10 m thick, 5 m s^{-1}; yellow: 5 m thick, 5 m s^{-1}.

The second batch of results deals with erosion rates into a substrate that is unconsolidated and modeled to have the thermophysical properties of granular regolith on the Moon. The density of the unconsolidated substrate (1600 kg m^{-3}) is much lower than the density (3100 kg m^{-3}) that characterizes the consolidated basaltic substrate. The lower density and the lower melting point (1100°C versus 1600°C) assumed in our simulations are together responsible for the increase in erosion rate observed across the entire range of values of eruption temperature and flow thickness. Results in Fig. 4.3 refer to both a consolidated and unconsolidated substrate. The flowing lava is still 5, 10 and 20 m in thickness though in this case flow rate is held constant at 10 m s^{-1} to aid in visualization and interpretation.

Maximum erosion rates of 2.8 m/day are associated with a superheated, 20-m thick lava flow that travels at a speed of 10 m s^{-1} over granular regolith materials. This value is a factor of ~2.3 higher than the erosion (1.2 m/day) caused by the same lava flowing at the same temperature over consolidated basaltic rock. A 10-m thick superheated lava traveling at the same speed will erode into the substrate at a rate of 2.3 m/day, a value within a factor of ~1.2 from the previous one. Finally, a 5-m thick flow with the same temperature will achieve a maximum erosion rate of 1.4 m/day – a value that is still higher than that associated with 20-m thick lava flowing at the same temperature over a consolidated substrate of basaltic composition. If we now look at maximum erosion rates into a substrate consisting of granular regolith materials for a 20-m thick flow erupted at the liquidus temperature, we find maximum values of 1.6 m/day. As a result, a superheated lava that is

erupted at a temperature that is almost 200°C higher than the liquidus value has a capability of eroding into the substrate that is a factor of ~1.6 higher than that associated with the same flow erupted at the liquidus temperature. Finally, a flow that is erupted at a sub-liquidus temperature of 1400°C can erode at a rate of 60 cm/day into an unconsolidated substrate. It is important to remember that in our model a flow that is erupted at a temperature of 1400°C is characterized by a flow dynamic viscosity of ~ 2 Pa s, a value that is still much lower than the average viscosity at which an average Hawaiian basalt is erupted. This explains the still comparatively high erosion rates that are associated with the investigated sub-liquidus lava.

The last results show how important is defining the characteristics of a lava substrate in studies of thermal erosion by lava (Fig. 4.3). Remarkably, our thermal erosion model does not account for any likely contribution coming from a process of mechanical erosion of the substrate. Mechanical erosion is expected to be especially important in the presence of an unconsolidated substrate and plays a far more important role than thermal erosion in the event of short-lasting eruptions.

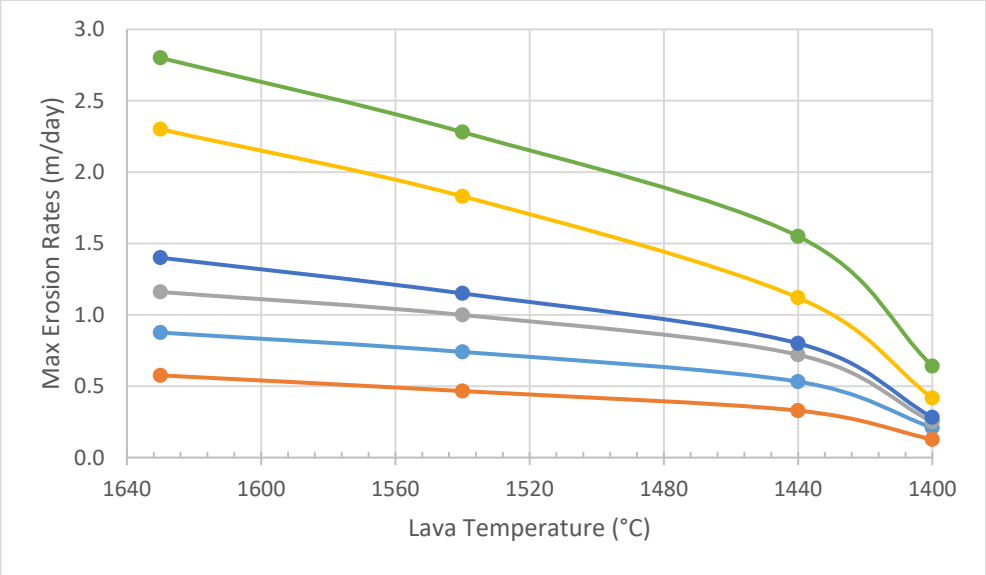

Fig 4.3. Graph showing how flow thickness and the presence of consolidated (CON) versus unconsolidated (UNCON) substrate affect maximum erosion rates at the chan -nel bed and banks. All values refer to lava thicknesses of 5, 10 and 20 m. The conso -lidated substrate is assumed to have a composition analogous to that of the flowing lava. The unconsolidated substrate is assumed to have the thermophysical properties of granular regolith material (*Robie et al*.,1970; *Colozza*, 1991; *Richter*, 1993). Flow rate is held constant at 10 m s^{-1}. Green: 20 m thick over UNCON; yellow:10 m thick over UNCON; blue: 5 m thick over UNCON; grey: 20 m thick over CON; pale blue: 10 m thick over CON; red: 5 m thick over CON.

Discussion

In this section, we will discuss a limitation of our modeling approach and discuss the processes we think might have led to the formation of the Vallis Schröteri rille that we see today. In our simulations, we aimed to obtain maximum erosion rates for flows of thickness comprised between 5 and 20 m and a range of eruption conditions. All of this while allowing for the lava to flow over both a consolidated and unconsolidated lava substrate. If we multiply the maximum erosion rate of 76 cm/day obtained for a 20-m thick flow that is erupted at the liquidus temperature (1440°C) by 920 days (2.5 years), we obtain a value of erosion depth of ~700 m, a value that is representative of the average depth of

the Vallis Schröteri primary rille at the Cobra Head (*Garry et al*., 2008; *Cataldo et al*., 2015). Instead, if we adopt the maximum erosion rate of 116 cm/day produced by superheated lava erupted at a temperature of 1630°C, we will achieve the required erosion depth in 604 days (1.6 years). Multiplying erosion rates by the time of flow duration is a procedure that can be used to provide a first-order estimate of the approximate length of time required to excavate the whole depth of a channel but cannot be used to derive an exact estimate of erosion depths for any modeled scenario. As a lava flows downstream of the source, it begins to incorporate progressively increasing portions of eroded substrate material. At least some of this material becomes assimilated (melted) into the flowing lava, which modifies the composition and physical properties of the flow. *Kerr* (2001) studied thermal erosion by laminarly flowing lava and found that the thermal budget of a flow must be higher than the energy required to melt the lava substrate by at least several factors for thermal erosion to remain effective. The time that it takes for any portions of incorporated substrate materials to become assimilated into the flow has the effect of lowering the Reynolds number of the flow and diminishing the erosive power of the lava.

An important source of uncertainty for our 3-D model has to do with the fact that eroded substrate materials do not become incorporated/assimilated into the flow. As a result, the model is unable to predict the geochemical and geophysical evolution of the flow over time and cannot be used to calculate erosion depths starting from any value of maximum erosion rate. For instance, an erosion rate of 2.8 m/day by a 20-m thick lava would imply that 14% of the actual thickness of the lava should become incorporated and fast-assimilated into the flowing lava every day. A similar amount of substrate material

would likely cause the flow to freeze! *Keszthelyi et al*. (2014) placed an upper limit on the amount of substrate material that was likely entrained in the lava that flowed at Athabasca Valles, Mars. Because substrate material is initially ~1000°C colder than lava, and the lava will freeze if cooled ~100°C, the entrained substrate material should be no more than 10% of the erupted volume. As a result, maximum erosion rates higher than ~1 m/day - assumed to be uniformly distributed over the boundaries of an individual 20-m thick flow emplaced across the whole cross-sectional area of the Vallis Schröteri primary rille – might be irrealistic as they would account for more than 10% of the erupted lava volume. By assuming for a flow to be able to entrain up to 1 m/day of substrate materials, it will take ~700 days (almost two years) for the flow to form a depression similar to that observed at the Cobra Head. That said, we must remember that a similar value of erosion rate will unlikely be preserved downstream of the lava source, especially if the flow is not thermally insulated. Besides, a flow that travels at a speed of 10 m s^{-1} will take ~4 hrs to reach the flow terminus. For the flow to be able to erode deeper into the lava substrate, an efficient mechanism of discharging for the lava is needed so that new lava will be able to flow over the same path and erode deeper into the same substrate. The two reasons outlined make it unlikely for a flow to be able to excavate the entire depth of the rille over a substantially long period of time.

Another important fact that should be taken into consideration is that most highland materials appear to outcrop at or near the Cobra Head (*Garry et al*., 2008) whereas LROC NAC images show that a large fraction of the primary rille walls consists of a sequence of lava layers (*Mustard et al*., 2011; *Campbell et al*., 2008), similar to the mare basalt layers

that were observed by the Apollo 15 crew at Hadley Rille (*Spudis et al*., 1988). As a result, the idea that the lava that flowed at the Vallis Schröteri primary rille might have eroded into an unconsolidated material for the entire depth of the rille is challenged by available imagery.

Was the primary rille of Vallis Schröteri entirely excavated by thermally and/or thermo-mechanically eroding lava? The results of our 3-D model and the thermal considerations previously discussed seem to challenge this idea. Furthermore, the regional geologic context of a given rille should be evaluated before it is determined to what degree mechanical and/or thermal erosion has been responsible for its development. As discussed on pp. 159-160, *Spudis et al*. (1988) noticed that numerous structural and depressions in the proximity of Hadley Rille were probably produced by regional deformation associated with Imbrium basin adjustment and were later followed by basalt flows that established the rille. The occurrence of scarps, cracks and grabens oriented in directions radial and concentric to Imbrium basin, and trends of individual segments of Hadley Rille which appear to be coincident with these regional structural patterns add support to their idea. Something similar can be seen in the Vallis Schröteri region. The two main trends of individual segments of the primary rille run in directions that are both perpendicular and parallel to the regional structural patterns associated with the adjustment that followed the formation of Imbrium basin. Finally, a closer inspection of the rille reveals the same evidence for erosion by lava that *Spudis et al*. (1988) found at Hadley Rille, which causes individual depression segments to connect, leading to smooth and rounded corners. An important difference we find between the observations carried out by

Spudis et al. (1988) at Hadley Rille and those made at the Vallis Schröteri primary rille is the absence of constructional features at or near the Vallis Schröteri primary rille. That said, evidence for at least a partly constructional origin for the primary rille might exist under the surface. The occurrence of subsurface radial dikes inferred from the "Gravity Recovery And Interior Laboratory" (GRAIL) data (*Andrew-Hanna et al.*, 2013) might potentially support this interpretation.

Conclusions

We have applied our new 3-D model of thermal erosion by turbulently flowing lava to the primary rille of Vallis Schröteri on the Moon. The purpose of this investigation was to find values of maximum erosion rates into the lava substrate at this lunar site and from there discuss the likely process or processes that might have led to the formation of the rille we see today. Eruption temperatures were assumed to vary from 1630°C (superheated lava) to 1440°C (liquidus) and 1400°C (sub-liquidus) and flow velocities of 5 and 10 m s^{-1} were considered in the simulations. The flowing lava was assumed to flow over both a consolidated and unconsolidated substrate. Maximum erosion rate values vary from a minimum of 6.9 cm/day for lava erupted at T = 1400°C and flowing over a consolidated substrate to 2.8 m/day for a 20-m thick lava erupted at T = 1630°C and flowing over an unconsolidated substrate of granular regolith. Thermal considerations pose a limit on the erosion rate values that can be used to calculate reliable values of erosion depths of the lava substrate, and we find that any such rates within 1 m/day are likely to better predict the geochemical and geophysical evolution of the lava over time, which is not a feature of the

current model. Assuming a constant erosion rate over time, it might have taken almost two years for the lava to excavate the Cobra Head, the lava source region of the primary rille.

The Vallis Schröteri rille outcrops on the Aristarchus Plateau, a tilted block that at least in part is thought to have formed in response to the adjustment that accompanied the formation of Imbrium basin. Structural patterms in the area appear to add support to the idea that the rille is partly tectonic in origin and was then partially excavated by thermally or thermo-mechanically eroding lava. Though we favor a combined tectonic and erosional origin for the rille, a constructional origin cannot be ruled out – especially when looking at the candidate dike structures inferred at depth by the (Gravity Recovery And Interior Laboratory" (GRAIL). A network of lava tubes might exist at depth, a network through which the lava might have been traveled out to the rille terminus while minimizing cooling rates. That said, an efficient mechanism of discharge for the lava would be required in such a scenario.

5 PAPER 3: MOON, VALLIS SCHRÖTERI INNER RILLE (CATALDO ET AL., IN PREPARATION)

Abstract

The first 3-D model of thermal erosion by turbulently flowing lava on the Moon addresses the formation of the inner rille of Vallis Schröteri and provides erosion rates at the rille bed and banks associated with 5-, 10- and 20-m-thick lavas erupted at liquidus, sub-liquidus and superheated temperatures. Two steady-state flow scenarios are considered: one in which lava is allowed to lose part of its internal heat by radiation from the flow top into the lunar environment (scenario 1) and another in which it flows insulated in a tube (scenario 2). Maximum erosion rates obtained from scenario 2 flows range from 3.6 cm/day for a 5-m-thick flow erupted at a sub-liquidus temperature of 1380°C and traveling at a velocity of 5 m s^{-1} to 98-105 cm/day for a 20-m-thick superheated lava traveling at a velocity of 10 m s^{-1}. All results consider a consolidated substrate of composition identical to that of the lava and an unconsolidated substrate with thermophysical properties analogous to those of lunar regolith (the latter for 10-m-thick flows erupted at the liquidus temperature). Flow durations and volumes required for the rille to develop fall within the range provided for high-volume eruptions at rille sites on the Moon. First-time evidence of secondary flow circulation is found in lava channels at meander bends. Secondary flow is well-studied in the river literature and appears to alter the magnitude and distribution of erosion rates at the bed and banks of rille sections that are cut along meander axes. The pressure gradients within the flow, which develop at

meander bends, are responsible for variations in mainstream as well as cross-stream lava velocities at the opposite sides of a bend. Secondary flow circulation is strongest in thick flows that travel at a faster velocity, and lava temperature does not appear to have control on it. Instead, increases in meander amplitude make secondary flow circulation stronger and faster. This suggests that, by analogy with what is observed in river channels, once a meander of a certain amplitude is generated, the amplitude of the same meander might grow larger in time. Some of the gooseneck meanders found along the path of the inner rille might have developed in a similar way over time. The found discrepancy in erosion rates at the opposite sides of a bend might be partially counterbalanced by a process of mechanical erosion acting at the outer bank (left bank in the simulations) of a meander bend. Evidence in support of this suggestion may be found when looking at the distribution of cross-stream velocities at rille cross-sections cut along meander axes. Mechanical erosion might have been especially effective for flows that are 10-20 m thick.

Introduction

Vallis Schröteri is the largest sinuous rille on the Moon and sits atop the Aristarchus Plateau. This plateau consists of a block of ancient highland crust that was uplifted during formation of the Imbrium basin (*Moore*, 1965; *Guest*, 1973; *Zisk et al.*, 1977) as the crust readjusted following the impact that occurred ~3.85 b.y. ago (*Wilhelms*, 1987). The Aristarchus Plateau lies just outside the main topographic ring of the Imbrium impact basin (*Mustard et al*., 2011), and rises 1-1.5 km above the surrounding Oceanus Procellarum sloping away from it to the west (*Zisk et al*., 1977). The actual rille site consists of a large,

primary outer rille and an inner rille that is much smaller and narrower and runs on the primary rille's floor. The larger rille is ~ 4.5 km in width (*Garry et al*., 2008) and runs from the lava source (Cobra Head) to the channel terminus out to a downstream distance of ~150 km. The inner rille originates in a distinct crater within the Cobra Head (*Zisk et al*., 1977) and is more sinuous than the primary rille and highly meandering. Before LROC imagery became available, it was measured to be ~170 km long, ~640 m wide and ~95 m deep on average (*Garry et al*., 2008). As regards the composition of the flowing lava, Clementine data shows that low-titanium basalts characterize the Aristarchus plateau region (*Zhang et al*., 2014), and the lava substrate is thought to have a composition of a "pure" ferroan anorthosite (PFA, *Warren*, 1990) or analogous to the upper anorthositic crust (*Mustard et al*., 2011). Alternatively, it might consist of the same lava that likely flowed within the primary rille (*Garry et al*., 2008).

As of today, no evidence exists as to whether the inner rille lava flowed insulated from the lunar environment (tubed flow) or uncrusted (open channel). Of course, tube-fed lava is more likely than uncrusted lava to flow farther from the source, holding other flow parameters equal because only a minimal amount of heat is dissipated (lost) into the surrounding environment. In contrast, a lava that is uncrusted or only partially crusted over dissipates part of its internal heat through the flow top, which causes the turbulent to laminar regime transition to occur much earlier and closer to the lava source. While there is no evidence that levees may exist along the edges of lunar rilles, *Chappaz et al*. (2014, 2017) found possible sub-lunarean extensions (potential tube structures) of surface sinuous rilles at the Vallis Schroteri site using a combination of gravity anomaly analysis techniques.

In this paper, we first present results obtained by applying the new 3-D model of thermal erosion by turbulently flowing lava to the emplacement of very low viscosity, low-Ti basaltic lava at the inner rille of Vallis Schröteri. Results refer to both uncrusted (scenario 1) and tube-fed (scenario 2) flow scenarios. The same results allow estimates of expected flow duration and total lava volume to be made, which are needed to explain the observed rille geometry. Finally, we show results of a theoretical study of erosion rate variations that are related to local variations in flow velocities and temperatures at two channel cross-sections cut parallel to two adjacent meander axes.

Objectives of current investigation

An important goal of the current investigation is that of obtaining values of maximum and minimum erosion rates at the channel bed and banks for eruption temperatures progressively decreasing from 1630°C to 1440°C (liquidus), and sub-liquidus temperatures. Whereas the highest modeled eruption temperatures are consistent with the previously modeled eruption and emplacement of superheated lavas on the Moon (*Williams et al*., 2000), the sub-liquidus temperature values at which flow regime might still be Newtonian are not known. Therefore, another important goal is to constrain such a minimum lava temperature by inspecting the soundness of model outputs from a physics standpoint. Investigating flow behavior and erosion rates at lava temperatures that are much lower than the liquidus temperature might potentially reveal how flow patterns relate to erosion rates at the channel bed and banks at downstream distances of several km from the lava source.

It is generally agreed that high effusion rates produce long lava flows (*Walker*, 1973; *Hulme*, 1974; *Crisp and Baloga*, 1990; *Pinkerton and Wilson*, 1994). Nevertheless, following observations and heat budget estimates obtained at the Waha'ula tube, Hawaii, *Keszthelyi* (1995) calculated that even basaltic tube-fed flows several hundred kilometers long could have been produced by eruptions with effusion rates of only a few tens of cubic meters per second. For such a scenario, lava cooling rates between ~0.5°C/km and 1°C/km could have been common (*Keszthelyi*, 1995). Because of the possibility that the inner rille lava might have flowed at both low and high effusion rates, all results shown here refer to flows traveling at speeds of 5 and 10 m s^{-1} (with the faster velocity value being used for 20-m-thick lavas only).

Another key objective of the present investigation is to conduct a fluid dynamic and thermal modeling study of the lava flows at rille segments that extend no more than a few km downstream of the lava source. The goal is to search for a potential correlation between variations in flow patterns, temperature and other flow physical parameters and the distribution of erosion rates at the channel bed and banks. Special emphasis is placed on investigating how erosion rates vary at meander bends for changing flow thickness, flow speed, channel width and meander geometry. To date, no assessment has yet been made on how channel bank erosion relates to erosion at the channel bed because this important aspect is not addressable by one- or two-dimensional models. When applied to sinuous rilles or curved channels in general, a 3-D model has the unique advantage of revealing the details of flow circulation and how flow velocity, viscosity and pressure at meander bends relate to the same flow parameters at the channel centerline and bed. How does flow

circulation at meander bends vary when varying temperature distribution within the lava? Will the details of flow circulations be the same for uncrusted versus tube-fed lava? These two different emplacement environments compel us to describe both scenarios and explore how the vertical distribution of temperature for the two case studies might have related to the details of flow circulation at the channel bed and banks. The other advantage of a three-dimensional model lies in its ability to reveal spatial variations of erosion rates with changing flow rate, flow temperature, and meander/channel geometry.

Method

A newly derived expression for the erosion rate into the lava substrate

Cataldo et al. (2022a, in revision) gave a concise yet complete description of the model and how the same is implemented in the OpenFOAM finite volume C++ library of solvers and utilities, a type of computational fluid dynamics (CFD) software. The same authors also described how the simpleFoam solver was chosen out of the several ones available within the OpenFOAM library itself and the modifications that were made to it. Those changes reflected a need to incorporate a temperature model and temperature-dependent viscosity into a solver that is commonly used in problems involving constant temperatures and viscosities. In coupling a temperature model to the simpleFoam solver that is used in steady-state turbulent flow scenarios, the first step is to find an energy equation that is applicable to a fixed control volume and fits a scenario of turbulently flowing lava. An energy equation can be written in terms of specific internal energy, specific enthalpy, specific total enthalpy, or temperature. An energy expression written in

terms of temperature assumes that the flow is Newtonian because the specific enthalpy of the flow is only a function of pressure and temperature variations (*Moukalled et al*., 2016). Such an assumption is consistent with a scenario of turbulently flowing lava for which lava temperatures are assumed to be above or near the liquidus value. The energy equation that is here normalized by density because lava can be treated as an incompressible fluid, is given by:

$$\nabla [\mathbf{v}\, T] = \nabla [\, \alpha_{eff} \nabla T \,] \qquad \text{Eq. (1)}$$

in which **v** is the velocity vector (**v** = v_x, v_y, v_z), T is lava temperature, and α_{eff} is defined as the effective thermal diffusivity in that it accounts for both laminar and turbulent contributions to diffusivity. The left- and right-hand sides of Eq. (1) are convection and diffusion terms, respectively. Specifically, the effective thermal diffusivity, α_{eff}, can be expressed as:

$$\alpha_{eff} = \frac{\upsilon}{Pr + \alpha t} \qquad \text{Eq. (2)}$$

in which υ is the kinematic viscosity of the flow (ratio of dynamic viscosity, μ, to density, ρ), Pr is the laminar or molecular Prandtl number of the flow and α_t is the turbulent thermal diffusivity, expressed as:

$$\alpha_t = \frac{\upsilon t}{Prt} \qquad \text{Eq. (3)}$$

in which υ_t is turbulent viscosity and Prt is the turbulent Prandtl number of the flow (a constant that takes the value of 0.85 at the bed and banks). The α_{eff} term plays a key role in determining variations of erosion rate at channel boundaries, as it will be shown later.

Eq. (1) enabled derivation of a new erosion rate expression that is suitable for use in the modified simpleFoam solver. The expression was obtained starting from the available 1-D expressions of *Hulme* (1973), *Huppert and Sparks* (1985) and *Williams et al*. (1998, 2000). Deriving an expression for erosion rate at the lava/substrate interface is a conduction/diffusion problem that can be solved effectively by adopting a one-dimensional approach (along the z or vertical axis perpendicular to the lava/substrate interface). By assuming thermal equilibrium at the lava/substrate interface (channel boundary), we can write:

$$-\rho\, C_P\, \alpha_{eff}\, \frac{\partial T}{\partial n} = h_T(T_l - T_m) \qquad \text{Eq. (4)}$$

in which the left-hand side of the expression represents the heat diffused through the interface and the right-hand side is the convective heat flux to the base of the flow. Specifically, ρ is the bulk density of the flow, C_p is the specific heat capacity of the lava, h_T is the convective heat transfer coefficient to the base of the flow, T_l is lava temperature and T_m is the temperature at which the lava substrate melts. *Hulme* (1973) first and then *Huppert and Sparks* (1985) and *Williams et al*. (1998, 2000) define the rate of advance of the ground/lava interface (i.e., the melting rate) as:

$$u_g = \frac{h_T(T_l - T_m)}{\rho_g[c_g(T_m - T_0) + L_g]} \quad \text{Eq. (5)}$$

in which u_g is the erosion rate expressed in m s^{-1}, ρ_g is the density of the lava substrate, C_g is the specific heat of the ground, T_0 is the temperature of the substrate away from the interface and L_g is the latent heat of fusion of the ground. Given that the h_T (T_l-T_m) convection term is found both in Eq. (5) and Eq. (4), by solving Eq. (5) for that term and then substituting it in Eq. (4), we get:

$$-\rho\, C_P\, \alpha_{eff}\, \frac{\partial T}{\partial n} = u_g\, \rho_g\, [C_g\, (T_m - T_0) + L_g] \quad \text{Eq. (6)}$$

And solving for u_g, we obtain:

$$u_g = \frac{-\rho\, c_p\, \alpha_{eff}\, \frac{\partial T}{\partial n}}{\rho_g[c_g(T_m - T_0) + L_g]} \quad \text{Eq. (7)}$$

This expression is only a short step away from the final equation adopted in our model. Due to the incompressibility requirement, both the numerator and denominator of Eq. (7) are normalized by density. As a result, the final expression that is used in our model is given by:

$$u_g = \frac{-c_p \alpha_{eff} \frac{\partial T}{\partial n}}{R[c_g(T_m - T_0) + L_g]} \quad \text{Eq. (8)}$$

in which R is a (ρ_g/ρ) density ratio, i.e., a dimensionless quantity. For any simulation, the only parameter that is not constant is the effective thermal diffusivity, α_{eff}. Because of this, any variation in effective thermal diffusivity is conducive to a proportional variation in erosion rate, u_g.

A newly-derived expression for the convective heat transfer coefficient h_T

The initial conditions of the model are to be specified at the lava source and channel boundaries. This is shown in appendix A, which is dedicated to the OpenFoam code and the key model input parameters. One of the boundary conditions introduced in this chapter section is the temperature (and associated viscosity) of the lava at the lava/bed and lava/banks interfaces. Previous models – though designed for laminarly flowing lava – predict that the thermal structure of a flow should be such that lava temperature is highest at the flow top and core and decreases down to the bottom of the channel (bed and banks) (*Kerr* 2001, 2009; *Siewert and Ferlito*, 2008). The fact that the flowing lava is cooler close to/at a channel boundary is intuitive because of the higher lava viscosity and much lower flow velocity that becomes equal to zero at the lava/substrate interface. *Siewert and Ferlito* (2008) provided an expression that enables determination of the temperature profile in lava that flows in a laminar fashion, but no expression and experimental data are available for a scenario of turbulently flowing lava. Even for lava that flows turbulently, thermal diffusivity is limited by the low conductivity of basaltic lava (~1 W m K^{-1}). In turbulently

flowing lava, most heat transfer occurs by advection and convection. Yet, regardless of how well-mixed a turbulent flow might be, convection will never be able to neutralize temperature differences between the top/core and bottom of a flow (if it did, convection would come to a halt). This is also true for the thickest flows, even though for a scenario of thick lava convection is stronger than for comparatively thinner flows (holding other factors equal). The coefficient that defines the ability to transfer heat upward and downward within a flow as well as from the flow bottom into the lava substrate is the convective heat transfer coefficient h_T, and we use it here to constrain - to a first order - the likely distribution of temperatures between the flow top/core and bottom for flows that vary in thickness between 5 and 20 m.

The numerator in Eq. (7) is identical to the left-hand size of Eq. (4) and both terms are equal to the convective heat flux to the base of the flow that is found on the right-hand size of Eq. (4). Starting from this, we can re-write Eq. (7) as:

$$u_g = \frac{h_T(T_l - T_m)}{\rho_g[c_g(T_m - T_0)+L_g]} \qquad \text{Eq. (9)}$$

and solving for h_T we obtain:

$$h_T = \frac{u_g \{\rho_g[c_g(T_m - T_0)+L_g]\}}{(T_l - T_m)} \qquad \text{Eq. (10)}$$

which is the expression adopted to determine the value of the heat transfer coefficient from the bottom of the flow into the lava substrate.

Flow scenario 1: Heat loss by radiation from lava top

On Earth, flowing lava loses heat by radiation and convection from the flow top and conduction into the ground. Due to the lack of an atmosphere, lunar flows cooled by radiating heat into the lunar vacuum environment and conducting it into the lava substrate. Even when modeling the cooling of thin and small Pahoehoe flow lobes in Hawaii, which lose internal heat by radiation faster than a large, thick lava flow, *Keszthelyi* (1994) showed that the first 5 minutes are dominated by cooling by radiation. We here provide a first order estimate of the amount of heat that was likely lost through the flow top from the lava that formed the Vallis Schröteri inner rille. We then derive an approximate rate of temperature decrease with time and downstream distance from the lava source. This task is applied to flows of different initial temperature (from 1630°C down to 1380°C) and thickness (5 and 20 m) and flow velocities of 5 and 10 m s^{-1}. The heat flux dissipated through the flow top or energy output, Q_r, can be estimated by the Stefan-Boltzmann relation:

$$Q_r = \sigma \varepsilon [T_{ft}^4 - T_a^4] \qquad \text{Eq. (11)}$$

in which σ is the Stefan-Boltzmann constant given as 5.67 x 10^{-8} W m^{-2} K^{-4}, ε is the emissivity for radiation and is taken as 0.93 in the present computations (*Harris*, 2013), T_{ft} is the temperature at the flow top and T_a is the temperature of the lunar environment. The

hotter a lava is, the higher is the loss of heat by radiation because temperature is a term raised to the power of 4 in Eq. (9). Q_r has dimensions of energy flux (energy per unit time per unit area) and is expressed in units of W m^{-2} or kg s^{-3}. The presence of a unit of time in the energy flux expression enables determination of flux at a downstream distance of 1 km from the lava source for flows that travel at 5 and 10 m s^{-1}. Of course, a radiation model accounts for how the convective heat transfer to the top of the flow relates to the heat lost by radiation, whereas only an estimate of the heat lost by radiation is provided here. In this study, it is shown how the vertical thermal structure of a flow that radiates heat into the lunar environment compares with that of a lava that flows in a tube. This information is then used to study how variations in the thermal and velocity structure of a flow (both vertically and horizontally) affect the distribution of erosion rates at one or two channel cross-sections. Appendix A (p. 372) shows the changes implemented in the temperature file within the 0 folder (initial conditions) to obtain a scenario in which lava loses heat by radiation into the lunar environment.

Flow scenario 2: Lava insulated from the lunar vacuum

As regards the tubed lava scenario, no heat is allowed to escape from the lava. The lowest cooling rates are obtained for tube-fed flows that travel insulated from the surrounding environment. Typical cooling rates of tube-fed lava are on the order of 1°C/km and can go down to ~0.4°C/km (*Keszthelyi*, 1995). Because of the above, flows are likely to travel a much greater distance from the lava source by keeping lava temperature high

and causing the turbulent/laminar flow regime transition to occur at much greater downstream distances. Appendix A (p. 373) shows the T file matching scenario 2 lavas.

Secondary Flow Circulation in Curved River Channels

Within the results section, mention is made of secondary flow circulation because there is evidence for it at two cross-sections of the 1200-m-long rille segment under study. The term is very common in the river literature. Water flowing through a bend must follow curved streamlines to remain with the banks of the river. The water surface is slightly higher near the concave bank than near the convex bank. As a result, at any elevation within the river, water pressure is slightly higher near the concave bank than near the convex bank. A pressure gradient results from the concave (outer) bank toward the convex (inner) bank (*Bowker*, 1988). The higher pressure near the concave bank is accompanied by slower water speed, and the lower pressure near the convex bank is accompanied by faster water speed, and all this is consistent with the Bernoulli principle.

A secondary flow results in the boundary layer along the floor of the riverbed. The boundary layer is not moving fast enough to balance the pressure gradient and so its path is partly downstream and partly across the stream from the concave bank toward the convex bank, driven by the pressure gradient (*Hickin*, 2003). The secondary flow is then upward toward the surface where it mixes with the primary flow or moves slowly across the surface, back toward the concave bank, a motion called helicoidal flow. On the floor of the riverbed the secondary flow sweeps sand, silt and gravel across the river and deposits the solids near

the convex bank, in similar fashion to sugar or tea leaves being swept toward the center of a bowl or cup (*Bowker*, 1988).

Input parameters: Lava temperatures and velocities

The input values of the new 3-D model encompass physical, thermo-physical and turbulence parameters of the flowing lava. The temperature of the lava at time of eruption is taken to vary from 1630°C (superheated) to 1440°C (liquidus), and anywhere from 1400°C to 1340°C (sub-liquidus). Given that the modified simpleFoam solver only works in the presence of Newtonian flow conditions, chosen sub-liquidus temperatures must comply with that flow regime requirement. One of our goals is to identify a minimum sub-liquidus temperature value for which obtained results are consistent with one another and remain sound from a physics standpoint. Clementine data shows that low-titanium basalts characterize the portion of the Aristarchus plateau where the rille is found (*Zhang et al*., 2014), and the chosen liquidus temperature of 1440°C is that of the lunar low-Ti picritic basalt sample 12002 (*Walker et al*., 1976). Superheated lavas might have been erupted on the lunar surface at temperatures up to ~200°C above their liquidus value, if their rising speed through the crust was sufficiently high to minimise heat loss to the surrounding rocks (*Arndt*, 1994; *Kerr et al.*, 1996). The 1630°C value was first suggested by *Wieczorek et al*. (2000) and then chosen by *Williams et al*. (2000) to calculate erosion rates into the lava substrate by superheated lavas on the Moon. The initial kinematic viscosity of the lava is taken to be equal to 1.38×10^{-4} m^2 s^{-1}, the equivalent of the dynamic viscosity value of 0.4 Pa s reported in *Williams et al*. (2000). Our model adopts the *Dragoni et al*. (1986)

temperature-dependent viscosity relationship that – though it was originally used for the purpose of investigating flow behavior in the Bingham laminar regime – can be used to model the evolution of temperature and viscosity in turbulently flowing lava so long as flow rate is fixed (a scenario for which flow height and velocity are both independent of lava yield stress and flow regime is Newtonian, *Dragoni et al*., 1986). The vertical distribution of temperatures within the flow is analogous to that modeled by previous authors (*Kerr*, 1996; *Siewert and Ferlito*, 1998), with higher temperature values at the flow top and core and lower values at the channel bed. Also, we assume for lava temperature and viscosity at the channel banks to be the same as those at the channel bed. As regards scenario 1 (lava radiating heat into the lunar environment), the choice of different initial temperature values for flows of different thickness was dictated by the fact that thick lava retains heat better than thin flows. As lava is erupted, exposure to the lunar vacuum causes lava temperatures to drop almost instantly to values that depend on the initial lava temperature and flow thickness. The temperature drop shown in Table 5.1a, which is always within 40°C of the eruption temperature, is probably underestimated. Yet, a limited temperature drop is here assumed because the simpleFoam solver can only deal with turbulent flow and, hence, temperatures that are consistent with that assumption. Of course, a lava that is erupted at a temperature of 1630°C will not have this problem until temperatures fall below the liquidus value. Nevertheless, the 40°C temperature drop is also applied to a scenario of superheated lava for the sake of consistency. The actual temperature values at the channel bed and banks were chosen based on our understanding of how convective heat flux is transported to the base of the flow. Holding the initial lava

temperature and viscosity equal, the higher the flow thickness the higher the convective heat transfer (the term found in the numerator of Eq. 7) through the flow and the temperature gap between flow core and channel boundaries. Also, the value of the heat transfer coefficient, h_T, is higher for a flow that is thicker than another one, holding other factors constant. The heat transfer coefficient expression (Eq. 8) was obtained by re-arranging the erosion rate expression. As a result, a range of temperature values are initially assigned at the channel boundary and only those values that turn out to provide physically consistent results for the chosen input parameters (lava temperatures, thicknesses, and velocities) are considered in the results section.

Initial flow velocities are determined by physical parameters such as the slope of the ground, lava thickness, acceleration due to gravity and friction coefficient. On the Moon, the acceleration due to gravity is a constant that is equal to 1.62 m s^{-2} and causes flows to travel at comparatively slower velocities than on Earth (holding other factors constant). Flow velocities are calculated for flows that are 5 and 20 m thick, according to the following re-arranged expression from *Jarvis* (1995) that was also adopted by *Williams et al*. (1998, 2000):

$$\sqrt{\frac{8\, g\, h\, sin\alpha}{\lambda}} \qquad \text{Eq. (12)}$$

in which h stands for flow thickness and λ is a friction factor expressed in terms of the Reynolds number of the flow, as follows:

$$\lambda = [0.79 \ln Re - 1.64]^{-2} \quad \text{Eq. (13)}$$

Here, we adopt the Reynolds number expression chosen by *Wilson and Head* (2017) in their paper discussing steady-state eruptions at lunar rille sites, which is given by:

$$Re = 4 U h \rho/\mu \quad \text{Eq. (14)}$$

in which U is lava horizontal velocity and μ is dynamic viscosity. By using Eqs. (12) and (13) combined, velocity values of 4.2, 6.6 and 10.2 m s^{-1} are found for lava thicknesses of 5, 10 and 20 m, respectively. The values adopted in our simulations are rounded up to 5, 7 and 10 m s^{-1}.

The thickness of individual flow units on the Moon has been a subject of debate over the last few decades. Astronauts on the Apollo 15 mission observed and photographed layered lava flows in the walls of Hadley Rille and found individual flow units < 1 m in thickness intercalated with units 10-20 m thick and even thicker (*Howard and Head*, 1972; *Howard et al*., 1972; *Swann et al*., 1972; *Spudis et al*., 1988; *Vaniman et al*., 1991). Recent Lunar Reconnaissance Orbiter (LRO) images of individual layers, interpreted to be sequences of mare basalt flow units, range between 2 and 14 m in thickness (*Robinson et al*., 2012). Considering these findings, the values of lava thickness adopted in this study are 5, 10 and 20 m.

Thermophysical parameters

Tables 5.1 (a, b) illustrate the key thermophysical parameters of the lava thought to have formed the Vallis Schröteri inner rille for the two scenarios of interest. The laminar or molecular Prandtl number of the flow ranges from a minimum of 570 for a superheated lava that is erupted at a temperature of 1630°C to a maximum of 64,069 for a lava that flows at a sub-liquidus temperature of 1340°C. The higher Prandtl value occurs at the lava/substrate interface of a 20-m-thick flow for which the kinematic viscosity calculated for a lava temperature of 1340°C is equal to 7.5 x 10^{-3} m^2 s^{-1} (equivalent to a dynamic viscosity of 21.8 Pa s). For the 20-m-thick insulated flow, the choice of lower freestream and interface temperatures compared to their radiating counterpart values was made for the purpose of testing whether flow conditions might still be Newtonian or not. The specific heat capacity of the lava is equal to 1570 J kg^{-1} $°C^{-1}$ at the liquidus temperature and above (*Williams et al*., 2000), and the specific heat of the lava substrate (consolidated) is chosen at the effective temperature of melting of the ground (T_{emg}=1160°C, from *Williams et al*., 2000). The value of the latent heat of fusion of the substrate, L_g, is taken to be equal to 4.25 x 10^5 J kg^{-1} (*Williams et al*., 2000).

Among the parameters that are not shown in the Table, the turbulent thermal diffusivity, α_t, is an input parameter of the model and we take it equal to 10^{-3} and 0 m^2 s^{-1} at the source and lava/substrate interface, respectively. The turbulent thermal diffusivity, α_t is equal to zero at the lava/substrate interface because flow velocity is zero there and, hence, there is no turbulent component of motion either. The temperature at which a basaltic substrate melts is T_{mg} = 1080°C (from *Williams et al*., 1998, 2000). The effective temperature (accounting for substrate viscosity) at which a basaltic substrate melts is T_{emg} = 1160°C (from *Williams et al*., 1998,

2000) and the ambient temperature of the ground, far from the lava/substrate interface, is T_a = 0°C. The turbulent Prandtl number can take values comprised between 0.7 and 0.9 and is here equal to 0.7 and 0.85. The former value applies to the freestream whereas the higher value is assumed to occur at the channel bed and banks.

Table 5.1a – Scenario 1 (flow radiating heat into the lunar environment). Model thermophysical parameters. Lava is assumed to be erupted at the liquidus temperature but, once in contact with the lunar environment, it cools down to sub-liquidus values. The last sub-scenario refers to lava that is erupted superheated. For each individual sub-scenario, lava is assumed to be 5 and 20 m in thickness, and travel at a horizontal velocity, U_x, that is equal to 5 m s^{-1} for the thinner flows and 5 and 10 m s^{-1} for 20-m-thick lava. The temperature drop (at time of eruption) that is undergone by the flowing lava is likely much higher than the one shown here (see text). The illustrated sub-liquidus values are calculated by the Stefan-Boltzmann expression and refer to a downstream distance of 1 km from the source. The decrease in temperature is higher for flows that are thinner and slower. The lava substrate is assumed to be consolidated and identical in composition to the flowing lava. The suffix "int" stands for interface (channel bed and banks); "T_l" stands for "lava temperature", "h" is lava thickness, "freestream" is the channel region that is farthest from channel boundaries. Pr is laminar (molecular) Prandtl number, C_p is specific heat capacity of the lava, C_g is specific heat capacity of the lava substrate, L_g is latent heat of fusion of the lava substrate. Values of the turbulent Prandtl number, Prt, are not shown here and are equal to 0.7 in the freestream and 0.85 at the channel bed and banks. The turbulent thermal diffusivity, α_t, is not shown and is equal to 10^{-3} m^2 s^{-1} and 0 at the lava source and the channel interface, respectively.

***Input thermophysical parameters* – Scenario 1. Lava radiating heat into the lunar vacuum**								
Sub-liquidus temperatures								
T_l	T_{int}	h	U_x	$Pr_{\_freestream}$	$Pr_{\_interface}$	L_g	$C_{p\_freestream}$	C_g
°C	°C	m	m s^{-1}	#	#	m^2 s^{-2}	m^2 s^{-2} °C^{-1}	m^2 s^{-2} °C^{-1}
1400	1380	5	5	6396	13,832	4.25 x 10^5	1550	1500
T_l	T_{int}	h	U_x	4391	20,256	4.25 x 10^5	1555	1500
°C	°C	m	m s^{-1}					
1410	1370	20	5					
T_l	T_{int}	h	U_x	3635	16,737	4.25 x 10^5	1557	1500
°C	°C	m	m s^{-1}					

1415	1375	20	10					
Superheated lava								
T_l	T_{int}	h	U_x	575	576	4.25×10^5	1570	1500
°C	°C	m	m s^{-1}					
1590	1570	5	5					
T_l	T_{int}	h	U_x	574	577	4.25×10^5	1570	1500
°C	°C	m	m s^{-1}					
1600	1560	20	5					
T_l	T_{int}	h	U_x	573	574	4.25×10^5	1570	1500
°C	°C	m	m s^{-1}					
1605	1565	20	10					

Table 5.1b – Scenario 2 (lava flowing insulated in a tube). Model thermophysical parameters. Values refer to three main sub-scenarios: a) Lava is erupted at the liquidus temperature; b) lava is erupted at sub-liquidus temperatures that are within 60°C of the liquidus value; c) lava is superheated and eruption temperature is 190°C higher than liquidus (*Wieczorek et al*., 2000). Each sub-scenario refers to flows that are 5 and 20 m thick and travel at horizontal velocities of 5 and 5 and 10 m s^{-1}, respectively. The latent heat of the flowing lava, L_l, is always equal to 425,000 m^2 s^{-2}. The turbulent thermal diffusivity, α_t, is equal to 10^{-3} m^2 s^{-1} and 0 at the lava source and the channel interface, respectively.

***Input thermophysical parameters* – Scenario 2. Lava flowing insulated (in a tube)**								
Liquidus temperature								
T_l	T_{int}	h	U_x	$Pr_{\_freestream}$	$Pr_{\_interface}$	L_g	$C_{p\_freestream}$	C_g
°C	°C	m	m s^{-1}	#	#	m^2 s^{-2}	m^2 s^{-2} °C^{-1}	m^2 s^{-2} °C^{-1}
1440	1420	5	5	1410	3016	4.25×10^5	1570	1500
T_l	T_{int}	h	U_x	1410	6473	4.25×10^5	1570	1500
°C	°C	m	m s^{-1}					
1440	1400	20	5					
T_l	T_{int}	h	U_x	1410	6389	4.25×10^5	1570	1500
°C	°C	m	m s^{-1}					
1440	1400	20	10					

Sub-liquidus temperatures								
T_l	T_{int}	h	U_x	13,711	29,654	4.25×10^5	1540	1500
°C	°C	m	m s^{-1}					
1380	1360	5	5					
T_l	T_{int}	h	U_x	13,693	64,069	4.25×10^5	1540	1500
°C	°C	m	m s^{-1}					
1380	1340	20	5					
T_l	T_{int}	h	U_x	13,693	64,069	4.25×10^5	1540	1500
°C	°C	m	m s^{-1}					
1380	1340	20	10					
Superheated lava								
T_l	T_{int}	h	U_x	570	572	4.25×10^5	1570	1500
°C	°C	m	m s^{-1}					
1630	1610	5	5					
T_l	T_{int}	h	U_x	570	572	4.25×10^5	1570	1500
°C	°C	m	m s^{-1}					
1630	1590	20	5					
T_l	T_{int}	h	U_x	570	570	4.25×10^5	1570	1500
°C	°C	m	m s^{-1}					
1630	1590	20	10					

The model assumes steady-state flow conditions, an assumption justified by the likely long-lasting duration of eruptive events associated with the formation of lunar sinuous rilles (*Wilson and Head*, 2017). The lava substrate is modeled as consolidated. For reference, the chapter dedicated to the sensitivity analysis describes the impact of an unconsolidated substrate on erosion rates. The thickness of individual lava layers is taken to be equal to 5 to 20 m for reasons that are well-explained in the sensitivity analysis chapter.

The geometry of the rille

As part of the current investigation, new measurements obtained from high-resolution LROC NAC images provide a length of ~200 km and an average width of ~160 m. The width value can locally increase up to ~320 m, although these higher values are only measured in the proximity of goose-neck meander axes, where the channel is always wider than at other rille sections. The inner rille extends ~50 km farther downstream of the primary rille, and cross cuts the distant wall of the larger channel before it finally reaches its terminus point in Oceanus Procellarum. As soon as the inner rille cross cuts the primary outer rille wall, the channel becomes narrower (~100 in width), meanders become rare, of shorter wavelength (~650 m) and lower amplitude (~250 m). The rille remains moderately sinuous until it reaches its terminus point in Oceanus Procellarum. The high-resolution LROC NAC images show that, out to a downstream distance of ~125-150 km from the Cobra Head (lava source), channel corners are well rounded (a likely sign of thermal/thermo-mechanical erosion) and meanders are similar to those located in the upstream portions of the rille.

The inner rille is locally characterized by very sinuous, goose-neck meanders out to a downstream distance of ~145 km from the lava source (only a few km upstream of the point where the inner rille cuts through the primary rille wall), and meanders that are more flattened in shape. The average meander wavelength is measured to be ~800 m, though values are found to vary down to ~650 within ~40 km of the rille terminus, and up to ~1200 m at rille portions that are closer to the lava source. A close inspection of goose-neck

meanders reveals that they occur in association with narrow mounds that might have acted as obstacles, thus compelling the flow to follow a loopy path around them.

Based on the recent measurements obtained from available high-resolution LROC NAC images of the Vallis Schröteri inner rille, a range of grid geometries was chosen and dealt with in the sensitivity analysis (S.A.) chapter. The baseline geometry adopted here consists of a channel that is 160 m wide and has meander wavelength and amplitude of 800 m and 300 m, respectively. The only difference is that lower- and upper-end values are used for lava thickness (5 and 20 m) instead of the 10-m value adopted in the S.A. This geometry displays channel meanders that are more flattened than the goose-neck meanders that characterize other portions of the rille.

Turbulence parameters

Table 5.2 shows the initial values of turbulent kinetic energy k and specific turbulent dissipation ω used in the SST k-ω model, calculated at the 1200-m-long rille section of interest. This mesh geometry is representative of a limited portion of the Vallis Schröteri primary rille though it is ideal for the purpose of determining maximum erosion rates at/near the lava source. Also, a 1.2-km-long mesh allows for a high cell resolution (the closest grid cell to the channel bed/banks is 0.5 m away from the walls) due to the much lower computational cost involved. The lower the values of k, the less kinetic energy is dissipated within the flow. As shown in Table 5.2, the lowest value of turbulent kinetic energy k is found for a 20-m-thick superheated lava whereas the highest belongs to a 5-m-thick flow that is erupted at a sub-liquidus temperature of 1380°C. A lava with a

temperature of 1380°C is associated with a flow viscosity that is more than an order of magnitude higher than that associated with a flow erupted at the liquidus temperature (4.4 Pa s versus 0.4 Pa s at T_{liq}). Another feature worth noticing is that k values are always equal to zero at channel boundaries because flow velocity is zero there. Because there is no lava motion, no turbulence dissipation processes take place at close contact with the lava/substrate interface. As regards specific turbulence dissipation (ω) values, the lowest is found at the inlet (lava source) of a 20-m-thick flow that travels at a horizontal velocity of 5 m s^{-1}. The highest ω value is found at the channel boundary (ω_{int} value), where flow viscosity is highest, and refers to a 20-m-thick flow that is erupted at a sub-liquidus temperature of 1380°C with an interface temperature of 1340°C and a dynamic viscosity of 21.8 Pa s.

Turbulence intensity values (not displayed in the table) are comprised between a minimum of 4.8 x 10^{-2} and a maximum of 2.8 x 10^{-2} and are indicative of a low turbulence intensity (lower than 0.5%). Turbulence intensity decreases for increasing flow rates and Reynolds number of the flow. As a result, it is higher for thinner lava flows and lower-temperature, higher-viscosity lavas. For flows of the same thickness, lower flow rates are characterized by slightly higher values of turbulence intensity and much lower values of k and ω than those associated with higher flow rates.

Table 5.2 - Model input parameters. Mesh properties and calculated turbulence parameters for the adopted SST k-ω turbulence model and the two investigated eruption scenarios. The length of the investigated rille segment is 1.2 km (from the lava source) and cell resolution is 0.5 m at channel boundaries. Variations in meander wavelength, λ, and amplitude, 2A, do not affect turbulence parameters values. All values refer to eruption temperatures in the range 1630°C-1380°C and flow kinematic viscosities in the range 1.4 x 10^{-4} m^2 s^{-1} (for superheated and liquidus lavas) to 7.5 x 10^{-3} m^2 s^{-1} (for T_{int}=1340°C). "Hydr. radius" stands for hydraulic radius (see sensitivity analysis chapter for a detailed description). As regards

turbulence parameters, k is turbulent kinetic energy and ω is specific turbulence dissipation (see sensitivity analysis chapter); the suffix "int_field" refers to the flow core or freestream lava that is far from boundaries (bed and banks); k_{inlet} is turbulent kinetic energy at the lava source; k_{top} and ω_{top} are not shown here because they are calculated in the model. Turbulence intensity values (not displayed in the table) are comprised between a minimum of 4.8×10^{-2} and a maximum of 2.8×10^{-2} and are indicative of a low turbulence intensity (always lower than 0.5%).

Geometry of the meandering channel					
Flow depth (h)	Length (l)	Width (w)	Hydr. radius	Meander λ	Meander 2A
m	m	m	m	m	m
5	1200	160	4.7	800	300
20	"	"	16.0	"	"

Scenario 1 (flow radiating heat). *Calculated input turbulence parameters - SST k-ω model (from Menter, 1993)*

h	T_l	$T_{int.}$	U_x	k_{int_field}	k_{inlet}	k_{int}	ω_{int_field}	ω_{inlet}	$\omega_{int.}$
m	°C	°C	m s^{-1}	$m^2\ s^{-2}$	$m^2\ s^{-2}$	$m^2\ s^{-2}$	s^{-1}	s^{-1}	s^{-1}
Subliquidus temperature									
5	1400	1380	5	3.6×10^{-5}	7.0×10^{-2}	0.0	4.8	1.5	4.9
20	1410	1370	5	7.2×10^{-6}	4.7×10^{-2}	0.0	1.4	3.5×10^{-1}	7.3
20	1415	1375	10	1.2×10^{-5}	1.5×10^{-1}	0.0	2.8	6.3×10^{-1}	5.9
Superheated lava									
5	1590	1570	5	7.3×10^{-6}	4.7×10^{-2}	0.0	4.8	1.2	0.4
20	1600	1560	5	2.1×10^{-6}	3.5×10^{-2}	0.0	1.4	3.0×10^{-1}	0.4
20	1605	1565	10	4.3×10^{-6}	1.2×10^{-1}	0.0	2.8	5.6×10^{-1}	0.4

Scenario 2 (insulated flow). *Calculated input turbulence parameters - SST k-ω model (from Menter, 1993)*

h	T_l	$T_{int.}$	U_x	k_{int_fld}	k_{inlet}	$k_{int.}$	ω_{int_fld}	ω_{inlet}	ω_{int}
m	°C	°C	m s^{-1}	$m^2\ s^{-2}$	$m^2\ s^{-2}$	$m^2\ s^{-2}$	s^{-1}	s^{-1}	s^{-1}
Liquidus temperature									
5	1440	1420	5	7.3×10^{-6}	4.7×10^{-2}	0.0	4.8	1.2	1.0
20	1440	1400	5	2.2×10^{-6}	3.5×10^{-2}	0.0	1.4	3.0×10^{-1}	2.2
20	1440	1400	10	8.6×10^{-6}	1.2×10^{-1}	0.0	2.8	6.0×10^{-1}	2.2
Subliquidus temperature									
5	1380	1360	5	8.1×10^{-5}	8.6×10^{-2}	0.0	4.8	1.6	10.8
20	1380	1340	5	2.4×10^{-5}	6.3×10^{-2}	0.0	1.4	4.1×10^{-1}	24.1

20	1380	1340	10	4.7×10^{-5}	2.1×10^{-1}	0.0	2.8	7.5×10^{-1}	24.1
Superheated lava									
5	1630	1610	5	7.3×10^{-6}	4.7×10^{-2}	0.0	4.8	1.2	0.4
20	1630	1590	5	2.1×10^{-6}	3.5×10^{-2}	0.0	1.4	3.0×10^{-1}	0.4
20	1630	1590	10	4.3×10^{-6}	1.2×10^{-1}	0.0	2.8	5.6×10^{-1}	0.4

Results

Erosional patterns at the rille bed and banks

The most consistent pattern observed in every single section considered, regardless of the geometric characteristics of the section itself, is the presence of two regions of thermal erosion enhancement that are located at or in proximity of meander troughs (the right bank at a channel cross-section cut parallel to bend 1 axis, in shown computer simulations) and over the bends. The lowest values of thermal erosion are found at meander apexes (the left bank at the mentioned channel cross-section), and this appears to always be the case regardless of channel geometry and assumed flow rates. Figs. 5.1 (a, b, c) show the described distribution of erosion rate changes at the bed and banks of a 1200-m-long and 20-m-thick channel section. Erosion highs at the bed are always found within a few meters of either of the two banks or within several meters (~25 m) of the right bank, as shown in Fig. 5.1a.

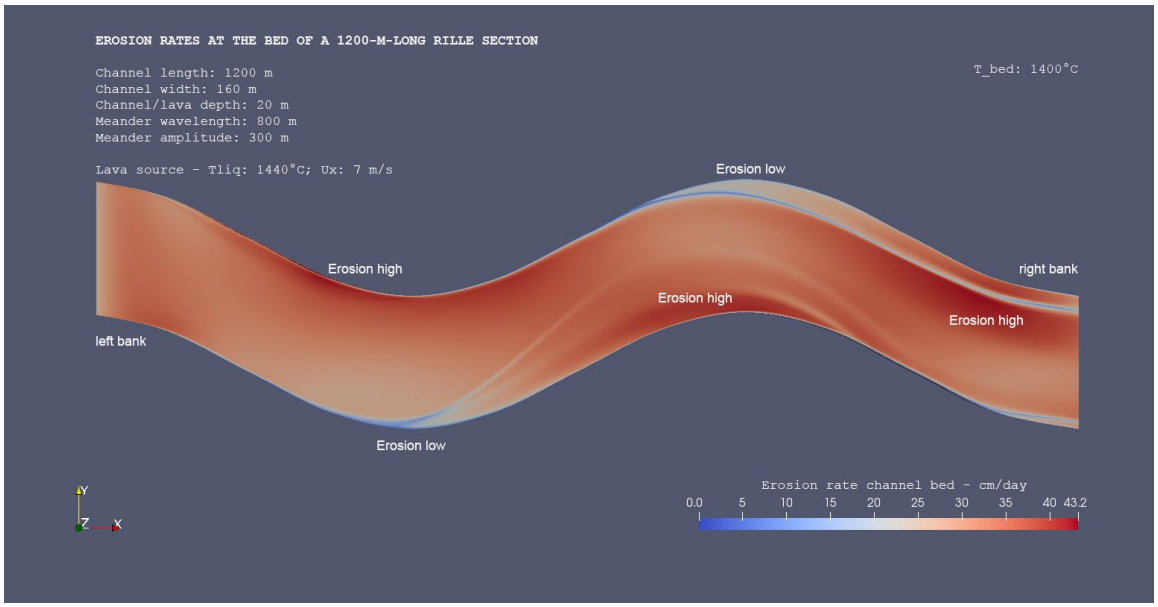

Figure 5.1a. Planar view that shows how erosion rate distribution varies at the bed of a 1200-m-long rille section. Lava source is on the left and flow motion is rightward. Erosion highs are concentrated at or near bend troughs whereas lows are found at bend apexes.

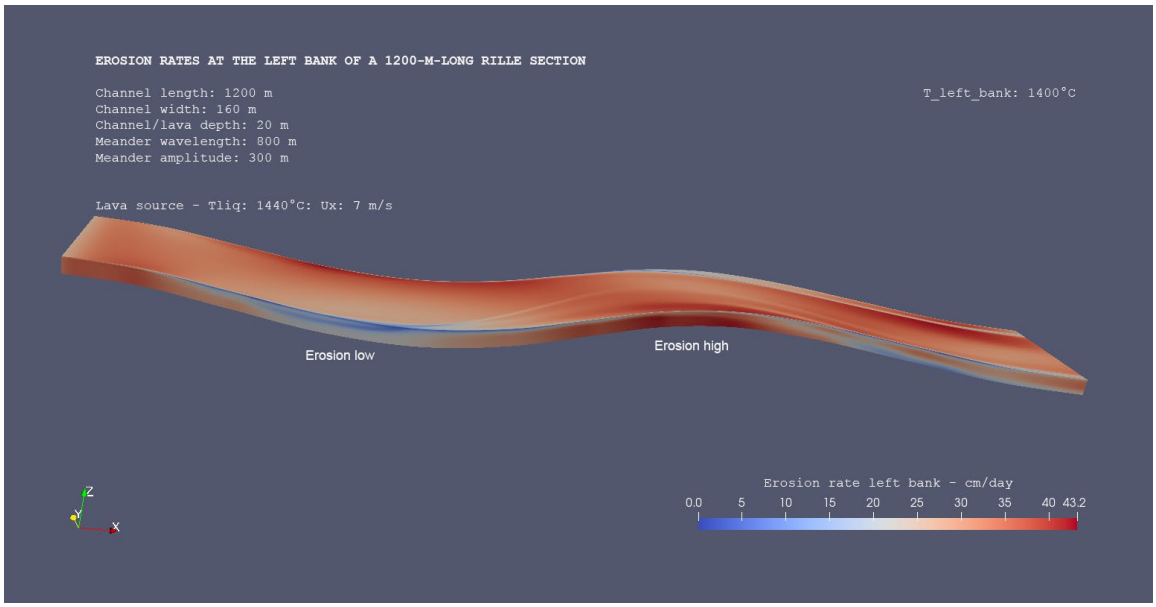

Figure 5.1b. Planar view that shows how erosion rate distribution varies at the left bank of a 1200-m-long rille section. Lava source is on the left and flow motion is rightward. Erosion highs are concentrated at or near bend troughs whereas erosion lows are found at bend apexes.

Figs. 5.1 (b, c) reveal a similar distribution of erosion rates at the left and right banks of the channel section of interest. Changing eruption conditions and flow parameters cause erosion highs and lows to migrate downstream or upstream of their original locations (as shown in the sensitivity analysis chapter) though such shifts are usually on the order of a few meters or tens of meters. Because of this, they are usually difficult to visualize at the image scale provided in Fig. 5.1.

In the sensitivity analysis chapter, a two-fold approach was adopted in the study of the distribution of erosion rates within the channel section of interest. Erosion rates were measured across the entire rille section and then at one or two cross-sections of the channel that were cut parallel to bend axes. The former approach provides a precise "mapping" of erosion highs and lows at the bed and reveals how those highs and lows relate to the highs and lows found at bed/bank contacts. While this approach proves especially useful in the context of a sensitivity study, it is not strictly needed in this analysis. The results obtained at one and occasionally two cross-sections of the rille will reveal the details of flow circulation at meander bends and how those affect erosion rate magnitudes and their distribution at the bed and banks of two adjacent rille bends or meanders.

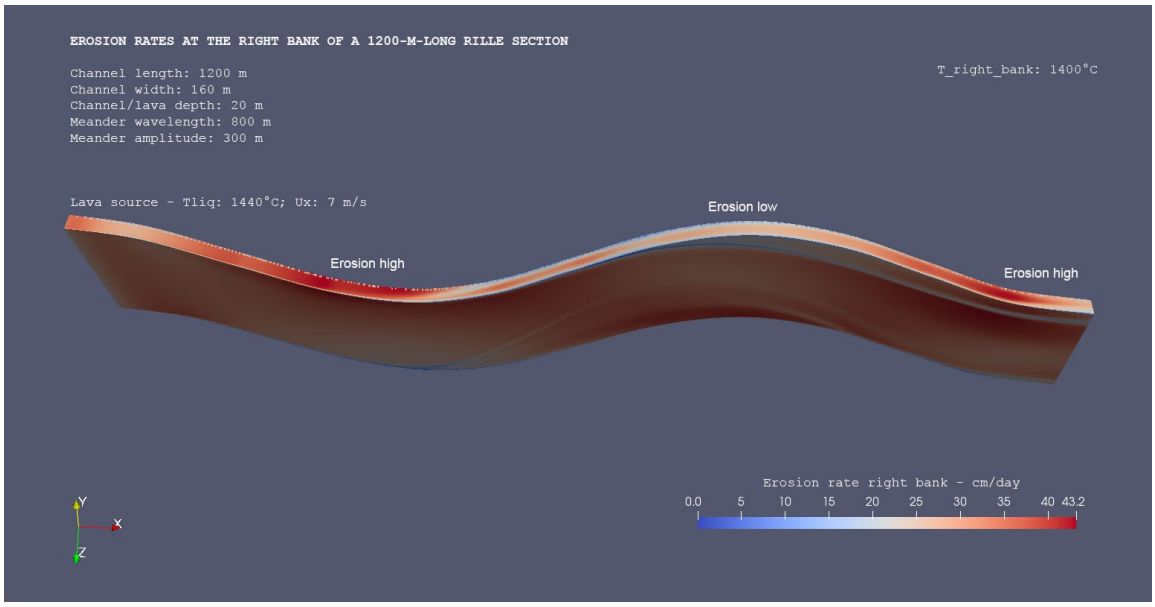

Figure 5.1c. Plan view that shows how the erosion rate distribution varies at the right bank of a 1200-m-long rille section. Lava source is on the left and flow motion is rightward. Erosion highs are concentrated at or near bend troughs whereas lows are found at bend apexes.

Scenario 1 - Cooling rates for the inner rille lava

In scenario 1, lava is assumed to lose heat through the flow top by radiation into the lunar environment. Here, Stefan-Boltzmann expression is used to provide a first order estimate of lava cooling rates (see Table 5.3) for flows that travel at velocities of 5 and 10 m s^{-1}. At time of eruption, lava temperature is assumed to be equal to 1440°C (liquidus), 1380°C (sub-liquidus) and 1630°C (superheated lava). The radiant emittance, Q_r, has dimensions of energy output (energy per unit time per unit area) and is calculated for both temperature values. Using this piece of information together with the previously calculated lava velocities of 5 and 10 m s^{-1}, the time taken by the flow to travel a downstream distance of 1 km from the source is found. The total energy output through the flow top (out to the traveled distance of 1 km) is then used to derive the cooling rate (°C/km) at the flow top.

Table 5.3 shows how the cooling rate through the flow top varies depending on the initial temperature of the lava and the flow rate. The higher the eruption temperature, the higher the radiant emittance through the flow top. Expectedly, the highest value at time of eruption (7.1×10^5 kg s^{-3} or W m^{-2}) refers to superheated lava and the lowest is obtained from sub-liquidus lava. Lava that flows at a horizontal velocity of 10 m s^{-1} takes a shorter time to travel the 1-km distance from the source and the total energy output through the flow top is lower than that produced by a flow that travels at a velocity of 5 m s^{-1}. The highest cooling rate of 10.1°C/km is thus associated with a flow that travels at 5 m s^{-1} and is erupted at a temperature of 1630°C whereas the lowest (5.2°C/km) is obtained from sub-liquidus lava that flows at 10 m s^{-1}. How do we provide an estimate of the distance to the turbulent/laminar transition? Simulations obtained by assuming an eruption temperature of 1340°C (and a corresponding dynamic viscosity of 21.8 Pa s) show that flow conditions are unlikely to be Newtonian because unrealistic and physically inconsistent results are obtained. Because of this, the 1340°C temperature value is used to mark the turbulent/laminar regime transition and the calculated cooling rates are used to obtain a first order estimate of the distance traveled by the lava till that temperature is reached. The approach adopted here – while being very simplistic – is applicable to a range of eruption temperatures and flow rates. As a result, lava that is erupted at a temperature of 1630°C and travels at a velocity of 10 m s^{-1} might be able to flow turbulently out to a downstream distance of ~48 km from the source. In contrast, a flow erupted at a sub-liquidus temperature of 1380°C and traveling at a velocity of 5 m s^{-1} might do so only for about 4.5 km.

Table 5.3 – Scenario 1 (lava radiating heat into the lunar vacuum). The lava is assumed to erupt at the liquidus temperature (1440°C), at a sub-liquidus temperature (1380°C) and at a temperature of 1630°C (superheated lava). This table provides a first-order estimate of lava cooling obtained by using Stefan-Boltzmann expression, three values of eruption temperature for the Vallis Schröteri inner rille lava and the calculated flow velocities of 5 and 10 m s^{-1}. T_e is temperature of eruption; T_e is here identical to T_{surf}, the initial lava temperature at the flow top; T_a is ambient temperature or temperature of the lunar environment; σ is Stefan-Boltzmann constant; ε is emissivity through flow top; Q_r is energy output through flow top; t_{1km} is the time taken by the flow to travel the 1-km distance from the lava source; $Q_{r\ at\ t=t1}$ is the total energy output through the flow top out to the 1-km distance from the source; C.R. is the cooling rate of the lava; D_{lam} is the distance to the turbulent/laminar regime transition.

Scenario 1 (flow radiating heat). *First order estimate of lava cooling rate from flow top. Estimate obtained by using Stefan-Boltzmann expression*									
U_x	$T_{e/surf}$	T_{surf}	σ	ε	$Q_{r\ at\ t=0}$	t_{1km}	$Q_{r\ at\ t=t1}$	C.R.	D_{lam}
m s^{-1}	°C	°C	W m^{-2} K^{-4}	#	kg s^{-3}	s	kg s^{-3}	°C/km	km
5	1440	1440	5.67×10^{-8}	0.93	4.6×10^{5}	200	3.7×10^{12}	9.1	11.0
10	1440	1440	5.67×10^{-8}	0.93	4.6×10^{5}	100	4.6×10^{11}	5.4	18.5
5	1380	1380	5.67×10^{-8}	0.93	4.0×10^{5}	200	3.2×10^{12}	8.8	4.6
10	1380	1380	5.67×10^{-8}	0.93	4.0×10^{5}	100	4.0×10^{11}	5.2	7.7
5	1630	1630	5.67×10^{-8}	0.93	7.1×10^{5}	200	5.7×10^{12}	10.1	28.7
10	1630	1630	5.67×10^{-8}	0.93	7.1×10^{5}	100	7.1×10^{11}	6.0	48.3

Scenario 1 - Erosion rates at channel cross-section 400

This section describes results relevant to a rille section that is identical to that considered in the sensitivity analysis chapter, i.e., cross-section 400, which is cut along bend 1 trough and is shown here again for the sake of completeness (see Fig. 5.2). As previously mentioned, lava temperatures are assumed to be 30-40°C lower than their values at time of eruption, the exact value depending on flow thickness. In this section, the erosional power of both sub-liquidus and superheated lavas will be explored. Fig. 5.3

illustrates the erosion rates distribution at the bed of a 5-m-thick lava with a sub-liquidus temperature of 1400°C and traveling at a horizontal velocity of 5 m s^{-1}. As for the other 5-m-thick flows, the temperature chosen at the lava/substrate interface is 20°C lower than the freestream value (i.e., equal to 1380°C).

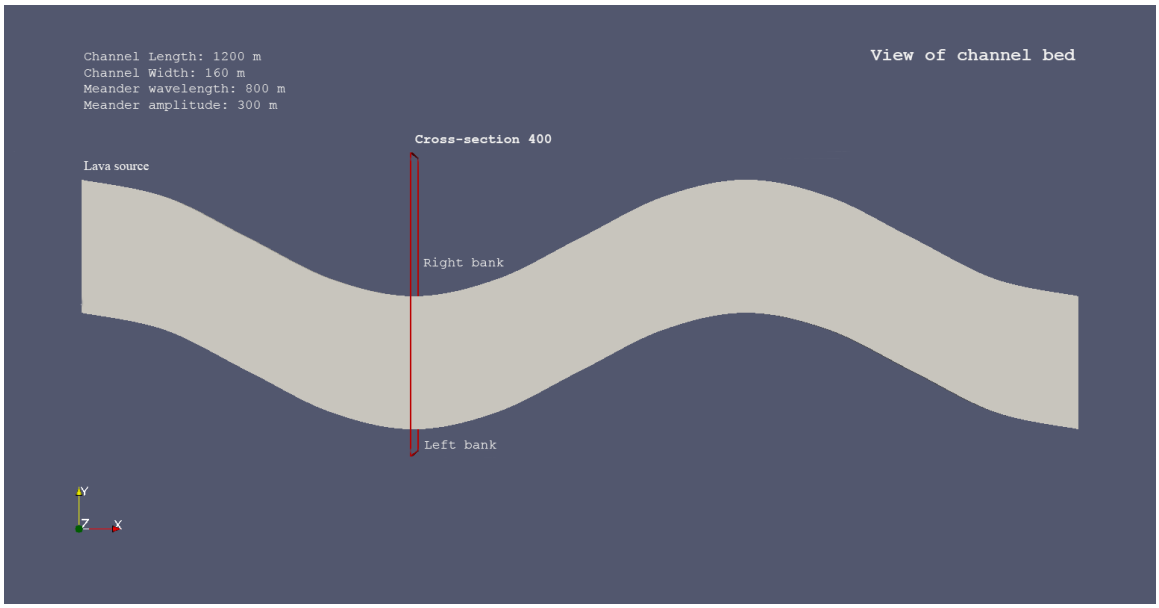

Figure 5.2. Plan view of rille bed for the 1200-m-long channel section of interest. Bend 1 axis is located at the lava source and cross-section 400 is cut through bend 1 trough at a downstream distance of 400 m from the lava source (left). The erupted lava flows toward the right end of the channel.

Maximum erosion rate values of 5.6 cm/day are obtained within ~10 m of the bed/right bank contact. While moving toward the bed/left bank contact, erosion into the substrate decreases at an almost constant rate till the distance of 40 m from the contact is reached. Within 40 m of the left bank, erosion rates decrease faster to a minimum of 0.1 cm/day that is obtained within 1 m of the bed/left bank contact.

Fig. 5.4a shows erosion rates at the left bank of channel cross-section 400. Maximum erosion rates of 0.37-0.38 cm/day are found at the bank top and from there down

to a vertical distance of ~2 m from the bank/bed contact. Within 2 m of the contact, erosion rates drop to a minimum of 0.09 cm/day. Erosion rates at the right bank are shown in Fig. 5.4b. For progressively decreasing vertical distances from the bank top to the underlying rille bank/bed contact, the erosion rate distribution appears very similar to the one shown in Fig. 5.4a (left bank), though the actual values are higher. Maximum values of 3.2-3.4 cm/day are found starting at the bank top and from there down to a vertical distance of ~2 m from the bank/bed contact. Within 2 m of the contact, erosion rates drop till a minimum value of 1.8 cm/day is reached at the contact itself.

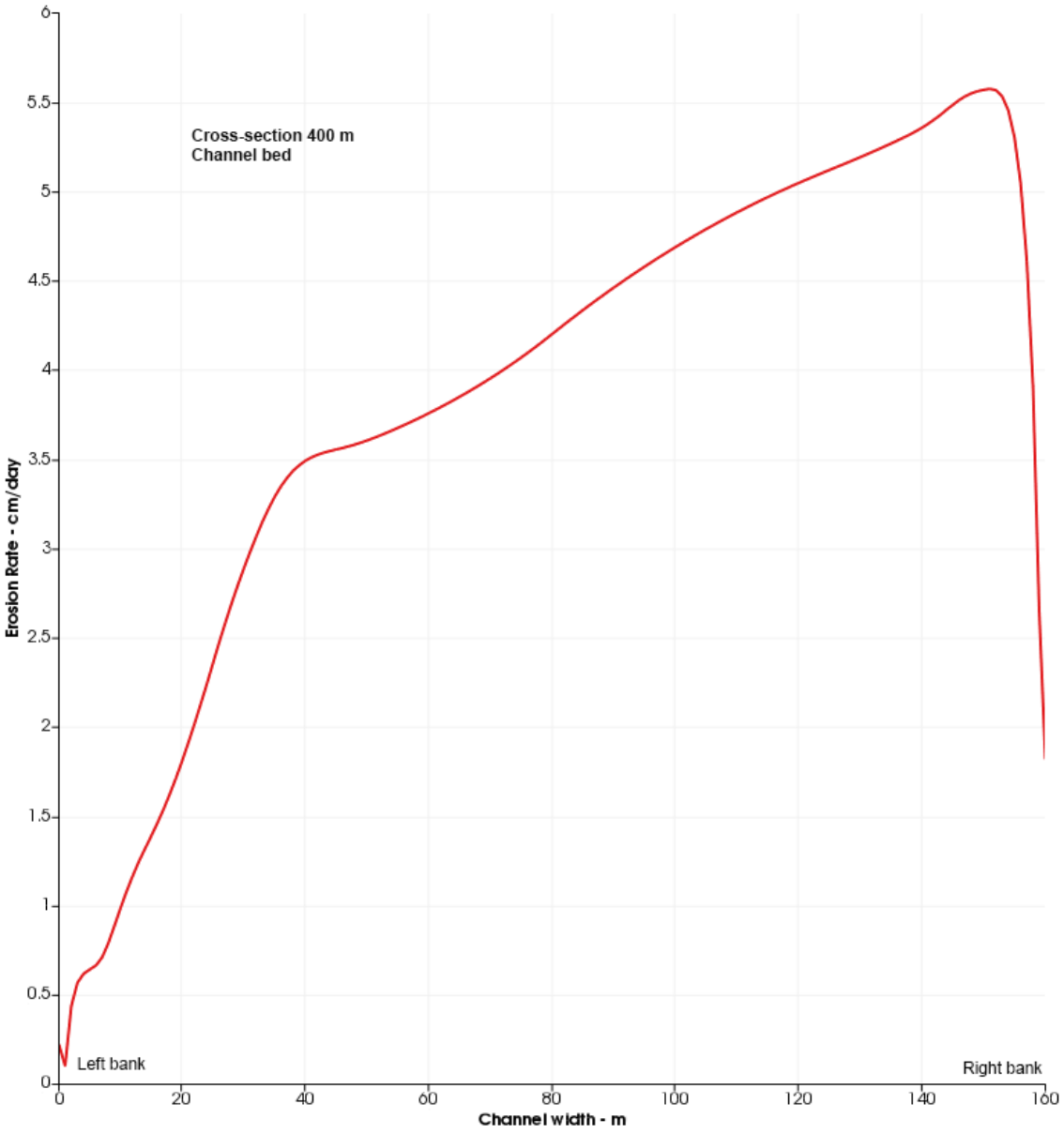

Figure 5.3. Scenario 1 (lava radiating heat through the flow top). Erosion rates at the bed of channel cross-section 400, a section cut through bend 1 trough. Results for a 5-m-thick lava flowing at the sub-liquidus temperature of 1400°C and a velocity of 5 m s^{-1}. Lava temperature at the bed is equal to 1380°C. Maximum erosion rate values of 5.6 cm/day are obtained within ~10 m of the bed/right bank contact. While moving toward that contact, erosion into the substrate decreases at an almost constant rate till the distance of 40 m from the contact is reached. Within 40 m of the left bank, erosion rates decrease faster to a minimum of 0.1 cm/day that is obtained within 1 m of the bed/left bank contact.

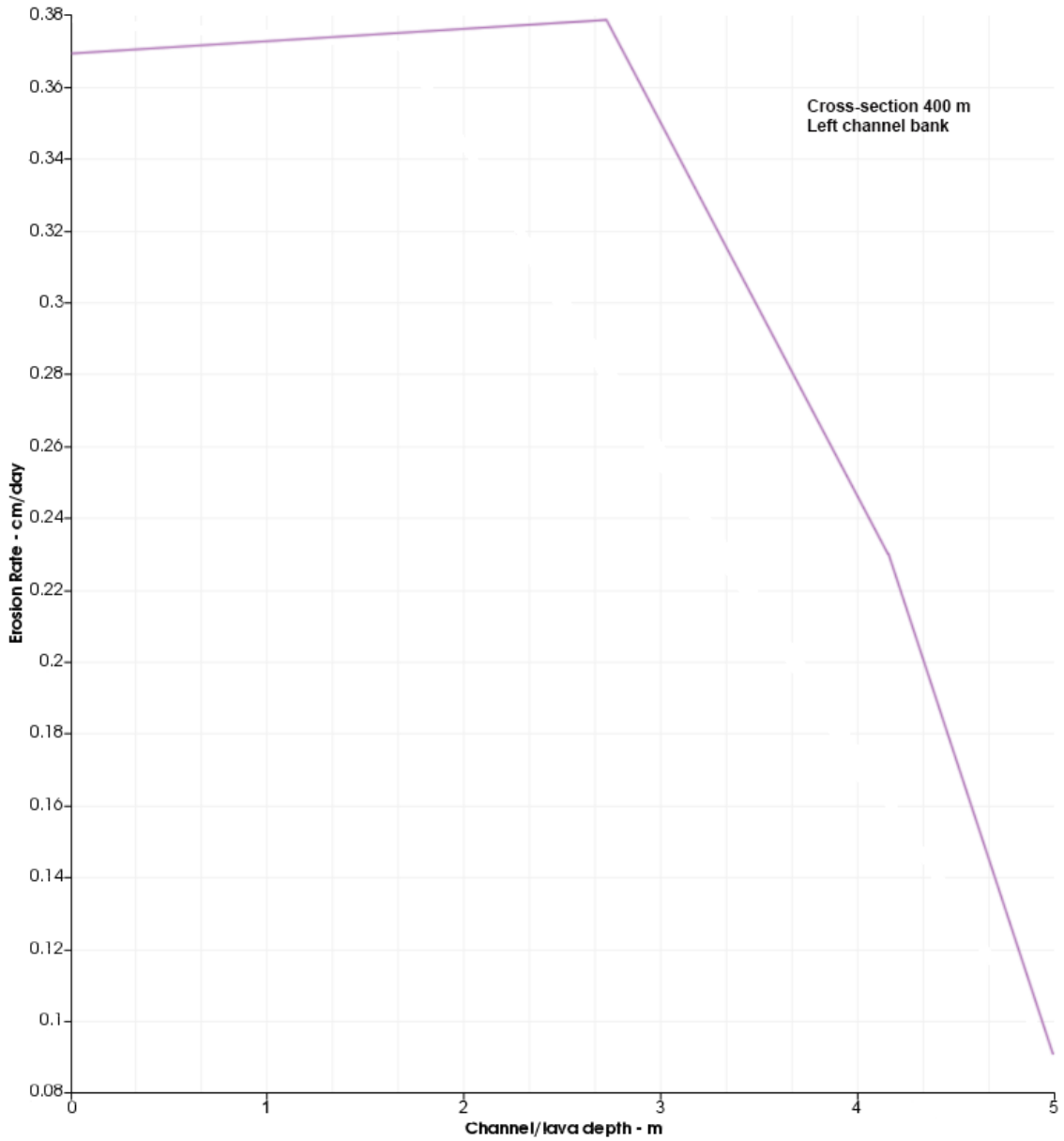

Figure 5.4a. Scenario 1 (lava radiating heat through the flow top). Erosion rates at the left bank of rille cross-section 400. A 5-m-thick lava flowing at the sub-liquidus temperature of 1400°C and a velocity of 5 m s^{-1}. Lava temperature at both channel banks is equal to 1380°C. Maximum erosion rates of 0.37-0.38 cm/day are found at the bank top and from there down to a vertical distance of ~2 m from the bank/bed contact. Within 2 m of the contact, erosion rates drop till a minimum value of 0.09 cm/day is reached at the contact itself.

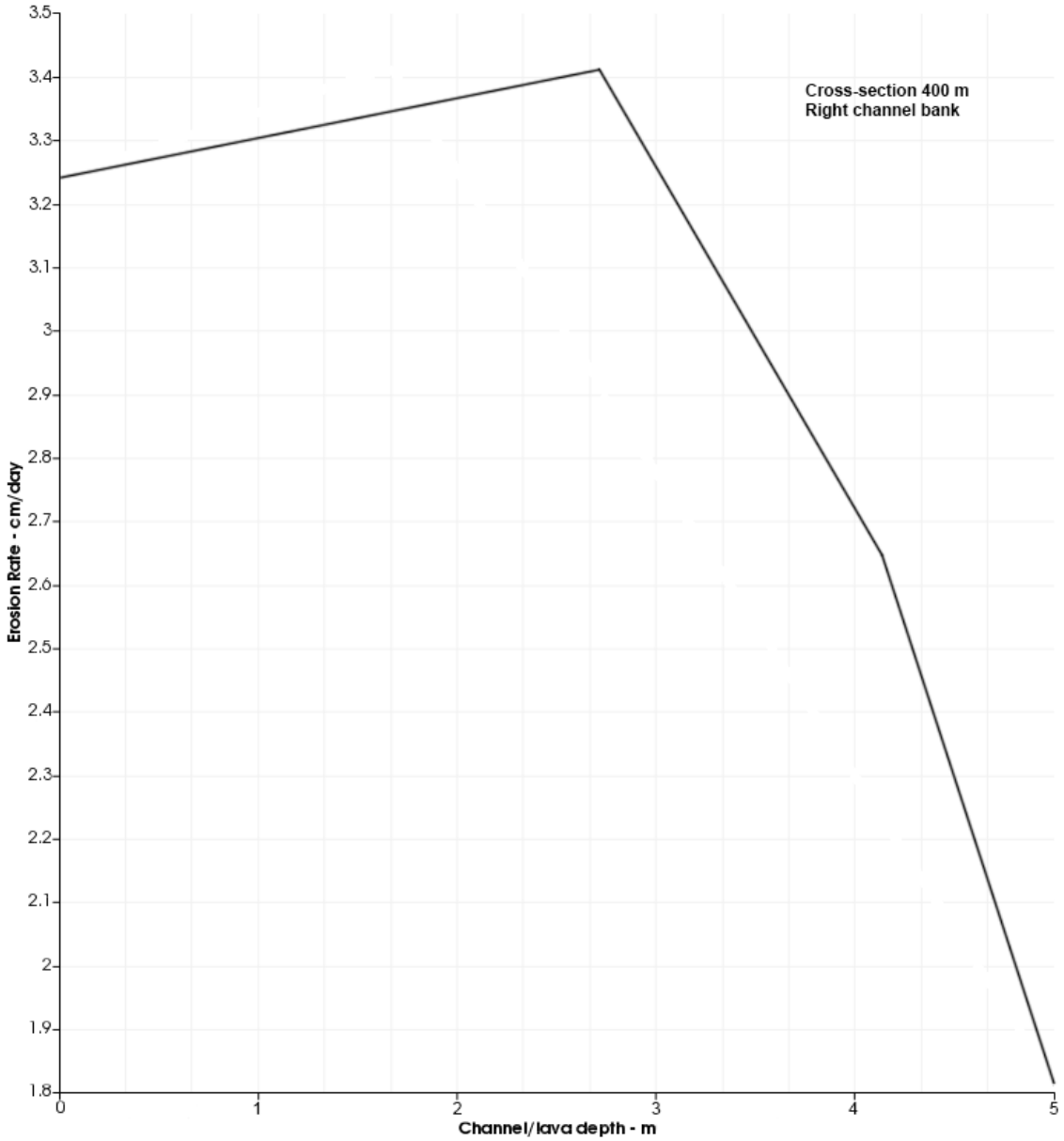

Figure 5.4b. Scenario 1 (lava radiating heat through the flow top). Erosion rates at the right bank of rille cross-section 400. Results refer to a 5-m-thick lava at the sub-liquidus temperature of 1400°C and flowing at a horizontal velocity of 5 m s^{-1}. Lava temperature at this bank is equal to 1380°C. The distribution of erosion rates with progressively decreasing vertical distances from the underlying rille bed appears very similar to the one shown in Fig. 4a (left bank). Erosion values are higher though. Maximum values of 3.25-3.41 cm/day are found at the bank top and from there down to a vertical distance of ~2 m from the bank/bed contact. Within 2 m of the contact, erosion rates drop till a minimum value of 1.8 cm/day is reached at the contact itself.

We next consider a 20-m-thick lava flowing at a temperature of 1410°C and a velocity of 5 m s^{-1}. Fig. 5.5 shows a plan view of the channel bed and the associated erosion rates. The source and freestream lava temperatures are assumed to have dropped 30°C below liquidus at time of eruption. The interface temperature is taken to be equal to 1370°C, i.e., 40°C lower than the lava freestream value. Lava source is on the left and flow motion is rightward. Once again, erosion highs (up to ~15.0 cm/day) are concentrated at or near bend troughs whereas lows are found at bend apexes.

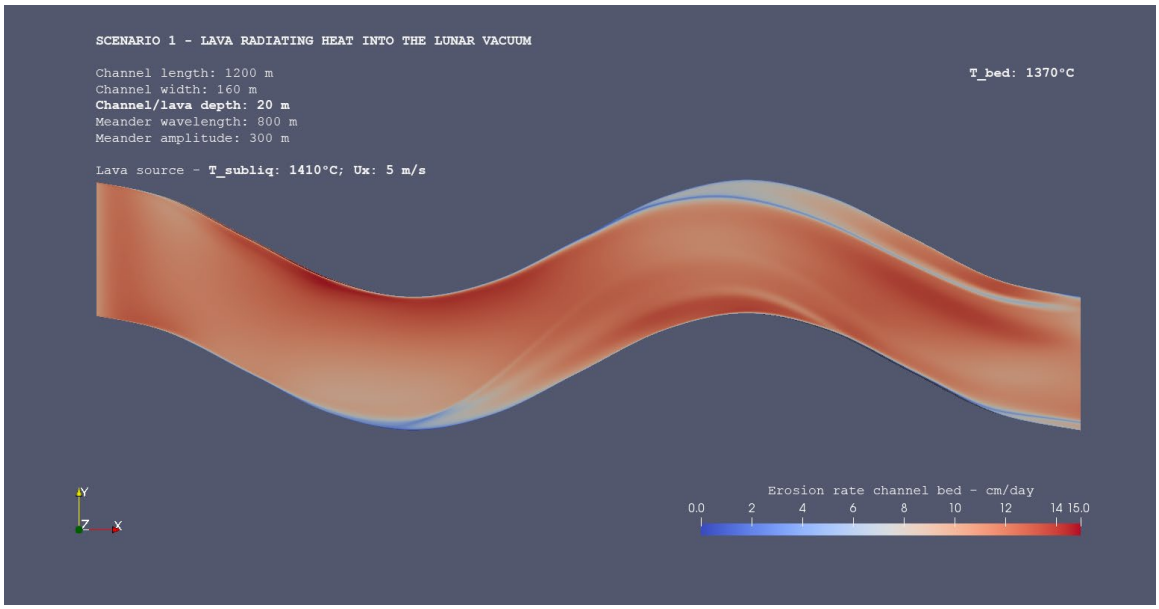

Figure 5.5. Plan view that shows how erosion rates vary at the bed of a 1200-m-long rille section. Scenario 1 (lava radiating heat into the lunar vacuum). Erosion rates are referred to a 20-m-thick lava of temperature equal to 1410°C (temperature dropped by 30°C at time of eruption) and flowing at a horizontal velocity of 5 m s^{-1}. The lava/substrate interface temperature is taken to be equal to 1370°C, i.e., 40°C lower than the lava freestream value. Lava source is on the left and flow motion is rightward. Once again, erosion highs (up to ~15.0 cm/day) are concentrated at or near bend troughs whereas lows are found at bend apexes.

Fig. 5.6 shows the erosion rates distribution at channel cross-section 400. Maximum erosion rates of 13.8 cm/day are obtained within ~10 m of the bed/right bank contact. While

moving toward the bed/left bank contact, erosion into the substrate decreases at an almost constant rate out to ~60 m from the same contact. Then, values level off out to ~30 m from the contact. From that point on, erosion rates decrease faster and then slowly increase again within 10 m of the contact. A minimum value of 0.2 cm/day is finally reached within 1 m of the bed/left bank contact.

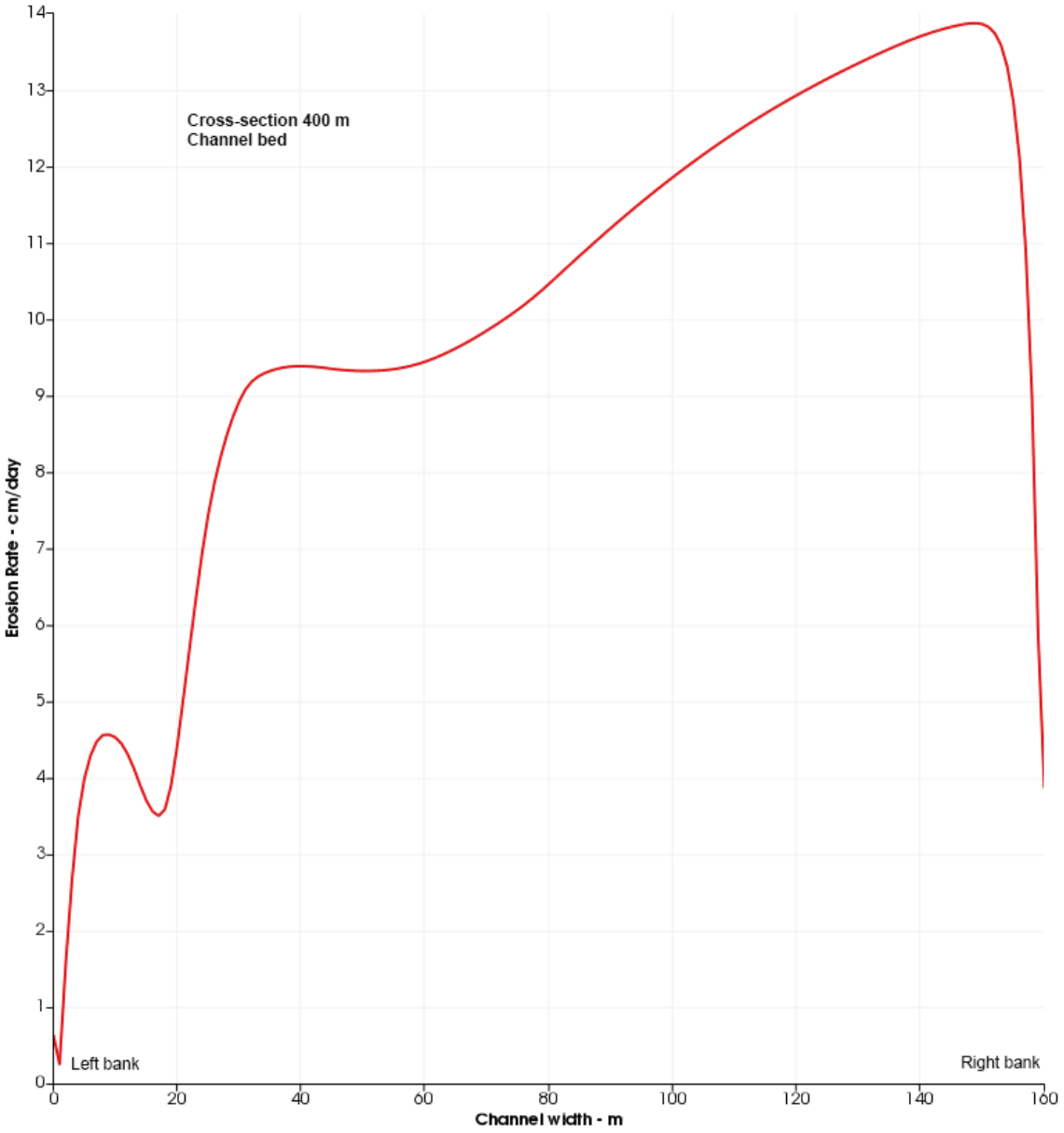

Figure 5.6. Scenario 1 (lava radiating heat through the flow top). Erosion rates at the bed of rille cross-section 400. Lava is 20 m thick and flows at the sub-liquidus temperature of 1410°C and a velocity of 5 m s^{-1}. Temperature at the bed is 1370°C. Maximum erosion rates of 13.8 cm/day are obtained within ~10 m of the bed/right bank contact. While moving toward the contact, erosion into the substrate decreases at an almost constant rate out to ~60 m from the contact itself. Then, values level off and remain almost constant out to ~30 m from the contact. From that point on, erosion rates decrease faster and then slightly increase within 10 m of the contact. A minimum value of 0.2 cm/day is finally reached within 1 m of the bed/left bank contact.

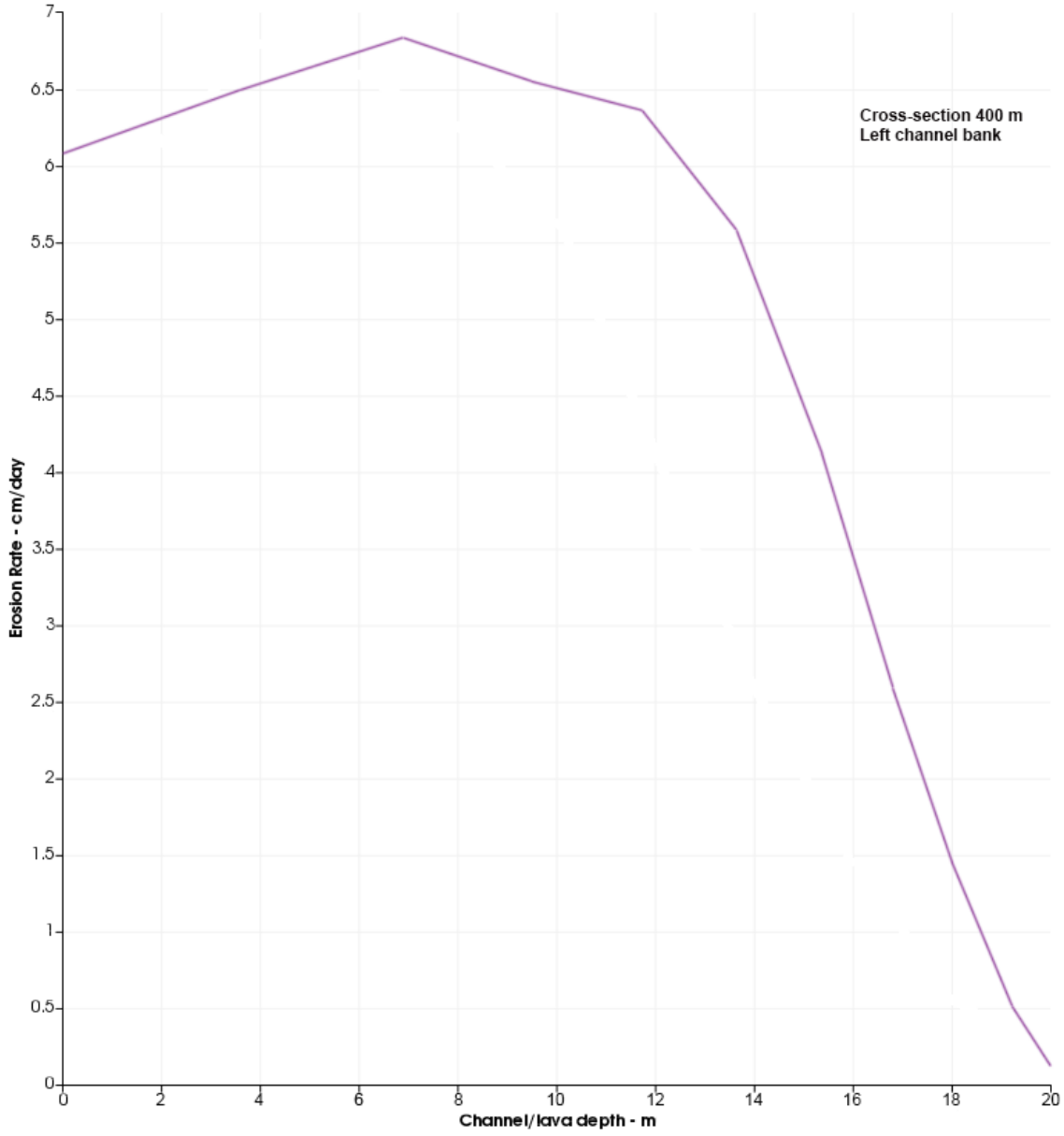

Figure 5.7a. Scenario 1 (lava radiating heat through the flow top). Erosion rates at the left bank of rille cross-section 400. Results refer to a 20-m-thick flow at 1410°C, which travels at a velocity of 5 m s^{-1}. Lava temperature at the bank is equal to 1370°C. Erosion rates increase from a value of 6.1 cm/day at the bank top to a maximum of 6.8 cm/day at a vertical distance of ~7 m from the bank top. From that point on, they decrease faster and faster until they literally drop to a minimum of 0.2 cm/day within ~6 m of the left bank/bed contact.

At the left bank of cross-section 400 (Fig. 5.7a), erosion rates increase from a value of 6.1 cm/day at the bank top to a maximum of 6.8 cm/day at a vertical distance of ~7 m from the bank top. From that point on, they decrease faster and faster until they literally drop to a minimum value of 0.2 cm/day. The sharpest drop occurs within ~6 m of the left bank/bed contact. Fig. 5.7b shows erosion rates on the opposite bank (right bank). Erosion rates increase from a value of 12.7 cm/day at the bank top to a maximum of 13.4 cm/day at a vertical distance of ~7 m from the bank top. Then, they decrease (first at a fast and then a slower rate) till a vertical distance of ~3 m from the underlying bank/bed contact is reached. The sharpest decrease in erosion rate finally occurs within ~3 m of the left bank/bed contact.

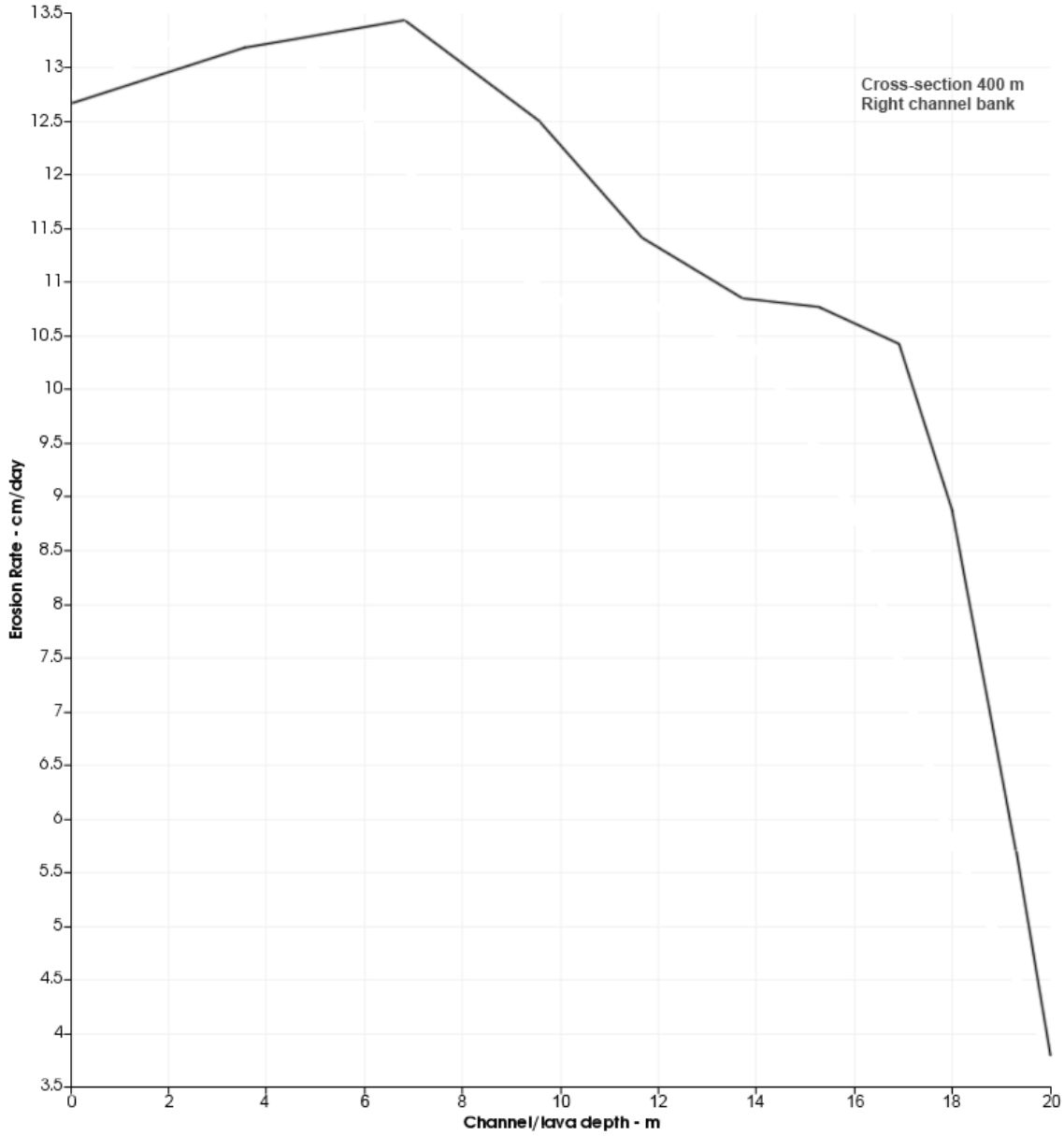

Figure 5.7b. Scenario 1 (lava radiating heat through the flow top). Erosion rates at the right bank of rille cross-section 400. Results refer to 20-m-thick lava at a temperature of 1410°C, which travels at a velocity of 5 m s^{-1}. Lava temperature at the bank is equal to 1370°C. Erosion rates increase from a value of 12.7 cm/day at the bank top to a maximum of 13.4 cm/day at a vertical distance of ~7 m from the bank top. Then, they decrease (first at a fast and then slower rate) till a vertical distance of ~3 m from the underlying bank/bed contact is reached. The sharpest decrease in erosion rate finally occurs within ~3 m of the left bank/bed contact.

Last, a 20-m-thick flow that travels at a velocity of 10 m s^{-1} is considered. Lava freestream and interface temperatures are 1415°C and 1375°C, respectively (Fig. 5.8).

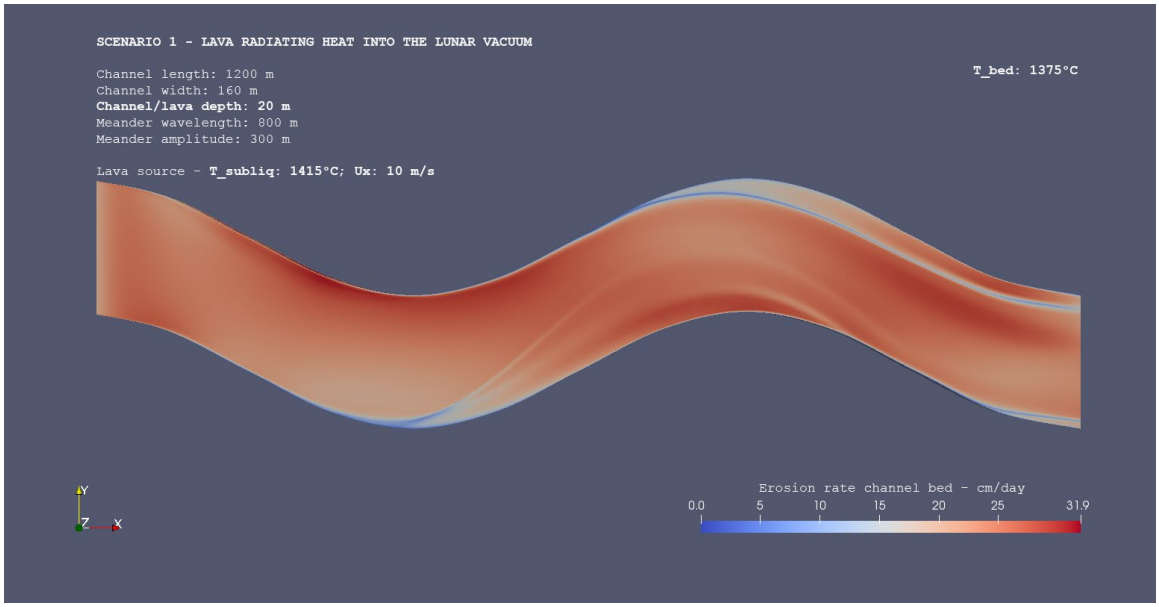

Figure 5.8. Plan view that shows how erosion rates vary at the bed of a 1200-m-long rille section. Scenario 1 (lava radiating heat into the lunar vacuum). Erosion rates are referred to a 20-m-thick lava of temperature equal to 1415°C (temperature dropped by 25°C at time of eruption) and flowing at a horizontal velocity of 10 m s^{-1}. The interface temperature is taken to be equal to 1375°C, i.e., 40°C lower than the lava freestream value. Lava source is on the left and flow motion is rightward. Once again, erosion highs (up to ~31.9 cm/day) are concentrated at or near bend troughs whereas lows are found at bend apexes. Erosion highs are doubled compared to those produced by lava of the same thickness that flows at 5 m s^{-1}.

For this sub-scenario, lava temperature is assumed to have dropped only 25°C below the liquidus value at time of eruption. Erosion rates reach maximum values of ~30 cm/day at the bed (at/near bend troughs), i.e., they are doubled compared to the values obtained for a 20-m-thick lava that flows at a slower velocity (5 m s^{-1}). Fig. 5.9 shows the distribution of erosion rates at the bed of channel cross-section 400. Maximum erosion rates of 29.0 cm/day are obtained within ~10 m of the bed/right bank contact. Values are higher by a factor of 2.1 than those produced by a 20-m-thick flow that travels at 5 m s^{-1}. While moving

toward the bed/left bank contact, erosion into the substrate fast decreases and then levels off within ~60 m of the interface and out to ~30 m from it. From that point on, erosion rates drop rapidly, then increase briefly and finally drop to a minimum of 3.8 cm/day within 1 m of the bed/left bank contact.

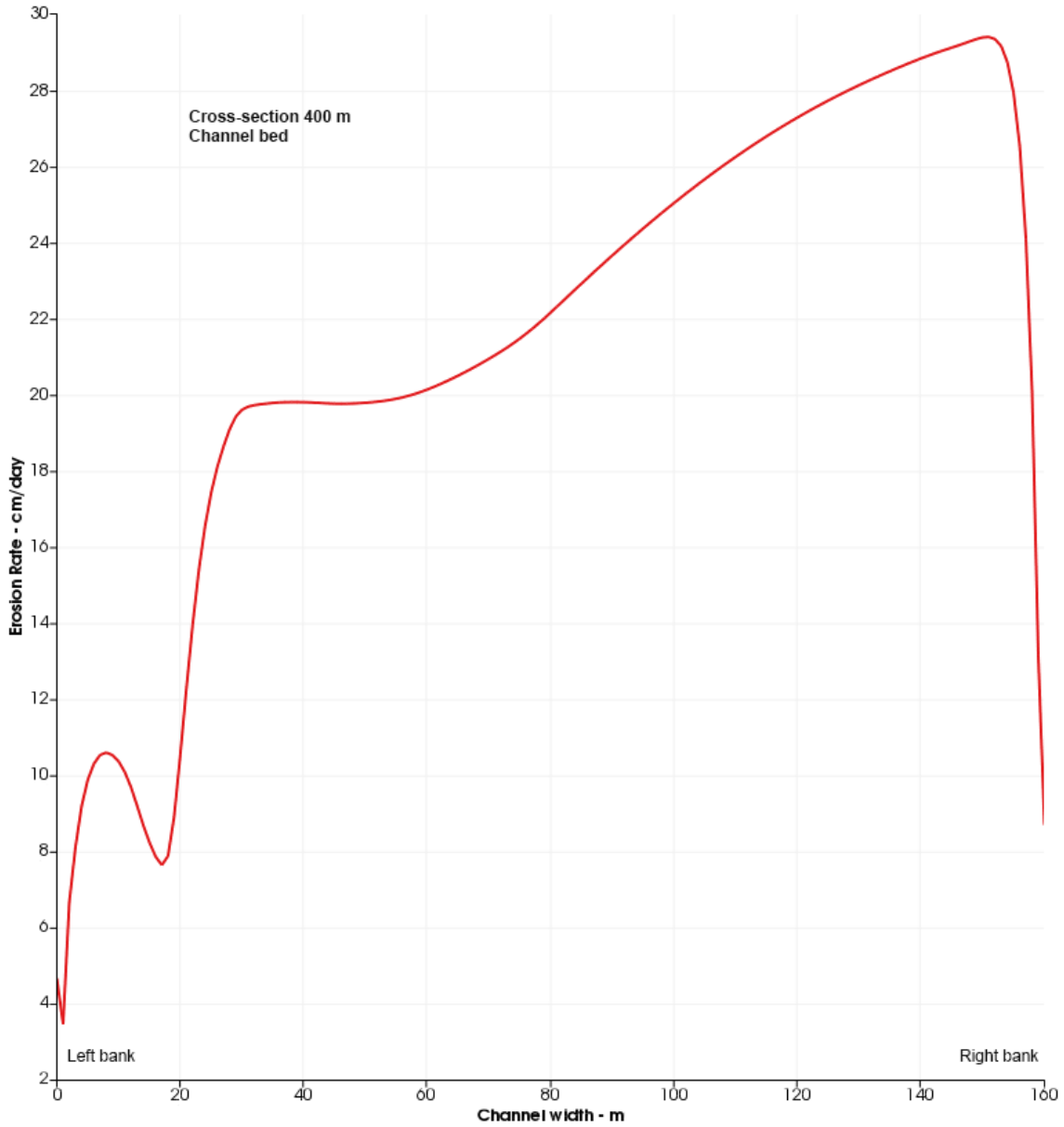

Figure 5.9. Scenario 1 (lava radiating heat through the flow top). Erosion rates at the bed of rille cross-section 400. Lava is 20 m thick and flows at the sub-liquidus temperature of 1415°C and a velocity of 10 m s^{-1}. Temperature at the bed is 1375°C. Maximum erosion

rates of 29.0 cm/day are obtained within ~10 m of the bed/right bank contact. Values are higher by a factor of 2.1 than those produced by a 20-m-thick flow that travels at 5 m s^{-1}. While moving toward the bed/left bank contact, erosion into the substrate fast decreases and then levels off at ~60 m from the contact and out to ~30 m from it. From that point on, erosion rates drop off and then increase briefly within 10 m of the contact. A minimum value of 3.8 cm/day is reached within 1 m of the bed/left bank contact.

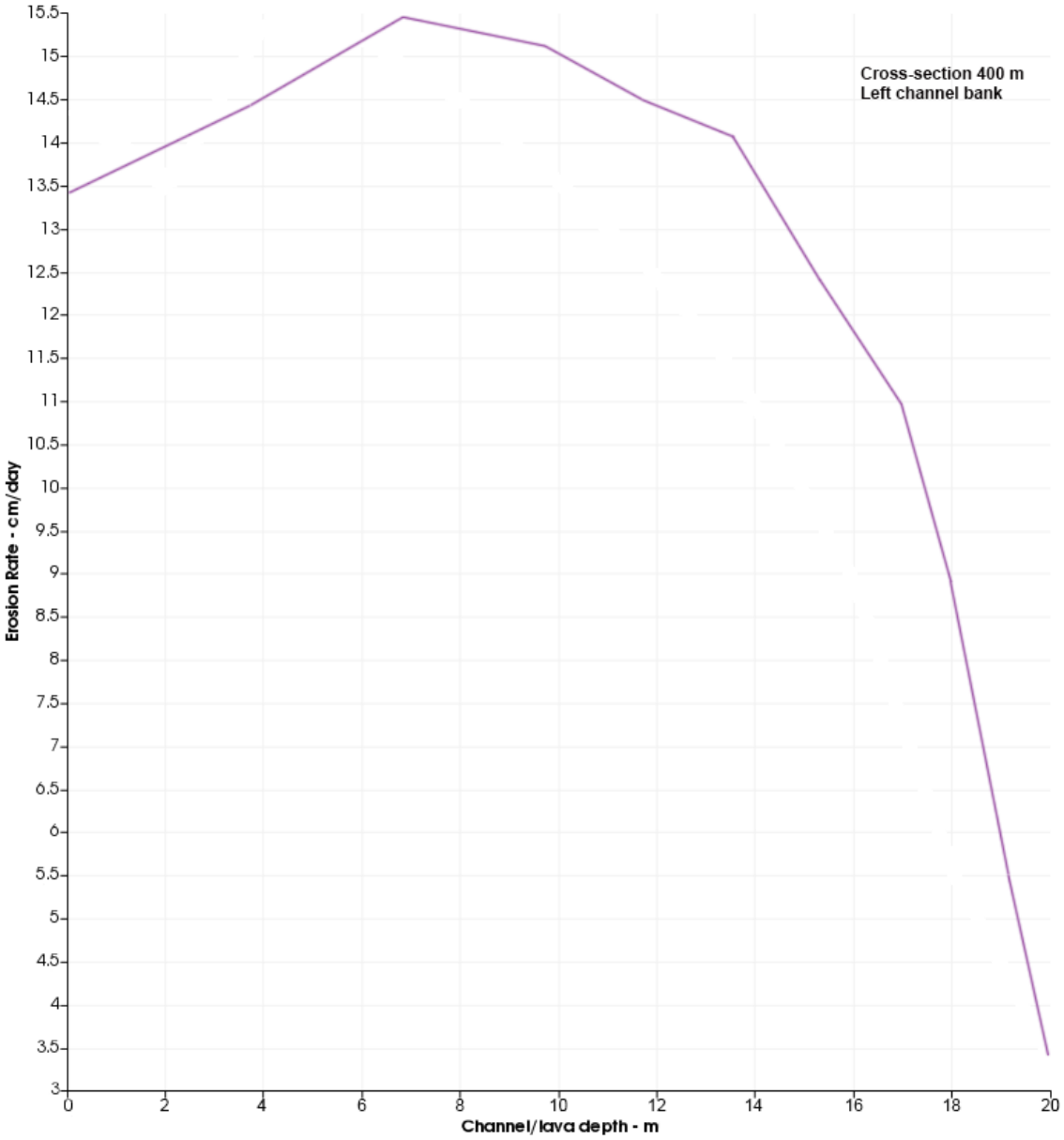

Figure 5.10a. Scenario 1 (lava radiating heat through the flow top). Erosion rates at the left bank of rille cross-section 400. Results refer to a 20-m-thick flow at 1415°C, which travels at a velocity of 10 m s^{-1}. Lava temperature at the bank is equal to 1375°C. Erosion rates increase from a value of 13.4 cm/day at the bank top to a maximum of 15.4 cm/day at a vertical distance of ~7 m from the bank top. From that point on, they decrease faster and faster until they drop to a minimum value of 3.4 cm/day at the left bank/bed contact. The fastest drop in erosion rates occurs within ~3 m of the contact. Erosion rates are doubled compared to those obtained at the left bank by the same flow traveling at a slower velocity (5 m s^{-1}).

At the left bank (Fig. 5.10a), erosion rates increase from a value of 13.4 cm/day at the bank top to a maximum of 15.4 cm/day at a vertical distance of ~7 m from the bank top. From that point on, they decrease faster and faster until they drop to a minimum value of 3.4 cm/day at the left bank/bed contact. The fastest drop in erosion rates is found within ~3 m

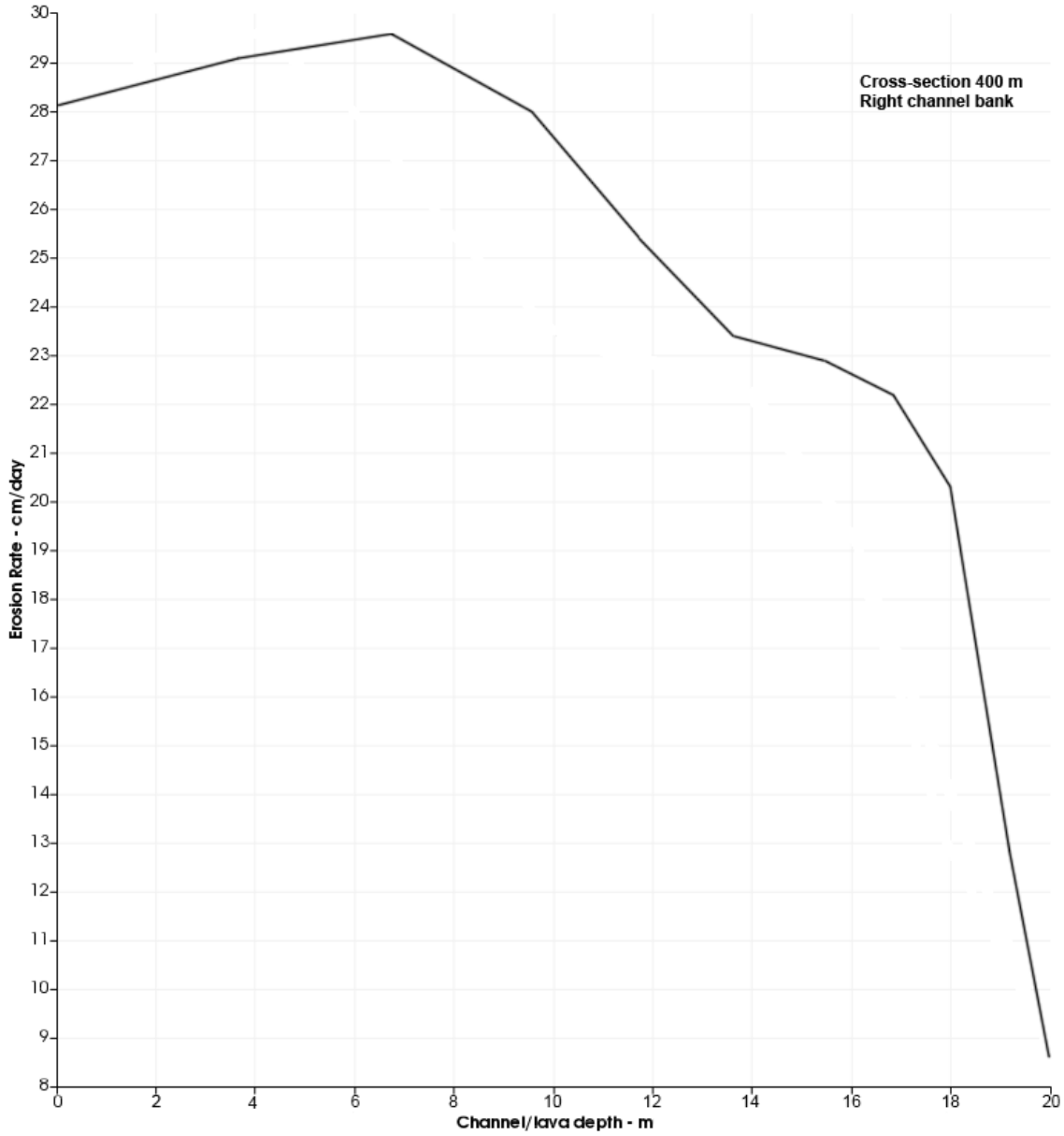

Figure 5.10b. Scenario 1 (lava radiating heat through the flow top). Erosion rates at the right bank of rille cross-section 400. Results refer to 20-m-thick lava with a temperature of 1415°C and a horizontal velocity of 10 m s^{-1}. Lava temperature at the bank is equal to 1375°C. Erosion rates increase from a value of 28.1 cm/day at the bank top to a maximum of 29.6 cm/day at a vertical distance of ~7 m from the bank top. Then, they decrease (first at a fast and then slower rate) till a vertical distance of ~3 m from the underlying bank/bed contact is reached. The sharpest decrease in erosion rate finally occurs within ~3 m of the contact. The minimum erosion rate of 8.5 cm/day is found at the contact itself.

of the bank/bed contact. Once again, erosion rate values are doubled compared to those generated at the left bank by the same flow traveling at a horizontal velocity of 5 m s^{-1}. Fig. 5.10b shows results referring to the right bank of cross-section 400. Erosion rates increase from a value of 28.1 cm/day at the bank top to a maximum of 29.6 cm/day at a vertical distance of ~7 m from the bank top. Then, they decrease (first at a fast and then slower rate) till a vertical distance of ~3 m from the underlying bank/bed contact is reached. The sharpest decrease in erosion rate finally occurs within ~3 m of the left bank/bed contact. The minimum erosion rate of 8.5 cm/day is found at the contact itself.

The next task is to explore the erosional power of superheated lava that radiates heat through the flow top. We start with a 5-m-thick flow that travels at a velocity of 5 m s^{-1}. Lava temperature is equal to 1590°C and the temperature at the lava/substrate interface is 1570°C. Fig. 5.11 shows the erosion rate distribution at the bed of cross-section 400. Maximum erosion rates of 27.2 cm/day are obtained within ~10 m of the bed/right bank contact. Values are higher by a factor of ~4.8 than those produced by the 5-m-thick sub-liquidus flow that travels at 5 m s^{-1} (see Fig. 5.3). While moving toward the bed/left bank contact, erosion into the substrate fast decreases and then levels off at ~40 m from the contact and out to ~35 m from it. From that point on, erosion rates drop very rapidly. A minimum value of 4.0 cm/day is reached within 1 m of the bed/left bank contact.

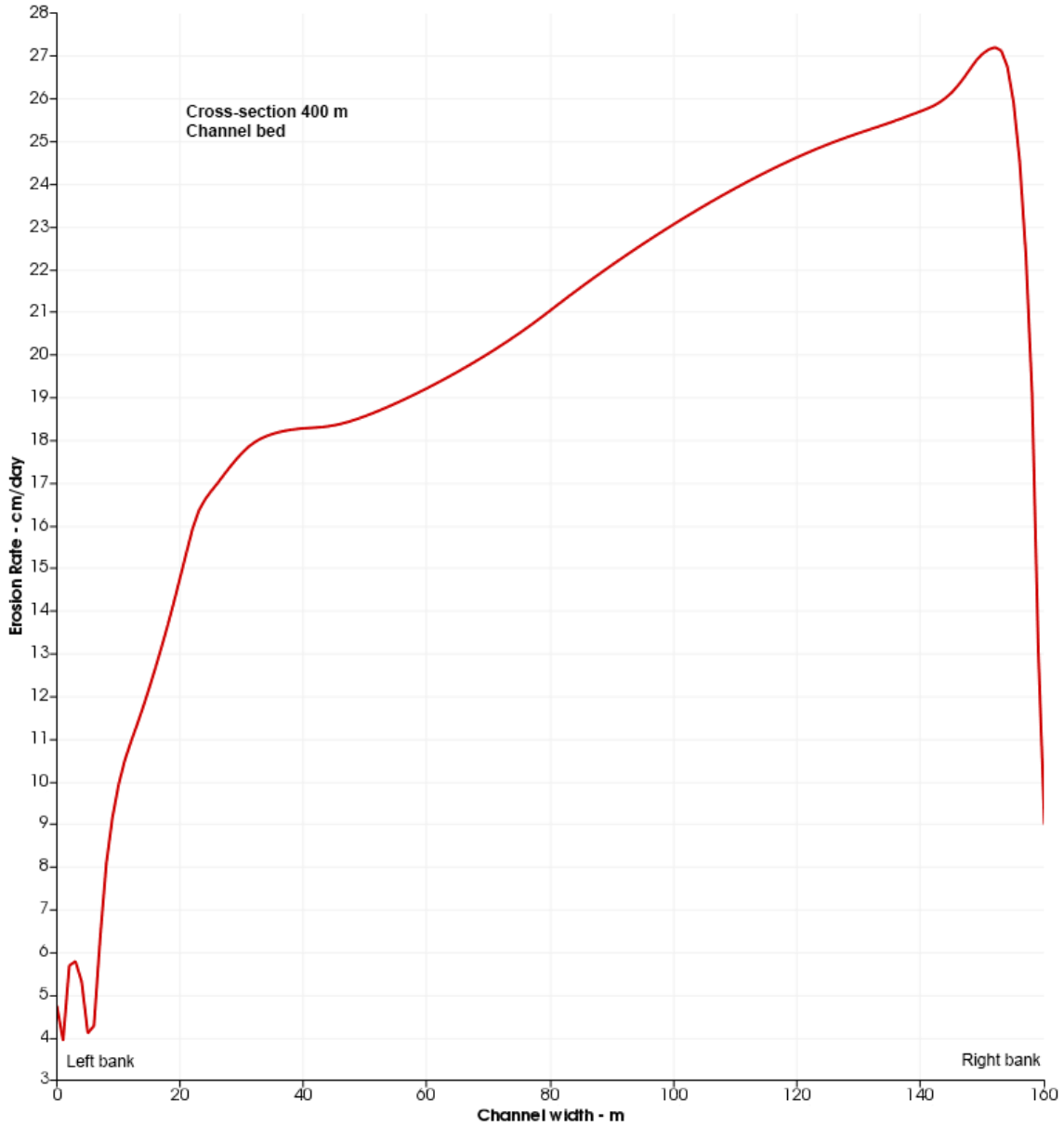

Figure 5.11. Scenario 1 (lava radiating heat through the flow top). Erosion rates at the bed of rille cross-section 400. A 5-m-thick superheated lava with a temperature of 1590°C and flowing at a velocity of 5 m s^{-1}. Temperature at the bed is 1570°C. Maximum erosion rates of 27.2 cm/day are obtained within ~10 m of the bed/right bank contact. Values are higher by a factor of ~4.8 than those produced by the 5-m-thick sub-liquidus flow that travels at 5 m s^{-1} (see Fig. 5.3). While moving toward the bed/left bank contact, erosion into the substrate fast decreases and then levels off at ~40 m from the contact and out to ~35 m from it. From that point on, erosion rates drop very rapidly. A minimum value of 4.0 cm/day is reached within 1 m of the bed/left bank contact.

Fig. 5.12a shows the erosion rate distribution at the left bank. Erosion rates rapidly increase from a value of 5.1 cm/day at the bank top to a maximum of 6.7 cm/day ~3 m down from the bank top. From that point on, they decrease and then drop to a minimum of 3.9 cm/day at the left bank/bed contact. The fastest drop in erosion rates occurs within ~1 m of the contact itself. Erosion rates are ~1.8 orders of magnitude higher than those obtained by a 5-m-thick lava with a temperature of 1400°C and a flow velocity of 5 m s^{-1}.

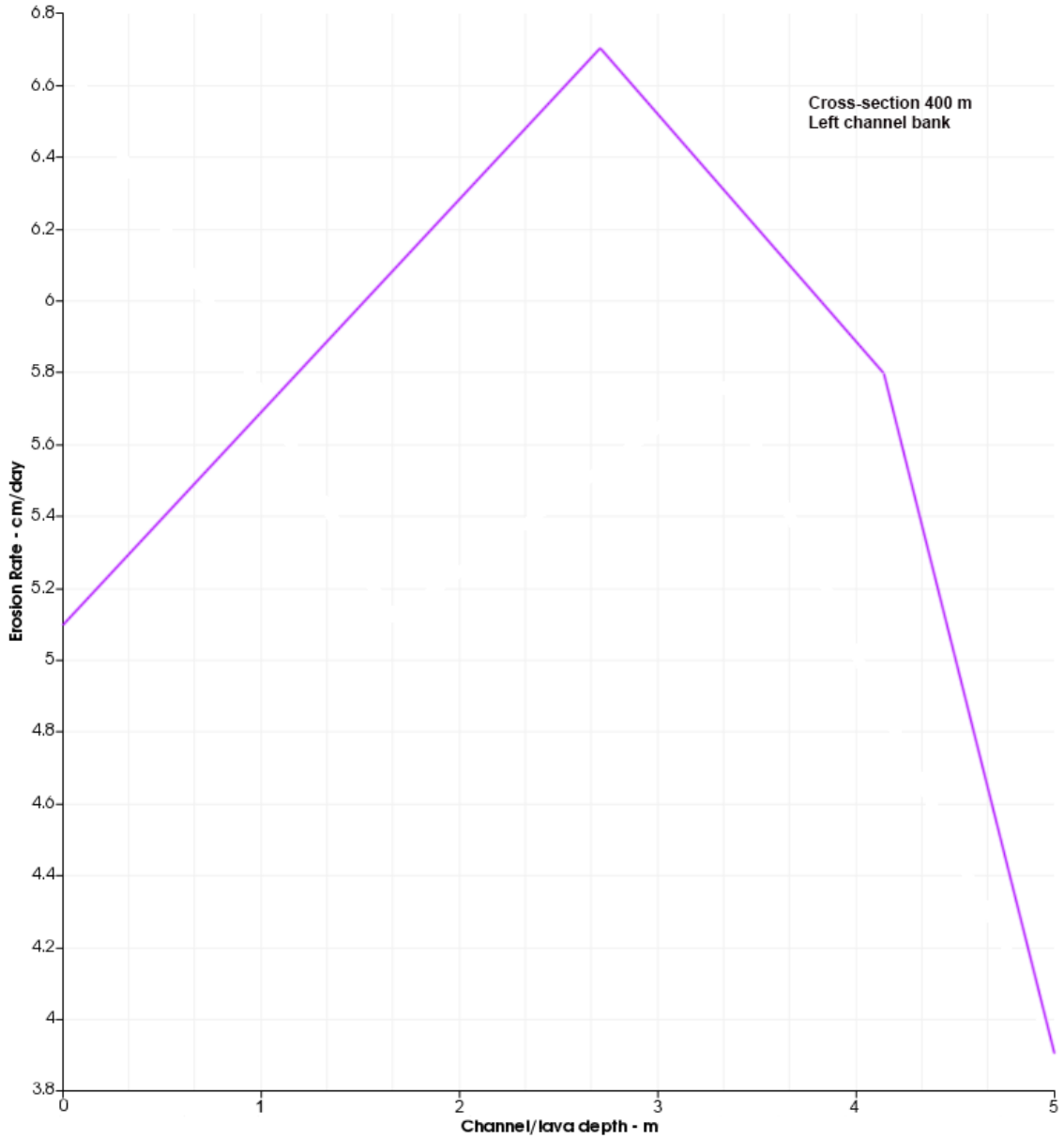

Figure 5.12a. Scenario 1 (lava radiating heat through the flow top). Erosion rates at the left bank of rille cross-section 400. Results refer to a 5-m-thick flow at 1590°C, which travels at a velocity of 5 m s^{-1}. Lava temperature at the bank is equal to 1570°C. Erosion rates rapidly increase from a value of 5.1 cm/day at the bank top to a maximum of 6.7 cm/day ~3 m down from the bank top. From that point on, they decrease and then drop to a minimum of 3.9 cm/day at the left bank/bed contact. The fastest drop in erosion rates occurs within ~1 m of that contact. Erosion rates are found to be higher by ~1.8 orders of magnitude than those obtained at the left bank by a flow of identical thickness, with a temperature of 1400°C and traveling at the same velocity.

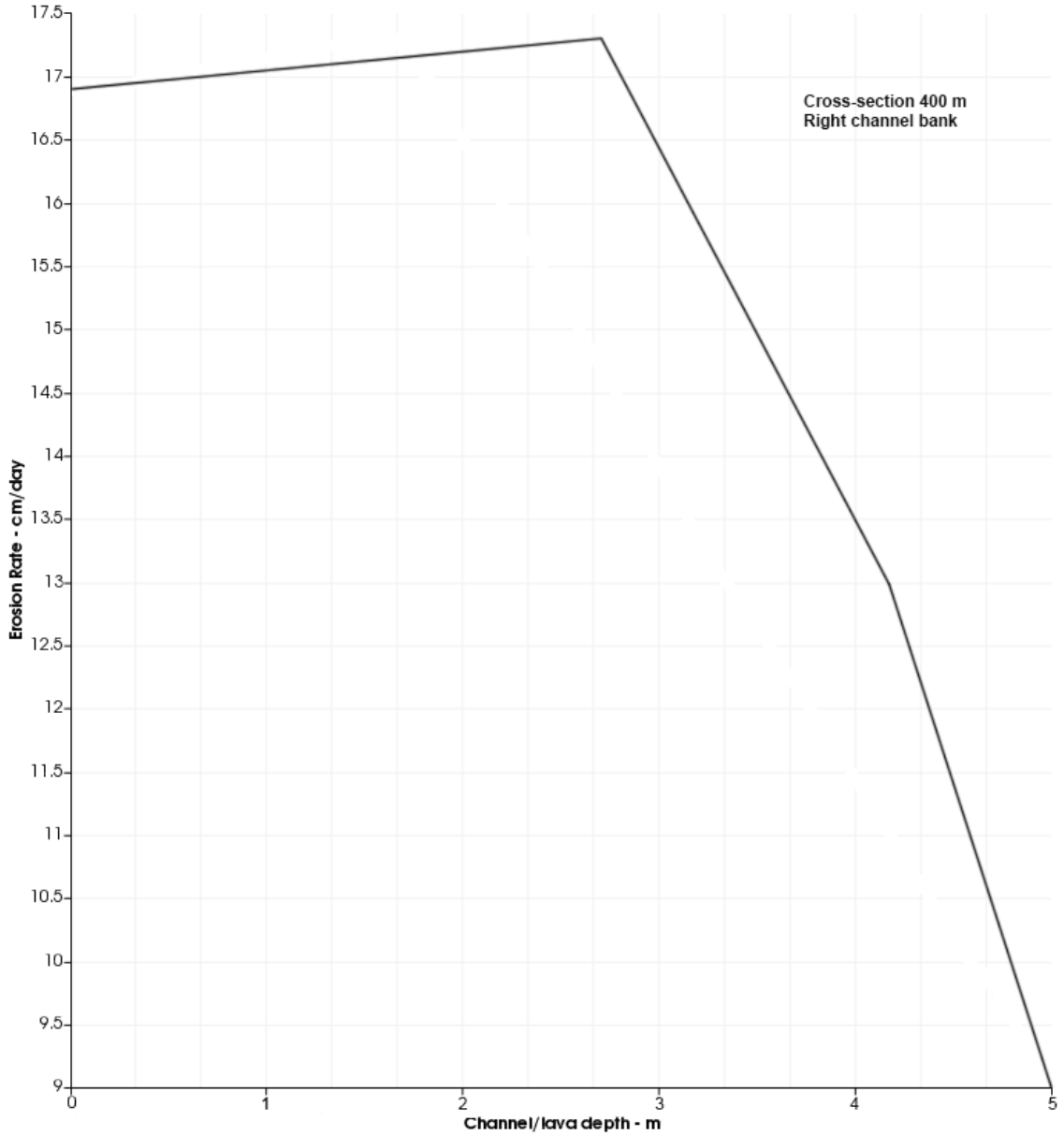

Figure 5.12b. Scenario 1 (lava radiating heat through the flow top). Erosion rates at the right bank of rille cross-section 400. Results refer to a 5-m-thick superheated lava at a temperature of 1590°C and flowing at a velocity of 5 m s^{-1}. Lava temperature at this bank is equal to 1570°C. Erosion rates slightly increase from a value of 16.9 cm/day at the bank top to a maximum of 17.3 cm/day ~3 m down from the bank top. From that point on, they fast decrease and then drop to a minimum of 9.0 cm/day at the left bank/bed contact. The fastest drop in erosion rates occurs within ~1 m of the contact. Erosion rates are found to be higher by a factor of ~5.1 than those obtained at the right bank by a flow of identical thickness, with a temperature of 1400°C and traveling at the same velocity.

Fig. 5.12b shows the erosion rate distribution at the right bank of cross-section 400. Erosion rates slightly increase from a value of 16.9 cm/day at the bank top to a maximum of 17.3 cm/day ~3 m down from the bank top. From that point on, they fast decrease and then drop to a minimum of 9.0 cm/day at the left bank/bed contact. The fastest drop in erosion rates occurs within ~1 m of the contact. Erosion rates are found to be higher by a factor of ~5.1 than those obtained at the right bank by a flow of identical thickness, with a sub-liquidus temperature of 1400°C and traveling at the same velocity.

The next sub-scenario deals with a 20-m-thick superheated lava at a temperature of 1600°C and flowing at a velocity of 5 m s^{-1}. Temperature at the flow boundaries (bed and banks) is taken to be equal to 1560°C. Max erosion rates of ~55.1 cm/day are found at the

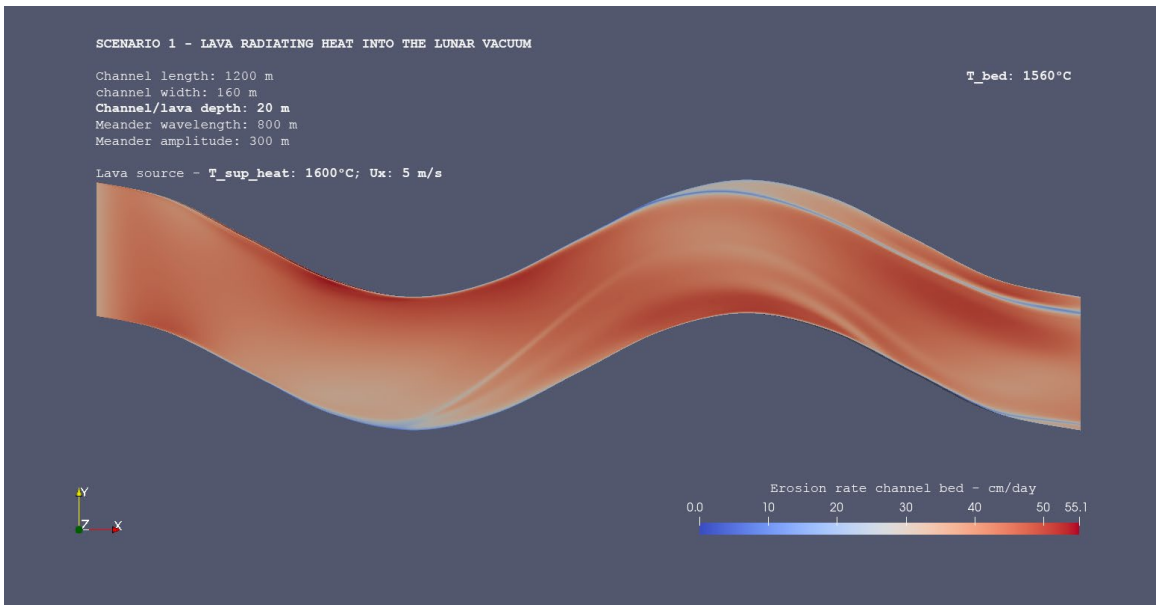

Figure 5.13. Plan view that shows how erosion rates vary at the bed of a 1200-m-long rille section. Scenario 1 (lava radiating heat into the lunar vacuum). Erosion rates are referred to a 20-m-thick superheated lava with T = 1600°C (temperature dropped by 30°C at time of eruption) and flowing at a velocity of 5 m s^{-1}. Temperature at channel boundaries is taken to be equal to 1560°C, i.e., 40°C lower than the freestream value. Lava source is on the left and flow motion is rightward. Once again, erosion highs (up to ~55.1 cm/day) are concentrated at or near bend troughs whereas lows are found at bend apexes. Erosion highs

are doubled compared to those produced by lava of identical thickness that flows at a temperature of 1410°C and a velocity of 5 m s^{-1}.

1200-m-long channel section of interest, as shown in Fig. 5.13. The distribution of erosion rates at the bed of cross-section 400 is shown in Fig. 5.14. Maximum erosion rates of 50.7 cm/day are obtained within ~10 m of the bed/right bank contact. While moving toward the contact, erosion into the substrate decreases at an almost constant rate out to ~70 m from the same contact. Then, it decreases at a slower rate out to ~30 m from the bed/left bank contact. From that point on, erosion rates decrease faster and then slightly increase again within 10 m of the bed contact with the left bank. A minimum value of 8.0 cm/day is finally found within 1 m of the contact. Compared to a sub-liquidus lava of temperature T=1410°C and identical thickness and flow velocity, erosion rates are found to be higher by a factor of 3.7. Fig. 5.15a shows erosion rates at the left bank of cross-section 400. Erosion rates increase from a value of 23.4 cm/day at the bank top to a maximum of 28.8 cm/day at a vertical distance of ~10 m from the bank top. From that point on, they decrease faster and faster until they drop to a minimum of 8.0 cm/day at the left bank/bed contact. The fastest drop in erosion rates occurs within ~3 m of the same contact. These values are higher by a factor of 4.2 than those obtained at the left bank by a flow of lower temperature (T=1410°C) and identical thickness and velocity. The distribution of erosion rates at the right bank is shown in Fig. 5.15b. Erosion rates increase from a value of 50.5 cm/day at the bank top to a maximum of 53.8 cm/day at a vertical distance of ~7 m from the bank top. Then, they decrease faster and faster to a minimum of 15.8 cm/day at the right bank/bed contact. The sharpest decrease in erosion rate occurs within ~3-2 m of that contact.

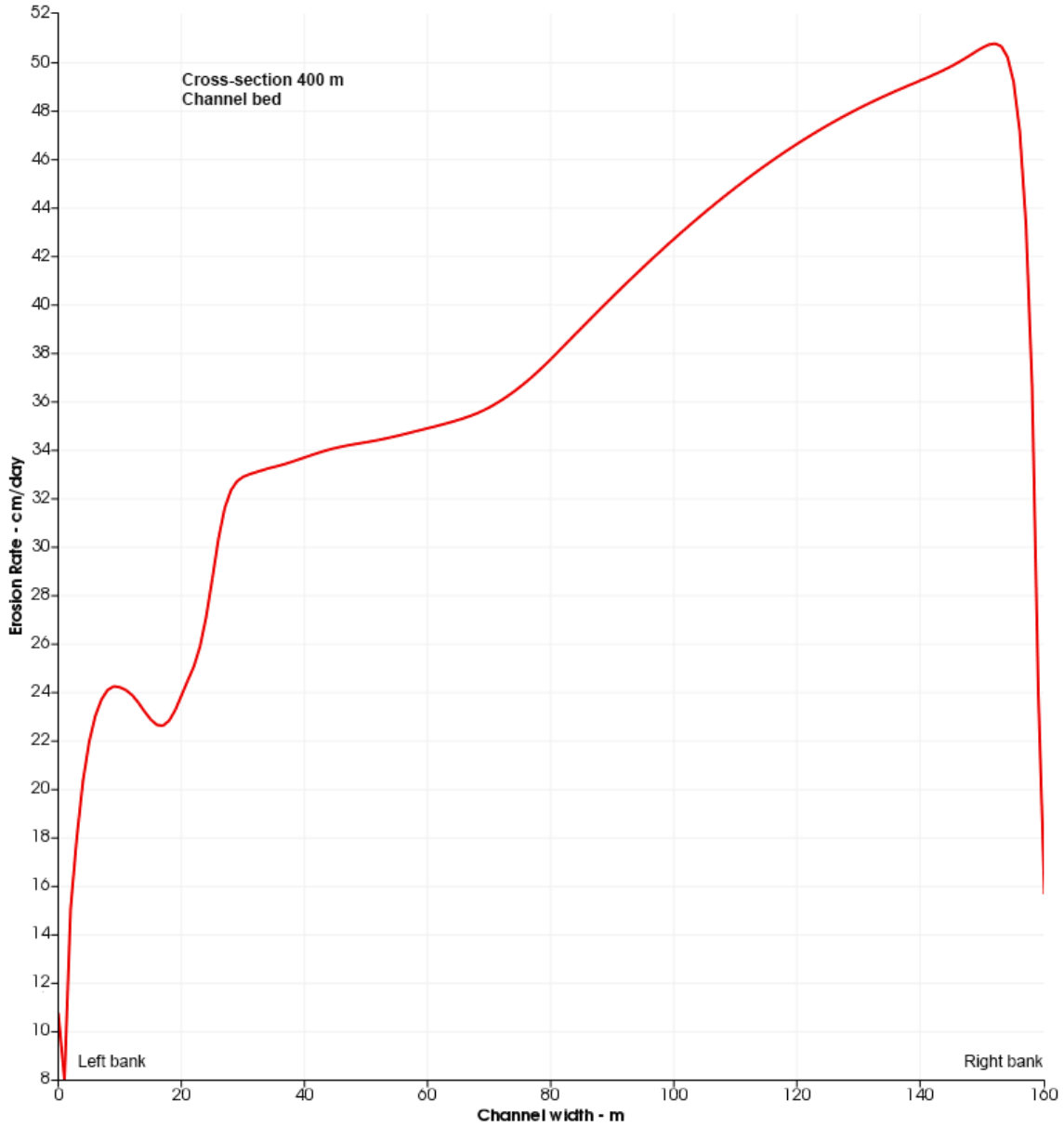

Figure 5.14. Scenario 1 (lava radiating heat through the flow top). Erosion rates at the bed of rille cross-section 400. The superheated lava is 20 m thick and flows at a temperature of 1600°C and velocity of 5 m s^{-1}. Temperature at the bed/banks is 1560°C. Maximum erosion rates of 50.7 cm/day are obtained within ~10 m of the bed/right bank contact. While moving toward the bed/left bank contact, erosion into the substrate decreases at an almost constant rate out to ~70 m from the contact. Then, it decreases at a slower rate out to ~30 m from the same contact. From that point on, erosion rates decrease faster and then slightly increase again within 10 m of the contact. A minimum value of 8.0 cm/day is finally reached within 1 m of that contact. Compared to a sub-liquidus lava of temperature T=1410°C and identical thickness and flow velocity, erosion rates are found to be higher by a factor of 3.7.

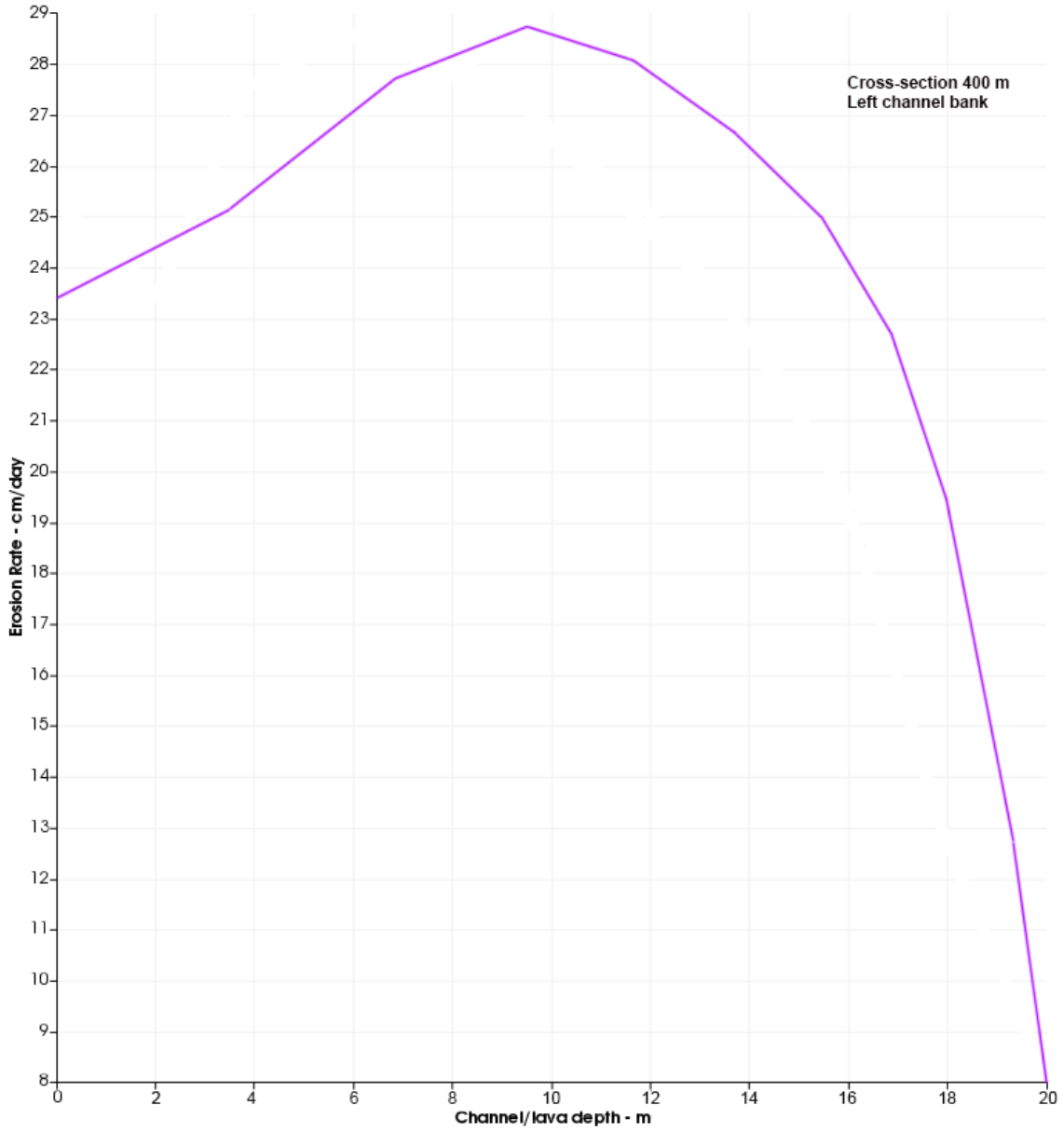

Figure 5.15a. Scenario 1 (lava radiating heat through the flow top). Erosion rates at the left bank of rille cross-section 400. Results refer to a 20-m-thick superheated lava of T=1600°C, which travels at a velocity of 5 m s^{-1}. Lava temperature at the bank is equal to 1560°C. Erosion rates increase from a value of 23.4 cm/day at the bank top to a maximum of 28.8 cm/day at a vertical distance of ~10 m from the bank top. From that point on, they decrease faster and faster until they drop to a minimum value of 8.0 cm/day at the left bank/bed contact. The fastest drop in erosion rates occurs within ~3 m of the bank/bed contact. These values are higher by a factor of 4.2 than those obtained at the left bank by a flow of lower temperature (T=1410°C) and identical thickness and velocity.

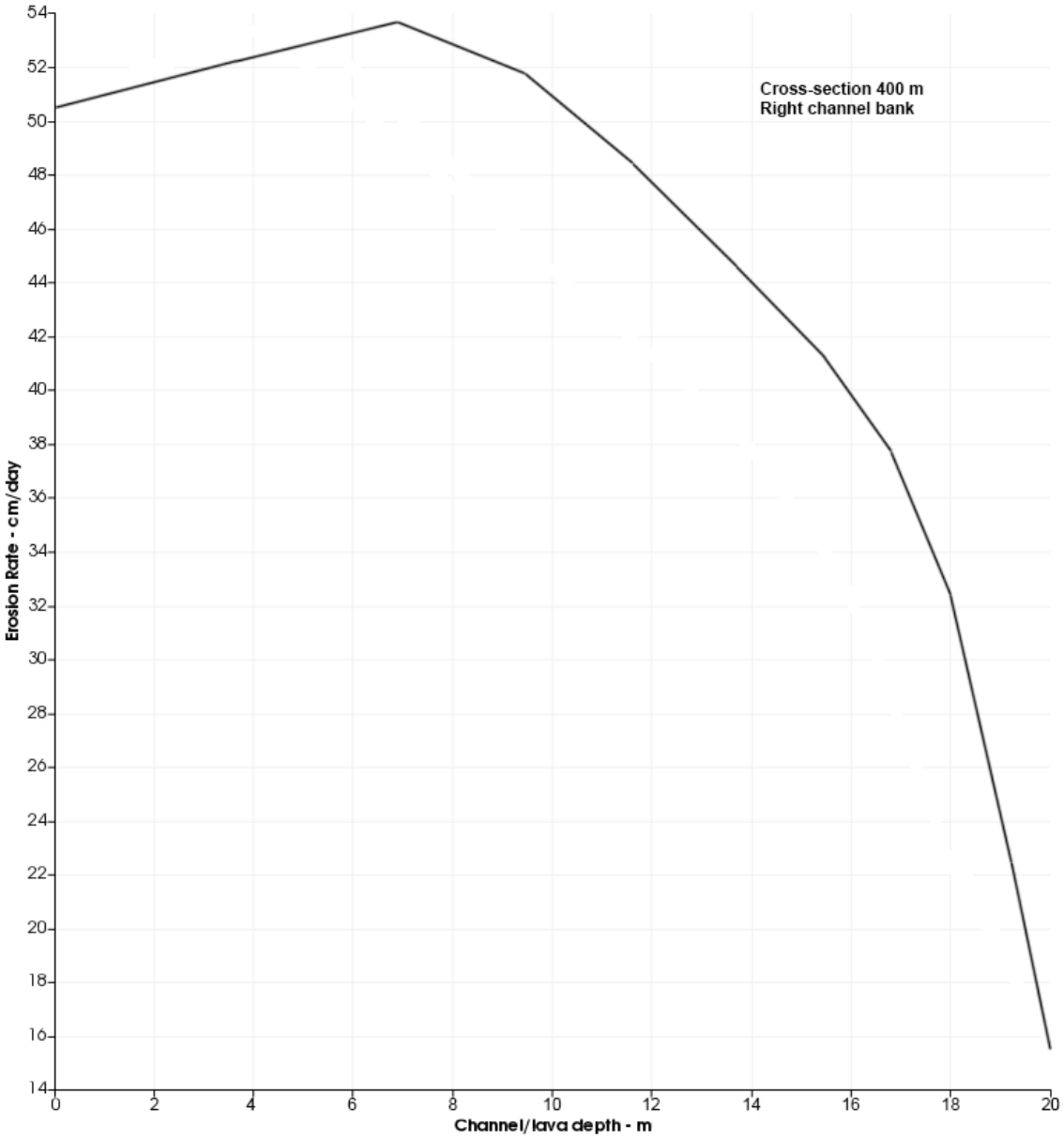

Figure 5.15b. Scenario 1 (lava radiating heat through the flow top). Erosion rates at the right bank of rille cross-section 400. Results refer to a 20-m-thick superheated lava at a temperature of 1600°C, which travels at a velocity of 5 m s^{-1}. Lava temperature at the bank is equal to 1560°C. Erosion rates increase from a value of 50.5 cm/day at the bank top to a maximum of 53.8 cm/day at a vertical distance of ~7 m from the bank top. Then, they decrease faster and faster to a minimum of 15.8 cm/day at the left bank/bed contact. The sharpest decrease in erosion rate occurs within ~3-2 m of the same contact.

The last sub-scenario has to do with superheated lava that is 20 m in thickness and flows at a velocity of 10 m s^{-1}. The freestream lava temperature is taken to be equal to 1605°C (a drop of 25°C from the prior-to-erupting value of 1630°C is assumed to have occurred), and the temperature at the bed and banks is T=1565°C (40°C lower than the freestream value). Fig. 5.16 shows a plan view of the bed with erosion rate values and their spatial distribution across the 1200-m-long rille section of interest.

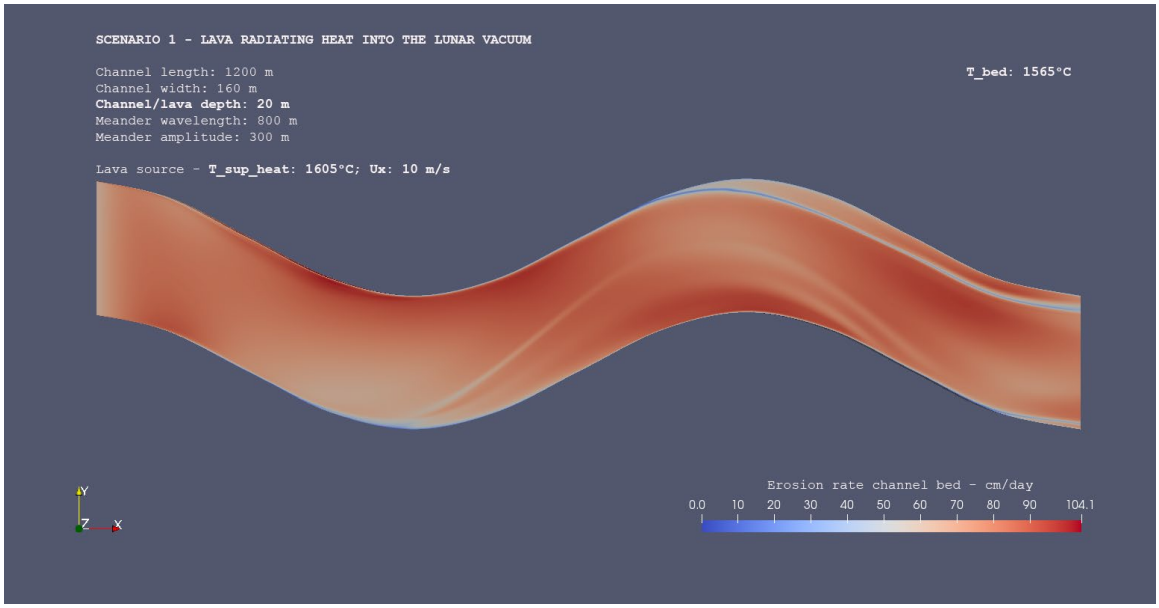

Figure 5.16. Plan view that shows how erosion rates vary at the bed of a 1200-m-long rille section. Scenario 1 (lava radiating heat into the lunar vacuum). Erosion rates are referred to a 20-m-thick superheated lava of T = 1605°C and flowing at a velocity of 10 m s^{-1}. The interface (bed and banks) temperature is taken to be equal to 1565°C. Lava source is on the left and flow motion is rightward. Once again, erosion highs (up to 104.1 cm/day) are concentrated at or near bend troughs whereas lows are found at bend apexes. Maximum erosion rates are higher by a factor of ~3.3 than those associated with a lava of identical thickness and velocity but lower in temperature (T=1415°C).

Fig. 5.17 shows the erosion rate distribution at the bed of cross-section 400. Maximum erosion rates of 96.0 cm/day are obtained within ~10 m of the bed/right bank contact. While moving toward the bed/left bank contact, erosion into the substrate decreases at an almost

constant rate out to ~70 m from the interface. Then, erosion rates level off out to ~50 m from the bed/left bank contact.

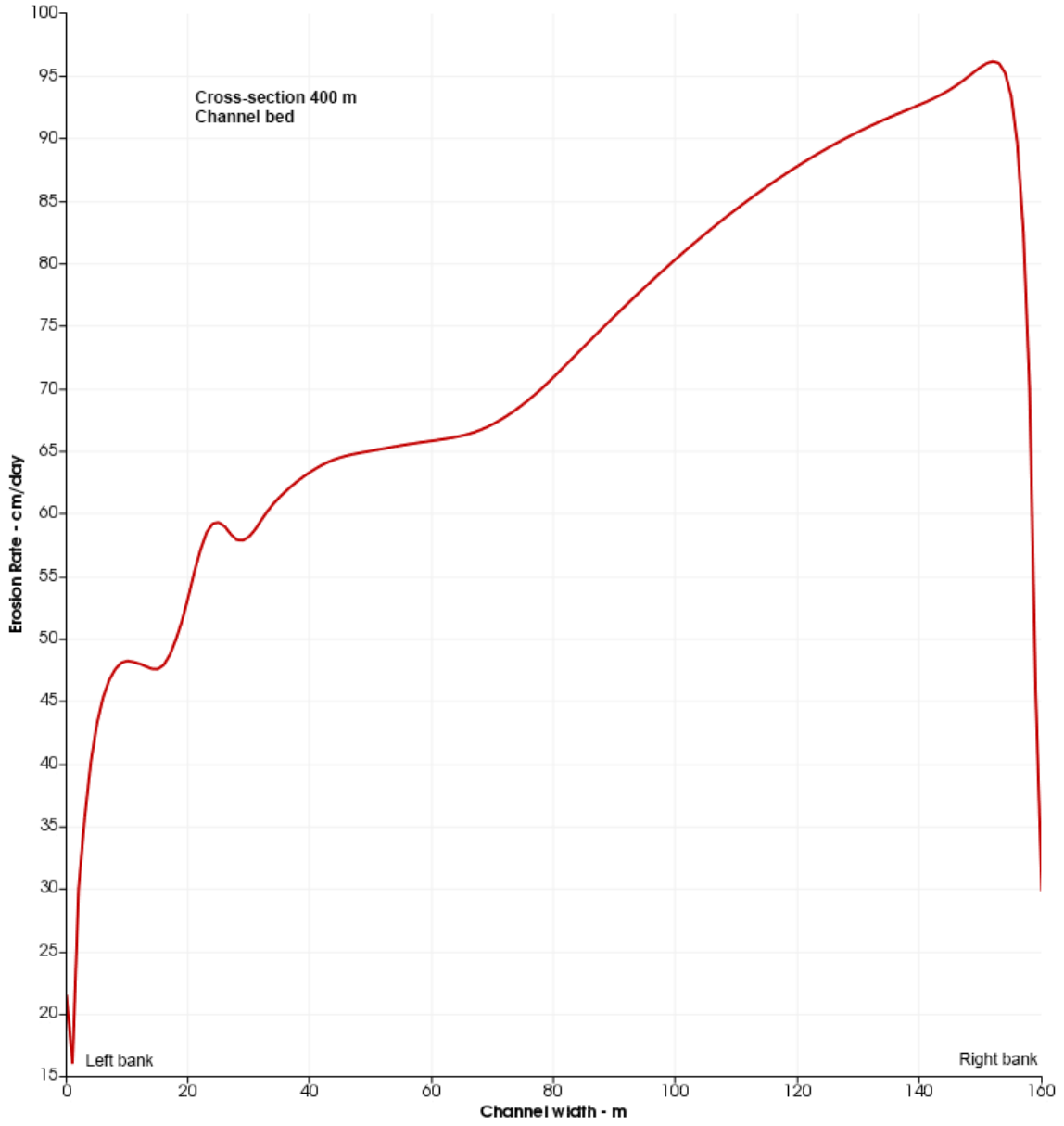

Figure 5.17. Scenario 1 (lava radiating heat through the flow top). Erosion rates at the bed of rille cross-section 400. The superheated lava is 20 m thick and flows at a temperature of 1605°C and a velocity of 10 m s^{-1}. Temperature at the bed/banks is 1565°C. Maximum erosion rates of 96.0 cm/day are obtained within ~10 m of the bed/right bank contact. While moving toward the bed/left bank contact, erosion into the substrate decreases at an almost constant rate out to ~70 m from the contact. Then, erosion rates level off out to ~50 m from the same contact. From that point on, erosion rates fluctuate a bit (while still decreasing)

until they drop to a minimum of ~16.0 cm/day at the bed/left bank contact. The sharpest drop occurs within ~10 m of the same contact. Compared to a sub-liquidus lava of temperature T=1415°C and identical thickness and flow velocity, erosion rates are found to be higher by a factor of 3.3.

From that point on, erosion rates fluctuate a bit (while still decreasing) until they drop to a minimum of ~16.0 cm/day at the bed/left bank contact. The sharpest drop occurs within ~10 m of the contact. Compared to a sub-liquidus lava of temperature T=1415°C and identical thickness and flow velocity, erosion rates are found to be higher by a factor of 3.3. The distribution of erosion rates at the left bank of cross-section 400 is shown is Fig. 5.18a. Erosion rates increase from a value of 44.4 cm/day at the bank top to a maximum of 54.8 cm/day at a vertical distance of ~10 m from the bank top. From that point on, they decrease faster and faster until they drop to a minimum value of 16.0 cm/day at the left bank/bed contact. The fastest drop in erosion rates occurs within ~3 m of the contact. Erosion rate values are higher by a factor of 3.6 than those obtained at the left bank by a flow of lower temperature (T=1415°C) and identical thickness and velocity. Fig 5.18b shows erosion rates at the right bank. Erosion rates increase from a value of 96.0 cm/day at the bank top to a maximum of 102.5 cm/day at a vertical distance of ~7 m from the bank top. Then, they decrease faster and faster to a minimum of 29.5 cm/day at the left bank/bed contact. The sharpest decrease in erosion rate occurs within ~3 m of the same contact.

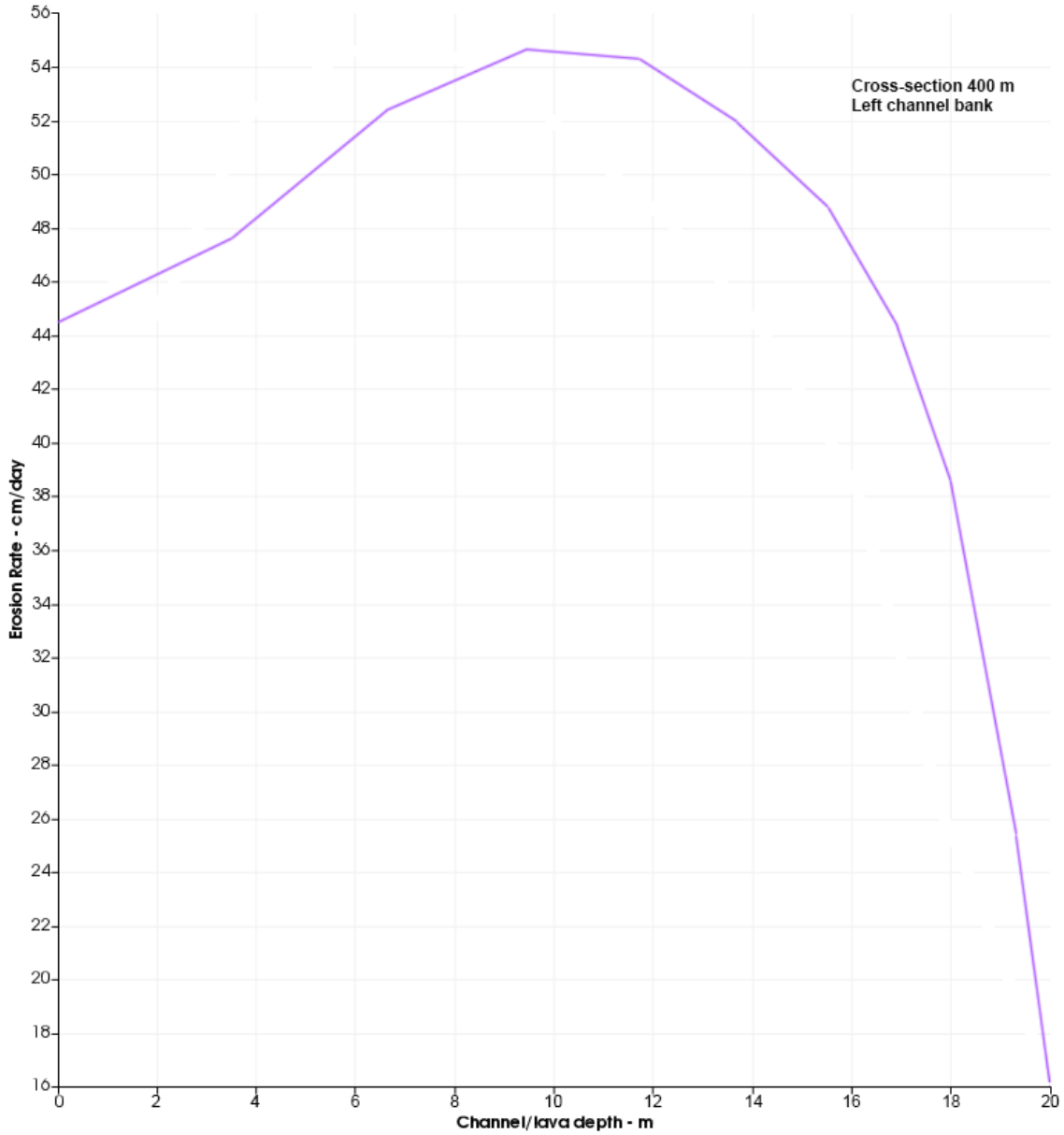

Figure 5.18a. Scenario 1 (lava radiating heat through the flow top). Erosion rates at the left bank of rille cross-section 400. Results refer to a 20-m-thick superheated lava of T=1605°C, which travels at a velocity of 10 m s^{-1}. Lava temperature at the bank is equal to 1565°C. Erosion rates increase from a value of 44.4 cm/day at the bank top to a maximum of 54.8 cm/day at a vertical distance of ~10 m from the bank top. From that point on, they decrease faster and faster until they drop to a minimum value of 16.0 cm/day at the left bank/bed contact. The fastest drop in erosion rates occurs within ~3 m of the bank/bed contact. Erosion rate values are higher by a factor of 3.6 than those obtained at the left bank by a flow of lower temperature (T=1415°C) and identical thickness and velocity.

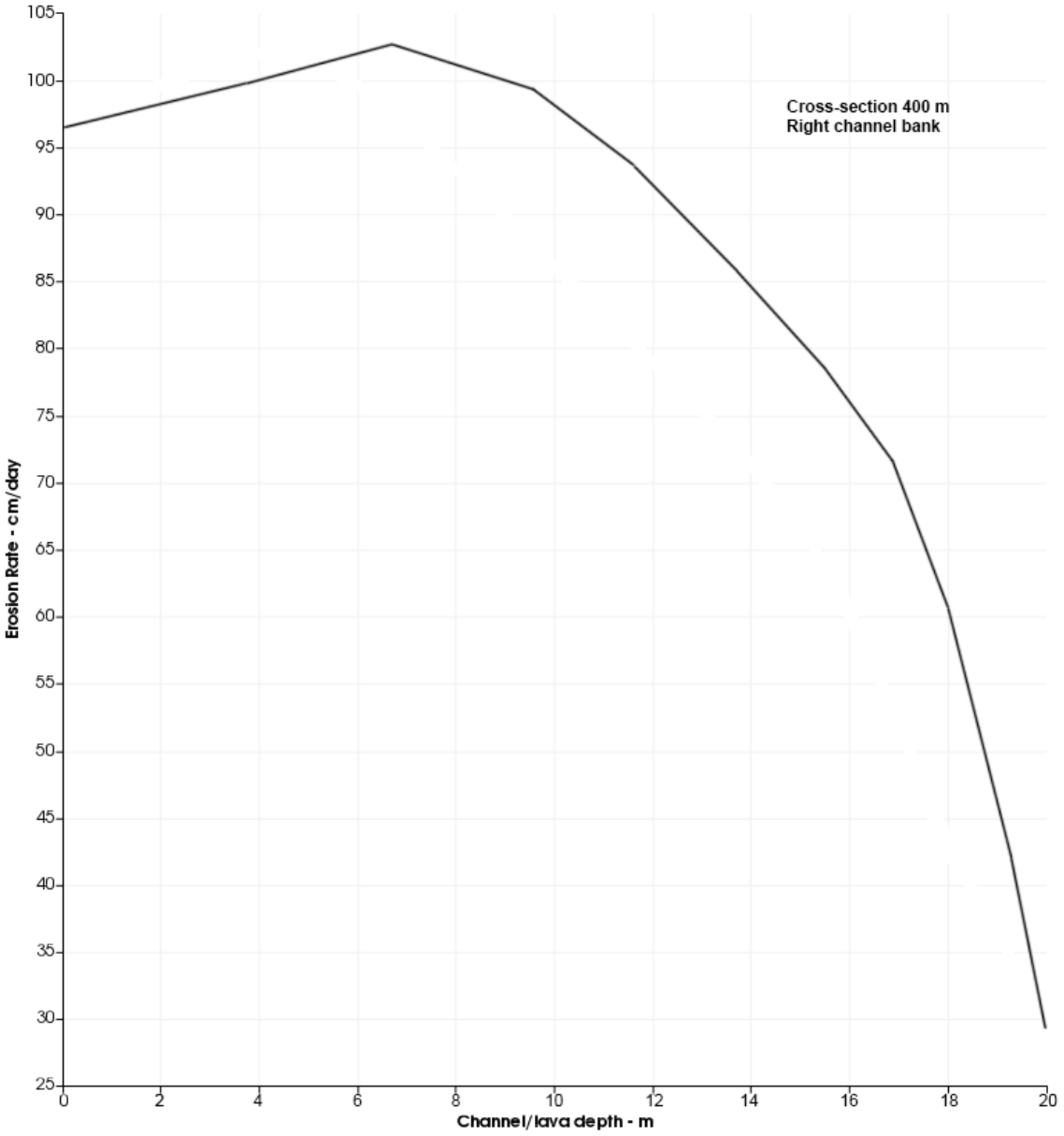

Figure 5.18b. Scenario 1 (lava radiating heat through the flow top). Erosion rates at the right bank of rille cross-section 400. Results refer to a 20-m-thick superheated lava of T=1605°C, which travels at a velocity of 10 m s^{-1}. Lava temperature at the bank is equal to 1565°C. Erosion rates increase from a value of 96.0 cm/day at the bank top to a maximum of 102.5 cm/day at a vertical distance of ~7 m from the bank top. Then, they decrease faster and faster to a minimum of 29.5 cm/day at the left bank/bed contact. The sharpest decrease in erosion rate occurs within ~3 m of the same contact.

Scenario 1 – The convective heat transfer coefficient h_T

In scenario 1, results pertaining to sub-liquidus and superheated lavas flowing at velocities of 5 and 10 m s^{-1} are shown. Values of the convective heat transfer coefficient h_T are calculated by Eq. (10) at the left and right bank tops as well as at the bed in the proximity of the bed/right bank contact. As a result, each value of h_T is associated with a specific erosion rate and the two values (h_T and erosion rate) vary in proportion. *Williams et al*. (1998, 2000) calculated values of the convective heat transfer coefficient, h_T, at the lava substrate for a range of lava temperatures and compositions while also accounting for viscosity variations within each substrate type. Here, different values of h_T are obtained at discrete locations along the axis of rille bend 1 (see Fig. 2.2a). The changes in the value of h_T reflect variations in flow properties that are explained in the theoretical section of this chapter. Table 5.4 illustrates values of the convective heat transfer coefficient, h_T, at the rille boundaries (bed and banks), calculated from erosion rate values obtained at the bed and banks of rille cross-section 400 (bend 1). Values of h_T vary drastically depending on the portion of cross-section 400 that is considered. If other things are equal, for a flow that

Table 5.4 – Scenario 1. Values of the heat transfer coefficient, h_T, at the lava substrate (bed and banks) at inner rille cross-section 400 (section cut parallel to the axis of bend 1). h_T values are obtained from Eq. (10). All results refer to the two sub-scenarios (sub-liquidus and superheated) in the text. Flow velocities are 5 m s^{-1} for the 5-m-thick lava and 5 and 10 m s^{-1} for the 20-m-thick flow. Suffixes "$_{5to10mfrb}$" stands for 5 to 10 meters from right bank; "$_{bed/left\ bank}$" indicates that the value is measured at the contact (where the two boundaries meet); "$_{right\ bank\ \#md}$" and "$_{left\ bank\ \#md}$" indicate that the h_T value is measured at the right or left bank, # meters down from the bank top (here 3, 7, or 10 meters down from the bank top).

SCENARIO 1 - Values of the heat transfer coefficient, h_T, at the lava substrate (bed and banks)									
T_{lava}	T_{interf}	h	U_x	$h_{T\_bed/5 to10mfrb}$	$h_{T\_bed/ left\ bank}$	$h_{T\_right\ bank\ top}$	$h_{T\_right\ bank\ \#md}$	$h_{T\_left\ bank\ top}$	$h_{T\_left\ bank\ \#md\_}$

°C	°C	m	m s^{-1}	J m^{-2} s^{-1} $°C^{-1}$					
1400	1380	5	5	19.8	0.4	11.5	12.0 $_{3md}$	1.3	1.4 $_{3md}$
1590	1570	5	5	51.5	7.6	32.0	32.8 $_{3md}$	9.7	12.7 $_{3md}$
1410	1370	20	5	51.0	0.7	47.0	49.6 $_{7md}$	22.6	25.2 $_{7md}$
1600	1560	20	5	98.5	15.5	98.1	104.5 $_{7md}$	45.4	55.9 $_{10md}$
1415	1375	20	10	104.8	13.7	101.5	106.9 $_{7md}$	48.4	55.6
1605	1565	20	10	184.1	30.7	184.1	196.6 $_{7md}$	85.2	105.1 $_{10md}$

is 5 m in thickness, the highest values are always found at the bed/right bank contact. For a 20-m-thick flow that travels at a velocity of 5 m s^{-1}, values of h_T at the bed and right bank are very similar if the temperature of the lava is below the liquidus. For a lava that is superheated, h_T values at the right bank become greater than those at the bed, which is even more so once the flow is allowed to travel at the velocity of 10 m s^{-1}. Another interesting result has to do with the noticeable discrepancy in h_T values between the left and right bank. Regardless of lava temperature and velocity, h_T values are always higher at the right bank than at the left bank. Besides, erosion rates at the bed are higher in the proximity of the bed/right bank contact, which suggests that some process is likely responsible for erosion enhancement in that portion of rille cross-section 400. This result is consistent with what found in the sensitivity analysis chapter.

Scenario 1 – Summary

Scenario 1 groups flow sub-scenarios for which lava is assumed to have been exposed to the lunar environment. As a result, lava underwent cooling by losing internal heat by radiation through the upper surface (flow top). Because of this assumption, no flow is assumed to have been erupted at the liquidus temperature and only sub-liquidus

temperatures are considered here. An exception is represented by lavas that might have been originally superheated, and erupted at temperatures much higher than the liquidus value. In the "Results" section and within the sub-section titled "Scenario 1 - Cooling rates for the inner rille lava", Table 5.3 shows that only superheated lavas might have traveled a non-negligible (28-43 km) distance downstream of the source prior to transitioning to laminar flow conditions. The sub-section titled "Scenario 1 - Erosion rates at channel cross-section 400" shows erosion rates into the rille bed and banks, produced by flows that are 5- and 20-m-thick and travel at velocities of 5 m s^{-1} (5- and 10-m-thick lavas) and 10 m s^{-1} (20-m-thick lavas only). All erosion rates refer to lava eruption temperatures that range from 1630°C (superheated lava) to 1400°C (sub-liquidus lava). The highest erosion rates (at the bed and banks) of ~96-102 cm/day are associated with 20-m-thick lavas erupted at a temperature of 1605°C (superheated lava) and traveling at a velocity of 10 m s^{-1} (Figs. 5.17 and 5.18 a, b). The lowest erosion rates of ~0.4-5.0 cm/day are produced by a 5-m-thick lava traveling at a velocity of 5 m s^{-1} and erupted at the sub-liquidus temperature of 1400°C (Figs. 5.3 and 5.4 a, b). Analogous to what shown in the sensitivity analysis chapter, the magnitude and spatial distribution of erosion rates at the rille bed and the two banks of channel cross-section 400 (section cut through bend 1 axis) is very heterogeneous for reasons that are explained at the end of this chapter in the section titled "Theoretical study". Neverthless, a consistent pattern of erosion is found at the rille bed and banks. The highest erosion rates are always located at the bed within a few meters of the bed/right bank contact and at the right bank, either at the bank top or within 4-6 m of the bank/bed contact. The latter scenario suggests that undercutting might have occurred over discrete portions of the

rille banks. The last section titled "Scenario 1 – The convective heat transfer coefficient h_T" illustrates the values of the convective heat transfer, h_T, into the rille bed and the two banks. The highest values of h_T (184.1-196.6 J m^{-2} s^{-1} $°C^{-1}$) are associated with a 20-m-thick superheated lava, the lowest (0.4-19.8 J m^{-2} s^{-1} $°C^{-1}$) with a 5-m-thick lava erupted at a sub-liquidus temperature. At the rille bed, the highest values of h_T are found within ~10 m of the bed/right bank contact, and at the right bank they are located either at the bank top or within 4-6 m of the bank/bed contact. The variation of h_T values is consistent with the illustrated magnitude and spatial distribution of erosion rates.

Scenario 2 – Erosion rates at channel cross-section 400

This section describes erosion rates obtained at cross-section 400 by assuming that lava flows were insulated from the lunar environment. For such lavas, there is no heat loss through the flow top and a larger amount of heat is retained within the flow, holding other factors equal. Results for the sub-scenarios illustrated in Table 5.1b and Table 5.2 are shown here: (1) flows erupted at the sub-liquidus temperature of 1380°C; (2) at the liquidus temperature of 1440°C; (3) at the temperature of 1630°C (superheated lava). Here, the two-fold objective is to first test the maximum erosion rates achieved by lavas that flow at liquidus and above-liquidus (superheated) temperatures and then identify the minimum sub-liquidus temperature at which Newtonian flow conditions may still apply. Because of the latter objective, the sub-liquidus lava is assumed to erupt at a temperature that is 20-30°C lower than that adopted in scenario 1. Fig. 5.19 shows a plan view of the bed at cross-section 400. A 5-m-thick flow is erupted at the sub-liquidus temperature of 1380°C and

travels at a velocity of 5 m s^{-1}. Temperature at channel boundaries is equal to 1360°C (20°C lower than the eruption value).

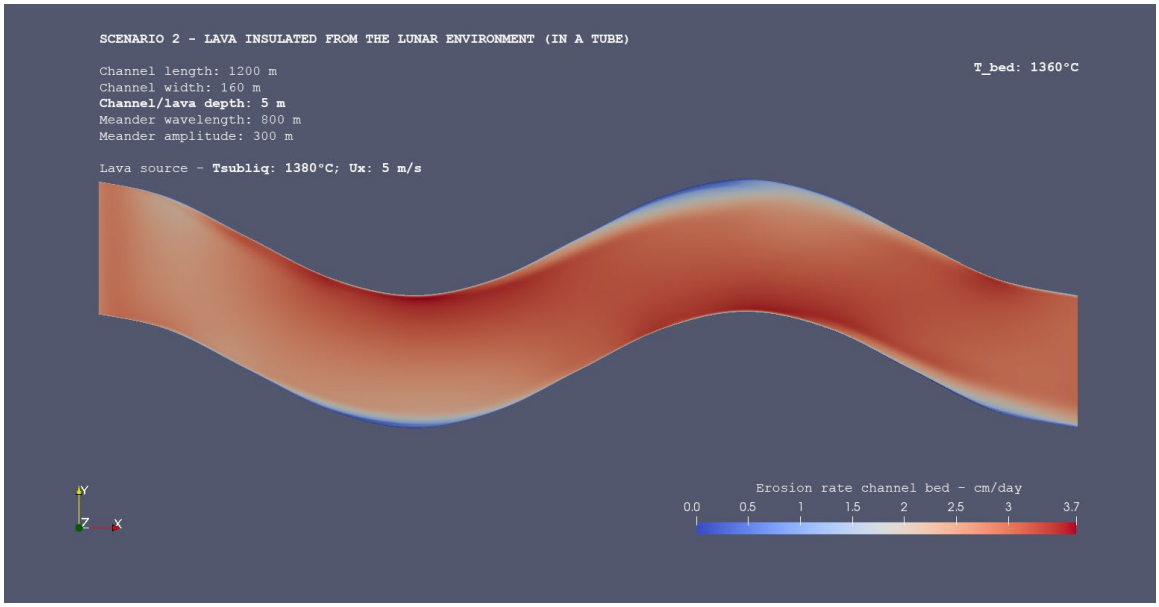

Figure 5.19. Plan view that shows how erosion rates vary at the bed of a 1200-m-long rille section. Scenario 2 (lava flowing insulated in a tube). Erosion rates are referred to a 5-m-thick lava of T = 1380°C and flowing at a velocity of 5 m s^{-1}. Temperature at channel boundaries is taken to be equal to 1360°C. Lava source is on the left and flow motion is rightward. Once again, erosion highs (up to 3.7 cm/day) are concentrated at or near bend troughs whereas lows are found at bend apexes.

Fig. 5.20 shows erosion rates at the bed of cross-section 400. Maximum erosion rate values of 15.3 cm/day are obtained within ~10 m of the bed/right bank contact. While moving toward the bed/left bank contact, erosion into the substrate decreases at an almost constant rate till the distance of ~50 m from that contact is reached. Within 25 m of the same contact, erosion rates decrease faster to a minimum of 2.0 cm/day that is obtained within 1 m of the bed/left bank contact.

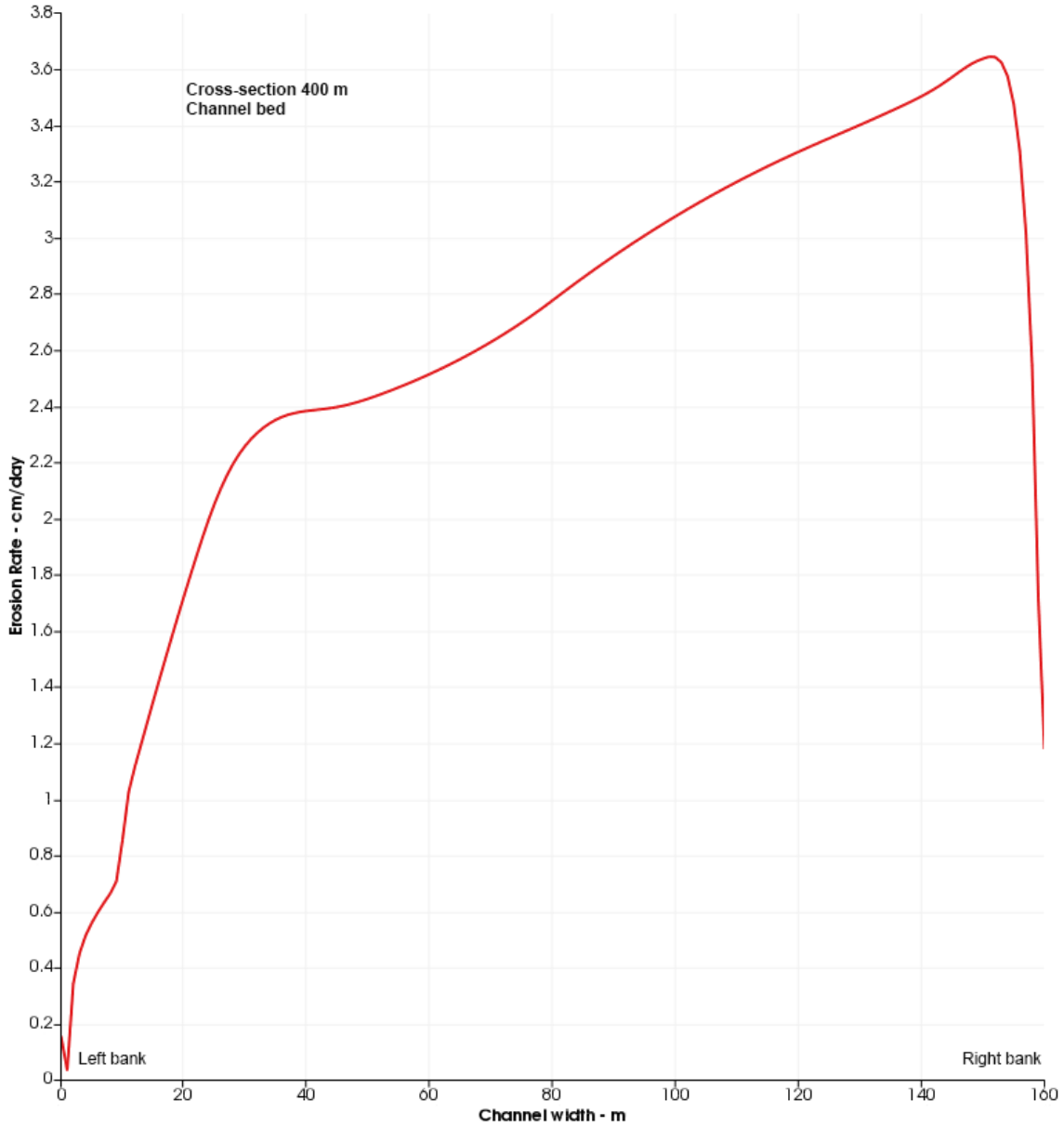

Figure 5.20. Scenario 2 (lava flowing insulated in a tube). Erosion rates at the bed of channel cross-section 400, a section cut through bend 1 axis. Results for a 5-m-thick lava at the sub-liquidus temperature of 1380°C and traveling at a velocity of 5 m s^{-1}. Lava temperature at the bed is equal to 1360°C. Maximum erosion rate values of ~3.6 cm/day are obtained within ~10 m of the bed/right bank contact. While moving toward the bed/left bank contact, erosion into the substrate decreases at an almost constant rate till the distance of ~45 m from that contact is reached. Within 30 m of the contact, erosion rates decrease faster till they reach a minimum of ~0.1 cm/day within 1 m of the contact itself. Despite flowing insulated from the lunar environment, the lower temperature of this lava (1380°C) compared to that assumed for the counterpart flow seen in scenario 1 (1400°C) produces erosion rates that are lower by a factor of 1.5.

Fig. 5.21a shows the distribution of erosion rates at the left bank. Maximum erosion rates of ~0.3 cm/day are found at the bank top and from there they decrease at a constant rate until a vertical distance of ~2 m from the bank/bed contact is reached. There, they have a value of ~0.3 cm/day. Within 2 m of the contact, erosion rates drop faster to a minimum of

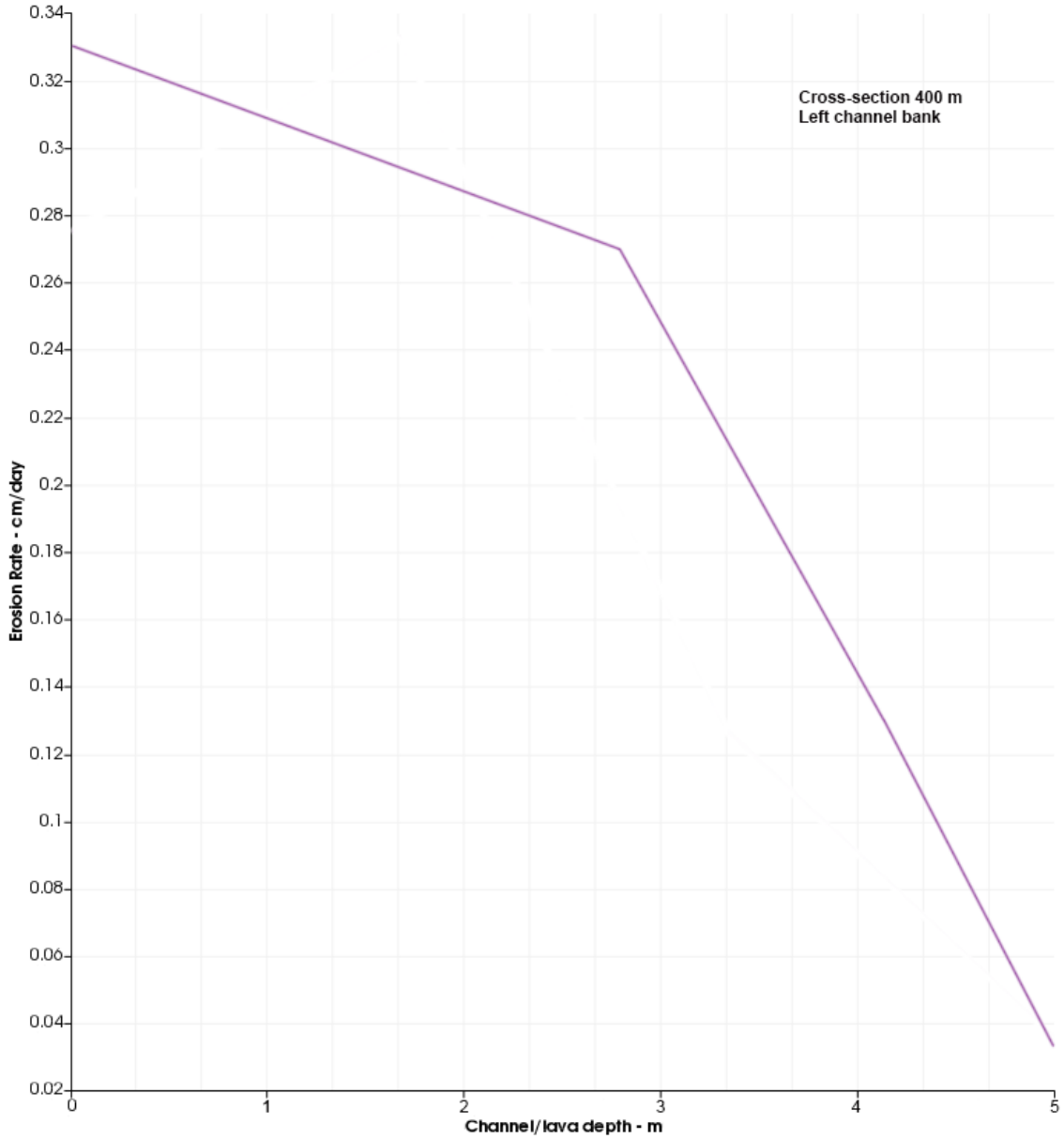

Figure 5.21a. Scenario 2 (lava flowing insulated in a tube). Erosion rates at the left bank

of rille cross-section 400. A 5-m-thick lava at the sub-liquidus temperature of 1380°C and flowing at a velocity of 5 m s^{-1}. Lava temperature at both banks is equal to 1360°C. Maximum erosion rates of 0.33 cm/day are found at the bank top and from there they decrease at a constant rate down to a vertical distance of ~2 m from the bank/bed contact, where they reach a value of ~0.27 cm/day. Within 2 m of the contact, erosion rates drop faster till a minimum value of 0.035 cm/day is obtained at the contact itself. Compared to the counterpart flow of scenario 1, erosion rates are lower by a factor of ~1.1, a likely consequence of the lower eruption temperature (even though the flow is insulated from the lunar environment).

~0.04 cm/day at the contact itself. Compared to the counterpart flow of scenario 1, erosion rates are lower by a factor of ~1.1, a likely consequence of the lower eruption temperature (even though the lava flows insulated from the lunar environment). Erosion rates at the right bank of cross-section 400 are shown in Fig. 5.21b. Erosion rates of 2.1 cm/day are found at the bank top and from there they increase until they reach a maximum of ~2.2 cm/day at a vertical distance of ~2 m from the underlying bank/bed contact. Within 2 m of the contact, erosion rates drop till a minimum value of 1.7 cm/day is reached at contact itself. The maximum erosion rate is lower than that produced by the analogous flow of scenario 1 by a factor of 1.5, a likely consequence of the lower temperature of the lava (1380°C versus 1400°C).

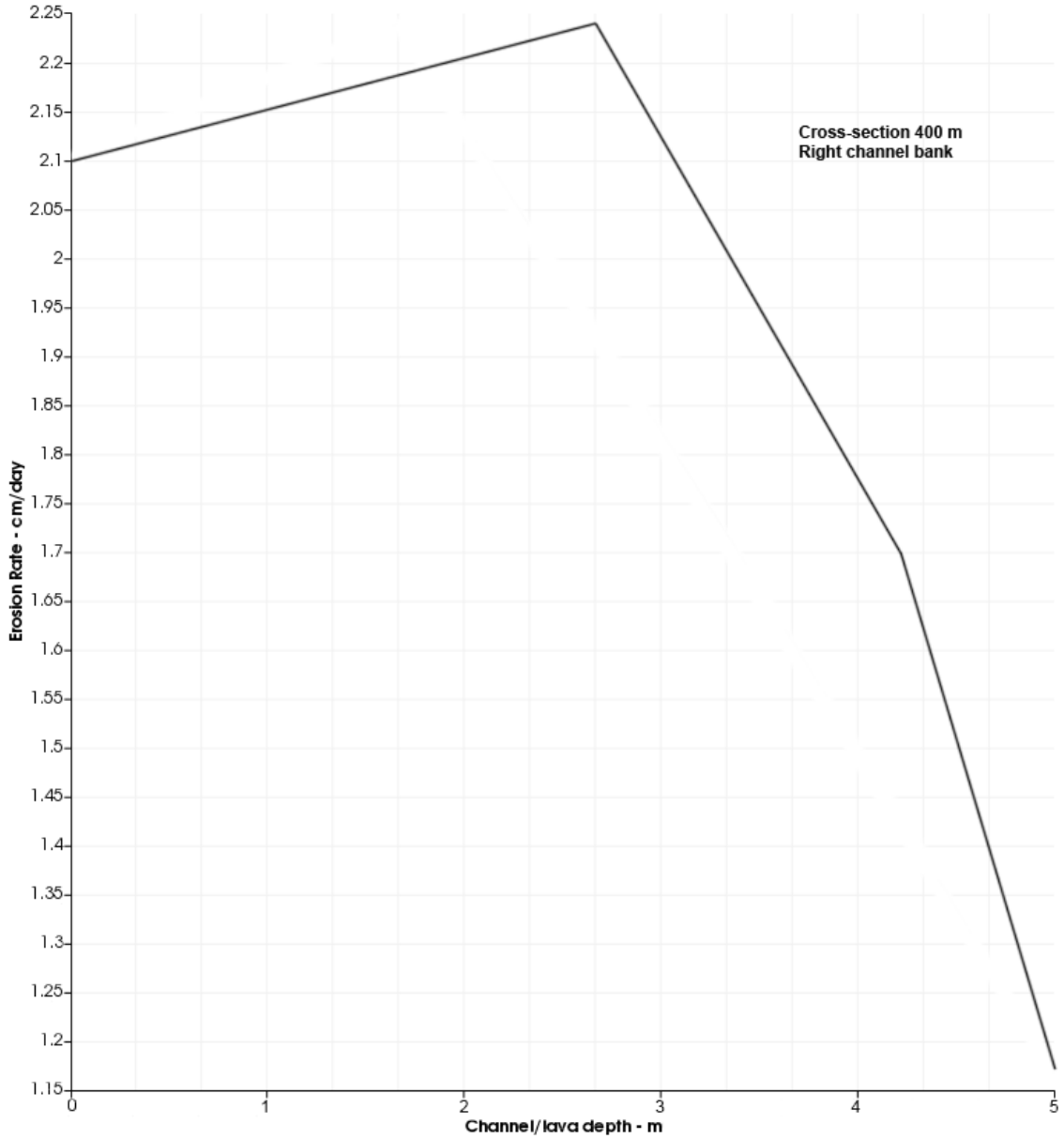

Figure 5.21b. Scenario 2 (lava flowing insulated in a tube). Erosion rates at the right bank of rille cross-section 400. Results refer to a 5-m-thick lava at the sub-liquidus temperature of 1380°C and flowing at a velocity of 5 m s^{-1}. Lava temperature at this bank is equal to 1360°C. Erosion rates of 2.1 cm/day are found at the bank top and from there they increase until they reach a maximum of 2.24 cm/day at a vertical distance of ~2 m from the underlying bank/bed contact. Within 2 m of the contact, erosion rates drop till a minimum value of 1.7 cm/day is obtained at the contact itself. The maximum erosion rate is lower than that associated with the analogous flow of scenario 1 by a factor of 1.5, a likely consequence of the lower temperature of the lava (1380°C versus 1400°C).

The next sub-scenario deals with a flow that is 20-m-thick, is erupted at a temperature of 1390°C and travels at a velocity of 5 m s^{-1} (Fig. 5.22). Temperature at channel boundaries is equal to 1350°C. Running a simulation for a 20-m-thick lava erupted at T=1380°C requires a boundary temperature of 1340°C, which leads to physically inconsistent results. In other words, the value of 1340°C appears to be incompatible with the assumption of Newtonian flow conditions. Fig. 5.22 shows a plan view of the bed with the associated erosion rate values. This run shows that even a temperature of 1350°C at the channel bed

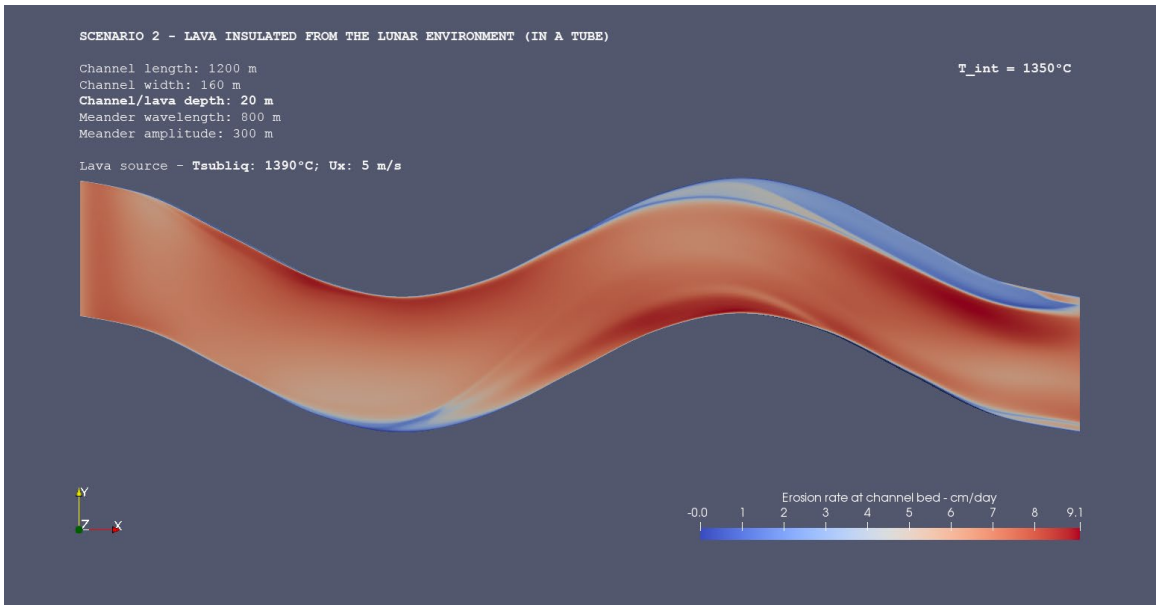

Figure 5.22. Plan view that shows erosion rates distribution at the bed of a 1200-m-long rille section. Scenario 2 (lava flowing insulated in a tube). Erosion rates are referred to a 20-m-thick lava of T = 1390°C, which travels at a velocity of 5 m s^{-1}. Temperature at rille boundaries is taken to be equal to 1350°C. Lava source is on the left and flow motion is rightward. Once again, erosion highs (up to 9.1 cm/day) are concentrated at or near bend troughs whereas lows are found at bend apexes.

and banks might be too low for flow conditions to still be Newtonian. To follow, evidence is provided in support of this statement. Fig. 5.23 shows erosion rates at the bed of cross-

section 400. Maximum erosion rates of 8.5 cm/day are obtained within ~10 m of the bed/right bank contact. While moving toward the bed/left bank contact, erosion into the substrate decreases at an almost constant rate out to ~65 m from the contact. Then, values level off and remain almost constant out to ~40 m from the same contact. From that point on, erosion rates decrease faster and then slightly increase again within 10 m of the contact. At the contact, a minimum value of 0.1 cm/day is found. Erosion rates are lower by a factor of 1.6 than those associated with the identical flow of scenario 1 that is erupted at a slightly

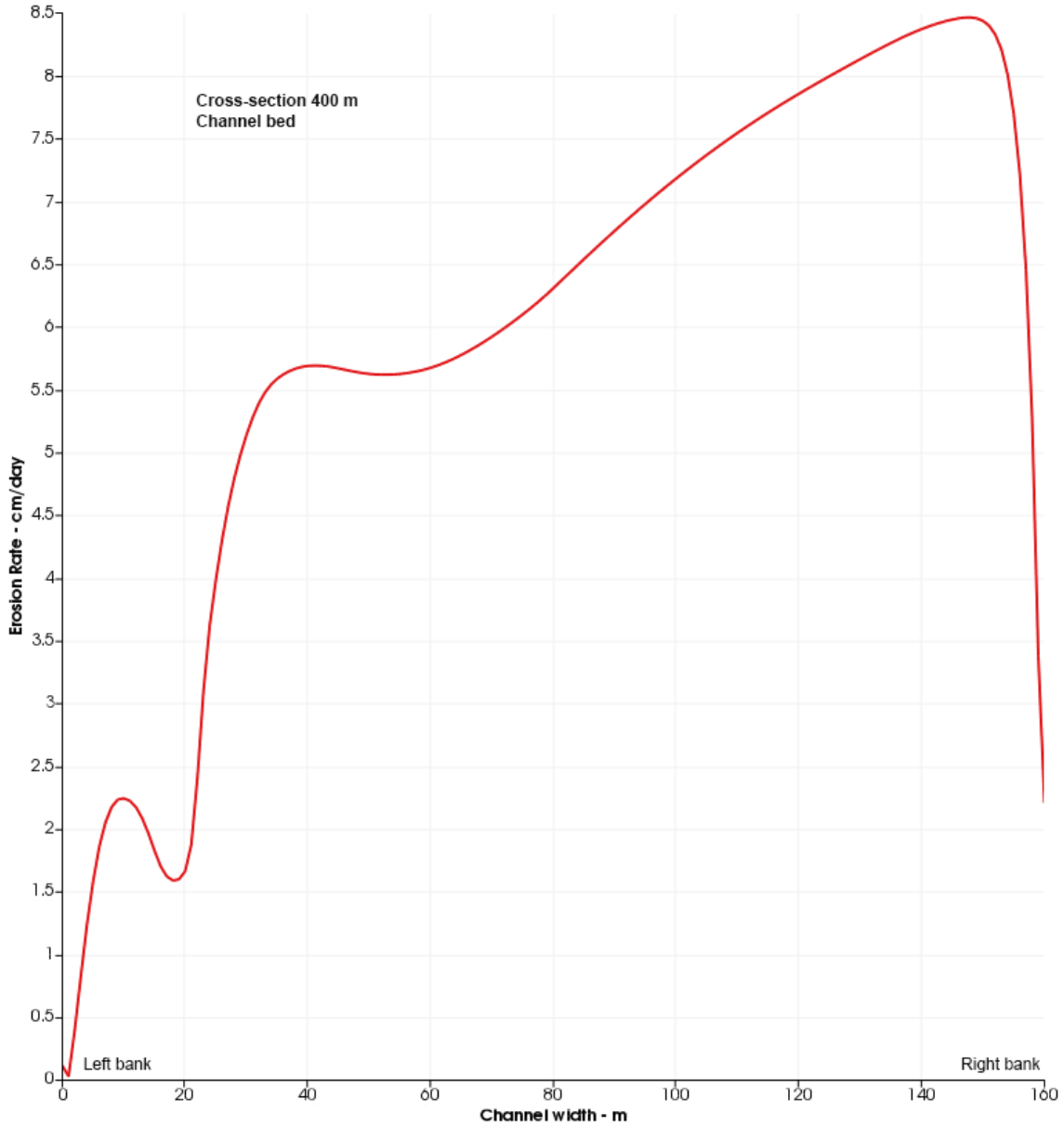

Figure 5.23. Scenario 2 (lava flowing insulated in a tube). Erosion rates at the bed of rille cross-section 400. Lava is 20 m thick, at the sub-liquidus temperature of 1390°C and travels at a velocity of 5 m s^{-1}. Temperature at the bed is 1350°C. Maximum erosion rates of 8.5 cm/day are found within ~10 m of the bed/right bank contact. While moving toward the bed/left bank contact, erosion into the substrate decreases at an almost constant rate out to a distance of ~65 m from the contact. Then, values level off and remain almost constant out to ~40 m from that contact. From that point on, erosion rates decrease faster and then slightly increase again within 10 m of the contact. A minimum value of 0.1 cm/day is finally reached within 1 m of the same contact. Erosion rates are lower by a factor of ~1.6 than those associated with the identical flow of scenario 1 erupted at a slightly higher temperature (1410°C) and traveling at the same velocity.

higher temperature (1410°C) and travels at the same velocity. The distribution of erosion rates at the left bank is shown in Fig. 5.24a. Maximum erosion rates of ~2.8 cm/day are found at the bank top and then decrease progressively faster till they reach a minimum value of ~0 cm/day at the bank/bed contact. This plot shows a trend that has not been seen in previous simulations, including those referred to the baseline model (see sensitivity analysis chapter). The trend suggests that a boundary temperature of 1350°C might be too low for flow conditions to still be Newtonian. Fig. 5.24b shows erosion rates at the right bank of cross-section 400. Maximum erosion rates of ~3.8 cm/day are found at a vertical distance of 2 m from the underlying bank/bed contact. At the bank top, erosion rates are equal to ~2.2 cm/day and then progressively decrease till they reach a value of 1.6 cm/day within ~8 m of the bank/bed contact. From that point on, they resume increasing till they reach the maximum of ~3.8 cm/day. The trend shown in this plot in unusual and, once again, it might suggest that a boundary temperature of 1350°C is inconsistent with the assumption of Newtonian flow conditions. Hence, displayed results might not be accurate.

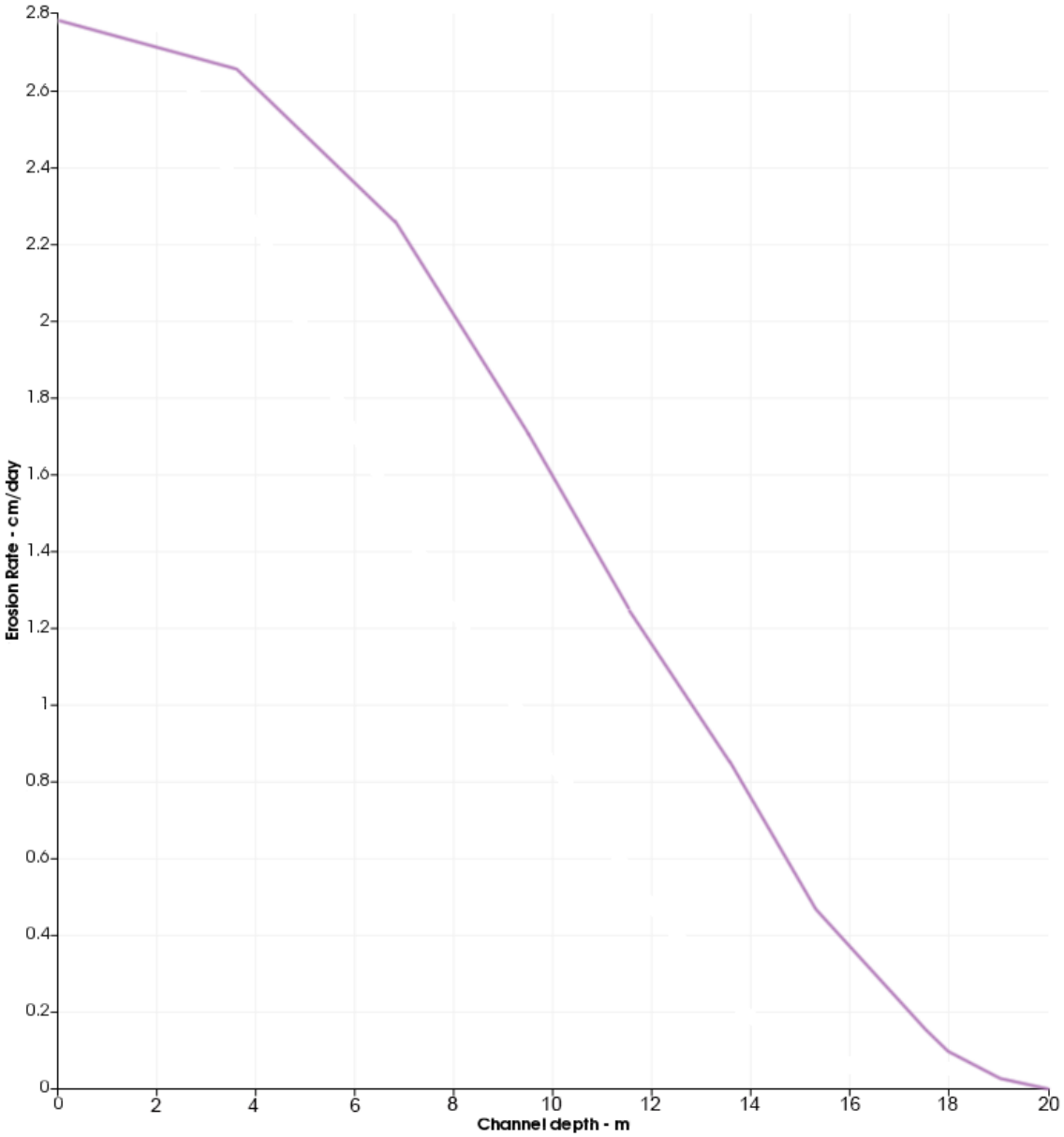

Figure 5.24a. Scenario 2 (lava flowing insulated in a tube). Erosion rates at the left bank of rille cross-section 400. A 20-m-thick flow erupted at the sub-liquidus temperature of 1390°C and traveling at a velocity of 5 m s^{-1}. Lava temperature at both banks is equal to 1350°C. Maximum erosion rates of 2.79 cm/day are found at the bank top and from there decrease progressively faster till they reach a minimum of ~0 cm/day at the bank/bed contact. This plot shows a trend that has not been seen in previous simulations, including those obtained from the baseline model (see sensitivity analysis chapter). The trend suggests that even a boundary temperature of 1350°C might be too low for flow conditions to still be Newtonian.

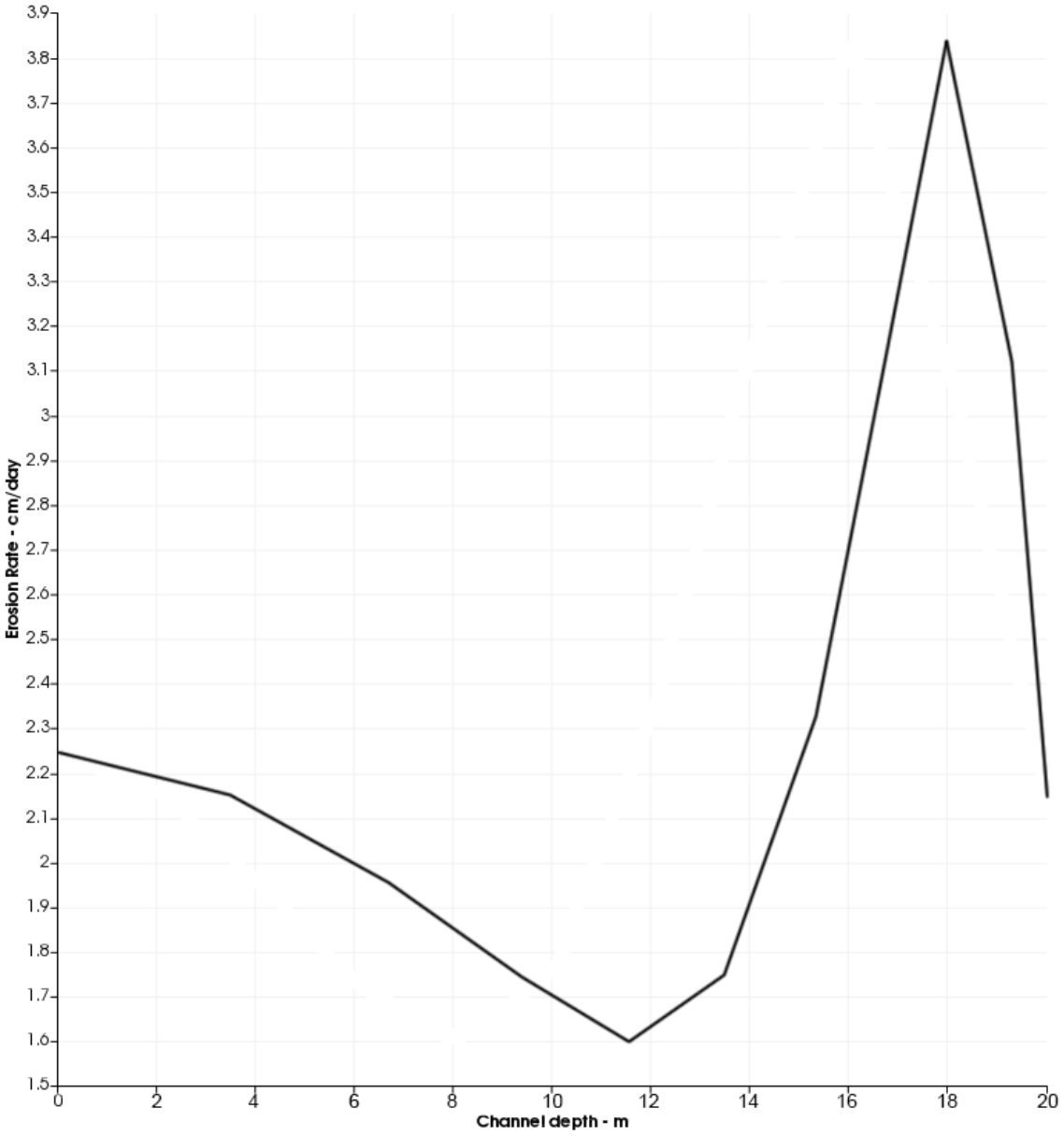

Figure 5.24b. Scenario 2 (lava flowing insulated in a tube). Erosion rates at the right bank of rille cross-section 400. A 20-m-thick lava erupted at the sub-liquidus temperature of 1390°C and flowing at a velocity of 5 m s^{-1}. Lava temperature at the two banks is equal to 1350°C. Maximum erosion rates of 3.83 cm/day are found at a vertical distance of ~2 m from the underlying bank/bed contact. At the bank top, erosion rates are equal to 2.24 cm/day and from there progressively decrease till they reach a minimum value of 1.6 cm/day within ~8 m of the bank/bed contact. From that point on, they resume increasing till they reach the maximum of 3.83 cm/day. This plot shows one more trend that has not been seen in previous simulations, including those referred to the baseline model (see

sensitivity analysis chapter). This unusual trend might also suggest that a boundary temperature of 1350°C is perhaps too low for flow conditions to still be Newtonian. Hence, results might be not 100% accurate.

The next sub-scenario deals with a flow that is erupted at the temperature of 1380°C, is 20 m in thickness and travels at a velocity of 10 m s^{-1}. Temperature at channel boundaries is taken to be equal to 1340°C. The intention is to test how increasing flow rates might impact flow conditions and, hence, the reliability of results. Fig. 5.25 shows the usual plan view of the bed with associated erosion rates and their spatial distribution.

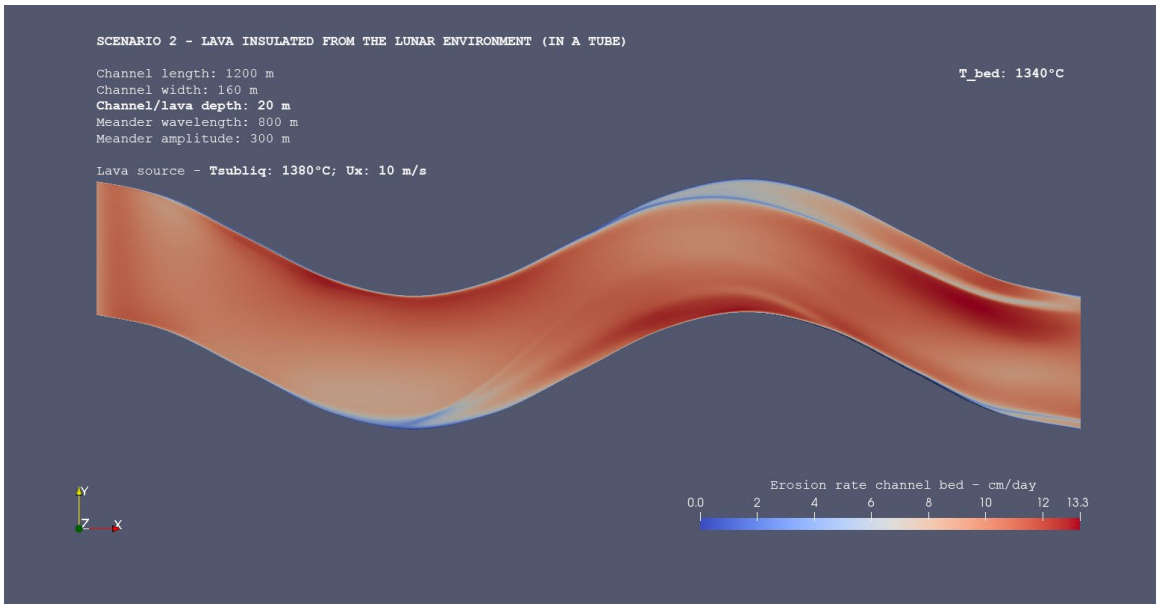

Figure 5.25. Plan view that shows erosion rates magnitude and their spatial distribution at the bed of a 1200-m-long rille section. Scenario 2 (lava flowing insulated in a tube). Erosion rates are referred to a 20-m-thick lava of T = 1380°C, which flows at a velocity of 10 m s^{-1}. Temperature at rille boundaries is taken to be equal to 1340°C. Lava source is on the left and flow motion is rightward. Once again, erosion highs (up to 13.3 cm/day here) are concentrated at or near bend troughs whereas lows are found at bend apexes.

The magnitude and spatial distribution of erosion rates at the bed of cross-section 400 are shown in Fig. 5.26. Maximum erosion rates of 12.3 cm/day are obtained within ~10 m of the bed/right bank contact. While moving toward the bed/left bank contact, erosion into the

substrate decreases at an almost constant rate out to ~60 m from the contact. Then, values remain almost constant out to ~35 m from the bed/left bank contact. From that point on, erosion rates decrease faster and then slowly increase again within 10 m of the same contact. A minimum value of 0.1 cm/day is finally reached within 1 m of the contact

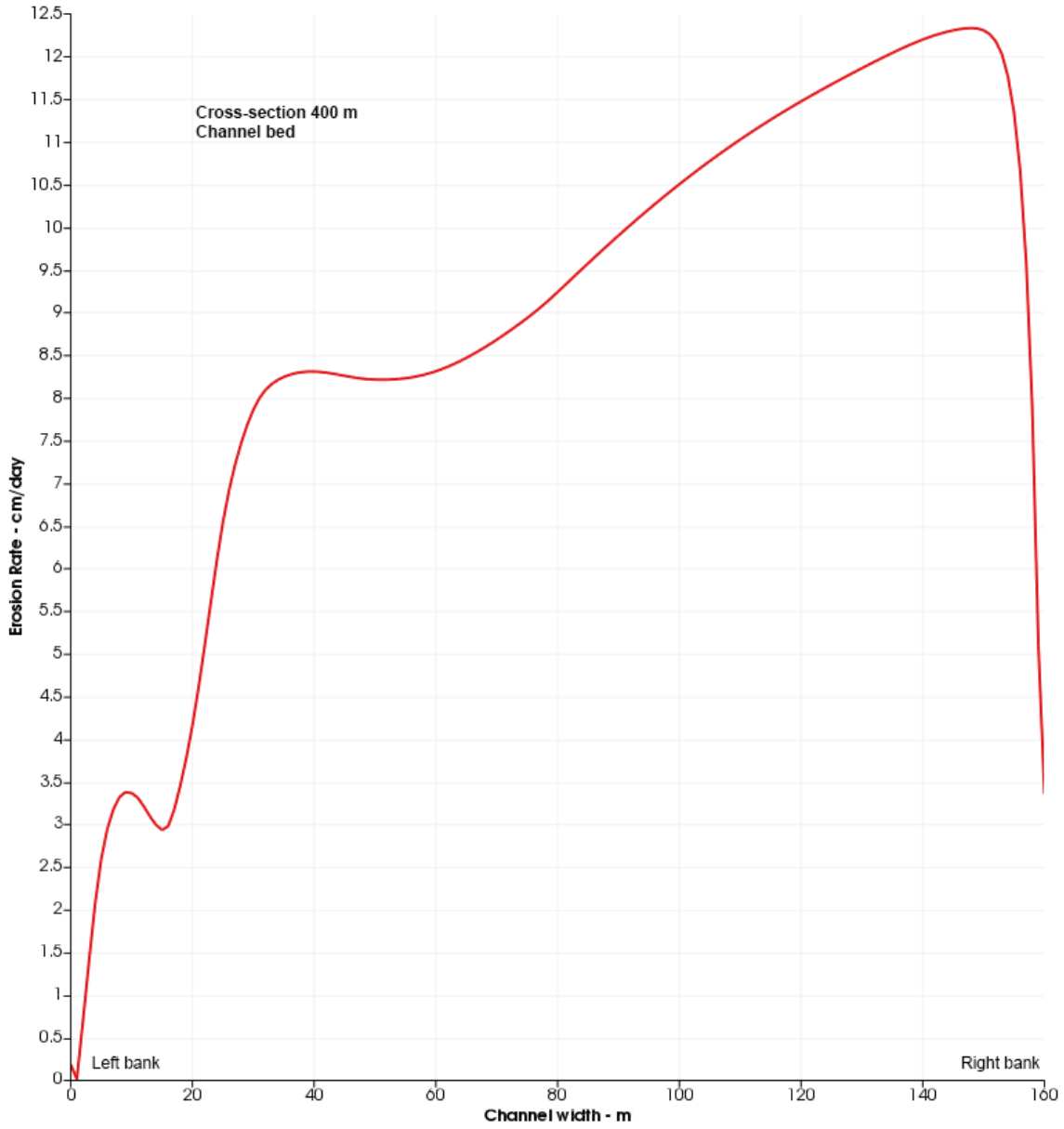

Figure 5.26. Scenario 2 (lava flowing insulated in a tube). Erosion rates at the bed of rille cross-section 400. Lava is 20 m thick, is erupted at the sub-liquidus temperature of 1380°C and travels at a velocity of 10 m s^{-1}. Temperature at the bed is 1340°C. Maximum erosion

rates of 12.3 cm/day are found within ~10 m of the bed/right bank contact. While moving toward the bed/left bank contact, erosion into the substrate decreases at an almost constant rate out to a distance of ~60 m from the contact. Then, values remain almost constant out to ~35 m from that contact. From that point on, erosion rates decrease faster and then slowly increase again within 10 m of the same contact. A minimum value of 0.1 cm/day is finally reached within 1 m of the bed/left bank contact.

Fig. 5.27a shows erosion rates at the left bank. Maximum erosion rates of ~4.7 cm/day are found at the bank top and from there they decrease to a minimum value that closely approaches 0 cm/day at the bank/bed contact. This plot shows a trend similar to that shown

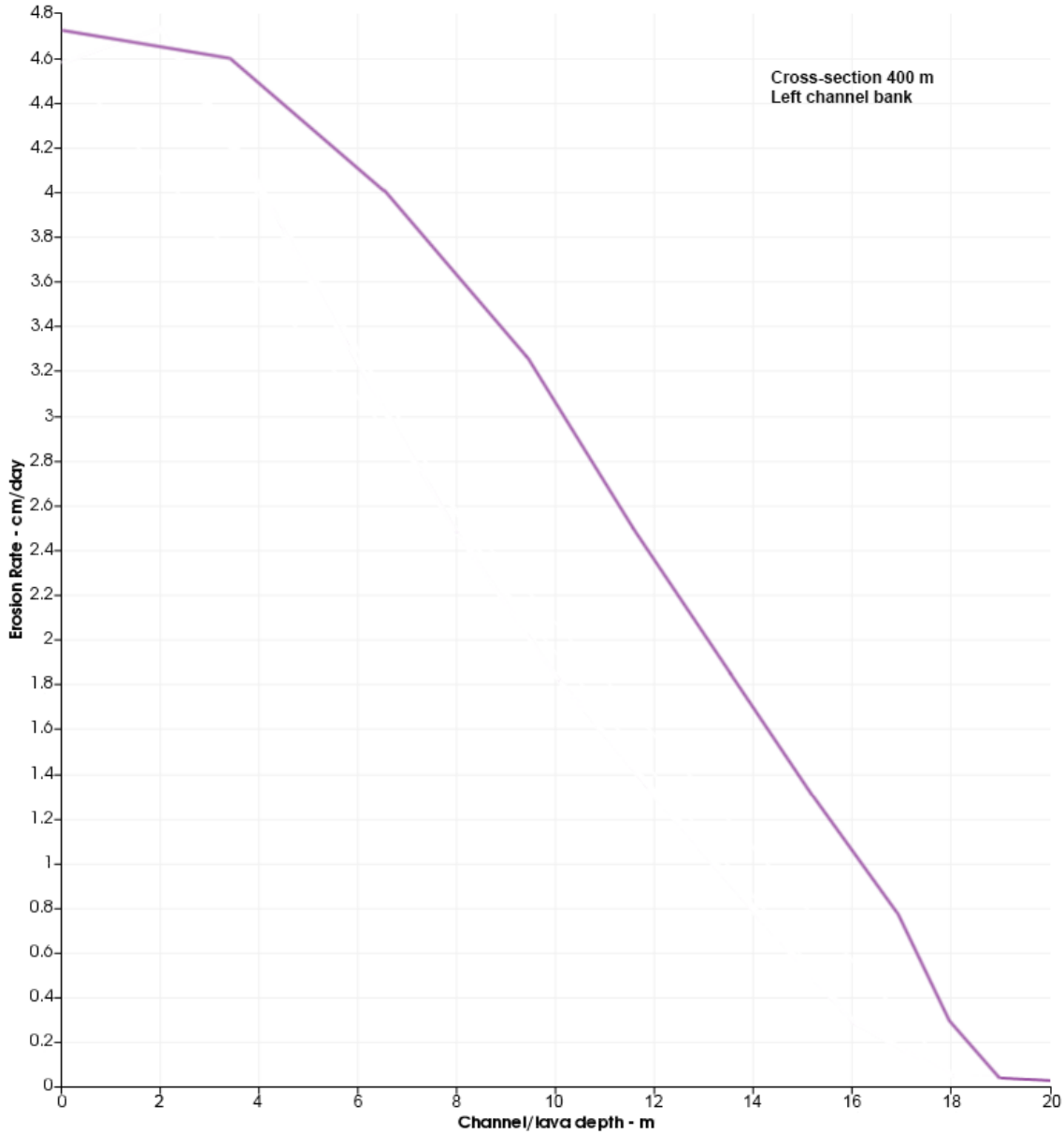

Figure 5.27a. Scenario 2 (lava flowing insulated in a tube). Erosion rates at the left bank of rille cross-section 400. A 20-m-thick lava is erupted at the sub-liquidus temperature of 1380°C and travels at a velocity of 10 m s^{-1}. Lava temperature at the two banks is equal to 1340°C. Maximum erosion rates of 4.74 cm/day are found at the bank top and from there they decrease to a minimum value that approaches 0 cm/day at the bank/bed contact. This plot shows a trend somewhat similar to that referred to a 20-m-thick lava erupted at a temperature of 1390°C and flowing at a velocity of 5 m s^{-1}.

by a 20-m-thick lava erupted at a temperature of 1390°C and flowing at a velocity of 5 m s^{-1}. The magnitude and distribution of erosion rates at the right bank is shown in Fig. 5.27b.

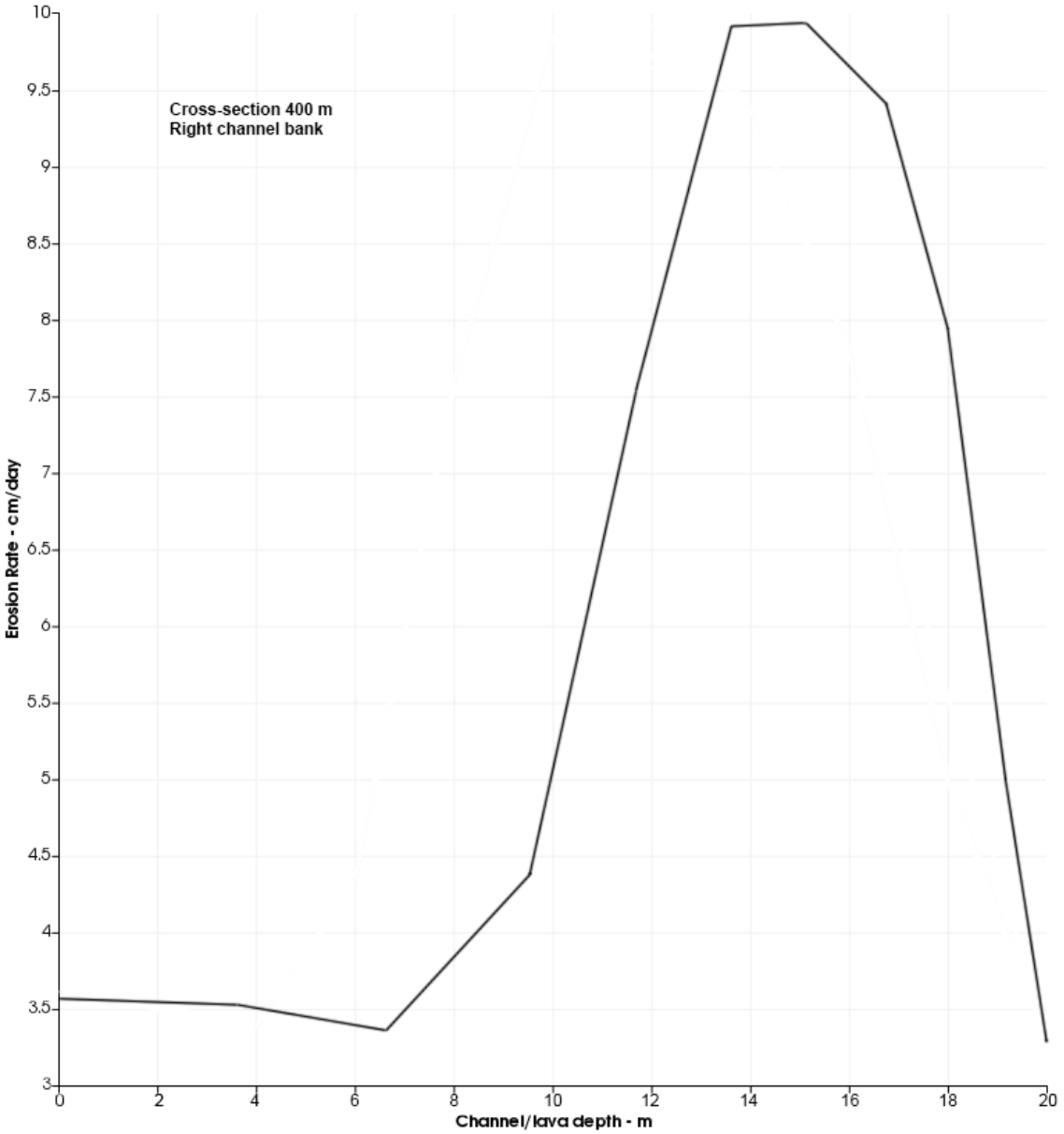

Figure 5.27b. Scenario 2 (lava flowing insulated in a tube). Erosion rates at the right bank of rille cross-section 400. A 20-m-thick lava is erupted at the sub-liquidus temperature of 1380°C and travels at a velocity of 10 m s^{-1}. Lava temperature at the banks is equal to 1340°C. Maximum erosion rates of 9.9 cm/day are found at a vertical distance of 5-7 m from the underlying bank/bed contact. At the bank top, erosion rates are equal to 3.55 cm/day and then decrease till they reach a value of 3.35 cm/day within ~7 m of the bank top. From that point on, they fast increase till they reach the maximum of 9.9 cm/day. Then,

they drop drastically till reaching a minimum value of 3.25 cm/day at the bank/bed contact. This plot shows a trend that is analogous to the one shown in the previously investigated flow sub-scenario.

Maximum erosion rates of 9.9 cm/day are found at a vertical distance of 5-7 m from the underlying bank/bed contact. At the bank top, erosion rates are equal to ~3.5 cm/day and, from there, slowly decrease till reaching a value of ~3.3 cm/day within ~7 m of the bank top. Then, they rapidly increase until they reach the maximum of 9.9 cm/day. At that point, they drop drastically till a minimum value of ~3.2 cm/day is found at the bank/bed contact. Once again, this plot shows a trend that is analogous to the one displayed in the previously investigated sub-scenario. In other words, it appears that an increase in lava velocity from 5 to 10 m s^{-1} allows for Newtonian flow conditions to be maintained even for a lava temperature of 1340°C, which is 100°C lower than the liquidus value. The faster flow rate allows for the simulation to run and produces results that look almost identical to those referred to a flow temperature of 1350°C (10°C higher).

The next scenario refers to a 5-m-thick lava that is erupted at the liquidus temperature (1440°C) and travels at a velocity of 5 m s^{-1}. Fig. 5.28 shows a plan view of the bed with erosion rates and their spatial distribution over the 1200-m-long rille section of interest. The highest values of 15.8 cm/day are higher than those associated with the previously investigated 5-m-thick sub-liquidus lava by a factor of 4.3, which represents a substantial increase.

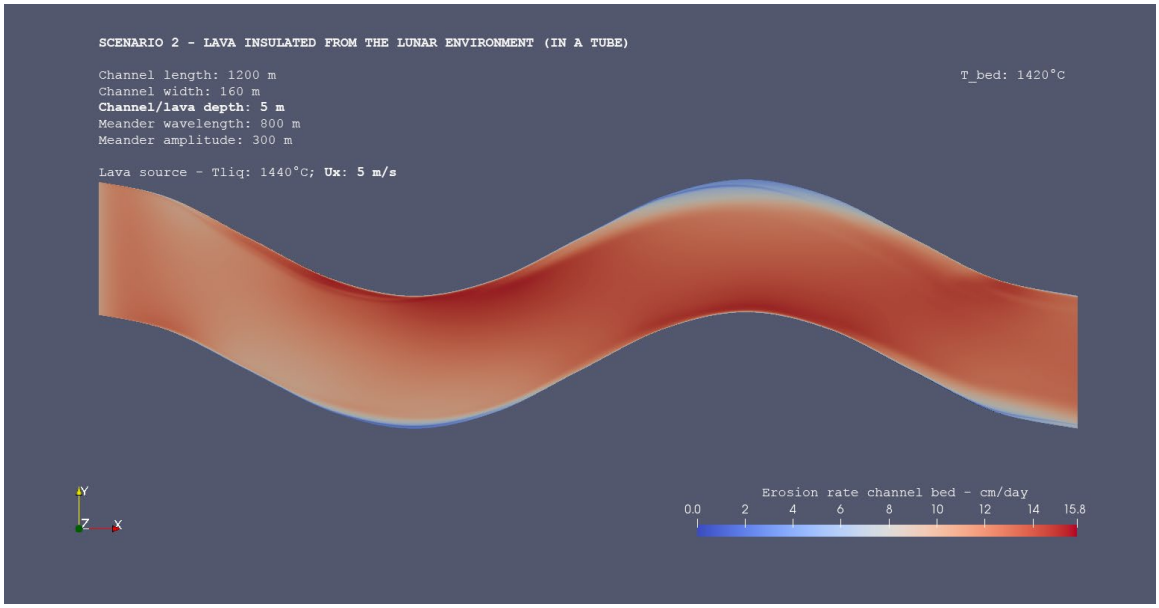

Figure 5.28. Plan view that shows erosion rate values and their spatial distribution at the bed of a 1200-m-long rille section. Scenario 2 (lava flowing insulated in a tube). Erosion rates are referred to a 5-m-thick lava of T = 1440°C (liquidus), and traveling at a velocity of 5 m s^{-1}. Temperature at rille boundaries is taken to be equal to 1400°C. Lava source is on the left and flow motion is rightward. Once again, erosion highs (up to 15.8 cm/day here) are concentrated at or near bend troughs whereas lows are found at bend apexes.

Erosion rates at the bed of cross-section 400 are shown in Fig. 5.29. Maximum erosion rates of 15.3 cm/day are found within ~10 m of the bed/right bank contact. While moving toward the bed/left bank contact, erosion into the substrate decreases at an almost constant rate out to a distance of ~55 m from the contact. Then, values remain almost constant out to ~25 m from the bed/left bank contact. From that point on, erosion rates decrease faster and then slowly increase within 5 m of the contact. A minimum value of 2.0 cm/day is reached within 1 m of the bed/left bank contact. Maximum erosion rates are higher by a factor of ~4.2 than those associated with the sub-liquidus lava (T=1380°C) of identical thickness and velocity.

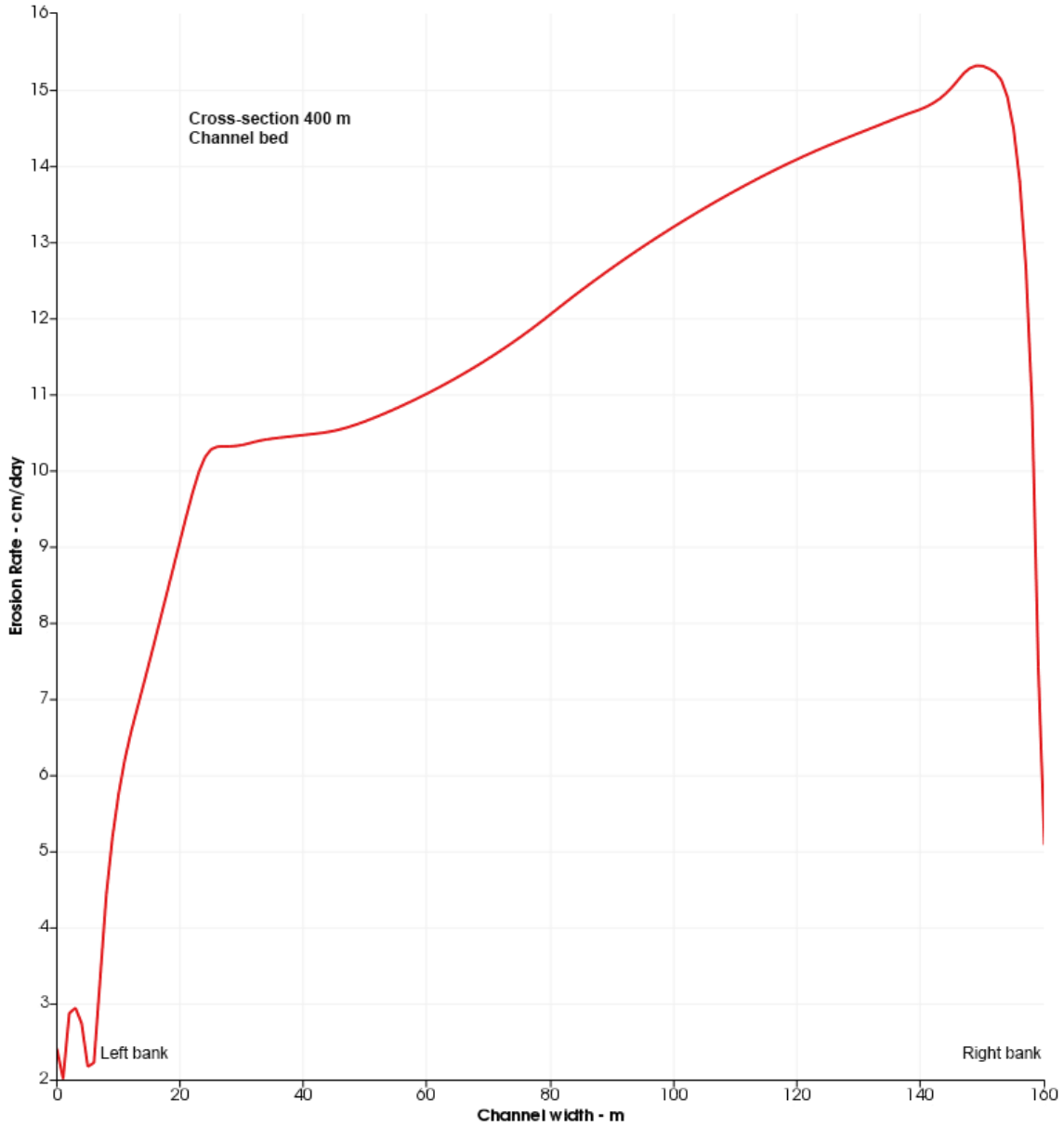

Figure 5.29. Scenario 2 (lava flowing insulated in a tube). Erosion rates at the bed of rille cross-section 400. Lava is 5 m thick, is erupted at the liquidus temperature (1440°C) and travels at a velocity of 5 m s^{-1}. Temperature at the bed is 1400°C. Maximum erosion rates of 15.3 cm/day are found within ~10 m of the bed/right bank contact. While moving toward the bed/left bank contact, erosion into the substrate decreases at an almost constant rate out to a distance of ~55 m from the contact. Then, values remain almost constant out to ~25 m from the contact. From that point on, erosion rates decrease faster and then slowly increase within 5 m of the same contact. Finally, a minimum value of 2.0 cm/day is reached within 1 m of the bed/left bank contact. Maximum erosion rates are higher by a factor of ~4.2 than those associated with the sub-liquidus lava (T=1380°C) of identical thickness and velocity.

Fig. 5.30a shows erosion rates at the left bank. Erosion rates rapidly increase from a value of ~2.9 cm/day at the bank top to a maximum of ~3.6 cm/day ~3 m down from the bank top. From that point on, they decrease and then drop to a minimum of 2.0 cm/day at the left bank/bed contact. The fastest drop in erosion rates occurs within ~1 m of the bank/bed contact. Erosion rates are found to be higher by a factor of 10.9 than those obtained at the left bank by a flow of identical thickness and velocity and with a temperature of 1380°C.

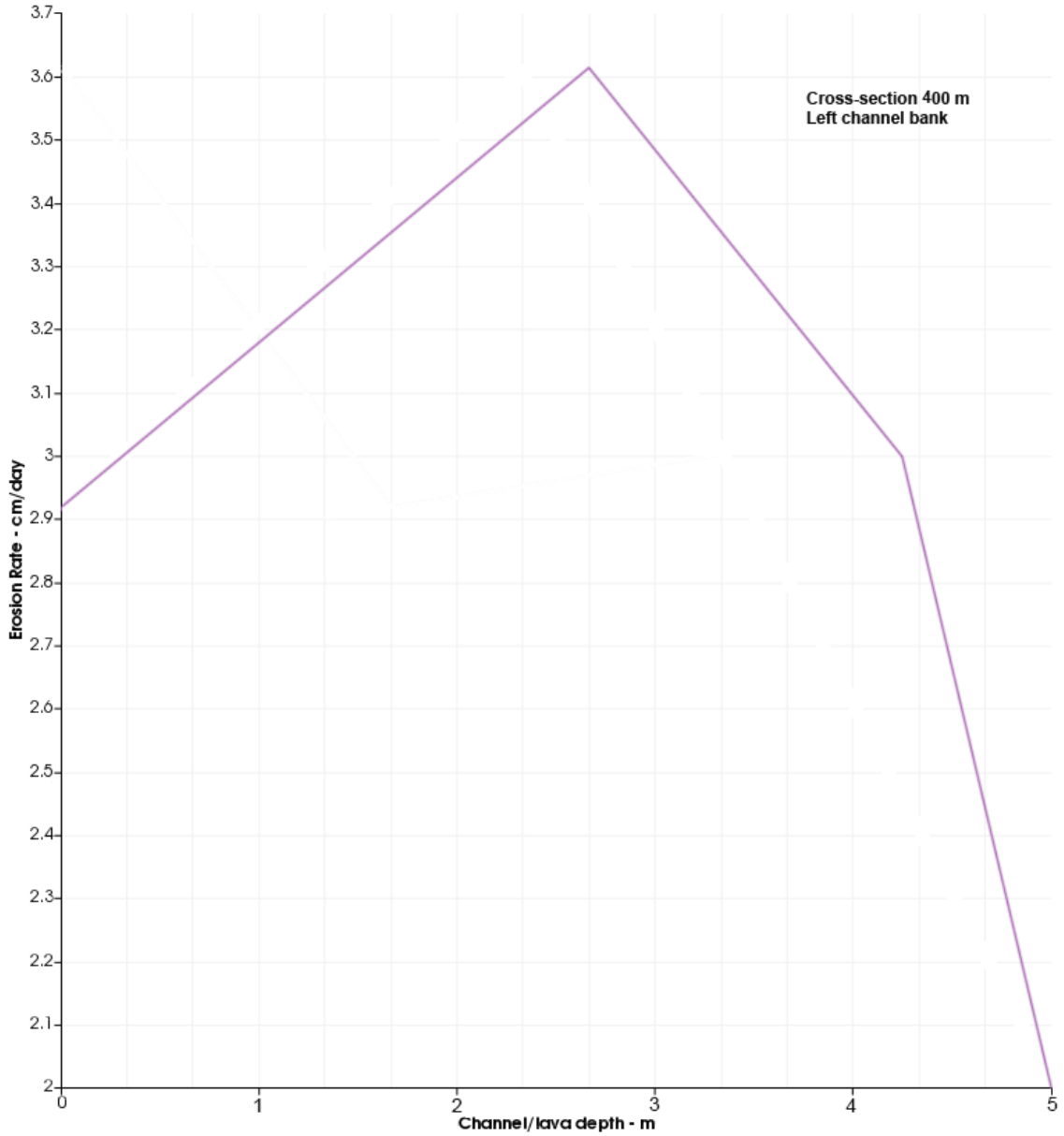

Figure 5.30a. Scenario 2 (lava flowing insulated in a tube). Erosion rates at the left bank of rille cross-section 400. Results refer to a 5-m-thick flow erupted at the liquidus temperature and traveling at a velocity of 5 m s^{-1}. Lava temperature at the bank is equal to 1400°C. Erosion rates rapidly increase from a value of 2.92 cm/day at the bank top to a maximum of 3.61 cm/day ~3 m down from the bank top. From that point on, they decrease and then drop to 2.0 cm/day at the left bank/bed contact. The fastest drop in erosion rates occurs within ~1 m of the bank/bed contact. Erosion rates are found to be higher by a factor of 10.9 (more than an order of magnitude) than those obtained at the left bank by a flow of identical thickness and velocity, and erupted at a temperature of 1380°C.

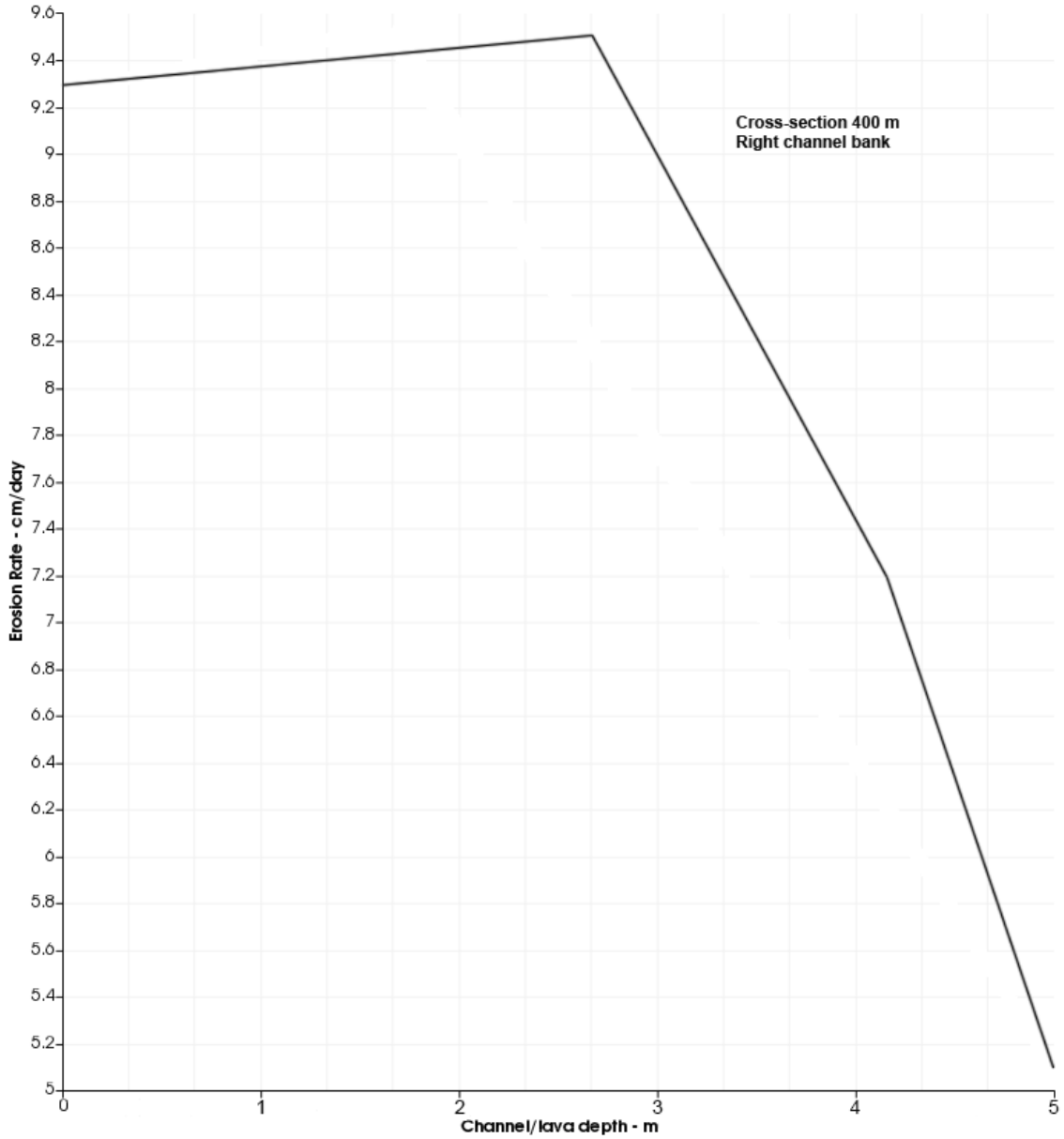

Figure 5.30b. Scenario 2 (lava flowing insulated in a tube). Erosion rates at the right bank of rille cross-section 400. Results refer to a 5-m-thick lava erupted at the liquidus temperature and flowing at a velocity of 5 m s^{-1}. Lava temperature at the two banks is equal to 1400°C. Erosion rates of 9.3 cm/day are found at the bank top and from there they increase until they reach a maximum of 9.52 cm/day at a vertical distance of ~2 m from the underlying bank/bed contact. Within 2 m of that contact, erosion rates drop till a minimum value of 5.1 cm/day is reached at the contact itself. The maximum erosion rate is higher than that produced by the sub-liquidus lava of identical thickness and velocity by a factor of 4.3.

The erosion distribution at the right bank is shown in Fig. 5.30b. Erosion rates of 9.3 cm/day are found at the bank top and from there they increase until they reach a maximum of ~9.5 cm/day at a vertical distance of ~2 m from the underlying bank/bed contact. Within 2 m of the contact, erosion rates drop till a minimum value of 5.1 cm/day is reached at the same contact. The maximum erosion rate is higher than that produced by the analogous sub-liquidus lava by a factor of 4.3.

The next flow is erupted at the liquidus temperature, travels at a velocity of 5 m s^{-1} and is 20 m thick (Fig. 5.31). Maximum erosion rates are higher by a factor of ~3.5 than those associated with the sub-liquidus lava (T=1390°C) of identical thickness and velocity.

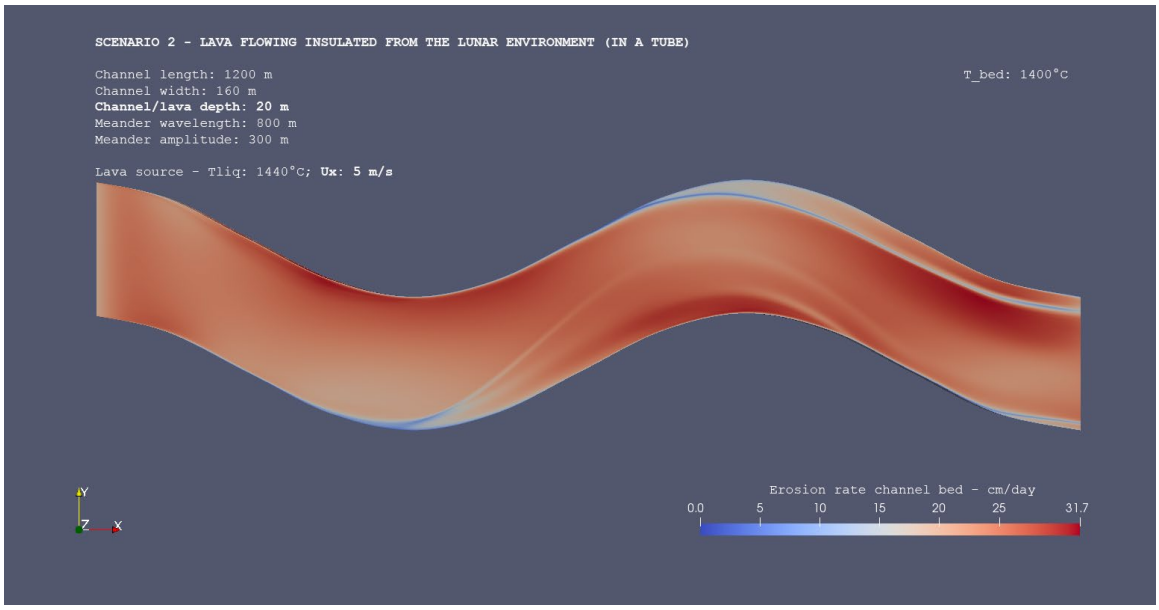

Figure 5.31. Plan view that shows erosion rates and their spatial distribution at the bed of a 1200-m-long rille section. Scenario 2 (lava flowing insulated in a tube). Erosion rates are referred to a 20-m-thick lava of T = 1440°C (liquidus), and traveling at a velocity of 5 m s^{-1}. The boundary temperature is taken to be equal to 1400°C. Lava source is on the left and flow motion is rightward. Once again, erosion highs (up to 31.7 cm/day) are concentrated at or near bend troughs whereas lows are found at/near bend apexes. Maximum erosion rates are higher by a factor of ~3.5 than those associated with the sub-liquidus lava (T=1390°C) of identical thickness and velocity.

Fig. 5.32 shows erosion rates magnitude and their distribution at the bed of cross-section 400. Maximum rates of 29.1 cm/day are found within 10 m of the bed/right bank contact.

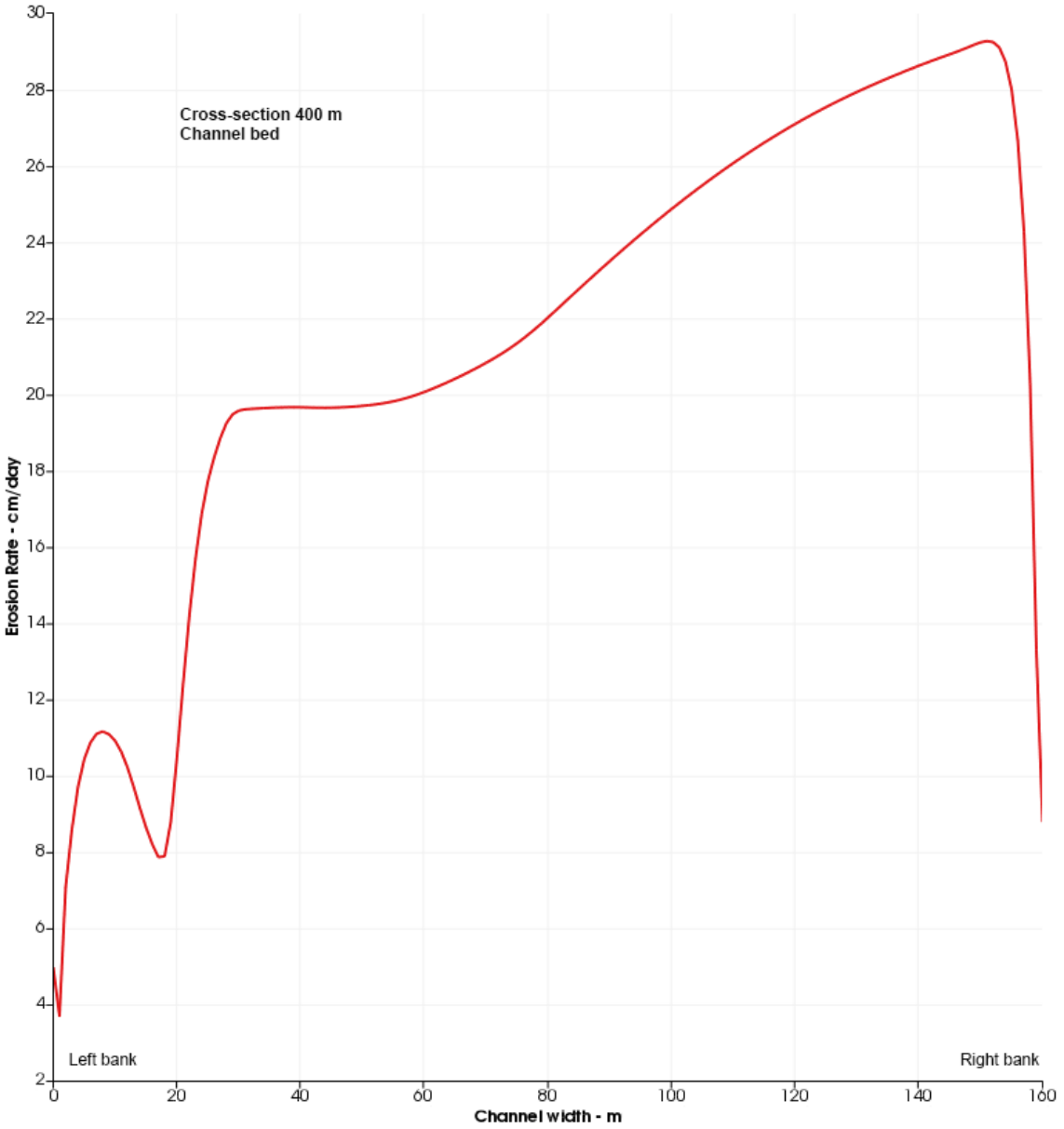

Figure 5.32. Scenario 2 (lava flowing insulated in a tube). Erosion rates at the bed of rille cross-section 400. Lava is 20 m thick and flows at the liquidus temperature (1440°C) and at a velocity of 5 m s^{-1}. Temperature at the bed is 1400°C. Maximum erosion rates of 29.1 cm/day are obtained within ~10 m of the bed/right bank contact. While moving toward the bed/left bank contact, erosion into the substrate decreases out to a distance of ~50 m from the contact. Then, values remain almost constant out to ~25 m from that contact. From that point on, erosion rates decrease faster and then slowly increase within 10 m of the contact.

A minimum value of 3.9 cm/day is reached within 1 m of the bed/left bank contact. Maximum erosion rates are higher by a factor of ~3.4 than those associated with the sub-liquidus lava (T=1390°C) of identical thickness and velocity.

While moving toward the bed/left bank contact, erosion into the substrate decreases out to a distance of ~50 m from the contact. Then, values remain almost constant out to ~25 m from that contact. From that point on, erosion rates decrease faster and then slowly increase. A minimum value of 3.9 cm/day is finally reached within 1 m of the bed/left bank contact. Maximum erosion rates are higher by a factor of ~3.4 than those associated with a sub-liquidus flow of identical thickness and velocity. Fig. 5.33a shows the magnitude and distribution of erosion rates at the left bank. Erosion rates increase from a value of 17.2 cm/day at the bank top to a maximum of ~17.3 cm/day at a vertical distance of ~4 m from the bank top. From that point on, they decrease faster and faster until they drop to a minimum value of 3.6 cm/day at the left bank/bed contact. The fastest drop in erosion rates occurs within ~3 m of the contact. Erosion rates are higher by a factor of ~6.2 than those produced at the left bank by a sub-liquidus lava (T=1390°C) of identical thickness and velocity. Erosion rates at the right bank are shown in Fig. 5.33b. Maximum erosion rates of 30.9 cm/day are found at the bank top and they decrease to a value of 23.4 cm/day down to a vertical distance of ~6 m from the underlying bank/bed contact. The sharpest decrease in erosion rate occurs within ~3 m of the same contact. Finally, the minimum erosion rate of 8.6 cm/day is found at the contact. Maximum erosion rates are higher by a factor of ~ 8.1 than those generated at the same bank by a sub-liquidus flow of identical thickness and velocity.

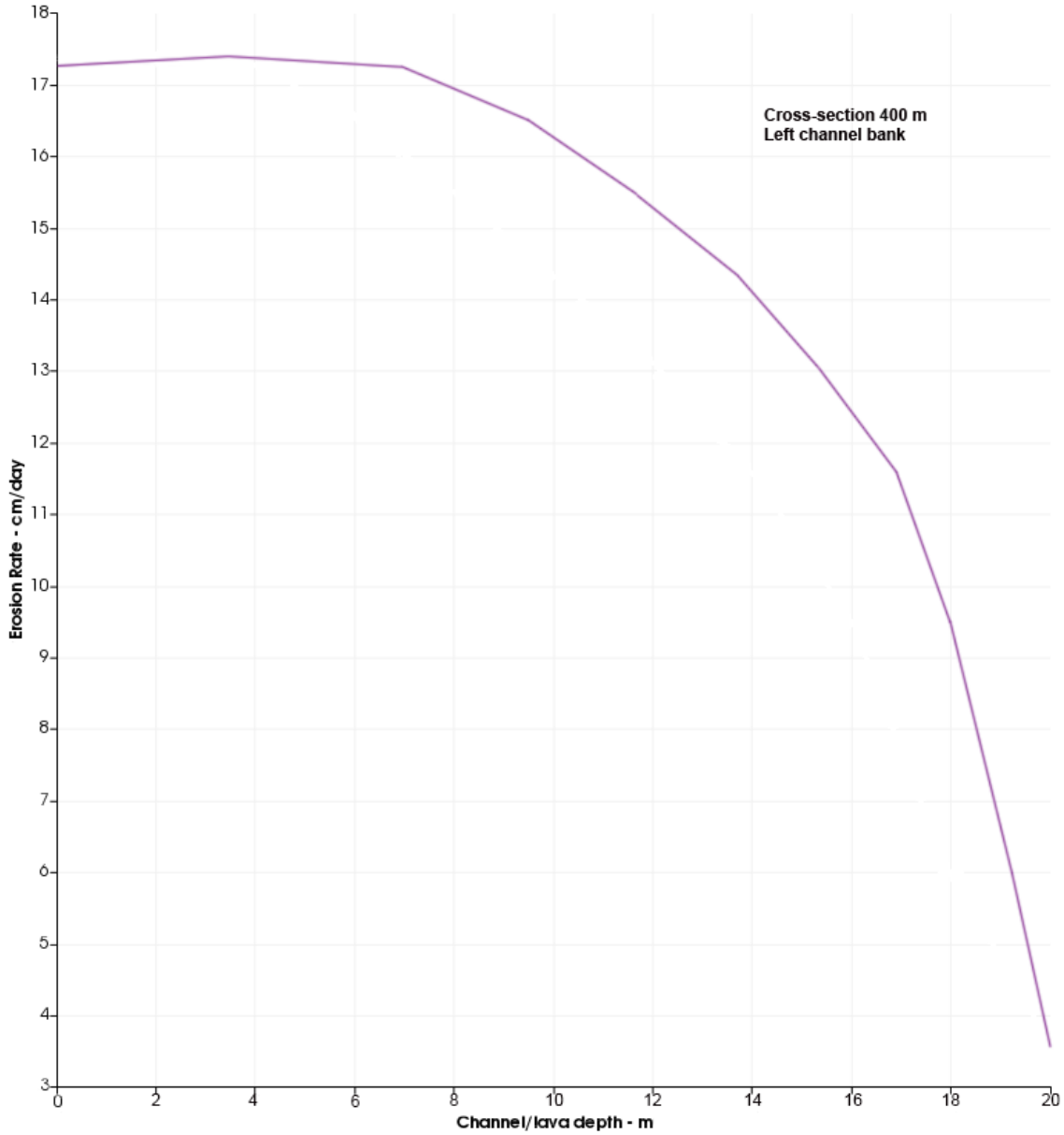

Figure 5.33a. Scenario 2 (lava flowing insulated in a tube). Erosion rates at the left bank of rille cross-section 400. Results refer to a 20-m-thick lava erupted at the liquidus temperature and traveling at a velocity of 5 m s^{-1}. Lava temperature at the bank is equal to 1400°C. Erosion rates increase from a value of 17.2 cm/day at the bank top to a maximum of 17.35 cm/day at a vertical distance of ~4 m from the bank top. From that point on, they decrease faster and faster until they drop to a minimum of 3.6 cm/day at the left bank/bed contact. The fastest drop in erosion rates occurs within ~3 m of the bank/bed contact. Erosion rates are higher by a factor of ~6.2 than those generated at the left bank by a sub-liquidus lava (T=1390°C) of identical thickness and velocity.

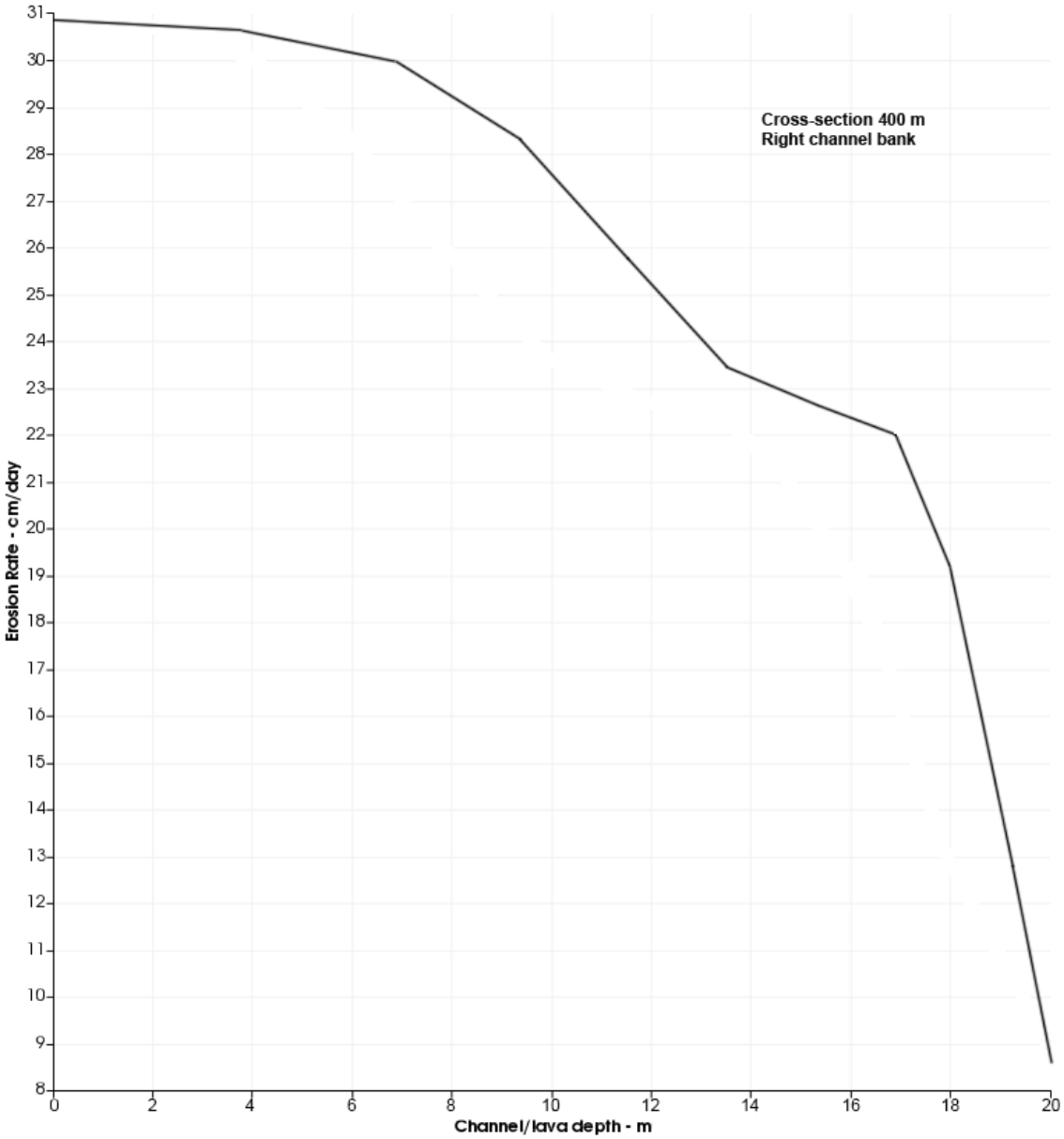

Figure 5.33b. Scenario 2 (lava flowing insulated in a tube). Erosion rates at the right bank of rille cross-section 400. Results refer to a 20-m-thick lava erupted at the liquidus temperature and flowing at a velocity of 5 m s^{-1}. Lava temperature at the bank is equal to 1400°C. Maximum erosion rates of 30.9 cm/day are found at the bank top and they decrease to a value of 23.4 cm/day down to a vertical distance of ~6 m from the underlying bank/bed contact. The sharpest decrease in erosion rate occurs within ~3 m of the contact and the minimum erosion rate of 8.6 cm/day is found at the contact itself. Maximum erosion rates are higher by a factor of ~ 8.1 than those produced at the same bank by a sub-liquidus flow of identical thickness and velocity.

The next sub-scenario deals with a 20-m-thick flow that is still erupted at the liquidus temperature but is now flowing at a faster velocity (10 m s^{-1}) (Fig. 5.34).

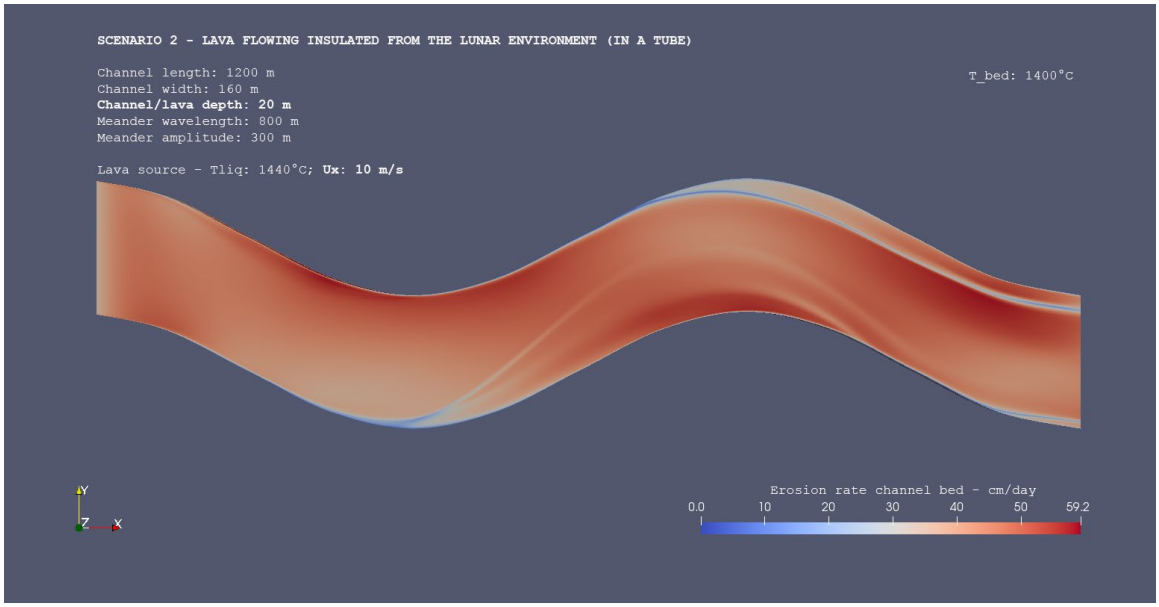

Figure 5.34. Plan view that shows erosion rates and their spatial distribution at the bed of a 1200-m-long rille section. Scenario 2 (lava flowing insulated in a tube). Erosion rates are referred to a 20-m-thick lava of T = 1440°C (liquidus), traveling at a velocity of 10 m s^{-1}. The boundary temperature is taken to be equal to 1400°C. Lava source is on the left and flow motion is rightward. Erosion highs (up to 59.2 cm/day) are concentrated at or near bend troughs whereas lows are found at/near bend apexes. Maximum erosion rates are higher by a factor of ~4.4 than those associated with a sub-liquidus lava of identical thickness and velocity.

Erosion rates at the bed of cross-section 400 are shown in Fig. 5.35. Maximum erosion rates of 54.5 cm/day are obtained within ~10 m of the bed/right bank contact. While moving toward the bed/left bank contact, erosion into the substrate decreases out to a distance of ~50 m from the contact. Then, values remain almost constant. From that point on, erosion rates drop and then slowly increase within 10 m of the contact. A minimum value of 7.9 cm/day is finally reached within 1 m of the bed/left bank contact. Maximum

erosion rates are higher by a factor of ~4.4 than those produced by a sub-liquidus flow of identical thickness and velocity.

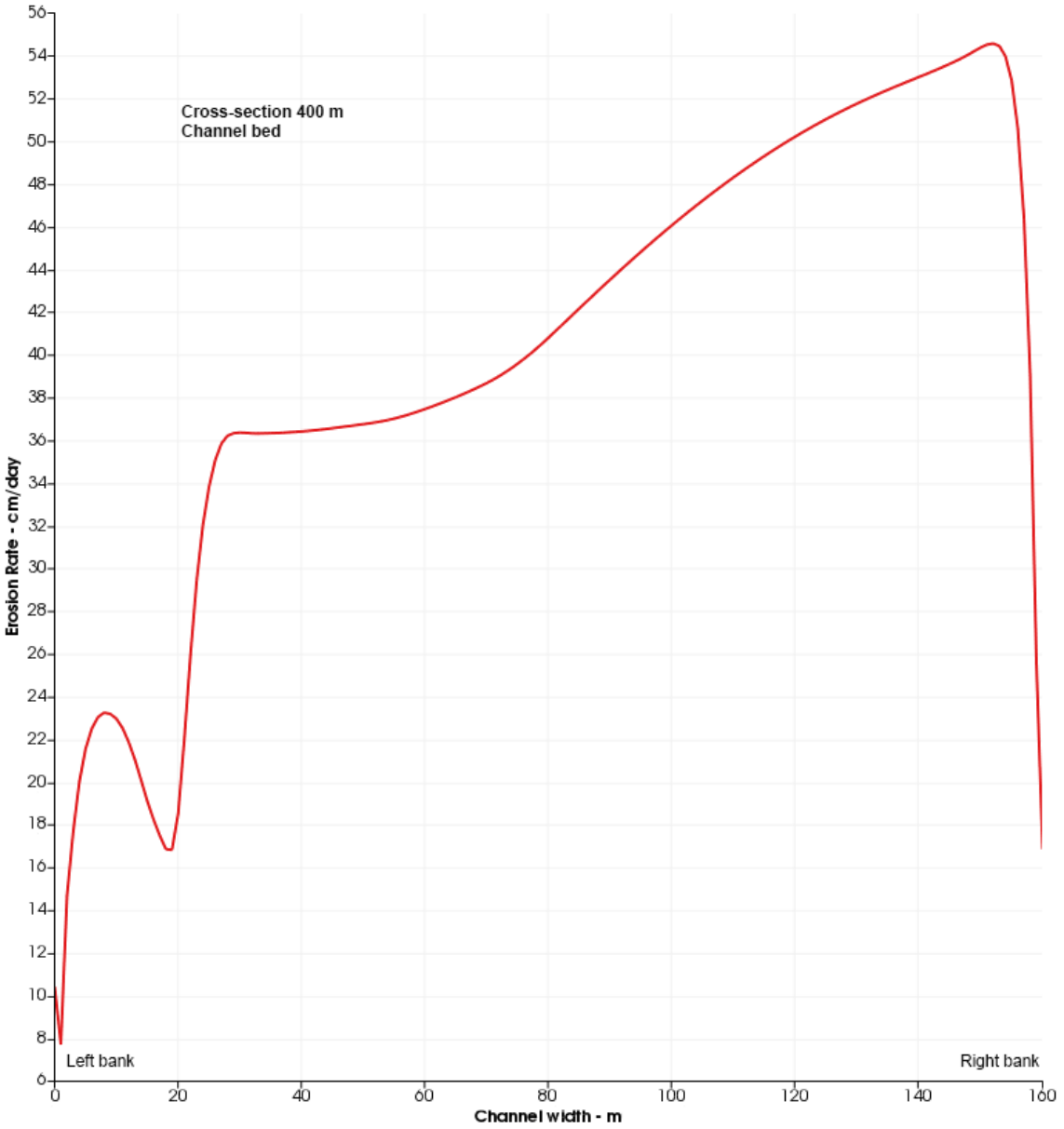

Figure 5.35. Scenario 2 (lava flowing insulated in a tube). Erosion rates at the bed of rille cross-section 400. Lava is 20 m thick and flows at the liquidus temperature (1440°C) and at a velocity of 10 m s^{-1}. Temperature at the bed is 1400°C. Maximum erosion rates of 54.5 cm/day are obtained within ~10 m of the bed/right bank contact. While moving toward the bed/left bank contact, erosion into the substrate decreases out to a distance of ~50 m from the contact. At that point, values remain almost constant. Then, they drop and slowly increase again within 10 m of the contact. A minimum value of 7.9 cm/day is finally

reached within 1 m of the bed/left bank contact. Maximum erosion rates are higher by a factor of ~4.4 than those associated with the sub-liquidus flow of identical thickness and velocity.

The distribution and magnitude of erosion rates at the left bank can be seen in Fig. 5.36a. Erosion rates increase from a value of 31.4 cm/day at the bank top to a maximum of 32.0 cm/day down to a vertical distance of ~7 m from the bank top. From that point on, they decrease faster and faster until they drop to a minimum value of 7.6 cm/day at the left bank/bed contact. The fastest drop in erosion rates occurs within ~2 m of the contact. Erosion rates are higher by a factor of 6.7 than those found at the left bank of a sub-liquidus

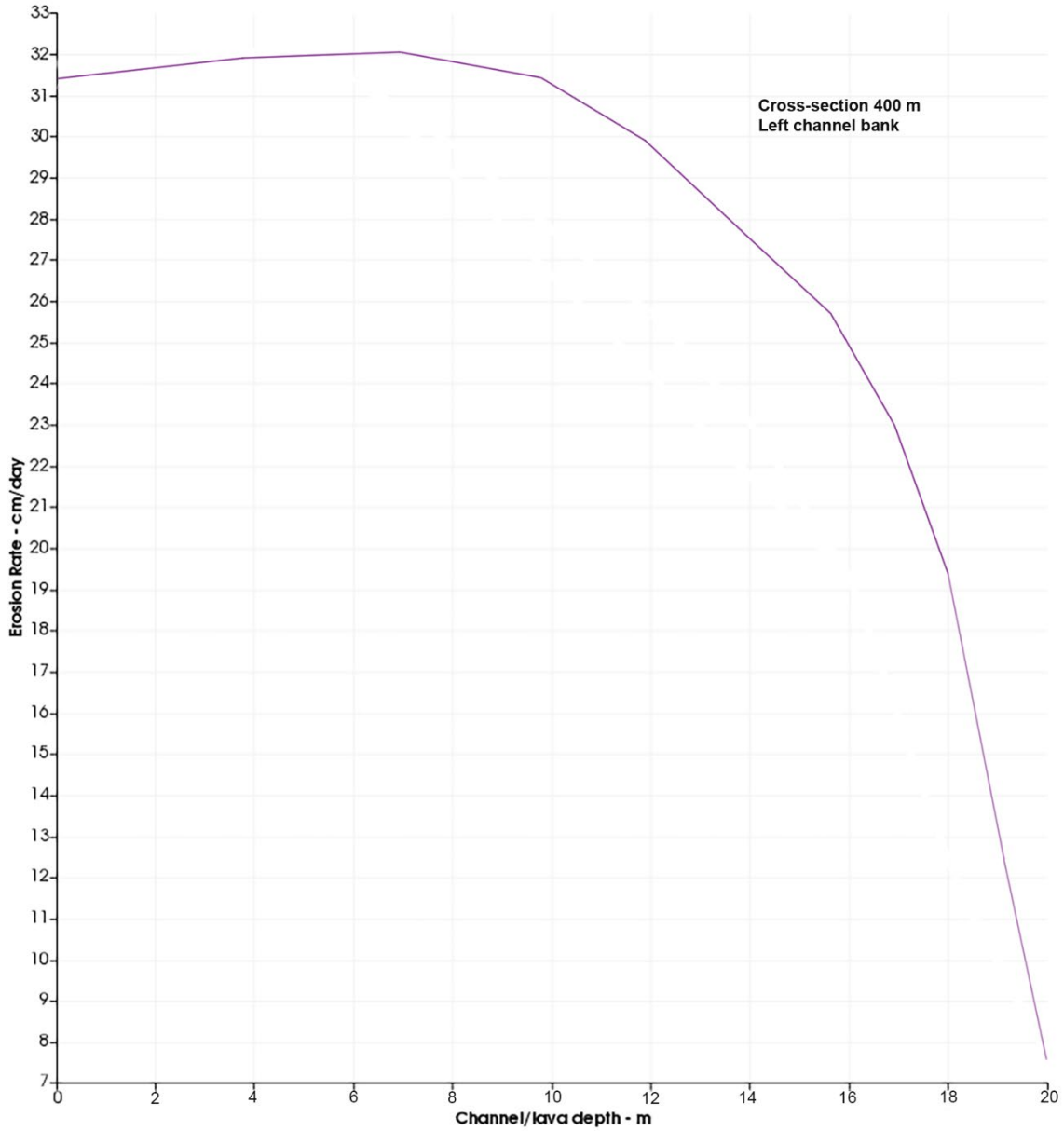

Figure 5.36a. Scenario 2 (lava flowing insulated in a tube). Erosion rates at the left bank of rille cross-section 400. Results refer to a 20-m-thick lava erupted at the liquidus temperature and traveling at a velocity of 10 m s^{-1}. Lava temperature at the bank is equal to 1400°C. Erosion rates increase from a value of 31.4 cm/day at the bank top to a maximum of 32.0 cm/day down to a vertical distance of ~7 m from the bank top. From that point on, they decrease faster and faster until they drop to a minimum value of 7.6 cm/day at the left bank/bed contact. The fastest drop in erosion rates occurs within ~2 m of the contact. Erosion rates are higher by a factor of ~6.7 than those generated at the left bank by a sub-liquidus lava (T=1390°C) of identical thickness and velocity.

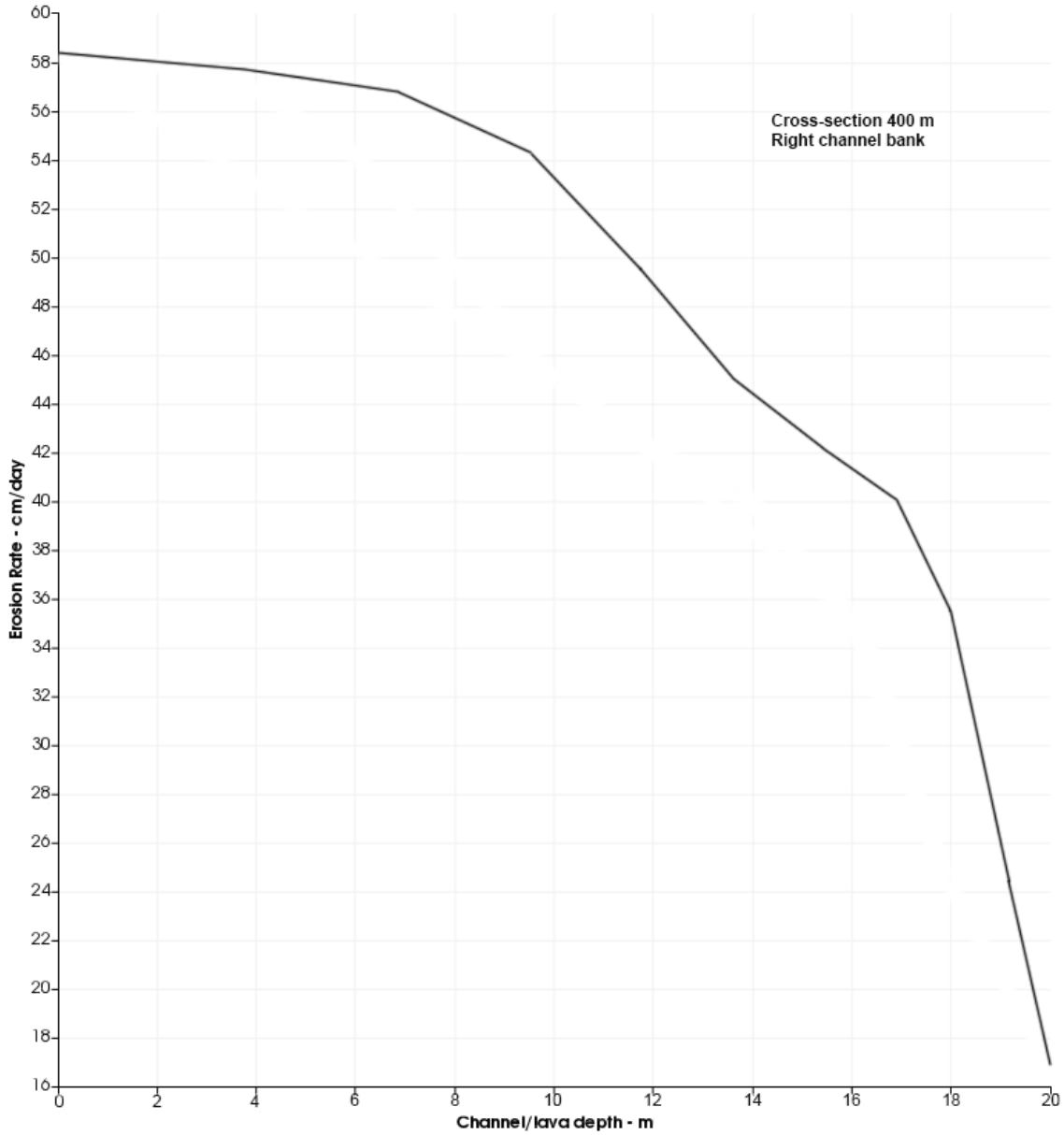

Figure 5.36b. Scenario 2 (lava flowing insulated in a tube). Erosion rates at the right bank of rille cross-section 400. Results refer to 20-m-thick lava erupted at the liquidus temperature and flowing at a velocity of 10 m s^{-1}. Lava temperature at the bank is equal to 1400°C. Maximum erosion rates of 58.3 cm/day are found at the bank top and they decrease to a value of 40.1 cm/day down to a vertical distance of ~3 m from the underlying bank/bed contact. The sharpest decrease in erosion rate occurs within ~3 m of the left bank/bed contact. Finally, the minimum erosion rate of 16.8 cm/day is found at the contact. Maximum erosion rates are higher by a factor of ~5.9 than those produced at the same bank by a sub-liquidus flow of identical thickness and velocity.

lava (T=1390°C) of identical thickness and velocity. Finally, Fig. 5.36b shows erosion rates at the right bank of cross-section 400. Maximum erosion rates of 58.3 cm/day are found at the bank top and they decrease to a value of 40.1 cm/day down to a vertical distance of ~3 m from the underlying bank/bed contact. The sharpest decrease in erosion rate occurs within ~3 m of the left bank/bed contact. Finally, the minimum erosion rate of 16.8 cm/day is found at the contact. Maximum erosion rates are higher by a factor of ~5.9 than those produced at the same bank by the sub-liquidus flow of identical thickness and velocity.

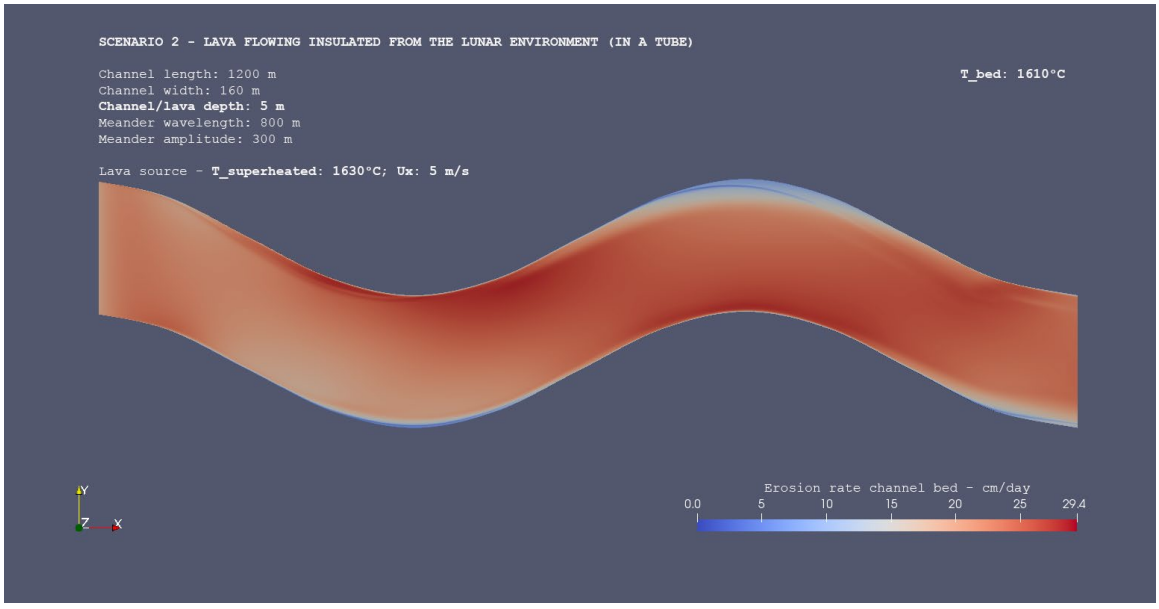

Figure 5.37. Plan view that shows erosion rates and their spatial distribution at the bed of a 1200-m-long rille section. Scenario 2 (lava flowing insulated in a tube). Erosion rates are referred to a 5-m-thick superheated lava of T = 1630°C, flowing at a velocity of 5 m s^{-1}. The boundary temperature is taken to be equal to 1610°C. Lava source is on the left and flow motion is rightward. Erosion highs (up to 29.4 cm/day) are concentrated at or near bend troughs whereas lows are found at/near bend apexes. Maximum erosion rates are higher by a factor of ~1.9 than those generated by the sub-liquidus lava of identical thickness and velocity.

The last sub-scenario deals with 5- and 10-m-thick flows that are erupted at the very high temperature of 1630°C (superheated lava) and flow at velocities of 5 m s^{-1} (5-m-thick lava)

and 5 and 10 m s^{-1} (20-m-thick lava). A plan view of the rille bed with erosion rates and their spatial distribution across the 1200-m-long rille section is shown in Fig. 5.37 and is referred to a 5-m-thick lava with initial velocity of 5 m s^{-1}. Fig. 5.38 shows the distribution and magnitude of erosion rates at the bed of cross-section 400. Maximum erosion rates of 27.9 cm/day are obtained within ~10 m of the bed/right bank contact. While moving toward the bed/left bank contact, erosion into the substrate decreases out to a distance of ~40 m from the contact. Then, values remain almost constant out to ~25 m from that contact. From that point on, erosion rates drop and then slowly increase within 5 m of the contact. A minimum value of 4.3 cm/day is finally reached within 1 m of the bed/left bank contact. Maximum erosion rates are higher by a factor of ~1.8 than those produced by a liquidus flow of identical thickness and velocity. Erosion rates at the left bank are shown in Fig. 5.39a. Erosion rates rapidly increase from a value of 6.1 cm/day at the bank top to a maximum of 7.6 cm/day ~3 m down from the bank top. From that point on, they decrease and then drop to a minimum of 4.3 cm/day at the left bank/bed contact. The fastest drop in erosion rates occurs within ~1 m of the contact. Erosion rates are found to be higher by a factor ~2.1 than those generated (at the left bank) by lava erupted at the liquidus temperature and of identical thickness and velocity.

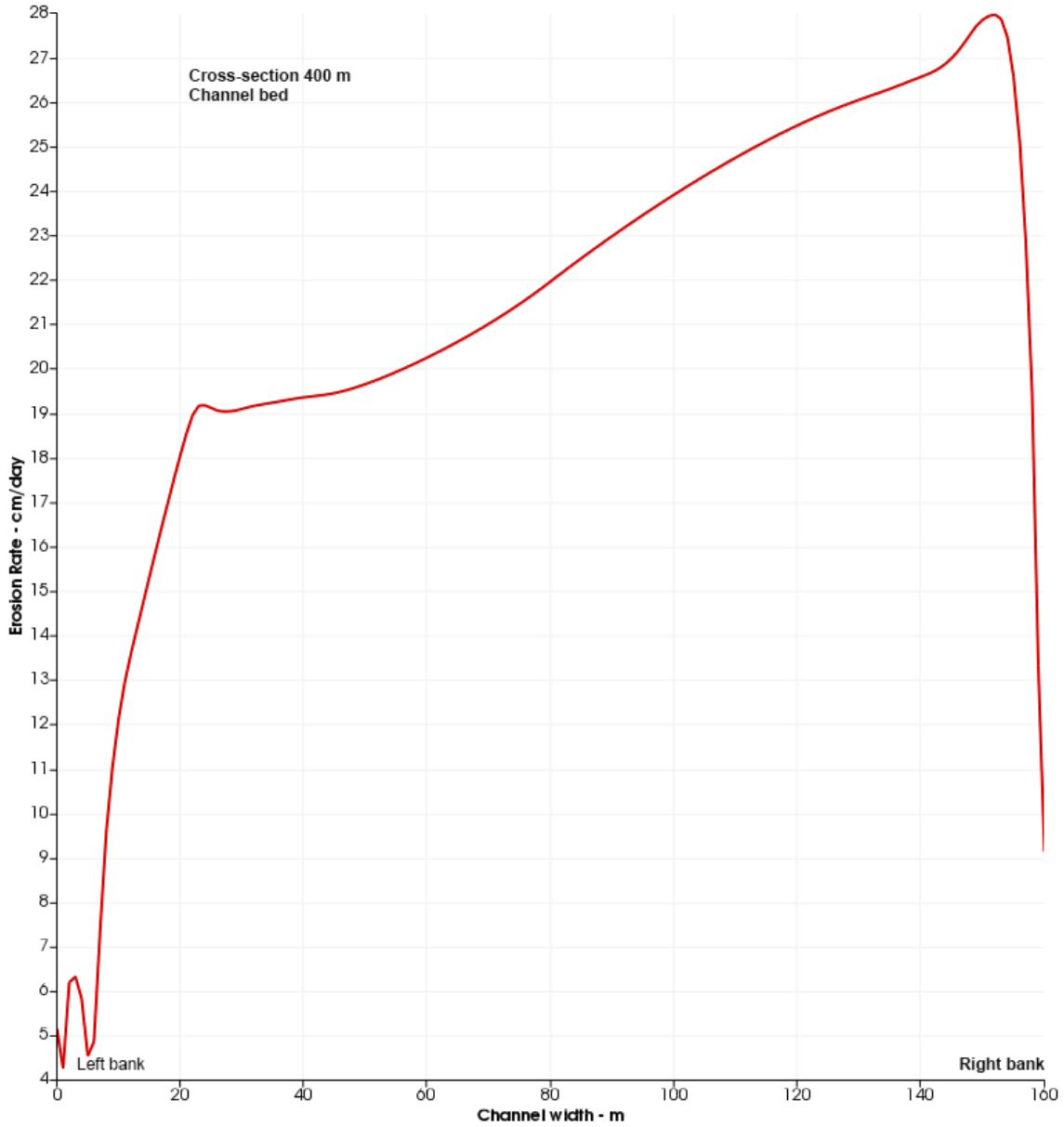

Figure 5.38. Scenario 2 (lava flowing insulated in a tube). Erosion rates at the bed of rille cross-section 400. Lava is 5 m thick and superheated (T=1630°C) and flows at a velocity of 5 m s^{-1}. Temperature at the bed is 1610°C. Maximum erosion rates of 27.9 cm/day are generated within ~10 m of the bed/right bank contact. While moving toward the bed/left bank contact, erosion into the substrate decreases. Then, values remain almost constant out to a distance of ~25 m from the contact. From that point on, erosion rates drop and then slowly increase within 5 m of the contact. A minimum value of 4.3 cm/day is finally reached within 1 m of the bed/left bank contact. Maximum erosion rates are higher by a factor of ~1.8 than those produced by a liquidus flow of identical thickness and velocity.

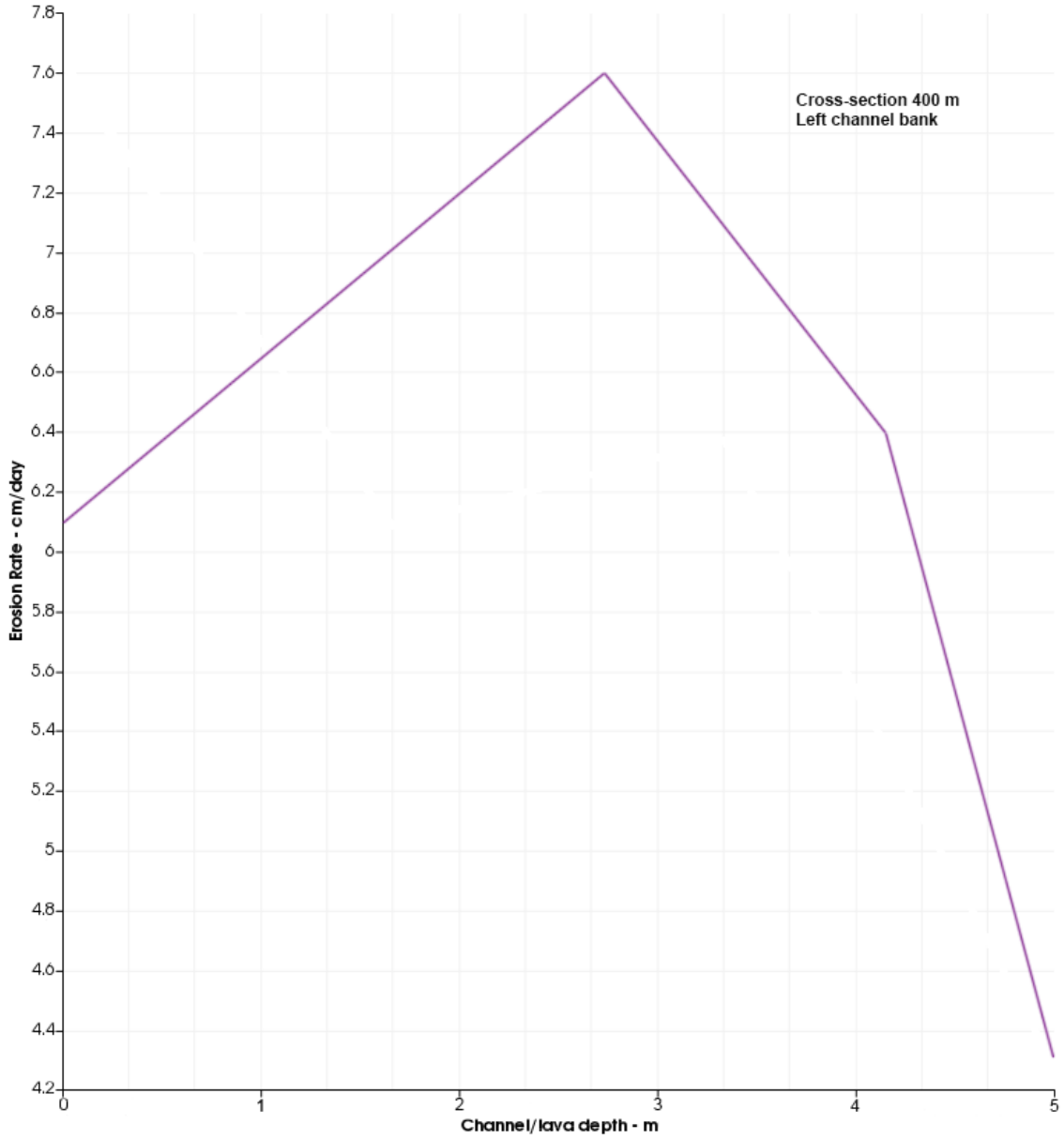

Figure 5.39a. Scenario 2 (lava flowing insulated in a tube). Erosion rates at the left bank of rille cross-section 400. Results refer to a 5-m-thick superheated lava (T=1630°C), which travels at a velocity of 5 m s^{-1}. Lava temperature at the bank is equal to 1610°C. Erosion rates rapidly increase from a value of 6.1 cm/day at the bank top to a maximum of 7.6 cm/day ~3 m down from the bank top. From that point on, they decrease and then drop to a minimum of 4.3 cm/day at the left bank/bed contact. The fastest drop in erosion rates occurs within ~1 m of the bank/bed contact. Erosion rates are found to be higher by a factor of ~2.1 than those generated at the left bank by liquidus lava of identical thickness and velocity.

Fig. 5.39b shows the distribution and magnitude of erosion rates at the right bank. Erosion rates of 17.6 cm/day are found at the bank top and from there they increase until they reach a maximum of ~17.7 cm/day at a vertical distance of ~2 m from the underlying bank/bed contact. Then, erosion rates drop till a minimum value of 9.2 cm/day is reached at the contact. The maximum erosion rate is higher by a factor of ~1.9 than that produced by a liquidus lava of identical thickness and velocity.

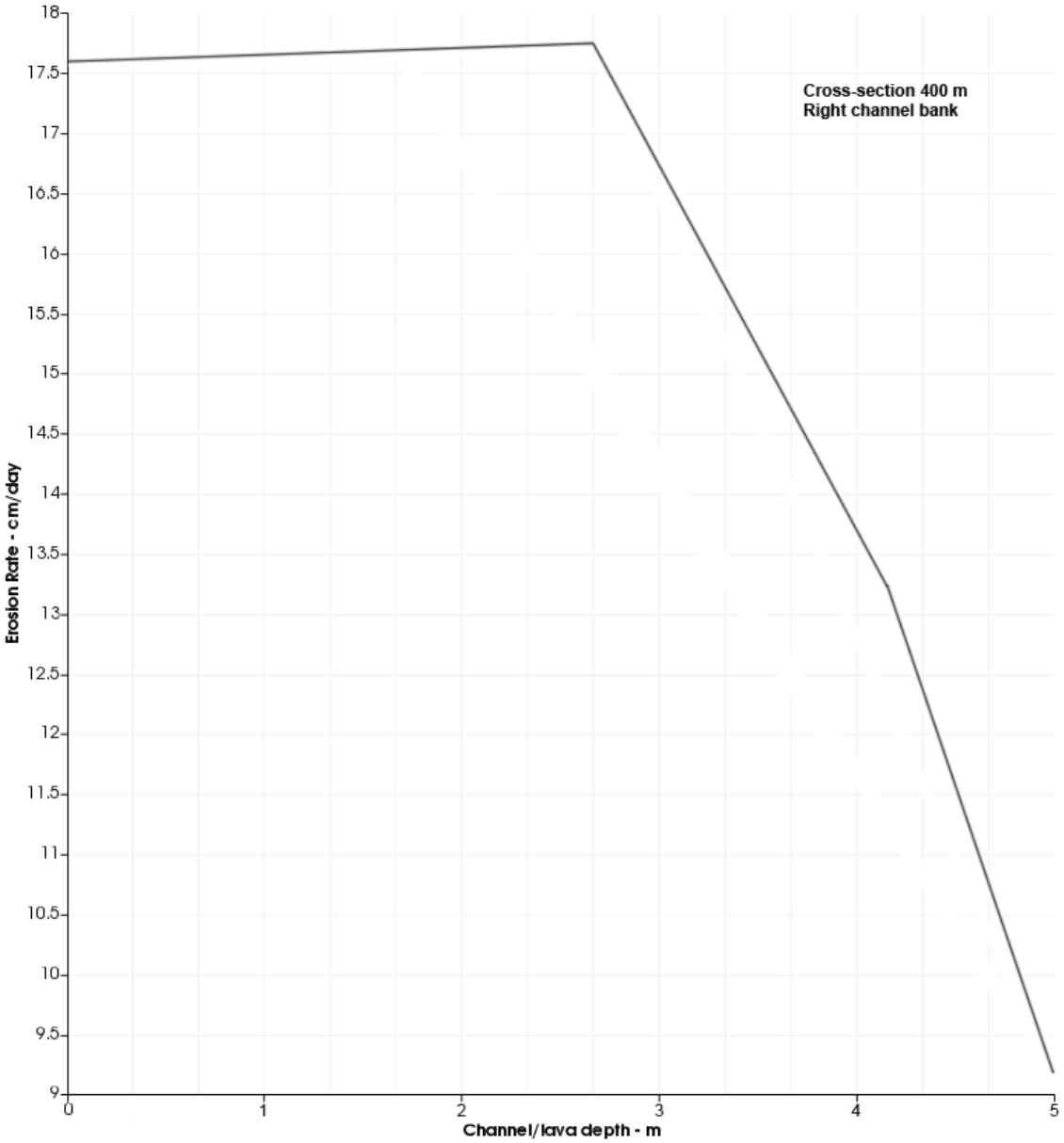

Figure 5.39b. Scenario 2 (lava flowing insulated in a tube). Erosion rates at the right bank of rille cross-section 400. Results refer to a 5-m-thick superheated lava (T=1630°C) flowing at a velocity of 5 m s^{-1}. Lava temperature at this bank is equal to 1610°C. Erosion rates of 17.6 cm/day are found at the bank top and from there they increase until they reach a maximum of 17.75 cm/day at a vertical distance of ~2 m from the underlying bank/bed contact. Then, erosion rates drop till a minimum value of 9.2 cm/day is reached at the right bank/bed contact. The maximum erosion rate is higher by a factor of ~1.9 than that produced by a liquidus lava of identical thickness and traveling at the same velocity.

The next sub-scenario deals with a 20-m-thick flow that is erupted at a superheated temperature of 1630°C and flows at a velocity of 5 m s^{-1}. The temperature at the bed and banks is equal to 1590°C (Fig. 5.40).

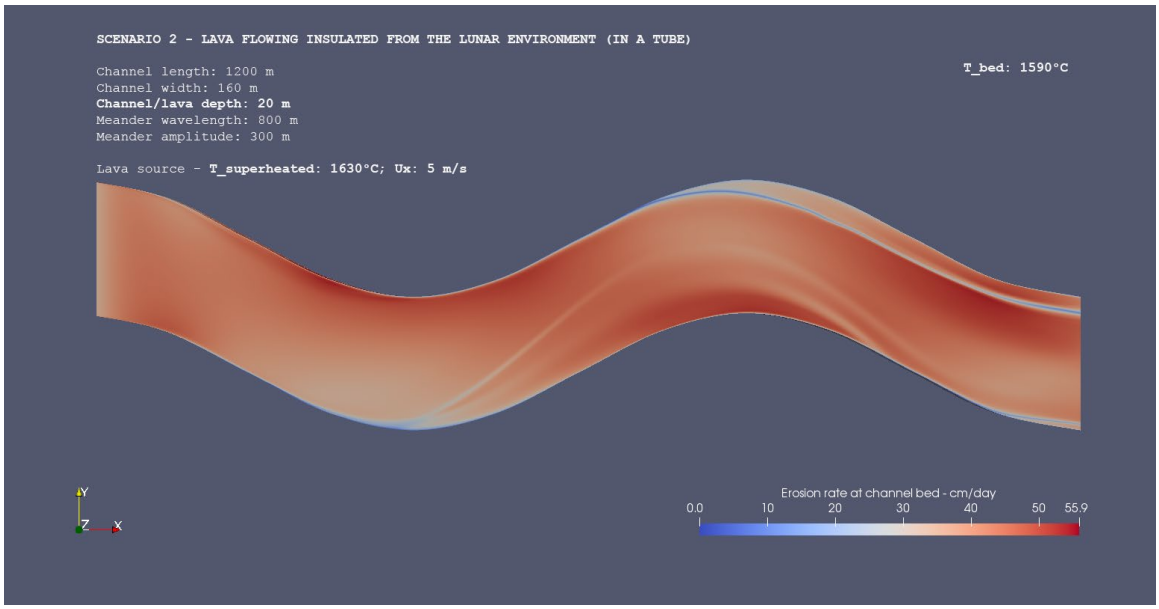

Figure 5.40. Plan view that shows erosion rate values and their spatial distribution at the bed of a 1200-m-long rille section. Scenario 2 (lava flowing insulated in a tube). Erosion rates are referred to a 20-m-thick superheated lava of T = 1630°C and flowing at a velocity of 5 m s^{-1}. The boundary temperature is taken to be equal to 1590°C. Lava source is on the left and flow motion is rightward. Erosion highs (up to 55.9 cm/day) are concentrated at or near bend troughs whereas lows are found at/near bend apexes. Maximum erosion rates are higher by a factor of ~1.8 than those associated with a liquidus lava of identical thickness and velocity.

Fig. 5.41 shows the erosion rate distribution and magnitude at the bed of cross-section 400. Maximum erosion rates of 50.7 cm/day are obtained within ~10 m of the bed/right bank contact. While moving toward the bed/left bank contact, erosion into the substrate decreases at an almost constant rate out to a distance of ~70 m from the contact. Then, values keep decreasing though at a slower rate out to ~25 m from the bed/left bank contact. From that point on, erosion rates drop and then slowly increase within 10 m of the contact.

A minimum value of 8.0 cm/day is finally reached within 1 m of the contact. Maximum erosion rates are higher by a factor of ~1.7 than those associated with a liquidus flow of identical thickness and velocity. Erosion at the left bank is shown in Fig. 5.42a. Erosion rates increase from a value of 28.5 cm/day at the bank top to a maximum of 29.7 cm/day down to a vertical distance of ~10 m from the bank top. From that point on, they decrease faster and faster and drop to a minimum value of 8.0 cm/day at the left bank/bed contact. The fastest drop in erosion rates occurs within ~3 m of the contact. Erosion rate values are higher by a factor of ~1.7 than those produced at the left bank by liquidus lava of identical thickness and velocity. Fig. 5.42b shows the magnitude and distribution of erosion rates at the right bank of cross-section 400. Erosion rates of 54.9 cm/day are found at the bank top and from there they decrease at a progressively faster rate and reach a minimum of 15.4 cm/day at the right bank/bed contact. The fastest decrease in erosion rate occurs within a vertical distance of 3-2 m of the contact. The maximum value is higher by a factor of ~1.8 than that obtained by the liquidus lava of identical thickness and velocity.

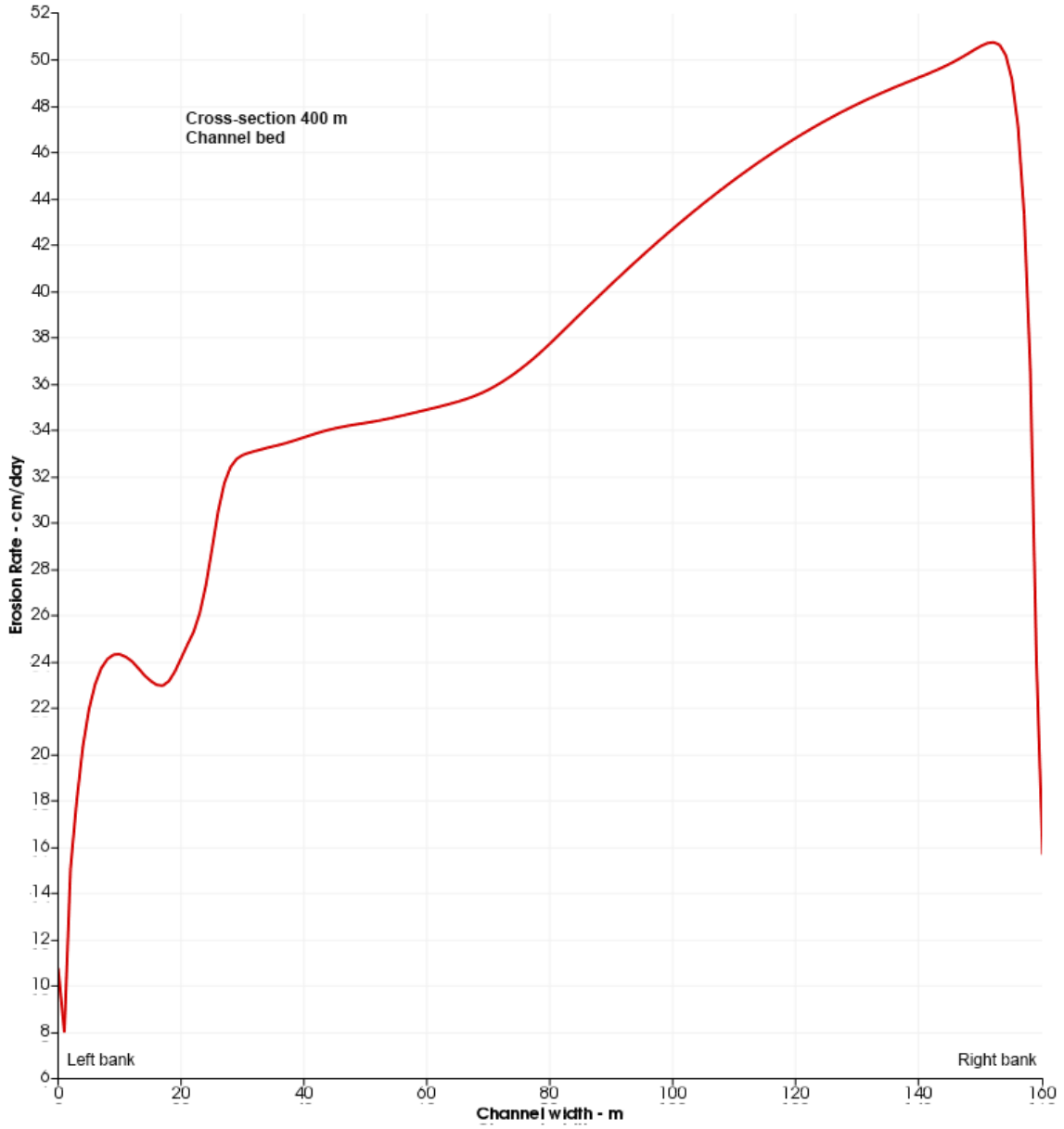

Figure 5.41. Scenario 2 (lava flowing insulated in a tube). Erosion rates at the bed of rille cross-section 400. Lava is 20 m thick and superheated (T=1630°C) and flows at a velocity of 5 m s^{-1}. Temperature at the bed is 1590°C. Maximum erosion rates of 50.7 cm/day are obtained within ~10 m of the bed/right bank contact. While moving toward the bed/left bank contact, erosion into the substrate decreases at an almost constant rate out to ~70 m from the contact. Then, values keep decreasing - though at a slower rate - out to ~25 m from the contact. From that point on, erosion rates drop and then slowly increase within 10 m of the contact. A minimum value of 8.0 cm/day is found within 1 m of the bed/left bank contact. Maximum erosion rates are higher by a factor of ~1.7 than those associated with a liquidus flow of identical thickness and velocity.

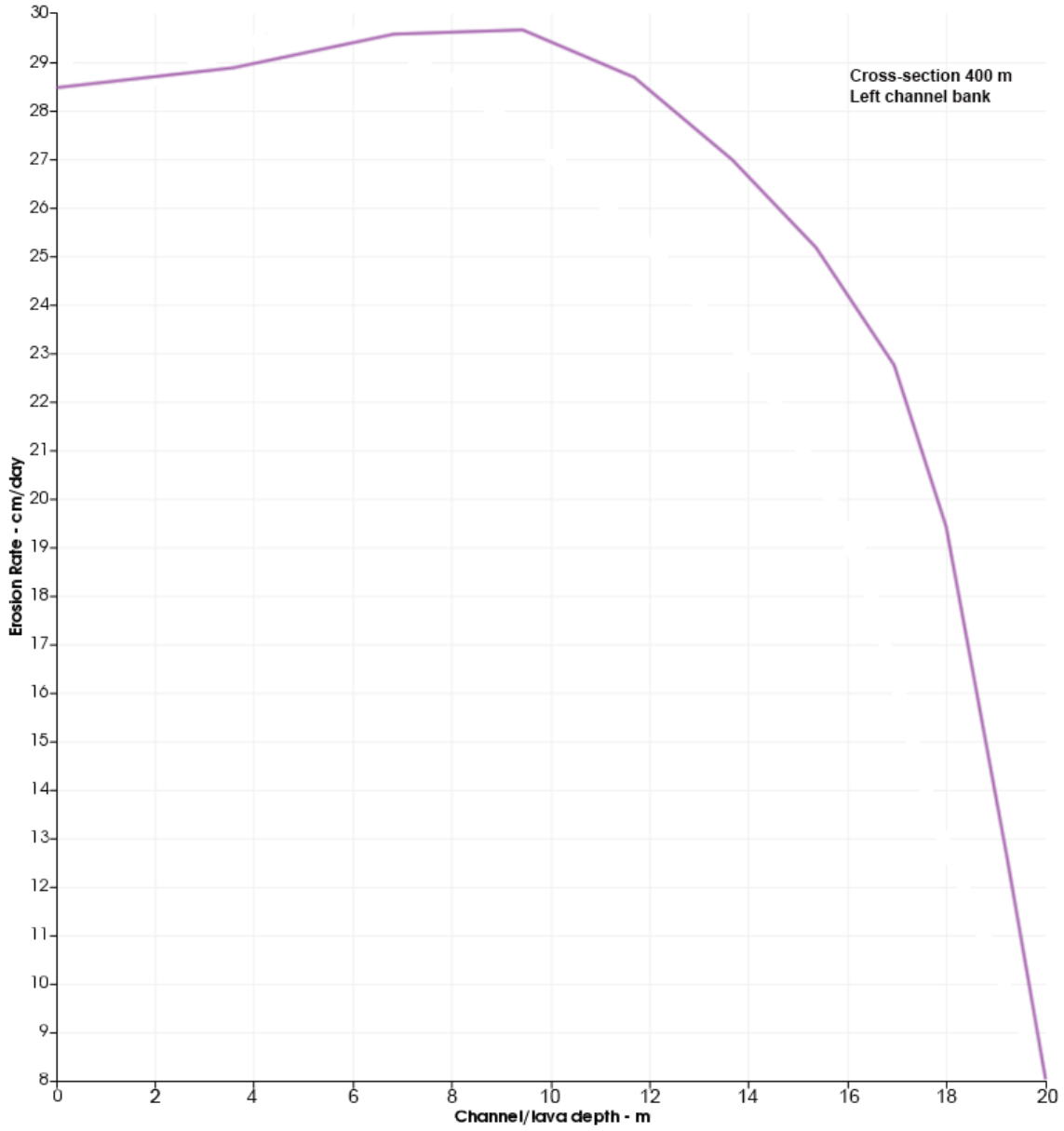

Figure 5.42a. Scenario 2 (lava flowing insulated in a tube). Erosion rates at the left bank of rille cross-section 400. Results refer to a 20-m-thick superheated lava (T=1630°C) that flows at a velocity of 5 m s^{-1}. Lava temperature at the bank is equal to 1590°C. Erosion rates increase from a value of 28.5 cm/day at the bank top to a maximum of 29.7 cm/day down to a vertical distance of ~10 m from the bank top. From that point on, they decrease faster and faster and drop to a minimum value of 8.0 cm/day at the left bank/bed contact. The fastest drop in erosion rates occurs within ~3 m of the contact. Erosion rates are higher by a factor of ~1.7 than those generated at the left bank by a liquidus lava of identical thickness and velocity.

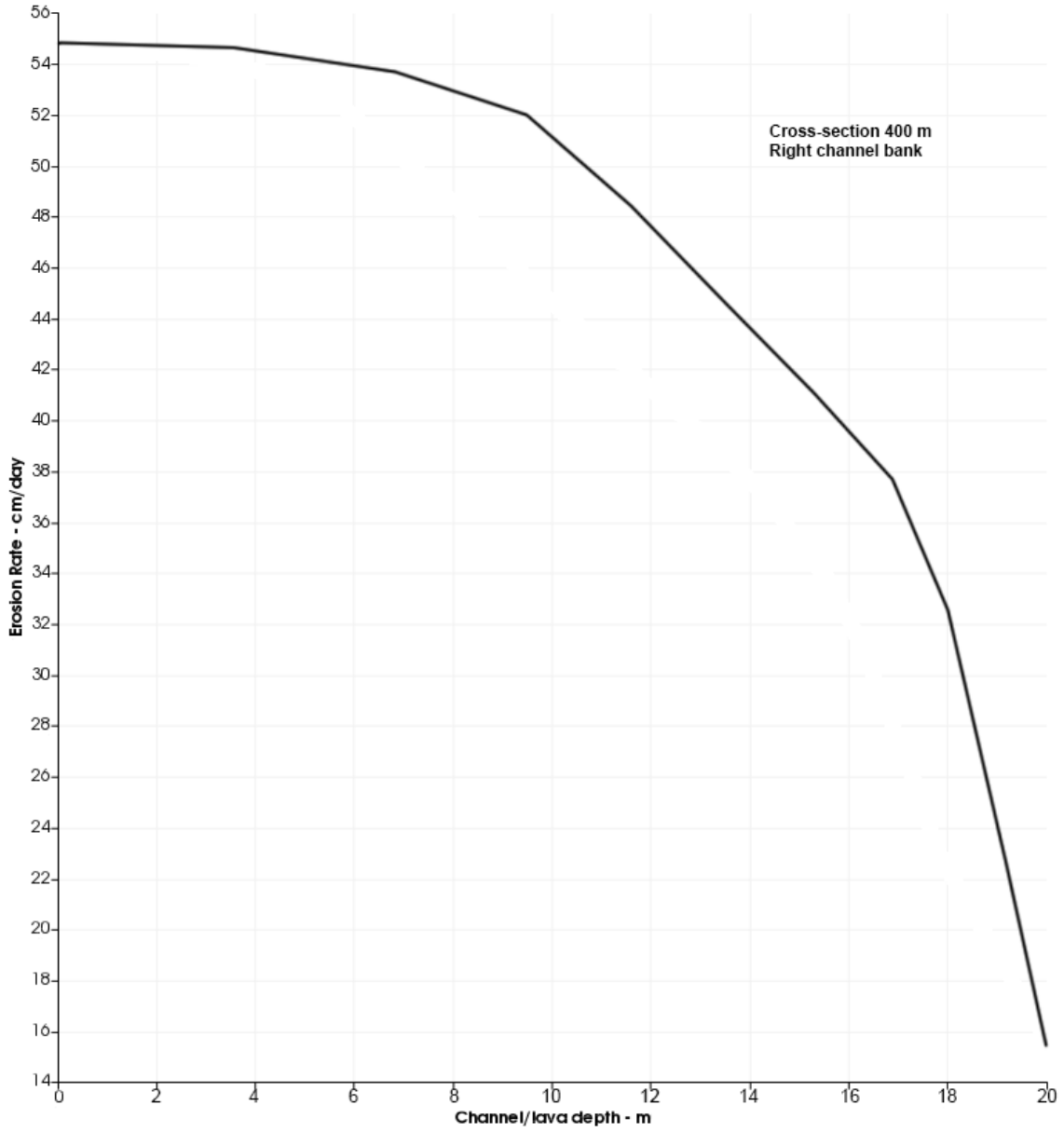

Figure 5.42b. Scenario 2 (lava flowing insulated in a tube). Erosion rates at the right bank of rille cross-section 400. Results refer to a 20-m-thick superheated lava (T=1630°C) flowing at a velocity of 5 m s^{-1}. Lava temperature at the bank is equal to 1590°C. Erosion rates of 54.9 cm/day are found at the bank top and from there they decrease at a progressively faster rate and reach a minimum of 15.4 cm/day at the right bank/bed contact. The fastest decrease in erosion rate occurs within a vertical distance of 3-2 m of the contact. The maximum value is higher by a factor of ~1.8 than that produced by a liquidus lava of identical thickness and velocity.

The last sub-scenario deals with a 20-m-thick superheated lava (T=1630°C) that flows at a velocity of 10 m s^{-1}. The temperature at the channel bed and banks is equal to 1590°C. This is by far the flow expected to produce the highest erosion rates among those considered until now. Fig. 5.43 shows a plan view of the bed with erosion rate magnitudes and their spatial distribution across the 1200-m-long rille section. At the 1200-m-long rille section,

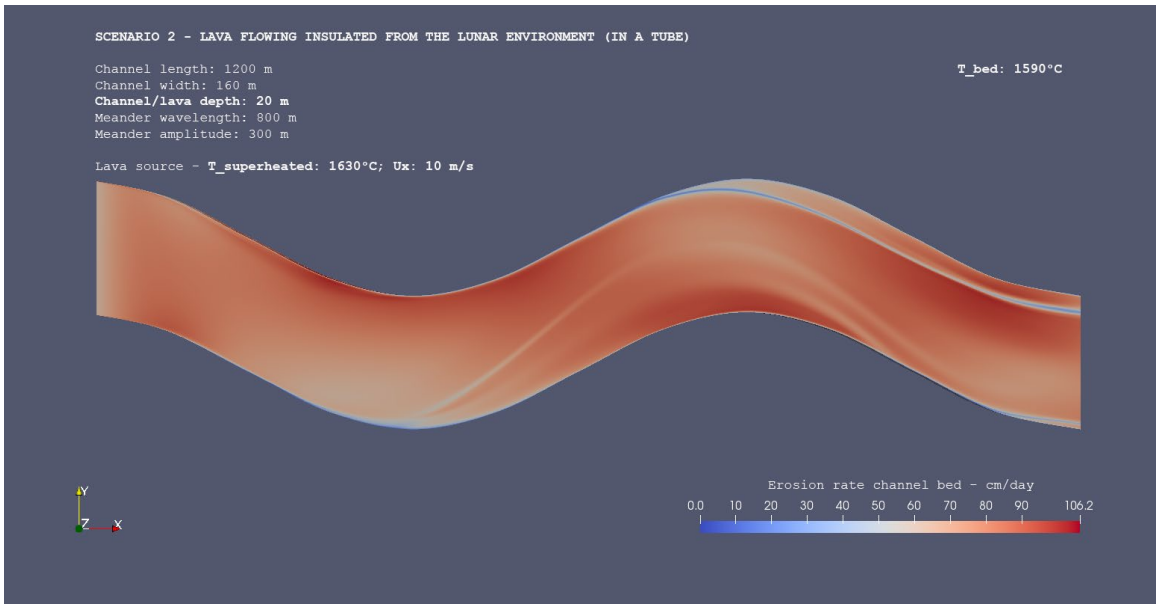

Figure 5.43. Plan view that shows erosion rate values and their spatial distribution at the bed of a 1200-m-long rille section. Scenario 2 (lava flowing insulated in a tube). Erosion rates are referred to a 20-m-thick superheated lava of T = 1630°C and flowing at a velocity of 10 m s^{-1}. The interface temperature is taken to be equal to 1590°C. Lava source is on the left and flow motion is rightward. Erosion highs (up to 106.2 cm/day) are concentrated at or near bend troughs whereas lows are found at/near bend apexes. Maximum erosion values are higher by a factor of ~1.8 than those associated with a liquidus lava of identical thickness and velocity.

maximum erosion values are higher by a factor of ~1.8 than those associated with the liquidus lava of identical thickness and velocity. Values of erosion at the rille bed are shown in Fig. 5.44. Maximum erosion rates of 96.0 cm/day are obtained within ~10 m of the bed/right bank contact. While moving toward the bed/left bank contact, erosion into the

substrate decreases at an almost constant rate out to a distance of ~70 m from the contact. Then, values keep decreasing - though at a slower rate - out to ~50 m from the bed/left bank contact. From that point on, erosion rates decrease at a faster rate even though the trend is discontinued due to the presence of a couple of steps in which erosion rates stop decreasing. A minimum value of 16.0 cm/day is finally reached within 1 m of the bed/left bank contact. Maximum erosion rates are higher by a factor of ~1.8 than those associated with the liquidus flow of identical thickness and velocity.

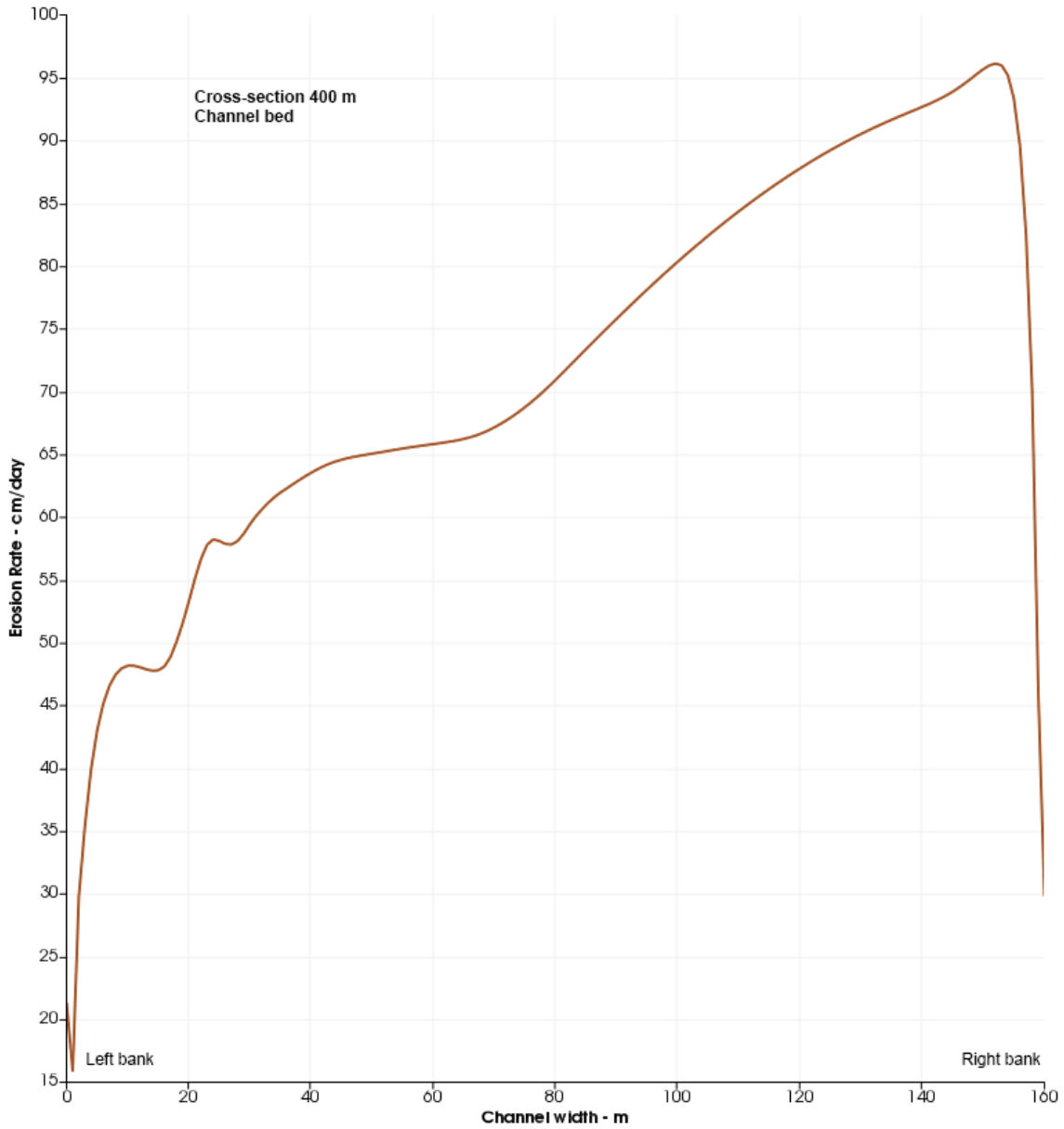

Figure 5.44. Scenario 2 (lava flowing insulated in a tube). Erosion rates at the bed of rille cross-section 400. Lava is 20 m thick and superheated (T=1630°C) and flows at a velocity of 10 m s^{-1}. Temperature at the bed is 1590°C. Maximum erosion rates of 96.0 cm/day are obtained within ~10 m of the bed/right bank contact. While moving toward the bed/left bank contact, erosion into the substrate decreases at an almost constant rate out to ~70 m from the contact. Then, values keep decreasing - though at a slower rate - out to ~50 m from the contact. From that point on, erosion rates decrease at a faster rate even though the trend is discontinued due to the presence of a couple of steps in which erosion rates stop decreasing. A minimum value of 16.0 cm/day is finally reached within 1 m of the bed/left bank contact. Maximum erosion rates are higher by a factor of ~1.8 than those associated with the liquidus flow of identical thickness and velocity.

Fig. 5.45a shows the distribution of erosion rates at the left bank. Erosion rates increase from a value of 53.4 cm/day at the bank top to a maximum of 56.0 cm/day at a vertical distance of ~10 m from the bank top. From that point on, they decrease faster and faster and drop to a minimum value of 15.9 cm/day at the left bank/bed contact. The fastest drop in erosion rates occurs within ~2 m of the same contact. Erosion rate values are higher by a factor of ~1.8 than those obtained at the left bank by liquidus lava of identical thickness and velocity. Finally, erosion rates at the right bank are shown in Fig. 5.45b. Values of 104.9 cm/day are found at the bank top and from there they decrease at a progressively faster rate and reach a minimum of ~29.9 cm/day at the right bank/bed contact. The fastest decrease in erosion rate occurs within a vertical distance of 3-2 m of the contact. The maximum value is higher by a factor of ~1.8 than that obtained by a liquidus lava of identical thickness and traveling at the same velocity.

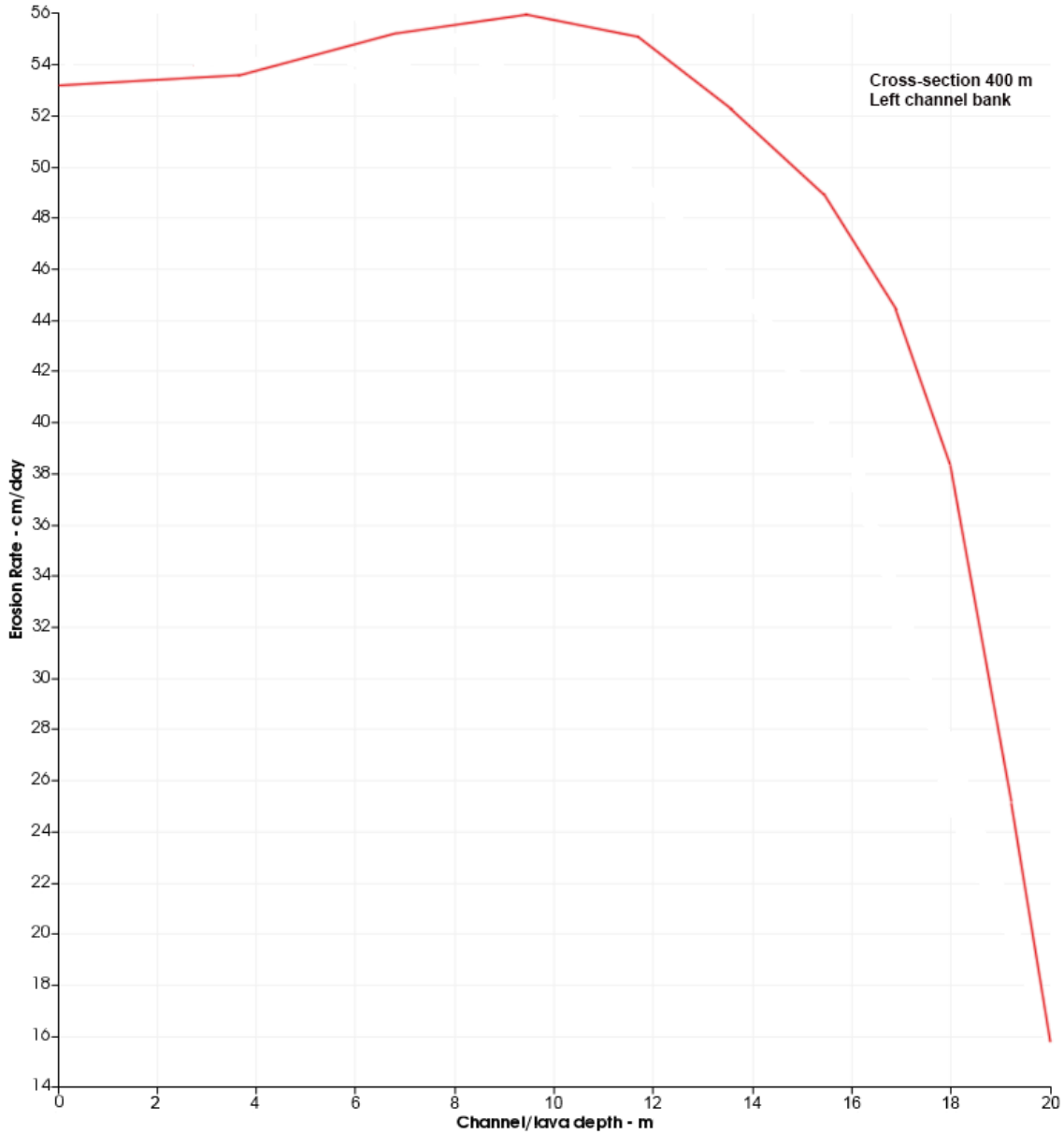

Figure 5.45a. Scenario 2 (lava flowing insulated in a tube). Erosion rates at the left bank of rille cross-section 400. Results refer to a 20-m-thick superheated lava (T=1630°C) that flows at a velocity of 10 m s^{-1}. Lava temperature at the bank is equal to 1590°C. Erosion rates increase from a value of 53.4 cm/day at the bank top to a maximum of 56.0 cm/day at a vertical distance of ~10 m from the bank top. From that point on, they decrease faster and faster and drop to a minimum value of 15.9 cm/day at the left bank/bed contact. The fastest drop in erosion rates occurs within ~2 m of the contact. Erosion rates are higher by a factor of ~1.8 than those obtained at the left bank by liquidus lava of identical thickness and velocity.

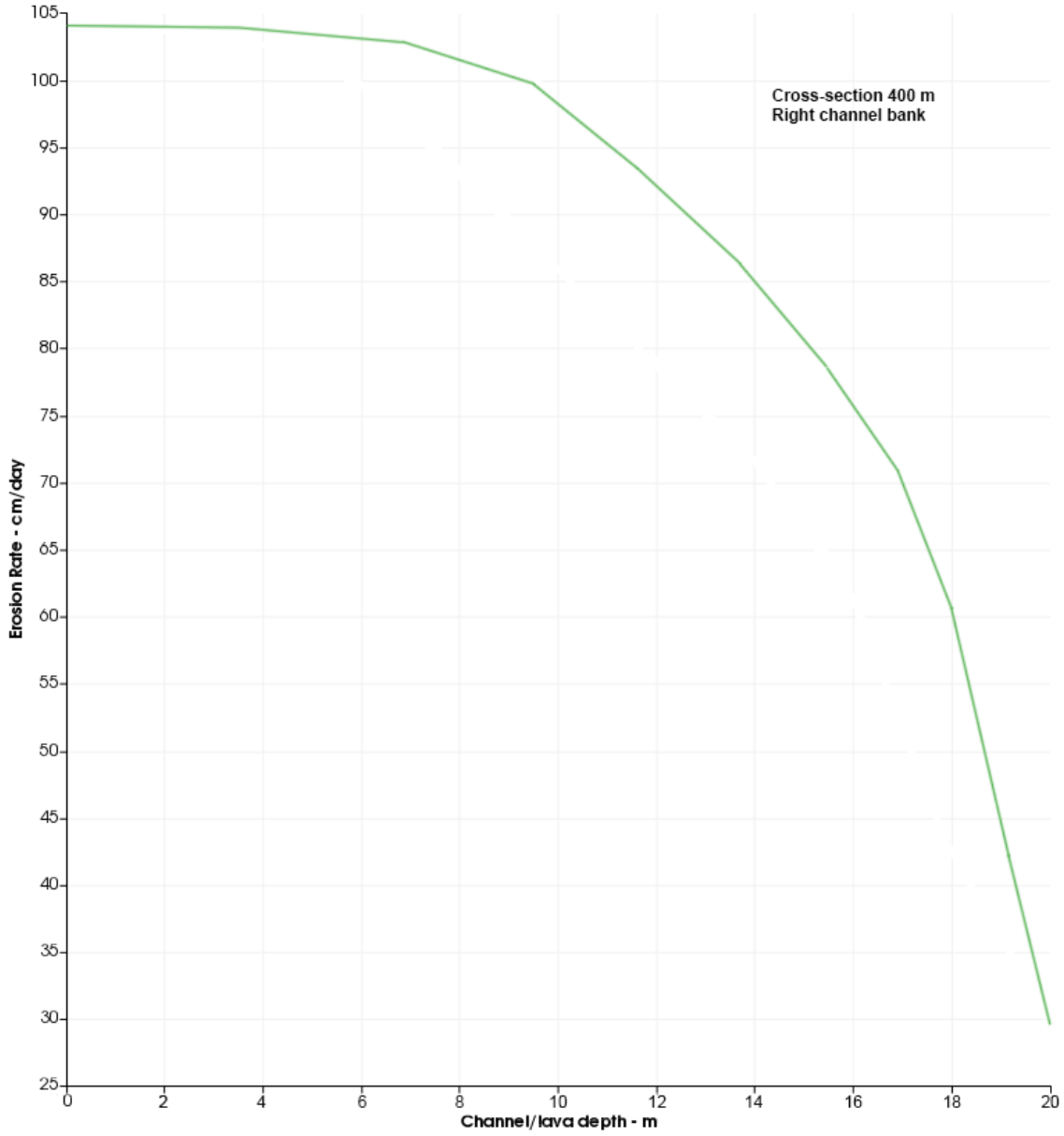

Figure 5.45b. Scenario 2 (lava flowing insulated in a tube). Erosion rates at the right bank of rille cross-section 400. Results refer to a 20-m-thick superheated lava (T=1630°C) flowing at a velocity of 10 m s^{-1}. Lava temperature at the bank is equal to 1590°C. Erosion rates of 104.9 cm/day are found at the bank top and from there they decrease at a progressively faster rate and reach a minimum of 29.95 cm/day at the bank/bed contact. The fastest decrease in erosion rate occurs within a vertical distance of 3-2 m of the contact. The maximum value is higher by a factor of ~1.8 than that generated by a liquidus lava of identical thickness and traveling at the same velocity.

Scenario 2 – The convective heat transfer coefficient h_T

This section shows how values of the convective heat transfer coefficient, h_T, vary depending on eruption conditions (temperature and flow velocity), lava thickness and location in the channel section of interest. As for scenario 1 flows, the h_T values shown in Table 5.5 are calculated at rille cross-section 400 (bend 1, see Fig. 2.2a). Results confirm that h_T values increase with increasing lava temperatures, thickness and flow rates.

Table 5.5 – Scenario 2. Values of the heat transfer coefficient, h_T, at the lava substrate (bed and banks) at inner rille cross-section 400 (section cut parallel to the axis of bend 1). h_T values are obtained from Eq. (10). All results refer to the three sub-scenarios (sub-liquidus, liquidus and superheated) in the text. Flow velocities are 5 m s^{-1} for the 5-m-thick lava and 5 and 10 m s^{-1} for the 20-m-thick flow. Suffixes "$_{5to10mfrb}$" stands for 5 to 10 meters from right bank; "$_{bed/left\ bank}$" indicates that the value is measured at the contact (where the two boundaries meet); "$_{right\ bank\ \#md}$" and "$_{left\ bank\ \#md}$" indicate that the h_T value is measured at the right or left bank, # meters down from the bank top (here 3, 7, or 10 meters down from the bank top).

SCENARIO 2 - Values of the heat transfer coefficient, h_T, at the lava substrate (bed and banks)									
T_{lava}	T_{interf}	h	U_x	$h_{T\_bed/5to10mfrb}$	$h_{T\_bed/left\ bank}$	$h_{T\_right\ bank\ top}$	$h_{T\_right\ bank\ \#md}$	$h_{T\_left\ bank\ top}$	$h_{T\_left\ bank\ \#md\_}$
°C	°C	m	m s^{-1}	J m^{-2} s^{-1} $°C^{-1}$					
1380	1360	5	5	14.1	0.7	8.2	8.7 $_{3md}$	1.3	< 1.3
1440	1420	5	5	45.7	6.9	27.8	28.4	8.7	10.8 $_{3md}$
1630	1610	5	5	52.2	9.5	32.9	33.2 $_{3md}$	11.4	14.2
1390	1350	20	5	34.8	0.4	9.2	15.7	11.4	< 11.4
1440	1400	20	5	94.2	15.9	100.0	< 100.0	55.7	56.2 $_{4md}$
1630	1590	20	5	99.2	21.1	107.4	< 107.4	55.8	58.1 $_{10md}$
1380	1340	20	10	53.1	0.9	15.8	42.7 $_{14md}$	20.5	< 20.5
1440	1400	20	10	176.4	33.0	188.7	< 188.7	101.6	103.6 $_{7md}$
1630	1590	20	10	187.8	42.5	205.3	< 205.3	104.5	109.6 $_{10md}$

A 5-m-thick lunar lava that flows over a substrate with a slope of the ground as low as 0.2° (value measured at the inner rille location) can only travel at a velocity that is no faster than

5 m s^{-1}. This constrains the amount of erosion attainable by 5-m-thick flows by making values of h_T smaller than those associated with flows that travel at a faster velocity. In other words, h_T and erosion rates vary in proportion, as can be inferred by looking at Eq. (10). The most intriguing result is the big difference in h_T values at different channel locations, which is remarkable even for the same flow. For a superheated lava that flows at a velocity of 10 m s^{-1}, h_T values jump from a value as small as 42.5 J m^{-2} s^{-1} °C^{-1} at the bed/left bank contact to a value of 205.3 J m^{-2} s^{-1} °C^{-1} at the top of the bank located on the opposite side of the channel, an increase by a factor of ~4.8. When considering a flow thickness of 5 m instead of 20 m, the ratio of the two values amounts to a factor of ~3.5. As seen before (in scenario 1 and in the sensitivity analysis chapter), there is a substantial difference in erosion rates at the two banks, with the right bank showing much higher values than the left bank. The maximum h_T values listed in Table 5.5 are higher than many of those shown in Table 5.4. This is partly a consequence of the higher initial temperatures assumed for scenario 2 lavas. *Williams et al*. (2000) found a value of h_T equal to 217 J m^{-2} s^{-1} °C^{-1} for a 10-m-thick flow of composition identical to that assumed here and erupted at the liquidus temperature. The maximum h_T value found for the baseline model, i.e., a 10-m-thick lava erupted at the liquidus temperature and flowing at a velocity of 7 m s^{-1}, is equal to 88.9 J m^{-2} s^{-1} °C^{-1}. This value is smaller by a factor of ~2.4 than that found by *Williams et al.* (2000).

Even if channel boundaries have identical lava temperature and viscosity, values of the convective heat transfer coefficient and the associated erosion rates are extremely heterogeneous. It is necessary to investigate flow circulation in detail and localize the areas

of thermal anomaly likely responsible for the heterogeneous distribution of h_T and erosion rates at channel boundaries. This is the subject of the following chapter section.

Scenario 2 – Summary

Scenario 2 includes flow sub-scenarios for which lava is assumed to have flowed insulated from the lunar environment, within a tube. The flowing lava is assumed to have preserved the temperature that originally had prior to erupting onto the lunar surface at the lava source or within a downstream distance of ~1 km from there. As a result, this section shows the highest erosion rates that might have been obtained by the flowing lava at the Vallis Schröteri inner rille site. The sub-section titled "Scenario 2 – Erosion rates at channel cross-section 400", shows erosion rates into the rille bed and banks, obtained by flows that are 5- and 20-m-thick and travel at velocities of 5 m s^{-1} (5- and 20-m-thick lavas) and 10 m s^{-1} (20-m-thick lavas only). All erosion rates refer to lava eruption temperatures of 1630°C (superheated lava), 1440°C (liquidus lava) and 1380°C (sub-liquidus lava). The highest erosion rates (at the bed and banks) of ~96-104.9 cm/day are associated with 20-m-thick lavas erupted at a temperature of 1630°C (superheated lava) and traveling at a velocity of 10 m s^{-1} (Figs. 5.44 and 5.45 a, b). The lowest erosion rates of ~0.3-3.6 cm/day are produced by a 5-m-thick lava traveling at a velocity of 5 m s^{-1} and erupted at the sub-liquidus temperature of 1380°C (Figs. 5.3 and 5.4 a, b). The sub-liquidus temperature assumed for scenario 2 flows (T=1380°C) is lower than that assumed for the counterpart scenario 1 lavas (T=1400°C), which explains the lower erosion rates associated with scenario 2 sub-liquidus lavas. Once again, the magnitude and spatial distribution of erosion

rates at the rille bed and the two banks of channel cross-section 1 are very heterogeneous for reasons that are explained at the end of this chapter in the section titled "Theoretical study". The identical pattern of erosion found for scenario 1 flows is found here because the highest erosion rates are always located at the bed within a few meters of the bed/right bank contact and at the right bank either at the bank top or within 4-6 m of the bank/bed contact. The latter scenario suggests that undercutting might have occurred over discrete portions of the rille banks. The last section titled "Scenario 2 – The convective heat transfer coefficient h_T" illustrates values of the convective heat transfer, h_T, into the rille bed and banks. The highest values of h_T (187.8-205.3 J m^{-2} s^{-1} $°C^{-1}$) are associated with a 20-m-thick superheated lava, the lowest (0.7-14.1 J m^{-2} s^{-1} $°C^{-1}$) with a 5-m-thick lava erupted at a sub-liquidus temperature. At the rille bed, the highest values of h_T are found within ~5-10 m of the bed/right bank contact, and at the right bank they are located at the bank top. As for scenario 2 lavas, the variation of h_T values is consistent with the illustrated magnitude and spatial distribution of erosion rates.

Theoretical study

Erosion rates and the thermophysical parameters diagnostic of change

This section aims to draw a connection between the erosion rates obtained at cross-section 400 and 800 of the 1200-m-long rille section of interest and the details of flow circulation and temperature distribution at rille bend axes. Only a few flow scenarios expected to aid in interpretation will be investigated and presented here. Before doing so, it might be worth looking at the erosion rate expression adopted in the 3-D model to gain

a better understanding of the flow parameters that determine variations of it. The erosion rate expression (Eq. 8) contains several flow parameters that, for a specific flow of interest, are constant. Specifically, the values of the density ratio, R, the specific heat capacity, C_g, the substrate melting temperature, T_m, the substrate ambient temperature far from the lava interface, T_0, and the latent heat of fusion, L_g are all constant for a single, individual The only values that are subject to change are the effective thermal diffusivity, α_{eff}, and the temperature gradient perpendicular to the interface, $\partial T/\partial n$. Temperature changes are tied to kinematic viscosity variations. Eqs. (2, 3) show that changes in the value of the effective thermal diffusivity, α_{eff}, are driven by variations in kinematic viscosity and turbulent viscosity. In the adopted SST k- ω model, kinematic and turbulent viscosity changes are tied to variations of the k (turbulent kinetic energy) and ω (specific dissipation rate) parameters. Both k and ω increase with increasing flow velocity (see Eqs. 4, 6 in chapter 2) and their increase is especially evident in regions of strong velocity gradients. At the bed and banks, the kinematic viscosity is held constant, and the turbulent viscosity is equal to zero because there is no flow motion at all. As we move away from channel boundaries (and prior to entering the region of freestream flow), both flow velocity and turbulent viscosity increase, whereas kinematic viscosity decreases. All these changes occur to various extents and cause variations in thermal diffusivity at the channel interface and, ultimately, erosion rate changes. The following sections show how tracking the change of the above-mentioned parameters at two channel cross-sections reveals the processes contributing to the observed variation in erosion rate. The study is based on results obtained from both the sensitivity analysis and the two scenarios presented before.

Contributor to erosion rates magnitude and distribution across the channel

For all the performed simulations, maximum attention was paid to minimize any discrepancy in initial flow conditions that might have a potential to affect downstream flow and, hence, the magnitude and spatial distribution of erosion rates at channel bed and banks. Notwithstanding this, the flowing lava is compelled to flow through a pre-defined channel geometry and a component of the measured erosion rate enhancement results from flow streamlines running into an obstacle represented by a specific bend portion. This has to do with the inertia of the flow that manifests itself soon after the flow enters a curve and causes lava to maintain the original direction of motion. It also appears to be the most important contributor to the observed erosional trend at bend/meander flanks and is known in the river literature as one of the leading forces behind meander migration (*Lawler*, 1993). These areas of erosion enhancement are usually located at some distance (~50-150 m) from meander axes in contrast to those associated with fluid processes occurring at meander axes, which are found at bend troughs or within 10-15 m of there. For all the simulations performed, the maximum erosion rates (at the bed and banks) that can be traced back to this cause are always higher than those resulting from processes occurring at channel cross-sections 400 and 800. In our simulations, the bend portions that show evidence for such a mechanism of erosion enhancement are located on the right flanks of bend 1 and 2, and the left flank of bend 2, as shown in Fig. 5.46.

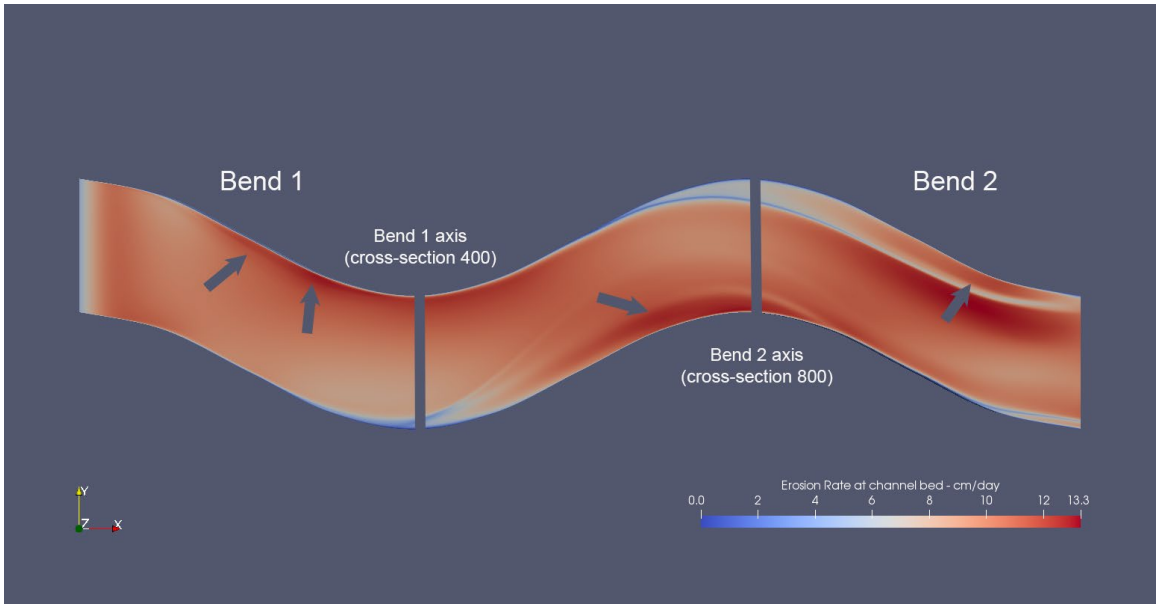

Figure 5.46. Plan view that shows erosion rates at the bed of a 1200-m-long rille section. This figure shows one of the contributors to the observed magnitude and spatial distribution of erosion rates. The arrows point at the bend portions flow streamlines run into and the associated areas of erosion enhancement. This mechanism is well-known in the river literature and is responsible for meander migration in rivers (*Lawler*, 1993). These areas of erosion enhancement are located ~50-150 m away from meander axes other than those associated with fluid processes occurring at meander axes, which are found at or within 10-15 m of bend axes.

While it is possible that, to some degree, this mechanism could also affect the magnitude and spatial distribution of erosion rates at bend axes, the pattern of flow circulation observed at channel cross-sections 400 and 800 is not found at bend flanks. Besides, the pattern shows striking similarities with that displayed at river meanders.

Contributor to erosion rates at meander bends: Secondary flow circulation

A brief introduction to secondary flow as applied to river meandering was given in the section titled “Secondary Flow Circulation in Curved River Channels”. The present section illustrates several sub-scenarios that display strong secondary flow circulation at

channel cross-sections 400 (bend 1) and 800 (bend 2) (see Figs. 2.2 a, b to locate cross-sections). Most of them concern scenario 2 flows that are insulated from the lunar environment. Referring to the sensitivity analysis chapter is needed for those lavas that flow in channels of different meander amplitude and width because results apply to 10-m-thick flows. The last few examples refer to scenario 1 flows (lava radiating heat through the flow top). For each case study presented, a brief overview is provided of how erosion rates at the bed and banks relate to changing fluid dynamic structures and lava temperatures at cross-section 400. Also, results at cross-section 800 are reported for one flow sub-scenario.

The first case study illustrates a 20-m-thick flow erupted at a sub-liquidus temperature of 1380°C and traveling at a horizontal velocity of 10 m s^{-1}. The reason behind this choice is that secondary flow circulation appears to be especially strong and well-developed in lavas that are thick and travel at fast speed. Though lava temperature is a key factor controlling the magnitude of erosion rates, it is not the driving force behind secondary flow circulation. The chosen scenario displays a large difference in erosion rates at the channel bed (Fig. 5.26) and at the left and right bank (Figs. 5.27 a, b). Values at the bed become progressively higher as the bed/right bank contact is approached and a maximum is reached within ~10 m of the contact. Erosion rates differ noticeably from one bank to the other, with right bank values that are higher by a factor of ~2.1 than those found on the opposite bank. At the right bank, the erosion enhancement is found within 5-7 m of the right bank/bed contact with values of ~9.9 cm/day that are much higher than the value found at the top of the bank (~3.3 cm/day).

Fig. 5.47 illustrates cross-stream or U_y velocity vectors that are perpendicular to the mainstream flow direction (entering the page). In the central portion of the cross-sectional view, flow vectors point in the direction of the left bank (left), whereas in the proximity of the channel bed (bottom) the red arrows point in the direction of the right bank. Red arrows mark presence of secondary circulation that is initiated at the left bank/bed contact where lava is slower and flow pressure is higher than elsewhere. At the bed/right bank contact, secondary flow reaches a maximum velocity of 1.9 m s^{-1} and is then diverted up the right bank. After reaching the flow top, it flows back in the direction of the left bank. There, it falls off the edge of the bank and mixes with the secondary flow that runs parallel to the bed. This section displays a well-developed scenario of helicoidal flow analogous to those

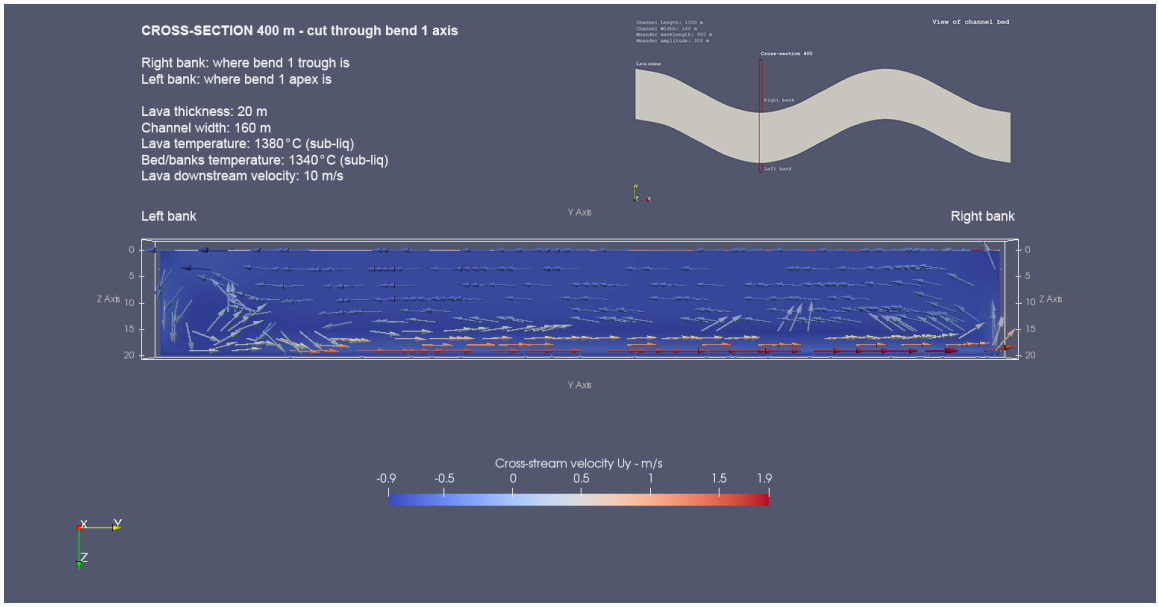

Figure 5.47. Cross-stream or U_y velocity vectors (perpendicular to direction of mainstream flow, which enters the page). Rille cross-section 400, bend 1 axis. Sub-scenario displaying a 20-m-thick flow that is erupted at the sub-liquidus temperature of 1380°C and travels at a velocity of 10 m s^{-1}. The inset up to the right (plan view of channel bed) shows where cross-section 400 is cut and the location of the right (up) and left (down) bank in the channel. In the central and upper portions of the cross-sectional view, flow streamlines point in the direction of the left bank (left) whereas in the proximity of the channel bed, red arrows point in the direction of the right bank (right). Red arrows mark presence of

secondary flow circulation that is initiated at the left bank (outer bend) where lava is slower and flow pressure is higher than elsewhere. Secondary flow reaches a maximum velocity of 1.9 m s^{-1} at the bed/right bank contact. At the right bank, secondary circulation moves upward and then flows back in the direction of the left bank. There, it falls off the edge of the bank and reaches the bed. This section displays a well-developed scenario of helicoidal flow analogous to those described in the river literature.

found at river meanders (*Lawler*, 1993). To better understand how the newly found secondary circulation relates to other flow parameters, Fig. 5.48 shows a cross-sectional view that illustrates how flow pressure varies throughout cross-section 400. Kinematic pressure is shown here because of the incompressibility requirement (pressure is normalized by lava density). When lava is slower, flow pressure is higher (on the left), in line with Bernoulli principle. Conversely, flow pressure is lower and flow velocity is higher in cross-sectional portions close to the right bank. Secondary circulation arises due to the pressure gradient that develops between the two section ends and flows parallel to the bed from left to right. Figs. 5.49 and 5.50 illustrate how downstream velocity and lava temperature vary at cross-section 400, channel bend 1. Fig. 5.49 confirms that downstream velocity is much higher close to the right bank than near the left bank. At the bed/right bank contact, flow velocity is faster than that found at the opposite end of the section by a factor of ~3.6. Fig. 5.50a displays the variation of flow temperature at cross-section 400. At the bed, lava temperatures progressively increase toward the right end of the section (Fig. 5.50b), and a maximum temperature of 1383.6°C (3.6°C higher than the eruption value) is reached within a few meters of the bed/right bank contact (at a location shown by the grey arrow). This temperature trend is responsible for the observed increase in erosion rates at the bed as the bed/right bank contact is approached (Fig. 5.26). The temperature

increase extends approximately halfway up the bank, a find that is consistent with the erosion rate enhancement shown in Fig. 5.27b. Interestingly, a minor increase in temperature is also observed at the bed/left bank contact, a likely consequence of the strong turbulent circulation occurring there (Fig. 5.47).

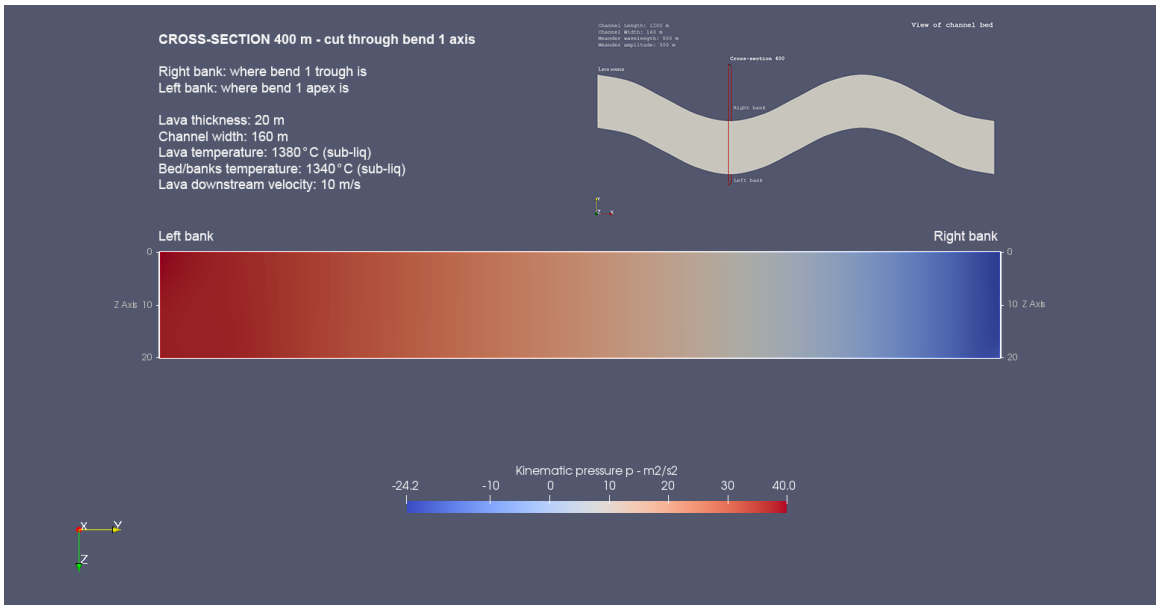

Figure 5.48. Flow pressure P variation from one end of bend 1 to the opposite at rille cross-section 400. Flow sub-scenario is described in Fig. 5.47. On the left side of the section, red color marks areas with the highest values of pressure and, on the right, blue color marks areas with the lowest values. Consistent with Bernoulli principle, lava flows slower on the left and faster on the right. The pressure gradient is the driving force behind secondary flow. Secondary flow circulation is initiated at the left end of the cross-section and runs along the channel bed toward the opposite end of the section (right bank). The gap in kinematic pressure between the left and right bank is equal to 64.2 m^2 s^{-2}, the largest value found in all the performed simulations.

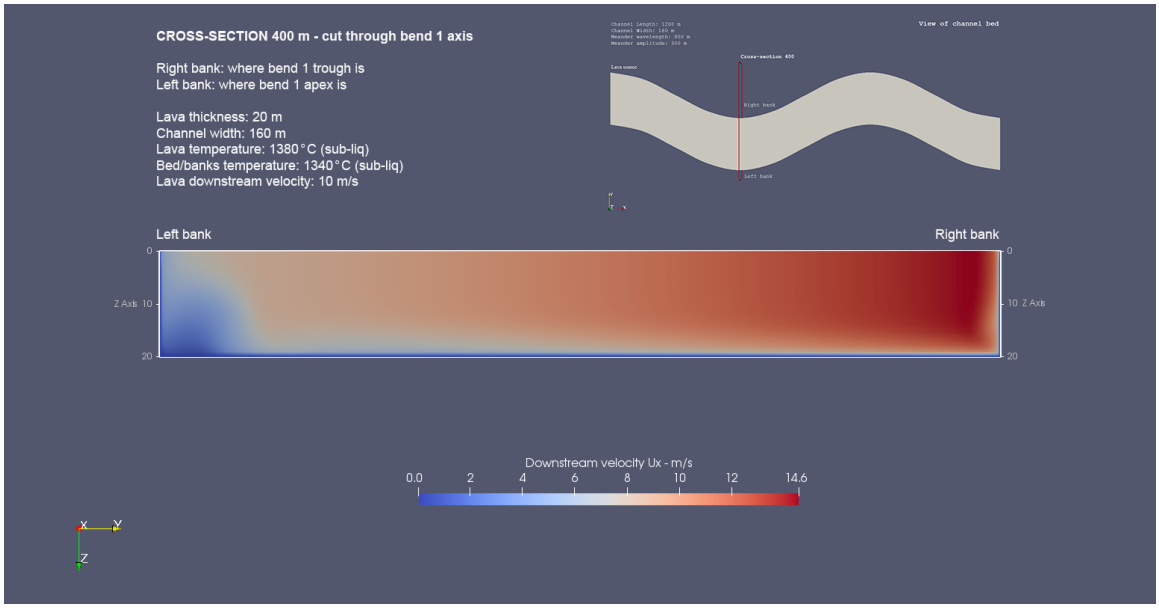

Figure 5.49. Downstream velocity U_x variation from one end of bend 1 to the opposite (flow is entering the page). Rille cross-section 400, flow sub-scenario described in Fig. 5.47. On the left end, lava velocity ranges from ~3 to 5 m s^{-1} whereas in the proximity of the right bank (where bend trough is) it is accelerated to a velocity of 14.6 m s^{-1}. Such a distribution in flow velocity arises from the pressure gradient that develops at the two bend ends (apex and trough) and is consistent with Bernoulli principle.

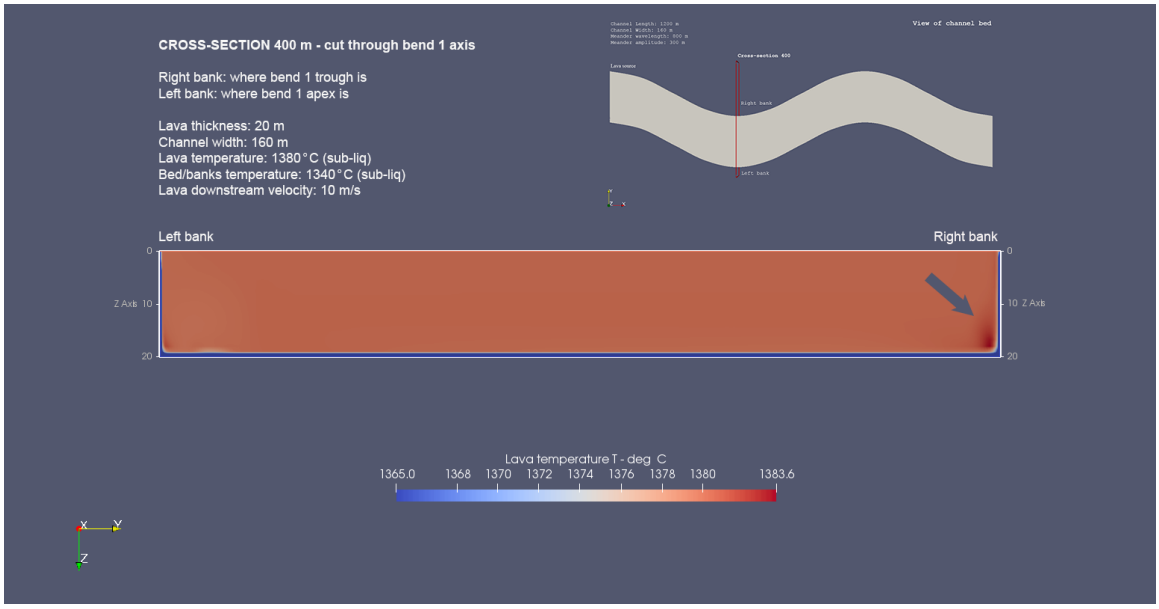

Figure 5.50a. Distribution of lava temperature T from apex (left bank) to trough (right bank) of bend 1 (mainstream flow is entering the page). Rille cross-section 400, flow sub-scenario described in Fig. 5.47. In the proximity of the right bank, a temperature increment of up to 3.6°C above the eruption value of 1380°C is obtained, as shown by the grey arrow. The temperature increase extends approximately halfway up the bank, a find that is

consistent with the erosion rate enhancement shown in Fig. 5.27b. A minor increase in temperature is also observed at the bed/left bank contact, a likely consequence of the strong turbulent circulation occurring there (Fig. 5.47).

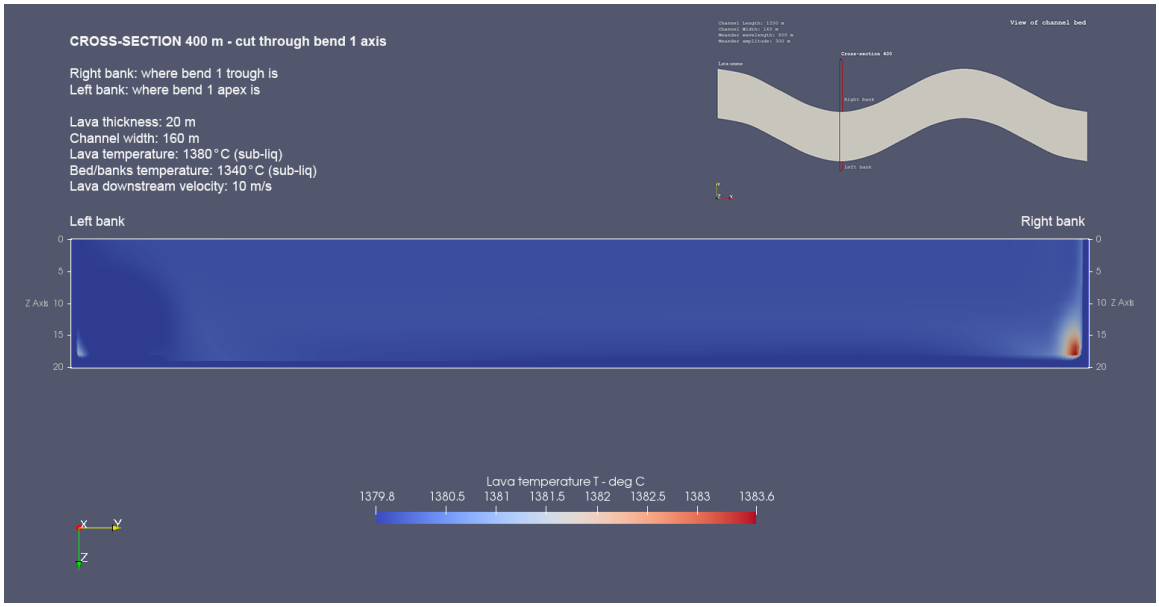

Figure 5.50b. Distribution of lava temperature T (enhanced view of Figure 5.50a). Cross-sectional temperature variations are easier to spot than in Fig. 5.50a. The same applies to lava temperature variations at the bed as bed/bank contacts are approached. The areas of temperature enhancement that occur at the two bed/bank contacts are better visible than in Fig. 5.50a.

These results confirm that, at the bed and bed/right bank contact of rille cross-section 400, secondary flow circulation is contributing to the observed increase in temperature and erosion enhancement. Will secondary flow circulation at cross-section 800 look the same as that at cross-section 400? The distribution of erosion rates at the bed of cross-section 800 is reversed and more irregular than that seen at cross-section 400 (Fig. 5.51). The maximum value is found within a few meters of the left bank and, as erosion rates decrease toward the bed/right bank contact, there are dips and fluctuations that are not seen at cross-section 400. At the left bank, erosion rates are higher than those at the right bank by a factor of ~3, with a maximum value of 11.0 cm/day at a vertical distance of ~5 m from the

bank/bed contact. From bank top to bottom, the distribution of erosion rates is far from homogeneous, with a value at the bank top that is a factor of ~3 smaller than the maximum erosion rate of 11.0 cm/day.

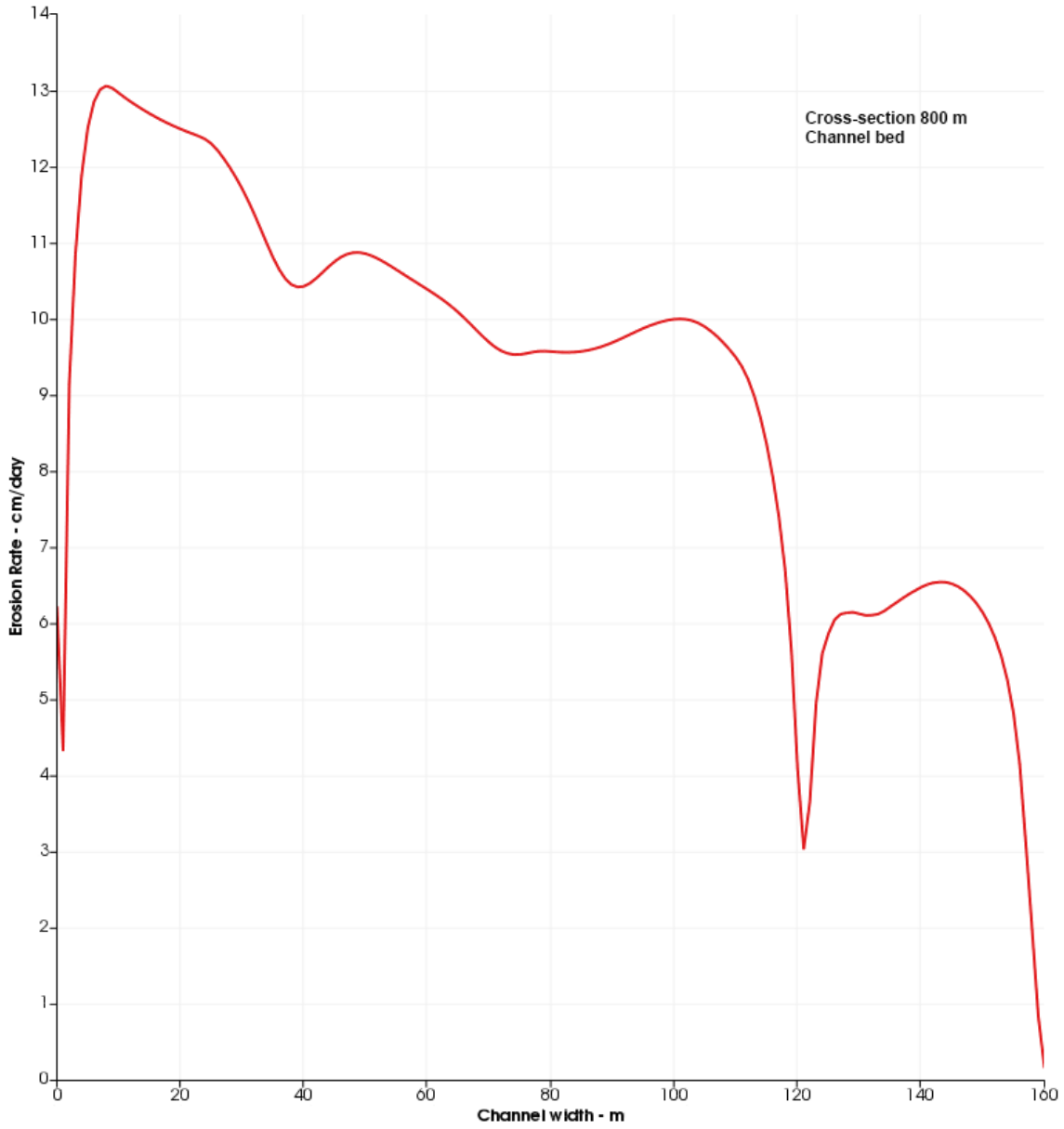

Figure 5.51. Erosion rate distribution at the bed of rille cross-section 800, bend 2 (800 m downstream of lava source). Flow sub-scenario is described in Fig. 5.47. Maximum erosion rates of 13.1 cm/day are found within ~7 m of the bed/left bank contact. The spatial distribution of erosion rates looks much more irregular than that found at channel cross-section 400. While values tend to decrease as the bed/right bank contact (from left to right)

is approached, fluctuations are more frequent than at bend 1 and even a dip occurs at a horizontal distance of ~40 m from the bed/right bank contact.

Fig. 5.52 displays the distribution of cross-stream velocities (U_y vectors) at cross-section 800 for the identical 20-m-thick flow erupted at a sub-liquidus temperature of 1380°C and traveling at a velocity of 10 m s^{-1}. At bend 2, secondary circulation flows parallel to the bed but, this time, toward the left bank.

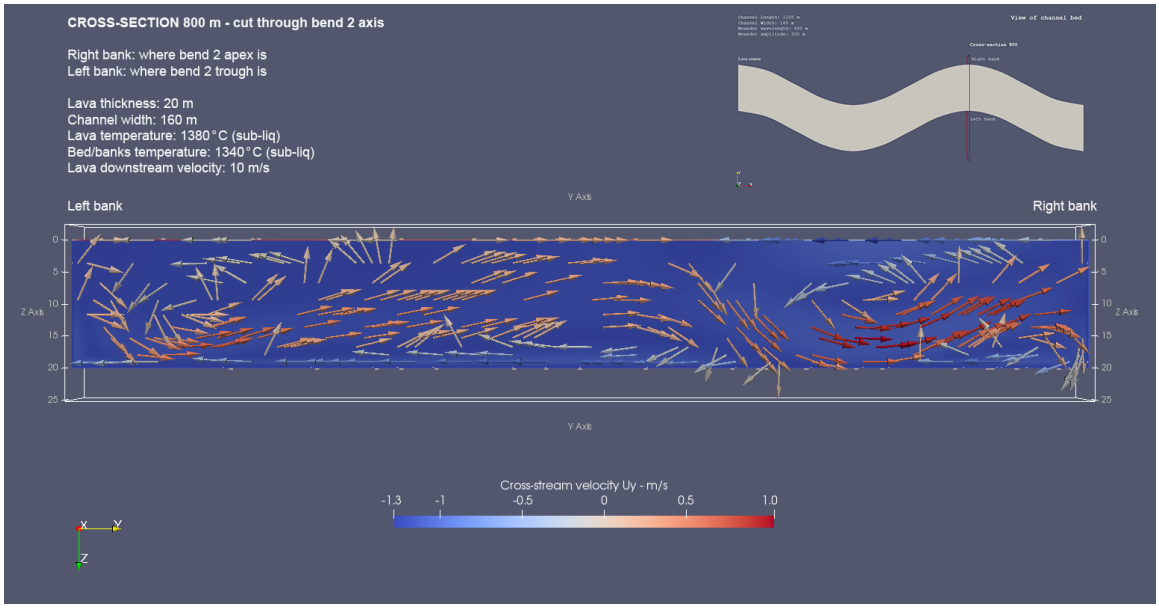

Figure 5.52. Cross-stream or U_y velocity vectors (perpendicular to mainstream flow that enters the page) at rille cross-section 800, bend 2 axis. Flow sub-scenario described in Fig. 5.47. The inset on the upper right shows where cross-section 800 is cut and the location of the right (up) and left (down) bank in the channel. In cross-section, bend apex is on the right (right bank) and trough is on the left (left bank). Flow is more turbulent and chaotic than that seen at cross-section 400 (Fig. 5.47). There is evidence for secondary flow circulation at the bed though blue arrows point toward the left bank (still where bend trough is). The highly turbulent motion in the proximity of the bend apex appears to locally disrupt secondary flow circulation that runs parallel to the bed. At the left bank, the maximum velocity reached by secondary flow is equal to 1.3 m s^{-1} and then flow is diverted upward. Near the right bank, flow lines separate and go both upward and downward, the latter ones mixing with secondary flow circulation at the bed. The helicoidal flow seen at cross-section 400 is disrupted by excess turbulence.

The aspect that is consistent with results obtained at cross-section 400 is that secondary flow runs parallel to bed and toward the bend trough. A more chaotic turbulent motion than that observed at cross-section 400 dominates cross-section 800 and helicoidal flow is disrupted by excess turbulence. Secondary flow circulation appears to be disrupted by excess turbulence in more than one area, which probably explains the irregular distribution of erosion rates at the bed shown in Fig. 5.51. Fig. 5.53 shows how flow pressure varies at cross-section 800.

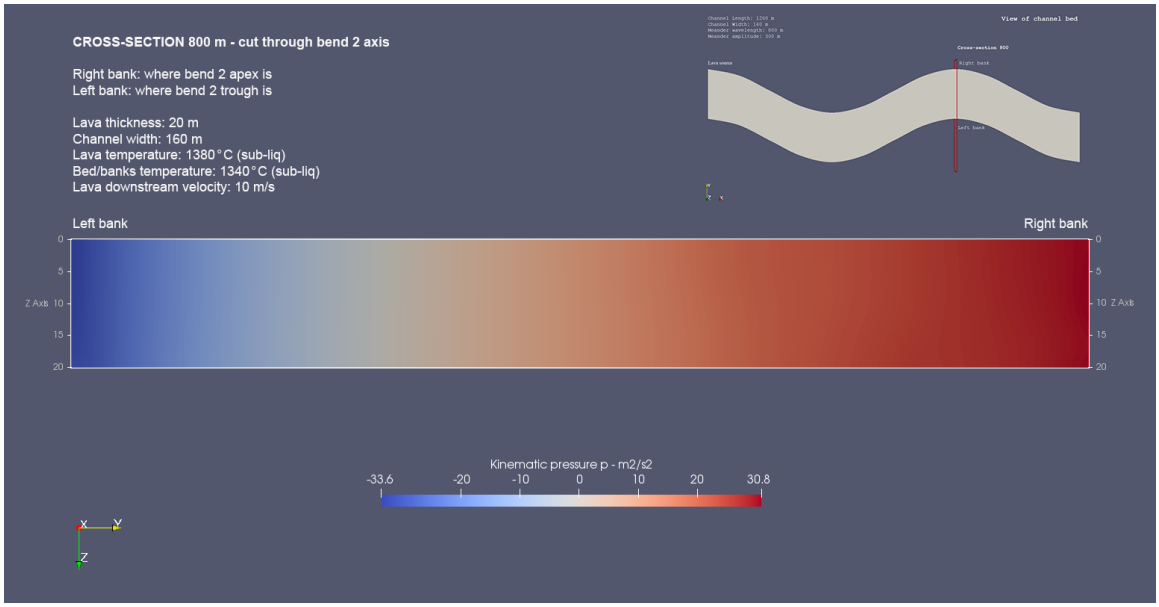

Figure 5.53. How flow pressure P varies from one end to the other of bend 2 (mainstream flow is entering the page). Rille cross-section 800, flow sub-scenario described in Fig. 5.47. The distribution of pressure is reversed compared to that shown in Fig. 5.48 (cross-section 400). On the left end (left bank), flow pressure is much lower than that found in the proximity of the right bank (right end of section).

The distribution of pressure is reversed compared to that shown in cross-section 400. On the left side of the section, which is where the trough of bend 2 is, pressure is much lower than the value found in proximity of the right bank (bend apex). Expectedly, the distribution of downstream velocity (Fig. 5.54) is also reversed compared to that shown in

Fig. 5.49 (cross-section 400). Lava travels much faster in the proximity of the left bank than near the right bank, and the maximum velocity of 14.3 m s^{-1} is slightly slower than the value of 14.6 m s^{-1} found at cross-section 400. Once again, the displayed distribution of downstream velocities arises from the pressure gradient that develops at the two bend ends (apex and trough) and is consistent with Bernoulli principle.

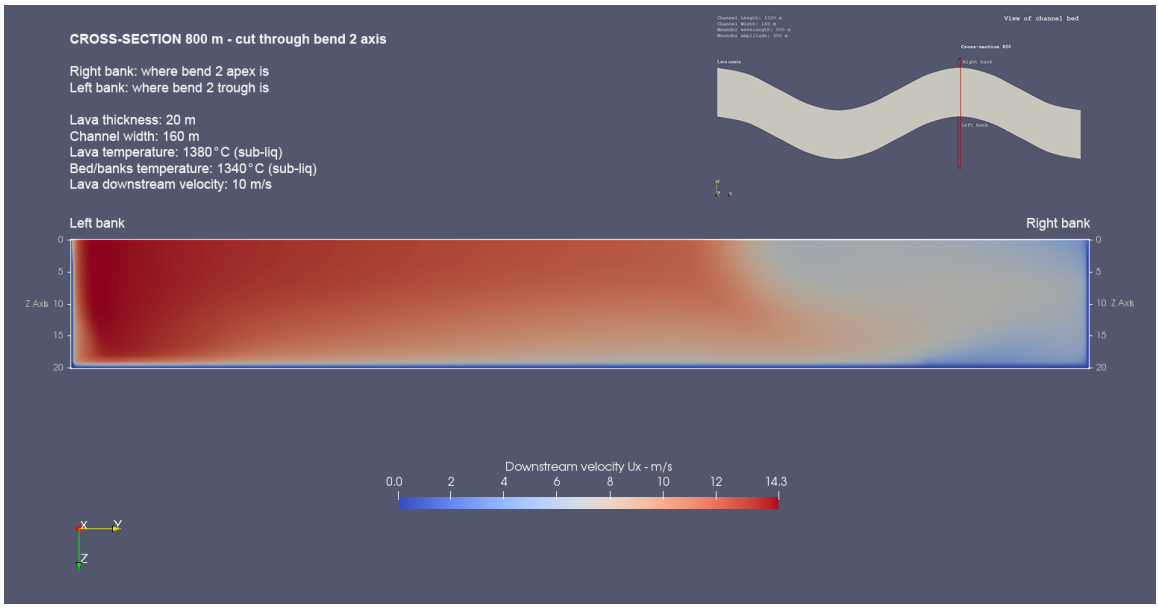

Figure 5.54. It is shown how downstream velocity U_x varies from one end of bend 2 to the opposite (mainstream flow enters the page) at rille cross-section 800. Flow sub-scenario is described in Fig. 5.47. Distribution of velocity is reversed compared to that shown in Fig. 5.49 (cross-section 400). Lava travels much faster in the proximity of the left bank than near the right bank, and the maximum velocity of 14.3 m s^{-1} is slightly slower than the one found at the right bank of cross-section 400 (14.6 m s^{-1}). The displayed distribution of flow velocity arises from the pressure gradient that develops at the two bend ends (apex and trough) and is consistent with Bernoulli principle.

Finally, lava temperature variations at cross-section 800 are shown in Figs. 5.55 (a, b). In the proximity of the left bank (where bend trough is), lava temperature is higher at the bank/bed contact, as shown by the dark arrow. An increase in temperature of 2.4°C above the original lava temperature (1380°C) is obtained at the bed/left bank contact, which is

lower than that observed at the bed/right bank contact of cross-section 400. The lower temperature increment is likely a consequence of the slower cross-stream (1.0 versus 1.9 m s^{-1}) and downstream (14.3 versus 14.6 m s^{-1}) velocities at bend 2, which arise from the lower pressure gradient that develops at the two bend ends. At the left bank of cross-section 800, the temperature increase extends approximately halfway up the bank, which is consistent with the observed distribution of erosion rates at the same bank. The other dark arrow points at another area of temperature increase (an increase that is lower than the one on the left) at the right bank/bed contact. This area is likely responsible for the erosion enhancement found at the right bank, halfway down from the bank top. Here, erosion rates increase from a value of 1.0 cm/day at the bank top to a value of 3.7 cm/day at a vertical distance of ~9.5 m from the bank/bed contact. The velocity gradients associated with the vigorous turbulent motion shown in the vicinity of the right bank are likely responsible for the observed increase in temperature and erosion rates. Finally, the green arrow points at an area located ~40 m to the left of the right bank/bed contact. Here, an elongated, narrow area of increased lava temperature sits on top of an area that is in contact with the bed and is much cooler than the surroundings. The occurrence of the latter probably explains the dip in erosion rates observed at the bed at a horizontal distance of ~40 m from the bed/right bank contact (Fig. 5.51). Once again, the vigorous turbulence that characterizes this portion of cross-section 800 along with the associated velocity gradients might be responsible for the observed non-homogeneous spatial distribution of temperatures and erosion rates at the channel bed. A higher level of complexity appears to characterize bend 2 compared to what

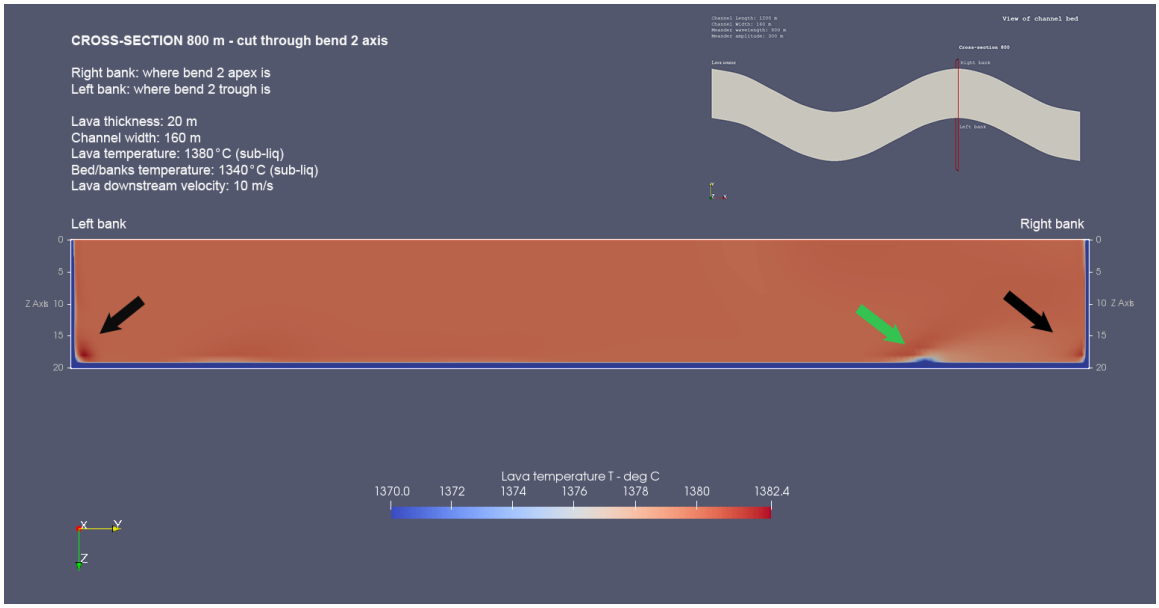

Figure 5.55a. It is shown how lava temperature T varies from one end of bend 2 to the opposite (mainstream flow enters the page). Rille cross-section 800, flow sub-scenario described in Fig. 5.47. In the proximity of the left bank (where bend trough is), lava temperature is higher at the bed/bank contact, in the area indicated by the dark arrow on the left. An increase in temperature of 2.4°C above the eruption value of 1380°C is obtained here, an increment that is lower than that observed at the bed/right bank contact of cross-section 400. The temperature increase extends approximately halfway up the bank, a find that is consistent with erosion rate distributions at the left bank. The other black arrow (on the right) points at another area of temperature increase (an increase lower than the one on the left) at the right bank/bed contact. This area is likely responsible for the erosion enhancement found at the right bank, halfway down from the bank top. Finally, the green arrow points at an area of low temperature close to the bed, which is likely responsible for the dip shown in Fig. 5.51.

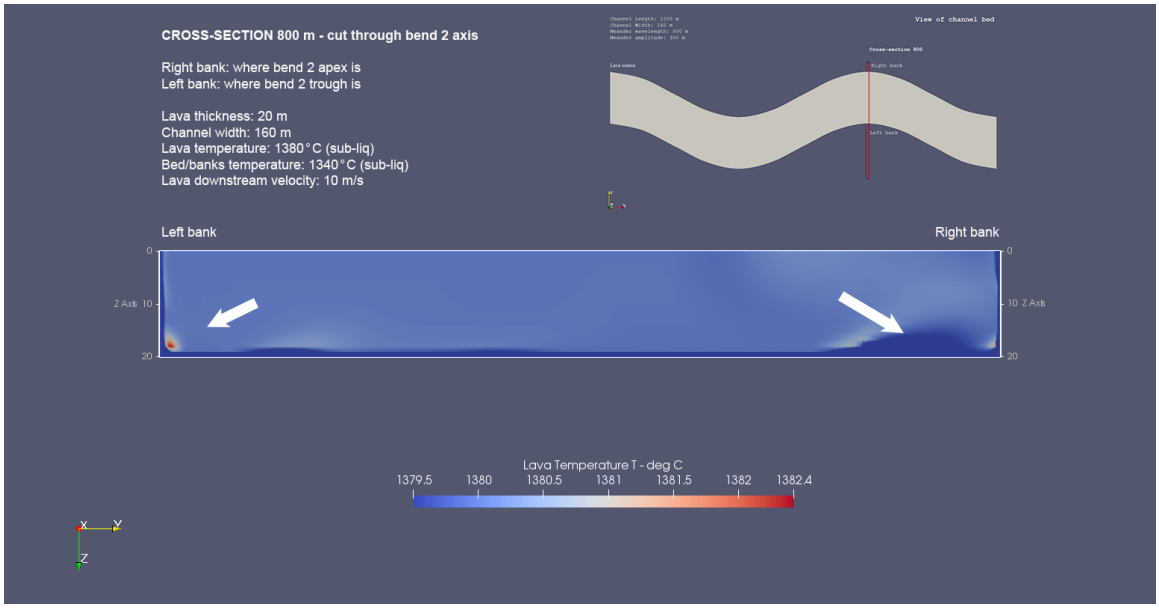

Figure 5.55b. Enhanced view of the temperature variations shown in Fig. 5.55a, which better shows how lava temperatures are irregularly distributed at the channel bed and explains the irregular distribution of erosion rates in Fig. 5.51. The white arrow on the right points at the cooler blue area indicated by the green arrow and described in Fig. 5.55a. The arrow on the left shows the hottest spot located at the bed/left bank contact.

observed at bend 1. Once again, secondary flow circulation and the local downstream velocity are likely responsible for the magnitude and spatial distribution of erosion rates at the bed and the two banks.

Let us now consider a 10-m-thick lava that is erupted at the liquidus temperature (1440°C) and flows at a velocity of 7 m s^{-1} in a channel with meanders of a higher amplitude (2A = 400 m, Fig. 5.56) compared to the amplitude adopted in the baseline model (2A = 300 m). At the bed (Fig. 2.24, chapter 2), the maximum peak of erosion is located at a horizontal distance of ~10 m (instead of ~6 m as in BM, Fig. 2.3) from the bed/right bank contact, and another peak of erosion is found ~50 m away from the bed/left bank contact. The latter peak is much smaller and only ~20 m away from the left bank in the lower amplitude BM scenario. The two peaks are higher in value (37.1 and 24.0 cm/day,

respectively) than those observed in the baseline model (28.8 and 18.9 cm/day). Figs. 2.25 (a, b) show that erosion maxima are found at the left bank top (Fig. 2.25a) and at a vertical distance of 2-4 m from the right bank/bed contact (Fig. 2.25b). The right bank displays the highest erosion rate value (25.6 cm/day versus 1.7 cm/day at the left bank). In the baseline model, the maximum of erosion at the right bank is at the bank top (Fig. 2.4a) and the left bank maximum is within 2-4 m of the left bank/bed contact (Fig. 2.4b). How does the observed variation in erosion rates relate to the spatial distribution of lava velocity and temperature at channel bend 1? Figs. 5.56 (a, b) show the velocity distribution at channel cross-section 400 for the higher amplitude version of the baseline model. In the central portion of cross-section 400 (Fig. 5.56a), flow lines point in the direction of the left bank (left). Red arrows point at secondary flow circulation that commences ~50 m away from the left bank compared to ~20 m away in the BM. The secondary flow travels faster and faster as it approaches the bed/right bank contact and reaches a maximum velocity of 1.7 m s^{-1}. This likely explains the maximum of erosion ~10 m away from the bed/right bank contact. The secondary circulation hits the lower-half of the right bank and flows upward at a velocity of 1.5 m s^{-1} (Fig. 5.56b), being likely responsible for the erosion enhancement observed half-way up the bank (Fig. 2.25b). Then, it flows away from the bank and toward the left bank (Fig. 5.56a). Flow lines hit the bed at a velocity of ~0.3 m s^{-1} (Fig. 5.56b), ~50 m away from the bed/left bank contact and are likely responsible for the secondary peak of erosion observed at the bed in Fig. 2.24. Then, they hit the lower-half portion of the left bank at a velocity of 0.9 m s^{-1} and move away from the upper-half portion of it (Fig.

5.56b). Overall, this section displays a high level of flow complexity, especially in the portion approaching the left bank (bend apex).

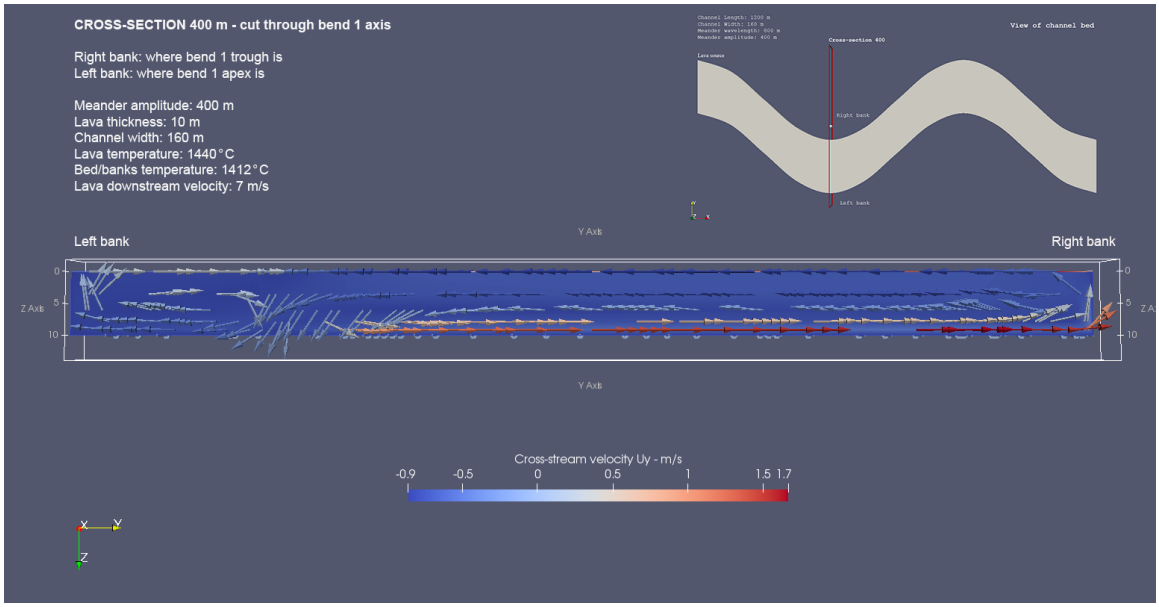

Figure 5.56a. Cross-stream or U_y velocity vectors (perpendicular to the downstream flow direction that enters the page), rille cross-section 400, bend 1 axis. Results refer to a 10-m-thick flow erupted at the liquidus temperature and traveling at a velocity of 7 m s^{-1}. Meander amplitude is higher (2A=400 m) than the 300-m value adopted in the baseline model and other simulations. In the central portion of the cross-section, flow lines point in the direction of the left bank. Secondary circulation (red arrows) commences ~50 m away from the left bank and flows in the direction of the right bank. At the left bank, lava is slow and flow pressure is high. Here, flow lines only hit the lower-half portion of the bank itself. The secondary flow reaches a velocity of 1.7 m s^{-1} in the proximity of the right bank, the second fastest value in all performed simulations. This section displays a high level of flow complexity, especially in the portion approaching the left bank (bend apex).

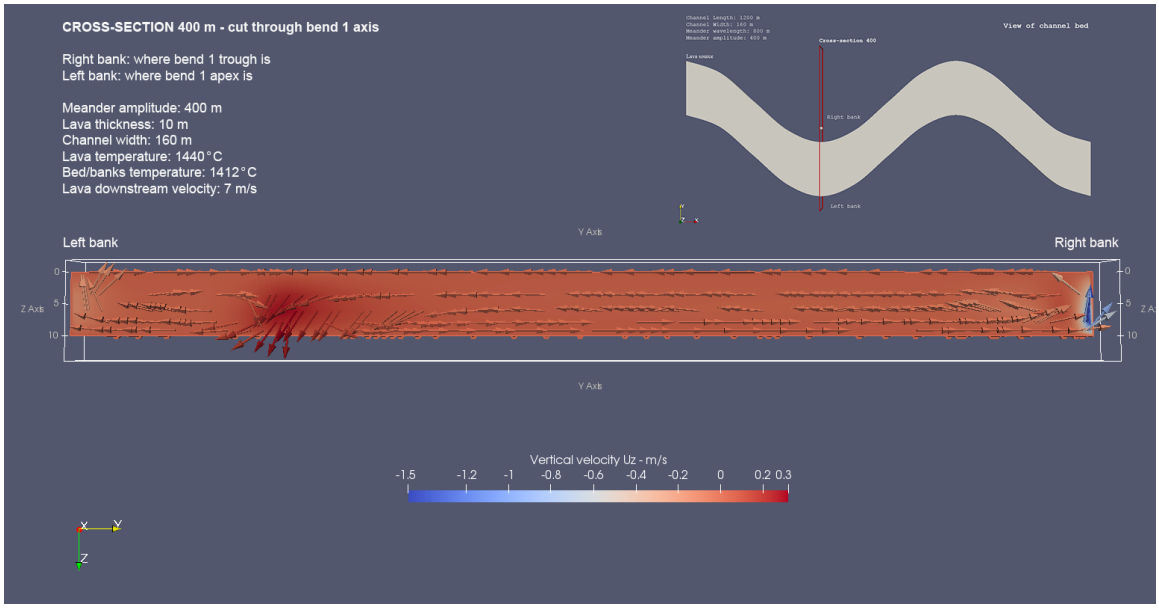

Figure 5.56b. Vertical velocity vectors or U_z vectors (flow moving up and down the two banks and at an angle from cross-stream flow elsewhere), rille cross-section 400, bend 1 axis. Results apply to the high-amplitude channel described in Fig. 5.56a. At the right bank, secondary flow moves upward at a velocity of 1.5 m s^{-1} (blue arrows), which explains the peak of erosion within ~10 m of the bank/bed contact. At the left bank, flow lines hit the lower-half portion of the bank and move away from the upper-half of the bank (pale orange arrows). This and the associated lava temperature variation (see Fig. 5.57) explain the observed erosion rate maximum at the bank top. Within ~50 m of the bed/left bank contact, flow lines hit the bed at a velocity of ~0.3 m s^{-1} (dark orange arrows), which leads to the secondary peak of erosion shown in Fig. 2.24.

Downstream velocity reaches a value of 11.5 m s^{-1} at/near the right bank and the difference in flow pressure between the two ends of the section is equal to 53.8 m^2 s^{-2}. The high downstream velocity is a consequence of the pronounced low-pressure zone (according to Bernoulli principle) that forms at the right bank in the presence of a high-amplitude bend, and significantly contributes to the erosion rate maximum observed at/near the right bank. The secondary flow circulation that develops from the pressure gradient at the two opposite banks of cross-section 400 - while also contributing to the magnitude of erosion - determines the spatial distribution of erosion at the bed and over the two banks. How does

flow velocity relate to lava temperature? Fig. 5.57 shows that lava temperature is highest at the bed/right bank contact (black arrow) where it increases by up to 4.2°C above the original value of 1440°C. The temperature increase extends approximately halfway up the bank, a find that is consistent with the erosion enhancement observed in Fig. 2.25b. The red arrow points at another area of temperature variation (a lower increase compared to the former) that is located at the bed/left bank contact. The presence of this area likely explains the low erosion enhancement seen within ~1 m of the left bank/bed contact in Fig. 2.25a. In general, temperature increments are highest where lava velocity is highest and flow lines hit the bed and/or the two banks.

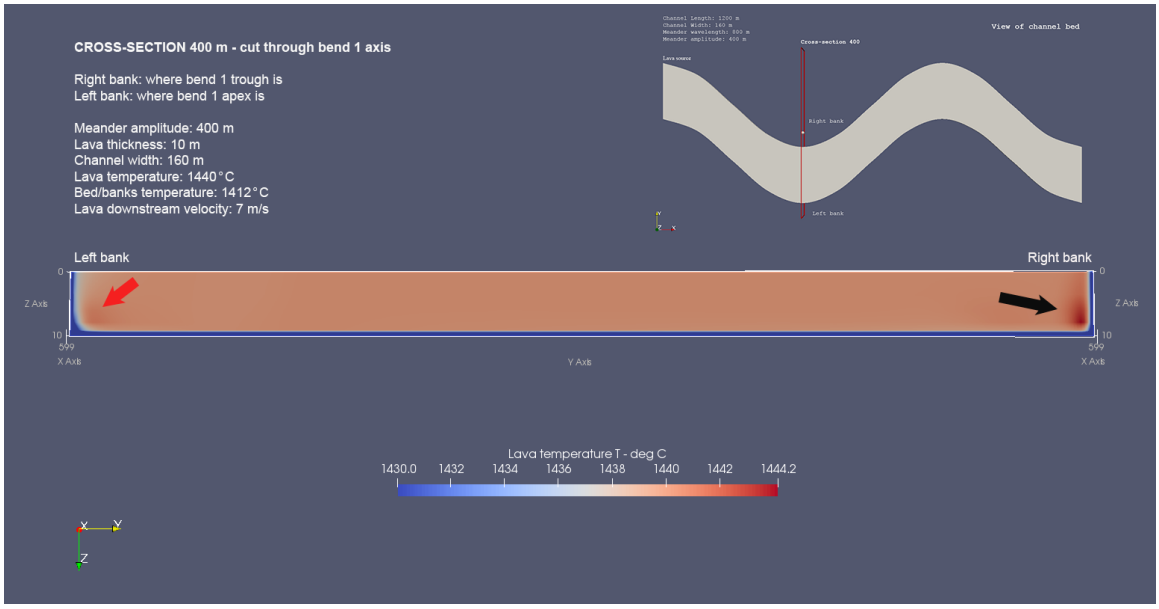

Figure 5.57. It is shown how lava temperature T varies from one end of bend 1 to the opposite (mainstream flow is entering the page), rille cross-section 400, baseline model with modified meander amplitude (2A=400 m). In the proximity of the right bank (where bend trough is, as shown in the upper right inset), lava temperature reaches a value of 1444.2°C (black arrow), a value 4.2°C higher than the original lava temperature. The temperature increase reaches up the bank top, but the peak value is found halfway up the bank, a find that is consistent with the erosion enhancement seen in Fig. 2.25b. The red arrow points at another area of temperature variation (a lower increase compared to the former) that is located at the bed/left bank contact. The presence of this area likely explains the erosion enhancement observed in Fig. 2.25a within ~1 m of the left bank/bed contact.

How different are flow velocities and temperatures at cross-section 400 for the lower-amplitude baseline model? Downstream velocity at the right bank is equal to 10.3 m s^{-1} and, thus, it is slower by a factor of ~1.1 than that associated with the higher-amplitude counterpart scenario. The pressure difference at the two banks is equal to 31.0 m^2 s^{-2} and is lower by a factor of ~1.7 than that found at the higher-amplitude bend. The lower pressure gradient is associated with slower secondary circulation and downstream velocities. Figs. 5.58 (a, b) show how cross-stream and vertical velocities differ from those seen in Figs. 5.56 (a, b). Secondary flow circulation (red arrows) commences ~50 m away from the bed/left bank contact (high-pressure, low-velocity zone) and reaches a maximum velocity of 0.9 m s^{-1} (Fig. 5.58a) in the proximity of the bed/right bank contact, a value lower by a factor of ~1.9 than that shown in Fig. 5.56a (higher amplitude bend). At the right bank, the secondary flow moves upward at a maximum velocity of 0.7 m s^{-1} (Fig. 5.58b), a value that is a factor of 2.1 lower than that obtained from the higher-amplitude scenario. All these finds explain the lower magnitude and different spatial distribution of erosion rates at the bed and banks of the lower-amplitude channel compared to the higher-amplitude rille section. How do flow velocities relate to lava temperature for the lower-amplitude baseline scenario? Fig. 5.59 shows that a temperature increment of 3.0°C above the original temperature of 1440°C is observed at the bed/right bank contact of cross-section 400.

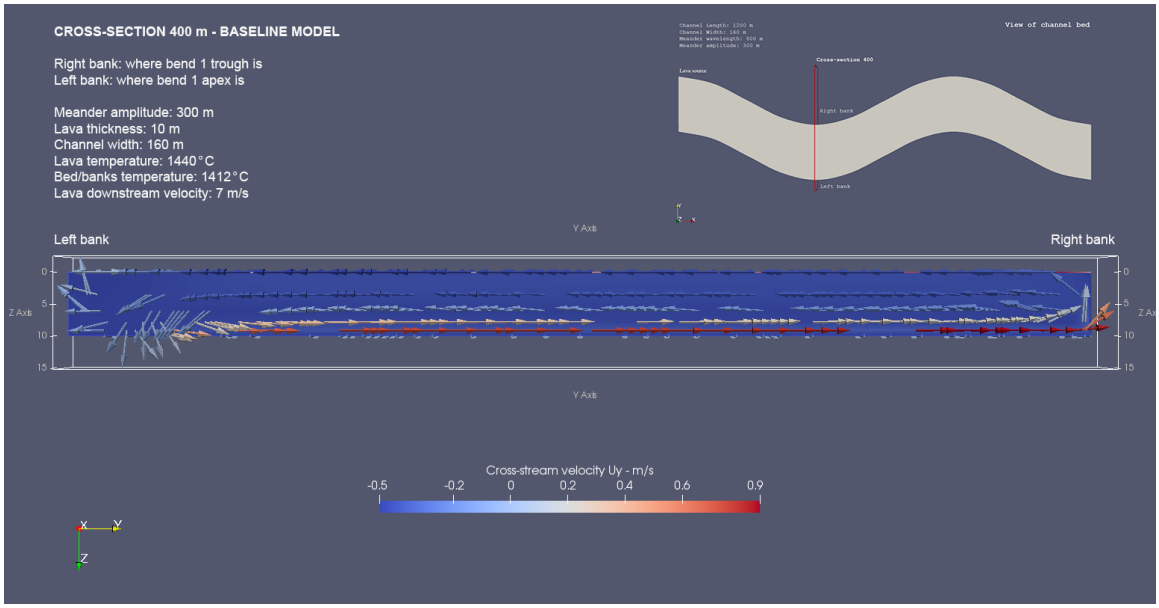

Figure 5.58a. Cross-stream velocity vectors or U_y vectors (perpendicular to the downstream flow direction that enters the page) for rille cross-section 400, bend 1 axis. Results refer to the baseline model, i.e., a 10-m-thick flow erupted at the liquidus temperature of 1440°C and traveling at a velocity of 7 m s^{-1}. Meander amplitude is 300 m. Secondary flow circulation (red arrows) commences ~20 m away from the bed/left bank contact. The secondary flow reaches a maximum velocity of 0.9 m s^{-1} in the proximity of the bed/right bank contact, a value lower by a factor of ~1.9 than that shown in Fig. 5.56 (higher amplitude channel). At the left bank, flow lines hit the bank head-on within ~4 m of the bed/bank contact and at an angle from there to the bank top.

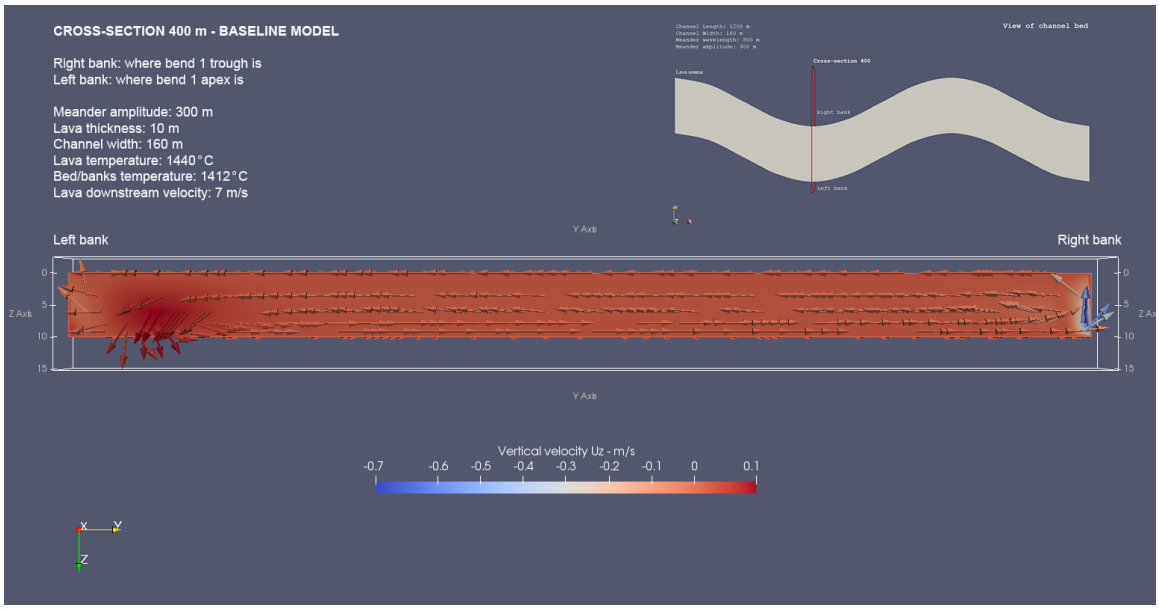

Figure 5.58b. View of vertical velocity vectors or U_z vectors (blue and dark orange) that

track flow up and down the two banks and at an angle from cross-stream flow elsewhere) at rille cross-section 400, bend 1 axis. Results refer to the low-amplitude BM scenario described in Fig. 5.58a. At the right bank, secondary flow moves upward at a maximum velocity of 0.7 m s^{-1} (blue arrows), a value that is a factor of 2.1 lower than that found at the higher-amplitude channel cross-section. The low U_z and U_y values found in Fig. 5.58a and the temperature results shown in Fig. 5.59 explain the lower erosion rates within ~4 m of the right bank/bed contact compared to those seen at the higher amplitude channel cross-section. At the left bank, no vertical motion is observed, and the erosional pattern is almost identical to the one observed at the higher amplitude cross-section.

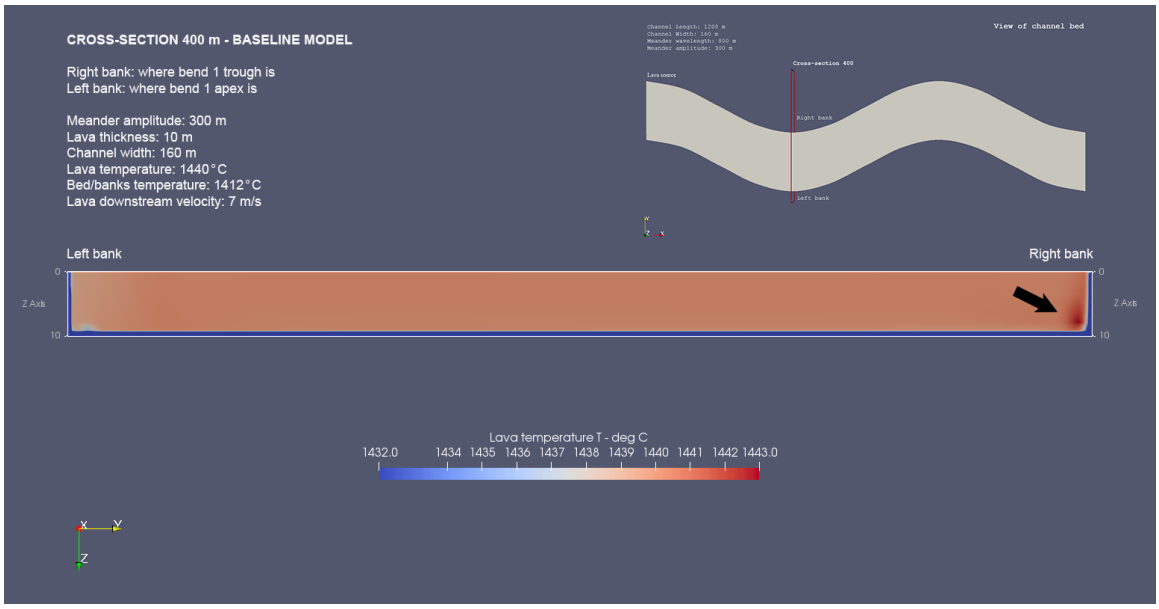

Figure 5.59. It is shown how lava temperature T varies from one end of bend 1 to the opposite (mainstream flow is entering the page), rille cross-section 400, baseline model with standard meander amplitude (2A=300 m). In the proximity of the right bank (where bend trough is), lava temperature reaches a value of 1443.0°C (black arrow), a value 3.0°C higher than the original lava temperature and 1.2°C lower than that found at the higher amplitude channel cross-section. The temperature increase extends all the way up the bank top where the erosion maximum is found.

By making the channel of meander amplitude 2A = 400 m thicker than 10 m, higher values of downstream and secondary flow velocities (compared to those found so far) are obtained at the bed/right bank contact of cross-section 400. The higher velocity values result in higher erosion rates at both the bed and the two banks. Nevertheless, the spatial distribution

of erosion rates at the two banks remains almost identical to that associated with the 10-m-thick high-amplitude channel.

For a 10-m-thick channel that is wider than the standard baseline channel (width = 200 m instead of 160 m), the distribution of downstream and cross-stream velocities at channel cross-section 400 changes dramatically. Fig. 2.31 (sensitivity analysis chapter) shows that erosion rates at the bed are slightly lower (27.1 cm/day) than their BM counterpart values (28.8 cm/day). At the left bank (Fig. 2.32a), a maximum erosion rate of 15.1 cm/day (higher than the BM counterpart value of 10.3 cm/day) is found at the bank top rather than within 2-4 m of the bank/bed contact. At the right bank (Fig. 2.32b), the maximum erosion rate is found at the bank top as well and is, once again, higher than its BM counterpart (26.1 versus 24.4 cm/day). In drawing a wider channel, channel sinuosity was held equal to ensure that any observed changes in erosion rate be tied to channel width variations only. Fig. 5.60 shows the pressure difference that develops at the ends of cross-section 400 for a channel that is 200 m instead of 160 m wide. The total difference in kinematic pressure is equal to 36.7 $m^2 s^{-2}$ and, thus, is a bit larger than that found at the same location in the narrower baseline channel (31.0 $m^2 s^{-2}$). The larger pressure difference translates into faster downstream velocities at both the right and left banks compared to the baseline counterpart velocities (Fig. 5.61).

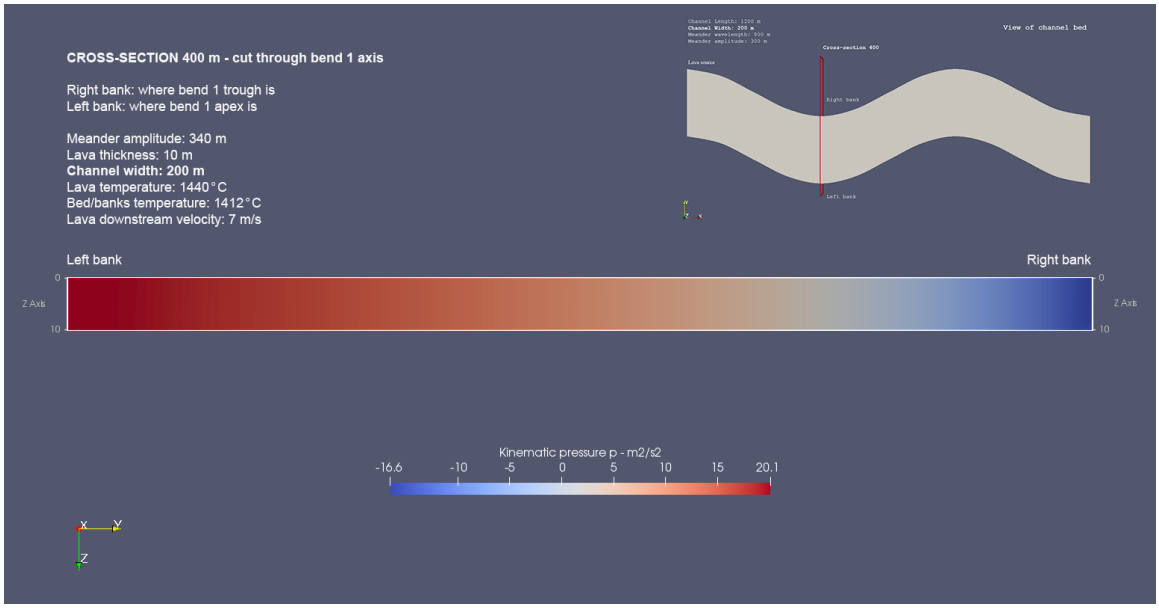

Figure 5.60. It is shown how flow pressure P varies from one end to the other of bend 1 (mainstream flow enters the page), rille cross-section 400. Results refer to a baseline model (BM) in which channel width is modified and taken to be equal to 200 m instead of 160 m. Left bank is a high-pressure (low-velocity) zone and right bank is a low-pressure (high-velocity) zone. The difference in kinematic pressure between the two cross-sectional ends is equal to 36.7 m^2 s^{-2} and, thus, is a bit higher than that measured at the two ends of cross-section 400 for the baseline model (31.0 m^2 s^{-2}).

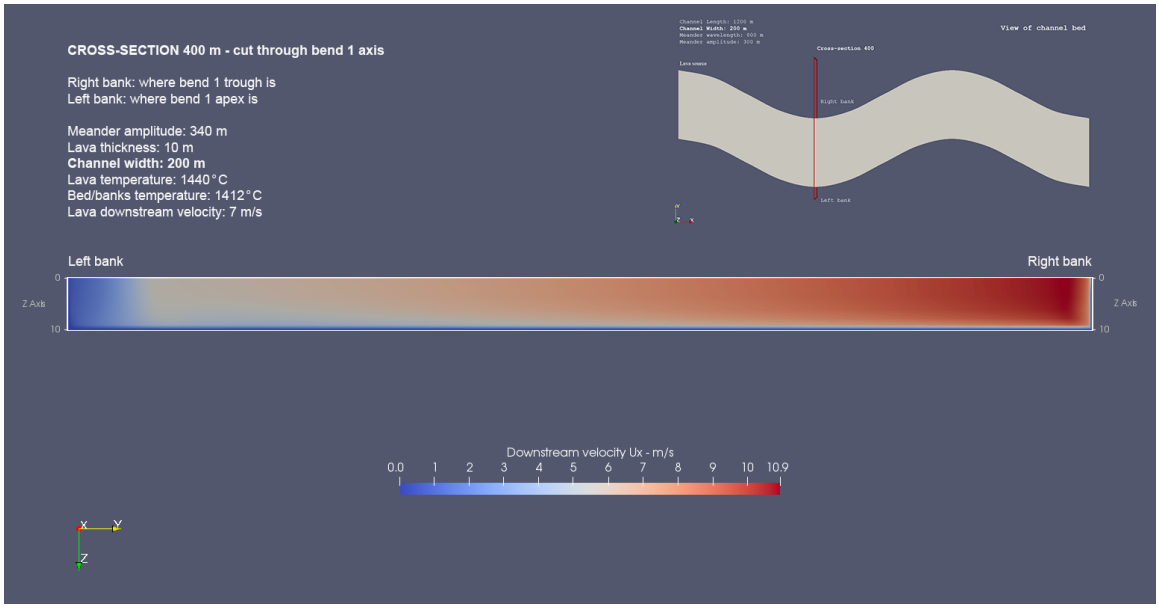

Figure 5.61. It is shown how downstream velocity U_x varies from one end to the other of bend 1 (mainstream flow enters the page), rille cross-section 400. Flow sub-scenario is described in Fig. 5.60. Lava travels much faster at the right bank than at the left bank, and the maximum velocity of 10.9 m s^{-1} measured at the right bank is slightly faster than that

found at the right bank of BM cross-section 400 (10.3 m s^{-1}). Velocity at the left bank is also slightly faster than its BM counterpart because flow pressure is not as high there, which allows for a slightly faster flow velocity.

The interesting find is that the magnitude and distribution of cross-stream and vertical velocities at section 400 are almost identical to those observed at cross-section 400 of the baseline model. As a result, any differences in the magnitude and distribution of erosion rates are likely due to differences in downstream velocities and lava temperature distribution at cross-section 400. Fig. 5.62 shows how lava temperature varies at cross-section 400. In the proximity of the right bank, which is where bend trough is, lava temperature reaches a value of 1443.03°C that is only slightly higher than the value of 1442.97°C (rounded up to 1443.0) found at cross-section 400 of the baseline model.

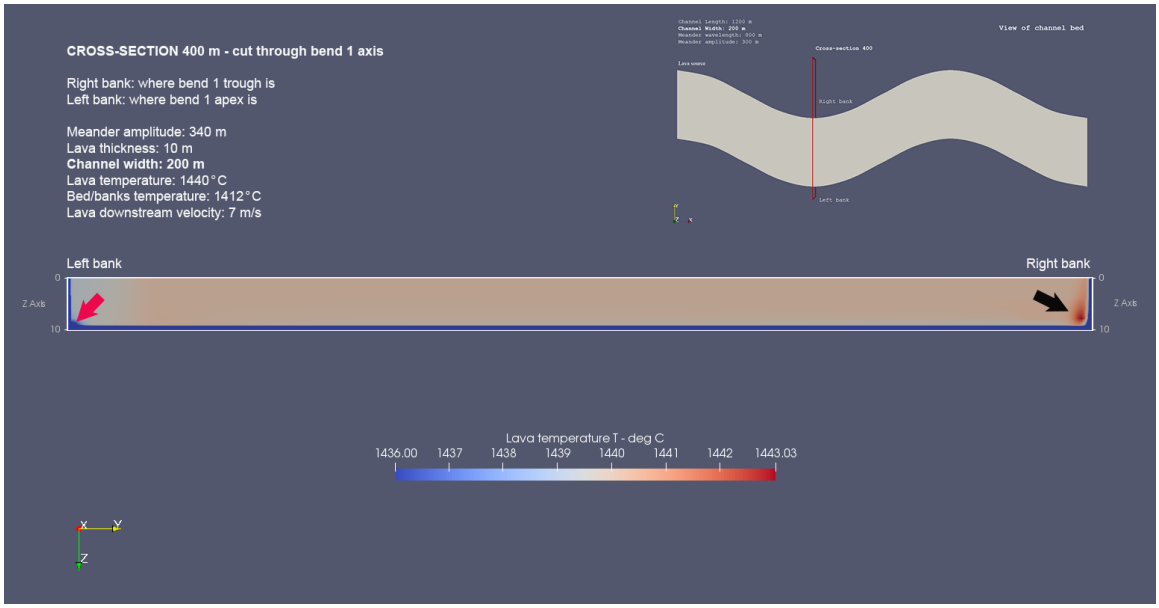

Figure 5.62. How lava temperature T varies from one end of bend 1 to the opposite (mainstream flow is entering the page), rille cross-section 400, baseline model with modified channel width (w=200 m instead of 160 m). In the proximity of the right bank (where bend trough is), lava temperature reaches a value of 1443.03°C (black arrow), which is only slightly higher than the value of 1442.97°C found at the same location in the baseline channel. The temperature increase extends all the way up to the bank top where the erosion maximum is. The higher erosion rate is likely a direct consequence of the faster

downstream velocity in the proximity of the right bank because, locally, the distribution of cross-stream and vertical velocities is identical to that found in BM. In the proximity of the left bank and, especially, at the bed/left bank contact (red arrow), a region of lower lava temperature is found, which explains the absence of a peak of erosion in the lower-half portion of the bank. A higher lava temperature is found toward the bank top, which explains the occurrence of the peak of erosion at the top of the left bank.

All results shown to this point pertain to scenario 2, i.e., they refer to flows for which no heat is lost by radiation to space because lava travels in a tube, hence, insulated from the lunar environment. Fig. 5.63 shows the cross-stream velocity distribution at channel cross-section 400 for a 5-m-thick flow that travels at a velocity of 5 m s^{-1} and flows at a sub-liquidus temperature of 1400°C. After erupting at the liquidus temperature of 1440°C, the flowing lava undergoes cooling through the flow top until its core temperature reaches a temperature of 1400°C. The fastest secondary flow velocity is achieved at the bed/right bank contact and is equal to 0.4 m s^{-1}, which confirms the dependence of secondary flow

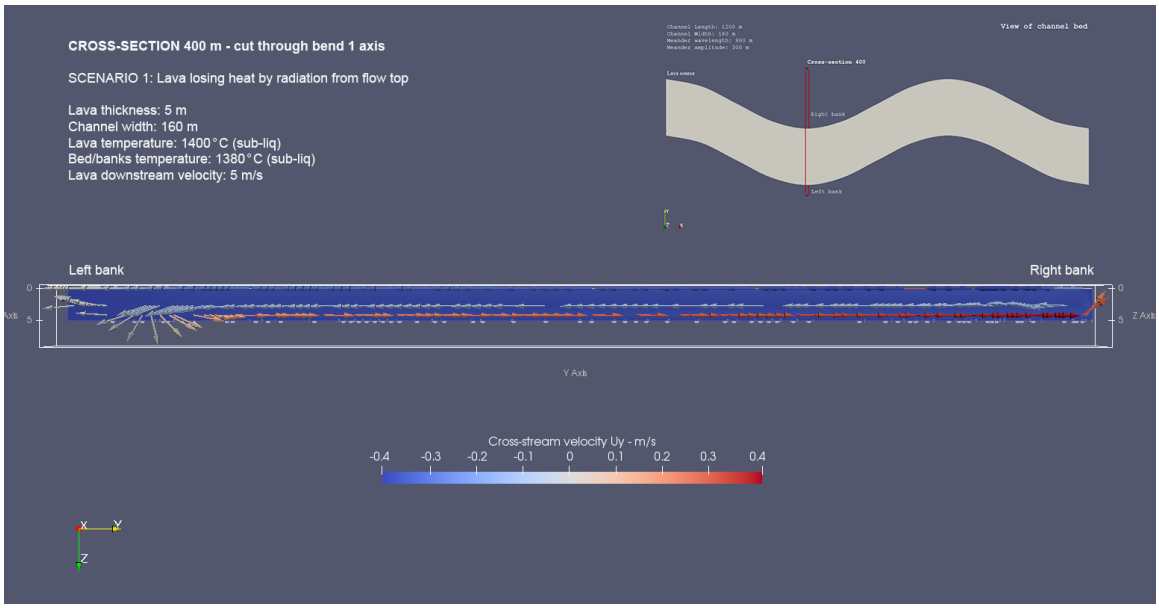

Figure 5.63. Cross-stream velocity vectors or U_y vectors (perpendicular to mainstream flow, which enters the page) for rille cross-section 400, bend 1 axis. Results refer to 5-m-thick lava that flows at a sub-liquidus temperature of 1400°C and travels at a velocity of 5 m s^{-1}. This lava undergoes cooling into the lunar environment through the flow top

(scenario 1). The secondary flow reaches a maximum velocity of 0.4 m s^{-1} in the proximity of the right bank. This low velocity value confirms how strong the dependence of cross-stream velocities is on lava thickness.

velocity on lava thickness. The distribution of cross-stream velocities is almost identical to that found at cross-section 400 for the counterpart lava that flows insulated from the lunar environment. Because heat is lost by radiation through the flow top, erosion rates measured at bank tops should never be the highest. Fig. 5.64 shows the distribution of lava temperatures at cross-section 400. A zone of lower lava temperature is found near the top of the cross-section and extends downward by ~1/3 of the vertical distance that separates the flow top from the bed. At the bed/right bank contact, the maximum temperature is equal to 1399.7°C, i.e., it is 0.3°C lower than the lava core temperature. This find confirms that the energy budget of the lava is reduced as heat is lost through the flow top. Near the left bank, lava temperatures are much lower than anywhere else in the cross-section. The details of flow circulation in this portion of the channel (Fig. 5.63) reveal that cooler lava flows

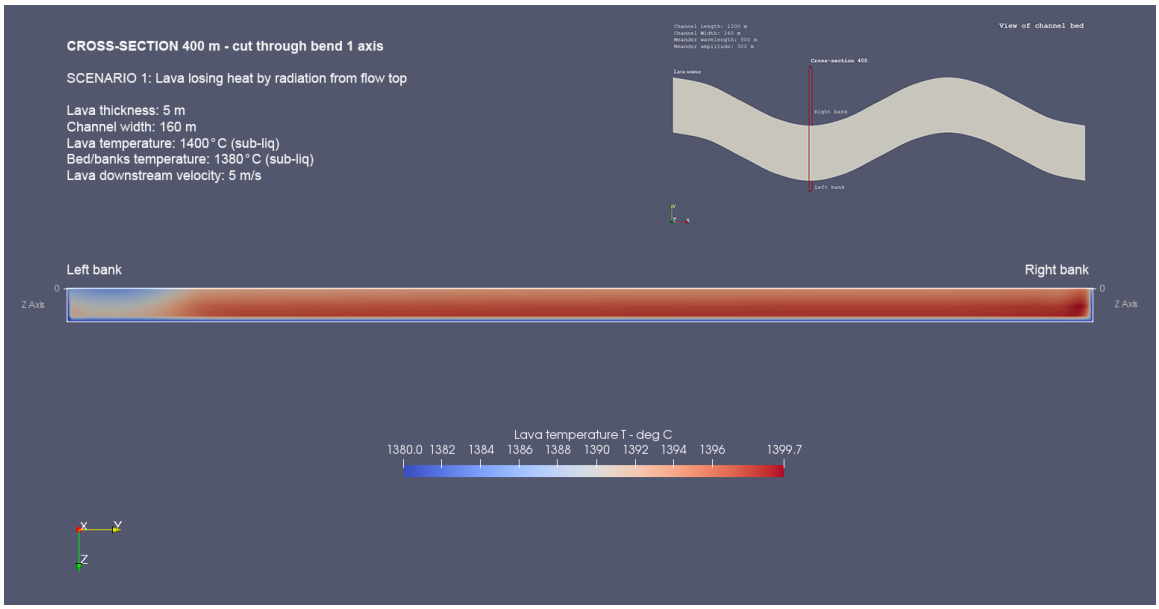

Figure 5.64. The distribution of lava temperature from one end of bend 1 to the opposite (mainstream flow is entering the page), rille cross-section 400, flow scenario described in Fig. 5.63. A zone of lower lava temperature extends from the flow top down to ~1/3 of the vertical distance that separates it from the bed. At the bed/right bank contact, the maximum lava temperature is 0.3°C lower than the original core temperature, which confirms that the energy budget of the lava is reduced as heat is lost through the flow top.

from the upper half of the cross-section downward to the bed. Fig. 5.65 shows the distribution of lava temperatures at the flow top and bed from one end to the other of cross-section 400.

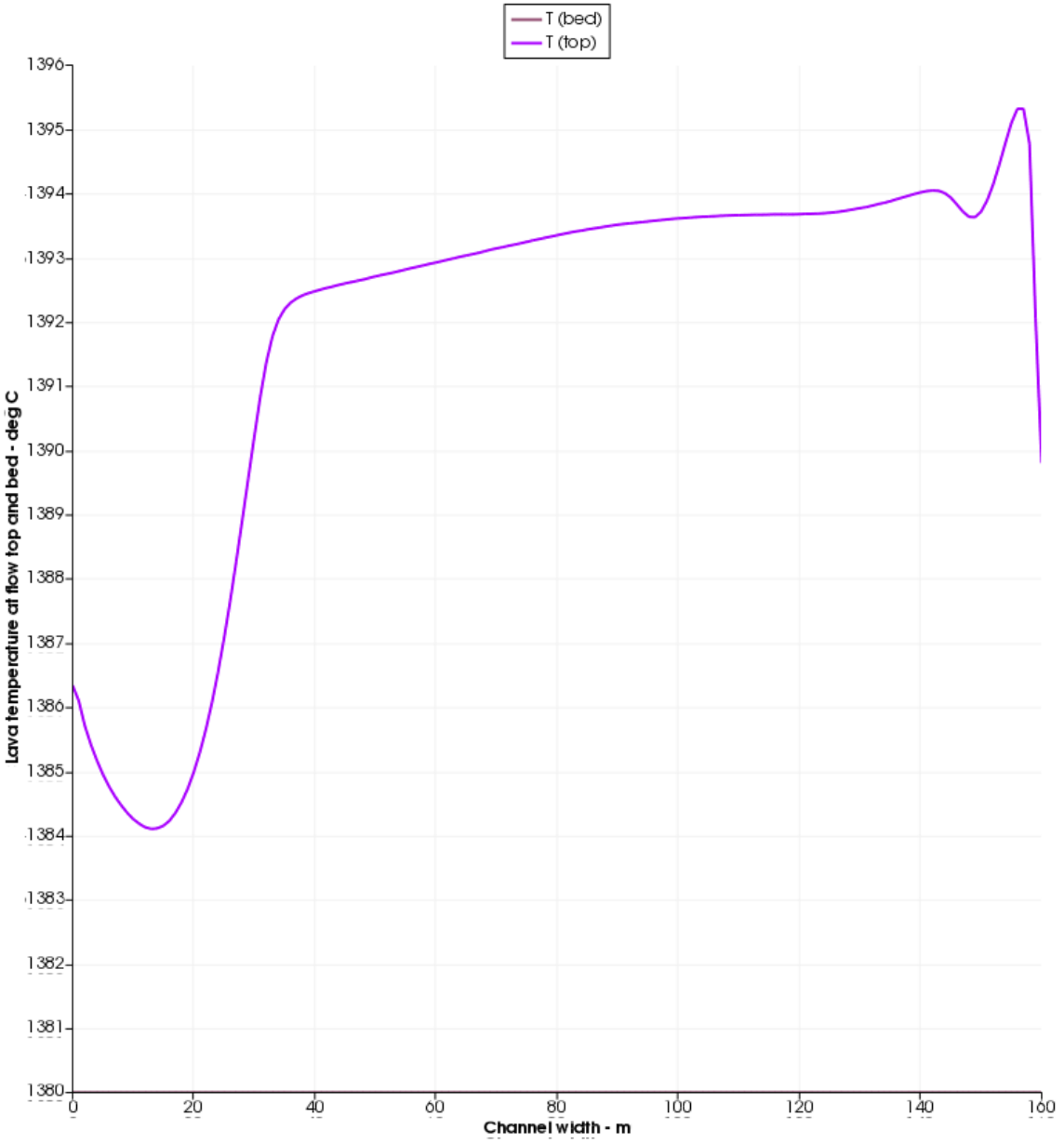

Figure 5.65. The distribution of lava temperatures at the flow top and bed of cross-section 400. Lava core temperature (input model parameter) is equal to 1400°C (sub-liquidus). At the bed, lava temperature is held constant at 1380°C whereas at the flow top it varies from a maximum of ~1395°C near the right bank to a minimum of ~ 1384°C within ~15 m of the left bank. Over the central portion of the section, flow top temperatures vary within ~1°C of 1393°C. Overall, flow top temperatures appear to vary within 5-16°C of the initial core temperature of 1400°C.

At the bed, lava temperature is held constant and equal to 1380°C (model input parameter), whereas temperatures at the flow top vary from >1395°C near the right bank to ~1384°C within ~15 m of the left bank. Over the central portion of cross-section 400, flow top temperatures vary within ~1°C of 1393°C, being ~7°C lower than the core temperature value of 1400°C.

Fig. 5.66 shows the distribution of velocities at bend 1 for a 20-m-thick superheated lava that flows at a temperature of 1605°C and travels at a velocity of 10 m s^{-1}. The lava, originally erupted at the superheated temperature of 1630°C, loses heat by radiation into the lunar environment. Secondary flow circulation reaches a maximum velocity of 1.4 m s^{-1} at the bed/right bank contact. The cross-stream velocity distribution is almost identical

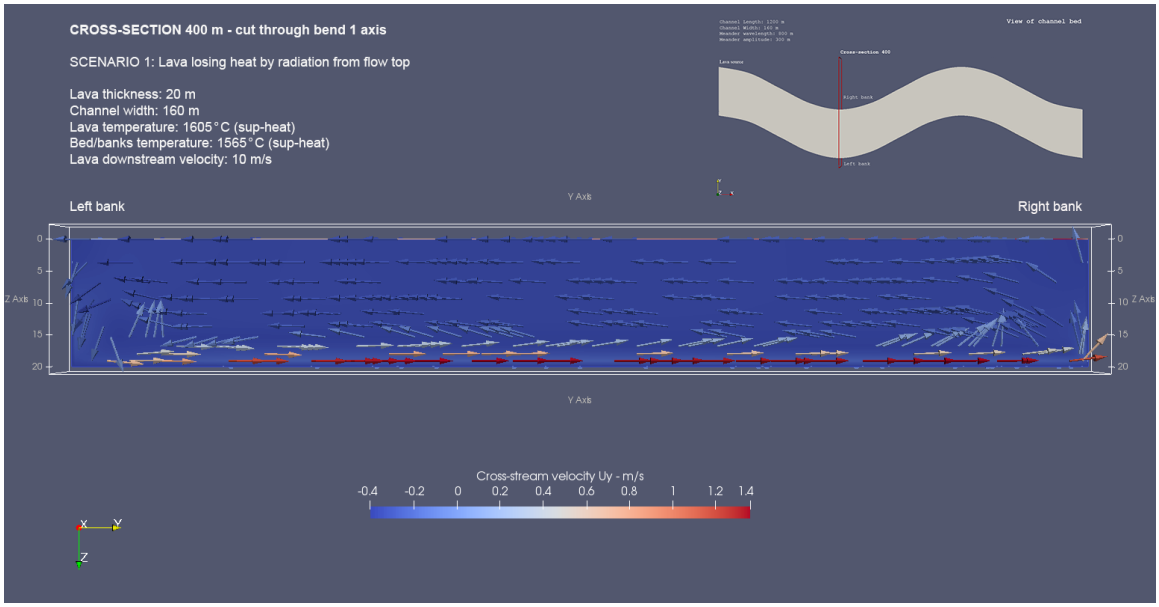

Figure 5.66. Cross-stream velocity vectors or U_y vectors (perpendicular to mainstream flow that enters the page) for rille cross-section 400, bend 1 axis. Results refer to 20-m-thick lava that undergoes cooling into the lunar environment through the flow top (scenario 1) and travels at a velocity of 10 m s^{-1}. The secondary flow reaches a maximum velocity of 1.4 m s^{-1} in the proximity of the right bank. The distribution of cross-stream velocities is almost identical to that found for the scenario 2 counterpart flow and once again shows evidence of a well-developed helicoidal flow.

to that found for the counterpart flow of scenario 2 (insulated lava). Fig. 5.67 shows the distribution of lava temperatures at cross-section 400. A low lava temperature zone extends

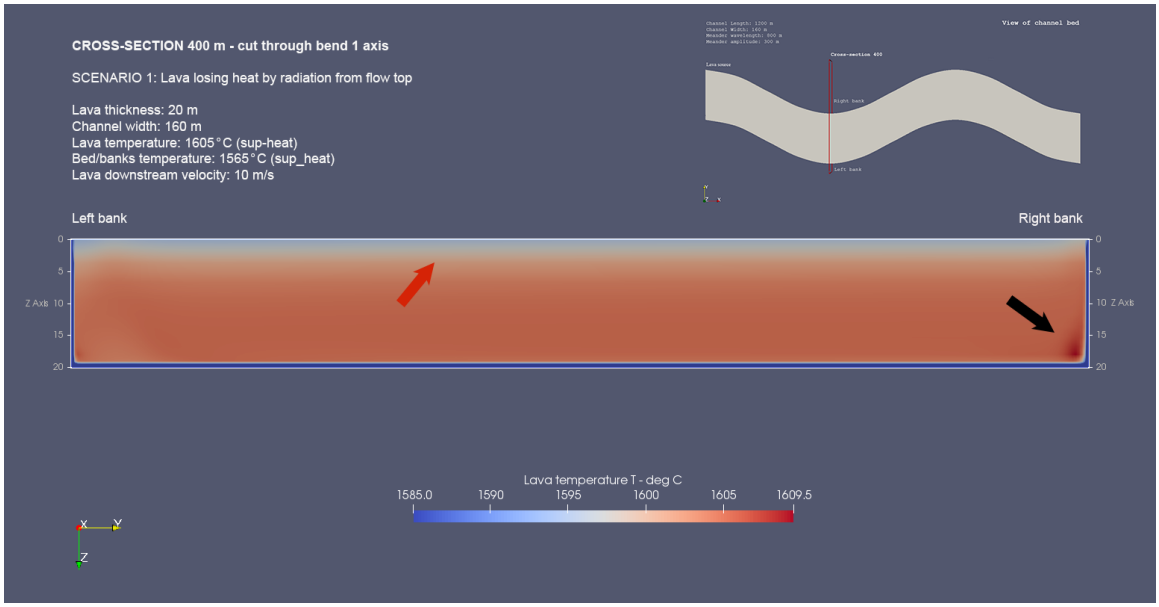

Figure 5.67. The distribution of lava temperature from one end of bend 1 to the opposite (mainstream flow enters the page), rille cross-section 400, flow scenario described in Fig. 5.66. A zone of lower lava temperature extends from the flow top down to ~1/4 of the vertical distance that separates it from the bed. At the bed/right bank contact (black arrow), the maximum lava temperature is 4.5°C higher than the core temperature value of 1605°C. The red arrow points at the low-temperature zone that forms because of lava losing heat by radiation into the lunar vacuum. The thickness of this zone is reduced compared to that observed in a 5-m-thick flow. The temperature enhancement at the bed/right bank contact and the lower thickness of the low-temperature zone at the flow top compared with that seen in a 5-m-thick flow confirm the better ability thick lava has to retain internal heat.

from the flow top down to ~1/4 of the vertical distance that separates it from the bed. At the bed/right bank contact, the maximum lava temperature is 4.5°C higher than the flow core temperature of 1605°C. This result is in stark contrast with the decrease in temperature observed at the same location in thin lava. The last two finds confirm that a 20-m-thick flow has a better ability to retain internal heat than a 5-m-thick lava. Finally, Fig. 5.68

shows the temperature distribution at the flow top and bed for the 20-m-thick superheated lava that travels at a velocity of 10 m s^{-1}.

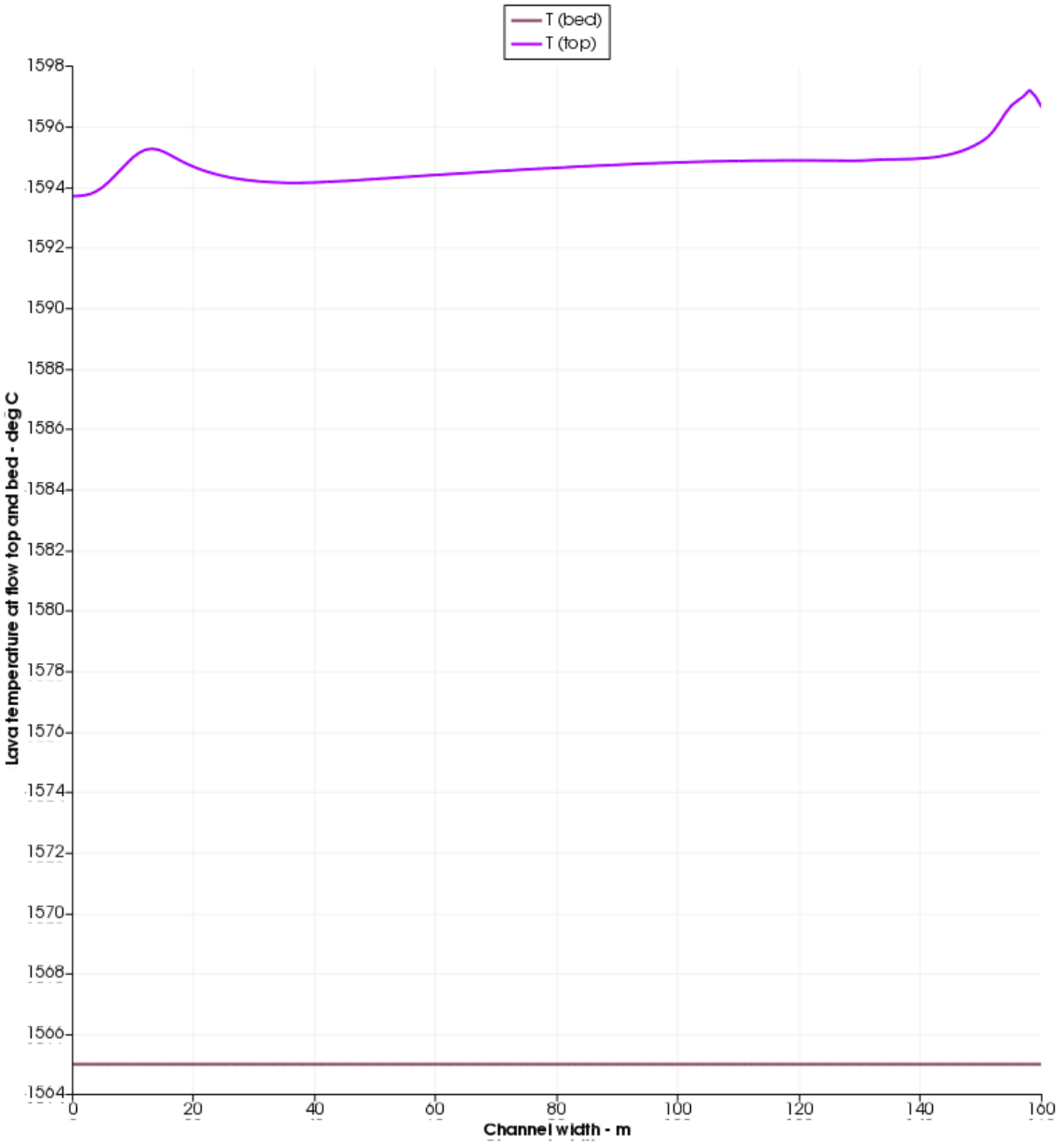

Figure 5.68. The distribution of lava temperatures at the flow top and bed of cross-section 400 for a 20-m-thick superheated lava (T=1605°C) traveling at a velocity of 10 m s^{-1}. At the bed, lava temperature is held constant at 1565°C, whereas at the flow top it varies from a maximum of ~1597°C near the right bank to a minimum of ~ 1594°C within ~15 m of the left bank. Over the central portion of the section, flow top temperatures vary within ~0.5°C of 1595°C. Overall, flow top temperatures appear to vary within 8-11°C of the

initial core temperature of 1605°C. In line with what seen in Fig. 5.67, a 20-m-thick flow has a much better ability to retain internal heat than a 5-m-thick flow.

At the flow top, the variation of temperature is much more contained than that underone by a 5-m-thick flow. Lava top temperatures only vary within 0.5°C of 1595°C across the central portion of the flow and there is a gap of only 3°C between maximum and minimum temperatures.

Physics behind the observed erosion rate enhancements

Figs. 5.47-5.66 show evidence for secondary flow circulation at two channel cross-sections that are cut parallel to two bend axes. For the thickest flows, secondary circulation forms a loopy pattern that closely reminds of helicoidal flow, as described in the river literature. Ultimately, secondary flow circulation appears to be responsible for a localized increase of lava temperatures and leads to erosion enhancement by impacting both magnitude and distribution of erosion rates at discrete portions of the channel bed and the two banks. How does this process work from a physics standpoint? At channel boundaries (bed and banks), flow velocity is held equal to zero. Also, lava temperature and viscosity are held constant. The SST k-ω turbulence model (*Menter*, 1993) adopts expressions for turbulent kinetic energy k and specific dissipation rate ω that contain velocity terms. If flow velocity increases, so do the values of k and ω. Besides, changes in flow velocity contribute to lava temperature variations because the convective term (term containing a velocity vector) is present in the temperature equation. Another important parameter that also changes with k and ω is turbulent viscosity, υ_t, as $\upsilon_t = k/\omega$ (*Menter*, 1993). Turbulent

and kinematic viscosity variations are also tied to lava temperature variations because the two viscosity terms are part of the effective thermal diffusivity term (α_{eff}) in the temperature equation. All results show that the channel segments that experience high velocity (and pressure) gradients are the meandering ones and, within those, the portions that are close to the bed and banks where flow velocities rapidly decrease to zero. As soon as the flowing lava enters a bend, the resulting pressure and velocity variations cause variations of k, ω, υ_t and T (lava temperature). Ultimately, variations of turbulent viscosity υ_t lead to variations in the effective thermal diffusivity of the lava (α_{eff}), which are responsible for variations of flow temperature and erosion rates at the interface (see Eqs. 2 and 3, this chapter).

Variations of k and υ_t at the rille bed and banks

Tracking down variations in turbulent kinetic energy and turbulent viscosity helps locate temperature variations and, ultimately, areas of erosion rate enhancement. Fig. 5.69

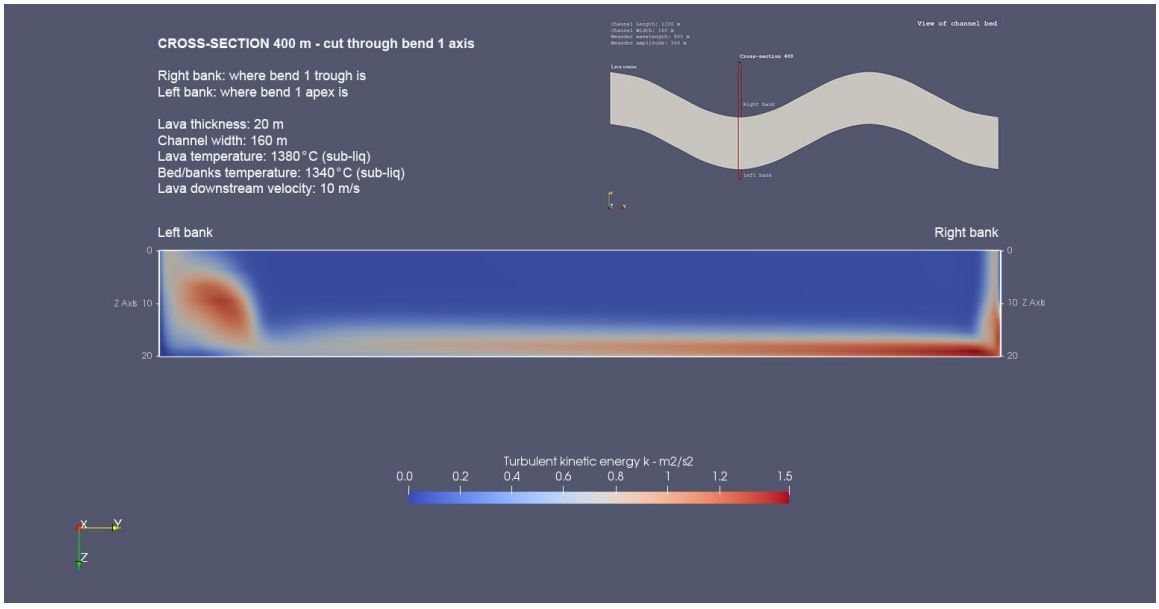

Figure 5.69. It is shown how turbulence kinetic energy k varies at cross-section 400 for a 20-m-thick lava erupted at the sub-liquidus temperature of 1380°C and traveling at a velocity of 10 m s^{-1}. The highest values of k are found at the bed in the proximity of the bed/right bank contact and at the right bank. At the latter location, values are highest from the bottom halfway up the bank top. From there, they drop and then remain almost constant up to the bank top. The oval-shaped region of high-k values on the left end of cross-section 400 is likely associated with the high-turbulence region observed in that channel portion. A high-turbulence region is characterized by strong velocity gradients and an increase of k is expected there.

shows the distribution of turbulence kinetic energy k at channel cross-section 400 for a 20-m-thick lava erupted at a sub-liquidus temperature of 1380°C and traveling at a velocity of 10 m s^{-1}. The highest values of k are found at the bed in proximity to the bed/right bank contact and at the right bank. At the latter location, values are highest from the bottom halfway up the bank top. From there, they drop and then remain almost constant up to the bank top. The oval-shaped region of high k values to the left appears to be associated with the high-turbulence region observed at the same location in Fig. 5.47 and is characterized by strong velocity gradients. Fig. 5.70 shows the other flow parameter that is diagnostic of

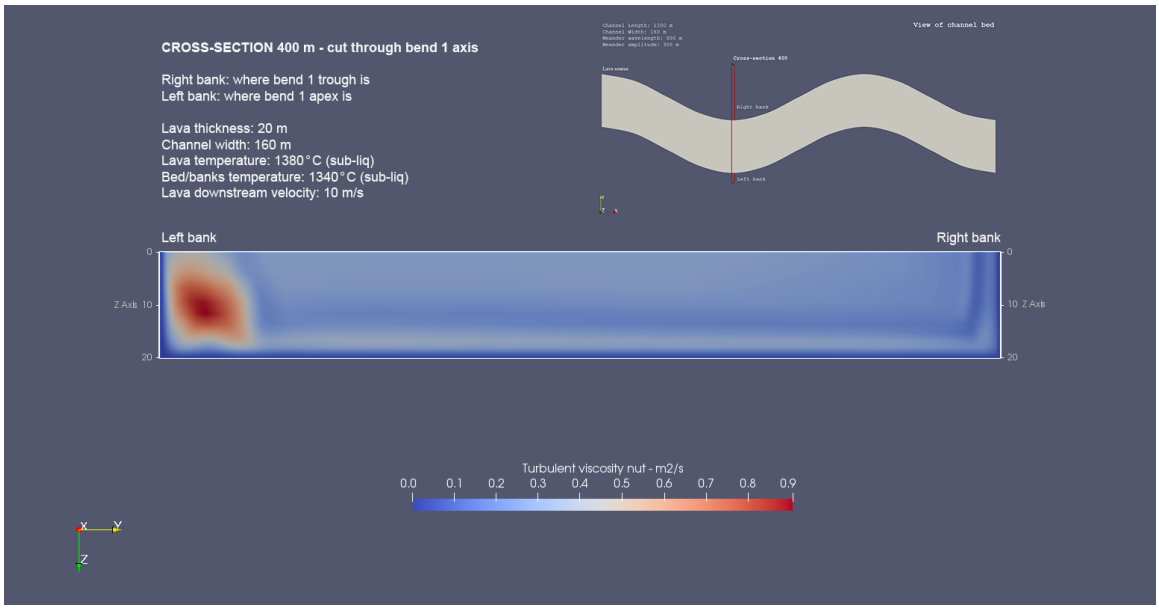

Figure 5.70. It is shown how turbulent viscosity, υ_t, varies for a 20-m-thick lava erupted at the sub-liquidus temperature of 1380°C and traveling at a velocity of 10 m s^{-1}. The highest values of υ_t are found at the center of the reddish area on the left end of the cross-section. This area is found in a portion of the channel that shows an oval-shaped increment of turbulent kinetic energy in Fig. 5.69, which is expected given that increments of k and υ_t tend to occur at the same location (they both develop in the presence of velocity gradients). That said, lower increments of υ_t (whitish in color) are seen right above the bed and to the immediate left of the right bank (locations of highest k values in Fig. 5.69). These increments are lower than the one seen on the left end of the cross-section because viscosity is a "resistance to flow" and, hence, that resistance is lower in those portions of the channel characterized by faster cross-stream velocities (regions parallel to the bed and up the right bank).

velocity and temperature variations at channel cross-section 400: turbulent viscosity, υ_t. The highest values of υ_t are found at the center of the reddish area on the left end of the cross-section. This area matches the location of an oval-shaped increment of turbulent kinetic energy in Fig. 5.69, which is expected given that increments of k and υ_t tend to occur at similar locations (they both develop in the presence of velocity gradients). That said, lower increments of υ_t (whitish in color) are seen right above the bed and to the immediate left of the right bank (locations of highest k values in Fig. 5.69). These increments are lower than the one seen on the left end of the cross-section because viscosity is a "resistance to flow" and, hence, that resistance is lower in those portions of the channel characterized by faster cross-stream velocities (regions parallel to the bed and up the right bank).

Discussion

This section is divided into two parts: the first aims to address the formation of the Vallis Schröteri inner rille and discusses the likelihood for this structure to have formed

due to a mechanism of thermal erosion or thermo-mechanical erosion. The second part discusses the limitations of the approach adopted. Results pertaining to scenario 1 lead to the conclusion that it is extremely unlikely for the lava that formed the inner rille of Vallis Schröteri to have flowed turbulently from lava source to terminus. Table 5.3 shows that, even allowing for a superheated temperature of 1630°C, the lava could have flowed turbulently probably no farther than ~48 km from the lava source. Of course, this is only a first-order estimate because the Stefan-Boltzmann relation that was used to determine cooling rates only accounts for initial lava temperatures and velocities. No account is taken of lava thickness. A lava that is thicker (i.e., of higher volumetric flow rate in 3-D modeling) has a better ability to retain internal heat than a thinner flow, holding other factors equal. Nevertheless, a lava that is 10- or 5-m-thick travels at a slower velocity than 10 m s^{-1} on the lunar surface and, thus, the error involved in this estimate is unlikely to be sufficiently large to alter the result. This might also be true for reasons that are discussed at the end of this section. Scenario 2 flows likely traveled greater distances from the Cobra Head, the source region for both the inner and outer rilles of Vallis Schröteri. Assuming cooling rates of 0.5-1.0°C/km (*Keszthelyi*, 1995), lavas 10-20 m in thickness, erupted at the liquidus temperature of 1440°C and flowing insulated from the lunar vacuum at velocities of 7-10 m s^{-1}, respectively, might have traveled downstream distances of 100-150 km. Finally, 10-20 m thick superheated lavas erupted at a temperature that is 190°C higher than the liquidus value might have been capable of flowing turbulently out to the rille terminus. Meanders of wavelength and amplitude analogous to those defining the meanders located in the upstream portions of the Vallis Schröteri inner rille occur at

downstream distances of ~100-150 km from the lava source. This seems to support the idea that thermal and/or thermo-mechanical erosion might have been very effective out to those distances from the Cobra Head.

How long might have taken for the lava to excavate the rille bed and banks, assuming thermal erosion only and a consolidated substrate of composition identical to that of the lava? For scenario 2 lavas, maximum erosion rates at the rille bed of 42.8 cm/day are found for a 20-m-thick lava erupted at the liquidus temperature and traveling at a velocity of 10 m s^{-1}. This flow would take 222 days to excavate the 95-m-deep (*Garry et al*., 2008) bed, whereas a superheated lava of identical thickness and speed would take 99 days. Estimated flow volumes for 20-m-thick liquidus and superheated lavas, given the rille length, width, and flow thickness, are equal to ~614 km^3 and ~274 km^3, respectively. A 10-m-thick lava erupted at the liquidus temperature and traveling at 7 m s^{-1} would take 330 days, whereas the superheated version of it would take 182 days. For this thinner flows, estimated lava volumes are equal to ~319 km^3 and ~176 km^3, respectively. Finally, a 5-m-thick lava erupted at the liquidus temperature and flowing at a velocity of 5 m s^{-1} would take 455 days, whereas its superheated version would take 340 days. The total volumes required for this 5-m-thick lavas to excavate the rille bed are equal to ~157 and 117 km^3. These newly calculated lava volumes are well within the 100-2000 km^3 range of values obtained by *Wilson and Head* (2017) for rilles of various size and excavated by flows inferred to be 10-m-thick. While a 5-m-thick flow could also have excavated the inner rille, 10-20-m-thick lavas pose less severe time and thermal constraints to accomplish the same goal. What would be the time required to carve a meander into the rock encasing the flow

– based on thermal erosion only? Secondary flow circulation affects the distribution of erosion rates at meander bends and, to a lesser extent, its magnitude (locally). The erosion rate discrepancy observed at the left and right bend of a meander might suggest that the two bends take different times to form. A 20-m-thick flow that is erupted at the liquidus temperature and travels at a velocity of 10 m s^{-1} would take ~324 days (duration obtained by averaging maximum erosion rates at the left and right bank) to excavate a 140-m-deep bend (average radius of bend curvature) into the rocks that encase the flowing lava. The superheated version of the same flow would take ~134 days instead. A 5-m-thick lava erupted at the liquidus temperature and traveling at a velocity of 5 m s^{-1} would take on average ~2.9 years (1085 days) to form a bend, whereas the same flow erupted at the superheated temperature of 1630°C would take ~2.2 years (791 days). The long durations associated with 5-m-thick lavas pose severe time and thermal challenges that might make these events not as likely as those featuring thicker flow units. The total lava volume a 20-m-thick flow would require to form a bend is equal to ~896 km^3 (if lava flows at the liquidus temperature) and ~371 km^3 (if lava is superheated). For a 5-m-thick flow, total lava volumes would range from ~375 km^3 (for lavas at the liquidus temperature) to ~273 km^3 (for superheated lavas). Once again, all of these values fall within the 100-2000 km^3 range of values obtained by *Wilson and Head* (2017). It is important to remember that time estimates are obtained from values of erosion rates that are assumed to remain constant over time. While this might hold true for a rille section located at a fixed downstream distance from the lava source (over a certain time), for increasing downstream distances from the Cobra Head, erosion rates will be lower and excavation times longer than those

illustrated here. Following the decrease in erosion rates with increasing downstream distances from the lava source, meander amplitude decreases. Moreover, as lava becomes progressively more viscous with decreasing temperatures and increasing distances from the vent, it travels at a slower velocity and meander wavelength decreases as well. Observational evidence obtained from LROC high-resolution NAC images shows that both the meander wavelength and amplitude decrease once a downstream distance of ~145 km is reached. This find strengthens the idea that the lava that formed the inner rille probably flowed insulated from the lunar environment. Otherwise, it would be extremely difficult to explain how meander amplitudes and wavelengths remain almost unchanged out to that large distance from the lava source.

A very important find of the theoretical study has to do with the impact of changes in meander amplitude on the strength and velocity of secondary flow circulation. Increases in meander amplitude make secondary flow circulation stronger and faster. This suggests that, by analogy with what happens in rivers, once a meander of a certain amplitude is generated, the amplitude of the same meander might grow larger with time. Some of the gooseneck meanders found along the path of the inner rille might have developed in a similar way over time.

Based on the presented thermal erosion results, how could a well-developed bend form in a lava channel? At both rivers and lava channels, the concave outer bend of a meander (left bank of bend 1 at cross-section 400 and right bank of bend 2 at cross-section 800) is a high-pressure zone characterized by slower water/lava velocities and the convex inner bend is a low-pressure zone with faster water/lava velocities. On the floor of a

riverbed, the secondary flow sweeps sand, silt and gravel across the river and deposits the solids near the convex, inner bank. This process leads to creation of D-shaped islands and meanders through creation of cut banks and opposing point bars (*Bowker*, 1988), which explains why the convex bank tends to be shallow and made up of these materials. On the contrary, the concave outer bank tends to be steep and elevated due to heavy mechanical erosion. Is there any evidence in the new 3-D model that could point at a potential role played by mechanical erosion at the concave, outer banks of a meander bend? All figures showing the distribution of cross-stream and vertical velocities at cross-section 400 reveal the occurrence of a region of high-turbulence in the proximity of the left bank. Flows that are 10-20 m in thickness reveal a high-turbulence region that is faster and better developed than that found in thinner flows. For 20-m-thick flows traveling at velocities of 5 and 10 m s^{-1}, each cross-section shows a well-developed vortex with cross-stream and vertical velocities in the range 0.5-1.2 m s^{-1} that are responsible for the observed enhancement in thermal erosion over specific portions of the left bank and at the bed (within 10-40 m of the bed/left bank contact). The same circulation could also promote a process of mechanical erosion at the concave, outer bank (high-pressure, low velocity zone), which could perhaps counterbalance (at least to some extent) the higher thermal erosion rates obtained at the convex, inner bank (low-pressure, high-velocity zone).

The 3-D model approach presented here suffers from a few limitations. First, it does not provide a real-time evolution of the flowing lava from source to terminus. Accurate and reliable transient simulations of lava evolution over distance and time (lava is a complex physical and chemical system) should require a treatment that be comprehensive

of the geochemical evolution of the flow. *Williams et al*. (1998, 2000) created a rigorous model of thermal erosion by turbulently flowing lava that, while suffering from the limitations imposed by the one-dimensional approach, it provides information on lava composition and its geochemical evolution over time. It also accounts for a mechanism of incorporation and assimilation of portions of eroded substrate into the flowing lava. A flow that incorporates and eventually assimilates portions of eroded substrate, changes composition. This lowers the Reynolds number of the flow, which, ultimately, leads to a decrease in erosion rates. The assimilation of substrate materials into the flowing lava takes up a part of the heat budget of the flow, which causes lava temperatures to decrease (at least locally) and viscosities to increase. Running a real-time simulation from lava source to terminus would introduce an error bar that is too large, until this level of complexity becomes incorporated into the model.

From a thermodynamic standpoint, the new model does not account for heat loss by conduction into the lava substrate. Thermal equilibrium is assumed at the lava/substrate interface, which implies that the temperature at the interface is held constant at the value of melting. For real-time flows, it takes about a week for the substrate to heat up and reach the melting temperature (Lionel Wilson, personal communication), which suggests that even a series of discrete, short-lasting events would likely be inefficient in excavating the lava substrate. Lava flowing at a velocity of 10 m s^{-1} could easily travel the entire distance separating the Cobra Head from the rille terminus in ~5.5 hours but the erosive power of the same flow would be negligible.

The lava substrate is assumed to be both consolidated and unconsolidated (the latter only applying to 10-m-thick flows erupted at the liquidus temperature and traveling at a velocity of 7 m s^{-1}). Regardless of substrate characteristics, the amount of eroded material that can become incorporated and eventually assimilated into the flowing lava depends on flow parameters such as lava temperature, velocity, and thickness. Specifically, one requirement must be met to prevent the flow from increasing its viscosity to the point that it may freeze. The available heat energy content in the eroding lava flow must be larger by at least several factors than the heat energy required to melt the substrate (*Kerr*, 2001, *Sewert and Ferlito*, 2008). Attention should be paid to this important aspect when modeling erosion by lava, especially when dealing with flows that are not thick and their ability to travel at high velocity is reduced compared to thicker lavas.

Conclusions

Chapter 5 presents results of the new 3-D model of thermal erosion by turbulently flowing lava, as applied to the inner rille of Vallis Schröteri on the Moon. Lava and substrate are assumed to be basaltic in composition, and the substrate is taken as consolidated. The SST k-ω turbulence model and OpenFOAM software are used for each steady-state simulation. Calculated maximum erosion rates refer to a ~1-km-long rille segment located at the Cobra Head (lava source) and are obtained from 5- and 20-m-thick uncrusted (scenario 1) and tube-fed (scenario 2) lavas. Flows are erupted at the liquidus temperature (1440°C) and at a range of superheated and sub-liquidus temperatures, all of which consistent with Newtonian flow conditions (solver requirement). Lower and upper

values of flow thickness – 5 and 20 m - are considered, and the initial flow velocities of 5 and 10 m s^{-1} are calculated from flow thickness and slope of ground. The highest erosion rates of ~1 m/day are associated with scenario 2 flows erupted at a temperature of 1630°C (superheated lava) and traveling at a velocity of 10 m s^{-1}. The lowest erosion rates are produced by 5-m-thick flows erupted at a temperature of 1380°C (sub-liquidus lava) and traveling at a velocity of 5 m s^{-1}. Flow durations required to excavate the 95-m-deep bed range from a minimum of 99 days for 20-m-thick superheated lavas traveling at 10 m s^{-1} to a maximum of 455 days for 5-m-thick liquidus lavas flowing at 5 m s^{-1}. To form an average-sized 140-m-wide bend, flow durations vary from 134 days (20-m-thick, superheated lava) to ~ 3 years (5-m-thick, liquidus lava). Mechanical erosion, which is unaccounted for in the presented model of thermal erosion, might have bridged the gap in flow durations at the bed and banks (at least, to some extent). Perhaps the most important result of the current investigation is the discovery of secondary flow circulation in lava channels and at meander bends. Secondary circulation is well known in meandering rivers and is responsible for meander generation and migration in time. At the Vallis Schröteri inner rille, secondary circulation appears to affect magnitude and spatial distribution of erosion rates at meander bends by first causing variations in downstream and cross-stream velocities than then translates into temperature variations. A consistent pattern is observed at any rille cross-sections that are cut parallel to meander axes. A cross-section cut parallel to bend 1 reveals a consistent increase in erosion rates at a portion of the rille bed close to the bed/right (inner) bank contact and at the right (inner) bank itself. In meandering rivers, the maximum of erosion (mechanical) is always found at the left (outer) bank but the

topography of river beds and banks changes both spatially and temporally. A new version of the 3-D model will resolve the apparent discrepancy in erosion rates distribution at lava and river meanders by incorporating the additional element of complexity that is unaccounted for in the current version of the 3-D model.

6 DISCUSSION, CONCLUSIONS AND FURTHER WORK

Discussion

The new 3-D model has revealed a level of complexity that is not accessible by available lower-dimensional models. It is the first model of thermal erosion by turbulently flowing lava that addresses erosion at the rille bed and banks, with special emphasis on erosion at meander bends. The model has revealed details of flow circulation that were only known in the river literature, which now appear to have a potential to explain how rille meanders might have formed and, possibly, evolved at the time lava was flowing at the Vallis Schröteri rille site on the Moon. At the primary rille of Vallis Schröteri, the model has added support to the idea that thermal erosion was unlikely responsible for the formation of the up-to 700-m-deep and 4-km-wide depression found at this lunar site. At the inner rille, it has shown that thermal erosion or thermo-mechanical erosion might have led to rille formation and placed key constraints on eruption durations and total lava volumes. Importantly, the model has provided first-time evidence for a mechanism of secondary flow circulation at meander bends, which affects erosion rate magnitude and distribution and might, at least, explain how meanders evolved over time. As a matter of fact, secondary circulation is responsible for meander generation in river channels, a process that is initiated prior to sediment transport from one bend to the opposite (*Olesen*, 1987; *Camporeale et al*., 2007).

Some of the implications of the modeling are here discussed. All results were obtained from steady-state simulations of lavas erupted at a range of temperatures and flow

velocities over a rille segment that extends for 1.0-1.5 km. As a result, no information on the physical and geochemical evolution of the lava is available at the present time. That said, specific results may cast light on the potential evolution of the lava in time. Specifically, the initial lava temperature poses severe constraints on the distance from the source an individual flow might be able to travel, while flowing in a turbulent fashion. The occurrence of well-formed meanders at downstream distances > 100 km from the lava source suggests that the erosive power of the lava might have still been high at those large distances from the Cobra Head (source). Another possibility is that the "distant" meanders might have developed from lava flowing laminarly and at slower flow rates than those associated with turbulently flowing lava. *Sakimoto and Gregg* (2019) support an origin from tube-fed and laminarly flowing lava for even large-scale sinuous rilles. What can be said about the observed changing geometry of rille meanders? As already stated in the section titled "The geometry of the rille" (Chapter 5), after the inner rille cross cuts the primary outer rille wall (at a distance from the lava source of ~150 km), the channel becomes shallower and narrower (~100 in width), meanders become rare, of shorter wavelength (~650 m) and lower amplitude (~250 m). Results of the sensitivity analysis chapter (Chapter 2) show that, for a flow of specified thickness, a reduction in lava temperature and/or flow velocity is accompanied by a reduced erosive power. As lava temperature decreases, flow viscosity increases and, at some point, flow regime transitions from turbulent to laminar (the Reynolds number decreases until it reaches a value of ~2000) and flow velocity decreases as well. The channel becomes shallower and narrower because the ability of the lava to erode vertically into the bed and sideways (laterally) into the banks

is reduced. Furthermore, a slower-traveling lava might likely develop meanders that are smaller in wavelength. In rivers, the slower the velocity of the flow, the shorter the meander wavelength. While affecting meander wavelength, a slower flow velocity also causes meander amplitude to decrease. The theoretical study section of Chapter 5 shows that a lower meander amplitude is associated with slower downstream and cross-stream velocities at channel cross-section 400 (a section cut through the bend axis). Conversely, a faster downstream and cross-stream velocity might have formed a rille with bends of a higher amplitude. The inner rille of Vallis Schröteri shows both meanders of low amplitudes and goose-neck meanders of very high amplitude. As already mentioned in the section titled "The geometry of the rille" (Chapter 5), a close inspection of goose-neck meanders reveals that they occur in association with narrow mounds that might have acted as obstacles, thus compelling the flow to follow a loopy path around them. If that is the case, the actual amplitude of, at least, a few goose-neck meanders might not have resulted from the interplay of lava velocity and erosion. Instead, it might be a reflection of changing topography. This interpretation is also consistent with the highly meandering nature of this rille, i.e., with the fact that rille wavelength is shorter than that seen at many other rille sites on the Moon. Meanders of very high amplitude might have required fast downstream and cross-stream velocities, which might be inconsistent with the frequent occurrence of meanders of a short wavelength along the inner rille path. Another possibility is that, at least, some goose-neck meanders could have resulted from local variations in the mechanical properties of the lava substrate. The goose-neck meanders that cannot be traced back to the occurrence of an obstacle in the lava path might have developed from a process

of differential erosion (likely mechanical because that would be more effective than thermal over a short time period) within the lava substrate. Topography might then exert a strong control on rille geometry.

The 3-D model has revealed how local variations in flow velocity and temperature at rille cross-sections cut parallel to meander axes affect the magnitude and spatial distribution of erosion rates over the bends. How could a meander form once lava starts flowing downstream of the source? Topography might still exert the strongest control on the onset of meandering. The occurrence of an obstacle in the way of the flowing lava or local variations of ground slope initially cause the flow to deviate from a straight line. As soon as water (or lava here) follows a curved trajectory, secondary flow circulation builds up, which then initiates the process of meander generation (*Bowker*, 1988).

In the presented 3-D model, erosion maxima (thermal) are found at the bed in the proximity of the bed/right bank contact and at the right bank, which is the equivalent of the convex or inner bend in river meanders. The problem is that in rivers the maximum of erosion (mechanical) is found at the concave or outer bend, which is where water travels faster than anywhere else in the bend. Furthermore, at the outer bend water is deeper than at the inner bend. In order to understand what is behind the observed discrepancy in flow behavior at river and lava meanders, it is important to remember that the 3-D model predicts the magnitude and distribution of erosion rates at meander bends before any changes in bed and bank topography may occur. As a result, all the simulations run by the 3-D model adopt a flat bed and flat bank geometry, and the thickness of the flowing lava is held constant from one meander bend to the opposite and through the entire channel segment.

In rivers, as soon as water follows a curved trajectory, secondary flow circulation induces a cross-stream component of the shear stress, which leads to a transverse bed slope and increases flow depth toward the outer bend (*Olesen*, 1987; *Camporeale et al.*, 2007). This redistributes momentum, causing velocities to increase toward the outer bend, which is then followed by sediment transport toward the inner bend (*Camporeale et al.*, 2007). Currently, no evidence for such a mechanism of velocity redistribution toward the outer bend exists at meandering lava channels. Nevertheless, the newly found evidence for secondary circulation at rille cross-sections cut parallel to meander axes suggests that a similar process might occur in lava channels as well. The described redistribution of momentum toward the outer bend should then cause the peak of erosion (both thermal and mechanical) to shift to the outer bend. Importantly, this may lay the foundations for further work, which is outlined in the next section.

Conclusions

The new 3-D model of thermal erosion by turbulently flowing lava has, for the first time, provided erosion rates at the bed and banks of a large, sinuous rille (the primary rille) and a highly meandering one (the inner rille) at the lunar site of Vallis Schröteri. It has shown that thermal erosion likely played a limited role in the formation of the primary rille while tectonics and, to a lower extent, constructional processes might have shaped the rille as it is. The model has also shown that thermal erosion was likely responsible for the formation of the inner rille and has allowed for flow durations and lava volumes to be constrained at this lunar site. Mechanical erosion might have led to the formation of, at

least, a few goose-neck meanders, by exploiting spatial variations in the mechanical properties of the lava substrate. Mechanical erosion could also have shortened flow durations based on thermal erosion only, especially at meander bends where flow durations were calculated to be slightly longer than at the rille bed. Last but not least, for the first time a theoretical study has found evidence for secondary flow circulation at the meander bends of a lava channel. This mechanism appears to be responsible for altering the magnitude and spatial distribution of erosion rates over the bends and might have had an important control in modifying bend geometry by analogy with what known from the river literature.

Further work

A new version of the 3-D model could include a number of improvements. Based on what described at the end of the discussion section, the first objective is that of building a model version that may reproduce a spatial distribution of erosion rates analogous to that shown in meandering river channels. The new version of the model should be able to correctly predict meander evolution over time, and will do so by accounting for variations in lava depth and friction at rille boundaries. The newly added level of complexity should redistribute momentum, causing lava velocities to increase toward the outer bend, which will lead to enhanced thermal erosion at the outer rille bend rather than at the inner bend or meander trough.

A new version of the model should also address the geochemical evolution of the flowing lava. To do so, it will allow for incorporation and assimilation of eroded materials

at the bed and banks. A concentration equation will be written and included within the code and boundary conditions will be modified so as to account for heat loss by conduction into the lava substrate. At that point, both steady-state and transient simulations over the entire rille length will better constrain the downstream distance at which the turbulent-laminar transition might have occurred at the Vallis Schröteri site.

REFERENCES

Andrews-Hanna, J.C., S.W. Asmar, J.W.III Head, W.S. Kiefer, A.S. Konopliv, F.G. Lemoine, I. Matsuyama, E. Mazarico, P.J. McGovern, H.J. Melosh, G.A. Neumann, F. Nimmo, R.J. Phillips, D.E. Smith, S.C. Solomon, G.J. Taylor, M.A. Wieczorek, J.G. Williams, and M.T. Zuber (2013), Ancient igneous intrusions and early expansion of the Moon revealed by GRAIL gravity gradiometry, *Science, 339*, 6120, 675-678, doi:10.1126/science.1231753.

Arndt, N. T. (1976), Melting relations of ultramafic lavas (komatiites) at one atmosphere and high pressure, *Year Book Carnegie Inst., 75,* Washington, pp. 555-562.

Arndt, N.T. (1994), Komatiites, ed. K.C. Condie, in: *Archean Crustal Evolution, Elsevier Sci.*, NY, pp. 11-44.

Baird, A. K. (1984), Did komatiitic lavas erode channels on Mars?, *Nature, 311*, 18.

Baker, V.R., G. Komatsu, T.J. Parker, V.C. Gulick, J.S. Kargel, and J.S. Lewis (1992), Channels and Valley on Venus: Preliminary analysis of Magellan data, *J. Geophys. Res., 97,* 13,421-13,444.

Baloga, S., and D. Pieri (1986), Time-dependent profiles of lava flows, *J. Geophys. Res., 91*, 9543-9552.

Bandfield, J. L., V. E. Hamilton, and P. R. Christensen (2000), A global view of Martian surface compositions from MGS-TES, *Science, 287,* 1626-1630.

Berman, D.C., and W. K. Hartmann (2002), Recent fluvial, volcanic, and tectonic activity on the Cerberus Plains of Mars, *Icarus, 159,* 1-17.

Bottinga, Y., and D. F. Weill (1970), Densities of liquid silicate systems calculated from partial molar volumes of oxide components, *Am. J. Sci., 269*, 169-182.

Bowker, K.A. (1988), Albert Einstein and meandering rivers, *Earth Science History, 1*, (1).

Boyd, A. K., H. Hiesinger, M.S. Robinson, T. Tran, C.H. Van der Bogert, R.V. Wagner, and the LROC Science Team (2011), Lunar pits: Sublunarean voids and the nature of mare emplacement, *Lunar Planet. Sci*., *42th* , abstract 2771.

Burr, D.M., J.A. Grier, A.S. McEwen, and L.P. Keszthelyi (2002), Repeated aqueous flooding from the Cerberus Fossae: Evidence for very recently extant, deep groundwater on Mars, *Icarus, 159,* 53-73.

Bussey, D.B.J., S.A. Sørensen, and J.E. Guest (1995), Factors influencing the capability of lava to erode its substrate: Application to Venus, *J. Geophys. Res., 100*, 16,941-16,948.

Campbell, B.A., L.M. Carter, B.R. Hawke, D.B. Campbell, and R.R. Ghent (2008), Volcanic and impact deposits of the Moon's Aristarchus Plateau: A new view from Earth-based radar images, *Geology*, *36(2),* 135–138, doi:10.1130/G24310A.1.

Camporeale, C., P. Perona, A. Porporato, and L. Ridolfi (2007), Hierarchy of models for meandering rivers and related morphodynamic processes, *Rev. Geophys., 45*, RG1001, doi:10.1029/2005RG000185.

Carslaw, H.S., and J.C. Jaeger (1959), Conduction of Heat in Solids, 2nd Ed., *Oxford Univ. Press,* New York, pp. 510.

Carr, M. H. (1974), The role of lava erosion in the formation of lunar rilles and Martian channels, *Icarus, 22*, 1-23.

Cataldo, V., D.A. Williams, and W.B. Garry (2015), Erosion by lava on the Moon: Application to the rille of Vallis Schröteri, *Lunar Planet. Sci.*, *46th*, abstract 1582.

Cataldo, V., M.H. Schmeeckle, and D.A. Williams (2022a), Vallis Schröteri, Moon: the likely role played by thermal erosion by lava in excavating the primary rille, *J. Volcanol. Geotherm. Res*., in revision.

Cataldo, V., M.H. Schmeeckle, and D.A. Williams (2022b), How the inner rille of Vallis Schröteri formed: Results of 1st lunar 3-D model of thermal erosion by turbulently flowing lava, manuscript in preparation.

Chappaz, L., H. Melosh, K. Howell, and the GRAIL mission team (2014), Surface and buried lava tube detection with GRAIL data, *Lunar Planet. Sci. Conf., 45th,* abstract 1746.

Chappaz, L., R. Sood, H.J. Melosh, K.C. Howell, D.M. Blair, C. Milbury, and M.T. Zuber (2017), Evidence of large empty lava tubes on the Moon using GRAIL gravity, *Geophys. Res. Lett., 44*, 105–112, doi:10.1002/2016GL071588.

Christensen, P. R., R. V. Morris, M. D. Lane, J. L. Bandfield, and M. C. Malin (2001), Global mapping of Martian hematite mineral deposits: Remnants of water-driven processes on early Mars, *J. Geophys. Res., 106* (E10), 23,873-23,885.

Ciesla, F. J., and L. Keszthelyi (2000), A simple model for lava flow quarrying: Mechanical erosion of the substrate, *Proc. Lunar and Planet. Sci. Conf., XXXI*, abstract 1647.

Colozza, A.J. (1991), Analysis of Lunar Regolith Thermal Energy Storage, *NASA CR-189073, 2*, 2.

Coombs, C.R., B.R. Hawke, and L. Wilson (1990), Terrestrial analogs to lunar sinuous rilles: Kauhako crater and channel, Kalaupapa, Molokai, and other Hawaiian lava conduit systems, *Proc. Lunar Planet. Sci. Conf., 20th*, 195-206.

Crisp, J., and S. Baloga (1990), A model for lava flows with two thermal components, *J. Geophys. Res., 95*, 1255-1270.

Crisp, J., and S. Baloga (1994), Influence of crystallization and entrainment of cooler material on the emplacement of basaltic aa lava flows, *J. Geophys. Res., 99*, 11,819-11,831.

Cruikshank, D.P., and C.A. Wood (1972), Lunar rilles and Hawaiian volcanic features: Possible analogs, *The Moon, 3*, 412-447.

Cutts, J. A., W. J. Roberts, and K. R. Blasius (1978), Martian channels formed by lava erosion, *Lunar and Planet. Sci. Conf., IX*, abstract 209.

Danês, Z.F. (1972), Dynamics of lava flows, *J. Geophys. Res., 77*, 1430-1432.

Dawson, J.B., H. Pinkerton, G.E. Norton, and D.M. Pyle (1990), Physicochemical properties of alkali carbonatite lavas: Data from the 1988 eruption of Oldoinyo Lengai, Tanzania, *Geology, 18*, 260-263.

Dragoni, M., M. Bonafede, and E. Boschi (1986), Downslope flow models of a Bingham liquid: Implications for a lava flow, *J. Volcanol. Geotherm. Res., 30*, 305-325.

Dragoni, M. (1988), A dynamical model of lava flows cooling by radiation, *Bull. Volcanol., 51*, p. 88-95.

Dragoni, M., A. Piombo, and A. Tallarico (1995), A model for the formation of lava tubes by roofing over a channel, *J. Geophys. Res., 100*, 8435-8447.

Dundas, C., and L. P. Keszthelyi (2013), Modeling steam pressure under martian lava flows, *Icarus, 226*, 1058-1067.

Dundas, C., and L.P. Keszthelyi (2014), Emplacement and erosive effects of lava in south Kasei Valles, Mars, *J. Volcanol. Geotherm. Res., 282*, 92-102.

Fagents, S., and R. Greeley (2001), Factors influencing lava-substrate heat transfer and implications for thermomechanical erosion, *Bull. Volcanol*., *62*, 519–532, doi:10.1007/s004450000113.

Garry, W.B., J.E. Bleacher, and N.A. Warner (2008), Emplacement scenarios for Vallis Schröteri, Aristarchus Plateau, the Moon, *Lunar Planet. Sci. Conf. 39th*, abstract 2261.

Gellert, R., et al. (2004), Chemistry of rocks and soils in Gusev crater from the Alpha Particle X-Ray Spectrometer, *Science, 305*, 829-832.

Ghiorso, M.S., and R.O. Sack (1995), Chemical mass transfer in magmatic processes IV. A revised and internally consistent thermodynamic model for the interpolation and extrapolation of liquid-solid equilibria in magmatic systems at elevated temperatures and pressures, *Contrib. Mineral. Petrol., 119*, 197-212.

Gifford, A.N. and F. El-Baz (1981), Thicknesses of mare flow fronts, *Moon Planet., 24*, 391-398.

Greeley, R. (1971a), Lunar Hadley Rille: Considerations of its origin, *Science*, *172*, 722–725, doi:10.1126/science.172.3984.722.

Greeley, R. (1971b), Observations of actively forming lava tubes and associated structures, Hawaii, *Modern Geol., 2*, 207-223.

Greeley, R. (1972), Additional observations of actively forming lava tubes and associated structures, Hawaii, *Mod. Geol., 3*, 157-160.

Greeley, R., S.W. Lee, D.A. Crown, and N. Lancaster (1990), Observations of industrial sulfur flows: Implications for Io, *Icarus, 84*, 374-402.

Greeley, R., S.A. Fagents, R.S. Harris, S.D. Kadel, D.A. Williams, and J.E. Guest (1998), Erosion by flowing lava: Field evidence, *J. Geophys. Res., 103,* 27,325-27,346.

Greeley, R., B.H. Foing, H.Y. McSween, G. Neukum, P. Pinet, M. Van Kan, S.C. Werner, D.A. Williams, and T.E. Zegers (2005), Fluid lava flows in Gusev crater, Mars, *J. Geophys. Res., 110*, doi:10.1029/2005JE02401.

Gregg, T.K.P., and R. Greeley (1993), Formation of Venusian Canali: Considerations of lava types and their thermal behaviors, *J. Geophys. Res*., *98*, 10873–10882, doi:10.1029/93JE00692.

Guest, J.E. (1973), Stratigraphy of ejecta from the lunar crater Aristarchus, *Geol. Soc. Am. Bull*., *84*, 2873–2894, doi:10.1130/0016-7606(1973) 84<2873:SOEFTL>2.0.CO;2.

Guest, J.E., C.R.J. Kilburn, H. Pinkerton, and A.M. Duncan (1987), The evolution of lava flow fields: Observations of the 1981 and 1983 eruptions of Mount Etna, Sicily, *Bull. Volcanol., 49*, 527-540.

Hallet, B. (1996), Glacial quarrying: a simple theoretical model, *Ann. Glaciol., 22*, 1-8.

Harris, A.J.L. (2013), Thermal Remote Sensing of Active Volcanoes: A User's Manual, *Cambridge University Press*, Cambridge, pp. 736.

Hartmann, W.K. (1964), Radial structures surrounding lunar basins, I: The Imbrium system, *Commun. Lunar and Planetary Lab*., *2*, 1-15.

Haruyama, J., K. Hioki, M. Shirao, T. Morota, H. Hiesinger, C.H. van der Bogert, H. Miyamoto, A. Iwasaki, Y. Yokota, M. Ohtake, T. Matsunaga, S. Hara, S. Nakanotani, and C.M. Pieters (2009), Possible lunar lava tube skylight observed by SELENE cameras, *Geophys. Res. Lett*., *36*, L21206, doi:10.1029/ 2009GL040635.

Head, J.W., and L. Wilson (1981), Lunar sinuous rille formation by thermal erosion: Eruption conditions, rates and durations, *Proc. Lunar Planet. Sci. Conf*., *12th*, 427–429.

Head, J.W., D.B. Campbell, C. Elachi, J.E. Guest, D.P. McKenzie, R.S. Saunders, G.G. Schaber, and G. Schubert (1991), Venus volcanism: Initial analysis from Magellan data, *Science, 252*, 276-288.

Head, J. W., et al. (2011), Flood volcanism in the northern high latitudes of Mercury revealed by MESSENGER, *Science, 333*, 1853-1856, doi:10.1126/science.1211997.

Hickin, E.J. (2003), Meandering Channels, ed. G.V. Middleton, in *Encyclopedia of Sediments and Sedimentary Rocks*, New York: Springer, pp. 432, ISBN 1-4020-0872-4.

Hon, K., J. Kauahikaua, R. Denlinger, and K. Mackay (1994), Observations and measurements of active lava flows on Kilauea volcano, Hawaii, *Geol. Soc. Am. Bull., 106*, 351-370.

Honda, C., T. Morota, Y. Yokota, Y. Ogawa, H. Demura, N. Hirata, T. Matsunaga, M. Ohtake, and J. Haruyama (2009), Morphologic characteristics of the Vallis Schröteri, *Lunar Planet. Sci. Conf.,40th,* abstract 1524.

Howard, K.A., and J. W. Head III (1972), Regional geology of Hadley Rille. in: *Apollo 15: Preliminary Science Report. NASA SP-289*, 53–58.

Howard, K.A., J.W. Head, and G.A. Swann (1972), Geology of Hadley Rille, *Proc. Lunar Sci. Conf., 3rd*, 1-14.

Huang, J., L. Xiao, X. He, L. Qiao, J. Zhao, and H. Li (2011), Geological characteristics and model ages of Marius Hills on the Moon, *J. Earth Sci., 22*, 601–609, doi:10.1007/s12583-011-0211-8.

Hulme, G. (1973), Turbulent lava flows and the formation of lunar sinuous rilles, *Mod. Geol., 4*, 107-117.

Hulme, G. (1974), The interpretation of lava flow morphology, *Geophys. J. Int., 39*, 361–383, doi:10.1111/j.1365-246X.1974.tb05460.x.

Hulme, G. (1982), A review of lava flow processes related to the formation of lunar sinuous rilles, *Surv. Geophys., 5*, 245–279, doi:10.1007/ BF01454018.

Huppert, H.E., R.S.J. Sparks, J.S. Turner, and N.T. Arndt (1984), Emplacement and cooling of komatiite lavas, *Nature, 309*, 19-22.

Huppert, H.E., and R.S.J. Sparks (1985), Komatiites, I, Eruption and flow, *J. Petrol. 26*, 694-725.

Hurwitz, D.M., C.I. Fassett, J.W. Head, and L. Wilson (2010), Formation of an eroded lava channel within an Elysium Planitia impact crater: Distinguishing between a mechanical and thermal origin, *Icarus, 210*, 626-634.

Jaeger, J.C. (1957), The temperature in the neighborhood of a cooling intrusive sheet, *Am. J. Science, 255*, 306-318.

Jaeger, J.C. (1959), Temperatures outside a cooling intrusive sheet, *Am. J. Science, 257*, 44-54.

Jaeger, J.C. (1964), Thermal effects of intrusions, *Rev. Geophys., 2*, 443-466.

Jaeger, J.C. (1968), Cooling and solidification of igneous rocks, eds. H.H. Hess and A. Poldervaart, in Basalts: The Poldervaart treatise on rocks of basaltic composition, *Intersci. Publ.,* New York, 503-536.

Jaeger, W.L., L.P. Keszthelyi, A.S. McEwen, C.M. Dundas, and P.S. Russell (2007), Athabasca Valles, Mars: A Lava-Draped Channel System, *Science, 317*, 1709-1711, doi:10.1126/science.1143315.

Jaeger, W.L., L.P. Keszthelyi, J.A. Skinner Jr., M.P. Milazzo, A.S. McEwen, T.N. Titus, M.R. Rosiek, D.M. Galuszka, E. Howington-Kraus, R.L. Kirk, and the HiRISE Team (2010), Emplacement of the youngest flood lavas on Mars: A short, turbulent story, *Icarus, 205*, 230-243.

Jarvis, R.A. (1995), On the cross-sectional geometry of thermal erosion channels formed by turbulent lava flows, *J. Geophys. Res., 100*, 10,127-10,140.

Jones, W.P. and B.E. Launder (1972), The prediction of laminarization with a two-equation model of turbulence, *Intern. J. of Heat and Mass Transfer, 15*, 301-314.

Kakaç, S., R.K. Shah, and W. Aung (1987), Handbook of Single-Phase Convective Heat Transfer, *John Wiley & Sons*, New York.

Kauahikaua, J. (1996), Observations on basaltic lava stream dynamics on tubes from Kilauea, Hawaii, *EOS, Trans. Am. Geophys. Union, 77*, F807, abstract.

Kerr, A.C., G.F. Marriner, N.T. Arndt, J. Tarney, A. Nivia, A.D. Saunders, and R.A. Duncan (1996), The petrogenesis of Gorgona komatiites, picrites and basalts: new field, petrographic and geochemical constraints, *Lithos, 37*, 245-260.

Kerr, R.C. (2001), Thermal erosion by laminar lava flows, *J. Geophys. Res*., *106* (B11), 26,453-26,465.

Kerr, R.C. (2009), Thermal erosion of felsic ground by the laminar flow of a basaltic lava, with application to the Cave Basalt, Mount St. Helens, Washington, *J. Geophys. Res., 114*, B09204, doi:10.1029/2009JB006430.

Keszthelyi, L. (1994), Calculated effect of vesicles on the thermal properties of cooling basaltic lava flows, *J. Volcanol. Geotherm. Res., 63*, 257-266.

Keszthelyi, L. (1995), Measurements of the cooling at the base of pahoehoe flows, *Geophys. Res. Lett., 22*, 2195-2198.

Keszthelyi, L., and R. Denlinger (1996), The initial cooling of pahoehoe flow lobes, *Bull. Volcanol., 58*, 5-18.

Keszthelyi, L., S. Self, and Th. Thordarson (2006), Flood lavas on Earth, Io, and Mars, *J. Geol. Soc. London, 163*, 253-264.

Keszthelyi, L., W.L. Jaeger, C.M. Dundas, D.A. Williams, and V. Cataldo (2014), Evidence for possible mechanical erosion by lava at Athabasca Valles, Mars from HiRISE and CTX images and topography, *Lunar Planet. Sci., 45*, abstract 1683.

Komatsu, G., and V.R. Baker (1992), Venusian sinuous rilles, *LPI Contrib., 789*, 60-61.

Komatsu, G., V.R. Baker, V.C. Gulick, and T.J. Parker (1993), Venusian channels and valleys: Distribution and volcanological implications, *Icarus, 102*, 1-25.

Komatsu, G., and V.R. Baker (1994), Meander properties of Venusian channels, *Geol., 22*, 67-70.

Lange, R. A., and A. Navrotsky (1992), Heat capacities of Fe2O3-bearing silicate liquids, *Contrib. Mineral. Petrol., 110,* 311-320.

Langseth, M.G., S.J. Keihm, and J.L. Chute (1973), Heat flow experiment. In: *Apollo 17: Preliminary Science Report. NASA SP-330*, Washington, DC, pp. 1–24.

Larsen, E.S. (1945), Time required for the crystallization of the great batholith of southern and lower California, *Am. J. Science, 243A*, 399-416.

Launder, B.E., and B.I. Sharma (1974), Application of the energy dissipation model of turbulence to the calculation of flow near a spinning disk, *Lett. Heat and Mass Transfer, 1*, 2, 131-138.

Lawler, D.M. (1993), The measurement of river bank erosion and lateral channel change: a review, *Earth Surf. Proc. & Landforms Tech. & Software Bull., 18*, 777-821.

Leverington, D.W. (2011), A volcanic origin for the outflow channels of Mars: Key evidence and major implications, *Geomorphol., 132*, 51-75.

Llewellin, E.W., H.M. Mader, and S.D.R. Wilson (2002), The rheology of a bubbly liquid, *Proc. R. Soc. A, 458(2020)*, 987–1016, doi:10.1098/ rspa.2001.0924.

Lovering, T.S. (1935), Theory of heat conduction applied to geological problems, *Geol. Soc. Am. Bull., 48*, 69-94.

Lovering, T.S. (1936), Heat conduction in dissimilar rocks and the use of thermal models, *Geol. Soc. Am. Bull., 47*, 87-100.

Malin, M.C. (1980), Lengths of Hawaiian lava flows, *Geol., 8*, 306-308.

Malin, M.C., et al. (2007), Context camera investigation on board the Mars Reconnaissance Orbiter, *J. Geophys. Res., 112,* doi:10.1029/2006JE002808.

McEwen, A.S., M.S. Robinson, E.M. Eliason, P.G. Lucey, T.C. Duxbury, and P.D. Spudis (1994), Clementine observations of the Aristarchus region of the Moon, *Science 266*, 1858–1862, doi:10.1126/ science.266.5192.1858.

McEwen, A.S., et al. (2007), Mars Reconnaissance Orbiter's High Resolution Imaging Science Experiment (HiRISE), *J. Geophys. Res., 112* (E5), doi:10.1029/2005JE002605.

McEwen, A.S., L.P. Keszthelyi, and J.A. Grant (2012), Have there been large recent (Mid-Late Amazonian) water floods on Mars?, *Lunar and Planet. Sci., 43,* abstract 1612.

McSween, H.Y., et al. (2004), Basaltic rocks analyzed by the Spirit rover in Gusev

crater, *Science, 305*, 842-845.

McSween, H.Y., et al. (2008), Mineralogy of volcanic rocks in Gusev crater, Mars: Reconciling Mossbauer, Alpha Particle X-Ray Spectrometer, and Miniature Thermal Emission Spectrometer spectra, *J. Geophys. Res., 113*, doi:10.1029/2007JE002970.

Melosh, H.J. (1976), On the origin of fractures radial to lunar basins, *Proc. Lunar Sci. Conf.,* 7th, 2967-2982.

Menter, F.R. (1993), Zonal two-equation k-ω turbulence models for aerodynamic flow, *AIAA paper*, 93-2906.

Mo, X., I.S.E. Carmichael, M. Rivers, and J. Stebbins (1982), The partial molar volume of Fe_2O_3 in multicomponent silicate liquids and the pressure dependence of oxygen fugacity in magmas, *Mineral. Mag., 45,* 237-245.

Moore, H.J. (1965), Geologic map of Aristarchus region of the Moon, *U.S. Geol. Surv.*, *Geol. Invest*. Map I-465.

Moukalled, F., L. Mangani, and M. Darwish (2016), The finite volume method in computational fluid dynamics: An advanced introduction with OpenFOAM and Matlab, Ed. 1, *Springer Internat. Publish*., ISBN: 978-3-319-16873-9, doi:10.1007/978-3-319-16874-6.

Murchie, S., et al. (2007), Compact Reconnaissance Imaging Spectrometer for Mars (CRISM) on Mars Reconnaissance Orbiter (MRO), *J. Geophys. Res., 112*, doi: 10.1029/2006JE002682.

Mustard, J.F., C.M. Peters, P.J. Isaacson, J.W. Head, S. Besse, R.N. Clark, R.L. Klima, N.E. Petro, M.I. Staid, J.M. Sunshine, C.J. Runyon, and S. Tompkins (2011), Compositional diversity and geologic insights of the Aristarchus crater from Moon Mineralogy Mapper data, *J. Geophys. Res., 116*, E00G12, 1-17, doi:10.1029/2010JE003726.

Navrotsky, A. (1995), Energetics of silicate melts, in *Structure, Dynamics and Properties of Silicate Melts,* ed. J.F. Stebbins, P.F. McMillan, and D.B. Dingwell, *Rev. Mineral., 32,* pp. 121-142, Mineralog. Soc. of Am., Chantilly, Va.

Nichols, R.L. (1939), Viscosity of lava, *J. Geol., 47*, 290-302.

Olesen, K.W. (1987), Bed topography in shallow river bends, *Commun. Hydraul. Geotech. Eng., 87-1*, Delft Univ. of Technol., Delft, NL.

Patankar, S.V. and D.B. Spalding (1972), A calculation procedure for heat, mass and

momentum transfer in three-dimensional parabolic flows, *Int. J. Heat and Mass Transfer, 15*, 10, 1787-1806.

Peitersen, M.N., S.M. Baloga, L.S. Glaze, and J.A. Crisp (2000), The influence of degassing on the emplacement of lava flows: implications for planetary modeling studies, *Lunar Planet. Sci.* [CD-ROM]*, 31,* abstract 1063.

Peterson, D.W., and D.A. Swanson (1974), Observed formation of lava tubes during 1970-71 at Kilauea Volcano, Hawaii, *Stud. Speleol., 2*, 209-222.

Peterson, D.W., R.T. Holcomb, R.I. Tilling, and R.L. Christiansen (1994), Development of lava tubes in the light of observations at Mauna Ulu, Kilauea Volcano, Hawaii, *Bull. Volcanol., 56*, 343-360.

Pinkerton, H., and R.J. Stevenson (1992), Methods of determining the rheological properties of magma at sub-liquidus temperatures, *J. Volcanol. Geotherm. Res., 53*, 47-66.

Pinkerton, H., and L. Wilson (1994), Factors controlling the lengths of channel-fed lava flows, *Bull. Volcanol., 56*, 108-120.

Plescia, J.B. (1990), Recent flood lavas in the Elysium region of Mars, *Icarus, 88*, 465-490.

Price, P.H., and M.R. Slack (1954), The effect of latent heat on numerical solutions of the Heat flow equation, *Brit. J. Appl. Physics, 5*, 285-287.

Richter, S.W. (1993), Experimental determination of in situ utilization of lunar regolith for thermal energy storage, *NASA CR-191050*, Brook Park, OH, pp. 3-4.

Robie, R.A., B.S. Hemingway, and W.H. Wilson (1970), Specific Heats of Lunar Surface Materials from 90 to 350 K, *Apollo 11 Lunar Sci. Conf. 1st*. Pergamon Press, 3, 2361-2367.

Robinson, M., J.W. Ashley, A.K. Boyd, R.V. Wagner, E.J. Speyerer, B. Ray Hawke, H. Hiesinger, and C.H. Van Der Bogert (2012), Confirmation of sublunarean voids and thin layering in mare deposits, *Planet. Space Sci., 69*, 18–27.

Rumpf, M.E., H. Needham, and S.A. Fagents (2020), Thicknesses of lava flows in satellite images: comparison of layered mare units with terrestrial analogs, *Icarus, 350*, 113853, 1-15, https://doi.org/10.1016/j.icarus.2020.113853.

Sakimoto, S.E.H., J. Crisp, and S.M. Baloga (1997), Eruption constraints on tube-fed planetary lava flows, *J. Geophys. Res., 102*, 6597-6613.

Sakimoto, S.E.H., and T.K.P. Gregg (2019), On the formation of lunar sinuous rilles: insights from multiphysics modelling techniques, *Lunar Planet. Sci., 50*, abstract 3108.

Schaber, G.G. (1973), Lava flows in Mare Imbrium: geological evaluation from Apollo orbital photography, In: *Proc. Lunar Sci. Conf., 4th,* Houston, TX, 73-92.

Schenk, P.M., and D.A. Williams (2004), A potential thermal erosion lava channel on Io, *Geophys. Res. Lett., 31*, L23702, doi:1029/2004GL021378.

Schultz, P.H., and D.A. Crawford (2016), Origin and implications of non-radial Imbrium sculpture on the Moon, *Nature, 535*, 391-394, https://doi.org/10.1038/nature18278.

Self, S., L.P. Keszthelyi, and Th. Thordarson (1998), The importance of pahoehoe, *Ann. Rev. Earth Planet. Sci., 26*, 81-110.

Serway, R.A., and J.W. Jewett (2014), Physics for scientists and engineers with modern physics, *9th Ed., Brooks/Cole*, Boston, MA, 1622 pp.

Shaw, H.R., and D.A. Swanson (1970), Eruption and flow rates of flood basalts, in *Proc. 2nd Columbia River Basalt Sympos.*, eds. E.H. Gilmore and D.F. Stradling, pp. 271–299, East. Wash. State Coll. Press, Cheney.

Shaw, H.R. (1972), Viscosities of magmatic silicate liquids: An empirical method of prediction, *Am. J. Sci., 272,* 870-893.

Sibree, J.O. (1934), The viscosity of froth, *Trans. Faraday Soc., 30*, 325-331, https://doi.org/10.1039/TF9343000325.

Siewert, J., C. Ferlito (2008), Mechanical erosion by flowing lava, *Contemp. Phys., 49*, 43 –54, doi:10.1080/00107510802077388.

Solomon, S.C., and E.D. Duxbury (1987), A test of the longevity of impact-induced faults as preferred sites for later tectonic activity, *J. Geophys. Res. – Solid Earth*, *92*, B4, E759-E768, doi.org/10.1029/JB092iB04p0E759.

Spera, F.J., A. Borgia, and J. Strimple (1988), Rheology of melts and magmatic Suspensions. 1. Design and calibration of concentric cylinder viscometer with application to rhyolitic magma, *J. Geophys. Res., 93* (B9), 10,273-10,294.

Spudis, P., G.A. Swann, and R. Greeley (1988), The formation of Hadley Rille and implications for the geology of the Apollo 15 region, *Proc. Lunar Planet. Sci. Conf. 18th*, Lunar Planet. Inst., 243-254.

Spudis, P.D. (2015), Volcanism on the Moon, eds. H. Sigurdsson, B. Houghton, H. Rymer, J. Stix, and S. McNutt, in *The Encyclopedia of Volcanoes*, 689-700. ISBN: 9780123859389.

Strom, R.G. (1964), Analysis of lunar lineaments I. Tectonic maps of the Moon, *Communic. lunar planet. lab., 2*, 205-216.

Swann, G.A., et al. (1972), Preliminary geologic investigation of the Apollo 15 landing site, in *Apollo 15: Prelim. Science Rep., NASA SP-289*, 21-31.

Swanson, D.A. (1973), Pahoehoe flows from the 1969-1971 Mauna Ulu eruption, Kilauea Volcano, Hawaii, *Geol. Soc. Am. Bull., 84*, 615-626.

Taylor, S.R. (1975), Lunar science: A post-Apollo view, *Pergamon Press*, New York, pp. 26.

Titus, M.R. , D.M. Rosiek Galuszka, E. Howington-Kraus, R.L. Kirk, and the HiRISE Team (2010), Emplacement of the youngest flood lavas on Mars: A short, turbulent story, *Icarus, 205*, 230-243.

Usselman, T.M., D.S. Hodge, A.J. Naldrett, and I.H. Campbell (1979), Physical constraints on the characteristics of nickel-sulfide ore in ultramafic lavas, *Can. Mineral., 17*, 361-372.

Vaniman, D.T., R. Reedy, G.H. Heiken, G. Olhoeft, and W.W. Mendell (1991), The lunar environment, eds., G.H. Heiken, D.T. Vaniman, and B.M. French, in: *The Lunar Source Book: A User's Guide to the Moon, Cambridge Univ. Press*, CB, pp. 27-60.

Wadge, G. (1978), Effusion rate and the shape of aa lava flow-fields on Mt Etna, *Geol., 6*, 503-506.

Wadge, G. (1981), The variation of magma discharge during basaltic eruptions, *J. Volcanol. Geotherm. Res., 11*, 139-168.

Walker, G.P.L. (1973), Lengths of lava flows, *Philos. Trans. Royal Soc. London, A274*, 107-118.

Walker, D., R.J. Kirkpatrick, J. Longhi, and J.F. Hays (1976), Crystallization history of lunar picrite basalt 12002: Phase equilibria and cooling rate studies, *Geol. Soc. Am. Bull., 87*, 646-656.

Warren, P.H. (1990), Lunar anorthosites and the magma-ocean plagioclase-flotation hypothesis: Importance of FeO enrichment in the parent magma, *Amer. Mineral., 75*, 1-2, 46-58.

Wieczorek, M.A., M.T. Zuber, and R.J. Phillips (2000), The control of magma buoyancy on the eruption of mare basalts, *Lunar Planet. Sci. Conf. 31st*, abstract 1520.

Wieczorek, M.A., M.T. Zuber, and R.J. Phillips (2001), The role of magma buoyancy on the eruption of lunar basalts, *Earth Planet. Sci. Lett., 185*, 71–83, doi:10.1016/S0012-821X(00)00355-1.

Wilhelms, D.E. (1987), The geologic history of the Moon, *U.S. Geol. Survey Prof. Paper, 1348*, 342 pp.

Williams, D.A., R.C. Kerr, and C.M. Lesher (1998), Emplacement and erosion by Archean komatiite lava flows at Kambalda: Revisited, *J. Geophys. Res., 103*, 27,533-27,550.

Williams, D.A., S.A. Fagents, and R. Greeley (2000), A reassessment of the emplacement and erosional potential of turbulent, low-viscosity lavas on the Moon, *J. Geophys. Res., 105* (E8), 20,189-20,205.

Williams, D.A., R. Greeley, E. Hauber, K. Gwinner, and G. Neukum (2005), Erosion by flowing Martian lava: New insights for Hecates Tholus from *Mars Express* and *MER* data, *J. Geophys. Res*., *110*, E05006, doi:10.1029/2004JE002377.

Wilson, L., and J.W.III Head (1981), Ascent and eruption of basaltic magma on the Earth and Moon, *J. Geophys. Res., 86*, 2971–3001, doi:10.1029/JB086iB04p02971.

Wilson, L., and P.J. Mouginis-Mark (1984), Martian sinuous rilles, *Lunar and Planet. Sci., XV*, 926-927, abstract.

Wilson, L., and P.J. Mouginis-Mark (2001), Estimation of volcanic eruptions conditions for a large flank event on Elysium Mons, Mars, *J. Geophys. Res., 106*, 20,621-20,628.

Wilson, L., and J.W. Head (2017), Generation, ascent and eruption of magma on the Moon: New insights into source depths, magma supply, intrusions and effusive/explosive eruptions (Part 1: Theory), *Icarus, 283*, 146-175.

Wood, C. (1981), Exploration and geology of some lava tube caves on the Hawaiian volcanoes, *Trans. Brit. Cave Res. Assoc., 8*, 111-129.

Zhang, F., Y.L. Zou, Y.C. Zheng, X. H. Fu, and Y.C. Zhu (2014), Lunar mare basalts in the Aristarchus region: Implications for the stratigraphic sequence from Clementine UVVIS Data, *Icarus, 227*, 132-151, doi: 10.1016/j.icarus.2013.09.011.

Zhang, F., and M.H. Zhu (2017), Resurfacing of Procellarum-Imbrium region by tectonism and volcanism: The role of the basin-radial fracture zones around the Imbrium basin, *Lunar Planet. Sci., 48th*, abstract 1710.

Zisk, S. H., C.A. Hodges, H.G. Moore, R.W. Shorthill, T.W. Thompson, E.A. Whitaker, and D.E. Wilhelms (1977), The Aristarchus–Harbinger region of the Moon: Surface geology and history from recent remote sensing observations, *Moon, 17*, 59 –99, doi:10.1007/BF00566853.

APPENDIX A

COMPUTER CODE AND 0 FOLDER

CODE: TEMPERATURE FILE

```
{
    alphat = turbulence->nut()/Prt;
    alphat.correctBoundaryConditions();

    volScalarField alphaEff("alphaEff", turbulence->nu()/Pr + alphat);

    volScalarField alphaEff2("alphaEff2", (turbulence->nu()/Pr +
    alphat)*Cp_int/((densityRatio*Lg)+densityRatio*Cg*tempDiff));

    /* Pr_interf = Cp*μb/Keff_interf */

    fvScalarMatrix TEqn
    (
        fvm::div(phi, T)
      - fvm::laplacian(alphaEff, T)
     ==
        fvOptions(T)
    );

    TEqn.relax();

    fvOptions.constrain(TEqn);

    TEqn.solve();

    fvOptions.correct(T);



    /* calculation of erosion rate at the lava/channel bed & bank
       interface */

            const fvPatchList& patches = mesh.boundary();
              forAll(erosionRate.boundaryFieldRef(), patchi)
            {
                const fvPatch& currPatch = patches[patchi];

                if (isA<wallFvPatch>(currPatch))
                {
                    erosionRate.boundaryFieldRef()[patchi]=-8640000*
                    alphaEff2.boundaryFieldRef()[patchi]*T.boundary
                    FieldRef()[patchi].snGrad();
                }
            }
}
```

0 FOLDER: SCENARIO 1 TEMPERATURE

```
FoamFile
{
    version     2.0;
    format      ascii;
    class       volScalarField;
    location    "0";
    object      T;
}
// * * * * * * * * * * * * * * * * * * * * * * * * * * * * * * * * * * * * //

dimensions      [0 0 0 1 0 0 0];

internalField   uniform 1415; // 25°C < T_erupt (1440°C)

boundaryField
{
    inlet
    {
        type            fixedValue;
        value           uniform 1415; // 25°C < T_erupt (1440°C)
    }
    outlet
    {
        type            zeroGradient;
    }
    top
    {
        type            fixedGradient;
        gradient        uniform -2.5; // heat loss by radiation
    }
    bed
    {
         type           fixedValue;
         value          uniform 1375; // 40°C < T_inlet (20 m flow)
    }
    leftbank
    {
         type           fixedValue;
         value          uniform 1375; // 40°C < T_inlet (20 m flow)
    }
    rightbank
    {
         type           fixedValue;
         value          uniform 1375; // 40°C < T_inlet (20 m flow)
    }
}
```

0 FOLDER: SCENARIO 2 TEMPERATURE

```
FoamFile
{
    version     2.0;
    format      ascii;
    class       volScalarField;
    location    "0";
    object      T;
}
// * * * * * * * * * * * * * * * * * * * * * * * * * * * * * * * * * * * * //

dimensions      [0 0 0 1 0 0 0];

internalField   uniform 1440;

boundaryField
{
    inlet
    {
        type            fixedValue;
        value           uniform 1440;
    }
    outlet
    {
        type            zeroGradient;
    }
    top
    {
        type            zeroGradient; // insulated flow
    }
    bed
    {
        type            fixedValue;
        value           uniform 1400; // 40°C < T_inlet (20 m flow)
    }
    leftbank
    {
        type            fixedValue;
        value           uniform 1400; // 40°C < T_inlet (20 m flow)
    }
    rightbank
    {
        type            fixedValue;
        value           uniform 1400; // 40°C < T_inlet (20 m flow)
    }
}
```

0 FOLDER: TURBULENT KINETIC ENERGY

```
FoamFile
{
    version     2.0;
    format      ascii;
    class       volScalarField;
    location    "0";
    object      k;
}
// * * * * * * * * * * * * * * * * * * * * * * * * * * * * * * * * * * * * //


dimensions      [0 2 -2 0 0 0 0]; // hydraulic radius h_R = 16 m

internalFielduniform 8.624e-06; // calcul. from Menter (1993)

boundaryField
{
    inlet
    {
        type            fixedValue;
        value           uniform 1.1702293e-01; // calculated
    }
    outlet
    {
        type            zeroGradient;
    }
    top
    {
        type            zeroGradient;
    }
   bed
    {
        type            kqRWallFunction;
        value           uniform 0; // from Menter (1993)
    }
    leftbank
    {
        type            kqRWallFunction;
        value           uniform 0; // from Menter (1993)
    }
    rightbank
    {
        type            kqRWallFunction;
        value           uniform 0; // from Menter (1993)
    }
}
```

0 FOLDER: TURBULENT DISSIPATION

```
FoamFile
{
    version     2.0;
    format      ascii;
    class       volScalarField;
    location    "0";
    object      omega;
}
// * * * * * * * * * * * * * * * * * * * * * * * * * * * * * * * * * * * * //

dimensions      [0 0 -1 0 0 0 0];

internalField   uniform 2.8125; // calcul., Menter (1993)

boundaryField
{
    inlet
    {
        type            fixedValue;
        value           uniform 0.557644; // calcul., Menter (1993)
    }
    outlet
    {
        type            zeroGradient;
    }
    top
    {
        type            zeroGradient;
    }
    bed
    {
        type            omegaWallFunction;
        value           uniform 2.1856; // calcul., Menter (1993)
    }
    leftbank
    {
        type            omegaWallFunction;
        value           uniform 2.1856; // calcul., Menter (1993)
    }
    rightbank
    {
        type            omegaWallFunction;
        value           uniform 2.1856; // calcul., Menter (1993)
    }
}
```

0 FOLDER: TURBULENT VISCOSITY

```
FoamFile
{
    version     2.0;
    format      ascii;
    class       volScalarField;
    location    "0";
    object      nut;
}
// * * * * * * * * * * * * * * * * * * * * * * * * * * * * * * * * * * * * //

dimensions      [0 2 -1 0 0 0 0];

internalField   uniform 1e-03;

boundaryField
{
    inlet
    {
        type           fixedValue;
        value          uniform 1e-03;
    }
    outlet
    {
        type           zeroGradient;
    }
    top
    {
        type           slip;
    }
    bed
    {
        type           nutkWallFunction;
        value          uniform 0;
    }
    leftbank
    {
        type           nutkWallFunction;
        value          uniform 0;
    }
    rightbank
    {
        type           nutkWallFunction;
        value          uniform 0;
    }
}
```

0 FOLDER: TURBULENT DIFFUSIVITY

```
FoamFile
{
    version     2.0;
    format      ascii;
    class       volScalarField;
    location    "0";
    object      alphat;
}
// * * * * * * * * * * * * * * * * * * * * * * * * * * * * * * * * * * //

dimensions      [0 2 -1 0 0 0 0];

internalField   uniform 0.001;

boundaryField
{
    inlet
    {
        type            fixedValue;
        value           uniform 0.001;
    }
    outlet
    {
        type            zeroGradient;
    }
    top
    {
        type            zeroGradient;
    }
    bed
    {
        type            alphatJayatillekeWallFunction;
        Prt             0.85;
        value           uniform 0;
    }
    leftbank
    {
        type            alphatJayatillekeWallFunction;
        Prt             0.85;
        value           uniform 0;
    }
    rightbank
    {
        type            alphatJayatillekeWallFunction;
        Prt             0.85;
        value           uniform 0;
    }
}
```